UNIVERSITÁ DEGLI STUDI DI PAVIA

Dipartimento di Scienze del Sistema Nervoso e del Comportamento

Dottorato in Scienze Biomediche

Direttore Prof. Egidio D'Angelo

Curriculum in Neuroscienze

Ciclo n. XXIX

UNIVERSITE PIERRE ET MARIE CURIE

Ecole doctorale de rattachement : ED 158 Cerveau, cognition, comportement

Laboratoire de Neuroncologie Expérimentale, Institut du Cerveau et de la Moelle

MOLECULAR MARKERS OF GLIOMAS

Implications for diagnosis and new target therapies

defended by Anna Luisa Di Stefano

under shared supervision of Prof. Marc Sanson and Prof. Mauro Ceroni

Composition of the Jury
President : Prof. Stefano Bastianello, Pavia
Reviewer : Prof. Francois Ducray, Lyon
Reviewer : Prof. Lorenzo Bello, Milano
Committee member : Dott. Enrico Marchioni, Pavia
Committee member : Prof. Jean-Philippe Spano, Paris
Committee member : Prof. Pierre Verrelle, Clermont Ferrand
Supervisor : Prof. Marc Sanson, Paris
Co-supervisor : Prof. Mauro Ceroni, Pavia

ACKNOWLEDGEMENTS

My Sincerest Thanks To:

Professor Marc Sanson, Director of Experimental Neuro-Oncology Lab at ICM, for the thoughtful support, constructive criticism, genuine enthusiasm and challenges we faced together over these last 3 years as well as the great opportunities he offered me for international collaborations that permitted the PhD project to advance.

I must also extend my gratitude to Professor Mauro Ceroni, my co-director and teacher, for his support and endless encouragement from the University of Pavia.

Regarding the three main projects that are presented in this thesis, a special thanks to Professor Richard Houlston, Victor Enciso Mora, Ben Kynnensley and Karim Larbreche from Institute of Cancer Research, for sharing results and advancements in GWA studies.

The project on *FGFR-TACC* fusions would not have been possible without Professors Antonio Iavarone and Anna Lasorella, for accepting me in their team in Columbia University and all their lab members, especially Alessandra Fucci, for her in-depth explanation of the genomic background of the spectrum of *FGFR-TACC* fusions and

her essential support on experiments and manuscript preparation. Regarding following studies on *FGFR-TACC* fusions, I have to especially thank Alberto Picca for his help, Julien Savatovsky for MRI analysis and Karima Mokhtari and Frank Bielle for their essential cooperation and their original and acute observations.

I thank all our collaborators from other institutions in the setting of ANOCEF for the interest shown in the enlargement of screening and identification of newly *FGFR-TACC* positive patients permitting the clinical trial, which is actually going on.

Regarding the project on 2 HG non-invasive detection, I have to especially thank Francesca Branzoli, physicist at CENIR, whose earnest, successful efforts on MEGA-PRESS were crucial to the success of the study. I also thank Chris Ottololenghi for his assistance on dosages of tumor 2 HG, Stephane Lehericy, Director of Cenir and Malgorzata Marjanska for their helpful suggestion of MRS sequence and Laurent Capelle for his collaboration on patients' enrolment.

I thank all present and former members of the Experimental Neuro-oncology Lab from ICM for their help and efforts, especially Marianne Labussiere, who supported and coached me from my very first moments in the lab, as well as Yohann Schmitt, Amithys Rahimian, Marine Giry, Catherine Carpentier and Blandine Boisselier.

I thank all my colleagues from Pitié Salpétrière Neuro-oncology Unit for their interest and collaboration on follow-up of *FGFR-TACC* patients and identification of new candidates for 2 HG detection. Your continual support during my clinical training in neuro-oncology is much appreciated.

I also owe thanks to all new colleagues from H. Foch for welcoming me: Dr. Frederic Bourdain and Dr. Stephane Gaillard enthusiastically and energetically supported my endeavours along with the whole multidisciplinary group, especially Chiara Villa, whose support for project development is crucial. To Betrand Baussart, Patrizia Farina and all members of our multidisciplinary group, you are deeply appreciated for all that you do.

I would be remiss to not mention Professor Jean Yves Delattre, who drove me and stoked my passion since I was a student and is, has been and will be my landmark in this field.

Of course I must also give a sincere thank you to Professor Hoang Xuan for giving me the opportunity to blossom as a clinician in his group, benefitting tremendously from his training and constant encouragement.

I thank Professor Stefano Bastianello and Doctor Enrico Marchioni for their precious help and the crucial discussions on neuro-oncology.

I thank also our collaborator and good friend Marica Eoli from Institute Besta, which made me grew up in neuroncology in first moments and Giulia Berzero which in turn joined us in this field for the constant help and sincere friendship.

Many thanks to the Association pour la Recherche sur les Tumeurs Cérébrales Malignes, the University of Pavia, the Department of Brain Behavioural Science, Premio Riquier, Fondazione Costa and Collegio Ghislieri for their support in developing research during these last three years.

Many thanks to Mme Isabelle Tounian and Mme Stephanie Girard who constantly assist me in daily clinical activity.

Last, but certainly not least, my sincerest thanks go to Giovanni, all my fantastic family, my nephews Anita and Ettore, friends, fellows and mates that shared this journey.
My sincerest thanks and gratitude go out to you all.

ABSTRACT

The 2016 WHO classification of gliomas integrates molecular alterations (ie *IDH* mutations, and 1p19q codeletion) to histological features, defining distinct histo-molecular entities: *IDH* wild-type gliomas (mostly glioblastomas), and *IDH* mutated gliomas, divided according to 1p19q status into astrocytomas (1p19q intact) and oligodendrogliomas (1p19q codeleted).

The first part of the manuscript is a contribution to molecular classification based on *TERT* promoter mutational status. We also contributed to GWAS analysis, and investigated the association between the risk loci and specific molecular entities, showing that some loci are associated with glioblastoma and *IDH* wild-type gliomas (rs2736100 near *RTEL1*, rs6010620 near *TERT*, rs3851634 near *POLR3B*) whereas others are associated to *IDH* mutated gliomas (rs4295627 and rs55705857 near *CCDC26*, rs498872 near *PHLDB1*, rs7572263 near *IDH1*, rs11196067 near *VTI1A*, rs648044, near *ZBTB16* and rs12230172). Notably, rs4295627 and rs55705857 near CCD26 resulted strongly associated to 1p19q codeletion and to risk of oligodendrogliomas (P=2.31 x10-^{94}).

The second part of this work is devoted to the characterization of a specific oncogenic fusion between *FGFR* and *TACC* genes, which initially reported 3% of glioblastoma (GBM) and other human cancers and is proposed as a new therapeutic target. Overall, we screened 907 gliomas for *FGFR3-TACC3* fusions. We found that *FGFR3-TACC3* fusions exclusively affect *IDH* wild-type gliomas (3%), and are mutually exclusive with the *EGFR* amplification and the *EGFR* vIII variant, whereas it co-occurs with *CDK4* amplification, *MDM2* amplification and 10q loss. *FGFR3–TACC3* fusions were associated with strong and homogeneous *FGFR3* immunostaining. We show that *FGFR3* immunostaining is a sensitive predictor of the presence of *FGFR3-TACC3* fusions. *FGFR3-TACC3* glioma patients had a longer overall survival than those patients with *IDH* wild-type glioma. We treated two patients with *FGFR3–*

TACC3 rearrangements with a specific FGFR-TK inhibitor and we observed a clinical improvement in both and a minor response in one patient. These data support the systematic screening for *FGFR-TACC* fusion in all *IDH* wild-type glioma patients who can benefit from *FGFR* inhibition.

In the third section, we developed a non-invasive diagnostic tool by 1H-magnetic resonance spectroscopy in *IDH* mutant gliomas. We optimized a uniquely different spectroscopy sequence called MEGA-PRESS for the detection of the oncometabolite *2-hydroxyglutarate* (2 HG) that specifically accumulates in *IDH* mutant gliomas. We analysed a prospective cohort of 25 patients before surgery for suspected grade II and grade III gliomas and we assessed specificity and sensitivity, correlation with 2 HG concentrations in the tumor and associations with grade and genomic background.

We found that MEGA-PRESS is highly specific (100%) and sensitive (95.2%) for the prediction of *IDH* mutation and correlated with 2 HG levels measured by gas chromatography-tandem mass spectrometry (GC-MS/MS) in frozen tissue. Preliminary follow-up during radio-chemotherapy regimen and anti-IDH therapy showed a decrease in 2 HG production. In conclusion, MEGA-PRESS is a reliable tool for *IDH* mutation prediction at pre-surgical stages and for measuring the activity of anti-cancer drugs. Long-term monitoring will help to clarify the prognostic and predictive value of 2 HG decrease during anti-cancer treatment.

RÉSUMÉ

La classification des gliomes OMS 2016 a récemment intégré aux caractéristiques histologiques deux principales altérations moléculaires (la mutation *IDH* et la codélétion 1p19) et a défini deux entités histo-moléculaires distincts : les gliomes *IDH* wild-type (principalement les glioblastomes, GBM) et les gliomes *IDH* mutés, séparés sur la base du statut 1p19q en astrocytomes (1p19q non codélétés) et oligodendrogliomes (1p19 codeletés).

La première partie du manuscrit est une contribution à la classification moléculaire des gliomes, basée sur la présence de la mutation du promoteur de *TERT* et de la mutation de *IDH*. Nous avons également contribués aux études de *genome-wide association* (GWAS), nous avons plus particulièrement exploré l'association entre les loci à risque et les sous-groupes moléculaires. Nous avons montré que certains loci sont associés aux gliomes *IDH* wild-type et aux glioblastomes (rs2736100 à proximité de *RTEL1*, rs6010620 à proximité de *TERT*, rs3851634 à proximité de *POLR3B*) et que d'autres sont associés aux gliomes *IDH* mutés (rs4295627 et rs55705857 à proximité de *CCDC26*, rs498872 à proximité de *PHLDB1*, rs7572263 à proximité de *IDH1*, rs11196067 à proximité de *VTI1A*, rs648044, à proximité de *ZBTB16* et rs12230172). Notamment rs4295627 et rs55705857 à proximité de *CCDC26* sont fortement associés à la codeletion 1p19q *(P*=2.31 x10-^{94})

La deuxième partie de mon travail est dédiée à la caractérisation de fusions spécifiques oncogéniques entre les gènes *FGFR* et *TACC*, qui avaient été initialement décrites dans 3% des GBM et dans d'autres cancers et identifiés comme une nouvelle cible thérapeutique.

Au total nous avons analysé 907 gliomes pour la présence du gène de fusion *FGFR3-TACC3*. Nous avons montré que les fusions *FGFR3-TACC3* ne touchent que les gliomes *IDH* wild-type (3%), sont mutuellement exclusives avec l'amplification de *EGFR* et avec la forme tronquée *EGFRvIII* et inversement, sont associées à l'amplification de *CDK4* et de *MDM2* et à la délétion du 10q.

Les fusions *FGFR3-TACC3* sont associées à une expression intense et diffuse de *FGFR3* en immunohistochimie (IHC). Nous avons montré que l'IHC pour *FGFR3* est un marqueur prédictif très sensible de la présence des fusions *FGFR3-TACC3*.

Les patients porteurs d'une fusion *FGFR3-TACC3* ont une survie globale significativement plus longue comparés aux patients avec gliome *IDH* wild-type. Nous avons traité deux patients porteurs d'un gène de fusion *FGFR3-TACC3* avec un inhibiteur tyrosine-kinase (TK) spécifique pour FGFR et nous avons observé une amélioration clinique avec stabilisation de maladie et une réponse mineur chez un patient.

Ces résultats justifient la réalisation d'un criblage systématique pour les gènes de fusions *FGFR3-TACC3* chez tout nouveau gliome *IDH* wild-type nouvellement diagnostiqué qui pourrait ainsi bénéficier d'un traitement par inhibiteur TK spécifique pour FGFR.

Dans la troisième section, nous avons développé une méthode diagnostique non invasive avec la 1-H spectroscopie en résonance magnétique (1H-MRS) chez les patients porteurs d'un gliome *IDH* muté. Nous avons optimisé une nouvelle séquence de spectroscopie différentielle-MEGA-PRESS- pour la détection de l'oncometabolite *2-hydroxyglutarate* (2 HG) qui s'accumule de manière spécifique dans les gliomes *IDH* mutés. Nous avons analysé de façon prospective une cohorte de 25 patients avant chirurgie pour probable gliome de grade II et grade III et nous avons calculé la sensibilité, la spécificité, la valeur prédictive positive et négative de la détection du pic de 2 HG, sa corrélation avec les concentrations de 2 HG dans le tissu et l'association avec le grade et le profil génomique.

Nous avons trouvé que la MEGA-PRESS est hautement spécifique (100%) et sensible (95.2%) dans la prédiction de la présence de la mutation *IDH*. Son taux est corrélé aux concentrations de 2 HG mesurés sur tissu congelé par spectrométrie de masse (gas chromatography-tandem mass spectrometry GC-MS/MS).

Des résultats préliminaires de suivi de patients traités pour un gliome *IDH* muté par radio-chimiothérapie ou par inhibiteur spécifique de IDH muté montrent une réduction sous traitement de la production de 2 HG. En conclusion la MEGA-PRESS est une technique fiable pour la prédiction de la mutation de *IDH* en phase préopératoire et également comme mesure d'activité des thérapies anticancéreuses. Le suivi à long terme pourra préciser la valeur d'une diminution du 2 HG aussi bien pronostique que prédictive de réponse aux traitements anti-cancéreux.

INDEX

1. INTRODUCTION

1.1 Histological and Molecular Background of Gliomas

Gliomas account for 30% of all primary brain tumors and are responsible for around 13,000 cancer-related deaths in the US each year (Ostrom, 2015; Siegel, 2011). Newly diagnosed gliomas are estimated around 20,000 in the US and 2500 to 3000 in France per year (Rigau, 2011)

For the past century, the classification of brain tumors has been based largely on concepts of histogenesis that tumors can be classified according to their microscopic similarities with different putative cells of origin and their presumed levels of differentiation (Louis, 2007). However, rresearch into glioma biology of the last two decades, has led to the discovery of molecular alterations that proved to better define biological entities and clinical aggressiveness.

As a result of the success of prognostic stratification according to genomic background of gliomas, the WHO (World Health Organization) recently updated the classification of brain tumors (Louis, 2016) and stated that two of them – the isocitrate dehydrogenase (*IDH*) mutations and chromosomes 1p19q codeletion – are determinant for the so-called "integrated" diagnosis, irrespective of morphological similarities of tumor cells to putative progenitors.

By now, brain tumor entities are broadly separated according to two main dichotomies:

- *IDH* mutations principally differentiate the more indolent lower-grade gliomas (grade II and grade III and progressive glioblastoma) from primary glioblastoma, the most aggressive of gliomas.
- 1p19q codeletion, which is tightly associated to *IDH* mutations, specifically tags oligodendrogliomas among lower-grades.

Isocitrate dehydrogenase is an enzyme with three isoforms, i.e., IDH1, IDH2, and IDH3 (Dang, 2010). Intra-cellularly, it catalyses the oxidative

decarboxylation of isocitrate to α-ketoglutarate (α-KG) (Arcaro, 2007; Dang, 2010). *IDH* mutations harbour in specific cancer entities: in gliomas (70–90% of low-grade gliomas and secondary glioblastoma), in haematological malignancies (~20% of acute myeloid leukaemia), in intrahepatic cholangiocarcinoma, chondrosarcoma and melanoma (Gross, 2010; Parsons, 2008; Waitkus, 2016; Yang, 2012). Glioma-specific mutations always affect the amino acid arginine in position 132 in *IDH1* and arginine at position 172 in *IDH2* (Hartmann, 2009).
The *IDH1* mutation is one of the earliest known genetic events in low-grade gliomas; it is thought to be a "driver" mutation for tumorigenesis (Suzuki, 2015) probably by accumulation of the onco-metabolite *2-hydroxyglutarate* (2 HG).
At a prognostic level, *IDH* mutations have revealed to have a major prognostic impact on morphological stratification based on the WHO's 2007 glioma grades, depicting a more favourable prognosis in *IDH* mutants compared to tumors with wild-type *IDH* in all glioma grades (Sanson, 2009) and recognizing a worse outcome common to the group of *IDH* wild-type gliomas independent of their grading (Louis, 2016).

Chromosome 1p/19q codeletion is strongly associated with classical oligodendroglial features. It results from an unbalanced translocation between the entire arm of 19p and 1q (Jenkins, 2006). At the genomic level, it corresponds to a complete loss of the 1p and 19q arms, which is important to distinguish from 1p partial distal deletions (typically 1p36) that occur in astrocytic tumors and are associated with a poor prognosis (Idbaih, 2005; Idbaih, 2008; Vogazianou, 2010).
1p19q codeletion is a strong favourable prognostic factor and since 1998 it has been associated with response and benefit to adjuvant chemotherapy with PCV after radiotherapy in anaplastic oligodendroglioma (Cairncross, 2014).
The reasons for this better prognosis are yet to be determined.
1p19q codeleted gliomas are systematically associated with *IDH1* or *IDH2* (Labussiere, 2010) and combinations of these molecular subgroups (*IDH*mutated+1p19q codeleted/*IDH*mutated+non codeleted and *IDH* wild-type

gliomas) correlate with marked differences in survival rates (**Figure 5.2, Chapter 5.1-Section 3)**.

The simplified algorithm of new integrated classification of gliomas from the WHO's 2016 (Louis, 2016) basing of *IDH* and 1p19q status, is reported in **Figure 1.1.**

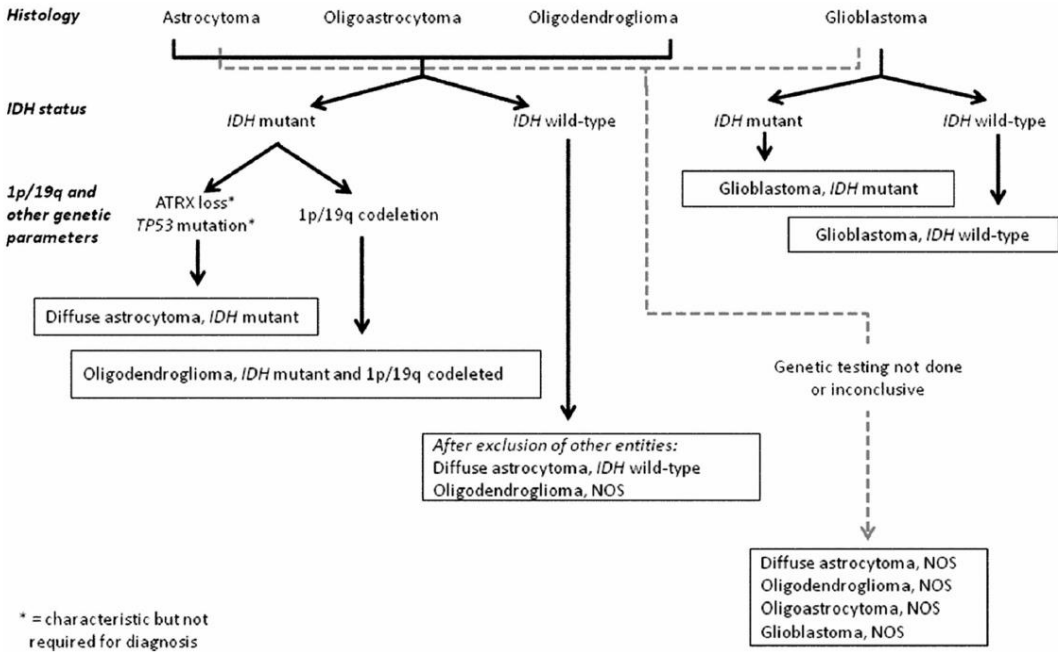

Figure 1.1 adapted from Louis et al. 2016. A simplified algorithm for classification of the diffuse gliomas based on histological and genetic features according to WHO 2016.

2. AIMS

The 3-year study in the present thesis is focused on implications for diagnosis and new therapies of two distinct driver molecular aberrations harbouring in the two principal entities discussed before: the *IDH* wild-type and *IDH*-mutant gliomas.

The study is articulated in three sections.

Section 1 correspond to our contribution to the molecular classification of gliomas basing on *IDH* and *TERT* mutational status and to correlations of glioma susceptibility germ line variants with tumor phenotype and molecular background.

Section 2 "Detection, Characterization, and Inhibition of *FGFR-TACC* Fusions in *IDH* Wild-type Glioma" is dedicated to a novel targetable aberration-the *FGFR-TACC* gene fusions-in *IDH* wild-type gliomas.
In this study, conducted with the collaboration of Dr. Iavarone and Dr. Lasorella's research group at Columbia University:

- we determine distribution and frequency of *FGFR-TACC* fusions in gliomas,
- we explore *FGFR-TACC* fusions, transcripts, repertoire and genomic background of *FGFR-TACC* positive gliomas,
- we validate a screening method and correlate with *FGFR3* expression
- we characterize clinical features and evolution of patients harbouring *FGFR-TACC* fusions, and
- we explore signals of activity of specific anti-*FGFR* therapies in two patients harbouring *FGFR-TACC* fusions.

First results of this study were published in Clinical Cancer Research (Di Stefano, 2015). The expansion study, not published to date, is developed in **Chapter 4.2**.

In Section 3, "In vivo non-invasive detection of *2-hydroxyglutarate* in *IDH* mutated gliomas" we focussed on the diagnostic implication of the *IDH* mutation in gliomas.

Aims of this study were:

- to develop and apply Magnetic Resonance Spectroscopy (MRS) protocols for non invasive detection of 2 HG accumulation in *IDH* mutant glioma patients,
- to explore correlations of 2 HG accumulation by MRS and 2 HG tissue dosages, and
- to follow 2 HG variations by MRS during convectional but also targeted anti-IDH therapies in *IDH* mutant patients.

Preliminary results correspond to the manuscript in preparation for publication.

3. SECTION 1-OUR CONTRIBUTION TO THE MOLECULAR CLASSIFICATION OF GLIOMAS

A supplementary molecular alteration that can enhance prognostic classification is the mutation in the promoter of *TERT*, which encodes telomerase. The increased telomerase activity seen in cancer leads to preservation of telomeres, allowing tumors to avoid induction of senescence.

Among other cancer, somatic mutations of the *TERT* promoter (*TERTp*-mut) have been documented in gliomas (Killela, 2013; Labussiere, 2014). The two most common mutations in *TERT*, C228T and C250T, map -124 and -146 bp, respectively, upstream of the *TERT* ATG site (chr5, 1,295,228 C4T and 1,295,250 C4T, respectively), creating binding sites for Ets/TCF transcription factors.

In the two following studies (Labussiere, 2014;Labussiere, 2014) we largely screened brain tumor banks from Pitié-Salpetriere (Onconeurotek) for *TERTp*-mutation (807 gliomas), and we explored the prognostic value and its association with main molecular aberrations in gliomas, such as *IDH* mutation, 1p19 codeletion and *EGFR* amplification.

As a result, in the first article (Labussiere, 2014) we reported that:

- prevalence of *TERTp*-mut is around 69% in gliomas
- we showed that *TERTp*-mut clusters specularly with *IDH* mutation in 89% of *IDH*+/1p19 codeleted gliomas (corresponding to oligodendrogliomas) and also with 75% of *IDH* wild-type glioblastoma
- we showed that *TERTp*-mut is a determinant prognostic factor but interestingly its prognostic impact is contextual and depends on the histologic and genomic background of the tumor
- we proposed a molecular stratification of tumors by both *IDH1*/2 and *TERTp*-mut status in gliomas.

In a second study (Labussiere, 2014) we focussed on glioblastoma:

- showing that *TERTp*-mut is an independent factor of poor prognosis in GBM, and even stronger in *IDH* mutated GBM
- we also proposed a refined prognostic classification of GBMs based on joint analyses of *TERT*, *EGFR*, and *IDH*.

Such molecular prognostic classification of gliomas have been reproduced by other groups (Killela, 2014) and became a paradigm to define five principal groups of gliomas with characteristic distributions of age at diagnosis, clinical behavior, acquired genetic alterations, and associated germ line variants (Eckel-Passow, 2015).

Articles we coauthored on *TERTp*-mutation in gliomas and molecular prognostic classifications (Labussiere, 2014; Labussiere, 2014) are reported in this section.

FULL PAPER

BJC

British Journal of Cancer (2014) 111, 2024–2032 | doi: 10.1038/bjc.2014.538

Keywords: gliomas; *TERT* promoter mutation; prognostic impact; *IDH* mutation; gliomas molecular classification

TERT promoter mutations in gliomas, genetic associations and clinico-pathological correlations

M Labussière[1,2,3], A L Di Stefano[1,2,3,4], V Gleize[1,2,3], B Boisselier[1,2,3,5], M Giry[1,2,3], S Mangesius[1,2,3], A Bruno[1,2,3], R Paterra[6], Y Marie[5,7], A Rahimian[1,2,3,7], G Finocchiaro[6], R S Houlston[8], K Hoang-Xuan[1,2,3,9], A Idbaih[1,2,3,9], J-Y Delattre[1,2,3,7,9], K Mokhtari[1,2,3,7,10] and M Sanson*[,1,2,3,7,9]

[1]*Sorbonne Universités, UMPC Univ Paris 06, Centre de Recherche de l'Institut du Cerveau et de la Moelle épinière, Paris 75013, France;* [2]*INSERM U 1127, Paris 75013, France;* [3]*CNRS, UMR 7225, Paris 75013, France;* [4]*National Neurological Institute C. Mondino, University of Pavia, 27100 Pavia, Italy;* [5]*Institut du Cerveau et de la Moelle épinière (ICM), Plateforme de Génotypage Séquençage, Paris 75013, France;* [6]*Dipartimento di Neuro Oncologia Molecolare Fondazione I.R.C.C.S. Istituto Neurologico C. Besta, Milano 20134, Italy;* [7]*Onconeurothèque, Paris 75013, France;* [8]*Division of Genetics and Epidemiology, Institute of Cancer Research, Surrey SM2 5NG, UK;* [9]*AP-HP, Groupe Hospitalier Pitié-Salpêtrière, Service de Neurologie 2, Paris 75013, France and* [10]*AP-HP, Groupe Hospitalier Pitié-Salpêtrière, Laboratoire de Neuropathologie R. Escourolle, Paris 75013, France*

Background: The role of telomerase reverse transcriptase (*TERT*) in gliomagenesis has been recently further strengthened by the frequent occurrence of *TERT* promoter mutations (*TERT*p-mut) in gliomas and evidence that the *TERT* SNP genetic rs2736100 influences glioma risk. *TERTp*-mut creates a binding site for Ets/TCF transcription factors, whereas the common rs2853669 polymorphism disrupts another Ets/TCF site on *TERT* promoter.

Methods: We sequenced for *TERT*p-mut in 807 glioma DNAs and in 235 blood DNAs and analysed *TERT* expression by RT-PCR in 151 samples. *TERT*p-mut status and *TERTp* polymorphism rs2853669 were correlated with histology, genomic profile, *TERT* mRNA expression, clinical outcome and rs2736100 genotype.

Results: *TERT*p-mut identified in 60.8% of gliomas (491 out of 807) was globally associated with poorer outcome (Hazard ratio (HR) = 1.50). We defined, based on *TERT*p-mut and *IDH* mutation status, four prognostic groups: (1) *TERT*p-mut and *IDH*-mut associated with 1p19q codeletion, overall survival (OS) > 17 years; (2) *TERT*p-wt and *IDH*-mut, associated with *TP53* mutation, OS = 97.5 months; (3) *TERT*p-wt and *IDH*-wt, with no specific association, OS = 31.6 months; (4) *TERT*p-mut and *IDH*-wt, associated with *EGFR* amplification, OS = 15.4 months. *TERT*p-mut was associated with higher *TERT* mRNA expression, whereas the rs2853669 variant was associated with lower *TERT* mRNA expression. The mutation of *CIC* (a repressor of ETV1-5 belonging to the Ets/TCF family) was also associated with *TERT* mRNA upregulation.

Conclusions: In addition to *IDH* mutation status, defining the *TERT*p-mut status of glial tumours should afford enhanced prognostic stratification of patients with glioma. We also show that *TERT*p-mut, rs2853669 variant and *CIC* mutation influence Tert expression. This effect could be mediated by Ets/TCF transcription factors.

The telomerase reverse transcriptase (*TERT*) gene encodes a highly specialised reverse transcriptase, which adds hexamer repeats to the 3' end of chromosomes (Aubert and Lansdorp, 2008; Cesare and Reddel, 2010). The increased telomerase activity seen in cancer leads to preservation of telomeres, allowing tumours to avoid induction of

*Correspondence: Dr M Sanson; E-mail: marc.sanson@psl.aphp.fr

Received 27 April 2014; revised 18 July 2014; accepted 12 September 2014; published online 14 October 2014

senescence (Smogorzewska and de Lange, 2004; Shay and Wright, 2011).

Somatic mutations of the *TERT* promoter (*TERT*p-mut) have recently been documented in various cancers (Griewank *et al*, 2013; Horn *et al*, 2013; Huang *et al*, 2013; Liu *et al*, 2013), but particularly in glioma (Aapola *et al*, 2000; Arita *et al*, 2013; Killela *et al*, 2013; Liu *et al*, 2013). The two most common mutations in *TERT*, C228T and C250T, map −124 and −146 bp, respectively, upstream of the *TERT* ATG site (chr5, 1,295,228 C>T and 1,295,250 C>T, respectively), creating binding sites for Ets/TCF transcription factors that are associated with a two- to four-fold increased transcriptional activity (Brennan *et al*, 2013; Huang *et al*, 2013).

There is increasing evidence that *TERT* variation also influences cancer susceptibility. Notably, the SNP rs2736100 is associated with glioblastoma (GBM) risk, especially for *IDH1* wild-type GBM (Shete *et al*, 2009; Simon *et al*, 2010; Di Stefano *et al*, 2013). Recently, germline mutation of the TERT promoter at position −57 has been shown to cause familial melanoma (Horn *et al*, 2013).

Here, we have (1) determined the prevalence and prognostic impact of *TERT* promoter mutations, in 807 patients with glioma (WHO grades II, III and IV). (2) examined the relationship between *TERT* promoter mutation and tumour subtype and (3) assessed the contribution of germline mutations in these patients and in familial glioma and patients with glioma and melanoma.

PATIENTS AND METHODS

Patients and tissue samples. Collection of patient samples and clinico-pathological information was undertaken with informed consent and ethical board approval in accordance with the tenets of the Declaration of Helsinki. Patients studied fulfilled the following criteria: histologic diagnosis of primary glial tumour according to the WHO classification; complete clinical data and follow-up information available within in the neuro-oncology database (Onconeurothèque Paris). Blood DNAs from 80 patients with familial glioma requited through the Onconeurothèque service were also studied. For controls we made use of data previously generated on 1090 French individuals, which have been described previously (Shete *et al*, 2009).

Molecular analysis. DNA was extracted from fresh-frozen tumours or formalin-fixed paraffin-embedded (FFPE) tumours using the QIAmp DNA minikit (Qiagen, Courtaboeuf, France) and the iPrep ChargeSwitch Forensic kit (Life Technologies, Saint Aubin, France), respectively, DNA was extracted from EDTA-venous blood samples using a standard saline method. DNAs were quantified using Nanodrop (Thermo Fisher Scientific, Villebon sur Yvette, France).

Genomic profiling was performed by CGH-array analysis or SNP array, as previously described (Idbaih *et al*, 2008; Gonzalez-Aguilar *et al*, 2012). Mutational status of *IDH1*, *IDH2* and *TP53* was determined by Sanger sequencing, as described (Sanson *et al*, 2009). *MGMT* promoter methylation status was determined by bisulphite modification and subsequent two-stage nested methylation-specific PCR (Everhard *et al*, 2006).

Mutation analysis of exons 1–20 of *CIC* was undertaken using 454 Sequencing Technology (Roche Applied Science, Meylan, France). Details of PCR primers are shown in Supplementary Table 1. All variations were then validated by Sanger sequencing using the same primers.

Genotyping of rs2736100 has been previously described (Shete *et al*, 2009).

The *TERT* promoter was amplified using GGCCGATTC GACCTCTCT (GTCCTGCCCCTTCACCTT for FFPE samples) and AGCACCTCGCGGTAGTGG primers and Sanger sequencing performed using an ABI Prism 3730 DNA Analyzer (Applied Biosystems, Villebon sur Yvette, France).

To determine *TERT* mRNA expression, tumours were lysed using Lysing Matrix D tube and FastPrep instrument (MP Biomedicals, Illkirch, France) and RNA extracted using the iPrep Trizol Plus RNA Kit (Life Technologies). In all, 300 ng of RNA was retrotranscribed with the Maxima First-Strand cDNA Synthesis Kit (Thermo Scientific, Villebon sur Yvette, France). The cDNA obtained was used as a template for the determination of *TERT* mRNA expression by qPCR using a QuantiFast assay (Qiagen). The ΔΔCp method was applied to normalise to the expression of *TERT* mRNA, using both the expression of β actin and a non-tumour brain tissue sample.

Statistical analysis. The χ^2 test was used to compare the distribution of categorical variables and unpaired *t*-test or Mann–Whitney test associations with continuous variables.

Overall survival (OS) was defined as the time between the diagnosis and death or last follow-up. Patients who were still alive at last follow-up were considered as a censored event in the analysis. Progression-free survival (PFS) was defined as the time between the diagnosis and recurrence or last follow-up. Patients who were recurrence free at last follow-up were considered as a censored event in analysis. To identify clinical and/or genomic factors associated with OS or PFS, survival curves were calculated by the Kaplan–Meier method and differences between curves assessed using the log-rank test. Variables with a significant *P*-value were then used to develop a multivariate Cox model. In all analyses a *P*-value of $\leqslant 0.05$ (two-sided) was considered to be statistically significant.

RESULTS

Somatic and constitutional *TERT*p-mut status. Tumours from 807 patients (451 male; median age at diagnosis 51.0 years, range, 17.3–89.1; 206 grade II, 206 grade III and 395 grade IV) were screened for *TERT*p-mut. Complete patient characteristics are shown in Supplementary Table 2.

Tumours from 491 of the 807 patients (60.8%) were *TERT*p-mut–355 C228T (72.3%) and 136 C250T (27.7%). One GBM and two grade II oligodendrogliomas carried both C250T and C228T. These three cases were considered as *TERT* C228T mutant in all subsequent analyses. To confirm the mutations were somatic, we screened germline DNA of 91 of the cases. No mutation was detectable in germline DNA. We also investigated for the presence of *TERT*p-mut, in 80 familial glioma patients and 64 glioma patients with a second cancer −14 with melanoma (Supplementary Table 2). In none of the cases was a −149, −124 or −57 mutation identified.

rs2853669 genotypes were available for 385 of the tumours. The distribution of genotypes showed no significant departure from HWE (39 CC, 161 CT, 185 TT $P=0.650$). There was no difference in the distribution of genotypes between the *TERTp* mut and the *TERTp* wt cases (TT 45.8 *vs* 53.5%, CT 44.3 *vs* 36.0% and CC: 10.0 *vs* 10.5%, respectively).

We then investigated a purported association between somatic *TERT*p-mut and rs2736100 genotype in 518 glioma patients, finding no association in the whole group (allele A frequency 371 out of 616=60% *vs* 249 out of 420=59%, $P=0.9$) or when stratifying by *IDH* status and tumour class (Supplementary Table 3).

Case–control comparison of showed a stronger association with rs2736100 with *IDH*-wt gliomas but not with *TERT*p-mut gliomas (Supplementary Table 4). Collectively, these data imply there is no association between *TERT*p-mut and rs2736100 genotype. In

addition, we did not find any significant association between *TERT* promoter mutation and the other gliomas susceptibility SNPs rs11979158, rs2252586, rs4295627, rs4977756, rs498872 and rs6010620 (data not shown).

***TERTp*-mut is associated with GBM and *EGFR* amplification, and with oligodendroglioma, *1p19q* codeletion and *CIC* mutation.** *TERTp*-mut was associated with an older age at diagnosis in all gliomas (median age 56.1 years for *TERT* mutated patients *vs* 40.0 years; *t*-test $P<0.0001$) and when stratified by grade (median age at diagnosis 40.4 years *vs* 36.1 for grade II, $P=0.008$; 53.3 *vs* 37.8 for grade III, $P<0.0001$ and 59.6 *vs* 53.6 years for grade IV, $P<0.0001$).

TERTp-mut was more frequent in GBM than in grade II or III tumours (299 out of 395 = 75.8% *vs* 189 out of 412 = 45.9%; χ^2 test $P<10^{-17}$), more frequent in oligodendrogliomas than in astrocytomas/oligoastrocytomas for grade III (52 out of 81 = 64.2% *vs* 46 out of 125 = 30.7%: χ^2 test $P=0.0001$) and for grade II (70 out of 119 = 58.8% *vs* 21 out of 87 = 24.1%; χ^2 test $P<10^{-6}$). Additionally, there was no difference in the ratio of C228T/C250T mutations among the different grades (Table 1).

Table 1. Distribution of *TERT* promoter mutations in gliomas according to WHO histological classification

		C250T mutations (%)	C228T mutations (%)	All TERT mutations (%)
Grade II		**26/206 (12.5)**	**65/206 (31.4)**	**91/206 (44.0)**
	AII	0/13 (0.0)	1/13 (7.7)	1/13 (7.7)
	OAII	7/74 (9.5)	13/74 (17.6)	20/74 (27.0)
	OII	19/119 (16.0)	51/119 (42.9)	70/119 (58.8)
Grade III		**30/206 (14.6)**	**68/206 (33.1)**	**98/206 (47.8)**
	AII	0/30 (0.0)	12/30 (40.0)	12/30 (40.0)
	OAIII	15/95 (15.8)	19/95 (20.0)	34/95 (35.8)
	OIII	15/81 (18.5)	37/81 (45.7)	52/81 (64.2)
Grade IV	GBM	**77/395 (19.5)**	**222/395 (56.2)**	**299/395 (75.7)**

Abbreviations: AII = diffuse astrocytoma; AIII = anaplastic astrocytoma; GBM = glioblastoma; OII = oligodendroglioma; OIII = anaplastic oligodendroglioma; OAII = oligoastrocytoma; OAIII = anaplastic oligoastrocytoma; TERT = telomerase reverse transcriptase; WHO = world health organisation.

*TERT*p-mut was identifiable in 87.9% (94 out of 107 of gliomas with 1p19q codeletion (90 oligodendrogliomas, 17 oligoastrocytomas; 26 (24.3%) on C250T and 68 (63.6%) on C228T) as compared with 58.8% of non-codeleted gliomas (341 out of 580, χ^2 test $P<0.0001$). *EGFR* amplification was present in 183 tumours (142 GBM) and was mutually exclusive with 1p19q codeletion: 163 (89.1%) having *TERT*p-mut (121, C228T) as compared with 51.8% (323 out of 624) of *EGFR* non-amplified tumours (χ^2 test $P<0.0001$). The association of *TERT* promoter mutations with other molecular alterations commonly seen in glioma is detailed in Supplementary Table 5 and Supplementary Figure 1. We investigated whether there was a relationship between *CIC* inactivating mutations and *TERT*p-mut in grades II and III. *CIC* mutation was associated with *TERT*p-mut in 85% of the cases (28 out of 33), compared with 61% (25 out of 41) in *CIC*-wt tumours (χ^2 test $P<0.04$).

***TERTp*-mut is associated with increased *TERT* mRNA expression.** We investigated the transcriptional consequences of *TERT*p-mut in 153 tumours for which mRNA was available. We found a three-fold increase in mRNA expression between *TERT*p-mut and non-mutated groups (mean ± s.e.m. 1.03 ± 0.37 *vs* 3.44 ± 0.88 AU; Mann–Whitney test $P<0.0001$. Figure 1A).

Since the presence of the rs2853669 -C allele disrupts an Ets2 binding site (Rachakonda *et al*, 2013), we investigated the effect of rs2853669 genotype on *TERT* mRNA expression. Tumours harbouring the variant allele (CC + CT) showed a two-fold reduction in *TERT* expression, as compared with TT homozygotes (respective means ± s.e.m. 2.97 ± 1.01 and 6.57 ± 2.04 AU; Mann–Whitney test $P=0.005$). This relationship was also seen in the *TERTp* mutant cohort, however we did not evidence any significant association in *TERTp* wt tumours (Figure 1B and C).

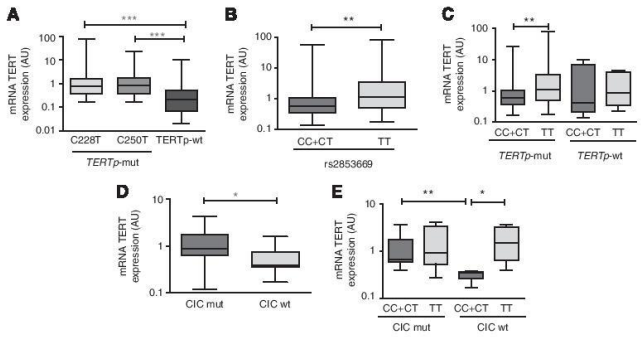

Figure 1. Expression of *TERT* mRNA in gliomas. The Mann–Whitney test was used to compare the expression of the different groups. (**A**) Expression of *TERT* mRNA according to *TERT* promoter mutation status. *TERTp* mutation (C228T $n=88$ or C250T $n=30$) is associated with higher *TERT* mRNA expression compared with *TERTp*-wt group ($n=35$) ($P\leqslant 0.0001$ in both cases). (**B**) Expression of *TERT* mRNA according to rs2853669 status. Variant allele carriers ($n=70$) present a lower *TERT* expression than TT homozygotes ($n=66$) ($P=0.0053$). (**C**) Expression of *TERT* mRNA according to *TERTp* and rs2853669 status. *TERT* mRNA expression is lower for the variant allele carriers ($n=62$) compared with TT ($n=56$) in *TERTp*-mut subgroup ($P=0.0079$). For *TERTp*-wt group, only seven CC + CT samples and eight TT samples were available. (**D**) Expression of *TERT* mRNA according to *CIC* mutation status. *TERT* mRNA expression is increased in *CIC* mutant tumours ($n=18$) compared with *CIC* wild type ($n=11$; $P=0.043$). (**E**) Impact of rs2853669 and *CIC* mutational status *TERT* expression. In the *CIC*-wt cohort, *TERT* expression was lower in CC + CT subgroup, as compared with TT subgroup ($P=0.0159$). For the variant allele carriers (CC + CT), expression of TERT was increased in the *CIC* mutant group ($n=8$), as compared with *CIC* wt ($n=5$) ($P=0.0016$). $^*P<0.05$; $^{**}P<0.01$; $^{***}P<0.0001$.

Since Ets/TCF transcription factors, including ETV1-4 transcription factors are controlled by *CIC* (Dissanayake *et al*, 2011), we also investigated a specific relationship with *CIC* mutation. We found *TERT* mRNA expression was two-fold higher in *CIC* mutant tumours, compared with *CIC* wild-type gliomas (Mann–Whitney test $P=0.043$) for the whole group (Figure 1D), and for the carriers of the variant allele (Figure 1E). The variant allele C was also associated with a decrease in *TERT* mRNA expression in the *CIC* wt group.

Prognostic impact of *TERT*p-mut is dependent on tumour grade. For patients with grade III and IV gliomas *TERT*p-mut was associated with a significantly shorter PFS and OS (Figure 2; Supplementary Table 6). For example in grade III gliomas, median OS of *TERT* promoter normal patients was twice longer (62.6 *vs* 29.4 months) than OS of *TERT* promoter mutated (log-rank test $P=0.013$). This was in sharp contrast with low-grade gliomas, where OS was better for patients with *TERT*p-mut (>16 years *vs* 97.5 months, $P=0.013$). There was no difference in outcome between C228T and C250T *TERT*p-mut in any of the analyses.

In a multivariate Cox model analysis incorporating *IDH* mutation, age at diagnosis, 1p19q codeletion, *MGMT* promoter methylation, Karnofsky performance status, WHO grade and extension of surgery (Table 2) *TERT*p-mut was seen to be an independent negative prognostic factor for OS (Hazard ratio (HR) = 1.50; 95% CI: 1.07–2.09, $P=0.018$).

***TERT*p-mut is associated with specific prognostic and molecular subgroups.** Given *TERT*p-mut is associated with both 1p19q codeletion and *EGFR* amplification, which are mutually exclusive alterations with opposite prognostic effects and *TERT*p-mut had a different effect in low- and high-grade gliomas, prompted us to refine our survival analysis (Figure 3). Gliomas can be stratified into four distinct prognostic groups according to *IDH* and *TERT*p-mut status: (1) *TERT*p-mut and *IDH*-mut, highly associated with 1p19q codeletion (83.9%, 94 out of 11), OS > 17 years; (2) *TERT*p-wt and *IDH*-mut, associated with *TP53* mutation (67.7%, 67 out of 99, OS = 97.5 months); (3) *TERT*p-wt and *IDH*-wt, with no specific association (all negative), OS = 31.6 months; (4) *TERT*p-mut and *IDH*-wt, highly associated with *EGFR* amplification (44.1%, 161 out of 365, OS = 15.0 months) (Figure 4).

***TERT*p-mut confers a poor prognosis except if associated with 1p19q codeletion.** We considered the prognostic impact of the above classification in grades II, III and IV (Figure 5; Supplementary Table 7). In grades II and III, *TERT*p-mut was predictive of a longer survival in the *IDH* mutated group, but shorter survival in the *IDH* wt group. This finding can be explained by the fact that 94 out of 114 of *TERT*p-mut-*IDH*-mut are 1p19q codeleted. Indeed in the GBM group that do not include any 1p19q codeletion, *TERT*p-mut is associated with a particularly poor prognosis in *IDH*-wt tumours (OS = 13.8 *vs*16.5 months, $P=0.006$) but surprisingly also in *IDH*-mut (OS = 13.8 *vs* 29.1

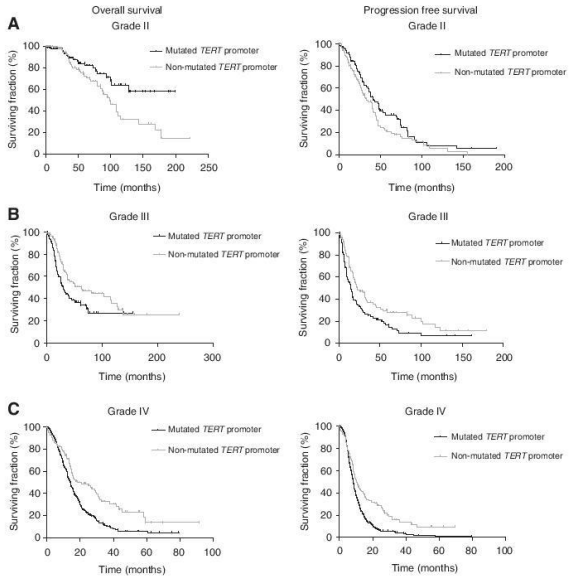

Figure 2. Prognostic impact of *TERT* promoter mutation status on overall survival and PFS, according to grade. Survivals were compared using the log-rank test (Mantel Cox). In grade II gliomas ($n=206$), *TERT*p mutation is associated with better survival (median >16 years *vs* 97.5 months; $P=0.013$). There is also a trend for better PFS (median 41.3 *vs* 33.3 months; $P=0.068$) (**A**) whereas in grade III (**B**; $n=206$) and grade IV gliomas (**C**; $n=395$), *TERT*p mutation is associated with poorer survival (median 29.4 *vs* 62.6 months $P=0.013$ and 13.8 *vs* 18.4 months $P<0.0001$) and PFS (median 15.1 *vs* 22.4 months $P=0.006$ and 8.3 *vs* 10.4 months $P<0.0001$).

Table 2. Cox model for overall survival and progression-free survival

	Overall survival			Progression-free survival		
Parameters	**HR**	**95% CI for HR**	***P***	**HR**	**95% CI for HR**	***P***
Age at diagnosis <60 years	0.631	0.470–0.848	*0.002*	0.798	0.610–1.044	*0.0991*
IDH mutation	0.586	0.369–0.930	*0.023*	0.707	0.473–1.056	*0.090*
1p19q codeletion	0.182	0.076–0.436	*<0.0001*	0.433	0.257–0.730	*0.002*
Surgery *vs* biopsy	0.586	0.435–0.791	*<0.0001*	0.896	0.682–1.178	*0.432*
MGMT promoter methylation	0.652	0.497–0.855	*0.002*	0.691	0.539–0.887	*0.004*
KPS >70	0.553	0.404–0.757	*<0.0001*	0.567	0.421–0.763	*<0.0001*
Grade	1.850	1.400–2.444	*<0.0001*	1.215	0.989–1.494	*0.064*
TERT promoter mutation	1.497	1.071–2.092	*0.018*	1.766	1.299–2.401	*<0.0001*

Abbreviations: CI = confidence interval; HR = hazard ratio; IDH = isocitrate dehydrogenase; KPS = Karnofsky Performance Status; TERT = telomerase reverse transcriptase. The analysis was conducted on 362 tumours with all parameters available.

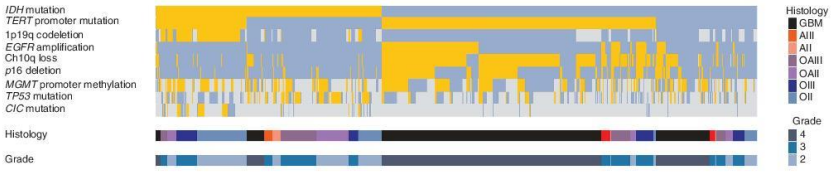

Figure 3. Association of *TERT* promoter mutations with the major genetic alterations in gliomas ($n = 806$). Each tumour is represented by a column. A yellow box indicates the presence of the genetic alteration, the absence in blue, and the cases not assessed are indicated in grey. The stratification has been done using four groups: *IDH* mut-*TERTp* mut, *IDH* mut-*TERTp* wt, *IDH* wt-*TERTp* wt and *IDH* wt *TERTp* mut. *TERTp* mutation is associated with two mutually exclusive alterations: 1p19q codeletion and *EGFR* amplification.

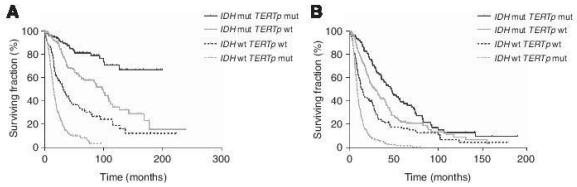

Figure 4. Prognostic stratification of gliomas according to *IDH* and *TERT* promoter mutation status ($n = 804$). (**A**) Overall survival. (**B**) Progression-free survival. We identified four prognostic subgroups, (1) *TERTp*-mut and *IDH*-mut (OS > 17 years, PFS 46.9 months), (2) *TERTp*-wt and *IDH*-mut (OS = 97.5 months, PFS 28.6 months), (3) *TERTp*-wt and *IDH*-wt, (OS = 31.6 months, PFS14.1 months) and (4) *TERTp*-mut and *IDH*-wt (OS = 15.0 months, PFS 8.5 months).

months, $P = 0.022$) (Figure 6). In contrast *TERTp*-mut was associated with a poorer outcome in *IDH*-wt gliomas irrespective of grade (OS: 76.2 *vs* 94.8 months in grade II $P =$ ns; 18.0 *vs* 36.5 months in grade III $P = 0.007$; 13.7 *vs* 17.5 months in grade IV $P = 0.006$).

DISCUSSION

Given that 60% of tumours being *TERTp*-mut, *TERT* is the most frequently mutated gene in gliomas thus far identified (Arita *et al*, 2013; Killela *et al*, 2013; Liu *et al*, 2013). We found *TERTp*-mut glioma patients were older, consistent with previous reports of other malignancies (Griewank *et al*, 2013; Killela *et al*, 2013). Unlike melanomas, in which germline *TERTp* mutations have been reported to cause familial melanoma (Horn *et al*, 2013), we found no evidence that *TERTp*-mut contributes substantially to predisposition to gliomas or the glioma/melanoma syndrome.

Our data showed that *TERTp*-mut is generally associated with poorer outcome in high-grade gliomas, consistently with previous data, on glioma (Killela *et al*, 2013, 2014), and other tumours (Rachakonda *et al*, 2013). In contrast, however we observed a trend for better outcome in low-grade gliomas. Stratifying tumours by both *IDH1/2* and *TERTp*-mut status provides insight into this apparent paradox, identified four molecular subtypes of gliomas with distinct prognosis, In *IDH* mutated tumours, *TERTp*-mut is largely confined to 1p19q codeleted oligodendroglial tumours that have the best outcome (Kaloshi *et al*, 2007; van den Bent *et al*, 2013). Mutation of *CIC*, recently identified (Bettegowda *et al*, 2011;

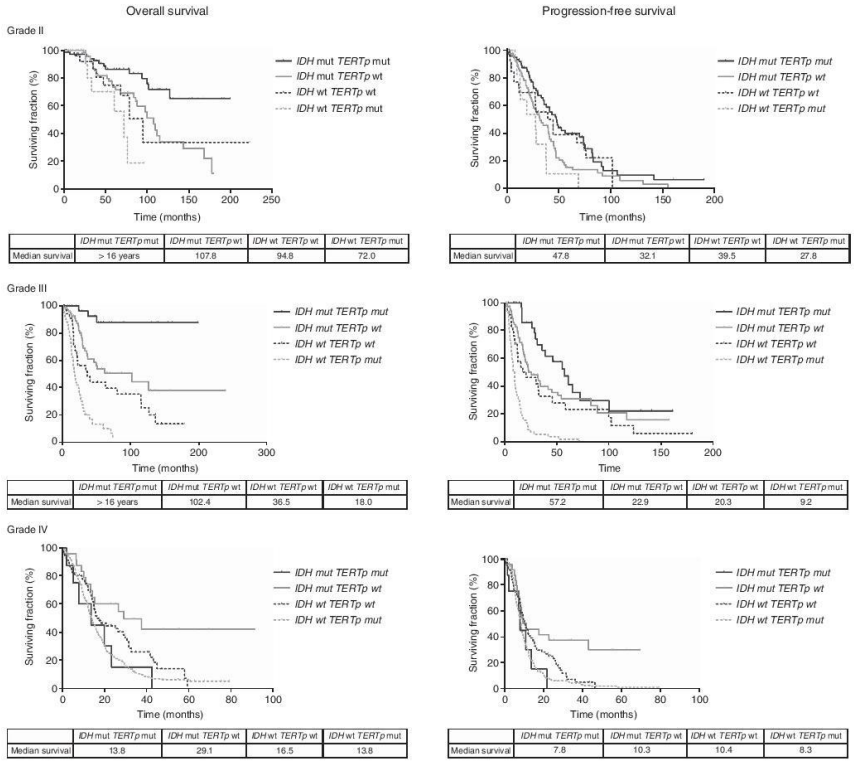

Figure 5. Prognostic stratification of gliomas according to *IDH* and *TERT* promoter mutation status (four subgroups) in grade II ($n=205$), grade III ($n=206$) and grade IV ($n=394$). Median survivals are indicated in months if not otherwise stated. *TERT*p mutation is associated with a poorer outcome in *IDH*-wt gliomas whatever the grade. *TERT*p mutation is associated with better outcome in *IDH* mut grades II and III (OS: >16 years *vs* 107.8 months in grade II $P=0.004$; >16 years *vs* 102.4 in grade III $P=0.0005$). In contrast, the survival of grade IV with *TERT*p mutation and *IDH*-mut is extremely poor compared with *TERT*p-wt (13.8 *vs* 29.1 months; $P=0.022$).

Yip *et al*, 2012) is also primarily a feature of this group (Figure 3). In contrast, if *TERT*p-mut is associated with *IDH1/2* wild-type tumours, then it is mainly seen in the context of GBM (276 out of 340) with almost half of them (124 out of 276) having an *EGFR* amplification which is associated with poor outcome. In our study, this subgroup also included 54 grade III gliomas that had a particularly poor OS of 20.1 months. Taken together, our data show that the prognostic impact of *TERT*p-mut is highly contextual and depends on the histologic and genomic background of the tumour.

From a mechanistic point of view, *TERTp* mutation leads to the creation of a putative binding site for Ets/TCF transcription factors (Huang *et al*, 2013), leading to a two- to four-fold higher expression of telomerase (Arita *et al*, 2013; Huang *et al*, 2013; Nault *et al*, 2013; Rachakonda *et al*, 2013). The activity of telomerase reverse transcriptase is closely correlated with *TERT* mRNA level. The expression of *TERT* is regulated by many transcription factors binding motives located in its promoter and by epigenetic and chromatin remodelling mechanisms (Kyo *et al*, 2008; Zhu *et al*, 2010). Among the complex regulation of telomerase expression, rs2853669 has been shown to modulate both *TERT* expression and impact on prognosis in bladder cancer (Rachakonda *et al*, 2013). Indeed, the presence of the variant allele disrupts a pre-existing Ets2 binding site and results in the decrease of *TERT* expression in our series. However, unlike bladder cancer, rs2853669 variant does not modify the prognostic impact of *TERTp* mutation in our glioma series (data not shown). Our data also suggest a link between *CIC* mutation and *TERT* expression in the context of glial tumours. Indeed, the presence of the variant allele of rs2853669 did not result in a reduction of *TERT* expression in the *CIC* mutant subgroup.

Among the 40% gliomas lacking *TERTp* mutation, ~50% harbour an *IDH* mutation (mostly astrocytomas (43 out of 180) and oligoastrocytomas (91 out of 180), which are frequently *TP53* mutated. In this group, mutations in the *ATRX* gene (alpha thalassaemia/mental retardation syndrome X-linked), or in its

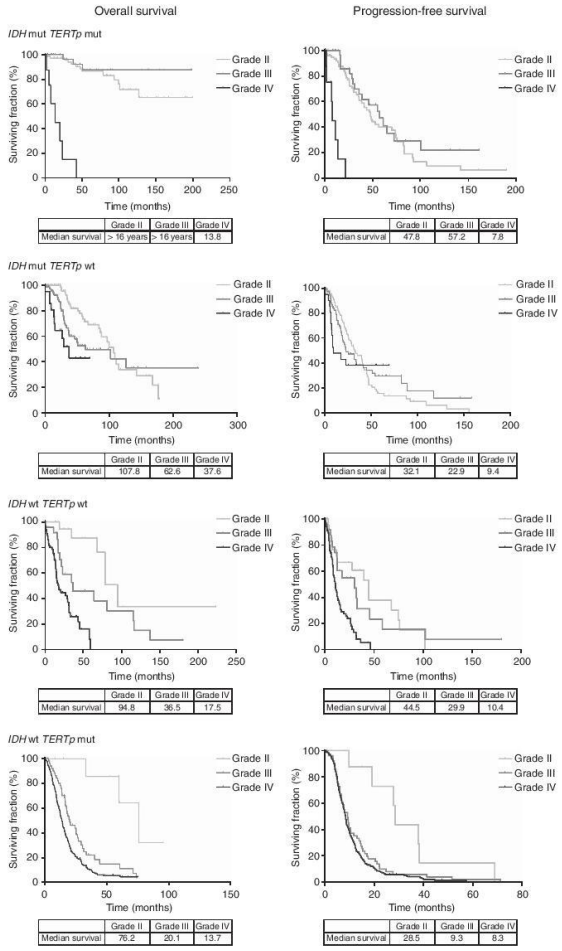

Figure 6. Prognostic stratification of gliomas according to grade in the four molecular subgroups (*IDH* mut *TERTp* mut $n=122$; *IDH* mut *TERTp* wt $n=180$; *IDH* wt *TERTp* wt $n=114$, *IDH* wt *TERTp* mut $n=340$). There is a dramatic difference of survival between grade IV (OS = 13.8 months) and grades II + III (OS > 16 years) in the *IDH*-mut-*TERT*-mut group ($P<0.0001$). In contrast, the group 2 (*IDH*-mut-*TERT*-wt) is much more homogeneous through grades II–IV.

partner death domain-associated protein (*DAXX*), which are involved in alternative lengthening telomere (ALT) phenotype, have been frequently documented (Jiao *et al*, 2012; Kannan *et al*, 2012; Liu *et al*, 2012; Killela *et al*, 2013) and are mutually exclusive with telomerase reactivation. The *IDH*-wt and *TERT*p-wt group includes mostly GBM tumours (58%, 66 out of 114). The 'triple negative' low-grade gliomas, characterised by a poorer outcome also conform to these categories (Metellus *et al*, 2010). Telomere maintenance mechanism has not been investigated yet in this subgroup.

A more detailed analysis shows the four group classification, recently reported (Killela *et al*, 2014) is an oversimplification (see Supplementary Figure 2 and Figure 5); for example, the *TERT*p-mut-*IDH*-mut is indicative of better outcome for grades II and III with an OS > 17 years, but is associated with a poorer outcome in GBM (OS = 13.8 months), whereas in GBM the best group

prognostic is those patients with *TERT*p-wt-*IDH*-mut group (OS = 29.1 *vs* 13.8 months for the *TERTp*-mut-*IDH* mut group). This discrepancy is unlikely to be solely explained by the relationship between *TERT*p mutation and 1p19q codeletion, present in 89% (94 out of 106) of our *TERT*p-mut-*IDH*-mut grades II and III, but none of our grade IV tumours. In fact, the survival of patients with *TERT*p-mut-*IDH*-mut grades II and III, without 1p19q codeletion was not significantly different from those with 1p19q codeleted tumours (median OS = 10 years) (Supplementary Figure 3).

In conclusion, our data confirm the high frequency of *TERT*p-mut in glioma and show that these mutations clusterise into specific entities, with distinct clinical significances. *TERT*p mutations are mostly associated with poor outcome, except for 1p19q codeleted grade II and grade III, and for *EGFR* amplified grade III and grade IV (Supplementary Figure 2A and B, respectively). A telomere maintenance mechanism (either *TERTp* mutation or *ATRX/DAXX* mutations) is involved in >80% of gliomas and appears therefore as a unique feature in these tumors, offering the prospect of new therapeutic approaches.

ACKNOWLEDGEMENTS

This study is supported by grants from the Institut National du cancer (INCa), the Association pour la Recherche contre le Cancer (ARC), the Ligue Nationale contre le Cancer (LNCC), and Association pour la Recherche sur les Tumeurs cérébrales (ARTC). ALDS is supported by an investigator fellowship from Collegio Ghislieri, Pavia, Italy. VG and SM are supported by a grant from the Association pour la Recherche contre le Cancer (ARC). SM is supported by a grant from the Ligue Nationale contre le Cancer (LNCC).

REFERENCES

Aapola U, Kawasaki K, Scott HS, Ollila J, Vihinen M, Heino M, Shintani A, Minoshima S, Krohn K, Antonarakis SE, Shimizu N, Kudoh J, Peterson P (2000) Isolation and initial characterization of a novel zinc finger gene, DNMT3L, on 21q22.3, related to the cytosine-5-methyltransferase 3 gene family. *Genomics* **65**(3): 293–298.

Arita H, Narita Y, Fukushima S, Tateishi K, Matsushita Y, Yoshida A, Miyakita Y, Ohno M, Collins VP, Kawahara N, Shibui S, Ichimura K (2013) Upregulating mutations in the TERT promoter commonly occur in adult malignant gliomas and are strongly associated with total 1p19q loss. *Acta Neuropathol* **126**(2): 267–276.

Aubert G, Lansdorp PM (2008) Telomeres and aging. *Physiol Rev* **88**(2): 557–579.

Bettegowda C, Agrawal N, Jiao Y, Sausen M, Wood LD, Hruban RH, Rodriguez FJ, Cahill DP, McLendon R, Riggins G, Velculescu VE, Oba-Shinjo SM, Marie SK, Vogelstein B, Bigner D, Yan H, Papadopoulos N, Kinzler KW (2011) Mutations in CIC and FUBP1 contribute to human oligodendroglioma. *Science* **333**(6048): 1453–1455.

Brennan CW, Verhaak RG, McKenna A, Campos B, Noushmehr H, Salama SR, Zheng S, Chakravarty D, Sanborn JZ, Berman SH, Beroukhim R, Bernard B, Wu CJ, Genovese G, Shmulevich I, Barnholtz-Sloan J, Zou L, Vegesna R, Shukla SA, Ciriello G, Yung WK, Zhang W, Sougnez C, Mikkelsen T, Aldape K, Bigner DD, Van Meir EG, Prados M, Sloan A, Black KL, Eschbacher J, Finocchiaro G, Friedman W, Andrews DW, Guha A, Iacocca M, O'Neill BP, Foltz G, Myers J, Weisenberger DJ, Penny R, Kucherlapati R, Perou CM, Hayes DN, Gibbs R, Marra M, Mills GB, Lander E, Spellman P, Wilson R, Sander C, Weinstein J, Meyerson M, Gabriel S, Laird PW, Haussler D, Getz G, Chin L (2013) The somatic genomic landscape of glioblastoma. *Cell* **155**(2): 462–477.

Cesare AJ, Reddel RR (2010) Alternative lengthening of telomeres: models, mechanisms and implications. *Nat Rev Genet* **11**(5): 319–330.

Di Stefano AL, Enciso-Mora V, Marie Y, Desestret V, Labussiere M, Boisselier B, Mokhtari K, Idbaih A, Hoang-Xuan K, Delattre JY, Houlston RS, Sanson M (2013) Association between glioma susceptibility loci and tumour pathology defines specific molecular etiologies. *Neuro Oncol* **15**(5): 542–547.

Dissanayake K, Toth R, Blakey J, Olsson O, Campbell DG, Prescott AR, MacKintosh C (2011) ERK/p90(RSK)/14-3-3 signalling has an impact on expression of PEA3 Ets transcription factors via the transcriptional repressor capicua. *Biochem J* **433**(3): 515–525.

Everhard S, Kaloshi G, Criniere E, Benouaich-Amiel A, Lejeune J, Marie Y, Sanson M, Kujas M, Mokhtari K, Hoang-Xuan K, Delattre JY, Thillet J (2006) MGMT methylation: a marker of response to temozolomide in low-grade gliomas. *Ann Neurol* **60**(6): 740–743.

Gonzalez-Aguilar A, Idbaih A, Boisselier B, Habbita N, Rossetto M, Laurenge A, Bruno A, Jouvet A, Polivka M, Adam C, Figarella-Branger D, Miquel C, Vital A, Ghesquieres H, Gressin R, Delwail V, Taillandier L, Chinot O, Soubeyran P, Gyan E, Choquet S, Houillier C, Soussain C, Tanguy ML, Marie Y, Mokhtari K, Hoang-Xuan K (2012) Recurrent mutations of MYD88 and TBL1XR1 in primary central nervous system lymphomas. *Clin Cancer Res* **18**(19): 5203–5211.

Griewank KG, Murali R, Schilling B, Scholz S, Sucker A, Song M, Susskind D, Grabellus F, Zimmer L, Hillen U, Steuhl KP, Schadendorf D, Westekemper H, Zeschnigk M (2013) TERT promoter mutations in ocular melanoma distinguish between conjunctival and uveal tumours. *Br J Cancer* **109**(2): 497–501.

Horn S, Figl A, Rachakonda PS, Fischer C, Sucker A, Gast A, Kadel S, Moll I, Nagore E, Hemminki K, Schadendorf D, Kumar R (2013) TERT promoter mutations in familial and sporadic melanoma. *Science (New York, NY)* **339**(6122): 959–961.

Huang FW, Hodis E, Xu MJ, Kryukov GV, Chin L, Garraway LA (2013) Highly recurrent TERT promoter mutations in human melanoma. *Science* **339**(6122): 957–959.

Idbaih A, Marie Y, Lucchesi C, Pierron G, Manie E, Raynal V, Mosseri V, Hoang-Xuan K, Kujas M, Brito I, Mokhtari K, Sanson M, Barillot E, Aurias A, Delattre JY, Delattre O (2008) BAC array CGH distinguishes mutually exclusive alterations that define clinicogenetic subtypes of gliomas. *Int J Cancer* **122**(8): 1778–1786.

Jiao Y, Killela PJ, Reitman ZJ, Rasheed AB, Heaphy CM, de Wilde RF, Rodriguez FJ, Rosemberg S, Oba-Shinjo SM, Marie SK, Bettegowda C, Agrawal N, Lipp E, Pirozzi C, Lopez G, He Y, Friedman H, Friedman AH, Riggins GJ, Holdhoff M, Burger P, McLendon R, Bigner DD, Vogelstein B, Meeker AK, Kinzler KW, Papadopoulos N, Diaz LA, Yan H (2012) Frequent ATRX, CIC, and FUBP1 mutations refine the classification of malignant gliomas. *Oncotarget* **3**(7): 709–722.

Kaloshi G, Benouaich-Amiel A, Diakite F, Taillibert S, Lejeune J, Laigle-Donadey F, Renard MA, Iraqi W, Idbaih A, Paris S, Capelle L, Duffau H, Cornu P, Simon JM, Mokhtari K, Polivka M, Omuro A, Carpentier A, Sanson M, Delattre JY, Hoang-Xuan K (2007) Temozolomide for low-grade gliomas: predictive impact of 1p/19q loss on response and outcome. *Neurology* **68**(21): 1831–1836.

Kannan K, Inagaki A, Silber J, Gorovets D, Zhang J, Kastenhuber ER, Heguy A, Petrini JH, Chan TA, Huse JT (2012) Whole-exome sequencing identifies ATRX mutation as a key molecular determinant in lower-grade glioma. *Oncotarget* **3**(10): 1194–1203.

Killela PJ, Pirozzi CJ, Healy P, Reitman ZJ, Lipp E, Rasheed BA, Yang R, Diplas BH, Wang Z, Greer PK, Zhu H, Wang CY, Carpenter AB, Friedman H, Friedman AH, Keir ST, He J, He Y, McLendon RE, Herndon 2nd JE, Yan H, Bigner DD (2014) Mutations in IDH1, IDH2, and in the TERT promoter define clinically distinct subgroups of adult malignant gliomas. *Oncotarget* **5**(6): 1515–1525.

Killela PJ, Reitman ZJ, Jiao Y, Bettegowda C, Agrawal N, Diaz Jr LA, Friedman AH, Friedman H, Gallia GL, Giovanella BC, Grollman AP, He TC, He Y, Hruban RH, Jallo GI, Mandahl N, Meeker AK, Mertens F, Netto GJ, Rasheed BA, Riggins GJ, Rosenquist TA, Schiffman M, Shih IeM, Theodorescu D, Torbenson MS, Velculescu VE, Wang TL, Wentzensen N, Wood LD, Zhang M, McLendon RE, Bigner DD, Kinzler KW, Vogelstein B, Papadopoulos N, Yan H (2013) TERT promoter mutations occur frequently in gliomas and a subset of tumors derived from cells with low rates of self-renewal. *Proc Natl Acad Sci USA* **110**(15): 6021–6026.

Kyo S, Takakura M, Fujiwara T, Inoue M (2008) Understanding and exploiting hTERT promoter regulation for diagnosis and treatment of human cancers. *Cancer Sci* **99**(8): 1528–1538.

Liu X, Wu G, Shan Y, Hartmann C, von Deimling A, Xing M (2013) Highly prevalent TERT promoter mutations in bladder cancer and glioblastoma. *Cell Cycle (Georgetown, Tex)* **12**(10): 1637–1638.

Liu XY, Gerges N, Korshunov A, Sabha N, Khuong-Quang DA, Fontebasso AM, Fleming A, Hadjadj D, Schwartzentruber J, Majewski J, Dong Z, Siegel P, Albrecht S, Croul S, Jones DT, Kool M, Tonjes M, Reifenberger G, Faury D, Zadeh G, Pfister S, Jabado N (2012) Frequent ATRX mutations and loss of expression in adult diffuse astrocytic tumors carrying IDH1/IDH2 and TP53 mutations. *Acta Neuropathol* **124**(5): 615–625.

Metellus P, Coulibaly B, Colin C, de Paula AM, Vasiljevic A, Taieb D, Barlier A, Boisselier B, Mokhtari K, Wang XW, Loundou A, Chapon F, Pineau S, Ouafik L, Chinot O, Figarella-Branger D (2010) Absence of IDH mutation identifies a novel radiologic and molecular subtype of WHO grade II gliomas with dismal prognosis. *Acta Neuropathol* **120**(6): 719–729.

Nault JC, Mallet M, Pilati C, Calderaro J, Bioulac-Sage P, Laurent C, Laurent A, Cherqui D, Balabaud C, Zucman-Rossi J (2013) High frequency of telomerase reverse-transcriptase promoter somatic mutations in hepatocellular carcinoma and preneoplastic lesions. *Nat Commun* **4**: 2218.

Rachakonda PS, Hosen I, de Verdier PJ, Fallah M, Heidenreich B, Ryk C, Wiklund NP, Steineck G, Schadendorf D, Hemminki K, Kumar R (2013) TERT promoter mutations in bladder cancer affect patient survival and disease recurrence through modification by a common polymorphism. *Proc Natl Acad Sci USA* **110**(43): 17426–17431.

Sanson M, Marie Y, Paris S, Idbaih A, Laffaire J, Ducray F, El Hallani S, Boisselier B, Mokhtari K, Hoang-Xuan K, Delattre JY (2009) Isocitrate dehydrogenase 1 codon 132 mutation is an important prognostic biomarker in gliomas. *J Clin Oncol* **27**(25): 4150–4154.

Shay JW, Wright WE (2011) Role of telomeres and telomerase in cancer. *Semin Cancer Biol* **21**(6): 349–353.

Shete S, Hosking FJ, Robertson LB, Dobbins SE, Sanson M, Malmer B, Simon M, Marie Y, Boisselier B, Delattre JY, Hoang-Xuan K, El Hallani S, Idbaih A, Zelenika D, Andersson U, Henriksson R, Bergenheim AT, Feychting M, Lonn S, Ahlbom A, Schramm J, Linnebank M, Hemminki K, Kumar R, Hepworth SJ, Price A, Armstrong G, Liu Y, Gu X, Yu R, Lau C, Schoemaker M, Muir K, Swerdlow A, Lathrop M, Bondy M, Houlston RS (2009) Genome-wide association study identifies five susceptibility loci for glioma. *Nat Genet* **41**(8): 899–904.

Simon M, Hosking FJ, Marie Y, Gousias K, Boisselier B, Carpentier C, Schramm J, Mokhtari K, Hoang-Xuan K, Idbaih A, Delattre JY, Lathrop M, Robertson LB, Houlston RS, Sanson M (2010) Genetic risk profiles identify different molecular etiologies for glioma. *Clin Cancer Res* **16**(21): 5252–5259.

Smogorzewska A, de Lange T (2004) Regulation of telomerase by telomeric proteins. *Annu Rev Biochem* **73**: 177–208.

van den Bent MJ, Brandes AA, Taphoorn MJ, Kros JM, Kouwenhoven MC, Delattre JY, Bernsen HJ, Frenay M, Tijssen CC, Grisold W, Sipos L, Enting RH, French PJ, Dinjens WN, Vecht CJ, Allgeier A, Lacombe D, Gorlia T, Hoang-Xuan K (2013) Adjuvant procarbazine, lomustine, and vincristine chemotherapy in newly diagnosed anaplastic oligodendroglioma: long-term follow-up of EORTC brain tumor group study 26951. *J Clin Oncol* **31**(3): 344–350.

Yip S, Butterfield YS, Morozova O, Chittaranjan S, Blough MD, An J, Birol I, Chesnelong C, Chiu R, Chuah E, Corbett R, Docking R, Firme M, Hirst M, Jackman S, Karsan A, Li H, Louis DN, Maslova A, Moore R, Moradian A, Mungall KL, Perizzolo M, Qian J, Roldan G, Smith EE, Tamura-Wells J, Thiessen N, Varhol R, Weiss S, Wu W, Young S, Zhao Y, Mungall AJ, Jones SJ, Morin GB, Chan JA, Cairncross JG, Marra MA (2012) Concurrent CIC mutations, IDH mutations, and 1p/19q loss distinguish oligodendrogliomas from other cancers. *J Pathol* **226**(1): 7–16.

Zhu J, Zhao Y, Wang S (2010) Chromatin and epigenetic regulation of the telomerase reverse transcriptase gene. *Protein Cell* **1**(1): 22–32.

Supplementary Information accompanies this paper on British Journal of Cancer website (http://www.nature.com/bjc)

Combined analysis of *TERT*, *EGFR*, and *IDH* status defines distinct prognostic glioblastoma classes

Marianne Labussière, PharmD, PhD
Blandine Boisselier, MSc
Karima Mokhtari, MD
Anna-Luisa Di Stefano, MD
Anais Rahimian, MSc
Marta Rossetto, MD
Pietro Ciccarino, MD
Olivier Saulnier, MSc
Rosina Paterra, PhD
Yannick Marie, MSc
Gaetano Finocchiaro, MD, PhD
Marc Sanson, MD, PhD

Correspondence to Dr. Sanson: marc.sanson@psl.aphp.fr

ABSTRACT

Objective: To identify the prognostic significance of *TERT* promoter mutations (*TERT*p-mut) and their associations with common molecular alterations in glioblastomas (GBMs).

Methods: We sequenced the *TERT*p-mut in DNA from 395 GBMs and analyzed the results with their respective histology, genetic profile (*IDH1* mutation, *EGFR* amplification, *CDKN2A* homozygous deletion, loss of chromosome 10, *TP53* mutation), and overall survival (OS).

Results: *TERT*p-mut were found in 299 of 395 GBMs (75.7%) and were associated with an older age (median 59.6 years for *TERT*p-mut vs 53.6 years for *TERT* promoter wild type [*TERT*p-wt], $p < 0.0001$). *TERT*p-mut was an independent factor of poor prognosis (OS = 13.8 vs 18.4 months), in both *IDH*-mutated (OS = 13.8 vs 37.6 months, $p = 0.022$) and *IDH*-wt GBMs (OS = 13.7 vs 17.5 months, $p = 0.006$). *TERT*p-mut was associated with *IDH*-wt, *EGFR* amplification, *CDKN2A* deletion, and chromosome 10q loss, but not with *MGMT* promoter methylation. In the *TERT*p-wt group, OS was twice longer in *EGFR*-wt than in *EGFR* amplification GBMs (OS = 26.6 vs 13.3 months; $p = 0.005$). In the *EGFR*-wt group, patients with *TERT*p-wt had a significantly better outcome (OS = 26.3 vs 12.5 months, $p < 0.0001$), whereas in the *EGFR* amplification group, patients with *TERT*p-mut survived longer (OS = 15.8 vs 13.3 months, $p = 0.05$). Taken together, the absence of both *EGFR* amplification and *TERT*p-mut is associated with longer survival in patients with GBM (26.5 months for patients with *IDH*-wt, 36.7 months for patients with *IDH* mutation).

Conclusions: The analysis of *TERT*p-mut, in combination with *EGFR* amplification and *IDH* mutation status, refines the prognostic classification of GBMs. *Neurology*® 2014;83:1200–1206

GLOSSARY

CDKN2A = cyclin-dependent kinase inhibitor 2A; ***EGFR*** = epidermal growth factor receptor; **GBM** = glioblastoma; ***IDH*** = isocitrate dehydrogenase; ***MGMT*** = methylguanine methyltransferase; **OS** = overall survival; **PFS** = progression-free survival; ***TERT*** = telomerase reverse transcriptase; ***TERT*p-mut** = *TERT* promoter mutation; ***TERT*p-wt** = *TERT* promoter wild type; ***TP53*** = tumor protein p53; **wt** = wild type.

Recently, mutations affecting the promoter region of the telomerase reverse transcriptase (*TERT*) gene have been reported in numerous cancers.[1–4] Gliomas and especially glioblastomas (GBMs) were among the most frequently affected tumors.[4–7] These mutations occurred in 2 hotspot positions (chr5, 1,295,228 C>T and chr5, 1,295,250 C>T), located −124 and −146 base pairs upstream from the ATG start site (−124 G>A and −146 G>A).[7] Both mutations conferred enhanced *TERT* promoter activity, possibly by generating a consensus binding site (CCTGAA>CCGGAA) for E-twenty-six transcription factors.[2,3]

The *TERT* gene codes for a highly specialized reverse transcriptase catalyzing, with other members of the telomerase complex, the 3′ extension of chromosome ends by adding hexamers repeats.[8,9] *TERT* expression and telomerase activity are usually low in normal tissues, and the constant shortening of telomeres finally leads to cell senescence. In contrast, most human

Supplemental data at Neurology.org

From Sorbonne Universités (M.L., B.B., K.M., A.-L.D.S., A.R., M.R., P.C., O.S., M.S.), UPMC Univ Paris 06, Inserm, CNRS, UM 75, U 1127, UMR 7225, ICM, Paris; Institut du Cerveau et de la Moelle épinière (ICM) (B.B., Y.M.), Plateforme de Génotypage Séquençage, Paris; Groupe Hospitalier Pitié Salpêtrière, Laboratoire de Neuropathologie R Escourolle (K.M.), Onconeurothèque (K.M., Y.M., M.S.), and Groupe Hospitalier Pitié-Salpêtrière, Service de Neurologie 2 (A.-L.D.S., M.S.), AP-HP, Paris, France; National Neurological Institute C. Mondino (A.-L.D.S.), Pavia; Department of Neuroscience (M.R., P.C.), University of Padova; and Unit of Molecular Neuro-Oncology (R.P., G.F.), Fondazione IRCCS Carlo Besta, Milan, Italy.

Go to Neurology.org for full disclosures. Funding information and disclosures deemed relevant by the authors, if any, are provided at the end of the article.

cancers are characterized by an increased activity of telomerase allowing the maintenance of telomere length, thus avoiding induction of senescence and conferring unrestricted growth properties to cancer cells.[10,11]

A number of genetic and genomic alterations have already been described in GBM, including epidermal growth factor receptor (*EGFR*) amplification, cyclin-dependent kinase inhibitor 2A (*CDKN2A*) homozygous deletion, methylguanine methyltransferase (*MGMT*) promoter methylation, and isocitrate dehydrogenase (*IDH*) mutation. To date, only *MGMT* promoter methylation and *IDH* mutation have been proven to be prognostic in GBMs.[12,13]

In this study, we investigated the prevalence and the prognostic impact of *TERT* promoter mutations (*TERT*p-mut), in a series of 395 patients with GBM treated in our department. We then correlated the *TERT*p-mut status with the other genetic alterations.

METHODS **Patients and tissue samples.** Selection of patients was based on the following criteria: histologic diagnosis of primary GBM according to the World Health Organization classification, and clinical data and follow-up available in the neuro-oncology database (Onconeurothèque Paris). We considered primary GBM when the first symptoms appeared less than 3 months before the patient was referred to the clinics. We excluded patients known to have a history of seizure or known low-grade gliomas.

The QIAamp DNA Mini Kit was used to extract tumor DNA from frozen tumors, as described by the manufacturer (Qiagen, Courtaboeuf, France). DNA was extracted from blood samples using a conventional saline method.

For the determination of *EGFR* amplification, *CDKN2A* homozygous deletion, and loss of chromosomes 9 and 10, genomic profiling was performed by comparative genomic hybridization array analysis or single nucleotide polymorphism array, as previously described.[14,15] Mutational status of *IDH1*, *IDH2*, and *TP53* (tumor protein p53) was determined using the Sanger technique, as previously described.[16] *MGMT* promoter methylation status was determined by 2-stage nested methylation-specific PCR after bisulfite modification.[17]

Standard protocol approvals, registrations, and patient consents. Collection of tumor and blood samples and clinicopathologic information was undertaken with informed consent and relevant ethical board approval in accordance with the tenets of the Declaration of Helsinki.

Determination of *TERT*p-mut status. The promoter region of the *TERT* gene was amplified as follows: TERT-F GGCCGATTCGACCTCTCT and TERT-R AGCACCTCGCGGTAGTGG; 3 minutes at 94°C; 35 cycles at 94°C 15 seconds, 60°C 45 seconds, 72°C 1 minute, with a final step at 72°C for 8 minutes. PCR products were then purified with the Agencourt AMPure XP PCR purification protocol (Beckman Coulter, Villepinte, France). Purified PCR products were then sequenced using the Big-Dye Terminator Cycle Sequencing Ready Reaction (PerkinElmer, Villebon sur Yvette, France). Sequences were purified with the Agencourt CleanSEQ protocol according to the manufacturer's instructions (Beckman Coulter) and analyzed on an ABI Prism 3730 DNA Analyzer (Applied Biosystems, Saint Aubin, France).

Statistical analysis. The χ^2 test was used to compare the genotypes' distribution. The association with continuous variables was calculated with a Mann–Whitney test.

Overall survival (OS) was defined as the time between the diagnosis and death or last follow-up. Patients who were still alive at the last follow-up were considered as a censored event in analysis. Progression-free survival (PFS) was defined as the time between the diagnosis and recurrence or last follow-up. Patients who were recurrence-free at the last follow-up were considered as a censored event in the analysis. To find clinical and/or genomic factors related to OS (or PFS), survival curves were calculated according to the Kaplan–Meier method, and differences between curves were assessed using the log-rank test. Variables with a significant p value were used to build a multivariate Cox model. Two-sided p values <0.05 were considered significant.

RESULTS **Somatic and constitutional *TERT*p-mut status.** A population of 395 primary GBMs was screened for the presence of *TERT*p-mut. Median age at diagnosis was 58.5 years (range 18.2–89.1). Median Karnofsky Performance Score was 80 (range 20–100). At diagnosis, 281 patients (71.1%) underwent partial or total surgical resection and 114 (28.9%) were biopsied. One hundred seventy-four patients were treated with radiotherapy and temozolomide. One hundred forty-four patients were treated upfront with radiotherapy alone, either because they were treated before 2005 (122 patients) or because they were older than 70 years (21 patients). Twenty-seven patients received upfront chemotherapy. Fourteen patients did not receive any specific oncology treatment. The information was missing for 36 patients, who have been excluded from all PFS analyses. Median OS was 14.8 months and median PFS was 8.6 months.

We found 299 (75.7%) *TERT*p-mut, including 222 C228T (74.2%) and 77 C250T (25.8%) mutations. One tumor had both C228T and C250T mutations. This patient was considered as C228T *TERT* mutant for all subsequent analyses. Patients with *TERT*p-mut were older than patients with *TERT* promoter wild type (*TERT*p-wt) GBMs: median age at diagnosis was 59.6 vs 53.6 years, respectively ($p < 0.0001$). There was no difference of age at diagnosis between patients harboring C228T and C250T *TERT* mutations (data not shown). To confirm that such mutations were all somatic events, we investigated the presence of the *TERT*p-mut in blood DNA corresponding to 56 *TERT*p-mut GBMs. No mutation was found in blood DNA (data not shown).

***TERT*p-mut is an independent factor of poor prognosis in GBM.** In patients with GBM, patients with *TERT*p-mut had significantly shorter OS and PFS than patients with *TERT*p-wt. Median OS was 13.8

Figure 1 Prognostic impact of *TERT* promoter mutational status in glioblastomas

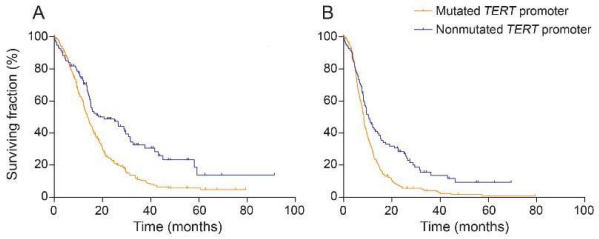

(A) Overall survival. (B) Progression-free survival. *TERT* = telomerase reverse transcriptase.

months in patients with *TERT*p-mut compared to 18.4 months in patients with *TERT*p-wt ($p < 0.0001$) (figure 1). Accordingly, PFS was 8.3 and 10.4 months, respectively ($p < 0.0001$). We did not find any difference in outcome between the C228T and C250T *TERT*p-mut (figure e-1 on the *Neurology*® Web site at Neurology.org).

We then input the following factors as candidate variables in the multivariate Cox proportional hazards regression model analysis: age at diagnosis, *IDH* mutation, extent of surgery, concomitant and adjuvant chemotherapy, Karnofsky Performance Score, *MGMT* promoter methylation status, and *TERT*p-mut. *TERT*p-mut appeared as an independent

Table 1 Multivariate analysis of prognostic factors for overall survival

	Univariate analysis		Multivariate analysis		
Parameters	Survival, mo	p	HR	95% CI for HR	p
KPS					
>70	17.1	<0.0001	0.801	0.569-1.127	0.2049
≤70	11.7				
IDH					
Mutated	26.6	0.005	0.603	0.332-1.094	0.0978
Nonmutated	14.5				
Extent of surgery					
Surgery	15.8	0.001	0.528	0.378-0.737	0.0002
Biopsy	10.1				
Age at diagnosis					
>60 y	10.7	<0.0001	1.720	1.272-2.325	0.0005
≤60 y	17.6				
Treatments					
Concomitant and adjuvant TMZ	19.0	<0.0001	0.478	0.351-0.651	<0.0001
Other	13.1				
MGMT promoter					
Methylated	15.8	0.022	0.684	0.515-0.908	0.0090
Nonmethylated	13.8				
TERT promoter					
Mutated	8.3	<0.0001	1.624	1.122-2.350	0.0105
Nonmutated	10.4				

Abbreviations: CI = confidence interval; HR = hazard ratio; *IDH* = isocitrate dehydrogenase; KPS = Karnofsky Performance Score; *MGMT* = methylguanine methyltransferase; *TERT* = telomerase reverse transcriptase; TMZ = temozolomide.

Table 2 Multivariate analysis of prognostic factors for progression-free survival

	Univariate analysis			Multivariate analysis	
Parameters	Survival, mo	p	HR	95% CI for HR	p
KPS					
>70	8.8	0.001	0.784	0.573-1.074	0.1321
≤70	7.4				
IDH					
Mutated	9.4	0.002	0.564	0.323-0.988	0.0439
Nonmutated	8.5				
Extent of surgery					
Surgery	8.8	0.275			
Biopsy	7.8				
Age at diagnosis					
>60 y	7.5	<0.0001	1.482	1.119-1.962	0.0063
≤60 y	9.5				
Treatments					
Concomitant and adjuvant TMZ	10.1	<0.0001	0.473	0.354-0.6733	<0.0001
Other	7.4				
MGMT promoter					
Methylated	9.2	0.012	0.660	0.504-0.865	0.0027
Nonmethylated	8.2				
TERT promoter					
Mutated	8.3	<0.0001	1.488	1.065-2.079	0.0204
Nonmutated	10.4				

Abbreviations: CI = confidence interval; HR = hazard ratio; *IDH* = isocitrate dehydrogenase; KPS = Karnofsky Performance Score; *MGMT* = methylguanine methyltransferase; *TERT* = telomerase reverse transcriptase; TMZ = temozolomide.

prognostic factor for both OS and PFS in GBM (tables 1 and 2).

***TERT* mutations are associated with specific prognostic and molecular subgroups.** The association of *TERT*p-mut with the other molecular alterations frequently found in GBMs is presented in table 3.

Table 3 Association of *TERT*p-mut with common molecular alterations found in gliomas

	*TERT*p-mut	*TERT*p-wt	p
EGFR amplification	131/299 (43.8)	13/96 (13.5)	<0.0001
Chr 10q loss	253/299 (84.6)	41/95 (43.2)	<0.0001
CDKN2A deletion	141/299 (47.2)	27/96 (28.1)	0.0013
IDH mutation	8/284 (2.8)	22/88 (25.0)	<0.0001
TP53 mutation	35/114 (30.7)	16/34 (47.1)	NS
MGMT promoter methylation	107/245 (43.7)	40/70 (50.6)	NS

Abbreviations: *CDKN2A* = cyclin-dependent kinase inhibitor 2A; Chr = chromosome; *EGFR* = epidermal growth factor receptor; *IDH* = isocitrate dehydrogenase; *MGMT* = methylguanine methyltransferase; NS = not significant; *TERT* = telomerase reverse transcriptase; *TERT*p-mut = *TERT* promotor mutation; *TERT*p-wt = *TERT* promoter wild type; *TP53* = tumor protein p53.
Data are n (%).

IDH mutation was associated with *TERT*p-wt GBM (22/88 [25%] vs 8/284 [2.8%] in *TERT*p-mut GBM). We therefore enquired whether the higher incidence of *IDH* mutation could explain the better outcome of *TERT*p-wt patients compared with *TERT*p-wt GBM. However, stratifying our population according to the *TERT*p status, we found that *TERT*p-mut was prognostic in both *IDH*-wt GBM (OS = 13.7 vs 17.5 months, $p = 0.006$) and *IDH*-mutation GBM (OS = 13.8 vs 37.6 months, $p = 0.02$). Moreover, it is particularly striking to note that *IDH* mutation was associated with a better outcome in *TERT*p-wt GBM (OS = 37.6 vs 17.5 months, $p = 0.04$) but not *TERT*p-mut GBM (OS = 13.8 vs 13.7 months, p = not significant) (figure 2).

In contrast to *IDH* mutation, *EGFR* amplification, present in 144 GBMs, was associated with *TERT*p-mut GBM (131/299 [43.8%] vs 13/96 [13.5%] in *TERT*p-wt GBM). We found that *EGFR* amplification had no prognostic impact per se (figure e-2). However, when stratifying according to *TERT*p status, we found that *EGFR* amplification was associated with shorter OS and PFS in the *TERT*p-wt group (OS = 13.3 vs

Figure 2 Prognostic impact of *TERT* promoter mutation in glioblastomas stratified according to *IDH* mutation

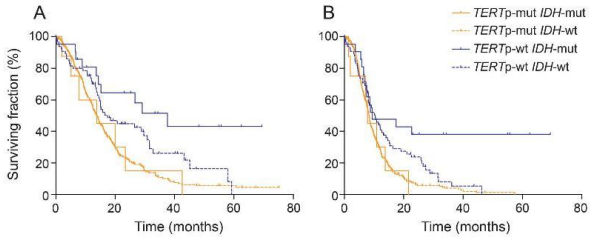

(A) Overall survival. (B) Progression-free survival. *IDH* = isocitrate dehydrogenase; *TERT* = telomerase reverse transcriptase.

26.6 months, $p = 0.005$) but not in the *TERT*p-mut group (OS = 15.8 vs 12.5 months, p = not significant) (figure 3). It is striking to note that in the *EGFR*-wt group, patients with *TERT*p-mut had a poorer outcome compared to patients with *TERT*p-wt (OS = 12.5 vs 26.6 months, $p < 0.0001$), whereas in the *EGFR* amplified group, patients with *TERT*p-mut had a better outcome than patients with *TERT*p-wt (OS = 15.8 vs 13.3 months, $p = 0.05$). To better understand this paradox, we compared the age of these different populations: there was no significant difference of age in the *EGFR* amplified group between *TERT*p-mut patients (59.1 years) and *TERT*p-wt patients (55.7 years) ($p = 0.5$), whereas *TERT*p-mut patients were significantly older than *TERT*p-wt patients (60 vs 49 years, $p < 0.0001$) in the *EGFR* nonamplified group. We therefore analyzed the impact of the *TERT*p-mut according to age in the *EGFR*-wt group. The results, reported in figure e-3, show that in each age category (<50 years; 50–65 years; >65 years), patients with *TERT*p-wt had a longer survival, but this was particularly relevant in the group of patients younger than 50 years.

We also found that *TERT*p-mut were associated with chromosome 10q loss and *CDKN2A* homozygous deletion, but these associations did not result in a prognostic stratification of our cohort.

Prognostic classification of GBMs based on *TERT*p, *EGFR*, and *IDH* status. Building on these results, we propose a 4-group molecular classification of GBMs: (1) GBMs with *TERT*p-mut constituting a homogeneous group (OS = 13.8 months); (2) GBMs with *EGFR* amplification and *TERT*p-wt (OS = 13.3 months), all of which are *IDH*-wt; (3) *IDH* mutation having no prognostic impact in this group; and (4) *EGFR*-wt and *TERT*p-wt, characterized by a much better prognosis particularly in the presence of the *IDH* mutation (OS = 37.6 months), but even in the absence of the *IDH* mutation (26.5 months) (figure 4).

Figure 3 Prognostic stratification of glioblastomas according to *TERT* promoter mutation and *EGFR* amplification status

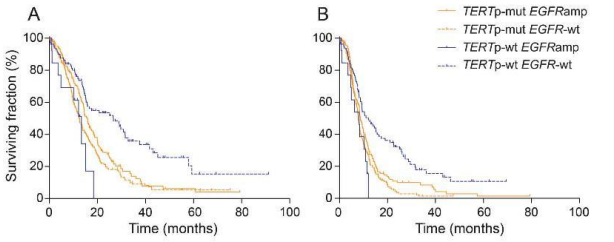

(A) Overall survival. (B) Progression-free survival. amp = amplification; *EGFR* = epidermal growth factor receptor; *TERT* = telomerase reverse transcriptase.

Figure 4 Survival curves corresponding to the 4 prognostic groups

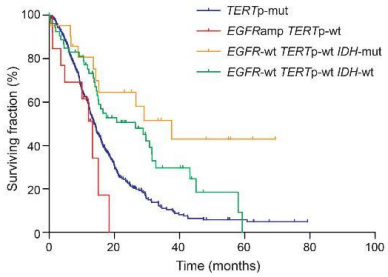

*TERT*p-mut (OS = 13.8 months); *EGFR* amp with *TERT*p-wt (OS = 13.3 months); *EGFR*-wt with *TERT*p-wt and *IDH*-wt (OS = 26.5 months); *EGFR*-wt with *TERT*p-wt *IDH* mutation (OS = 37.6 months). amp = amplification; *EGFR* = epidermal growth factor receptor; *IDH* = isocitrate dehydrogenase; mut = mutation; OS = overall survival; *TERT* = telomerase reverse transcriptase; *TERT*p-mut = *TERT* promoter mutation; *TERT*p-wt = *TERT* promoter wild type; wt = wild type.

DISCUSSION *TERT* is the most frequently mutated gene in GBMs,[4,6,7] suggesting that it may be an early event in the development of these tumors. These mutations create a putative binding site for the E-twenty-six/ternary complex factor transcription factors and increase 2- to 4-fold transcriptional activity of the promoter.[3,18] Increasing telomerase activity confers a selective advantage and promotes immortalization of cells by preventing the senescence induced by telomere shortening.

In our series, *TERT*p-mut were associated with an older age at diagnosis, as previously reported in medulloblastomas,[7] conjunctival melanomas,[1] and recently in gliomas.[19] Telomeres are shorter in the GBMs of older patients,[20] and preventing telomere shortening may therefore be more critical in older patients. Accordingly, the polymorphism rs2736100, which maps to the *TERT* locus, has also been associated with the *IDH*-wt and older age gliomas.[21]

In this work, we show that *TERT*p-mut is an independent factor of poor outcome in GBMs. Indeed, we clearly show here that this effect is not due to the association of *IDH* mutation with *TERT*p-wt status as previously believed.[22] Moreover, the impact of *TERT*p-mut is even stronger in patients with *IDH* mutation than in patients with *IDH*-wt, with a median OS decreasing from 37.6 months in *TERT*p-wt to 13.8 months in *TERT*p-mut. In other words, our data suggest that the favorable prognostic impact of the *IDH* mutation in GBMs is lost in the presence of an associated *TERT* mutation, because the survival in *IDH* mutation *TERT*p-mut GBMs is identical to standard (i.e., *IDH*-wt) GBMs.

We further dissected the prognostic impact of the *TERT*p-mut in the context of different genetic backgrounds. *EGFR* amplification is a hallmark of GBM. It affects 40% of GBMs and is mutually exclusive with *IDH* mutation. In line with previous reports, we show here that *EGFR* amplification has no prognostic impact in the whole GBM population.[23,24] However, determination of the *TERT*p-mut status revealed that in the *TERT*p-wt group, patients with *EGFR*-wt had a median survival twice superior to that of patients with *EGFR* amplification. Consequently, we show a very sharp and opposite effect of the *TERT*p-mut on survival according to *EGFR* status. Similar results have been obtained in medulloblastomas, also showing an opposite prognostic effect of *TERT*p-mut according to different genetic subtypes.[25] Our study also makes it clear that the difference of age—a well-known prognostic factor in GBM—is not a valid explanation, because in the *EGFR* amplified subgroup, patients with *TERT*p-mut were older but still had a better outcome (OS = 15.8 vs 13.3 months, $p = 0.05$).

Finally, we propose a 4-group molecular classification that summarizes our results: when either *EGFR* amplification or *TERT*p-mut is present, the prognosis is poor with median survival ranging from 12 to 16 months. Median survival is much better when none of these 2 alterations is present, ranging from more than 2 years for patients with *IDH*-wt, to more than 3 years for patients with *IDH* mutation.

In this study, we found that the *TERT*p-mut is a strong and independent prognostic marker in GBM, and is not related to *IDH* status. We also show an opposite prognostic effect of *TERT*p-mut in *EGFR*-wt GBM. Finally, we propose a refined prognostic classification of GBMs based on the joint analyses of *TERT*, *EGFR*, and *IDH*.

AUTHOR CONTRIBUTIONS

M.L. and M.S. designed the study and wrote the manuscript. M.L., B.B., A.R., A.-L.D.S., M.R., P.C., O.S., R.P., and G.F. performed genes analysis. K.M. performed the histologic analysis. Clinical data were collected and analyzed by Y.M., M.R., and M.S. All contributed to the data analysis and interpretation. All read and approved the manuscript.

ACKNOWLEDGMENT

The authors are indebted to Alexandru Agachi for editing the manuscript.

STUDY FUNDING

Supported by the Ligue Nationale contre le Cancer (LNCC) and the Institut National du Cancer (INCa). Anna-Luisa Di Stefano is supported by an investigator fellowship from Collegio Ghislieri, Pavia, Italy.

DISCLOSURE

The authors report no disclosures relevant to the manuscript. Go to Neurology.org for full disclosures.

Received December 29, 2013. Accepted in final form July 2, 2014.

REFERENCES

1. Griewank KG, Murali R, Schilling B, et al. TERT promoter mutations in ocular melanoma distinguish between conjunctival and uveal tumours. Br J Cancer 2013;109:497–501.
2. Horn S, Figl A, Rachakonda PS, et al. TERT promoter mutations in familial and sporadic melanoma. Science 2013;339:959–961.
3. Huang FW, Hodis E, Xu MJ, Kryukov GV, Chin L, Garraway LA. Highly recurrent TERT promoter mutations in human melanoma. Science 2013;339:957–959.
4. Liu X, Wu G, Shan Y, Hartmann C, von Deimling A, Xing M. Highly prevalent TERT promoter mutations in bladder cancer and glioblastoma. Cell Cycle 2013;12:1637–1638.
5. Aapola U, Kawasaki K, Scott HS, et al. Isolation and initial characterization of a novel zinc finger gene, DNMT3L, on 21q22.3, related to the cytosine-5-methyltransferase 3 gene family. Genomics 2000;65:293–298.
6. Arita H, Narita Y, Fukushima S, et al. Upregulating mutations in the TERT promoter commonly occur in adult malignant gliomas and are strongly associated with total 1p19q loss. Acta Neuropathol 2013;126:267–276.
7. Killela PJ, Reitman ZJ, Jiao Y, et al. TERT promoter mutations occur frequently in gliomas and a subset of tumors derived from cells with low rates of self-renewal. Proc Natl Acad Sci USA 2013;110:6021–6026.
8. Aubert G, Lansdorp PM. Telomeres and aging. Physiol Rev 2008;88:557–579.
9. Cesare AJ, Reddel RR. Alternative lengthening of telomeres: models, mechanisms and implications. Nat Rev Genet 2010;11:319–330.
10. Smogorzewska A, de Lange T. Regulation of telomerase by telomeric proteins. Annu Rev Biochem 2004;73:177–208.
11. Shay JW, Wright WE. Role of telomeres and telomerase in cancer. Semin Cancer Biol 2011;21:349–353.
12. Ducray F, Idbaih A, Wang XW, Cheneau C, Labussiere M, Sanson M. Predictive and prognostic factors for gliomas. Expert Rev Anticancer Ther 2011;11:781–789.
13. Ricard D, Idbaih A, Ducray F, Lahutte M, Hoang-Xuan K, Delattre JY. Primary brain tumours in adults. Lancet 2012;379:1984–1996.
14. Gonzalez-Aguilar A, Idbaih A, Boisselier B, et al. Recurrent mutations of MYD88 and TBL1XR1 in primary central nervous system lymphomas. Clin Cancer Res 2012;18:5203–5211.
15. Idbaih A, Marie Y, Lucchesi C, et al. BAC array CGH distinguishes mutually exclusive alterations that define clinicogenetic subtypes of gliomas. Int J Cancer 2008;122:1778–1786.
16. Sanson M, Marie Y, Paris S, et al. Isocitrate dehydrogenase 1 codon 132 mutation is an important prognostic biomarker in gliomas. J Clin Oncol 2009;27:4150–4154.
17. Everhard S, Kaloshi G, Criniere E, et al. MGMT methylation: a marker of response to temozolomide in low-grade gliomas. Ann Neurol 2006;60:740–743.
18. Brennan CW, Verhaak RG, McKenna A, et al. The somatic genomic landscape of glioblastoma. Cell 2013;155:462–477.
19. Koelsche C, Sahm F, Capper D, et al. Distribution of TERT promoter mutations in pediatric and adult tumors of the nervous system. Acta Neuropathol 2013;126:907–915.
20. Lotsch D, Ghanim B, Laaber M, et al. Prognostic significance of telomerase-associated parameters in glioblastoma: effect of patient age. Neuro Oncol 2013;15:423–432.
21. Walsh KM, Rice T, Decker PA, et al. Genetic variants in telomerase-related genes are associated with an older age at diagnosis in glioma patients: evidence for distinct pathways of gliomagenesis. Neuro Oncol 2013;15:1041–1047.
22. Nonoguchi N, Ohta T, Oh JE, Kim YH, Kleihues P, Ohgaki H. TERT promoter mutations in primary and secondary glioblastomas. Acta Neuropathol 2013;126:931–937.
23. Batchelor TT, Betensky RA, Esposito JM, et al. Age-dependent prognostic effects of genetic alterations in glioblastoma. Clin Cancer Res 2004;10:228–233.
24. Weller M, Felsberg J, Hartmann C, et al. Molecular predictors of progression-free and overall survival in patients with newly diagnosed glioblastoma: a prospective translational study of the German Glioma Network. J Clin Oncol 2009;27:5743–5750.
25. Remke M, Ramaswamy V, Peacock J, et al. TERT promoter mutations are highly recurrent in SHH subgroup medulloblastoma. Acta Neuropathol 2013;126:917–929.

3.1 Glioma Susceptibility Loci Reflect a "*IDH*-Based Watershed" in Gliomagenesis

Understanding of the genetic susceptibility of glioma has been transformed by recent genome-wide association studies (GWAS), which recently disclosed a dichotomy between *IDH* mutated and *IDH* wild-type gliomas in heritability of gliomas.

Starting from 2009, GWAS have progressively identified single nucleotide polymorphisms (SNPs) at 26 loci influencing glioma risk and have provided evidence for a polygenic basis of genetic susceptibility of gliomas (Shete, 2009; Sanson, 2011; Wrensch, 2009; Kinnersley, 2015; Walsh, 2014; Enciso-Mora, 2013; Jenkins, 2012).

Inherited predisposition to glioma is also suggested by a number of rare inherited cancer syndromes, such as Turcot's and Li–Fraumeni syndromes, and neurofibromatosis, which however, even collectively, account for little of the two-fold familial risk of glioma and for <5% of glioma cases (Hemminki, 2009).

Giving heterogeneity of gliomas, in 2012 we started exploring associations between the first known 7 glioma-risk SNPs at that time, and tumor histological and molecular genetic profile (Di Stefano, 2013).

Interestingly, in this study we found that certain SNPs -rs2736100 (annotating *TERT*) and rs6010620 (*RTEL1*) are associated with high-grade phenotype and molecular aberrations and that rs4295627 (*CCDC26*) and rs498872 (*PHLDB1*) are associated with low-grade disease, *IDH* mutation, and 1p-19q codeletion.

We then proposed for the first time a model of case-control analyses based on four tumor molecular classes by *IDH* status, 1p19q codeletion and *EGFR* amplification **[Figure 3.1** adapted from (Di Stefano, 2013)].

In this study, we found that susceptibility alleles on TERT, *RTEL1*, *CCDC26*, *PHLDB1* predispose to different molecular subgroups of gliomas and that *IDH* somatic mutation is the most robust watershed for these distinct etiologic pathways **[Figure 3.1**; (Di Stefano, 2013)].

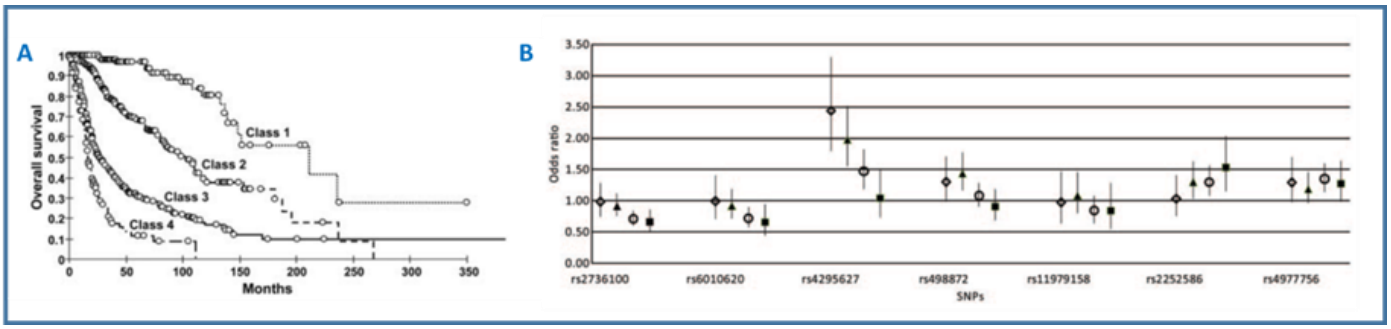

Figure 3.1 adapted from (Di Stefano, 2013). Glioma susceptibility loci predispose to specific molecular classes of gliomas. In A) Kaplan–Meier curves in 1372 glioma patients show significant overall survival difference between tumor class 1-*IDH* mut/1p-19q codel/*EGFR* normal-(median OS 211.2 months), tumor class-2 *IDH* mut/1p-19q normal/*EGFR* normal-(median OS 103.9 months), tumor class 3-*IDH* wt/1p-19q normal/*EGFR* normal-(median OS 26.5 months), and tumor class 4-*IDH* wt/1p-19q normal/*EGFR* amplification-(median OS 16.6 months). In B) Glioma risk, stratified by specific tumor class, is represented (OR and 95% CI) for each single SNP. *IDH* mutation/1p-19q codeletion/*EGFR* normal status; *IDH* mutation/1p-19q normal status/*EGFR* normal status; *IDH* wild-type/1p-19q normal status/*EGFR* normal status; *IDH* wild-type/1p-19q normal status/*EGFR*amplification.

More recently, others and we have reported supplementary susceptibility variants for gliomas using an imputation based approach and genotyping confirmation.

We reported a rare variant rs78378222 (minor allele frequency 0.013) annotating *TP53*, which is strongly associated to glioma risk (P=6.86 x10 $^{-24}$) (Enciso-Mora, 2013). This locus does not show a differential association between rs78378222 histological phenotype (GBM versus non-GBM tumors) and is not associated with *TP53* somatic mutation.

In a following study, thanks to advances in high-density genotyping and imputation reference panels we were able (Enciso-Mora, 2013) to deeply examine 8q24.21, the region encompassing the rs4295627 (*CCDC26*), which correspond to the region with the highest signal of association with *IDH* mutation and 1p19 codeleted gliomas (OR 2.44 P=10^{-9}). Analysis revealed an imputed low-frequency SNP rs55705857 (P=2.24 x10^{-38}) and stratifying by glioma subtype, we showed that the association with rs55705857 is confined to non-glioblastoma (non-GBM) tumors with the tightest association ever found in GWAS (P=1.07x10^{-67}; P=2.31 x10^{-94}in the pooled analysis, of three additional datasets).

rs55705857 maps to a highly evolutionarily conserved sequence within the long non-coding RNA *CCDC26*, raising the possibility that this region (8q24.21) contains a germ line alteration that facilitates the initiation or progression of gliomas with *IDH* mutations (Enciso-Mora, 2013).

More recently, to expand the repertoire of glioma susceptibility loci, others and we recently performed the following:

- a first meta-analysis of four GWAS (totalling 4,147 cases and 7,435 controls), reporting new risk loci for glioblastoma (GBM) at 12q23.33 (rs3851634, near *POLR3B*, $P=3.02x10^{-9}$) and non-GBM at 10q25.2 (rs11196067, near *VTI1A*, $P=4.32x10^{-8}$), 11q23.2 (rs648044, near *ZBTB16*, $P=6.26x10^{-11}$), 12q21.2 (rs12230172, $P=7.53x10^{-11}$) and 15q24.2 (rs1801591, near *ETFA*, $P=5.71x10^{-9}$) (Kinnersley, 2015).
- a second larger meta-analysis, in the setting of the Glioma International Case Control Consortium, including past published GWAS and a new GWAS with replication comprising 12,496 cases and 18,190 controls (Melin et al. Nat Genet, in press)

This study identified 13 new risk loci, reaching a total of 26 glioma risk loci identified so far.

Among them, rs7572263, mapping to 2q33.3, is associated with non-GBM ($P=2.18\times10^{-10}$, Odds Ratio=1.20) and interestingly localizes ~50 kb telomeric to the gene encoding *IDH1*. Since *IDH* mutation is predominate, as mentioned before, in non-GBM glioma, the association at 2q33.3 could potentially disclose additional insights into the aetiological basis of *IDH* mutant gliomagenenesis.

Reported articles are included in this section.

nature COMMUNICATIONS

ARTICLE

Received 8 May 2015 | Accepted 4 Sep 2015 | Published 1 Oct 2015

DOI: 10.1038/ncomms9559 OPEN

Genome-wide association study identifies multiple susceptibility loci for glioma

Ben Kinnersley[1], Marianne Labussière[2], Amy Holroyd[1], Anna-Luisa Di Stefano[2,3,4], Peter Broderick[1], Jayaram Vijayakrishnan[1], Karima Mokhtari[2,3,5], Jean-Yves Delattre[2,3,4], Konstantinos Gousias[6], Johannes Schramm[6], Minouk J. Schoemaker[1], Sarah J. Fleming[7], Stefan Herms[8,9], Stefanie Heilmann[8], Stefan Schreiber[10,11], Heinz-Erich Wichmann[12,13], Markus M. Nöthen[8], Anthony Swerdlow[1,14], Mark Lathrop[5,15,16], Matthias Simon[6], Melissa Bondy[17], Marc Sanson[2,3,4] & Richard S. Houlston[1]

Previous genome-wide association studies (GWASs) have shown that common genetic variation contributes to the heritable risk of glioma. To identify new glioma susceptibility loci, we conducted a meta-analysis of four GWAS (totalling 4,147 cases and 7,435 controls), with imputation using 1000 Genomes and UK10K Project data as reference. After genotyping an additional 1,490 cases and 1,723 controls we identify new risk loci for glioblastoma (GBM) at 12q23.33 (rs3851634, near *POLR3B*, $P = 3.02 \times 10^{-9}$) and non-GBM at 10q25.2 (rs11196067, near *VTI1A*, $P = 4.32 \times 10^{-8}$), 11q23.2 (rs648044, near *ZBTB16*, $P = 6.26 \times 10^{-11}$), 12q21.2 (rs12230172, $P = 7.53 \times 10^{-11}$) and 15q24.2 (rs1801591, near *ETFA*, $P = 5.71 \times 10^{-9}$). Our findings provide further insights into the genetic basis of the different glioma subtypes.

[1] Division of Genetics and Epidemiology, The Institute of Cancer Research, London SM2 5NG, UK. [2] Sorbonne Universités UPMC Univ Paris 06, INSERM CNRS, U1127, UMR 7225, ICM, F-75013 Paris, France. [3] Onconeurotek, F-75013 Paris, France. [4] AP-HP, GH Pitié-Salpêtrière, Service de Neurologie 2, F-75013 Paris, France. [5] AP-HP, GH Pitié-Salpêtrière, Laboratoire de neuropathologie R Escourolle, F-75013 Paris, France. [6] Department of Neurosurgery, University of Bonn Medical Center, Sigmund-Freud-Straße 25, 53105 Bonn, Germany. [7] Centre for Epidemiology and Biostatistics, Faculty of Medicine and Health, University of Leeds, Leeds LS2 9JT, UK. [8] Department of Biomedicine, Institute of Human Genetics, University of Bonn, 53127 Bonn, Germany. [9] Division of Medical Genetics, Department of Biomedicine, University of Basel, 4056 Basel, Switzerland. [10] 1st Medical Department, University Clinic Schleswig-Holstein, Campus Kiel, House 6, Arnold-Heller-Straße 3, Kiel 24105, Germany. [11] Institute of Clinical Molecular Biology, Christian-Albrechts-University Kiel, Arnold-Heller-Straße 3, Kiel 24105, Germany. [12] Institute of Epidemiology I, Helmholtz Zentrum München, German Research Center for Environmental Health, Ingolstädter Landstraße 1, 85764 Neuherberg, Germany. [13] Institute of Medical Informatics, Biometry and Epidemiology, Chair of Epidemiology, Ludwig-Maximilians-Universität, 81377 Munich, Germany. [14] Division of Breast Cancer Research, The Institute of Cancer Research, Sutton, Surrey SM2 5NG, UK. [15] Foundation Jean Dausset-CEPH, 27 Rue Juliette Dodu, 75010 Paris, France. [16] Génome Québec, Department of Human Genetics, McGill University, Montreal, Quebec, Canada H3A 0G1. [17] Division of Hematology-Oncology, Department of Pediatrics, Dan L. Duncan Cancer Center, Baylor College of Medicine, Houston, Texas 77030, USA. Correspondence and requests for materials should be addressed to R.S.H. (email: richard.houlston@icr.ac.uk).

Gliomas account for ~40% of all primary brain tumours and cause around 13,000 deaths in the United States of America each year[1]. Gliomas are heterogeneous and different tumour subtypes, defined in part by malignancy grade (for example, pilocytic astrocytoma World Health Organization (WHO) grade I, diffuse 'low-grade' glioma WHO grade II, anaplastic glioma WHO grade III and glioblastoma (GBM) WHO grade IV) can be distinguished[2]. Gliomas are typically associated with a poor prognosis irrespective of clinical care, with the most common type, GBM, having a median overall survival of only 10–15 months[1].

While the glioma subtypes have distinct molecular profiles resulting from different aetiological pathways[3], no environmental exposures have, however, consistently been linked to risk except for ionizing radiation, which only accounts for a very small number of cases[1]. Direct evidence for inherited predisposition to glioma is provided by a number of rare inherited cancer syndromes, such as Turcot's and Li–Fraumeni syndromes, and neurofibromatosis[4]. Even collectively, these diseases however account for little of the twofold increased risk of glioma seen in first-degree relatives of glioma patients[5]. Support for polygenic susceptibility to glioma has come from genome-wide association studies (GWASs) that have identified single-nucleotide polymorphisms (SNPs) at eight loci influencing glioma risk—3q26.2 (near *TERC*), 5p15.33 (near *TERT*), 7p11.2 (near *EGFR*), 8q24.21 (near *CCDC26*), 9p21.3 (near *CDKN2A/CDKN2B*), 11q23.3 (near *PHLDB1*), 17p13.1 (*TP53*) and 20q13.33 (near *RTEL1*) (refs 6–10). Perhaps not surprisingly there is variability in genetic effects on glioma by histology with subtype-specific associations at 5p15.33, 20q13.33 and 7p11.2 for GBM and at 11q23.3 and 8q24 for non-GBM glioma[6,7].

Recovery of untyped genotypes via imputation has enabled fine mapping and refinement of association signals, for example, in identification of rs55705857 as the basis of the 8q24 association signal in glioma[11]. Recently, the use of the 1000 Genomes Project and the UK10K projects as a combined reference panel has been shown to improve accuracy compared with using the 1000 Genomes Project data alone, allowing imputation of alleles with frequencies ~0.5% to be viable[12].

Here we report a meta-analysis of four GWASs totalling 4,147 cases and 7,435 controls to identify new glioma susceptibility loci, after imputation using the 1000 Genomes and the UK10K Project data as reference. After genotyping an additional series of 1,490 cases and 1,723 controls we identified new risk loci for GBM at 12q23.33 and non-GBM at 10q25.2, 11q23.2, 12q21.2 and 15q24.2. Our findings provide further insights into the genetic basis of the different glioma subtypes.

Results

Association analysis. To identify additional glioma susceptibility loci we conducted a pooled meta-analysis of four GWASs in populations of European ancestry, the UK-GWAS, the French-GWAS, the German-GWAS and the US-GWAS, that were genotyped using either Illumina HumanHap 317, 317 + 240S, 370Duo, 550, 610 or 1M arrays (Supplementary Table 1). After filtering, the studies provided genotypes on 4,147 cases and 7,435 controls of European ancestry (Supplementary Table 1, Supplementary Fig. 1). Consistent with our previous analysis[6], quantile–quantile (Q–Q) plots for the German and the US series showed some evidence of inflation (inflation factor based on the 90% least-significant SNPs, $\lambda_{90} = 1.15$ and 1.11, respectively), however after correcting for population substructure using principal-component analyses as implemented in Eigenstrat[13], λ_{90} for all four studies was ≤ 1.05 (combined $\lambda_{90} = 1.05$, Supplementary Fig. 2). To achieve consistent and dense genome-wide coverage, we imputed unobserved genotypes at >10 million SNPs using a combined reference panel comprising 1,092 individuals from the 1000 Genomes Project and 3,781 individuals from the UK10K project. Q–Q plots for all SNPs (minor allele frequency (MAF) >0.5%) post-imputation did not show evidence of substantive over-dispersion introduced by imputation after Eigenstrat adjustment (combined $\lambda_{90} = 1.07$, λ_{90} for individual studies = 1.04–1.06; Supplementary Fig. 2).

Pooling data from each GWAS into a joint discovery data set, we derived joint odds ratios (ORs) and 95% confidence intervals (CIs) under a fixed-effects model for each SNP with MAF >0.005 and associated per allele Eigenstrat-corrected *P* values. Overall and histology-specific ORs were derived for all glioma, GBM and non-GBM. In the pooled data set, associations at the established risk loci for glioma at 5p15.33, 7p11.2, 8q24.21, 9p21.3, 11q23.3, 17p13.1 and 20q13.33 showed a consistent direction of effect with previously reported studies ($P < 5.0 \times 10^{-8}$, Fig. 1 and Supplementary Table 2). In contrast we found no significant support for the association between rs1920116 near *TERC* (3q26.2) and risk of high-grade glioma recently reported by Walsh *et al.*[10] (combined *P* value for GBM = 0.179; Supplementary Table 2 and Supplementary Fig. 3). While the UK-GWAS and the study of Walsh *et al.* share use of UK 1958 Birth Cohort controls, the other three GWAS we analysed are fully independent.

After filtering at $P < 5.0 \times 10^{-6}$ in either all glioma, GBM or non-GBM, we selected 14 SNPs for follow-up, mapping to distinct loci not previously associated with glioma risk (Fig. 1 and Supplementary Table 2). rs141035288, rs117527984, rs138170678 were not taken forward as there was poor concordance between imputed and sequenced genotypes (Supplementary Table 3), and rs145034266 could not be genotyped as it mapped within a highly repetitive region.

The 10 remaining SNPs underwent replication genotyping in an additional set of 1,490 glioma cases and 1,723 controls (UK replication series, Supplementary Table 4). Meta-analysis was then conducted across discovery and replication stages, with genotype data available on 5,637 cases and 9,158 controls. In the combined analysis five SNPs showed an association with tumour risk, which was genome-wide significant (Table 1)—rs3851634 (12q23.3, $P_{GBM} = 3.02 \times 10^{-9}$), rs11196067 (10q25.2, $P_{Non\text{-}GBM} = 4.32 \times 10^{-8}$), rs648044 (11q23.2, $P_{Non\text{-}GBM} = 6.26 \times 10^{-11}$), rs12230172 (12q21.2, $P_{Non\text{-}GBM} = 7.53 \times 10^{-11}$) and rs1801591 (15q24.2, $P_{Non\text{-}GBM} = 5.71 \times 10^{-9}$). We tested for secondary signals at each locus by adjusting for the sentinel SNP in each region, but found no evidence for independent associations (Supplementary Fig. 4).

The association signal at 12q23.3 defined by rs3851634 was specific for GBM. The rs3851634 maps to intron 12 of the gene encoding polymerase III, RNA, subunit b (*POLR3B*; Fig. 2a) within a ~350-kb block of linkage disequilibrium (LD) at 12q23.3, which also contains the genes *CKAP4* and *TCP1L2*. The other four SNP associations defined by rs11196067, rs648044, rs12230172 and rs1801591 were specific to non-GBM glioma. rs11196067 (10q25.2) is located in intron 7 of *VTI1A* (vesicle transport through interaction with t-SNAREs 1A, Fig. 2b). Similarly rs648044 (11q23.2) is also intronic mapping within ZBTB16 (zinc finger and BTB domain-containing protein 16, alias PLZF; Fig. 2c). The rs12230172 (12q21.2) maps within the lincRNA *RP11-114H23.1* and is centromeric to the gene encoding *PHLDA1* (centromeric pleckstrin homology-like domain, family a, MEMBER 1, Fig. 2d). rs1801591 (15q24.2) is responsible for the p.Thr171Ile substitution in *ETFA* (electron transfer flavoprotein, alpha polypeptide gene, which resides within a 500-kb region of LD to which *ISL2*, *TYRO3P* and *SCAPPER* genes also map Fig. 2e).

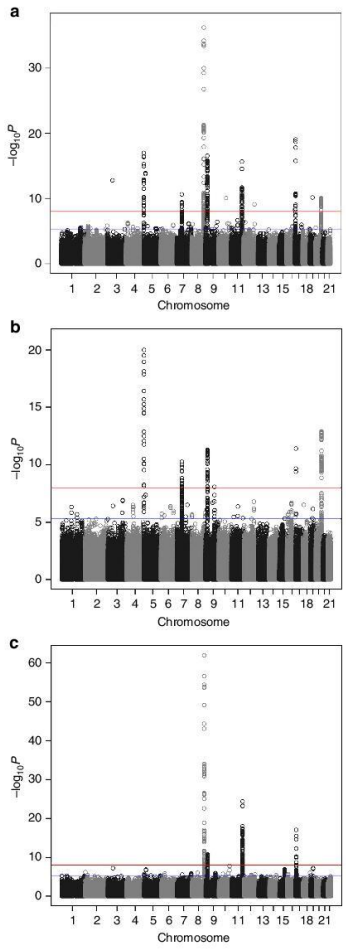

Figure 1 | Genome-wide meta-analysis *P* values (-log$_{10}$*P*, *y* axis) plotted against their chromosomal positions (*x* axis). (**a**) All glioma, (**b**) GBM (**c**) non-GBM. The red and blue horizontal lines represent significance thresholds of $P = 5.0 \times 10^{-8}$ and $P = 5.0 \times 10^{-6}$, respectively.

Relationship between the new glioma SNPs and tumour profile. To investigate the impact of the new risk SNPs on glioma subtype we examined rs11196067, rs648044, rs12230172, rs1801591 and rs3851634 genotypes in the French case series for which comprehensive histology and molecular phenotyping had been performed (Supplementary Data 1). The GBM SNP rs3851634 was associated with 10q-deleted glioma ($P = 0.016$). In the case of non-GBM SNPs rs11196067 showed the strongest association with grade II glioma ($P = 3.2 \times 10^{-5}$) and *TP53* non-mutated glioma ($P = 5.82 \times 10^{-5}$); rs648044 with grade II oligodendroglioma ($P = 0.026$) and 10q non-deleted glioma ($P = 0.006$); rs1801591 with grade II astrocytoma ($P = 0.001$) and *IDH1/IDH2* mutated glioma ($P = 0.005$) and rs12230172 with grade II oligodendroglioma ($P = 0.009$), *IDH1/IDH2* mutated ($P = 0.009$) and 10q non-deleted glioma ($P = 0.003$).

Functional annotation of risk variants. For each of the sentinel risk SNPs at the five risk loci (as well as correlated variants, $r^2 > 0.8$) we examined published data[14,15] and made use of the online resources HaploReg v3, RegulomeDB and SeattleSeq for evidence of functionality and regulatory motifs at genomic regions (Supplementary Table 5). rs1801591, which is responsible for the *ETFA* p.Thr171Ile substitution, resides within a highly conserved region of the genome (genomic evolutionary rate profiling (GERP) = 5.65) and the amino-acid change is predicted to be damaging (PolyPhen = 1). Although rs648044 exhibits low evolutionary conservation (GERP = − 9.32) it maps within a strong DNase hypersensitivity site and predicted enhancer/super-enhancer element for multiple tissues including the brain. The region surrounding rs648044 is also predicted to interact with the *ZBTB16* promoter, which combined with alteration of a Pax-5 motif is suggestive of direct functional impact. rs12230172 localizes within a moderately conserved region (GERP = 3.41) and occupies promoter histone marks in the brain as well as enhancers predicted to associate with transcriptional start sites for *PHLDA1* and *GLIPR1*. rs11196067 in *VTI1A*, while having a low conservation score (GERP = 0.719), occupies enhancer histone marks in embryonic stem cells although not in brain cells. Similarly, rs3851634 maps to a moderately conserved region (GERP = 2.37) and occupies enhancer histone marks in 18 organs including the brain.

eQTL analysis of the five new glioma SNPs. To gain further insight into the functional basis of rs11196067, rs648044, rs12230172, rs1801591 and rs3851634 associations we performed an expression quantitative trait loci (eQTL) analysis using RNA-Seq expression data on 389 low-grade gliomas (LGGs) and 138 GBMs from The Cancer Genome Atlas (TCGA), together with lymphoblastoid cell line RNA-Seq data on 363 samples from GEUVADIS[16]. We examined for an association between SNP genotype and expression of genes mapping within 1 Mb of the sentinel SNP (Supplementary Data 2). After adjusting for multiple testing within each region no statistically significant eQTL was seen for rs11196067, rs12230172, rs1801591 or rs3851634. The strongest association between rs648044 genotype and gene expression was with *ZW10* in LGG ($P = 5.7 \times 10^{-5}$), with the risk allele (T) associated with lower expression, remaining significant after adjustment for multiple testing. To explore the possibility that rs648044 is correlated with a SNP exhibiting a stronger association with *ZW10*, we examined associations with *ZW10* expression in LGG tumours in all SNPs in LD ($r^2 > 0.4$) with rs648044. All of the proxy SNPs examined were more weakly associated with *ZW10* than rs648044 (Supplementary Table 6). Following on from these analyses we made use of publically available eQTL mRNA expression array data on adipose tissue, lymphoblastoid cell lines and skin from 856 twins (MuTHER[17]) and 5,311 non-transformed peripheral blood samples using the blood eQTL browser[18]. The risk allele (C) of rs3851634 was associated with significantly lower levels of *POLR3B* ($P = 7.49 \times 10^{-6}$) in peripheral blood analysis with a nominally significant association in skin ($P = 0.0052$). The risk allele (T) of rs1801591, was associated with significantly lower

Table 1 | Association between SNP and glioma risk in discovery and replication data sets for rs11196067, rs648044, rs12230172, rs3851634 and rs1801591.

	MAF			All glioma		GBM		Non-GBM	
SNP	**Case**	**Control**	**Study**	***P***	**OR (95% CI)**	***P***	**OR (95% CI)**	***P***	**OR (95% CI)**
rs111696067	0.38	0.41	FRE	5.00×10^{-5}	0.79 (0.71-0.89)	0.26	0.91 (0.78-1.07)	2.54×10^{-6}	0.74 (0.66-0.84)
(*VTI1A*)			GER	0.44	0.95 (0.83-1.08)	0.88	1.01 (0.86-1.19)	0.15	0.88 (0.75-1.04)
10q25.2			UK	0.012	0.85 (0.75-0.96)	0.34	0.91 (0.76-1.10)	8.11×10^{-3}	0.81 (0.69-0.95)
A/**T**			USA	0.016	0.88 (0.80-0.98)	0.097	0.90 (0.79-1.02)	0.033	0.87 (0.76-0.99)
			Replication	0.56	0.97 (0.88-1.07)	0.91	0.99 (0.89-1.11)	0.33	0.93 (0.81-1.07)
			Combined	4.32×10^{-6}	0.89 (0.85-0.93)	0.11	0.95 (0.89-1.01)	4.32×10^{-8}	0.84 (0.79-0.89)
rs648044	0.40	0.38	FRE	0.019	1.15 (1.02-1.30)	0.93	0.99 (0.83-1.18)	1.76×10^{-3}	1.23 (1.08-1.41)
(*ZBTB16*)			GER	0.043	1.16 (1.00-1.34)	0.39	1.08 (0.90-1.30)	0.016	1.25 (1.04-1.50)
11q23.2			UK	0.78	1.02 (0.89-1.16)	0.044	0.82 (0.67-0.99)	0.037	1.20 (1.01-1.42)
C/**T**			USA	0.088	1.10 (0.99-1.23)	0.62	0.97 (0.86-1.09)	1.02×10^{-3}	1.27 (1.10-1.46)
			Replication	0.97	1.08 (0.97-1.19)	0.59	0.97 (0.86-1.09)	4.16×10^{-4}	1.29 (1.12-1.48)
			Combined	5.29×10^{-4}	1.10 (1.04-1.16)	0.32	0.97 (0.90-1.03)	6.26×10^{-11}	1.25 (1.17-1.34)
rs12230172	0.45	0.46	FRE	0.054	0.90 (0.81-1.00)	0.72	1.03 (0.88-1.20)	4.40×10^{-3}	0.84 (0.74-0.95)
(intergenic)			GER	0.043	0.88 (0.77-1.00)	0.84	0.98 (0.84-1.16)	2.17×10^{-3}	0.78 (0.66-0.91)
12q21.2			UK	0.44	0.95 (0.84-1.09)	0.77	0.97 (0.85-1.11)	0.42	0.94 (0.80-1.10)
G/**A**			USA	0.30	0.95 (0.86-1.05)	0.55	1.04 (0.92-1.18)	0.018	0.85 (0.75-0.97)
			Replication	1.84×10^{-6}	0.79 (0.70-0.86)	7.00×10^{-3}	0.85 (0.76-0.96)	3.59×10^{-8}	0.67 (0.58-0.77)
			Combined	1.57×10^{-6}	0.88 (0.84-0.93)	0.22	0.96 (0.91-1.02)	7.53×10^{-11}	0.81 (0.76-0.86)
rs3851634	0.27	0.30	FRE	0.053	0.89 (0.79-1.00)	0.020	0.81 (0.69-0.97)	0.25	0.93 (0.81-1.06)
(*POLR3B*)			GER	0.18	0.91 (0.73-1.04)	0.12	0.87 (0.73-1.04)	0.59	0.95 (0.80-1.14)
12q23.3			UK	0.058	0.88 (0.60-0.89)	1.56×10^{-3}	0.73 (0.60-0.89)	0.92	1.01 (0.85-1.20)
T/**C**			USA	2.84×10^{-4}	0.81 (0.73-0.91)	7.21×10^{-4}	0.79 (0.68-0.90)	0.021	0.84 (0.73-0.98)
			Replication	0.022	0.88 (0.79-0.98)	5.00×10^{-3}	0.83 (0.74-0.95)	0.57	0.96 (0.83-1.11)
			Combined	4.07×10^{-7}	0.87 (0.82-0.92)	3.02×10^{-9}	0.81 (0.76-0.87)	0.037	0.93 (0.87-1.00)
rs1801591	0.10	0.09	FRE	6.67×10^{-3}	1.32 (1.08-1.61)	0.29	1.17 (0.87-1.58)	2.51×10^{-3}	1.40 (1.13-1.74)
(*ETFA*)			GER	0.037	1.25 (1.01-1.53)	0.17	1.20 (0.93-1.56)	0.052	1.31 (1.00-1.72)
15q24.2			UK	0.44	1.08 (0.88-1.33)	0.93	0.99 (0.73-1.33)	0.23	1.17 (0.90-1.53)
G/**A**			USA	0.016	1.23 (1.04-1.46)	0.97	1.00 (0.80-1.24)	5.13×10^{-5}	1.56 (1.26-1.94)
			Replication	0.16	1.13 (0.95-1.33)	0.89	1.01 (0.83-1.23)	0.013	1.31 (1.06-1.63)
			Combined	2.75×10^{-5}	1.20 (1.10-1.30)	0.32	1.06 (0.95-1.18)	5.71×10^{-9}	1.36 (1.23-1.51)

ORs derived with respect to the minor allele, highlighted in bold. The SNPs rs3851634 and rs1801591 were directly genotyped while rs1196067, rs648044 and rs12230172 were imputed with imputation information scores (Is) of 0.99, 0.87 and 1.00, respectively. Sample sizes in the individual data sets are as follows: FRE (French-GWAS), 1,423 cases and 1,190 controls; GER (German-GWAS), 846 cases and 1,310 controls; UK (UK-GWAS), 631 cases and 2,699 controls; USA (USA-GWAS), 1,247 cases and 2,236 controls; replication, 1,490 cases and 1,723 controls; combined, 5,637 cases and 9,158 controls. MAF, minor allele frequency in discovery series.

ETFA levels in peripheral blood ($P=7.90\times10^{-12}$); there was a nominally significant association in MuTHER lymphoblastoid cell lines ($P=0.037$).

Somatic mutation of newly implicated risk genes in glioma. We examined mutation data from TCGA for evidence of recurrent mutation in genes annotated by the new GWAS signals. Collectively *POLR3B*, *ETFA*, *VTI1A*, *ZBTB16* and *PHLDA1* are altered in 8% (22/286) of LGG as compared with 3% (8/273) of GBM ($P=0.014$, Supplementary Table 7) providing support for these genes having a role in glioma tumorigenesis.

Individual variance in risk associated with glioma SNPs. To explore the relative contributions of previously reported and newly described loci to glioma risk, we applied the method of Pharoah *et al.*[19] to eight previously reported SNPs as well as the five new risk SNPs (Supplementary Table 8). The variance in risk attributable to all 12 SNPs is 26%, 27% and 43% for all glioma, GBM and non-GBM, respectively.

Pathway enrichment of glioma GWAS SNPs. To gain further insights into the biological basis of associations we performed a pathway analysis on GWAS associations in all glioma, GBM and non-GBM. Applying a false discovery rate (FDR) threshold of <0.1 revealed enrichment for 14 pathways in all glioma, 8 in GBM and 9 in non-GBM tumours (Supplementary Table 9). Pathways implicated in GBM tumours primarily include DNA repair and Notch-signalling, whereas for non-GBM tumours pathways were primarily associated with cell-cycle progression and energy metabolism (Supplementary Table 9).

Discussion

To our knowledge we have performed the largest GWAS of glioma to date, identifying five novel glioma susceptibility loci at 12q23.33, 10q25.2, 11q23.2, 12q21.2 and 15q24.2 and taking the total count of risk loci to 12. Through making use of a combined reference panel from the UK10K and the 1000 Genomes Projects we were able to recover genotypes from $\sim$8 million SNPs for association analysis, a significant increase from using array SNPs alone. In addition, we have provided further evidence that genetic susceptibility to glioma can be subtype specific, emphasising the importance of searching for histology-specific risk variants.

While deciphering the functional impact of these SNP associations on glioma development requires additional analyses, a number of the genes implicated have relevance to the biology of this cancer *a priori*. As well as participating in regulating insulin-stimulated trafficking of secretory vesicles[20], *VTI1A* plays a key role in neuronal development and in selectively maintaining spontaneous neurotransmitter release[21]. Intriguingly recent GWAS have identified associations between the *VTI1A* SNPs rs7086803 and lung cancer[22] and between rs12241008 and colorectal cancer[23]; rs7086803 and rs12241008 are not

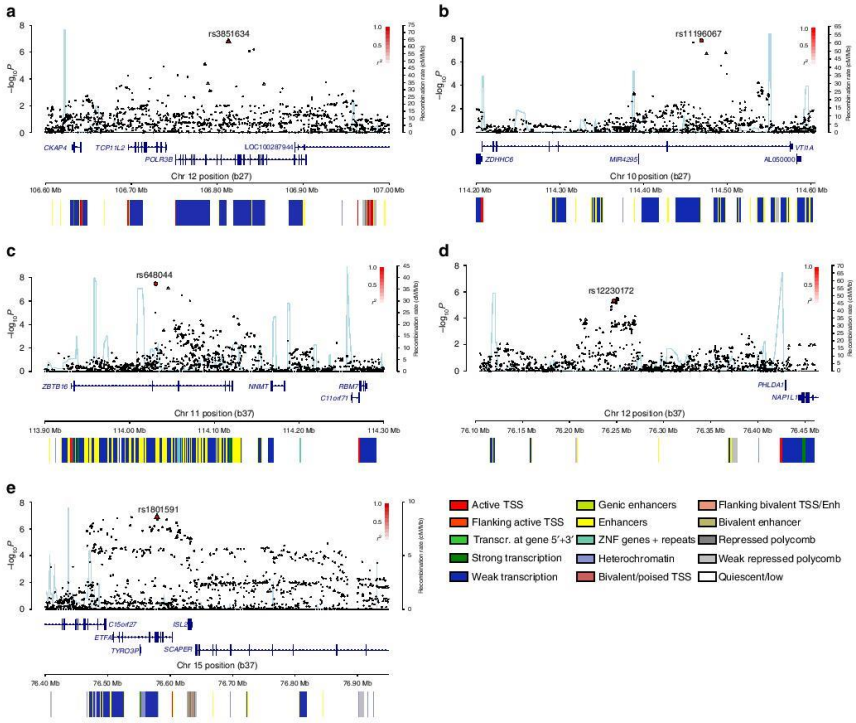

Figure 2 | Regional plots of discovery-phase association results, recombination rates and chromatin state segmentation tracks for five glioma-risk loci. Results for: (**a**) 12q23.33, rs3851634 (GBM); (**b**) 10q25.2, rs11196067 (non-GBM); (**c**) 11q23.2, rs648044 (non-GBM); (**d**) 12q21.2 rs12230172 (non-GBM); and (**e**) 15q24.2, rs1801591 (non-GBM). Plots show discovery association results of both genotyped (triangles) and imputed (circles) SNPs in the GWAS samples and recombination rates. The $-\log_{10} P$ values (*y* axes) of the SNPs are shown according to their chromosomal positions (*x* axes). The lead SNP in each combined analysis is shown as a large circle or triangle (if imputed or directly genotyped, respectively) and is labelled by its rsID. The colour intensity of each symbol reflects the extent of LD with the top genotyped SNP, white ($r^2=0$) to dark red ($r^2=1.0$). Genetic recombination rates, estimated using HapMap samples from Utah residents of western and northern European ancestry (CEU), are shown with a light blue line. Physical positions are based on NCBI build 37 of the human genome. Also shown are the relative positions of University of Carolina, Santa Cruz (UCSC) genes and transcripts mapping to the region of association. Genes have been redrawn to show their relative positions; therefore, maps are not to physical scale. Below each plot is a diagram of the exons and introns of the genes of interest, the associated SNPs and the chromatin state segmentation track (ChromHMM) for H1 neural progenitor cells derived from the epigenome roadmap project, as per legend. TSS, transcriptional start sites.

correlated with each other ($r^2=0.22$, $D'=0.72$) and are also not correlated with rs11196067 ($r^2=0.03/0.00$ $D'=1.00/0.22$, respectively), suggesting the existence of multiple risk loci within the region with different tumour specificities.

ZBTB16 is highly expressed in undifferentiated, multipotential progenitor cells and its expression has been shown to influence resistance to retinoid-mediated re-differentiation in *t*(11;17)(q23;21) acute promyelocytic leukaemia[24]. The BTB domain of *ZBTB16* has transcriptional repression activity and interacts with components of the histone deacetylase complex thereby linking the transcription factor with regulation of chromatin conformation[25]. Although rs648044 lies within an enhancer active in brain and is predicted to interact with the *ZBTB16* promoter, providing an attractive functional basis for the 11q23.2 association through differential ZBTB16 expression, we found a strong association between rs648044 and *ZW10* expression in LGG ($P=5.7\times10^{-5}$). Since *ZW10* plays a role in chromosome segregation[26] it also represents a plausible candidate for the 11q23.2 association.

We also observed a strong association between *ETFA* expression and rs1801591 in peripheral blood ($P=7.90\times10^{-12}$). *ETFA* participates in mitochondrial fatty acid beta oxidation; shuttling electrons between flavoprotein dehydrogenases and the membrane-bound electron transfer flavoprotein ubiquinone oxidoreductase[27]. Mutations of *ETFA* have been reported to be a cause of recessive glutaric acidaemia IIA (refs 28,29), which

features gliosis. While the p.Thr171Ile change is reported to decrease thermal stability of *ETFA*[30] thereby providing evidence for a direct functional effect the strong eQTL data is consistent with the functional basis for the 15q24.2 association being mediated through differential expression.

RNA polymerase III (*POLR3B*) is involved in the transcription of small noncoding RNAs and short interspersed nuclear elements, as well as all transfer RNAs[31]. Although mutations in *POLR3B* have been shown to cause recessive hypomyelinating leukoencephalopathy[32] thus far there is no evidence implicating the gene in the development of glioma. Albeit in peripheral blood there was a strong association between *POLR3B* expression and rs3851634 ($P = 7.49 \times 10^{-6}$), providing a possible functional basis of the 12q23.2 association.

At 12q21.2 rs12230172 maps within *RP11-114H23.1*, a lincRNA of currently unknown function. Although only lying adjacent to *PHLDA1*, the known 11q23.3 association maps to the related gene *PHLDB1*, which is also specific to non-GBM tumours[7]. Although a role for *PHLDA1* in glioma has yet to be established downregulation of *PHLDA1* in neuronal cells has been shown to enhance cell death without Fas induction[33], additionally *PHLDA1* expression may be involved in regulation of anti-apoptotic effects of *IGF1* (ref. 34).

Intriguingly across all of the four GWAS data sets we analysed we did not replicate the association between rs1920116 (near *TERC*) at 3q26.2 and risk of high-grade glioma recently reported by Walsh *et al.*[10] ($P = 8.3 \times 10^{-9}$, OR = 1.30 versus $P = 0.18$, OR = 1.06 relative to the G-allele in our GBM data set), despite our study having a similar power to demonstrate a relationship (1,783 GBM cases, 7,435 controls in our study as compared with 1,644 cases, 7,736 controls). It is, however noteworthy that the Walsh *et al.* analysed both anaplastic astrocytoma and GBM. While we could not demonstrate a significant association with either subtype we did see an association between rs1920116 and *TP53*-mutated glioma ($P = 0.016$, Supplementary Data 1) suggesting that the association might be restricted to a specific molecularly defined subtype of glioma.

Our findings provide further evidence for an inherited genetic susceptibility to glioma. Future investigation of the genes targeted by the risk SNPs we have identified is likely to yield increased insight into the development of this malignancy. We estimate that the risk loci so far identified for glioma account for 27 and 43% of the familial risk of GBM and non-GBM tumours, respectively, of which 0.8% and 7.6% can be explained by the loci newly reported in this study (Supplementary Table 8). Although the power of our study to detect the major common loci (MAF > 0.2) conferring risk ≥ 1.2 was high ($\sim$80%), we had low power to detect alleles with smaller effects and/or MAF < 0.1. By implication, variants with such profiles probably represent a much larger class of susceptibility loci for glioma because of the truly small effect sizes or submaximal LD with tagging SNPs. Thus, it is probable that a large number of variants remain to be discovered. In addition, as we have recently shown, stratified analysis of glioma by molecular profile may lead to the discovery of additional subtype-specific risk variants. However, such subtype analyses can increase the statistical burden of adjusting for multiple testing. For example, if applying an additional Bonferroni correction for GBM and non-GBM subtypes, the rs11196067 (*VTI1A*) association at $P = 8.64 \times 10^{-8}$ would not be declared genome-wide significant. An issue in future subtype analyses of glioma will therefore be to have sufficient study power to mitigate type II error given the additional constraints of multiple testing. Further efforts to expand the scale of GWAS meta-analyses through international consortia and increasing the number of SNPs taken forward to large-scale replication will be required to address this challenge.

Methods

Ethics. Collection of blood samples and clinico-pathological information from patients and controls was undertaken with informed consent and relevant ethical review board approval in accordance with the tenets of the Declaration of Helsinki. Ethical committee approval for this study was obtained from relevant study centres (UK: South East Multicentre Research Ethics Committee (MREC) and the Scottish Multicentre Research Ethics Committee; France: APHP Ethical Committee-CPP (comité de Protection des Personnes); Germany: Ethics Commission of the Medical Faculty of the University of Bonn; and USA: University of Texas MD Anderson Cancer Institutional Review Board).

Genome-wide association studies. We used GWAS data previously generated on four non-overlapping case–control series of Northern European ancestry, which have been the subject of previous studies[6,7]; summarized in Supplementary Table 1. Briefly, the UK-GWAS was based on 636 cases (401 males; mean age 46 years) ascertained through the INTERPHONE study[35]. Individuals from the 1958 Birth Cohort ($n = 2{,}930$) served as a source of controls. The US-GWAS was based on 1,281 cases (786 males; mean age 47 years) ascertained through the MD Anderson Cancer Center, Texas, between 1990 and 2008. Individuals from the Cancer Genetic Markers of Susceptibility (CGEMS, $n = 2{,}245$) studies served as controls[36,37]. The French-GWAS study comprised 1,495 patients with glioma ascertained through the Service de Neurologie Mazarin, Groupe Hospitalier Pitié-Salpêtrière Paris. The controls ($n = 1{,}213$) were ascertained from the SU.VI.MAX (SUpplementation en VItamines et Mineraux Antioxydants) study of 12,735 healthy subjects (women aged 35–60 years; men aged 45–60 years)[38]. The German-GWAS comprised 880 patients who underwent surgery for a glioma at the Department of Neurosurgery, University of Bonn Medical Center, between 1996 and 2008. Control subjects were taken from three population studies: KORA (Co-operative Health Research in the Region of Augsburg; $n = 488$) (ref. 39); POPGEN (Population Genetic Cohort; $n = 678$) (ref. 40) and from the Heinz Nixdorf Recall study ($n = 380$) (ref. 41).

Replication genotyping. For replication we made use of DNA from 1,490 glioma cases recruited to an ongoing UK study of primary brain tumours (National Brain Tumour Study). Controls were healthy individuals that had been recruited to the National Study of Colorectal Cancer Genetics[42] and the GEnetic Lung CAncer Predisposition Study[43]. All cases and controls were UK residents and had self-reported European ancestry. Controls reported no personal history of cancer at the time of ascertainment. Genotyping of rs76178334, rs4432939, rs182521816, rs12780046, rs11196067, rs648044, rs12230172, rs3851634, rs1801591 and rs78543262 was performed using competitive allele-specific PCR KASPar chemistry (LGC, Hertfordshire, UK, primer sequences detailed in Supplementary Table 10). Conditions used are available on request. Call rates for SNP genotypes were >95%. To ensure quality of genotyping in all assays, at least two negative controls and 1–10% duplicates (showing a concordance >99%) were genotyped. For SNPs with MAF<5%, at least two known heterozygotes were included per genotyping plate, to aid clustering.

Statistical and bioinformatic analysis. Data were imputed for all scans for over 10 million SNPs using IMPUTE2 v2.3.0 (ref. 44) software and the 1000 Genomes Project (Phase 1 integrated release 3, March 2012 (ref. 45)) and the UK10K data (ALSPAC, EGAS00001000090/EGAD00001000195, and TwinsUK, EGAS00001000108/EGAD00001000194, studies only) as reference panels (Supplementary Table 1). Genotypes were aligned to the positive strand in both imputation and genotyping. Imputation was conducted separately for each scan in which before imputation each GWAS data set was pruned to a common set of 425,190 SNPs. Poorly imputed SNPs defined by an information score (Is) <0.70 and Hardy–Weinberg equilibrium $P < 1.0 \times 10^{-5}$ were excluded from the analyses. Tests of association between imputed SNPs and glioma was performed under a probabilistic dosage model in SNPTEST v2.5 (ref. 46).

Eigenvectors for the GWAS data sets were inferred using *smartpca* (part of EIGENSOFTv2.4 (refs 13,47)) using $\sim$100,00 ld-pruned SNPs. Eigenstrat adjustment was carried out in SNPTEST by including the first 10 eigenvectors as covariates. The adequacy of the case–control matching and possibility of differential genotyping of cases and controls was evaluated using Q–Q plots of test statistics. The inflation factor λ was based on the 90% least-significant SNPs as previously advocated[48]. Testing for secondary signals was carried out in SNPTEST, adjusting for the sentinel SNP using the '-condition_on' option. Visualization of population ancestry was carried out in *smartpca* by projecting query samples onto eigenvectors inferred from the 1000 Genomes Project populations (Supplementary Fig. 1). Meta-analysis of GWAS data sets under a fixed-effects model was undertaken in META v1.6 (ref. 49) using the inverse-variance approach. Cochran's *Q*-statistic to test for heterogeneity and the I^2 statistic to quantify the proportion of the total variation due to heterogeneity were calculated[50]. P_{het} values <0.05 are considered characteristic of large heterogeneity[50]. In addition, analyses stratified by glioma tumour histology and molecular characteristics were performed. All statistical *P* values were two sided.

Estimates of individual variance in risk associated with glioma-risk SNPs was carried out using the method described in Pharoah *et al.*[19] assuming the familial

risk of glioma to be 1.77 (ref. 51). Briefly, for a single allele (i) of frequency p, relative risk R and ln risk r, the variance (V_i) of the risk distribution due to that allele is given by:

$$V_i = (1-p)^2E^2 + 2p(1-p)(r-E)^2 + p^2(2r-E)^2$$

Where E is the expected value of r given by:

$$E = 2p(1-p)r + 2p^2r$$

For multiple risk alleles the distribution of risk in the population tends towards the normal with variance:

$$V = \sum V_i$$

The total genetic variance (V) for all susceptibility alleles has been estimated to be $\sqrt{1.77}$. Thus the fraction of the genetic risk explained by a single allele is given by:

$$V_i/V$$

LD metrics were calculated in vcftools v0.1.12b (ref. 52) using UK10K data and plotted using visPIG (ref. 53). LD blocks were defined on the basis of HapMap recombination rate (cM/Mb) as defined using the Oxford recombination hotspots and on the basis of distribution of confidence intervals defined by Gabriel *et al.*[54]

SNPs were annotated for putative functional effect using RegulomeDB[55], HaploReg v3 (ref. 56) and SeattleSeq Annotation 138 (ref. 57). These servers make use of data from ENCODE[58], GERP[59] conservation metrics, combined annotation-dependent depletion (CADD)[60] scores and PolyPhen 2 (ref. 61) scores. We searched for overlap of associated SNPs with enhancers defined by the FANTOM5 enhancer atlas[15], annotating by ubiquitous enhancers as well as enhancers specifically expressed in astrocytes, neurons, neuronal stem cells and brain tissue. Similarly, we searched for overlap with 'super-enhancer' regions as defined by Hnisz *et al.*[14], restricting analysis to U87 GBM cells, astrocyte cells and brain tissue. We additionally made use of 15-state chromHMM data from H1-derived neuronal progenitor cells available from the Epigenome roadmap project[62]. Mutation data in LGG and GBM tumours from TCGA was assessed using the cBioPortal for cancer genomics[63].

To search for biological pathways enriched for glioma SNP associations we made use of Improved Gene Set Enrichment Analysis for Genome-wide Association Study (i-GSEA4GWAS v1.1) (ref. 64). SNPs up to 5 kb upstream and downstream of a given gene were mapped to that gene, with the maximum P value of all SNPs mapping to a gene used to represent the gene. Gene sets used were: canonical pathways, gene ontology (GO) biological process, GO molecular function, GO cellular component. As recommended we applied an FDR cutoff of <0.10 on all reported gene sets. In the case of multiple identical pathways, that with the lower FDR value is retained.

Imputation concordance assessment. The fidelity of imputation as assessed by the concordance between imputed and directly genotyped SNPs was examined in 192 cases and 187 controls from the UK-GWAS discovery series (Supplementary Table 3). Targeted sequencing for the SNPs rs141035288, rs117527984, rs76178334, rs4432939, rs182521816, rs138170678, rs145034266, rs12780046, rs11196067, rs648044, rs12230172 and rs78543262 was performed by Sanger on an ABI3700 analyser (Applied Biosystems; Supplementary Table 10, conditions are available on request). For SNPs with MAF <0.05, samples were included to ensure at least 10 predicted heterozygotes were sequenced. Imputed genotypes were considered for concordance assessment if exhibiting probability >0.9.

Tumour genotyping. Tumour samples were available from a subset of the patients ascertained through the Service de Neurologie Mazarin, Groupe Hospitalier Pitié-Salpêtrière Paris. Tumours were snap frozen in liquid nitrogen and DNA was extracted using the QIAmp DNA minikit, according to the manufacturer's instructions (Qiagen, Venlo, LN, USA). DNA was analysed for large-scale copy number variation by CGH array as previously described[65,66]. In the cases not analysed by CGH array, 9p, 10q, 1p and 19q status was assigned using PCR microsatellites, and *EGFR* amplification and *CDKN2A-p16-INK4a* homozygous deletion by quantitative PCR. *IDH1*, *IDH2* and *TERT* promoter mutation status was determined by sequencing as previously described[67,68].

Expression quantitative trait loci analysis. To examine the relationship between SNP genotype and gene expression, we made use of tumour RNA sequence data and blood Affymetrix 6.0 SNP Array data for 389 low-grade and 138 GBM tumours of European ancestry from TCGA (accession number phs000178.v9.p8), as well as RNA sequence data from lymphoblastoid cells (GEUVADIS project[16]) and genotype data for 363 European individuals from the 1000 Genomes Project[45]. Sequence reads from downloaded FASTQ files were aligned to the human hg19 reference genome and GRCh37 Ensembl transcriptome using TopHat v2.0.7 and Bowtie v2.0.6. Read counts per gene were generated for 62,069 Ensembl genes using featureCounts[69] as part of the Rsubread Bioconductor package[70]. For TCGA samples, European ancestry was assessed through visualization of clustering with CEU samples after principal components analysis (data not shown). Untyped genotypes were imputed from the Affymetrix 6 array using similar methods to those discussed previously. Genotypes with probability >0.9 were taken forward for eQTL analysis. The association between SNP and gene expression was quantified using the Kruskal–Wallis trend test.

We additionally queried publically available eQTL mRNA expression data using MuTHER, and the Blood eQTL browser. MuTHER contains expression adipose tissue, lymphoblastoid cells and skin expression data from 856 healthy twins[17]. rs500629 was used as a proxy for rs648044 ($r^2 = 0.52$, $D' = 0.85$). The blood eQTL browser contains expression data from 5,311 non-transformed peripheral blood samples[18]. Putative eQTLs were thresholded at FDR <0.1.

References

1. Bondy, M. L. *et al.* Brain tumor epidemiology: consensus from the Brain Tumor Epidemiology Consortium. *Cancer* **113,** 1953–1968 (2008).
2. Louis, D. N. *et al.* The 2007 WHO classification of tumours of the central nervous system. *Acta Neuropathol.* **114,** 97–109 (2007).
3. Ostrom, Q. T. *et al.* The epidemiology of glioma in adults: a "state of the science" review. *Neuro Oncol.* **16,** 896–913 (2014).
4. Hodgson, S. V., Maher, E. R. & Hodgson, S. *A Practical Guide to Human Cancer Genetics* (Springer, 1999).
5. Hemminki, K., Tretli, S., Sundquist, J., Johannesen, T. B. & Granstrom, C. Familial risks in nervous-system tumours: a histology-specific analysis from Sweden and Norway. *Lancet Oncol.* **10,** 481–488 (2009).
6. Sanson, M. *et al.* Chromosome 7p11.2 (EGFR) variation influences glioma risk. *Hum. Mol. Genet.* **20,** 2897–2904 (2011).
7. Shete, S. *et al.* Genome-wide association study identifies five susceptibility loci for glioma. *Nat. Genet.* **41,** 899–904 (2009).
8. Wrensch, M. *et al.* Variants in the CDKN2B and RTEL1 regions are associated with high-grade glioma susceptibility. *Nat. Genet.* **41,** 905–908 (2009).
9. Enciso-Mora, V. *et al.* Low penetrance susceptibility to glioma is caused by the TP53 variant rs78378222. *Br. J. Cancer* **108,** 2178–2185 (2013).
10. Walsh, K. M. *et al.* Variants near TERT and TERC influencing telomere length are associated with high-grade glioma risk. *Nat. Genet.* **46,** 731–735 (2014).
11. Enciso-Mora, V. *et al.* Deciphering the 8q24.21 association for glioma. *Hum. Mol. Genet.* **22,** 2293–2302 (2013).
12. Huang, J. *et al.* Improved imputation of low-frequency and rare variants using the UK10K haplotype reference panel. *Nat. Commun.* **6,** 8111 (2015).
13. Price, A. L. *et al.* Principal components analysis corrects for stratification in genome-wide association studies. *Nat. Genet.* **38,** 904–909 (2006).
14. Hnisz, D. *et al.* Super-enhancers in the control of cell identity and disease. *Cell* **155,** 934–947 (2013).
15. Andersson, R. *et al.* An atlas of active enhancers across human cell types and tissues. *Nature* **507,** 455–461 (2014).
16. Lappalainen, T. *et al.* Transcriptome and genome sequencing uncovers functional variation in humans. *Nature* **501,** 506–511 (2013).
17. Grundberg, E. *et al.* Mapping cis- and trans-regulatory effects across multiple tissues in twins. *Nat. Genet.* **44,** 1084–1089 (2012).
18. Westra, H. J. *et al.* Systematic identification of trans eQTLs as putative drivers of known disease associations. *Nat. Genet.* **45,** 1238–1243 (2013).
19. Pharoah, P. D., Antoniou, A. C., Easton, D. F. & Ponder, B. A. Polygenes, risk prediction, and targeted prevention of breast cancer. *N. Engl. J. Med.* **358,** 2796–2803 (2008).
20. Bose, A. *et al.* The v-SNARE Vti1a regulates insulin-stimulated glucose transport and Acrp30 secretion in 3T3-L1 adipocytes. *J. Biol. Chem.* **280,** 36946–36951 (2005).
21. Ramirez, D. M., Khvotchev, M., Trauterman, B. & Kavalali, E. T. Vti1a identifies a vesicle pool that preferentially recycles at rest and maintains spontaneous neurotransmission. *Neuron* **73,** 121–134 (2012).
22. Lan, Q. *et al.* Genome-wide association analysis identifies new lung cancer susceptibility loci in never-smoking women in Asia. *Nat. Genet.* **44,** 1330–1335 (2012).
23. Wang, H. *et al.* Trans-ethnic genome-wide association study of colorectal cancer identifies a new susceptibility locus in VTI1A. *Nat. Commun.* **5,** 4613 (2014).
24. Chen, S. J. *et al.* Rearrangements of the retinoic acid receptor alpha and promyelocytic leukemia zinc finger genes resulting from t(11;17)(q23;q21) in a patient with acute promyelocytic leukemia. *J. Clin. Invest.* **91,** 2260–2267 (1993).
25. Ahmad, K. F., Engel, C. K. & Prive, G. G. Crystal structure of the BTB domain from PLZF. *Proc. Natl Acad. Sci. USA* **95,** 12123–12128 (1998).
26. Vallee, R. B., Varma, D. & Dujardin, D. L. ZW10 function in mitotic checkpoint control, dynein targeting, and membrane trafficking: is dynein the unifying theme? *Cell Cycle* **5,** 2447–2451 (2014).
27. Frerman, F. E. Acyl-CoA dehydrogenases, electron transfer flavoprotein and electron transfer flavoprotein dehydrogenase. *Biochem. Soc. Trans.* **16,** 416–418 (1988).
28. Indo, Y., Glassberg, R., Yokota, I. & Tanaka, K. Molecular characterization of variant alpha-subunit of electron transfer flavoprotein in three patients with glutaric acidemia type II—and identification of glycine substitution for valine-157 in the sequence of the precursor, producing an unstable mature protein in a patient. *Am. J. Hum. Genet.* **49,** 575–580 (1991).

29. Freneaux, E., Sheffield, V. C., Molin, L., Shires, A. & Rhead, W. J. Glutaric acidemia type II. Heterogeneity in beta-oxidation flux, polypeptide synthesis, and complementary DNA mutations in the alpha subunit of electron transfer flavoprotein in eight patients. *J. Clin. Invest.* **90,** 1679–1686 (1992).
30. Bross, P. *et al.* A polymorphic variant in the human electron transfer flavoprotein α-chain (α-T171) displays decreased thermal stability and is overrepresented in very-long-chain acyl-CoA dehydrogenase-deficient patients with mild childhood presentation. *Mol. Genet. Metab.* **67,** 138–147 (1999).
31. Dieci, G., Fiorino, G., Castelnuovo, M., Teichmann, M. & Pagano, A. The expanding RNA polymerase III transcriptome. *Trends Genet.* **23,** 614–622 (2007).
32. Saitsu, H. *et al.* Mutations in POLR3A and POLR3B encoding RNA Polymerase III subunits cause an autosomal-recessive hypomyelinating leukoencephalopathy. *Am. J. Hum. Genet.* **89,** 644–651 (2011).
33. Johnson, E. O. *et al.* PHLDA1 is a crucial negative regulator and effector of Aurora A kinase in breast cancer. *J. Cell Sci.* **124,** 2711–2722 (2011).
34. Sellheyer, K., Nelson, P., Kutzner, H. & Patel, R. M. The immunohistochemical differential diagnosis of microcystic adnexal carcinoma, desmoplastic trichoepithelioma and morpheaform basal cell carcinoma using BerEP4 and stem cell markers. *J. Cutan. Pathol.* **40,** 363–370 (2013).
35. Cardis, E. *et al.* The INTERPHONE study: design, epidemiological methods, and description of the study population. *Eur. J. Epidemiol.* **22,** 647–664 (2007).
36. Hunter, D. J. *et al.* A genome-wide association study identifies alleles in FGFR2 associated with risk of sporadic postmenopausal breast cancer. *Nat. Genet.* **39,** 870–874 (2007).
37. Yeager, M. *et al.* Genome-wide association study of prostate cancer identifies a second risk locus at 8q24. *Nat. Genet.* **39,** 645–649 (2007).
38. Hercberg, S. *et al.* The SU.VI.MAX Study: a randomized, placebo-controlled trial of the health effects of antioxidant vitamins and minerals. *Arch. Intern. Med.* **164,** 2335–2342 (2004).
39. Wichmann, H. E., Gieger, C. & Illig, T.MONICA/KORA Study Group. KORA-gen—resource for population genetics, controls and a broad spectrum of disease phenotypes. *Gesundheitswesen* **67**(Suppl 1): S26–S30 (2005).
40. Krawczak, M. *et al.* PopGen: population-based recruitment of patients and controls for the analysis of complex genotype-phenotype relationships. *Community Genet* **9,** 55–61 (2006).
41. Schmermund, A. *et al.* Assessment of clinically silent atherosclerotic disease and established and novel risk factors for predicting myocardial infarction and cardiac death in healthy middle-aged subjects: rationale and design of the Heinz Nixdorf RECALL Study. Risk factors, evaluation of coronary calcium and lifestyle. *Am. Heart J.* **144,** 212–218 (2002).
42. Penegar, S. *et al.* National study of colorectal cancer genetics. *Br. J. Cancer* **97,** 1305–1309 (2007).
43. Eisen, T., Matakidou, A., Houlston, R. & Consortium, G. Identification of low penetrance alleles for lung cancer: the GEnetic Lung CAncer Predisposition Study (GELCAPS). *BMC Cancer* **8,** 244 (2008).
44. Howie, B. N., Donnelly, P. & Marchini, J. A flexible and accurate genotype imputation method for the next generation of genome-wide association studies. *PLoS Genet.* **5,** e1000529 (2009).
45. 1000 Genomes Project Consortium. A map of human genome variation from population-scale sequencing. *Nature* **467,** 1061–1073 (2010).
46. Marchini, J., Howie, B., Myers, S., McVean, G. & Donnelly, P. A new multipoint method for genome-wide association studies by imputation of genotypes. *Nat. Genet.* **39,** 906–913 (2007).
47. Patterson, N., Price, A. L. & Reich, D. Population structure and eigenanalysis. *PLoS Genet.* **2,** e190 (2006).
48. Clayton, D. G. *et al.* Population structure, differential bias and genomic control in a large-scale, case-control association study. *Nat. Genet.* **37,** 1243–1246 (2005).
49. Liu, J. Z. *et al.* Meta-analysis and imputation refines the association of 15q25 with smoking quantity. *Nat. Genet.* **42,** 436–440 (2010).
50. Higgins, J. P., Thompson, S. G., Deeks, J. J. & Altman, D. G. Measuring inconsistency in meta-analyses. *BMJ* **327,** 557–560 (2003).
51. Scheurer, M. E. *et al.* Familial aggregation of glioma: a pooled analysis. *Am. J. Epidemiol.* **172,** 1099–1107 (2010).
52. Danecek, P. *et al.* The variant call format and VCFtools. *Bioinformatics* **27,** 2156–2158 (2011).
53. Scales, M., Jager, R., Migliorini, G., Houlston, R. S. & Henrion, M. Y. visPIG—a web tool for producing multi-region, multi-track, multi-scale plots of genetic data. *PLoS ONE* **9,** e107497 (2014).
54. Gabriel, S. B. *et al.* The structure of haplotype blocks in the human genome. *Science* **296,** 2225–2229 (2002).
55. Boyle, A. P. *et al.* Annotation of functional variation in personal genomes using RegulomeDB. *Genome Res.* **22,** 1790–1797 (2012).
56. Ward, L. D. & Kellis, M. HaploReg: a resource for exploring chromatin states, conservation, and regulatory motif alterations within sets of genetically linked variants. *Nucleic Acids Res.* **40,** D930–D934 (2012).
57. Ng, S. B. *et al.* Targeted capture and massively parallel sequencing of 12 human exomes. *Nature* **461,** 272–276 (2009).
58. de Souza, N. The ENCODE project. *Nat. Methods* **9,** 1046 (2012).
59. Cooper, G. M. *et al.* Distribution and intensity of constraint in mammalian genomic sequence. *Genome Res.* **15,** 901–913 (2005).
60. Kircher, M. *et al.* A general framework for estimating the relative pathogenicity of human genetic variants. *Nat. Genet.* **46,** 310–315 (2014).
61. Adzhubei, I. A. *et al.* A method and server for predicting damaging missense mutations. *Nat. Methods* **7,** 248–249 (2010).
62. Roadmap Epigenomics Consortium *et al.* Integrative analysis of 111 reference human epigenomes. *Nature* **518,** 317–330 (2015).
63. Gao, J. *et al.* Integrative analysis of complex cancer genomics and clinical profiles using the cBioPortal. *Sci. Signal.* **6,** pl1 (2013).
64. Zhang, K., Cui, S., Chang, S., Zhang, L. & Wang, I. i-GSEA4GWAS: a web server for identification of pathways/gene sets associated with traits by applying an improved gene set enrichment analysis to genome-wide association study. *Nucleic Acids Res.* **38,** W90–W95 (2010).
65. Idbaih, A. *et al.* BAC array CGH distinguishes mutually exclusive alterations that define clinicogenetic subtypes of gliomas. *Int. J. Cancer* **122,** 1778–1786 (2008).
66. Gonzalez-Aguilar, A. *et al.* Recurrent mutations of MYD88 and TBL1XR1 in primary central nervous system lymphomas. *Clin. Cancer Res.* **18,** 5203–5211 (2012).
67. Sanson, M. *et al.* Isocitrate dehydrogenase 1 codon 132 mutation is an important prognostic biomarker in gliomas. *J. Clin. Oncol.* **27,** 4150–4154 (2009).
68. Labussiere, M. *et al.* TERT promoter mutations in gliomas, genetic associations and clinico-pathological correlations. *Br. J. Cancer* **111,** 2024–2032 (2014).
69. Liao, Y., Smyth, G. K. & Shi, W. featureCounts: an efficient general purpose program for assigning sequence reads to genomic features. *Bioinformatics* **30,** 923–930 (2014).
70. Liao, Y., Smyth, G. K. & Shi, W. The Subread aligner: fast, accurate and scalable read mapping by seed-and-vote. *Nucleic Acids Res.* **41,** e108 (2013).

Acknowledgements

In the UK, funding was provided by Cancer Research UK (C1298/A8362 supported by the Bobby Moore Fund), the Wellcome Trust and the DJ Fielding Medical Research Trust. B.K. is supported by a PhD studentship funded by the Sir John Fisher Foundation. The National Brain Tumour Study is supported by the National Cancer Research Network and we acknowledge the contribution of all clinicians and health-care professionals to this initiative. The UK INTERPHONE study was supported by the European Union Fifth Framework Program 'Quality of life and Management of Living Resources' (QLK4-CT-1999-01563) and the International Union against Cancer (UICC). The UICC received funds from the Mobile Manufacturers' Forum and GSM Association. Provision of funds via the UICC was governed by agreements that guaranteed INTERPHONE's scientific independence (http://www.iarc.fr/ENG/Units/RCAd.html) and the views expressed in the paper are not necessarily those of the funders. The UK centres were also supported by the Mobile Telecommunications and Health Research (MTHR) Programme and the Northern UK Centre was supported by the Health and Safety Executive, Department of Health and Safety Executive and the UK Network Operators. In France, funding was provided by the Ligue Nationale contre le Cancer, the fondation ARC, the Institut National du Cancer (INCa; PL046), the French Ministry of Higher Education and Research and the program 'Investissements d'avenir' ANR-10-IAIHU-06. This study was additionally supported by a grant from Génome Québec, le Ministère de l'Enseignement supérieur, de la Recherche, de la Science et de la Technologie (MESRST) Québec and McGill University. In Germany, funding was provided to M.S. and J.S. by the Deutsche Forschungsgemeinschaft (Si552, Schr285), the Deutsche Krebshilfe (70-2385-Wi2, 70-3163-Wi3, 10-6262) and BONFOR. Funding for the WTCCC was provided by the Wellcome Trust (076113&085475). The KORA Ausburg studies are supported by grants from the German Federal Ministry of Education and Research (BMBF) and were mainly financed by the Helmholtz Zentrum München, German Research Center for Environmental Health, Neuherberg. This work was financed by the German National Genome Research Network (NGFN) and supported within the Munich Center of Health Sciences (MC Health) as part of LMUinnovativ. Generation of the German control data was partially supported by a grant of the German Federal Ministry of Education and Research (BMBF) through the Integrated Network IntegraMent (Integrated Understanding of Causes and Mechanisms in Mental Disorders), under the auspices of the e:Med research and funding concept (01ZX1314A). Markus M. Nöthen received support from the Alfried Krupp von Bohlen und Halbach-Stiftung and is a member of the DFG-funded Excellence Cluster ImmunoSensation. We are grateful to all the patients and individuals for their participation and we would also like to thank the clinicians and other hospital staff, cancer registries and study staff in respective centres who contributed to the blood sample and data collection. For the UK study, we acknowledge the funders who contributed to the blood sample and data collection for this study. We also thank colleagues from the UK National Cancer Research Network (for NSCCG). MD Anderson acknowledges the work on the USA GWA study of Phyllis Adatto, Fabian Morice, Hui Zhang, Victor Levin, Alfred W.K. Yung, Mark Gilbert, Raymond Sawaya, Vinay Puduvalli, Charles Conrad, Fredrick Lang and Jeffrey Weinberg from the Brain and Spine Center. For the French study, we are indebted to A. Rahimian (Onconeurotek),

A.M. Lekieffre and M Brandel for help in collecting data, and Y Marie for database support. For the German study, we are indebted to B. Harzheim (Bonn), S. Ott and Dr A. Müller-Erkwoh (Bonn) for help with the acquisition of clinical data, and R. Mahlberg (Bonn) who provided technical support. The UK study made use of control genotyping data generated by the Wellcome Trust Case–Control Consortium. A full list of the investigators who contributed to the generation of the data is available from www.wtccc.org.uk. The US-GWA study made use of control genotypes from the Cancer Genetic Markers of Susceptibility (CGEMS) prostate and breast cancer studies. A full list of the investigators who contributed to the generation of the data is available from http://cgems.cancer.gov/. French controls were taken from the SU.VI.MAX study. The German GWA study made use of genotyping data from three population control sources: KORA-gen, The Heinz Nixdorf RECALL study and POPGEN. The HNR cohort was established with the support of the Heinz Nixdorf Foundation. Franziska Degenhardt received support from the BONFOR Programme of the University of Bonn, Germany. We are grateful to all investigators who contributed to the generation of this data set. UK10K data generation and access was organized by the UK10K consortium and funded by the Wellcome Trust. The results here are in part based on data generated by the TCGA Research Network: http://cancergenome.nih.gov/.

Author contributions

R.S.H. and B.K. designed the study, drafted the manuscript with contributions from all other authors; B.K. performed statistical and bioinformatics analyses; P.B. performed laboratory management and oversaw replication genotyping and sequencing of UK cases and controls by B.K., A.H. and J.V.; in the UK, A.S., M.J.S., S.J.F. and R.S.H. developed patient recruitment, sample acquisition and performed sample collection of cases; in the US, M.B. developed protocols and patient recruitment; in Germany, M.S., M.M.N., H.-E.W., S.S. and J.S. developed patient recruitment and blood sample collection, M.S. oversaw DNA isolation and storage and performed case and control ascertainment and supervision of DNA extractions, S. Herms, S. Heilmann and K.G. performed experimental work; in France, M.S. and J.-Y.D. developed patient recruitment, M.L. and A.-L.D.S performed tumour genotyping and K.M. performed the neuropathological analysis; M. Lathrop performed laboratory management and oversaw genotyping of the French samples; all authors contributed to the final paper.

Additional information

Supplementary Information accompanies this paper at http://www.nature.com/naturecommunications

Competing financial interests: The authors declare no competing financial interests.

Reprints and permission information is available online at http://npg.nature.com/reprintsandpermissions/

How to cite this article: Kinnersley, B. *et al.* Genome-wide association study identifies multiple susceptibility loci for glioma. *Nat. Commun.* 6:8559 doi: 10.1038/ncomms9559 (2015).

Genome-wide association study reveals specific differences in genetic susceptibility to glioblastoma and non-glioblastoma

Beatrice Melin*#, Jill Barnholtz-Sloan#, Margaret R. Wrensch#, Christoffer Johansen#, Dora Il'yasova#, Ben Kinnersley#, Quinn Ostrom, Karim Labreche, Yanwen Chen, Georgina Armstrong, Yanhong Liu, Jeanette E Eckel-Passow, Paul A Decker, Marianne Labussière, Anna-Luisa Di Stefano, Peter Broderick, Pilar Galan, Karima Mokhtari, Jean-Yves Delattre, Konstantinos Gousias, Johannes Schramm, Minouk J. Schoemaker, Sarah J Fleming, Stefan Herms, Stefanie Heilmann, Markus M Nöthen, Heinz-Erich Wichmann, Stefan Schreiber, Anthony Swerdlow, Mark Lathrop, Matthias Simon, Marc Sanson, Ulrika Andersson, Preetha Rajaraman, Stephen Chanock, Martha Linet, Zhaoming Wang, Meredith Yeager,(on behalf on the glioma scan group), John Wiencke, Helen Hansen, Lucie McCoy, Terri Rice, Matthew L Kosel, Thomas M Kollmeyer, Hugues Sicotte, Chris Amos, Jonine Bernstein, Faith Davis, Dan Lachance, Ching Lau, Ryan T Merrell , Joellen Shildkraut, Ali Osman, Siegal Sadetzki, Michael Scheurer, Sanjay Shete, Rose Lai+, Elizabeth B Claus+, Sara Olson+, Robert B Jenkins+, Richard S Houlston+*, Melissa L Bondy+*

*Corresponding authors
shared first authors
+shared last authors

Author affiliations:
Department of Radiation Sciences, Faculty of Medicine, Umeå University, Umeå, Sweden (Beatrice S. Melin, Ulrika Andersson)

Case Comprehensive Cancer Center, School of Medicine, Case Western Reserve University, Cleveland, Ohio (Jill S. Barnholtz-Sloan Quinn Ostrom, Yanwen Chen)

Department of Neurological Surgery, School of Medicine, University of California, San Francisco, San Francisco, California, USA (Margaret R. Wrensch, John Wiencke, Helen Hansen, Lucie McCoy, Terri Rice)

Institute of Cancer Epidemiology, Danish Cancer Society, Copenhagen, Denmark , Rigshospitalet, University of Copenhagen, Copenhagen, Denmark (Christoffer Johansen)

Department of Epidemiology and Biostatistics, School of Public Health, Georgia State University, Atlanta, Georgia< USA (Dora Il'yasova)

Cancer Control and Prevention Program, Depart- ment of Community and Family Medicine, Duke University Medical Center, Durham, North Carolina,USA (Dora Il'yasova, Joellen Schildkraut)

Departments of Neurology, Neurosurgery, and Preventive Medicine, Keck School of Medicine, University of Southern California, Los Angeles, California, USA (Rose Lai)

							All glioma		GBM glioma		Non-GBM glioma	
Locus	**Subtype**	**SNP**	**Position**	**Alleles**	**RAF**	**INFO**	***P***	**Odds ratio**	***P***	**Odds ratio**	***P***	**Odds ratio**
1p31.3	GBM	rs12752552	65229299	**T**/C	0.870	0.994	**4.07×10^{-9}**	1.18 (1.11-1.24)	**2.04×10^{-9}**	1.22 (1.15-1.31)	4.78×10^{-3}	1.11 (1.03-1.18)
1q32.1	non-GBM	rs4252707	204508147	G/**A**	0.220	0.990	2.97×10^{-7}	1.12 (1.07-1.17)	0.015	1.07 (1.01-1.13)	**3.34×10^{-9}**	1.19 (1.12-1.26)
1q44	non-GBM	rs12076373	243851947	**G**/C	0.837	0.992	4.97×10^{-4}	1.09 (1.04-1.15)	0.846	0.99 (0.94-1.06)	**2.63×10^{-10}**	1.23 (1.16-1.32)
2q33.3	non-GBM	rs7572263	209051586	**A**/G	0.756	0.998	2.58×10^{-6}	1.11 (1.06-1.15)	0.019	1.06 (1.01-1.12)	**2.18×10^{-10}**	1.20 (1.13-1.26)
3p14.1	non-GBM	rs11706832	66502981	A/**C**	0.456	0.991	1.06×10^{-5}	1.08 (1.05-1.12)	0.158	1.03 (0.99-1.08)	**7.66×10^{-9}**	1.15 (1.09-1.20)
10q24.33	non-GBM	rs11598018	105661315	**C**/A	0.462	0.957	3.07×10^{-7}	1.10 (1.06-1.14)	0.0103	1.06 (1.01-1.11)	**3.39×10^{-8}**	1.14 (1.09-1.20)
11q14.1	GBM	rs11233250	82397014	**C**/T	0.868	0.988	5.40×10^{-6}	1.14 (1.08-1.21)	**9.95×10^{-10}**	1.24 (1.16-1.33)	0.592	0.98 (0.91-1.05)
11q21	non-GBM	rs7107785	95747337	**T**/C	0.479	0.995	2.96×10^{-4}	1.07 (1.03-1.11)	0.844	1.00 (0.95-1.04)	**3.87×10^{-10}**	1.16 (1.11-1.21)
14q12	non-GBM	rs10131032	33250081	**G**/A	0.916	0.996	2.33×10^{-6}	1.17 (1.09-1.24)	0.247	1.05 (0.97-1.13)	**5.07×10^{-11}**	1.33 (1.22-1.44)
16p13.3	GBM	rs2562152	123896	A/**T**	0.850	0.930	1.18×10^{-3}	1.09 (1.04-1.15)	**1.93×10^{-8}**	1.21 (1.13-1.29)	0.948	1.00 (0.93-1.07)
16p13.3	non-GBM	rs3751667	1004554	C/**T**	0.208	0.992	**8.75×10^{-10}**	1.14 (1.09-1.19)	5.95×10^{-6}	1.13 (1.07-1.19)	**2.61×10^{-9}**	1.18 (1.12-1.25)
16q12.1	GBM	rs10852606	50128872	T/**C**	0.713	0.993	**3.66×10^{-11}**	1.14 (1.10-1.19)	**1.29×10^{-11}**	1.18 (1.13-1.24)	2.42×10^{-3}	1.08 (1.03-1.14)
22q13.1	GBM	rs2235573	38477930	**G**/A	0.507	0.995	8.64×10^{-7}	1.09 (1.06-1.13)	**1.76×10^{-10}**	1.15 (1.10-1.20)	0.325	1.02 (0.97-1.07)

Table 1: Association statistics for top SNP at each of the newly-reported glioma risk loci. Associations at $P<5\times10^{-8}$ are highlighted in bold. Odds ratios were derived with respect to the risk allele underlined and highlighted in bold. Risk allele frequency (RAF) is according to European samples from 1000 genomes project. The INFO column indicates the average imputation info score across the studies in the discovery phase, with a score of 1 indicating the SNP is directly genotyped in all studies.

Figure 2: Forest plots of effect size and direction for the new SNPs associated with glioma risk.

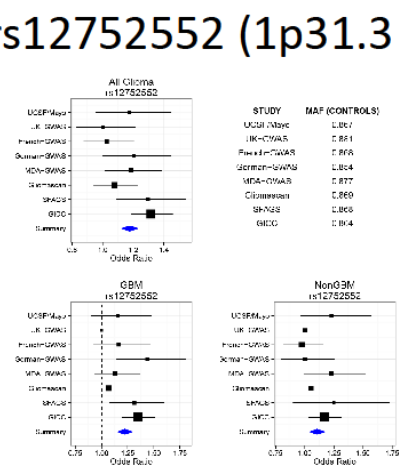

Figure 3: Regional plots of discovery-phase association results, recombination rates and chromatin state segmentation tracks for the new glioma risk loci.

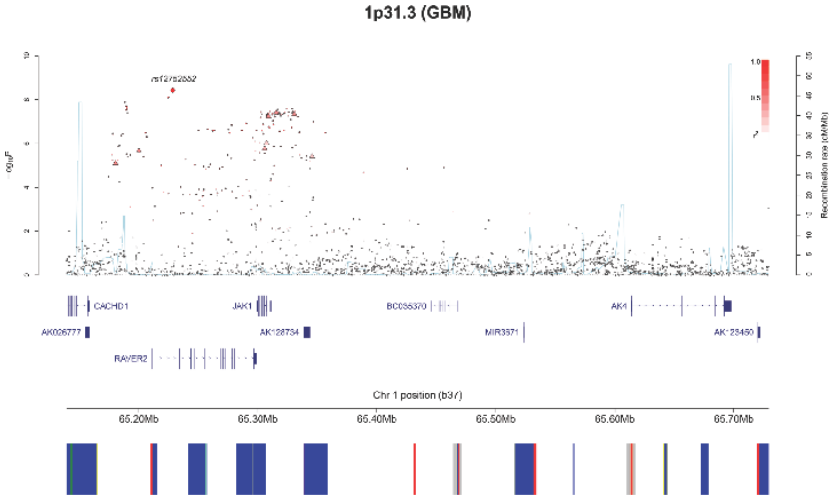

Figure 4 -Relative impact of SNP associations at known and newly identified risk loci for GBM and non-GBM tumours

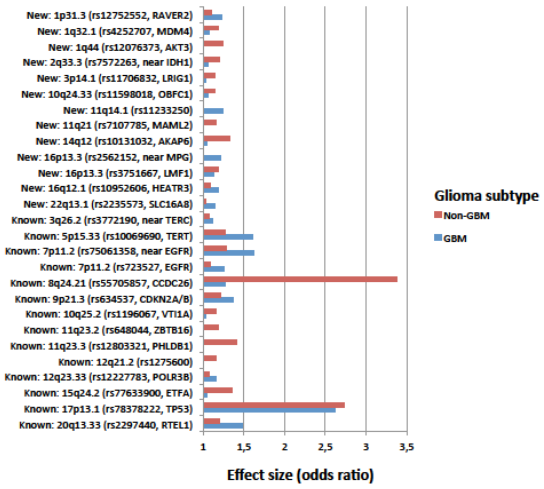

Supplementary Figure 1: Q-Q plots of association statistics for the GWAS datasets pre- and post-imputation.

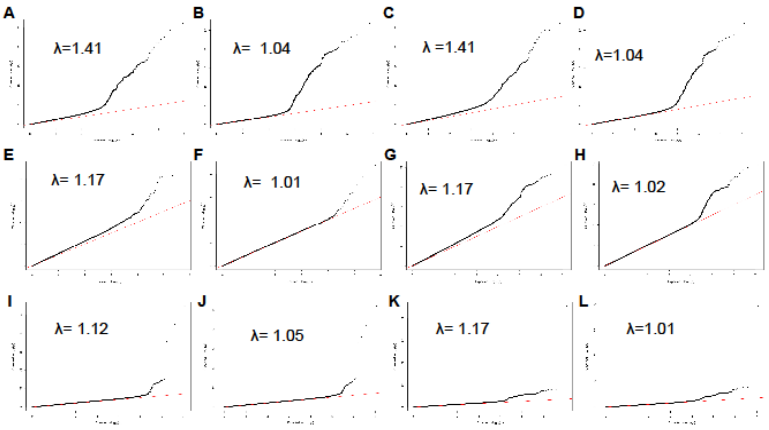

A. GICC Genotyped (unadjusted), B. GICC Genotyped (adjusted for first 2 PC), C. GICC Genotyped and Imputed (unadjusted), D. GICC Genotyped and Imputed (adjusted for first 2 PC), E. UCSF genotyped (unadjusted), F. UCSF genotyped (adjust for first 4 PCs), G. UCSF genotyped and imputed (unadjusted), H. UCSF genotyped and imputed (adjust for first 4 PCs), I. MDA Genotyped and imputed (unadjusted), J. MDA genotyped and imputed (adjust for first 2 PCS), K. NIH genotyped and imputed (unadjusted), L. NIH genotyped and imputed (adjusted for first 4 PCs)

	All Glioma						GBM			Non-GBM		
	Pre-QC			Post QC**			Post QC			Post QC		
	Total	Cases	Controls	Total	Cases	Controls	Total	Cases	Controls	Total	Cases	Controls
Baylor College of Medicine	40	40	0	11	11	0	6	6	0	5	5	0
Brigham and Women's Hospital	247	225	22	215	193	22	123	101	22	98	76	22
Columbia	215	64	151	166	40	126	150	24	126	141	15	126
Case Western Reserve University	74	60	14	67	56	11	44	33	11	34	23	11
Denmark	1,054	522	532	1,008	496	512	811	299	512	706	194	512
Duke	876	622	254	782	578	204	627	423	204	338	134	204
Mayo	833	376	457	803	358	445	639	194	445	604	159	445
MD Anderson	1,783	1,505	278	1,140	921	219	571	352	219	774	555	219
Memorial Sloan Kettering	652	283	369	531	239	292	416	124	292	396	104	292
North Shore	306	133	173	264	123	141	217	76	141	187	46	141
Sweden	1,400	476	924	1,356	465	891	1,162	270	891	1,079	188	891
University of California, San Francisco	673	333	340	506	277	229	381	152	229	350	121	229
UK	914	798	116	874	766	108	491	383	108	366	258	108
University of Southern California	297	98	199	135	49	86	115	29	86	105	19	86
GICC*	**9,364**	**5,535**	**3,829**	**7,858**	**4,572**	**3,286**	**5,754**	**2,466**	**3,286**	**5,183**	**1,897**	**3,286**

* Israeli samples and whole genome amplified samples were excluded at the initial QC regarding DNA quality control.
** Samples were excluded for call rate < 99%, mismatch between reported sex and genotyped sex chromosomes, European ancestry < 80% (as estimated using FastPop). When two individuals' samples were identified as having high IBD, the sample with the lower call rate was excluded.

Supplementary Table 1: Summary characteristics of the GICC substudies

Supplementary Figure 1: PCA plots of the GWAS datasets

(a) GICC study

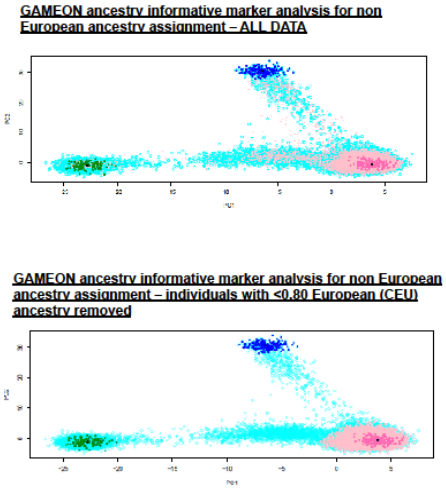

Supplementary Figure 3: Forest plots of effect size and direction for the SNPs from previously reported loci associated with glioma risk.

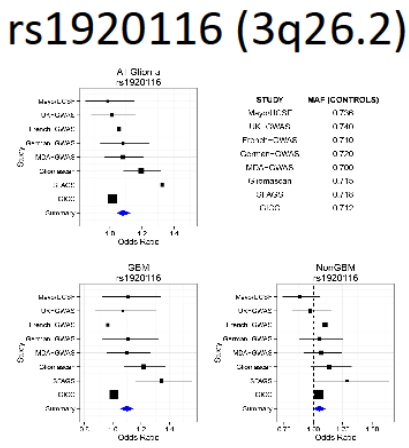

Locus	SNP	Position	r^2	D'	GERP	CADD	Gene	Annotation	RegulomeDB	FANTOM5	Super-enhancer
1p31.3	rs12127031	65224965	0.97	0.99	0.118	1.378	*RAVER2*	intronic	6	None	None
	rs12752552	65229299	1	1	0.225	3.011	*RAVER2*	intronic	NA	None	None
1q32.1	rs16853822	204450341	0.87	0.97	-3.78	2.514	*PIK3C2B*	intronic	4	enhancer_tss	brain (many)
	rs6668637	204452295	0.87	0.97	-1.79	1.802	*PIK3C2B*	intronic	6	enhancer_tss	brain (many)
	rs35634264	204454570	0.87	0.97	NA	NA	*PIK3C2B*	intronic	6	enhancer_tss	brain (many)
	rs12036042	204469314	0.89	0.98	2.04	9.248	5.5kb 5' of *PIK3C2B*	intergenic	4	enhancer_tss	brain (many)
	rs12031912	204476113	0.92	0.98	-0.646	2.013	9.4kb 5' of *MDM4*	intergenic	4	enhancer_tss	brain (many)
	rs12028476	204476361	0.92	0.98	-2.43	3.44	9.1kb 5' of *MDM4*	intergenic	4	enhancer_tss	brain (many) astrocyte_cell
	rs12039365	204488687	0.89	0.98	0.427	8.685	*MDM4*	intronic	1f	enhancer_tss	
	rs12041243	204490470	0.89	0.98	-0.866	5.68	*MDM4*	intronic	1b	enhancer_tss	
	rs12039968	204490674	0.89	0.98	0.954	2.816	*MDM4*	intronic	4	enhancer_tss	
	rs61817959	204492522	0.88	0.96	NA	0.333	*MDM4*	intronic	6	enhancer_tss	
	rs898388	204500257	0.93	0.98	-2.38	4.643	*MDM4*	intronic	4	enhancer_tss	
	rs4252697	204501383	0.91	0.98	2.06	12.99	*MDM4*	intronic	5	enhancer_tss	
	rs4252704	204506174	0.94	0.99	NA	NA	*MDM4*	intronic	NA	enhancer_tss	
	rs4252707	**204508147**	**1**	**1**	**-0.766**	**0.498**	***MDM4***	**intronic**	**NA**	**enhancer_tss**	
	rs4252733	204516918	0.89	0.96	0.628	2.139	*MDM4*	intronic	NA	enhancer_tss	
	rs11801299	204529084	0.87	0.96	-2.22	0.925	*MDM4*	intronic	6	enhancer_tss	
	rs12029692	204532323	0.87	0.96	-0.102	1.725	*MDM4*	intronic	5	enhancer_tss	
	rs6689629	204539291	0.86	0.95	0.217	4.751	*MDM4*	intronic	2b	enhancer_tss	
	rs61817460	204543579	0.87	0.96	0.994	8.78	707bp 3' of *MDM4*	intergenic	5	enhancer_tss	
1q44	rs320337	243814548	0.8	0.99	NA	1.406	*AKT3*	intronic	NA	enhancer_tss	
	rs2345993	243815373	0.93	0.98	NA	0.131	*AKT3*	intronic	NA	enhancer_tss	
	rs10803150	243822600	0.91	0.96	-2.06	1.805	*AKT3*	intronic	3a	enhancer_tss	
	rs200593524	243826003	0.84	0.96	NA	NA	*AKT3*	intronic	6	enhancer_tss	
	rs320320	243835186	0.82	1	1.76	9.429	*AKT3*	intronic	5	enhancer_tss	
	rs1843655	243837150	0.95	0.99	0.149	0.975	*AKT3*	intronic	5	enhancer_tss	
	rs4478795	243844576	0.95	0.99	1.44	3.716	*AKT3*	intronic	6	enhancer_tss	

							All glioma		GBM glioma		Non-GBM glioma	
Locus	Source	SNP	Position	Alleles	RAF	INFO	*P*	Odds ratio	*P*	Odds ratio	*P*	Odds ratio
3q26.2	Published	rs1920116	169579971	G/A	0.710	1.000	7.36×10^{-5}	1.08 (1.04-1.13)	1.46×10^{-4}	1.10 (1.05-1.15)	0.049	1.05 (1.00-1.11)
3q26.2	This study	rs3772190	169500487	G/A	0.757	0.998	2.25×10^{-6}	1.11 (1.06-1.15)	2.68×10^{-5}	1.11 (1.06-1.17)	0.012	1.07 (1.02-1.13)
5p15.33	Published	rs2736100	1286516	C/A	0.499	1.000	2.34×10^{-45}	1.29 (1.25-1.34)	1.20×10^{-53}	1.41 (1.35-1.47)	7.26×10^{-30}	1.16 (1.10-1.21)
5p15.33	This study	rs10069690	1279790	C/T	0.276	0.816	2.71×10^{-66}	1.45 (1.39-1.51)	8.33×10^{-74}	1.61 (1.53-1.69)	1.14×10^{-36}	1.27 (1.20-1.34)
7p11.2	Published	rs2252586	54978924	C/T	0.281	1.000	1.38×10^{-13}	1.16 (1.11-1.20)	7.89×10^{-15}	1.20 (1.15-1.26)	1.89×10^{-4}	1.10 (1.05-1.16)
7p11.2	This study	rs75061358	54916280	T/G	0.099	0.909	3.62×10^{-27}	1.42 (1.33-1.52)	4.94×10^{-34}	1.63 (1.50-1.76)	1.54×10^{-8}	1.28 (1.18-1.40)
7p11.2	Published	rs11979158	55159349	A/G	0.831	1.000	1.21×10^{-17}	1.24 (1.18-1.30)	1.94×10^{-19}	1.31 (1.24-1.39)	7.73×10^{-9}	1.16 (1.08-1.23)
7p11.2	This study	rs723527	55134872	A/G	0.573	0.954	5.83×10^{-17}	1.17 (1.13-1.21)	4.79×10^{-23}	1.25 (1.20-1.31)	8.25×10^{-4}	1.08 (1.03-1.14)
8q24.21	Published	rs55705857	130645692	A/G	0.057	0.795	9.53×10^{-79}	1.99 (1.85-2.13)	9.45×10^{-7}	1.27 (1.16-1.40)	7.28×10^{-149}	3.39 (3.09-3.71)
9p21.3	Published	rs4977756	22068652	G/A	0.400	1.000	1.46×10^{-41}	1.28 (1.23-1.32)	4.24×10^{-40}	1.34 (1.29-1.40)	2.28×10^{-14}	1.20 (1.15-1.26)
9p21.3	This study	rs634537	22032152	T/G	0.411	0.976	1.24×10^{-45}	1.30 (1.25-1.34)	7.23×10^{-45}	1.37 (1.31-1.43)	1.05×10^{-15}	1.21 (1.16-1.27)
10q25.2	Published	rs11196067	114469065	A/T	0.579	0.983	3.79×10^{-5}	1.08 (1.04-1.12)	0.182	1.03 (0.99-1.08)	3.53×10^{-9}	1.15 (1.10-1.21)
10q25.2	This study	rs11599775	114459697	G/A	0.620	0.965	4.34×10^{-5}	1.08 (1.04-1.12)	0.299	1.02 (0.98-1.07)	3.44×10^{-9}	1.16 (1.10-1.22)
11q23.2	Published	rs648044	114030799	A/G	0.390	0.886	3.55×10^{-3}	1.06 (1.02-1.10)	0.363	0.98 (0.93-1.03)	4.66×10^{-12}	1.19 (1.13-1.25)
11q23.3	Published	rs498872	118477367	A/G	0.307	1.000	4.09×10^{-11}	1.14 (1.10-1.18)	0.715	1.01 (0.96-1.06)	8.46×10^{-13}	1.35 (1.28-1.41)
11q23.3	This study	rs12803321	118480115	G/C	0.643	0.976	9.93×10^{-16}	1.17 (1.27-1.22)	0.769	1.01 (0.96-1.05)	6.33×10^{-13}	1.42 (1.35-1.49)
12q21.2	Published	rs12230172	76242675	A/G	0.543	0.998	0.012	1.05 (1.01-1.08)	0.541	0.99 (0.94-1.03)	5.50×10^{-6}	1.11 (1.06-1.17)
12q21.2	This study	rs1275600	76263551	T/A	0.595	0.983	2.67×10^{-4}	1.07 (1.03-1.11)	0.862	1.00 (0.96-1.05)	3.72×10^{-9}	1.16 (1.10-1.21)
12q23.33	Published	rs3851634	106812902	T/C	0.702	0.998	3.96×10^{-3}	1.06 (1.02-1.10)	5.41×10^{-4}	1.09 (1.04-1.14)	0.492	1.02 (0.97-1.07)
12q23.33	This study	rs12227783	107041782	A/T	0.851	0.978	5.86×10^{-5}	1.12 (1.06-1.18)	1.60×10^{-5}	1.16 (1.08-1.24)	0.058	1.07 (1.00-1.15)
15q24.2	Published	rs1801591	76578762	G/A	0.088	1.000	3.56×10^{-7}	1.17 (1.10-1.24)	0.343	1.04 (0.96-1.12)	6.36×10^{-13}	1.33 (1.23-1.44)
15q24.2	This study	rs77633900	76538459	G/C	0.086	0.992	1.48×10^{-7}	1.18 (1.11-1.25)	0.258	1.04 (0.97-1.13)	1.60×10^{-13}	1.35 (1.25-1.46)
17p13.1	Published	rs78378222	7571752	T/G	0.013	0.910	8.64×10^{-38}	2.53 (2.19-2.91)	4.82×10^{-29}	2.63 (2.22-3.11)	4.70×10^{-17}	2.73 (2.27-3.28)
20q13.33	Published	rs6010620	62309839	A/G	0.794	1.000	2.81×10^{-40}	1.34 (1.29-1.40)	5.49×10^{-44}	1.46 (1.38-1.54)	2.60×10^{-9}	1.19 (1.12-1.25)
20q13.33	This study	rs2297440	62312299	T/C	0.796	0.993	1.60×10^{-42}	1.36 (1.30-1.42)	3.66×10^{-46}	1.48 (1.40-1.56)	6.90×10^{-10}	1.20 (1.13-1.26)

Supplementary Table 2: Best association signals from previously published risk loci discovered in European populations. Shown for each region are the GWAS tagSNP as well as the most associated variant within a 500kb window in the imputation and the associated odds ratio and *P*-values associated with each. Odds ratios derived with respect to the allele underlined and highlighted in bold. Shown are the association statistics for previously published SNPs in each locus, as well as the most associated SNP in this study if differing from the published SNP. Risk allele frequency (RAF) is according to European samples

			All glioma		GBM		Non-GBM	
Locus	**SNP**	**RAF**	**Odds ratio**	**% risk**	**Odds ratio**	**% risk**	**Odds ratio**	**% risk**
Previously reported loci								
3q26.2	rs3772190	0.757	1.11	0.30	1.11	0.30	1.07	0.13
5p15.33	rs10069690	0.276	1.45	4.15	1.61	6.81	1.27	1.72
7p11.2	rs75061358	0.099	1.42	1.65	1.63	3.20	1.28	0.82
7p11.2	rs723527	0.573	1.17	0.91	1.25	1.83	1.08	0.22
8q24.21	rs55705857	0.057	1.99	3.83	1.27	0.46	3.39	12.04
9p21.3	rs634537	0.411	1.30	2.51	1.37	3.61	1.21	1.32
10q25.2	rs11599775	0.620	1.08	0.21	1.02	0.01	1.16	0.78
11q23.2	rs648044	0.390	1.06	0.12	0.98	0.01	1.19	1.08
11q23.3	rs12803321	0.643	1.17	0.85	1.01	0.00	1.42	4.24
12q21.2	rs1275600	0.595	1.07	0.17	1.00	0.00	1.16	0.80
12q23.33	rs12227783	0.851	1.12	0.24	1.16	0.42	1.07	0.09
15q24.2	rs77633900	0.086	1.18	0.32	1.04	0.02	1.35	1.06
17p13.1	rs78378222	0.013	2.53	1.66	2.63	1.80	2.73	1.95
20q13.33	rs2297440	0.796	1.36	2.31	1.48	3.75	1.20	0.81
		TOTAL		**19.22**		**22.24**		**27.06**
Loci first reported in this study								
1p31.3	rs12752552	0.870	1.18	0.47	1.22	0.67	1.11	0.19
1q32.1	rs4252707	0.220	1.12	0.33	1.07	0.12	1.19	0.78
1q44	rs12076373	0.837	1.09	0.15	0.99	0.00	1.23	0.88
2q33.3	rs7572263	0.756	1.11	0.30	1.06	0.09	1.20	0.92
3p14.1	rs11706832	0.456	1.08	0.22	1.03	0.03	1.15	0.73
10q24.33	rs11598018	0.462	1.10	0.34	1.06	0.13	1.14	0.64
11q14.1	rs11233250	0.868	1.14	0.30	1.24	0.80	0.98	0.01
11q21	rs7107785	0.479	1.07	0.17	1.00	0.00	1.16	0.83
14q12	rs10131032	0.916	1.17	0.29	1.05	0.03	1.33	0.94
16p13.3	rs2562152	0.850	1.09	0.14	1.21	0.70	1.00	0.00
16p13.3	rs3751667	0.208	1.14	0.43	1.13	0.37	1.18	0.68
16q12.1	rs10852606	0.713	1.14	0.53	1.18	0.84	1.08	0.18
22q13.1	rs2235573	0.507	1.09	0.28	1.15	0.73	1.02	0.01
		TOTAL		**3.94**		**4.51**		**6.79**
		OVERALL		**23.16**		**26.75**		**33.84**

Supplementary Table 4: Individual variance in risk associated with glioma SNPs. For each glioma risk locus, the relative risk per risk allele of the highest associated SNP is given. Risk allele frequency (RAF) is according to European samples from 1000 genomes project.

Figure 1: Genome-wide meta-analysis *P*-values ($-\log_{10}P$, y axis) plotted against their chromosomal positions (x axis)

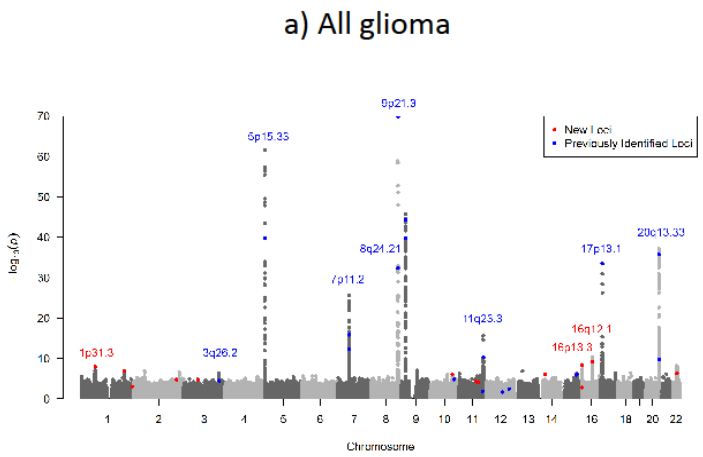

4. SECTION 2-THERANOSTIC MARKERS

4.1 Detection, Characterization, and Inhibition of *FGFR-TACC* Fusions in *IDH* Wild-type Glioma

Glioblastoma multiforme (GBM) is among the most lethal and frequent primary brain tumors. Targeted therapies against common genetic alterations in GBM have not changed the dismal outcome of the disease (Weathers, 2014; Omuro, 2013).

The genetic background of glioblastoma is commonly characterized by the absence of the *IDH* mutation (94%), recurrent chromosomal abnormalities (7p gain, 10q loss, 13q loss), oncogenes amplifications (*EGFR*, *CDK4*) and oncosuppressors deletions (Brennan, 2013).

This same genetic background, notably the absence of the *IDH* mutation, may be recapitulated in a small percentage of lower grade gliomas (grade III and grade II), showing an aggressive clinical behaviour (Sanson, 2009).

As discussed in the introduction section, the recent update of the WHO classification of brain tumors dichotomized the classification and prognostication of gliomas according to the *IDH* status (Louis, 2016) and recognized a worse outcome common to the group of *IDH* wild-type gliomas independent of their grading.

Because of the failure of conventional therapies in the control of *IDH* wild-type gliomas, there is a major need for new druggable targets in this subgroup of patients.

In 2012, Singh et al. reported that a small subset of GBMs (3.1%; 3 of 97 tumors examined) harbours oncogenic chromosomal translocations that fuse in-frame the tyrosine kinase coding domains of fibroblast growth factor receptor (*FGFR*) genes (*FGFR1* or *FGFR3*) to the transforming acidic coiled-coil (*TACC*) coding domains of *TACC1* or *TACC3*, respectively (**Figure 4.1**) (Singh, 2012).

The FGFR-TACC fusion protein displays oncogenic activity when introduced into astrocytes or stereotactically transduced in the mouse brain. The fusion protein, which localizes to mitotic spindle poles, has constitutive kinase activity and induces mitotic and chromosomal segregation defects and triggers aneuploidy (**Figure 4.1**) (Singh, 2012).

Inhibition of FGFR kinase corrects the aneuploidy, and oral administration of an FGFR inhibitor prolongs survival of mice harbouring intracranial *FGFR3-TACC3*–initiated glioma (Figure 4.1.1) (Singh, 2012).

However, the full repertoire of the structural variants of *FGFR-TACC* fusions is incomplete as well as the genetic and phenotypic signature of *FGFR-TACC* positive gliomas. Clinical activity of specific inhibition with anti-FGFR therapies in patients harbouring this oncogenic alteration is also incomplete.

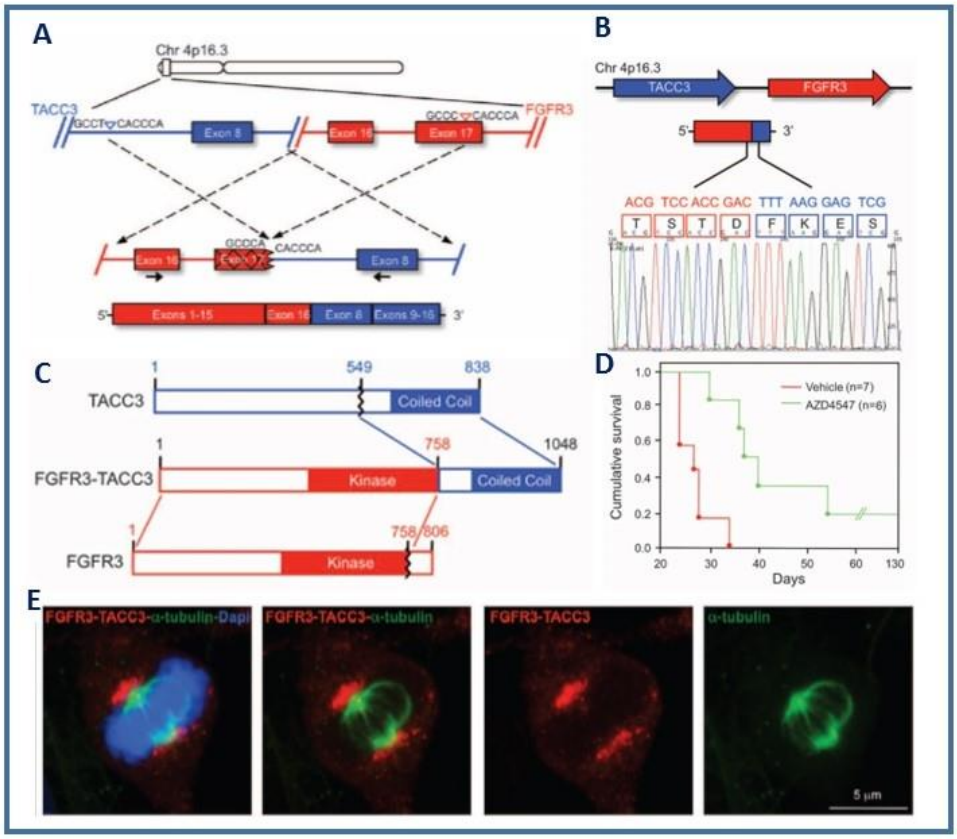

Figure 4.1 Adapted from *Singh et al. 2012. FGFR3-TACC3* gene fusion.
A) Genomic fusion of *FGFR3* exon 17 with intron 7 of *TACC3*. In the fused mRNA, exon 16 of *FGFR3* is spliced 5′ to exon 8 of *TACC3*. Solid black arrows indicate the position of the fusion-genome primers. **B)** Sanger sequencing chromatogram showing the reading frame at the breakpoint and putative translation of the fusion protein. T, threonine; S, serine; D, aspartic acid; F, phenylalanine; E, glutamic acid. **C)** Schematics of the FGFR3-TACC3 protein. Regions corresponding to FGFR3 or TACC3 are shown in red or blue, respectively. The fusion protein joins the tyrosine kinase domain of FGFR3 to the TACC domain of *TACC3*. **D)** Survival of glioma-bearing mice was tracked after intracranial implantation of Ink4A; Arf−/− astrocytes transduced with *FGFR3-TACC3*. After tumor engraftment, mice were treated with vehicle or AZD4547 (50 mg/kg) for 20 days (vehicle, n = 7 animals; AZD4547, n = 6; *P*=0.001) **E)** FGFR3-TACC3 localizes to spindle poles, delays mitotic progression, and induces chromosome segregation defects and aneuploidy. (A) Confocal microscopy analysis of FGFR3-TACC3 (red) covering the spindle poles of a representative mitotic cell. α-tubulin, green; DNA [stained with 4′,6-diamidino-2-phenylindole (DAPI)], blue.

Since 2013, in the collaborative setting with research group led by Dr. Lasorella and Dr. Iavarone, we have been able to perform the largest screening for this therapeutic target in up to 907 patients to date.

Results from first analysis in a dataset of 584 GBM and 211 grade II and grade III gliomas were published in Clinical Cancer Research in 2015 (Di Stefano, 2015). In this article:

- we confirmed that RT-PCR sequencing is a sensitive and specific method to identify *FGFR–TACC*–positive patients,
- we detected for the first time *FGFR3–TACC3* fusions in about 3% of *IDH* wild-type non-GBM (grade II and grade III) and we confirmed the frequency of 3% of *IDH* wild-type glioblastoma,
- we found that *FGFR3–TACC3* fusions are associated with uniform intratumor expression of the fusion protein
- we found that the presence of *FGFR–TACC* fusions are mutually exclusive of the *IDH* mutation, *EGFR* amplification, *EGFR* vIII variant and that it is associated with higher frequency of *MDM2* and *CDK4* amplifications, and
- we observed a clinical benefit in two *FGFR3–TACC3*–positive patients treated with a FGFR inhibitor.

The corresponding article is included in this section.

Next, we started three supplementary studies, based on the prospectical screening for *FGFR-TACC* fusions at *Pitié-Salpetriere Hospital* of new diagnosed *IDH*-wild type glioma cases.

This screening accounts for 907 analysed cases, of which 40 *FGFR3-TACC3* positive patients have been identified so far, corresponding to the largest series ever identified.

Expansion studies are focused on:

- an extensive characterisation of new *FGFR3-TACC3* transcripts and molecular features, together with clinical and histological phenotypes in a larger repertoire of 40 *FGFR3-TACC3* positive gliomas patients (**Section 4.2**)

- an exploratory study on the presence of new acquired mutations associated with resistance in one *FGFR3-TACC3* positive patient recurring after specific anti-FGFR therapy (**Section 4.3**)

- a "phase Ib/phase II clinical trial testing efficacy and tolerability of an anti-FGFR therapy-AZD4547-in glioma patients harbouring *FGFR-TACC* fusions at recurrence" (NCT02824133, *TARGET* trial, PI Prof Marc Sanson) which is the first world-wide phase II trial, testing the efficacy of the anti-FGFR therapy AZD4547 in this selected subgroup of patients. The *TARGET* trial started in September 2015, which included 12 patients, and is now on the expansion phase. Preliminary results of this trial are not shown in this thesis.

Published OnlineFirst January 21, 2015; DOI: 10.1158/1078-0432.CCR-14-2199

Biology of Human Tumors

Clinical Cancer Research

Detection, Characterization, and Inhibition of FGFR–TACC Fusions in IDH Wild-type Glioma

Anna Luisa Di Stefano[1,2,3], Alessandra Fucci[4], Veronique Frattini[4], Marianne Labussiere[1], Karima Mokhtari[1,5,6], Pietro Zoppoli[4], Yannick Marie[1,7], Aurelie Bruno[1], Blandine Boisselier[1], Marine Giry[1], Julien Savatovsky[8], Mehdi Touat[9], Hayat Belaid[10], Aurelie Kamoun[11], Ahmed Idbaih[1,2], Caroline Houillier[2], Feng R. Luo[12], Jean-Charles Soria[9], Josep Tabernero[13], Marica Eoli[14], Rosina Paterra[14], Stephen Yip[15], Kevin Petrecca[16], Jennifer A. Chan[17], Gaetano Finocchiaro[14], Anna Lasorella[4,18], Marc Sanson[1,2,6], and Antonio Iavarone[4,19]

Abstract

Purpose: Oncogenic fusions consisting of fibroblast growth factor receptor (FGFR) and TACC are present in a subgroup of glioblastoma (GBM) and other human cancers and have been proposed as new therapeutic targets. We analyzed frequency and molecular features of FGFR–TACC fusions and explored the therapeutic efficacy of inhibiting FGFR kinase in GBM and grade II and III glioma.

Experimental Design: Overall, 795 gliomas (584 GBM, 85 grades II and III with wild-type and 126 with *IDH1/2* mutation) were screened for *FGFR–TACC* breakpoints and associated molecular profile. We also analyzed expression of the FGFR3 and TACC3 components of the fusions. The effects of the specific FGFR inhibitor JNJ-42756493 for FGFR3–TACC3–positive glioma were determined in preclinical experiments. Two patients with advanced FGFR3–TACC3–positive GBM received JNJ-42756493 and were assessed for therapeutic response.

Results: Three of 85 *IDH1/2* wild-type (3.5%) but none of 126 *IDH1/2*-mutant grade II and III gliomas harbored FGFR3–TACC3 fusions. *FGFR–TACC* rearrangements were present in 17 of 584 GBM (2.9%). FGFR3–TACC3 fusions were associated with strong and homogeneous FGFR3 immunostaining. They are mutually exclusive with *IDH1/2* mutations and *EGFR* amplification, whereas they co-occur with *CDK4* amplification. JNJ-42756493 inhibited growth of glioma cells harboring FGFR3–TACC3 *in vitro* and *in vivo*. The two patients with FGFR3–TACC3 rearrangements who received JNJ-42756493 manifested clinical improvement with stable disease and minor response, respectively.

Conclusions: RT-PCR sequencing is a sensitive and specific method to identify FGFR–TACC–positive patients. *FGFR3–TACC3* fusions are associated with uniform intratumor expression of the fusion protein. The clinical response observed in the FGFR3–TACC3–positive patients treated with an FGFR inhibitor supports clinical studies of FGFR inhibition in FGFR–TACC–positive patients. *Clin Cancer Res; 21(14); 3307–17. ©2015 AACR.*

See related commentary by Ahluwalia and Rich, p. 3105

Introduction

The history of successful targeted therapy of cancer largely coincides with the inactivation of recurrent, oncogenic, and addicting gene fusions in hematologic malignancies and recently in some types of epithelial cancer (1, 2). Glioblastoma multiforme (GBM) is among the most lethal forms of human cancer, and targeted therapies against common genetic alterations in GBM have not changed the dismal outcome of the disease

[1]Sorbonne Universités UPMC Univ Paris 06, INSERM CNRS, U1127, UMR 7225, ICM, Paris, France. [2]AP-HP, Groupe Hospitalier Pitié-Salpêtrière, Service de Neurologie 2, Paris, France. [3]Department of Brain and Behavioral Sciences, University of Pavia, Pavia, Italy. [4]Institute for Cancer Genetics, Columbia University Medical Center, New York, New York. [5]AP-HP, Groupe Hospitalier Pitié Salpêtrière, Laboratoire de Neuropathologie R Escourolle, Paris, France. [6]AP-HP Onconeurothèque, Groupe Hospitalier Pitié-Salpêtrière, Paris, France. [7]Institut du Cerveau et de la Moelle épinière (ICM), Plateforme de Génotypage Séquençage, Paris, France. [8]Fondation Ophtalmologique A. de Rothschild, Paris, France. [9]Drug Development Department, Gustave Roussy Cancer Center, Paris, France. [10]AP-HP, Groupe Hospitalier Pitié Salpêtrière, Department of Neurosurgery, Paris, France. [11]Programme Cartes d'Identité des Tumeurs (CIT), Ligue Nationale Contre Le Cancer, Paris, France. [12]Janssen Pharmaceutical Companies of Johnson and Johnson, Titusville, New Jersey. [13]Vall d'Hebron University Hospital and Vall d'Hebron Institute of Oncology (VHIO), Universitat Autònoma de Barcelona, Barcelona, Spain. [14]Fondazione I.R.C.C.S Istituto Neurologico C. Besta, Milan, Italy. [15]Department of Pathology and Laboratory Medicine, University of British Columbia, Vancouver, Canada. [16]Montreal Neurological Institute and Hospital, McGill University, Montreal, Canada. [17]University of Calgary, Calgary, Canada. [18]Department of Pediatrics and Pathology, Columbia University Medical Center, New York, New York. [19]Department of Neurology and Pathology, Columbia University Medical Center, New York, New York.

Note: Supplementary data for this article are available at Clinical Cancer Research Online (http://clincancerres.aacrjournals.org/).

A.L. Di Stefano and A. Fucci contributed equally to this article.

Corresponding Authors: Marc Sanson, Groupe Hospitalier Pitié-Salpêtrière, 47 Boulevard de l'Hôpital, Cedex 13, 75651 Paris, France. Phone: 33-142 160573; Fax: 33-142-160375; E-mail: marc.sanson@psl.aphp.fr; and Antonio Iavarone, Institute for Cancer Genetics, Columbia University Medical Center, 1130 St. Nicholas Avenue, 10032 New York. Phone: 1 212 851 5245; Fax: 1 212 851 5267; E-mail: ai2102@columbia.edu

doi: 10.1158/1078-0432.CCR-14-2199

Published OnlineFirst January 21, 2015; DOI: 10.1158/1078-0432.CCR-14-2199

Translational Relevance

This article reports an unbiased screening assay for FGFR–TACC fusions in glioma that overcomes the great variability of variants that are generated by FGFR–TACC chromosomal translocation in human cancer. FGFR–TACC fusions occur in grade II and III glioma harboring wild-type IDH1 with frequency similar to glioblastoma (GBM), therefore providing a clue to the aggressive clinical behavior of this glioma subtype. The molecular characterization of fusion-positive glioma revealed that *FGFR–TACC* is mutually exclusive with *EGFR* amplification but co-occurs with *CDK4* amplification. FGFR–TACC –positive glioma displays strikingly uniform and strong expression of the fusion protein at the single-cell level. Preclinical experiments with FGFR3–TACC3–positive glioma cells treated with the fibroblast growth factor receptor (FGFR) inhibitor JNJ-42756493 showed strong antitumor effects, and treatment of two patients with recurrent GBM harboring FGFR3–TACC3 resulted in clinical improvement and radiologic tumor reduction. These findings validate the treatment with FGFR inhibitors of patients with glioma harboring FGFR–TACC chromosomal translocations.

(3, 4). Underlying biologic features, including infiltrative growth behavior, intratumoral heterogeneity, and adaptive resistance mechanisms, coupled with the unique challenges of intracranial location present significant problems in its effective management. Despite surgery and chemoradiotherapy, most patients rapidly recur and no effective treatment options are available at that stage. Besides GBM, which features the highest grade of malignancy among glioma (grade IV), lower grade gliomas, which include grades II and III, are a heterogeneous group of tumors in which specific molecular features are associated with divergent clinical outcome. The majority of grade II and III glioma (but only a small subgroup of GBM) harbor mutations in *IDH* genes (*IDH1* or *IDH2*), which confer a more favorable clinical outcome. Conversely, the absence of *IDH* mutations is associated with the worst prognosis (5).

We have recently identified *FGFR–TACC* gene fusions (mostly *FGFR3–TACC3* and rarely *FGFR1–TACC1*) as the first example of highly oncogenic and recurrent gene fusions in GBM. The FGFR–TACC fusions that have been identified so far include the tyrosine kinase (TK) domain of FGFR and the coiled-coil domain of TACC proteins, both necessary for the oncogenic function of FGFR–TACC fusions. We also tested tumor dependency on FGFR–TACC fusions in preclinical mouse models of FGFR–TACC glioma and observed marked antitumor effects by FGFR inhibition (6). After our report, *FGFR3–TACC3* fusions have been identified in pediatric and adult glioma, bladder carcinoma, squamous lung carcinoma, and head and neck carcinoma, thus establishing *FGFR–TACC* fusions as one of the chromosomal translocation most frequently found across multiple types of human cancers (6–15).

From a mechanistic standpoint, we discovered the unexpected capacity of FGFR–TACC fusions to trigger aberrant chromosome segregation during mitosis, thus initiating chromosome instability (CIN) and aneuploidy, 2 hallmarks of cancer. However, we still have an incomplete understanding of the full repertoire of the structural variants of *FGFR–TACC* fusions occurring in GBM and lower grade glioma. Furthermore, it remains unknown whether *FGFR–TACC* fusions mark distinct grades of glioma and GBM subtypes.

To date, 8 variants of the *FGFR3–TACC3* fusion have been reported that mostly differ for the breakpoint in the *TACC3* gene (6–15). Because of the close proximity of *FGFR3* and *TACC3* (the 2 genes map at a distance of 70 Kb on chromosome 4p16.3), detection of *FGFR3–TACC3* rearrangements by FISH is not a feasible option with the currently available methods. Here, we report a screening method for *FGFR–TACC* fusions that include a RT-PCR assay designed to identify the known and novel *FGFR3–TACC3* fusion transcripts, followed by confirmation of the *in-frame* breakpoint by Sanger sequencing. Using this assay, we have analyzed a dataset of 584 GBM and 211 grade II and III gliomas.

A crucial question with fundamental clinical relevance for any novel candidate target mutation is the frequency of the alteration in the cancer cell population, thus discriminating between a clonal or subclonal origin of the mutation. In fact, GBM is characterized by a formidable degree of subclonal heterogeneity, whereby neighboring cells display amplification and expression of different receptor tyrosine kinase (RTK)-coding genes (16–19). This notion poses major therapeutic challenges for targeting any individual RTK will result, at best, in the eradication of a limited tumor subclone. In this study, we determine that brain tumors harboring *FGFR–TACC* fusions manifest strong and homogeneous intratumor expression of the FGFR3 and TACC3 component invariably included in the fusion protein, when analyzed by immunostaining. We also report a significant clinical benefit following treatment with a specific inhibitor of FGFR-TK in 2 patients with GBM who harbored *FGFR3–TACC3* rearrangement.

Materials and Methods

Patients and tissue samples

This study includes a cohort of 746 untreated patients with histologic diagnosis of glioma from 5 institutions. Forty-nine recurrent gliomas from Pitié-Salpêtrière Hospital and one recurrent glioma from the University of Calgary (Calgary, Canada) were also included. A summary of the patient cohort is provided in Table 1.

Tumor specimens, blood samples, and clinicopathologic information were collected with informed consent and relevant ethical board approval in accordance with the tenets of the Declaration of Helsinki. For the samples from the Pitié-Salpêtrière Hospital, clinical data and follow-up are available in the neuro-oncology database (Onconeurotek, GH Pitié-Salpêtrière, Paris).

Two recurrent patients with GBM harboring *FGFR3–TACC3* were enrolled in the dose escalation part of JNJ-42756493 trial (NCT01962532) at the Gustave Roussy Institute (Paris, France).

Identification of fusion transcripts and analysis of genomic breakpoints

Total RNA was extracted from frozen tissues using TRIzol (Invitrogen) according to manufacturer instructions. Two to three hundred nanograms of total RNA was retrotranscribed with the Maxima First Strand cDNA Synthesis Kit (Thermo Scientific) or SuperScript II (Invitrogen). RT-PCR was performed using AccuPrime Taq DNA Polymerase (Invitrogen). Primer pairs used for the FGFR3–TACC3 fusions screening were: FGFR3ex12-FW: 5′-CGTGAAGATGCTGAAAGACGATG-3 and TACC3ex14-RV: 5′-AAACGCTTGAAGAGGTCGGAG; amplification conditions were 94°C-3 minutes (94°C-30 seconds/61°C-30 seconds/68°C-1

Published OnlineFirst January 21, 2015; DOI: 10.1158/1078-0432.CCR-14-2199

Table 1. Frequency of FGFR3–TACC3 fusions in GBM and grade II–III glioma

Tumor sample source	Cases (GBM), *n*	Detected fusions, *n*	Immunostaining FGFR3 positive/sample analyzed
Pitié-Salpêtrière Hospital	380	9	9/9
Besta Neurological Institute	85	5	2/2
University of Calgary	60 + 1R[a]	2 + 1R[a]	1/1 +1/1R[a]
Montreal Neurological Institute	51	1	—
University of British Columbia	8	0	—
Total	584 (100%)[b]	17 (2.9%)	

Tumor sample source	IDH status	Cases (grades II–III), *n*	Detected fusions, *n*	Immunostaining FGFR3 positive/sample analyzed
Pitié-Salpêtrière Hospital	IDH wt	85[c] (100%)	3 (3.5%)	3/3
	IDH1/IDH2 Mut	126 (100%)	0 (0%)	0

NOTE: Distribution of the FGFR3–TACC3 fusions in GBM (top) and lower grade glioma (bottom) samples stratified according to the institution of origin. The table reports number of cases analyzed, number of tumors harboring FGFR3–TACC3 fusion transcripts, and results of FGFR3 immunostaining. Lower grade glioma samples are further classified according to *IDH* status (*IDH1* and *IDH2*). The respective frequency of FGFR3–TACC3 in GBM, glioma grades II–III *IDH* wild type (wt), and *IDH* mutant (Mut) glioma is reported in parentheses.

[a]R, recurrent GBM.

[b]Recurrent GBM from the University of Calgary Dataset is not included in the total count of GBM.

[c]Twenty-five cases of 85 are unknown for *IDH2* status.

minute 40 seconds) for 35 cycles, 68°C-7 minutes. FGFR1–TACC1 fusions were amplified with FGFR1ex16-FW: 5′-TGCCTGTGGAGGAACTTTTCA-3′ and TACC1ex13-RV: 5′-CCCAAACTCAGCAGCCTAAG-3′ primers (94°C-30 seconds/60°C-30 seconds/68°C-1 minute 40 seconds for 35 cycles). PCR products were subjected to Sanger sequencing.

FGFR3–TACC3 genomic breakpoints were analyzed in 6 *FGFR3–TACC3*–positive samples, 5 of which from the Pitié-Salpêtrière Hospital and 1 from Montreal Neurological Institute (Montreal, Canada). Three additional samples (MB-22, TCGA 27-1835, and TCGA 06-6390) available from our previous study (6) were also included in the analysis. Fifty nanograms of gDNA was used in the PCR reaction, performed with Accuprime Taq Polymerase (Invitrogen) and PCR products were Sanger sequenced. Primers used in genomic PCR were designed according to the breakpoint sequence in the mRNA; the list of primers used are: FGFR3ex17-FW 5′-TGGACCGTGTCCTTACCGT-3′ (PCR samples 3048, 4373, 4867, 4451, MB-22, OPK-14, 06-6390, 27-1835 and sequencing sample 3048, 4373, 4867, 4451, MB-22, OPK14, 06-6390, 27-1835); FGFR3ex16-FW 5′-GGTCCTTTGGGGTCCTGCT-3′ (PCR and sequencing sample 3808); TACC3ex6-RV 5′-CCTCTTTCAGCTCCAAGGCA-3′ (PCR and sequencing samples PCR 4451 and OPK-14); TACC3ex8-RV 5′-TCTACCAGGACTGTCCCTCAG-3′ (sequencing samples 3048 and 4373); TACC3ex9-RV 5′-GGGAGTCTCATTTGCACCGT-3′ (PCR samples 3048,4373,4867 and sequencing sample 4867); TACC3ex10-RV 5′-CTGCATCCAGGTCCTTCTGG-3′ (PCR and sequencing samples MB-22 and 06-6390); TACC3ex11-RV 5′-CCAGTTCCAGGTTCTTCCCG-3′ (sequencing samples 27-1837 and 3808); TACC3ex12-RV 5′-CAACCTCTTCGAACCTGTCCA-3′ (PCR and sequencing samples 27-1837 and 3808). PCR conditions were 94°C-30 seconds/60°C-30 seconds/68°C-2 minute 30 seconds for 40 cycles. For amplifications performed with the primer TACC3ex9-RV, the program was 94°C-30 seconds/56°C-30 seconds/68°C-2 minute 30 seconds) for 40 cycles.

Quantitation of *FGFR3* and *TACC3* transcripts in GBM

The relative expression of *FGFR3* and *TACC3* regions included in or excluded from the fusion transcript was assessed by qRT-PCR. Primer pairs with comparable efficiency of amplification were identified, and efficiency was assessed using serial dilutions of cDNA (20) prepared from OAW28 ovarian carcinoma cells that contain wild-type *FGFR3* and *TACC3* (21). Primers used are: N-terminal region of *FGFR3*, FGFR3-N: Forward 5′-AAGACGATGCCACTGACAAG-3′, Reverse 5′-CCCAGCAGGTTGATGATGTTTTTG-3′; C-terminal region of TACC3, TACC3-C: Forward 5′-TCCTTCTCCGACCTCTTCAAGC-3′, Reverse 5′-TAATCCTCCACGCACTTCTTCAG-3′. To amplify transcripts in regions excluded from FGFR3–TACC3 fusion, primers were designed in the C-terminal region of FGFR3, FGFR3-C: Forward 5′-TACCTGGACCTGTCGGCG-3′, Reverse 5′-TGGGCAAACACGGAGTCG-3′ and N-terminal domain of TACC3, TACC3-N: Forward 5′-CCACAGACGCACAGGATTCTAAGTC-3′, Reverse 5′-TGAGTTTTCCAGTCCAAGGGTG-3′. All reactions were performed in triplicate and the data are reported as fold change ± SD.

Immunofluorescence and immunohistochemistry

For immunofluorescent (IF) staining of FGFR3, 5-μm formalin-fixed, paraffin-embedded (FFPE) sections were subjected to antigen retrieval with citrate buffer for 8 minutes. Primary antibodies were: FGFR3-N (1:400, sc-13121, Santa Cruz Biotechnology), FGFR3-C (1:2000, sc-123, Santa Cruz Biotechnology), TACC3-N (1:600, ab134153, Abcam), and TACC3-C (1:300, NBP1-01032, Novus Biological). Secondary biotinylated antibodies were used at 1:50,000 followed by streptavidin and TSA Cy3-conjugated. Nuclei were counterstained with 4′,6-diamidino-2-phenylindole (DAPI). For immunohistochemical (IHC) analysis of FGFR3 expression, antigen retrieval was performed for 12 minutes and FGFR-3 antibody (sc-13121, Santa Cruz Biotechnology) was diluted 1:500. Biotinylated anti-mouse antibody (1:30,000) and streptavidin were added before incubation with the chromogen. Nuclei were counterstained with hematoxylin.

Molecular characterization of tumor samples

Mutational status of *IDH1*, *IDH2*, *TERT* promoter, as well as the methylation status of the *MGMT* promoter was analyzed in the Pitié-Salpêtrière cohort. Expression of IDH1-R132H mutant was analyzed by IHC in 500 cases as previously described (22). *IDH1* and *IDH2* gene mutations were identified by Sanger sequencing in 464 and 388 gliomas, respectively (5). *IDH* wild-type tumors are

Published OnlineFirst January 21, 2015; DOI: 10.1158/1078-0432.CCR-14-2199

defined according to the absence of IDH1-R132H immunopositivity and/or mutations in *IDH1* and *IDH2* genes. *TERT* promoter status was determined by the same technique in 277 samples (23). Hypermethylation of the *MGMT* promoter was tested in 242 samples by bisulfite pyrosequencing (24). The presence of *EGFR-vIII* was evaluated by RT-PCR in 118 samples using EGFR-FW 5′-CTTCGGGGAGCAGCGATGCGAC-3′ and EGFR-RV 5′CTGTCC-ATCCAGAGG AGGAGTA-3′ primers (25).

Copy number variations analyses have been performed on 192 tissue samples using CGH arrays using BAC arrays ($n = 187$), Agilent 4 × 180 K ($n = 2$), Nimblegen 3 × 720 K ($n = 2$), and Agilent 8 × 60 K ($n = 1$). Results were normalized using control DNA from matched blood samples as previously described (26). Additional analyses of 193 tumor specimens were performed by SNP array, using Illumina Omni ($n = 110$), Illumina HumCore ($n = 32$), Illumina 370 K ($n = 27$), or Illumina 610 K ($n = 24$), as previously described (27). Array processing was outsourced to Integragen. Raw copy numbers were estimated at each of the SNP and copy number markers. Biodiscovery property SNP-FASST2 algorithm was then used to segment copy number data. Segments were mapped to hg18 genome assembly (28). Copy number alterations magnitudes called log-R ratio (LRR) were classified using simple thresholds: deletion ($x \leq -1$), loss ($-1 < x \leq -0.2$), gain ($0.2 \leq x < 1$), or amplification ($x \geq 1$) according to default Nexus 7.5 software. For additional 56 gliomas, 10q loss was assessed on tumor and blood DNA by microsatellite analysis, whereas amplification of *EGFR*, *MDM2*, and *CDK4*, and deletion of *CDKN2A* gene, were determined by qPCR, as previously reported (29, 30).

The molecular profiles obtained in Pitié-Salpêtrière dataset were combined with those available in The Cancer Genome Atlas (TCGA) data portal. TCGA GBM segmented copy number variation profile was downloaded from The UCSC Cancer Genomics Browser (31). Copy number variations (CNV) were measured experimentally using the Affymetrix Genome-Wide Human SNP Array 6.0 platform at the Broad TCGA genome characterization center (32). Raw copy numbers were estimated at each of the SNP and copy number markers. Circular binary segmentation was then used to segment the copy number data (28). Segments are mapped to hg18 genome assembly at Broad.

For CNV analysis of the regions across *FGFR3* and *TACC3* genes, we considered samples for which RNAseq and CNV data were available or samples for which only CNV data were available and RT-PCR sequencing of *FGFR3–TACC3* fusion had been performed. Overall, 158 GBM (all with a wild-type *IDH1* gene) satisfied these criteria. Among them, 5 harbored an *FGFR3–TACC3* fusion, whereas 153 were *FGFR—TACC*–negative. The CNV magnitudes, called LRR, were classified using the following thresholds: deletion ($x < -1$), loss ($-1 \leq x \leq -0.2$), gain ($0.2 \leq x \leq 1$), or amplification ($x > 1$), according to the Atlas-TCGA (32). The analysis of the genomic regions encompassing *EGFR*, *MDM2*, *CDK4*, *CDKN2A*, *7p*, *10q*, according to *hg18* genome assembly, was performed to evaluate their CNV. *EGFRvIII* mutation status was inferred according to Brennan and colleagues (32). The frequencies of the aberrations of these genes in *FGFR3–TACC3*–positive and -negative samples were calculated and the obtained data were then combined with the Pitié-Salpêtrière Hospital dataset.

Statistical analysis

Differences in the distribution on categorical variables were analyzed using the Fisher exact test. The *P* values were adjusted for multiple testing according to Benjamini and Hochberg false discovery rate (FDR). A *q* value ≤ 0.05 (2-sided) was considered to be statistically significant.

Overall survival (OS) was defined as the time between the diagnosis and death or last follow-up. Patients who were still alive at the last follow-up were considered as censored events in the analysis. Progression-free survival (PFS) was defined as the time between the diagnosis and recurrence or last follow-up. Patients who were recurrence-free at the last follow-up were considered as censored events in the analysis. Survival curves were calculated by the Kaplan–Meier method and differences between curves assessed using the log-rank test. A log-rank test $P \leq 0.05$ (2-sided) was considered to be statistically significant.

Cell culture and cell growth assay

GIC-1123 gliomaspheres were cultured in neurobasal medium (Invitrogen) supplemented with B27, N2 (Invitrogen), EGF, and FGF2 (20 ng/mL, PeproTech). Mouse astrocytes *Ink4A-Arf*$^{-/-}$ were cultured in DMEM supplemented with 10% FBS. Cells were seeded at 1,000 cells per well in a 96-well plate and treated with JNJ-42756493 (Active Biochem, #A-1278). After 72 hours, cell viability was assessed using the MTT assay. Data are mean ± SEM of 6 replicates. Experiments were performed 3 times.

Subcutaneous xenografts and drug treatment

GIC-1123 cells (5×10^5) were injected subcutaneously in the flank of athymic nude (*nu/nu*) mice (Charles River Laboratories). Mice carrying about 200 mm^3 subcutaneous tumors were randomized to receive 12 mg/kg JNJ-42756493 (Active Biochem, #A-1278) or dimethyl sulfoxide (DMSO) in 1% Tween 80 by oral gavage. Tumor diameters were measured with caliper and tumor volumes estimated using the formula: 0.5 × length × width^2. Data are mean ± SD of 9 mice in each group. Mice were sacrificed when tumors in the control group reached the maximal size allowed by the IACUC Committee at Columbia University (New York, NY).

MRI imaging and evaluation of clinical response to JNJ-42756493

Baseline and follow-up imaging assessments were performed on 1.5-Tesla MR imaging systems, including at least axial T1-weighted images before gadolinium injection, Axial or 3D FLAIR (fluid-attenuated inversion recovery), dynamic susceptibility contrast MR perfusion (0.1 mmol/kg of gadobutrol), axial and 3D T1-weighted images after gadolinium injection. Tumor response was assessed according to the RANO criteria (33). Contrast-enhancing lesion volume was assessed with the help of a semiautomated volumetry tool (SegmentiX), based on shape detection and thresholding, with control and manual correction of edges when necessary. Because exclusion of cystic or necrotic portions of the lesion may be affected by operator subjectivity, we included them both for volumetric and axial measurements.

DSC (dynamic susceptibility contrast) perfusion datasets were processed with vendor's software suite (Neuroperfusion, Philips), including coregistration and rCBV (relative cerebral blood volume) parametric maps generation with 3 different algorithms (Gamma-variate fitting, Arterial Input Function–based deconvolution and Model Free).

Published OnlineFirst January 21, 2015; DOI: 10.1158/1078-0432.CCR-14-2199

Results

Detection of *FGFR1–TACC1* and *FGFR3–TACC3* fusions in GBM and grade II–III glioma

To determine the frequency and molecular features of *FGFR–TACC* fusions in human patients with glioma, we screened a cohort of 584 GBM and 211 grade II–III glioma treated at 5 neuro-oncology centers (Table 1). One hundred eight were grade III (49 *IDH* wild-type, 52 *IDH1* mutant, and 7 *IDH2* mutant) and 103 were grade II (36 *IDH* wild-type, 63 *IDH1* mutant, and 4 *IDH2* mutant). We also established the *IDH* mutational status of 333 GBM and determined that 303 harbored wild-type *IDH1/2* and 30 were mutated at codon 132 of *IDH1*. We designed a RT-PCR assay for the detection of all known and possibly new variants of *FGFR1–TACC1* and *FGFR3–TACC3* fusions that retain the mRNA sequences coding for the key FGFR-TK and TACC domains required for the oncogenic activity of the fusion protein (Figs. 1 and 2A–D). Overall, we found 20 tumors with an *FGFR3–TACC3* fusion, of which 17 were GBM (2.9% positives) and 3 lower grade glioma harboring wild-type *IDH1/2* genes (3.5% positives). The size of the *FGFR3–TACC3* RT-PCR amplicons ranged from 928 bp (for *FGFR3ex18-TACC3ex13*) to 1,706 bp (for *FGFR3ex18-TACC3ex4*). The *FGFR1–TACC1* fusion was detected in one grade II *IDH* wild-type glioma (Fig. 1). Conversely, we did not find any *IDH1/2*-mutant glioma harboring *FGFR–TACC* fusions ($P < 0.02$). Sanger sequencing of the fusion amplicons revealed that each *FGFR–TACC* cDNA joined *in-frame* the sequence coding for the entire TK domain upstream of *TACC*-coding sequences that invariably include the coiled-coil TACC domain (Fig. 1). However, we detected a notable variability among *FGFR3–TACC3* fusion isoforms, whereby 5 of the identified variants occurred only in individual cases (Fig. 1). Furthermore, 6 fusion transcripts emerged as new variants that have not been reported before in human cancer (marked in red in Fig. 1).

Next, we designed suitable PCR primers to map the genomic breakpoint coordinates for 9 *FGFR3–TACC3*–positive samples for which gDNA was available (Supplementary Figs. S1 and S2). We successfully reconstructed the genomic breakpoints by Sanger sequencing and found that they differ for each of the 9 positive cases. Interestingly, even cases harboring the same *FGFR3–TACC3* transcript splice variants (#4451 and #OPK-14 joining exon 17 of *FGFR3* to exon 6 of *TACC3*; #3048 and #4373 joining exon 17 of *FGFR3* to exon 8 of *TACC3*; #3808 and #27-1835 joining exon 17 of *FGFR3* to exon 11 of *TACC3*) had different genomic breakpoints (Supplementary Fig. S2). Taken together, the above findings indicate that the noticeable variability among *FGFR3–TACC3* fusion transcripts and genomic breakpoints is efficiently resolved by the RT-PCR screening assay.

Immunostaining analysis of FGFR3–TACC3–positive tumors

We analyzed the expression of the FGFR3 fusion protein by IHC or IF using an antibody that recognizes the N-terminal region of FGFR3 (FGFR3-N) in 12 GBM and 3 lower grade glioma harboring *FGFR3–TACC3* fusions for which sufficient tissue was available. Remarkably, each of the 15 positive tumors but none of those that had scored negative in the RT-PCR assay, displayed strong positivity for FGFR3 in the vast majority of tumor cells but

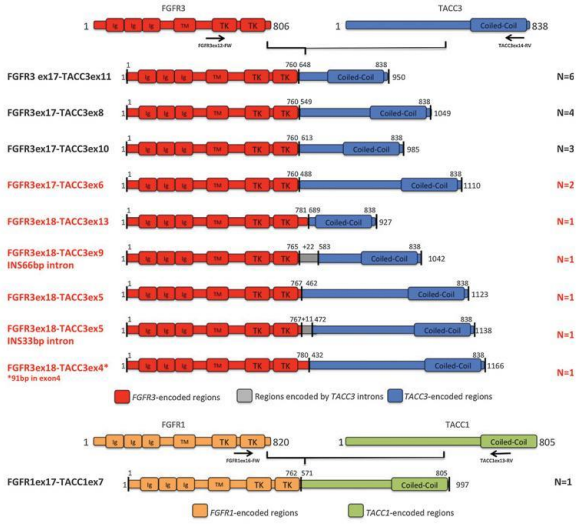

Figure 1.
Structure of *FGFR–TACC* fusions identified by RT-PCR Sanger sequencing. Predicted FGFR–TACC fusion proteins encoded by the transcripts identified by RT-PCR. Regions corresponding to FGFR3 or TACC3 are shown in red or blue, respectively. FGFR1 and TACC1 corresponding regions are shown in yellow and green. On the left are indicated the *FGFR* and *TACC* exons joined in the fused mRNA; the presence of *TACC3* introns is also reported when they are spliced in the fusion cDNA. On the right, the number of patients harboring the corresponding fusion variant is indicated. The novel transcripts discovered in this study are highlighted in red. Black arrows indicate the position of the primers used for the *FGFR–TACC* fusion screening.

Published OnlineFirst January 21, 2015; DOI: 10.1158/1078-0432.CCR-14-2199

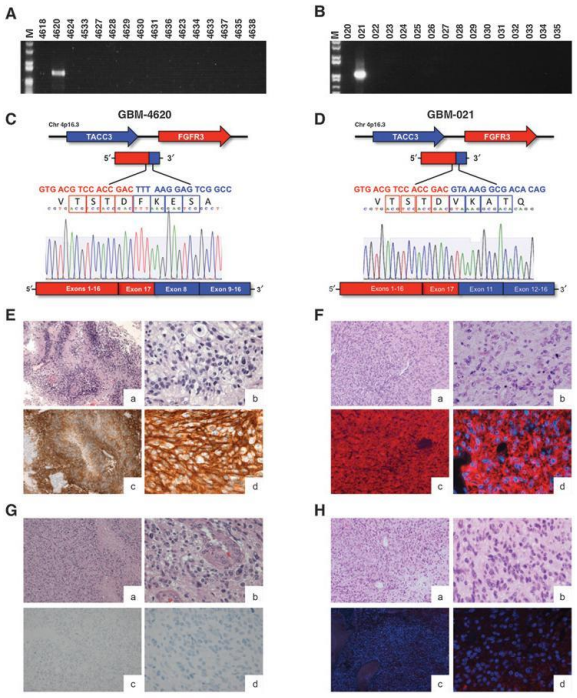

Figure 2.
Identification and immunostaining of FGFR3–TACC3–positive tumors. Results from RT-PCR screening in representative samples from the Pitié-Salpêtrière Hospital (A and C) and the Besta (B and D) datasets. M, DNA ladder. Schematic representation of the FGFR3–TACC3 fusion transcripts identified in samples GBM-4620 (C) and GBM-021 (D). The junction sequences on the mRNA and the reading frame at the breakpoint are reported. Representative microphotographs of hematoxylin and eosin (H&E) and FGFR3 immunostaining in the FGFR3–TACC3–positive samples GBM-4620 (E) and GBM-021 (F) and 2 FGFR3–TACC3–negative samples (G and H). a, H&E, 10× magnification; b, H&E, 40× magnification; c, FGFR3, 10× magnification; d, FGFR3, 40× magnification.

not endothelial cells throughout the analyzed tumor section (Fig. 2A–H). Notably, IF using an antibody that recognizes an epitope at the C-terminus of TACC3, which is invariably retained within FGFR3–TACC3 variants (TACC3-C), reproduced the staining pattern of the FGFR3-N antibody in FGFR3–TACC3–positive tumors. Conversely, negative or very weak staining was obtained in *FGFR3–TACC3*–positive tumors with antibodies recognizing the regions of FGFR3 (FGFR3 C-terminal region, FGFR3-C) and TACC3 (TACC3 N-terminal region, TACC3-N) constantly excluded from FGFR3–TACC3 fusion proteins (Supplementary Fig. S3A). Consistently, quantitative RT-PCR of GBM harboring *FGFR3–TACC3* fusions showed that the expression of the N-terminal coding region of *FGFR3* and the C-terminal coding region of *TACC3* (which are included in the fusion genes) is markedly higher than the expression of the C-terminal coding region of *FGFR3* and the N-terminal coding region of *TACC3*, which are excluded from the fusion transcripts (Supplementary Fig. S3B). We also analyzed one recurrent GBM from a patient whose tumor had been found positive for *FGFR3–TACC3* at the initial diagnosis and who had recurred after concurrent radiotherapy and temozolomide treatment. The recurrent tumor retained the same *FGFR3–TACC3* fusion gene and protein that was present in the untreated GBM as determined by RT-PCR sequencing and FGFR3 IF, respectively (Supplementary Fig. S4). Although this requires additional evaluation, the retained uniform positivity for FGFR3 in this recurrent GBM suggests that targeting the FGFR3–TACC3 fusion protein at relapse is a valid therapeutic strategy.

Clinical and molecular characteristics of glioma patients with *FGFR3–TACC3* fusions

Clinical and molecular profiling data were available for 591 patients, including 380 GBM (9 with *FGFR3–TACC3* fusions) and all 211 lower grade glioma (3 with *FGFR3–TACC3* fusions). Of these 12 patients, 5 are males and 7 females, aged 48 to 82 years (median = 61 years). We sought to determine the molecular

Published OnlineFirst January 21, 2015; DOI: 10.1158/1078-0432.CCR-14-2199

Table 2. Molecular alterations in *IDH* wild-type glioma harboring *FGFR3–TACC3* fusions

	FGFR3–TACC3 positive, *n*	% of FGFR3–TACC3 positive	FGFR3–TACC3 negative, *n*	% of FGFR3–TACC3 negative	*P* (Fisher test)	*q* (FDR)
EGFR amplification	**0/16**	**0.0%**	**166/411**	**40.4%**	**4.E−04**	**0.0012**
CDK4 amplification	**7/16**	**43.7%**	**41/408**	**10.0%**	**8.E−04**	**0.0024**
MDM2 amplification	**4/16**	**25.0%**	**24/408**	**5.9%**	**0.016**	**0.048**
EGFRvIII	0/16	0.0%	37/219	16.9%	0.083	0.25
CDKN2A deletion	4/16	25.0%	188/411	45.7%	0.13	0.39
Chr. 7p gain	12/15	80.0%	242/374	64.7%	0.28	0.84
Chr. 10q deletion	12/16	75.0%	253/420	60.2%	0.3	0.9
TERT promoter mutation	9/11	81.8%	128/163	78.5%	0.8	1
MGMT promoter hypermethylation	6/12	50.0%	73/160	45.6%	0.7	1

NOTE: The table reports the absolute number and frequency (percentage) of individual glioma-specific molecular alterations in tumors scoring positive or negative for *FGFR3–TACC3* fusions. The analysis is done on the Union dataset (TCGA and "Pitié-Salpètrière Hospital" datasets, see Materials and Methods for details). Statistically significant associations are indicated in bold (Fisher exact test, *q* values adjusted with FDR).

profile of *FGFR3–TACC3*–positive glioma. To do so, we combined the analysis of CNVs and somatic mutations of key GBM genes in our dataset with the SNP6.0 high-density genomic array analysis of 158 TCGA-derived GBM samples fully annotated for *FGFR3–TACC3* fusion genes (the RNA-seq and/or RT-PCR analysis of these samples had revealed that 5 of them harbor *FGFR3–TACC3* fusions; ref. 6). Patients with *FGFR3–TACC3* fusions displayed unique characteristics (Table 2). *FGFR3–TACC3* fusions were mutually exclusive with *EGFR* amplification (0 of 16 vs. 166 of 411; $P = 0.0004$, FDR q value corrected for multiple comparisons $= 0.0012$) and showed a clear trend against the presence of the *EGFRvIII* transcript variant (0 of 16 vs. 37 of 219; $P = 0.083$). Conversely, *CDK4* amplification was significantly more frequent in *FGFR3–TACC3*–positive tumors (7 of 16 vs. 41 of 408, $P = 0.0008$; FDR q value $= 0.0024$). A less significant association of *FGFR3–TACC3* fusions was also seen with amplification of *MDM2*, which as *CDK4*, maps to chromosome 12q (4 of 16 vs. 24 of 408, $P = 0.016$; FDR $q = 0.048$). We found no statistical association between *FGFR3–TACC3* fusions and other genetic and epigenetic alterations that commonly occur in gliomas harboring wild-type *IDH* genes (*CDKN2A* deletion, *TERT* promoter mutations, gain of chromosome 7p, loss of chromosome 10q, and methylation of the *MGMT* promoter; Table 2). When compared with the *IDH* wild-type patient population of grade II and III glioma and GBM, there was no significant difference in PFS or OS between patients positive or negative for *FGFR3–TACC3* (Supplementary Fig. S5A and S5B).

Finally, we sought to establish whether the CNV analysis of the *FGFR3* and *TACC3* genomic loci could be used to predict positivity for *FGFR3–TACC3* fusions. The analysis of high-density SNP6.0 arrays of the 158 GBM samples from TCGA revealed that 10 samples displayed different degrees of copy number gains encompassing the entire *FGFR3* and *TACC3* loci (Supplementary Fig. S6). However, none of them harbored *FGFR3–TACC3* fusions. Conversely, the 5 *FGFR3–TACC3*–positive samples in the dataset harbor microamplification events involving only the exons of the *FGFR3* gene that are included in the fusion breakpoint. This finding suggests that any CNV survey that is less accurate than high-density SNP arrays could fail to identify the genomic marks associated with true *FGFR3–TACC3*–positive cases.

Preclinical and clinical relevance of targeting *FGFR3–TACC3* fusions

JNJ-42756493 is a potent, oral pan-FGFR tyrosine kinase inhibitor with IC_{50} values in the low nanomolar range for all members of the FGFR family. It has demonstrated potent antitumor activities in nonclinical models with FGFR aberrations, including squamous non–small cell lung cancer, gastric cancer, breast cancer, hepatocellular cancer, endometrial, and bladder cancers (34, 35). To ask whether JNJ-42756493 is effective in targeting specifically FGFR–TACC–positive cells, we treated with JNJ-42756493 mouse astrocytes expressing FGFR3–TACC3, FGFR3–TACC3 containing a mutation that inactivates the kinase activity of FGFR3 (FGFR3–TACC3-KD) or the empty vector. We also studied the effect of JNJ-42756493 on human glioma stem cells GIC-1123 that harbor the *FGFR3–TACC3* gene fusion (6). These experiments revealed that both mouse astrocytes and GIC-1123 that express FGFR3–TACC3 but not cells expressing the KD mutant fusion or the empty vector are highly sensitive to FGFR inhibition by JNJ-42756493 with an IC_{50} of 3.03 and 1.55 nmol/L, respectively (Fig. 3A and B). Next, we tested whether oral treatment with JNJ-42756493 of mice-bearing xenografts of human GIC-1123 affects tumor growth. Mice were randomized to receive vehicle or JNJ-42756493 (12 mg/kg). Mirroring the *in vitro* results, JNJ-42756493 elicited a potent growth inhibition of GIC-1123 tumor xenografts (Fig. 3C and D) with a statistically significant tumor regression after 2 weeks (P value of the slope calculated from the treatment starting point $= 0.04$). The above findings provide a strong foundation for the treatment of patients with GBM harboring *FGFR–TACC* rearrangements with JNJ-42756493.

Two patients with recurrent GBM harboring *FGFR3–TACC3* fusions were treated with JNJ-42756493 in a first-in-man phase I trial. Patient 1, male aged 52 years, underwent partial surgical resection of a right parietal GBM, followed by fractionated radiotherapy and concomitant temozolomide as first-line treatment (36). The RT-PCR sequencing analysis of the GBM specimen revealed positivity for the *FGFR3–TACC3* fusion (*FGFR3-exon17-TACC3-exon 6*, sample 4451, Supplementary Figs. S1 and S2) and the immunostaining using FGFR3 antibody on paraffin-embedded sections showed strong positivity in a large fraction of tumor cells (not shown). After 5 cycles of temozolomide, the patient presented with dizziness and headache and brain MRI revealed tumor progression (Fig. 4A). At this time, the patient was enrolled in the JNJ-42756493 trial and received JNJ-42756493 (12 mg/d administered in cycles of 7 days followed by 7 days off-treatment). After 3 weeks, the patient reported a marked clinical improvement (complete regression of dizziness and headache). On MRI, the sum of product diameters (RANO criteria, Fig. 4B) and volumetry (Fig. 4C) measured without excluding cystic and necrotic components showed disease stabilization. However, the tumor mass underwent significant decrease of the enhancing

Published OnlineFirst January 21, 2015; DOI: 10.1158/1078-0432.CCR-14-2199

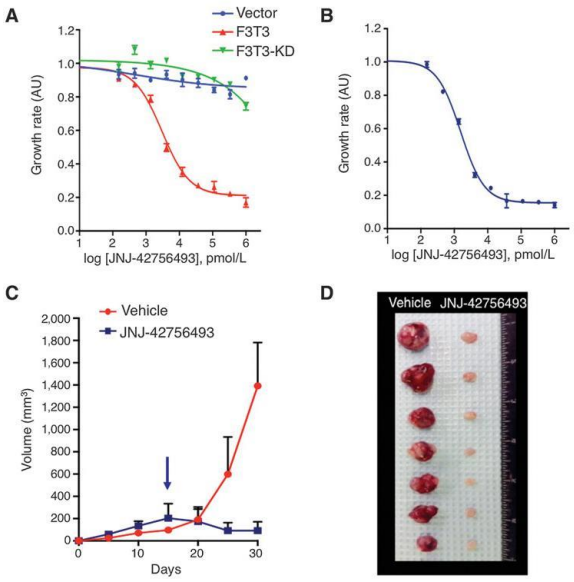

Figure 3.
Preclinical evaluation of FGFR3–TACC3 inhibition by JNJ-42756493. A, mouse astrocytes expressing FGFR3–TACC3 (F3T3), FGFR3–TACC3-KD (F3T3-KD), or the empty vector (Vector) were treated with the indicated concentration of JNJ-42756493. Cell viability was determined by the MTT assay. Error bars show mean ± SEM ($n = 6$). B, survival analysis of GIC-1123 treated with JNJ-42756493. C, the FGFR-TK inhibitor JNJ-42756493 suppresses tumor growth of subcutaneous tumors generated by GIC-1123. After tumor establishment (arrow), mice were treated with vehicle or JNJ-42756493 (12 mg/kg) for 14 days. Values are mean tumor volumes ± SD ($n = 9$ mice per group). *P* value of the slope calculated from the treatment starting point (arrow) is 0.04. D, photograph showing tumors dissected from vehicle or JNJ-42756493–treated mice after 2 weeks of treatment.

parenchyma (−44%) with formation of a cystic portion in the central core (33). The objective response was further corroborated by the marked reduction of the extent of tumor vascularity estimated by quantitative analysis of rCBV (relative cerebral blood volume) from dynamic susceptibility MR perfusion maps (37) (Fig. 4D). Stabilization lasted for 115 days. During JNJ-42756493 treatment, mild and manageable toxicity was observed (grade I hyperphosphatemia, asthenia, dysgueusia, dry mouth, keratitis, and grade II nail changes). After 4 months, tumor progressed on MRI locally both on T1 contrast-enhanced area and T2/FLAIR hypersignal. The patient was reoperated and subsequently treated with CCNU. He is still alive, but in progression after 21 months from diagnosis and 287 days from the start of the anti-FGFR therapy.

Patient 2 is a 64-year-old woman, affected by left parietal GBM, diagnosed by stereotactic biopsy. The tumor was positive for *FGFR3–TACC3* gene fusion by RT-PCR sequencing and showed diffuse FGFR3 expression in most tumor cells (Fig. 2A, C and E, sample 4620). The patient received as first-line treatment fractionated radiotherapy and temozolomide according to the Stupp protocol (36), but after 2 cycles of monthly temozolomide, she presented with clinical deterioration including progressive headaches, right homonymous hemianopsia, and memory impairment. Brain MRI performed 3 and 4 months after the completion of concomitant chemoradiotherapy revealed tumor progression with increase of the left parietal mass and the appearance of a small contralateral lesion (Fig. 4E). The patient was thus enrolled in the JNJ-42756493 trial (12 mg/d administered in cycles of 7 days followed by 7 days off-treatment) and showed clinical improvement after 4 weeks (regression of headaches, visual field defect, and memory impairment). Best response was observed after 104 days of treatment with a 22% reduction of tumor size according to the RANO criteria (Fig. 4F) and 28% according to volumetry (Fig. 4G). Grade I hyperphosphatemia, nail changes, and mucositis were observed. Clinical status remained stable until disease progression occurring 134 days after the start of the anti-FGFR therapy. The patient is still alive and is receiving a third-line chemotherapy with nitrosoureas and bevacizumab.

Discussion

FGFR–TACC fusions are potent oncogenic events that when present in brain tumor cells confer sensitivity to FGFR inhibitors (6). Since our original identification of recurrent *FGFR–TACC* fusions in GBM, small subgroups of patients harboring *FGFR–TACC* translocations have been identified in several other tumor types (7–15). Here, we report an unbiased RT-PCR-sequencing analysis for the identification of all possible functional *FGFR–TACC* fusion transcripts. The screening of a large glioma dataset from multiple institutions not only confirmed that *FGFR–TACC*

Published OnlineFirst January 21, 2015; DOI: 10.1158/1078-0432.CCR-14-2199

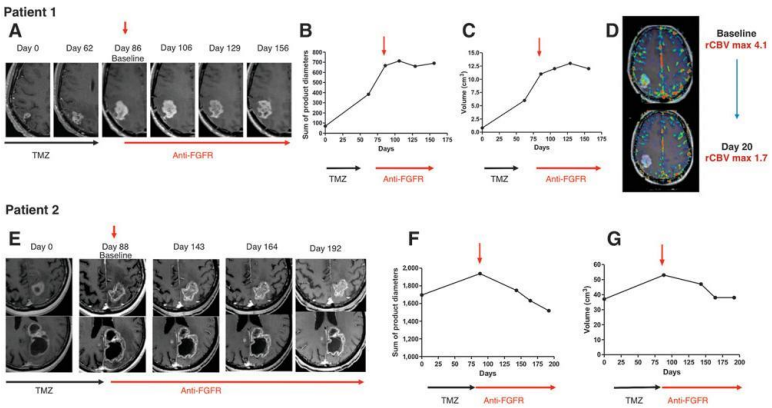

Figure 4.

Baseline and posttreatment MRI of patients treated with JNJ-42756493. Patient 1 (A–D). A, post-gadolinium T1-weighted images show the target lesion on the right parietal lobe. The interval (days) from the beginning of follow-up is indicated above each MRI. B, analysis of sum of product diameters (SPD) before and during the anti-FGFR treatment (RANO criteria). C, analysis of tumor volume (cm^3) before and during the anti-FGFR treatment. During anti-FGFR treatment, a stabilization of the tumor was observed according to RANO criteria and volumetry. D, perfusion images at baseline and after 20 days of anti-FGFR treatment. rCBV post-gadolinium T1-weighted images with color overlay of rCBV are shown. Patient 2 (E–G). E, two different MRI slice levels of superior and middle part of the lesion are presented. F, analysis of SPD before and during the anti-FGFR treatment. During the anti-FGFR treatment, a reduction of 22% of tumor size was observed. G, volumetric evaluation showed a 28% tumor reduction. Vertical red arrow indicates the start of anti-FGFR treatment (baseline).

rearrangements occur in about 3% of human GBM but also revealed that *FGFR–TACC* fusions are present in the subgroup of *IDH* wild-type lower grade glioma (grades II–III) with prevalence similar to that of GBM. *IDH* wild-type grade II and III glioma have a significantly worse clinical outcome than the *IDH*-mutant glioma and manifests molecular and clinical features that resemble GBM (5). Our finding that *FGFR–TACC* fusions occur in *IDH* wild-type but not in *IDH*-mutant glioma provides an important clue for the molecular characterization of this glioma subtype. Furthermore, the clustering of such potent oncogenic events in *IDH* wild-type glioma underscores the particularly aggressive nature of this group of glioma. While we showed that *FGFR–TACC* fusions cluster within the poor clinical outcome subgroup of *IDH* wild-type glioma, these translocations do not seem to carry prognostic value within the *IDH* wild-type subgroup of patients with glioma. However, the sample size of patients harboring *FGFR–TACC* fusions is too small to draw definitive conclusions with respect to the impact on survival, and larger studies will be necessary to clarify the prognostic role of *FGFR–TACC* fusions in *IDH* wild-type glioma.

Besides mutual exclusivity between *IDH1* mutations and *FGFR–TACC* fusions, our results showed that patients with *FGFR3–TACC3* rearrangements lack *EGFR* amplification and *EGFRvIII* but are significantly enriched for amplification of *CDK4* (and *MDM2* to a lesser extent). Knowledge of these molecular characteristics will help select those patients who most likely harbor *FGFR–TACC* rearrangements and design combinatorial targeted therapies that might be more effective in the *FGFR–TACC*–positive glioma subgroup.

The molecular screen uncovered 6 new *FGFR3–TACC3* fusion events. Together with the previously identified variants, others and we have reported 12 distinct isoforms of *FGFR3–TACC3*, thus revealing a remarkable variability of *FGFR3–TACC3* transcripts in human cancer (see Supplementary Table S1 summarizing the structure of all the *FGFR–TACC* variants identified to date). The structural heterogeneity of *FGFR3–TACC3* fusions is yet more pronounced at the genomic level, whereby each fusion event harbors distinct genomic breakpoints, even for identical fusion transcripts. This finding underscores the notion that targeted genomic analyses are unlikely to be suitable approaches for the molecular diagnosis of *FGFR3–TACC3* positivity. Conversely, the unbiased identification of *FGFR3–TACC3*–positive tumors with the RT-PCR sequencing assay reported here overcomes the limitations of screening only for previously identified *FGFR3–TACC3* fusions and provides a simple molecular diagnostic assay.

Rather than displaying uniform amplifications of the *FGFR3* and *TACC3* genomic loci, *FGFR3–TACC3*–positive samples harbor small, intragenic microamplification events typically encompassing only the exons of the *FGFR3* and *TACC3* genes included in the breakpoint (6). This finding is consistent with the notion that a "fusion breakpoint principle" sustains the CNVs of driver gene fusions such as *FGFR3–TACC3* in which local CNVs target exclusively the breakpoint region (38). We note that such small and irregular CNVs may easily go undetected from CNV analyses performed using platforms less-sensitive than the high-density SNP6.0 genomic arrays. Furthermore, the notion that *FGFR3–TACC3*-negative GBM may harbor uniform amplifications across

Published OnlineFirst January 21, 2015; DOI: 10.1158/1078-0432.CCR-14-2199

the *FGFR3* and *TACC3* loci argues against the standard analysis of *FGFR3* and/or *TACC3* CNVs as a method for the selection of *FGFR3–TACC3*–positive tumors.

There is a growing body of evidence supporting the notion that GBM is a markedly heterogeneous tumor. The formidable degree of intratumor heterogeneity of GBM is a potential cause of failure of targeted therapies in these tumors. In particular, the intratumor heterogeneity of GBM has previously been recognized in light of the mosaic expression of the RTK genes *EGFR*, *PDGFRA*, and *MET* by neighboring cells (16–19). Thus, in the majority of GBM, amplification or overexpression of individual RTK genes are present in a subclonal fraction of tumor cells and co-exist with amplification/expression of other RTK-coding genes within the tumor mass. Therefore, it was essential to determine whether such heterogeneity was also present in gliomas harboring *FGFR–TACC* translocations. The immunostaining of FGFR3–TACC3–positive tumors revealed that positive specimens manifest strong and uniform expression of the fusion protein, which is also retained after recurrence. This behavior is reminiscent of other driver chromosome translocations (*BCR-ABL*, *EML4-ALK*) and is compatible with the glioma-initiating functions of FGFR–TACC fusions (6). It is also the scenario expected for a driver oncogene whose activity remains essential for tumor maintenance regardless of secondary genetic alterations that occur during tumor progression.

The strong antitumor effects obtained with JNJ-42756493 in glioma cells harboring *FGFR3–TACC3* fusions have built a compelling rationale for the treatment of patients with glioma positive for *FGFR–TACC* rearrangements. JNJ-42756493 is an oral ATP-competitive pan-FGFR selective inhibitor that inhibits tyrosine phosphorylation of activated FGFR at nanomolar concentrations (34, 35). The enrollment of 2 patients with recurrent *FGFR3–TACC3*–positive GBM in a phase I trial with JNJ-42756493 showed that this treatment has tolerable toxicity and clear antitumor activity, thus validating FGFR–TACC as a therapeutic target. Therefore, targeted inhibition of FGFR-TK in preselected *IDH* wild-type FGFR–TACC–positive glioma may provide clinical benefits for patients with recurrent glioma who currently lack valuable therapeutic options. In conclusion, we have shown the importance and feasibility of prospective genotyping for *FGFR–TACC* fusions in patients with glioma and provided a preliminary evidence of clinical response that warrants the investigation of the sensitivity of gliomas harboring *FGFR–TACC* rearrangements to FGFR kinase inhibition in clinical trials.

Disclosure of Potential Conflicts of Interest

J. Savatovsky reports receiving speakers bureau honoraria from Bayer and Philips Healthcare. J.-C. Soria and J. Tabernero are consultant/advisory board members for Johnson & Johnson. No potential conflicts of interest were disclosed by the other authors.

Authors' Contributions

Conception and design: A.L. Di Stefano, M. Labussiere, A. Lasorella, M. Sanson, A. Iavarone

Development of methodology: A. Fucci, J.-C. Soria, A. Lasorella

Acquisition of data (provided animals, acquired and managed patients, provided facilities, etc.): A.L. Di Stefano, A. Fucci, V. Frattini, M. Labussiere, K. Mokhtari, Y. Marie, A. Bruno, B. Boisselier, M. Giry, J. Savatovsky, M. Touat, H. Belaid, A. Idbaih, C. Houillier, F.R. Luo, J. Tabernero, S. Yip, K. Petrecca, J.A. Chan, G. Finocchiaro, A. Lasorella, M. Sanson, M. Eoli

Analysis and interpretation of data (e.g., statistical analysis, biostatistics, computational analysis): A.L. Di Stefano, A. Fucci, V. Frattini, M. Labussiere, P. Zoppoli, B. Boisselier, J. Savatovsky, A. Kamoun, J.-C. Soria, A. Lasorella, M. Sanson, A. Iavarone

Writing, review, and/or revision of the manuscript: A.L. Di Stefano, A. Fucci, P. Zoppoli, M. Touat, F.R. Luo, J.-C. Soria, J. Tabernero, G. Finocchiaro, A. Lasorella, M. Sanson, A. Iavarone

Administrative, technical, or material support (i.e., reporting or organizing data, constructing databases): A.L. Di Stefano, M. Labussiere, M. Giry, R. Paterra, A. Lasorella

Study supervision: A. Lasorella, M. Sanson, A. Iavarone

Other (histologic diagnosis and immunochemical analysis of the tumoral samples): K. Mokhtari

Grant Support

This work was supported by National Cancer Institute grants R01CA101644 and R01CA131126 (to A. Lasorella) and R01CA178546 (to A. Iavarone), National Institute of Neurological Disorders and Stroke R01NS061776 (to A. Iavarone), and a grant from The Chemotherapy Foundation (to A. Iavarone), the French national program Cartes d'Identité des Tumeurs (CIT) (http://cit.ligue-cancer.net/; to M. Sanson), the Association pour la Recherche sur les Tumeurs cérébrales (ARTC; to M. Sanson). The research leading to these results received funding from the program "Investissements d'avenir" ANR-10-IAIHU-06. A. Fucci is supported by a fellowship from the Italian Ministry of Welfare/Provincia di Benevento. V. Frattini is supported by a fellowship from the American Brain Tumor Association (ABTA). A.L. Di Stefano was supported by the Fondation ICM and PRIN 2010–2011, 2010ZESJWN_008. S. Yip is supported by the mentored scientist award from the Vancouver Coastal Health Research Institute (VCHRI). Banking and distribution of brain tumor samples from UBC is made possible by generous financial support of BrainCare BC.

The costs of publication of this article were defrayed in part by the payment of page charges. This article must therefore be hereby marked *advertisement* in accordance with 18 U.S.C. Section 1734 solely to indicate this fact.

Received August 22, 2014; revised December 16, 2014; accepted January 4, 2015; published OnlineFirst January 21, 2015.

References

1. Medves S, Demoulin JB. Tyrosine kinase gene fusions in cancer: translating mechanisms into targeted therapies. J Cell Mol Med 2012;16:237–48.
2. Mitelman F, Johansson B, Mertens F. The impact of translocations and gene fusions on cancer causation. Nat Rev Cancer 2007;7:233–45.
3. Weathers SP, Gilbert MR. Advances in treating glioblastoma. F1000Prime Rep 2014;6:46.
4. Omuro A, DeAngelis LM. Glioblastoma and other malignant gliomas: a clinical review. JAMA 2013;310:1842–50.
5. Sanson M, Marie Y, Paris S, Idbaih A, Laffaire J, Ducray F, et al. Isocitrate dehydrogenase 1 codon 132 mutation is an important prognostic biomarker in gliomas. J Clin Oncol 2009;27:4150–4.
6. Singh D, Chan JM, Zoppoli P, Niola F, Sullivan R, Castano A, et al. Transforming fusions of FGFR and TACC genes in human glioblastoma. Science 2012;337:1231–5.
7. Cancer Genome Atlas Research N. Comprehensive molecular characterization of urothelial bladder carcinoma. Nature 2014;507:315–22.
8. Majewski IJ, Mittempergher L, Davidson NM, Bosma A, Willems SM, Horlings HM, et al. Identification of recurrent FGFR3 fusion genes in lung cancer through kinome-centred RNA sequencing. J Pathol 2013;230:270–6.
9. Parker BC, Annala MJ, Cogdell DE, Granberg KJ, Sun Y, Ji P, et al. The tumorigenic FGFR3-TACC3 gene fusion escapes miR-99a regulation in glioblastoma. J Clin Invest 2013;123:855–65.
10. Wang R, Wang L, Li Y, Hu H, Shen L, Shen X, et al. FGFR1/3 tyrosine kinase fusions define a unique molecular subtype of non-small cell lung cancer. Clin Cancer Res 2014;20:4107–14.
11. Williams SV, Hurst CD, Knowles MA. Oncogenic FGFR3 gene fusions in bladder cancer. Hum Mol Genet 2013;22:795–803.

Published OnlineFirst January 21, 2015; DOI: 10.1158/1078-0432.CCR-14-2199

12. Wu YM, Su F, Kalyana-Sundaram S, Khazanov N, Ateeq B, Cao X, et al. Identification of targetable FGFR gene fusions in diverse cancers. Cancer Discov 2013;3:636–47.
13. Zhang J, Wu G, Miller CP, Tatevossian RG, Dalton JD, Tang B, et al. Whole-genome sequencing identifies genetic alterations in pediatric low-grade gliomas. Nat Genet 2013;45:602–12.
14. Capelletti M, Dodge ME, Ercan D, Hammerman PS, Park SI, Kim J, et al. Identification of recurrent FGFR3-TACC3 fusion oncogenes from lung adenocarcinoma. Clin Cancer Res 2014;20:6551–8.
15. Stransky N, Cerami E, Schalm S, Kim JL, Lengauer C. The landscape of kinase fusions in cancer. Nat Commun 2014;5:4846.
16. Inda MM, Bonavia R, Mukasa A, Narita Y, Sah DW, Vandenberg S, et al. Tumor heterogeneity is an active process maintained by a mutant EGFR-induced cytokine circuit in glioblastoma. Genes Dev 2010;24:1731–45.
17. Snuderl M, Fazlollahi L, Le LP, Nitta M, Zhelyazkova BH, Davidson CJ, et al. Mosaic amplification of multiple receptor tyrosine kinase genes in glioblastoma. Cancer Cell 2011;20:810–7.
18. Ene CI, Fine HA. Many tumors in one: a daunting therapeutic prospect. Cancer Cell 2011;20:695–7.
19. Sottoriva A, Spiteri I, Piccirillo SG, Touloumis A, Collins VP, Marioni JC, et al. Intratumor heterogeneity in human glioblastoma reflects cancer evolutionary dynamics. Proc Natl Acad Sci U S A 2013;110:4009–14.
20. Kindich R, Florl AR, Jung V, Engers R, Muller M, Schulz WA, et al. Application of a modified real-time PCR technique for relative gene copy number quantification to the determination of the relationship between NKX3.1 loss and MYC gain in prostate cancer. Clin Chem 2005;51:649–52.
21. Bulusu KC, Tym JE, Coker EA, Schierz AC, Al-Lazikani B. canSAR: updated cancer research and drug discovery knowledgebase. Nucleic Acids Res 2014;42:D1040–7.
22. Reyes-Botero G, Giry M, Mokhtari K, Labussiere M, Idbaih A, Delattre JY, et al. Molecular analysis of diffuse intrinsic brainstem gliomas in adults. J Neurooncol 2014;116:405–11.
23. Labussière M, Boisselier B, Mokhtari K, Di Stefano AL, Rahimian A, Rossetto M, et al. Combined analysis of TERT, EGFR and IDH status defines distinct prognostic glioblastoma classes. Neurology 2014;83:1200–6.
24. Quillien V, Lavenu A, Karayan-Tapon L, Carpentier C, Labussiere M, Lesimple T, et al. Comparative assessment of 5 methods (methylation-specific polymerase chain reaction, MethyLight, pyrosequencing, methylation-sensitive high-resolution melting, and immunohistochemistry) to analyze O6-methylguanine-DNA-methyltranferase in a series of 100 glioblastoma patients. Cancer 2012;118:4201–11.
25. Idbaih A, Aimard J, Boisselier B, Marie Y, Paris S, Criniere E, et al. Epidermal growth factor receptor extracellular domain mutations in primary glioblastoma. Neuropathol Appl Neurobiol 2009;35:208–13.
26. Idbaih A, Marie Y, Lucchesi C, Pierron G, Manie E, Raynal V, et al. BAC array CGH distinguishes mutually exclusive alterations that define clinicogenetic subtypes of gliomas. Int J Cancer 2008;122:1778–86.
27. Gonzalez-Aguilar A, Idbaih A, Boisselier B, Habbita N, Rossetto M, Laurenge A, et al. Recurrent mutations of MYD88 and TBL1XR1 in primary central nervous system lymphomas. Clin Cancer Res 2012;18:5203–11.
28. Olshen AB, Venkatraman ES, Lucito R, Wigler M. Circular binary segmentation for the analysis of array-based DNA copy number data. Biostatistics 2004;5:557–72.
29. Hoang-Xuan K, He J, Huguet S, Mokhtari K, Marie Y, Kujas M, et al. Molecular heterogeneity of oligodendrogliomas suggests alternative pathways in tumor progression. Neurology 2001;57:1278–81.
30. Houillier C, Lejeune J, Benouaich-Amiel A, Laigle-Donadey F, Criniere E, Mokhtari K, et al. Prognostic impact of molecular markers in a series of 220 primary glioblastomas. Cancer 2006;106:2218–23.
31. Goldman M, Craft B, Swatloski T, Ellrott K, Cline M, Diekhans M, et al. The UCSC cancer genomics browser: update 2013. Nucleic Acids Res 2013;41:D949–54.
32. Brennan CW, Verhaak RG, McKenna A, Campos B, Noushmehr H, Salama SR, et al. The somatic genomic landscape of glioblastoma. Cell 2013;155:462–77.
33. Wen PY, Macdonald DR, Reardon DA, Cloughesy TF, Sorensen AG, Galanis E, et al. Updated response assessment criteria for high-grade gliomas: response assessment in neuro-oncology working group. J Clin Oncol 2010;28:1963–72.
34. Bahleda R, Dienstmann R, Adamo B, Gazzah A, Infante JR, Zhong B, et al. Phase 1 study of JNJ-42756493, a pan-fibroblast growth factor receptor (FGFR) inhibitor, in patients with advanced solid tumors. J Clin Oncol 2014;32:suppl; abstr 2501.
35. Squires M, Ward G, Saxty G, Berdini V, Cleasby A, King P, et al. Potent, selective inhibitors of fibroblast growth factor receptor define fibroblast growth factor dependence in preclinical cancer models. Mol Cancer Ther 2011;10:1542–52.
36. Stupp R, Mason WP, van den Bent MJ, Weller M, Fisher B, Taphoorn MJ, et al. Radiotherapy plus concomitant and adjuvant temozolomide for glioblastoma. N Engl J Med 2005;352:987–96.
37. Law M, Yang S, Babb JS, Knopp EA, Golfinos JG, Zagzag D, et al. Comparison of cerebral blood volume and vascular permeability from dynamic susceptibility contrast-enhanced perfusion MR imaging with glioma grade. AJNR Am J Neuroradiol 2004;25:746–55.
38. Wang XS, Prensner JR, Chen G, Cao Q, Han B, Dhanasekaran SM, et al. An integrative approach to reveal driver gene fusions from paired-end sequencing data in cancer. Nat Biotechnol 2009;27:1005–11.

Published OnlineFirst January 21, 2015; DOI: 10.1158/1078-0432.CCR-14-2199

AACR American Association for Cancer Research

Clinical Cancer Research

Detection, Characterization, and Inhibition of FGFR–TACC Fusions in IDH Wild-type Glioma

Anna Luisa Di Stefano, Alessandra Fucci, Veronique Frattini, et al.

Clin Cancer Res 2015;21:3307-3317. Published OnlineFirst January 21, 2015.

4.1.1 SUPPLEMENTARY MATERIALS

Supplementary Figures and Tables

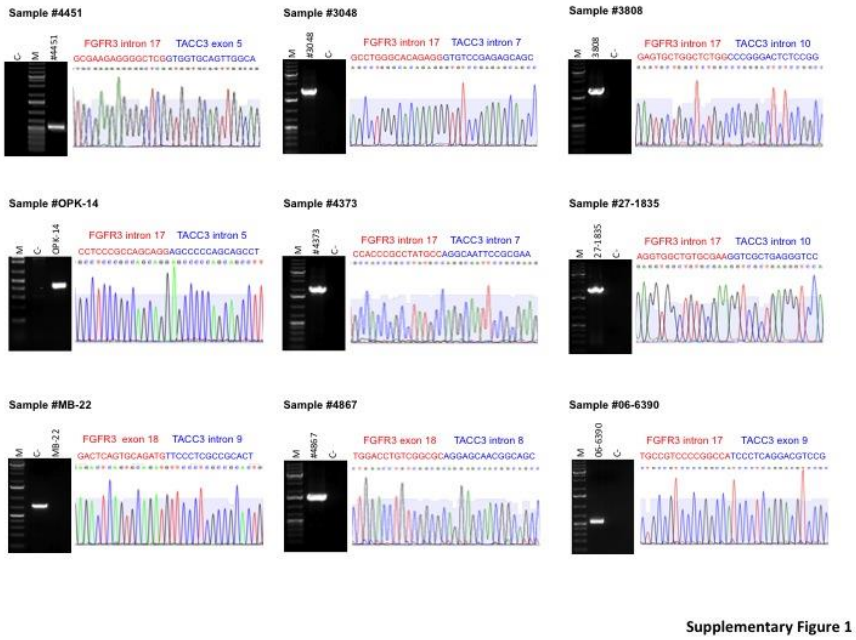

Supplementary Figure 1 from article (Di Stefano, 2015).
Genomic PCR images and Sanger sequences of *FGFR3-TACC3* genomic breakpoints. Fusion specific PCR products and Sanger sequencing chromatograms showing the *FGFR3-TACC3* genomic breakpoints. The genomic sequences corresponding to *FGFR3* and *TACC3* are indicated in red or blue, respectively. M, DNA adder; C-, Negative Control.

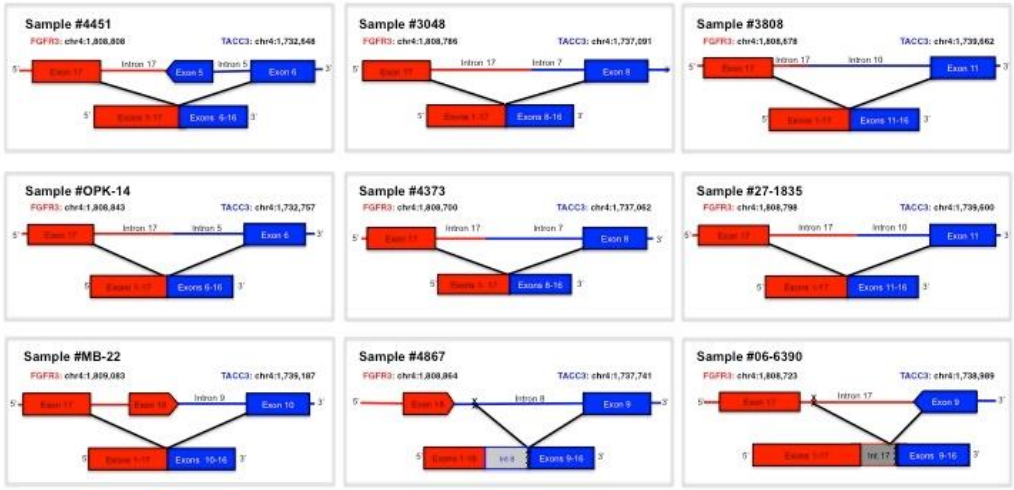

Supplementary Figure 2 from article (Di Stefano, 2015).
Schematics of *FGFR3-TACC3* genomic break points. Schematic representation of the genomic fusions between *FGFR3* and *TACC3* compared to the corresponding mRNA in red and blue report the regions belonging to *FGFR3* and *TACC3*, respectively. The genomic breakpoint coordinates, according to the genome build GRCh37/hg19, are indicated above each fusion gene.

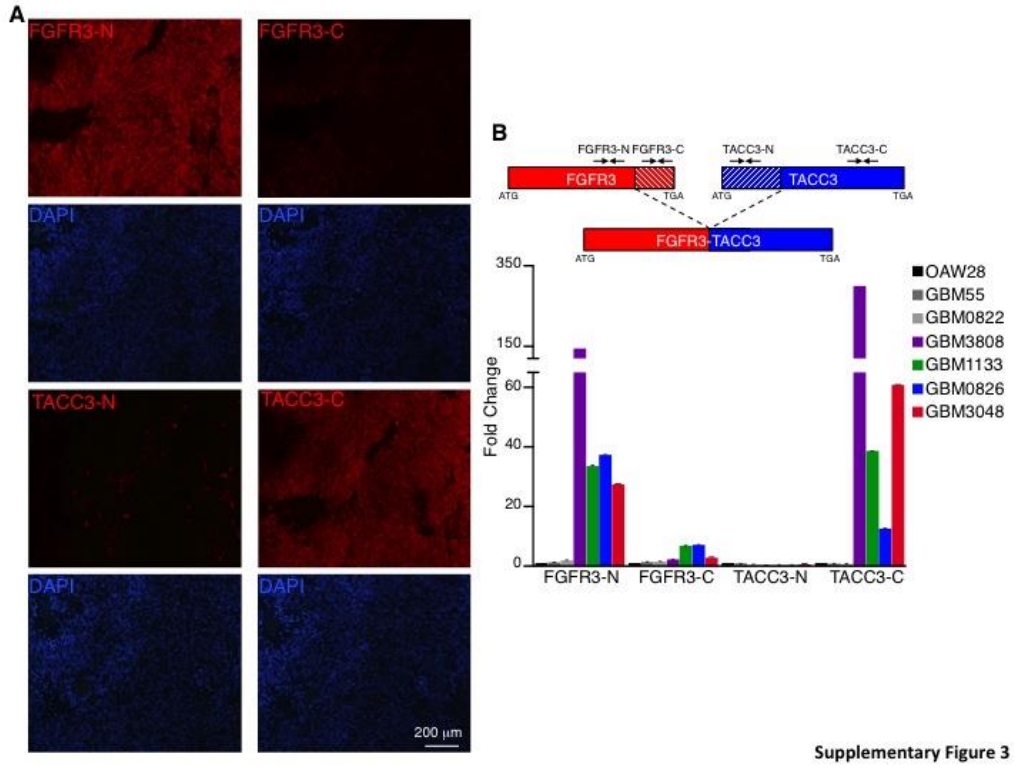

Supplementary Figure 3 from article (Di Stefano, 2015).
Evaluation of the expression of *FGFR3-TACC3* fusion elements. (A) Microphotographs of immunofluorescence staining of a representative GBM harboring *FGFR3-TACC3* fusion using antibodies that recognize the N- and C- termini of FGFR3 (FGFR3-N, FGFR3-C) and TACC3 (TACC3-N, TACC3-C), are in red. Nuclei are counterstained with DAPI, shown in blue. (B) Quantitative RT-PCR of four representative GBM carrying *FGFR3-TACC3* fusion and three negative controls using primer pairs that amplify *FGFR3* and *TACC3* regions included in or excluded from the fusion transcripts, as indicated in the diagram. OAW28: ovarian cystoadenocarcinoma cell line harboring wild-type *FGFR3* and *TACC3* genes; GBM55 and GBM0822: GBM harboring wild-type *FGFR3* and *TACC3* genes; GBM3808; GBM1133; GBM0826; GBM3048: GBM harboring *FGFR3-TACC3* (*F3-T3*) fusion. Error bars are SD of triplicate samples.

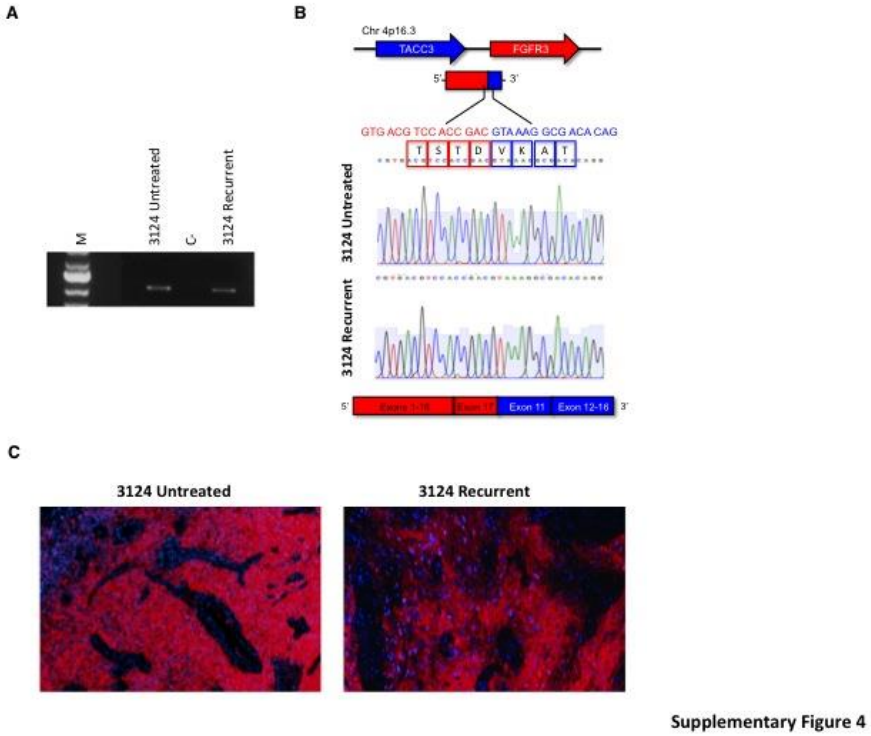

Supplementary Figure 4

Supplementary Figure 4 from article (Di Stefano, 2015).
The *FGFR3-TACC3* fusion gene and protein are retained in recurrent GBM. (A) *FGFR3-TACC3* fusion specific RT-PCR product from untreated and recurrent GBM from patient #3124. (B) Sanger sequencing chromatogram showing the identical reading frame at the breakpoint and the putative translation of the fusion protein in the untreated and recurrent tumor from the same patient. The fused exons at mRNA level are shown. Regions corresponding to *FGFR3* and *TACC3* are indicated in red and blue, respectively. T = threonine; S = serine; D = aspartic acid; V = valine; K = lysine; and A = alanine. (C) Representative microphotographs of FGFR3 immunofluorescence (IF) staining in both untreated and recurrent GBM. Blue staining indicates DAPI; Red staining indicates *FGFR3*. Magnification is 10x.

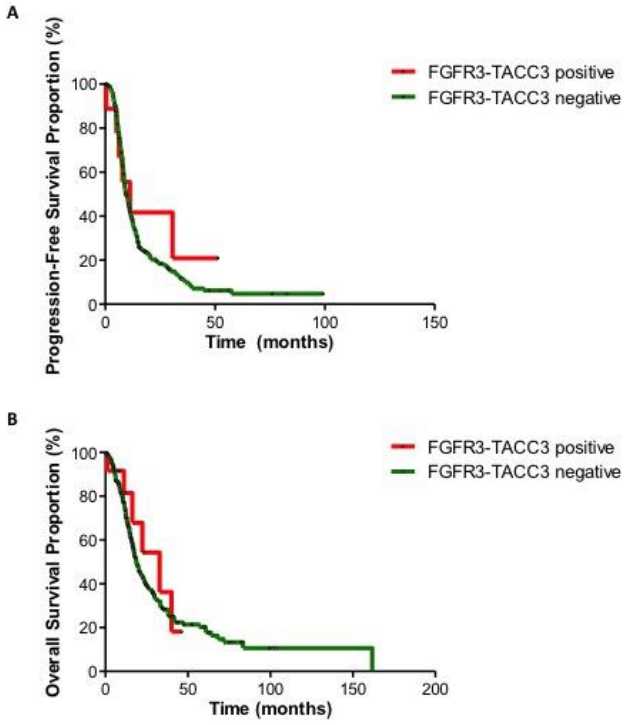

Supplementary Figure 5 from article (Di Stefano, 2015).
PFS and OS of *FGFR3-TACC3*-positive glioma patients. (A) Kaplan-Meier curves in *IDH* wild-type glioma patients don't show significant differences in Progression Free Survival (PFS) between *FGFR3-TACC3* positive (N=12, median PFS=11.20 months) and *FGFR3-TACC3* negative (N=274, Median PFS= 12.27 months) (*P*=0.85). (B) Kaplan-Meier curves in *IDH* wild-type glioma patients don't show significant differences in Overall Survival (OS) between *FGFR3-TACC3* positive (N=12, Median OS=32.80 months) and *FGFR3-TACC3* negative (N=326, Median OS=18.60 months) (*P*=0.6). Red indicates *FGFR3-TACC3* positive patients and green indicates *FGFR3-TACC3* negative patients. Open circles represent censored patients.

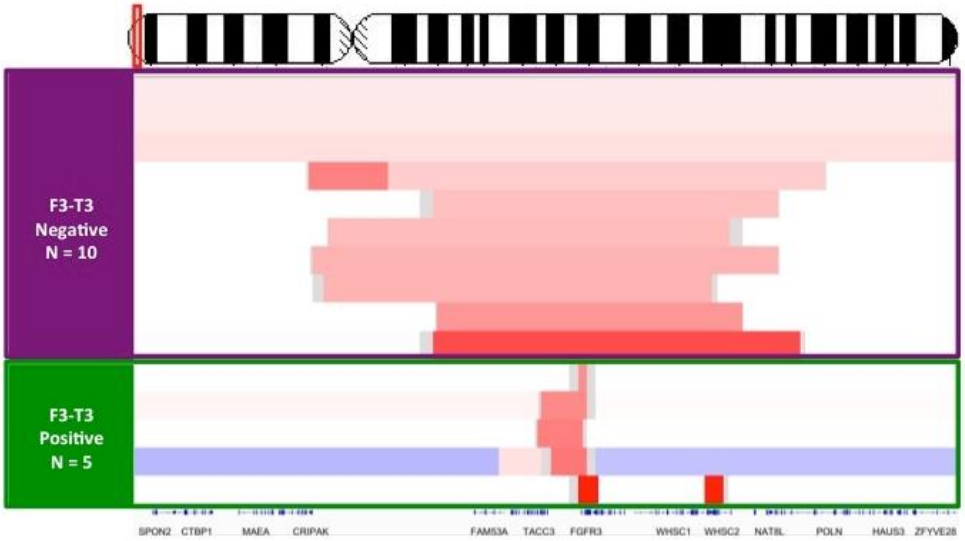

Supplementary Figure 6

Supplementary Figure 6 from article (Di Stefano, 2015). Analysis of SNP6.0 arrays of GBM harboring CNVs of *FGFR3* and *TACC3* genomic loci. CNVs of the *FGFR3*/*TACC3* genomic loci in "gain labeled" (LRR > 0.2) TCGA samples. The CNA magnitudes (expressed as log2 ratio) were classified using simple thresholds:
deletion ($x < -1$), loss ($-1 < x \leq -0.2$), gain ($0.2 \leq x <$) or amplification ($x >$). Gains are in gradients of red, losses in gradients of blue. Samples with uniform gains/amplification of *FGFR3* and *TACC3* lack *FGFR3-TACC3* fusions. Samples harboring *FGFR3-TACC3* fusions (*F3-T3*) show microamplifications involving the first *FGFR3* exons, which are spliced in the fusion gene.

FGFR-TACC Fusion Variant		N Cases	Tumor Type
FGFR3-TACC3	FGFR3exon17-TACC3exon11	29	**Brain Tumors, N=10** (N=2,[6]. N=2,[9]. N=6, Present Study).
			Bladder Cancer, N=6 (N=3,[12]. N=3,[11]).
			Lung Cancer, N=13 (N=4,[17]. N=9,[10]).
	FGFR3exon17-TACC3exon10	17	**Brain Tumors, N=5** (N=1,[6]. N=1,[9]. N=3, Present study).
			Oral Cancer, N=1,[12].
			Head and Neck Cancers, N=2,[12].
			Bladder Cancer, N=3,[7].
			Lung Cancer, N=5 (N=4,[8]. N=2,[10]).
	FGFR3exon17-TACC3exon8	7	**Brain Tumors, N=6** (N=2,[6]. N=4, Present study).
			Lung Cancer, N=1,[10].
	FGFR3exon17-TACC3exon4	3	**Brain Tumors, N=2** (N=1,[9]. N=1,[13]).
			Bladder Cancer, N=1[9].
	FGFR3exon17-TACC3exon6	2	**Brain Tumors, N=2,** Present study.
	FGFR3exon18-TACC3exon4	1	**Brain Tumors, N=1,** Present study.
	FGFR3exon17-TACC3exon9 INS63bp	1	**Brain Tumors, N=1,**[6].
	FGFR3exon18-TACC3exon9 INS66bp	1	**Brain Tumors, N=1,** Present study.
	FGFR3exon18-TACC3exon5	1	**Brain Tumors, N=1,** Present study.
	FGFR3exon18-TACC3exon5 INS33bp	1	**Brain Tumors, N=1,** Present study.
	INS71bp	1	**Lung Cancers, N=1,**[10].
	FGFR3exon18-TACC3exon13	1	**Brain Tumors, N=1,** Present study.
	FGFR3exon18-TACC3exon11	1	**Lung Cancers, N=1,**[10].
FGFR1-TACC1	FGFR1exon17-TACC1exon7	5	**Brain Tumors, N=5** (N=1,[6]. N=3,[13]; N=1, Present study).

Supplementary Table 1

Supplementary Table 1 from article (Di Stefano, 2015). Summary of *FGFR-TACC* fusion transcripts identified in all cancer types. *FGFR3-TACC3* fusion variants are ranked according to their prevalence across any cancer type. The number of *FGFR-TACC* fusions identified in each tumor type, including those identified in the present study, is also indicated.

4.2 Clinical Phenotype, Genetic Background and Correlations with *FGFR3* Expression of *FGFR-TACC* Positive Gliomas

4.2.1 BACKGROUND

FGFR-TACC fusions are potent oncogenic events that when present in brain tumor cells confer sensitivity to *FGFR* inhibitors (Singh, 2012) that had been detected as a recurrent event in about 3% of *IDH*-wild type gliomas.

We have recently reported an unbiased screening assay for *FGFR–TACC* fusions by RT-PCR in glioma that overcomes the great variability of variants that are generated by *FGFR–TACC* chromosomal translocation and we described the spectrum of transcripts, genomic breakpoints and molecular features of the 15 gliomas (12 GBMs and 3 lower grade gliomas) identified at that time (Di Stefano, 2015). However, exhaustivity was affected by the rarity of this aberration and the small sample size collected.

In the same study, we observed that all the 15 *FGFR–TACC*–positive glioma displayed strikingly uniform and strong expression of the FGFR3-N terminus as a result of accumulation of the fusion protein, suggesting that *FGFR-TACC* fusions are early events compatible with the glioma-initiating functions (Di Stefano, 2015).

Based on this observation we hypothesized that immunostaining using an antibody that recognized the N-terminus of FGFR3 might be useful as a pre-screening method on paraffin embedded samples, but no data on sensitivity and specificity were available from a prospective cohort.

In this study we perform an institutional prospectic binary screening for *FGFR-TACC* fusions by IHC and by RT-PCR in all new diagnosed *IDH* wild-type gliomas in *Pitié-Salpétrière Hospital*. We calculate predictive values of IHC regarding the presence of the *FGFR-TACC* fusion transcripts, and we depict clinical features of a multicentric case series of 40 *FGFR3-TACC3* positive glioma patients, the largest series identified to date.

4.2.2 METHODS

Patient and Tissue Samples

This study includes a cohort of patients with histologic diagnosis of glioma from 9 institutions in the setting of ANOCEF (Association des Neuro-Oncologue d'Expression Française) and POLA French Networks (Hopital Pitié-Salpétrière, Onconeurotek, Paris; Hopitaux Civils de Lyon; Hopital Foch Suresnes; Institut du Cancers d'Angers; Hopital la Timone, Marseille; CHU Bordeaux, Hôpital Roger Salengro, Lille; CHU de Toulouse).

This cohort included a retrospective series of glioma patients from *Pitié-Salpétriere Hospital*, being the object of a previous publication (Di Stefano, 2015), a new prospective series of newly diagnosed glioma patients starting from January 2014 from *Pitié-Salpétriere Hospital*, and cases from other institutions.

In the prospective cohort, all cases underwent parallel-blinded analysis by FGFR3 IHC and RT-PCR while cases from other institutions were addressed at our centre in order to perform RT-PCR, screening for the fusion transcripts after local detection of FGFR3 expression by IHC.

Tumor specimens, blood samples and clinico-pathological information were collected with informed consent and relevant ethical board approval in accordance with the tenets of the Declaration of Helsinki. For the samples from the *Pitié-Salpêtrière Hospital*, clinical data and follow-up are available in the neuro-oncology database (Onconeurotek, GH Pitié-Salpêtrière, Paris).

Identification of Fusion Transcripts and analysis of Genomic Breakpoints

Total RNA was extracted from frozen tissues using Trizol (Invitrogen) according to manufacturer instructions. Two to three hundred nanograms of total RNA were

retro-transcribed with the Maxima First Strand cDNA Synthesis Kit (Thermo Scientific) or SuperScript II (Invitrogen). RT-PCR was

Performed using AccuPrime Taq DNA Polymerase (Invitrogen). Primer pairs used for the *FGFR3-TACC3* fusions screening were: *FGFR3*ex12-FW: 5'-CGTGAAGATGCTGAAAGACGATG-3 and *TACC3*ex14-RV: 5'-AAACGCTTGAAGAGGTCGGAG; amplification conditions were 94°C-3min, (94°C-30sec/61°C-30sec/68°C-1min40sec) for 35 cycles, 68°C-7min. *FGFR1-TACC1* fusions were amplified with *FGFR1*ex16-FW: 5'-TGCCTGTGGAGGAACTTTTCA-3' and *TACC1*ex13-RV: 5'-CCCAAACTCAGCAGCCTAAG-3' primers (94°C-30sec/60°C-30sec/68°C-1min40sec for 35 cycles). PCR products were subjected to Sanger sequencing.

Immunohistochemistry and Histological Diagnosis

For the immunohistochemical analysis (IHC) of FGFR3 expressions, deparaffinization and immunolabeling of the sections were performed by a fully automated immunohistochemistry system Ventana benchmark XT system® (Roche, Basel, Switzerland) using as primary antibody the mouse monoclonal anti-FGFR-3 diluted 1:500 (clone B9, Santa Cruz Biotechnology), and using as chromogen: streptavidin–peroxidase complex with diaminobenzidin. The percentage of immunopositive tumor cells among the total number of tumor cells together with the maximal intensity of the immunolabelling were evaluated by visual semi-quantitative examination and tumor samples were then classified according to "weak", "moderate" and "intense" staining for FGFR3. Integrated diagnosis was reviewed according to WHO 2016 (Louis, 2016) by two independent expert pathologists (KM and FB).

Molecular Characterization of Tumor Samples

Mutational status of *IDH1*, *IDH2*, *TERT* promoter, Histones *H3B* and *H3F3A*, *PTEN*, *BRAF* V600, was analysed as well as the methylation status of the *MGMT* promoter.

Expression of *IDH1-R132H* mutation was analyzed by IHC as previously described (Reyes-Botero, 2014) and *IDH1* and *IDH2* gene mutations were identified by Sanger sequencing (Sanson, 2009).

IDH wild-type tumors are defined according to the absence of IDH1-R132H immunopositivity and/or mutations in *IDH1* and *IDH2* genes. *TERT* promoter status was determined by the Sanger sequencing (Labussiere, 2014; Labussiere, 2014).

Hyper-methylation of the *MGMT* promoter was tested by bisulphite pyro-sequencing (Quillien, 2012). The presence of *EGFRvIII* was evaluated by RT-PCR using *EGFR*- FW5′- TTCGGGGAGCAGCGATGCGAC-3′and *EGFR*-RV ′CTGTCCATCCAGAGG AGGAGTA-3′ primers (Idbaih, 2009).

Copy number variations analyses have been performed using CGH arrays using BAC arrays (N=235). Results were normalized using control DNA from matched blood samples as previously described (Idbaih, 2008). Additional analyses of 154 tumor specimens were performed by SNP array, using Illumina Omni (Gonzalez-Aguilar, 2012). Array processing was outsourced to Integragen. Raw copy numbers were estimated at each of the SNP and copy-number markers. The bio-discovery property SNP-FASST2 algorithm was then used to segment copy number data. Segments were mapped to hg18 genome assembly (Olshen, 2004). Copy number alterations (CAN) magnitudes called log-R ratio (LRR) were classified using simple thresholds: deletion ($x \leq -1$), loss ($-1 < x \leq -0.2$), gain ($0.2 \leq x <$) or amplification ($x \geq$) according to default Nexus 7.5 software.

Targeted gene capture followed by sequencing with parallel next-generation sequencing (NGS) for *IDH1*, *IDH2*, *TERT* promoter, *H3B* and *H3F3A*, *BRAF*

V600 mutations, *EGFR*, *CDK4*, *MDM2* amplifications, p16 deletions and chromosomal gain and losses was performed in 29 glioma cases.

Statistical Analysis

Differences in the distribution on categorical variables were analyzed using Fisher Exact test. The *P* values were adjusted for multiple testing according to the Benjamini and Hochberg false discovery rate (FDR). A q-value of 0.05 (2-sided) was considered to be statistically significant.
Overall survival (OS) was defined as the time between the diagnosis and death or last follow-up. Patients who were still alive at the last follow-up were considered as censored events in the analysis. Progression-free survival (PFS) was defined as the time between the diagnosis and recurrence or last follow-up. Patients who were recurrence-free at the last follow-up were considered as censored events in the analysis. Survival curves were calculated by the Kaplan-Meier method and differences between curves assessed using the Log-Rank test. A Log-Rank test p-value ≤ 0.05 (two-sided) was considered to be statistically significant. Chi-square tested sensitivity, specificity, and positive and negative predictive values of FGFR3 staining to detect the presence of *FGFR3-TACC3* fusions.

4.2.3 RESULTS

To determine the frequency and features of *FGFR–TACC* fusions in human patients with glioma, we screened a cohort of 907 gliomas (655 grade IV, 144 grade III and 108 grade II).

This cohort included a retrospective series of 591 glioma patients from Pitié Salpétriere, being object of a previous publication (Di Stefano et al. 2015), a new prospective series of 236 newly diagnosed glioma patients starting from January 2014 from *Pitié Salpétriere Hospital* and 80 supplementary cases from other institutions.

176 cases had *IDH* mutations (36 grade IV, 72 grade III and 68 grade IV).
The RT-PCR assay was used for screening, as previously reported (Di Stefano, 2015), which allows for the detection of possible variants of *FGFR3–TACC3* fusions that retain the mRNA sequences coding for the key FGFR-TK and TACC domains required for the oncogenic activity of the fusion protein.
Overall, we found 40 tumors harbouring *FGFR3–TACC3* fusions. According to the 2016 WHO classification, 34 were glioblastoma *IDH* wild-type, 3 anaplastic astrocytoma *IDH* wild-type and 3 diffuse astrocytoma grade II *IDH* wild-type (see **Table 4.2.1**).
In this cohort, results were consistent with what we previously discovered in that all glioma harbouring *FGFR3-TACC3* fusions are *IDH* wild-type.
Conversely, all 176 *IDH* mutated gliomas of the cohort were negative for *FGFR3-TACC3* fusions.

Sanger sequencing of the fusion amplicons revealed that each *FGFR–TACC* cDNA joined in-frame the sequence coding for the entire TK domain upstream of *TACC* coding sequences that invariably include the coiled-coil TACC.
We confirmed, in these larger series', that *FGFR3–TACC3* fusion isoforms are notably variable, even though isoforms *FGFR3*-exon 17-*TACC3*-exon 11 (17/40, 42%), *FGFR3*-exon 17-*TACC3*-exon 10 (12/40, 30%) and *FGFR3*-exon 17-*TACC3*-exon 8 (4/40, 10%) occurred more frequently. Seven supplementary variants occurred only in individual cases (**Table. 4.2.1**). Among them, we identified two new fusion transcripts (*FGFR3*-exon 17-*TACC3*-exon 13 and *FGFR3*-exon 17-*TACC3*-exon 4) as new variant currently unreported (underlined in **Table 4.2.1**).
Range of size of the *FGFR3–TACC3* RT-PCR amplicons was comprised between 805 bp (for *FGFR3*ex18-*TACC3*ex13) and 1706 bp (for *FGFR3*ex18-*TACC3*ex4), comparing to our previous findings (Di Stefano, 2015).

Clinical and histo-molecular features (according to WHO 2016) of patients harbouring *FGFR3-TACC3* fusions in this series are detailed in **Table 4.2.1**.

Sex ratio was 0.9 (21 females and 19 males); median age at diagnosis was 61 years old (range 35-87).

Information on tumor location was available for all patients harbouring *FGFR3-TACC3* fusions**.** In all 40 patients, *FGFR3-TACC3* gliomas are supra-tentorial and located in cerebral lobes. No patients present tumors in the deep structures of the cerebrum, ventricles, cerebellum or in the brainstem**.** Gliomas in the frontal lobe accounted for 40% (16/40), temporal lobe for 27% (11/40), parietal/parieto-occipital lobe for 30% (12/40) and occipital lobe for 1 out of 40.

Gliomas were located more frequently in the right hemisphere (58%; 23/40) than in the left (42%; 17/40).

Pt	Sex	Age at diagnosis	Location	Histological diagnosis	FGFR3 IHC max intensity	FGFR3-TACC3 fusion variant	Outcome at end of follow-up	OS months	Series
1	M	75	Right Parieto-occipital lobes	glioblastoma IDH wild-type	Moderate	FGFR 3 EX17 TACC3 EX 11	Dead	11.2	Di Stefano et al. 2015
2	M	64	Right Temporal lobe	glioblastoma IDH wild-type	Intense	FGFR 3 EX17 TACC3 EX 11	Dead	18.4	Present study
3	M	64	Right Frontal lobe	glioblastoma IDH wild-type	Intense	FGFR 3 EX17 TACC3 EX 11	Alive	56.9	Present study
4	M	41	Right Frontal lobe	glioblastoma IDH wild-type	Intense	FGFR 3 EX17 TACC3 EX 11	Alive	39.4	Present study
5	F	60	Left Frontal lobe	glioblastoma IDH wild-type	Intense	FGFR 3 EX17 TACC3 EX 11	Alive	18.9	Present study
6	F	44	Left Frontal lobe	glioblastoma IDH wild-type	Intense	FGFR 3 EX17 TACC3 EX 11	Alive	23.2	Present study
7	F	61	Left Frontal lobe	glioblastoma IDH wild-type	Intense	FGFR 3 EX17 TACC3 EX 11	Alive	16.2	Present study
8	F	72	Right Frontal lobe/Corpus callosum	glioblastoma IDH wild-type	Intense	FGFR 3 EX17 TACC3 EX 11	Alive	3.9	Present study
9	M	55	Left Parieto-occipital lobes	glioblastoma IDH wild-type	Intense	FGFR 3 EX17 TACC3 EX 11	Alive	20.4	Present study
10	F	64	Right Temporo-insular lobes	glioblastoma IDH wild-type	Intense	FGFR 3 EX17 TACC3 EX 11	Alive	5.5	Present study
11	F	68	Left Temporo-parietal lobes	glioblastoma IDH wild-type	Weak	FGFR 3 EX17 TACC3 EX 11	Alive	14.1	Present study
12	M	41	Right Frontal lobe	anaplastic astrocytoma IDH wild-	Intense	FGFR 3 EX17 TACC3 EX 11	Dead	15.1	Present study
13	M	75	Right Parieto-occipital lobes	glioblastoma IDH wild-type	Intense	FGFR 3 EX17 TACC3 EX 11	Alive	8.0	Present study
14	M	46	Left Frontal lobe	glioblastoma IDH wild-type	Intense	FGFR 3 EX17 TACC3 EX 11	Alive	13.9	Present study
15	F	44	Left Frontal lobe	anaplastic astrocytoma IDH wild-	na	FGFR 3 EX17 TACC3 EX 11	Dead	50.5	Present study
16	M	76	Right Parietal lobe	glioblastoma IDH wild-type	Intense	FGFR 3 EX17 TACC3 EX 11	Dead	10.0	Present study
17	F	66	Left Frontal lobe	glioblastoma IDH wild-type	Intense	FGFR 3 EX17 TACC3 EX 11	Dead	40.1	Di Stefano et al. 2015
18	F	79	Right Frontal lobe	glioblastoma IDH wild-type	Moderate	FGFR 3 EX17 TACC3 EX 13	Alive	8.9	Present study
19	M	46	Right Parietal lobe	glioblastoma IDH wild-type	Intense	FGFR 3 EX17 TACC3 EX 4	Alive	28.5	Present study
20	M	53	Right Parieto-occipital lobes	glioblastoma IDH wild-type	Intense	FGFR 3 EX17 TACC3 EX 6	Dead	28.4	Di Stefano et al. 2015
21	M	50	Right Parieto-occipital lobes	glioblastoma IDH wild-type	Intense	FGFR 3 EX17 TACC3 EX 8	Alive	77.8	Di Stefano et al. 2015
22	F	64	Left Parietal lobe	glioblastoma IDH wild-type	Intense	FGFR 3 EX17 TACC3 EX 8	Alive	18.3	Di Stefano et al. 2015
23	M	58	Left Parieto-occipital lobes	glioblastoma IDH wild-type	Intense	FGFR 3 EX17 TACC3 EX 8	Alive	40.2	Di Stefano et al. 2015
24	F	51	Left Fronto-insular lobes	glioblastoma IDH wild-type	Intense	FGFR 3 EX17 TACC3 EX 8	Alive	4.1	Present study
25	F	49	Right Temporal lobe	glioblastoma IDH wild-type	Intense	FGFR3 EX18 TACC3 EX 4	Dead	32.7	Di Stefano et al. 2015
26	M	51	Right Temporal lobe	glioblastoma IDH wild-type	na	FGFR3 EX17 TACC3 EX 10	Alive	22.7	Present study
27	M	60	Right Frontal lobe	glioblastoma IDH wild-type	Intense	FGFR3 EX17 TACC3 EX 10	Dead	16.3	Di Stefano et al. 2015
28	M	62	Right Fronto-temporal lobes	glioblastoma IDH wild-type	Moderate	FGFR3 EX17 TACC3 EX 10	Dead	18.2	Present study
29	F	67	Left Occipital lobe	glioblastoma IDH wild-type	Intense	FGFR3 EX17 TACC3 EX 10	Alive	17.6	Present study
30	M	46	Left Parieto-occipital lobes	glioblastoma IDH wild-type	Intense	FGFR3 EX17 TACC3 EX 10	Alive	6.8	Present study
31	F	77	Left Parieto-occipital lobes	glioblastoma IDH wild-type	Intense	FGFR3 EX17 TACC3 EX 10	Dead	16.5	Present study
32	F	63	Right Temporal lobe	glioblastoma IDH wild-type	Moderate	FGFR3 EX17 TACC3 EX 10	Alive	14.6	Present study
33	M	35	Right Temporal lobe	glioblastoma IDH wild-type	Intense	FGFR3 EX17 TACC3 EX 10	Alive	23.2	Present study
34	F	87	Right Parietal lobe	glioblastoma IDH wild-type	Intense	FGFR3 EX17 TACC3 EX 10	Dead	14.1	Present study
35	M	49	Right Frontal lobe	anaplastic astrocytoma IDH wild-	na	FGFR3 EX17 TACC3 EX 10	Dead	54.1	Present study
36	F	74	Left Frontal lobe	diffuse astrocytoma IDH wild type	na	FGFR3 EX17 TACC3 EX 10	Dead	46.2	Di Stefano et al. 2015
37	F	72	Right Temporal lobe	diffuse astrocytoma IDH wild type	Intense	FGFR3 EX17 TACC3 EX 10	Dead	22.4	Di Stefano et al. 2015
38	F	59	Left Temporal lobe	diffuse astrocytoma IDH wild type	Moderate	FGFR3 EX18 TACC3 EX 5	Alive	40.6	Di Stefano et al. 2015
39	F	43	Right Temporal lobe	glioblastoma IDH wild-type	Intense	FGFR3 EX18 TACC3 EX 13	Alive	46.8	Present study
40	F	82	Left Temporal lobe	glioblastoma IDH wild-type	Intense	FGFR3 INT17 TACC3 EX 7	Dead	0.9	Di Stefano et al. 2015

Table 4.2.1 Clinical and histological diagnosis of patients harboring FGF3-TACC3 fusions. Details about FGFR3-TACC3 variant and FGFR3 staining are reported. Underlined FGFR3-TACC3 isoformes emerged as new variants in the present study. Abbreviations: M=male; F=female; EX=exon; INT=intron; OS=overall survival from diagnosis; na=not available

Next, we explored if *FGFR3-TACC3* positive patients had a different clinical course and outcome. We compared overall survival from time of diagnosis of *FGFR3-TACC3* positive patients with the *IDH* wild-type glioma of this cohort (including grade II, grade III and grade IV). Remarkably, we observed that survival is significantly longer in *FGFR3-TACC3* patients than *FGFR3-TACC3* negatives (median OS 40.1 and 20.0 months respectively) (*P*=0.03) and this difference is confirmed, even more pronouncedly, in the grade IV glioma subgroup (median OS *FGFR3-TACC3* positives 40.1 months versus *FGFR3-TACC3* negatives OS 19.0; *P*=0.006), as showed in **Figure 4.2.1**. *FGFR3-TACC3* isoforms did not correlate with different survival ranges.

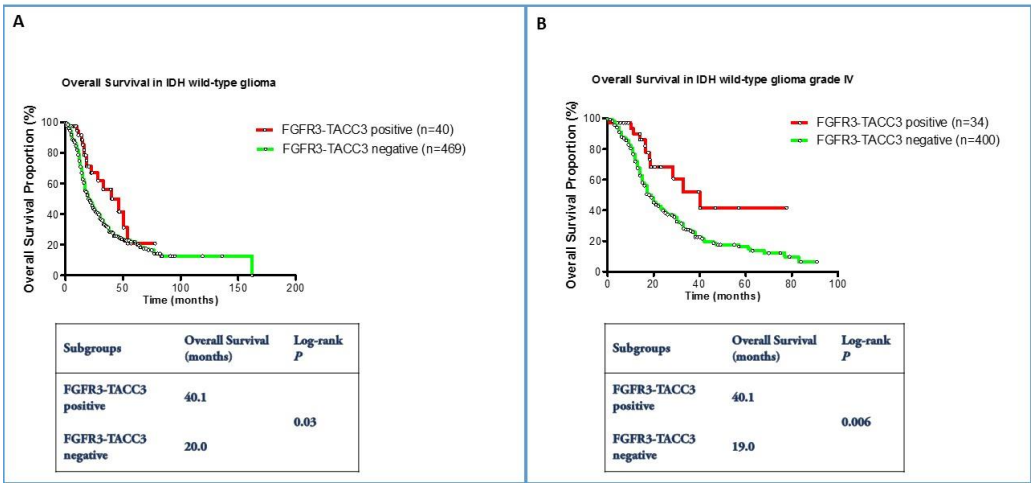

Figure 4.2.1 OS of *FGFR3-TACC3*-positive glioma patients. (A) Kaplan-Meier curves in *IDH* wild-type glioma patients show significant differences in between *FGFR3-TACC3* positive (N=40, median OS=40.1 months) and *FGFR3-TACC3* negative (N=469, Median OS= 20.0 months) (*P*=0.03). (B) Kaplan-Meier curves in *IDH* wild-type glioma grade IV subgroup show significant differences in Overall Survival (OS) between *FGFR3-TACC3* positive (N=34, Median OS=40.1 months) and *FGFR3-TACC3* negative (N=400, Median OS=19.0 months) (*P*=0.006). Red indicates *FGFR3-TACC3* positive patients, green indicates *FGFR3-TACC3* negative patients and open circles represent censored patients.

FGFR3 Immunostaining is Highly Specific of the Presence of *FGFR3-TACC3* Fusions

In the previous study, we observed that all gliomas harbouring *FGFR3-TACC3* fusions strong and homogeneous FGFR3 immunostaining, with an antibody that recognized the N-terminus of FGFR3 which is retained and overexpressed in the fusion protein. To determine sensitivity and specificity of FGFR3 imunostaining to predict the presence of *FGFR3-TACC3* fusions we analysed a prospective cohort of 236 subjects using parallel-blinded immunostaining and RT-PCR assay. Results are detailed in **Table 4.2.2**. FGFR3 immunostaining was positive in all patients harbouring the *FGFR3-TACC3* fusions and, conversely, any *FGFR3-TACC3* positive glioma scored negative at immunostaining. Then, sensitivity of FGFR3 immunostaining to predict the *FGFR3-TACC3* fusions was 100%, specificity was 81.8%, positive predictive value (VPP) was 19.6%, and negative predictive value (VPN) 100% (chi2 37.9).

80 cases from other institutions were addressed at our centre in order to perform RT-PCR screening for the fusion transcripts after local detection of FGFR3 expression by IHC. Of them, RT-PCR analysis was contributive in 77 patients while in the remaining 3, RNA concentration was too low and no supplementary frozen tumor was available. We added these supplementary 77 cases from other institutions to the prospective institutional cohort in order to calculate the positive predictive value in a larger sample. Adding these 77 supplementary patients, scoring positive for FGFR3 staining (59 *FGFR3-TACC3* negative and 18 *FGFR3-TACC3* positive by RT-PCR), the positive predictive value increased to 21.8%.

	FGFR3 IHC +	FGFR3 IHC -	Total
FGFR3-TACC3 negative	41	185	226
FGFR3-TACC3 positive	10	0	10
Total	51	185	236

Table 4.2.2 Parallel-blinded analysis by FGFR3 immunostaining (IHC) and RT-PCR assay in an institutional prospective cohort of 236 patients. FGFR3 immunostaining proved highly sensitive 100%. Specificity was 81.8%.

Regarding the intensity of FGFR3-N immunostaining 30 out of the 40 gliomas harbouring *FGFR3-TACC3* fusions scored "intense" expression of FGFR3, 5 "moderate" (Patients 1, 18, 28, 32 and 38 in **Table 4.2.1**) and 1 "weak" (Patient 11 in **Table 4.2.1**). No information *of FGFR3* IHC was available for four of the patients (Patients 15, 26, 35 and 36).

While in our previous study we observed that all *FGFR3-TACC3* positive gliomas shared a diffuse an intense pattern *of FGFR3* expression, in this larger series we observe that rarely *FGFR3-TACC3* fusions may present a weaker expression of FGFR3, suggesting that weak *FGFR3* staining does not rule out the presence of *FGFR3-TACC3* fusion transcript. Transcript sequencing and FGFR3 immunostaining of the only patient showing a "weak" expression of FGFR3 in this series (Patient 11) are shown in **Figure 4.2.2.**

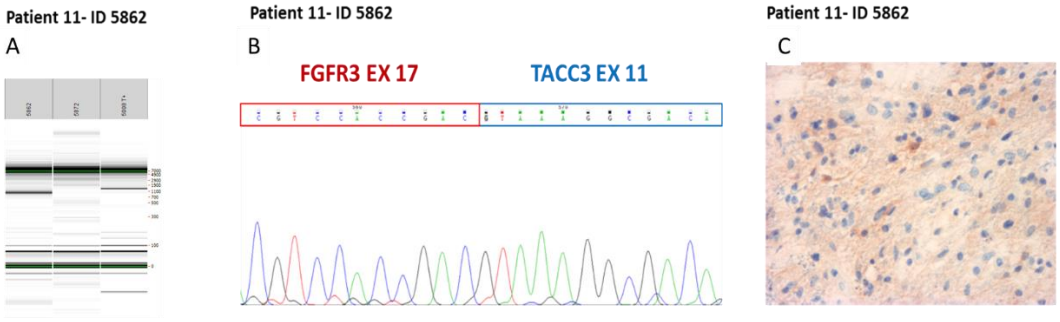

Figure 4.2.2 Representation of FGFR3 expression in Patient 11. (A) *FGFR3-TACC3* fusion specific RT-PCR product from untreated GBM from Patient 11, glioma sample ID 5862; 5008 Positive control. (B) Sanger sequencing chromatogram for *FGFR3-TACC3* transcript showing a breakpoint at *FGFR3* Exon 17 and *TACC3* Exon 11. Regions corresponding to *FGFR3* and *TACC3* are indicated in red and blue, respectively. (C) Is a representative microphotograph of FGFR3 immunostaining scoring 20% of labeled tumor cells. Magnification is 200x.

Molecular Alterations in *IDH* Wild-Type Gliomas Harbouring *FGFR3-TACC3* Fusions

We sought to update and extend to a larger series and a larger panel of chromosomal aberration than what was previously reported on the molecular profile of *FGFR3-TACC3*-positive glioma and to compare to *IDH* wild-type *FGFR3-TACC3* negative gliomas.

Genomic data were available for up to 595 *IDH* wild-type gliomas, and 40 *FGFR3-TACC3* positives are presented in **Table 4.2.3**.

According to our previous analysis, we confirmed in a larger series the mutual exclusivity of *EGFR* amplifications and *FGFR3-TACC3* fusions (0/34 cases with *EGFR* amplification in *FGFR3.TACC3* positives versus 139/358 (62%) in *IDH* wild-type *FGFR3-TACC3* negatives; *P*=0.0001), and the higher frequency of *CDK4* amplification in *FGFR3-TACC3* positives gliomas (5/29, 17% vs. 24/337, 7% in *FGFR3-TACC3* negatives; *P*=0.06).

Moreover, we confirm that *MDM2* amplifications are more frequent in *FGFR3-TACC3* fusions (5/30, 16% in *F3-T3* positives versus 17/380, 4% in *F3-T3* negatives; *P*=0.01) and that *EGFRvIII* is not represented in *FGFR3-TACC3* fusions (*P*=0.01).

Interestingly, as a new result we found a significantly higher frequency of 10q loss in *FGFR3-TACC3* gliomas compared to *FGFR3-TACC3* negative gliomas (23/25, 92% versus 225/346, 65%; *P*=0.004).

In these series' we could extend analysis to other rare molecular aberrations such as *PTEN* mutation, *MET* amplification, histones *H3F3A* and *H3B* mutations and *BRAF V600E* mutations, and we did not find any *FGFR3-TACC3* positive gliomas harbouring these alterations.

We found no statistical association between *FGFR3-TACC3* fusions and other genetic and epigenetic alterations that commonly occur in gliomas harbouring wild-type *IDH* genes (*TERT* promoter mutations, gain of chromosome 7p, loss of chromosomes 13q and 14q and methylation of the *MGMT* promoter, **Table 4.2.3**).

Alteration	N° of *FGFR3-TACC3* positive	*% of FGFR3-TACC3* positive	N of *FGFR3-TACC3* negative	% of FGFR3-TACC3 negative	*P* (Fisher test)	q (FDR)
EGFR amplification	0/34	0%	139/358	38%	0.0001	0.01
CDK4 amplification	5/29	17%	24/337	7%	0.06	0.14
MDM2 amplification	5/30	16%	17/380	4%	0.01	0.04
EGFRvIII	0/12	0%	29/82	35%	0.01	0.04
p16 deletion	9/28	32%	163/358	45%	0.23	0.43
10q loss	23/25	92%	225/346	65%	0.004	0.03
7p gain	19/23	83%	213/310	69%	0.23	0.43
13q loss	3/22	13%	53/318	17%	1	1
14q loss	3/21	14%	45/297	15%	1	1
TERT promoter mutation	19/25	76%	234/301	78%	0.80	0.98
MGMT promoter hypermethylation	6/15	40%	82/180	45%	0.79	0.97
H3B and *H3F3A* mutations	0/8	0%	7/99	7%	1	1
BRAFV600E mutation	0/12	0%	3/224	1%	1	1
MET amplification	0/9	0%	0/31	0%	-	-
PTEN mutation	3/9	33%	21/108	19%	0.38	0.53

Table 4.2.3 Molecular alterations in *IDH* wild type glioma harboring *FGFR3-TACC3* fusions (635 *IDH* wild-type gliomas; 40 *FGFR3-TACC3* positive vs. 595 *FGFR3-TACC3* negative). The table reports the absolute number and frequency (percentage) of individual glioma-specific molecular alterations in tumors scoring positive or negative for *FGFR3-TACC3* fusions. Statistically significant associations are indicated in red (Fisher Exact test). Comparing to our previous study, we found a significant higher frequency of 10q loss in *FGFR3-TACC3* positive and lower of *EGFRvIII* variant (underlined). q-values adjusted with FDR are reported.

4.2.4 DISCUSSION

FGFR-TACC fusions are potent oncogenic events that specifically recur in the setting of *IDH* wild-type gliomas.

Knowledge of specific histological and clinical characteristics of gliomas harbouring *FGFR3-TACC3* fusions is affected by the rarity of this alteration and the small sample size of positive cases of *FGFR3-TACC3*.

Beginning with the RT-PCR-sequencing assay, we have previously validated all possible functional *FGFR3-TACC3* fusion transcripts; in this study we have extended the screening up to 907 cases and increased the number of identified *FGFR3-TACC3* positive cases to 40.

The first relevance of our findings is that, among them, 24 patients are alive at the end of this follow-up and could potentially benefit from anti-FGFR therapies, concurrent with the example we have previously reported of the two patients treated with anti-FGFR therapy at recurrence (Di Stefano, 2015).

According to the remarkable variability of *FGFR3-TACC3* fusion events we have previously reported (Di Stefano, 2015), in this larger series we were able to detect two new isoforms of *FGFR3-TACC3* fusions (*FGFR3* EX17-*TACC3* EX13 and *FGFR3* EX17-*TACC3* EX4), occurring in individual cases. Adding these novel identified variants, the numbers of isoforms that others and we have reported so far, increase to 14 (**Supplementary Table 1** from Di Stefano, 2015). However, by increasing the repertoire of variants in this study, we observe that two variants *FGFR3* EX17-*TACC3* EX11 and *FGFR3* EX17-*TACC3* EX10 are highly recurrent and cover 42% and 30% of the series, respectively.
From our previous study we know that structural heterogeneity of *FGFR3-TACC3* fusions is yet more pronounced at the genomic level, whereby even identical fusions transcripts (*FGFR3* EX17-*TACC3* EX11; *FGFR3* EX17-*TACC3* EX8; *FGFR3* EX17-*TACC3* EX6) harbours distinct genomic breakpoints [**Supplementary Figure 2** from (Di Stefano, 2015)]. Further studies might elucidate why these translocation events involve more frequently specific genomic regions in *FGFR* and *TACC3* genes.

We were able to collect clinical records on the 40 patients harbouring *FGFR3-TACC* fusions identified so far.
We did not observe specific differences in sex ratio and median age at diagnosis. Regarding tumor location we found that all 40 patients of this series were affected by supra-tentorial hemispheric brain tumors: none of them affected deep structures of the cerebrum, ventricles, cerebellum, brainstem and/or spine.
Given the recognized role of *FGFR3* as a regulator caudo-lateral (occipito-temporal) cortex development (Thomson, 2009), we wondered if *FGFR3-*

TACC3 initiated glioma occurred specifically in posterior lobes. In this series of 40 *FGFR3-TACC3* positive glioma patients, we found that *FGFR3-TACC3* glioma do not occur specifically in caudo-lateral lobes but rather in all cerebral lobes. However, we observed a slightly higher frequency in partieto-occipital lobes (12/40; 30%) compared to what was reported about glioma in the literature of around 17% (Larjavaara et al. 2007). This observation is affected by the small sample size of *FGFR3-TACC3* cases. We plan to analyse in a larger series, with case-controlled analyses that may also illustrate if cortical location is predominant in *FGFR3-TACC3* gliomas.

To determine if *FGFR3-TACC3* fusion events were associated with difference on survival, we extend follow-up and survival analysis to novel identified patients of this study. In our previous study, we failed to observe difference in survival (Di Stefano, 2015). Inversely, in this second analysis performed in a larger number of patients and a longer follow-up, we found a clearly longer median survival of up to 40 months in *FGFR3-TACC3* glioma patients, as compared with *FGFR3-TACC3* negative-*IDH*-wild-type patients. Difference in overall survival resulted yet more pronouncedly in the GBM subgroup, where we observed strikingly long survival rates (longer than 24 months) in 9 patients out of the 34 GBM harbouring *FGFR3-TACC3* fusions (26%), independent of the transcript isoforms.

The majority of patients in both groups received standard radio-chemotherapy at first line in both groups (Stupp, 2005). Eight GBM patients harbouring *FGFR3-TACC3* fusions were recently included in a phase II trial testing AZD4547, an ATP-competitive pan-*FGFR* selective inhibitor, at recurrence. Enrolment in this clinical trial does not explain the longer survival we observed in *FGFR3-TACC3* positive GBM because:

- patients with the longest survivals did not match with those who received or are receiving AZD4547

- longest survivals correspond to patients with especially long remission intervals after first line treatment
- enrolments in *TARGET* trial are relatively recent, starting from September 2015.

The reason for this better prognosis remains to be determined.

However, this finding highlights a supplementary relevance of usefulness of specific therapies targeting FGFR3-TK in this selected subgroup of patients. We previously reported a clinical improvement and a minor response in two patients treated with an anti-*FGFR* ATP-competitive pan-FGFR selective inhibitor (JNJ42756493) (Di Stefano, 2015). Other anti-FGFR specific reversible and covalent inhibitors are being tested in the setting of phase I and phase II trials in selected patients harbouring activating aberrations of FGFR receptors.

In perspective, the enrichment of therapeutic armamentarium against *FGFR* oncogenic drivers may be particularly interesting in this subset of patients given their longer evolution, by rechallenging or combining specific therapies targeting *FGFR3* that might finally lead to a relevant clinical benefit.

In our previous study, we observed that all glioma harbouring *FGFR3-TACC3* fusions presented an intense and diffuse staining for FGFR3 as a result of the accumulation of the fusion protein. In this study we determined, prospectively, sensitivity and specificity of FGFR3 staining to predict the presence of *FGFR-TACC* fusions. While constant in all cases harbouring the fusion (100% sensitivity), FGFR3 expression predicts the presence of the fusion in only 20% of the cases.

Despite the majority of FGFR3 showing an intense and diffuse staining for FGFR3, a small fraction of *FGFR3-TACC3* gliomas had a weak expression of FGFR3, with 20 to 50% FGFR3 positive tumor cells.

This data shows that IHC for FGFR3 is an efficient and reliable pre-screening method and can be integrated in histological routine work-up: when positive, it raises the attention level of pathologists, clinicians and biologists for

biomolecular analysis on frozen samples that can be performed in reference laboratories.

Finally, by the extension of molecular characterization in a larger case series with a larger panel of molecular aberrations, we confirmed that *FGFR3-TACC3* positive glioma harbour a specific genomic background principally characterized by the absence of *EGFR* amplification and *EGFRViii* variant, a higher frequency of *MDM2* and *CDK4* amplification and 10q loss.

Overall, our findings have shown the importance and feasibility of prospective genotyping for *FGFR3-TACC3* fusions and provide preliminary elements on clinical and histological phenotype of *FGFR3-TACC3* glioma patients. Further studies should answer the question on radiological and histological signatures linked to this driver oncogenic alteration, on efficacy FGFR-TK inhibitors and on eventual factors of resistance to this promising target therapy.

4.3 Exploratory Analysis on Mechanism of Resistance to Anti-*FGFR* Therapies

FGFRs/FGFs are key molecules involved in embryogenesis, tissue homeostasis, tissue repair, wound healing, and inflammation (Powers, 2000). The main effects of the FGFR pathway include proliferation, migration, and antiapoptotic signals. Proliferation is mainly achieved through the MAPK cascade, whereas antiapoptotic signals are mediated by PI3K/AKT with cross talk between both pathways (Turner, 2010).

FGF signalling is deregulated in many cancer types. Activating mutations and amplification occurring in 50-60% of non muscle invasive bladder cancers (van Rhijn, 2002) and translocations t(4;14) (p16.3;q32.3) occurring in 15-20% in multiple myeloma are the most frequent *FGFR* activating alterations reported so far (Chesi, 1997).

At a therapeutic level, the most clinically advanced anti-FGFR drugs are small-molecule TKIs, targeting the ATP-binding site of the intracellular tyrosine kinase domain of FGFRs.

In our previous study (Di Stefano, 2015), we treated two patients harbouring *FGFR3-TACC3* recurrent glioblastoma with JNJ-42756493 an oral ATP-competitive pan-FGFR selective inhibitor that inhibits tyrosine phosphorylation of activated FGFR at nanomolar (Tabernero, 2015). We observed a clinical improvement in both patients, a stabilization of tumor growth and one minor response.

Next, 4 months after starting anti-FGFR therapy, Patient 1 showed tumor progression on MRI and underwent surgery 4 weeks after discontinuation of JNJ-42756493. Expression of FGFR3 was maintained in recurring GBM, scoring highly positive (Id 5008 in **Figure 4.3.1**). We confirmed the presence of *FGFR3-TACC3* fusions transcript with the same breakpoint as the initial GBM *FGFR3* EX17-*TACC3*EX6 (Id 4451) **Figure 4.3.1**. At a genomic level, we found

FGFR3-TACC3 in the recurrent GBM with the same breakpoint as the initial tumor (*FGFR3* EX17+INT17-*TACC3*EX5+INT5+EX6) **Figure 4.3.1**.

Recent data indicates that the *FGFR* pathway is a potential driver of a number of mechanisms of resistance to various targeted drugs. Interestingly, Chell et al. generated a derivative of the KMS-11 myeloma cell line (*FGFR*(Y373C)) with acquired resistance to AZD4547 (KMS-11R cells) an inhibitor of *FGFR1*-3 and they identified the presence of a secondary heterozygous mutation at the gatekeeper residue, encoding *FGFR3*(V555M) as a mechanism of acquired resistance to *FGFR* inhibitors [(Chell, 2013); **Figure 4.3.2** adapted from the article].

Basing on this observation we looked for new acquired mutations of *FGFR3-TACC3* in the recurrent GBM.

We performed PCR and Sanger sequencing of all 18 exons of *FGFR3* and 16 exons of *TACC3* in the initial GBM and in the recurrent GBM after anti-FGFR therapy. By comparison of *FGFR3* and *TACC3* genomic DNA in exonic regions, we did not find any new acquired mutation in the recurrent GBM. In particular, no mutations at *FGFR3* (V555M) were present in the primary, nor in the recurrent GBM. Only 6 common-indexed non funtional SNPs were found in both the initial and the recurrent GBM (*FGFR3*-Exon 14: SNV G>A; *FGFR3*-Exon 18: SNV A>G, *FGFR3*-Exon 18: deletion of 2bp (TG>/-); *FGFR3*-Exon 18: SNV C>T ; *TACC3*-Exon 1: SNV T>C ; *TACC3*-Exon 4: SNV A>G).

Additional studies, including % of *FGFR3* cells expressing and exome sequencing of recurrent resistant tumors after anti-FGFR therapy are planned.

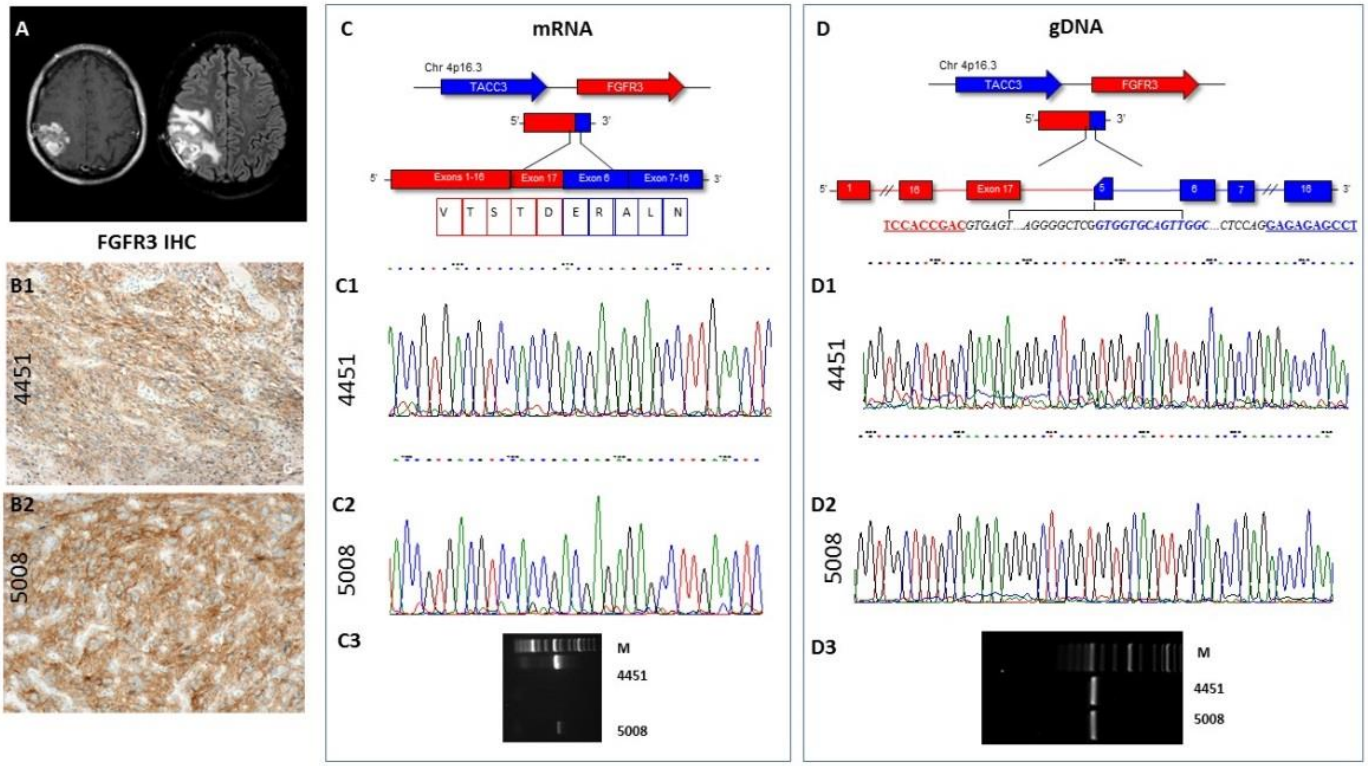

Figure 4.3.1 FGFR3 expression and *FGFR3-TACC3* gene fusions in Patient 1, before and post-treatment with JNJ-42756493. In A) Post-gadolinium T1-weighted and FLAIR imaging show the target lesion on the right parietal lobe corresponding to progression disease (see Figure 4 from Di Stefano et al. (2015) for baseline imaging).
B) Representative microphographs of FGFR3 immunostaining of untreated GBM (4451) in B1 and recurring GBM after JNJ-42756493 (5008) in B2. 10 X magnification in B1 and 40 X magnification in B2.
C) Schematic representation of the *FGFR3–TACC3* fusion transcripts in untreated GBM (4451) in C1 and recurring GBM (5008) in C2. The junction sequences of *FGFR3* EX17-*TACC3* EX 6 isoform in mRNA and the reading frame at the breakpoint are reported.
D) Schematic representation of the genomic fusions between *FGFR3* and *TACC3 FGFR3* EX17+INT17-*TACC3*EX5+INT5+EX6 in untreated GBM (4451 in D1) and recurrent GBM (5008) in D2.
The reported regions belonging to *FGFR3* and *TACC3* are in red and blue, respectively.
C3 and D3: results from RT-PCR screening: M, DNA ladder.

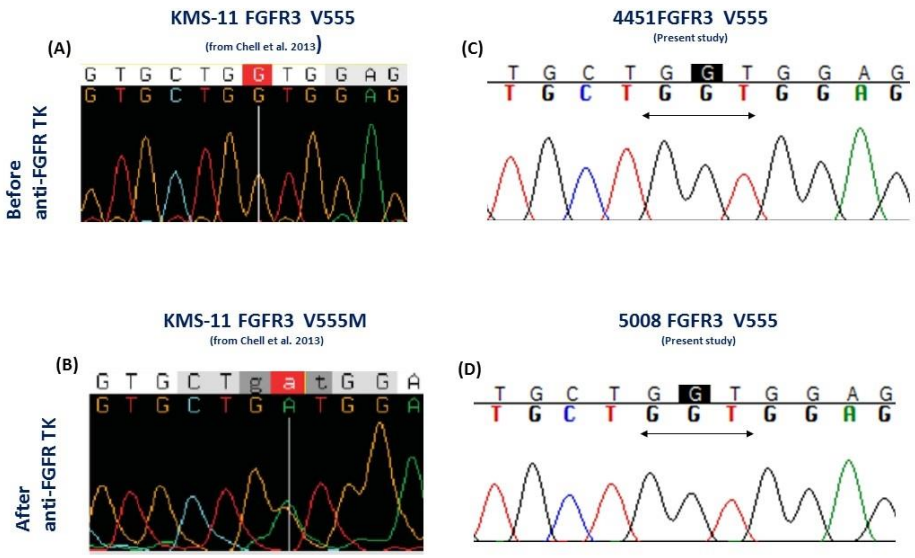

Figure 4.3.2 Analysis of *FGFR3* Val555 in KMS-11R cells [A and B; images adapted from (Chell, 2013)] and untreated GBM (4451 in C) and post treatment GBM in (5008 D) after anti-*FGFR*-therapy ATP-binding inhibitor. While resistant KMS-11R cells after AZD4547 showed a gatekeeper mutation in *FGFR3*Va555Met, both untreated GBM (4451) and the recurrent (5008) after JNJ-42756493 show wild-type sequence at Val555. Sequence chromatograms of genomic DNA at codon 555 (exon 13) of *FGFR3* are shown.

5. SECTION 3 – DIAGNOSTIC MARKERS

In Vivo Non-Invasive Detection of 2-Hydroxyglutarate in *IDH* Mutated Gliomas

5.1 INTRODUCTION

Proton magnetic resonance spectroscopy (1H-MRS) is used in the metabolic research of gliomas, and as a supplemental tool to magnetic resonance imaging (MRI) in the diagnosis of gliomas (Law, 2003; Zonari, 2007). However, 1H-MRS presents certain limitations that can be attributed to the intrinsically low concentrations of metabolites yielding limited signal-to-noise ratio (SNR), to the low spectral resolution at clinical fields, and to the lack of specificity of the metabolites that have been previously proposed as biomarkers of gliomas.

In this regard, the emergence of *2-hydroxyglutarate* (2 HG) as an onco-metabolite overproduced in isocitrate dehydrogenase *IDH*-mutated gliomas (Dang, 2010; Parsons, 2008; Yan, 2009), the substantially longer survival duration of *IDH*-mutated gliomas patients (Sanson, 2009) and recent pioneering studies on the feasibility of non-invasive detection of 2 HG by 1H-MRS (Pope, 2012; Andronesi, 2012; Choi, 2012), have recently drawn attention of neuro-oncologists.

Reportedly, due to severe spectral overlap with its background signal, the quantification of 2 HG is challenging (Andronesi, 2012; Choi, 2012).

5.1.1 Overproduction of 2-Hydroxyglutarate in *IDH*-Mutated Gliomas

Isocitrate dehydrogenase is an enzyme with three isoforms, i.e., IDH1, IDH2, and IDH3 (Dang et al. 2010). Intra-cellularly, it catalyses the oxidative decarboxylation of isocitrate to α-ketoglutarate (α-KG) in cytoplasm and peroxisomes (IDH1) and in mitochondria (IDH2 and IDH3) (**Figure 5.1**) (Arcaro, 2007; Dang, 2010).

Mutations in *IDH1* were detected initially by a whole-genome sequence analysis in a small subset of glioblastoma patients (Parsons, 2008). Subsequent studies confirmed the presence of *IDH* mutations in 70–90% of low-grade glioma and secondary glioblastoma, in ~20% of acute myeloid leukaemia, and in intrahepatic cholangiocarcinoma, chondrosarcoma, and melanoma (Gross, 2010; Waitkus, 2016; Yang, 2012).

Glioma-specific mutations in *IDH1* always affect the amino acid arginine in position 132 of the amino acid sequence belonging to a high, evolutionarily conserved region located at the binding site for isocitrate (Hartmann, 2009). Mutations in *IDH2* affect arginine at position 172, which is the analogous site to arginine 132 in *IDH1* (Hartmann, 2009). Mutations in both *IDH1* and *IDH2* are heterozygous and of somatic origin.

The predominant amino acid sequence alteration in *IDH1* was R132H, accounting for 92.7% of the detected mutations. For this specific mutation, an immunostaining with a mutant protein recognition antibody has been proven to be highly sensitive and specific and successfully introduced in clinical practice (Capper, 2009). Less frequently, other amino acid sequence alteration *IDH1* mutation may occur in codon 132 (R132C for 4.1%, R132S for 1.5%, R132G for 1.4% and R132L for 0.2% of all *IDH1* mutations). *IDH2* mutations occur with a frequency of 3% in non-glioblastoma tumors and interestingly seem to be associated with tumors with an oligodendroglial component (Hartmann, 2009). Type and distribution of *IDH1* and *IDH2* mutations are given in **Table 5.1**.

The *IDH1* mutation is one of the earliest known genetic events in low-grade gliomas, and it is thought to be a "driver" mutation for tumorigenesis (Suzuki, 2015). Presence of the *IDH1* is associated with a more favourable prognosis compared to tumors with wild-type *IDH1* in all glioma grades and it is also predictive of response to anti-cancer therapy (Cairncross, 2014; Sanson, 2009; Houillier, 2006). The reasons for this better prognosis remain to be determined. *IDH* mutations cluster with other molecular aberrations such as codeletion of 1p19q: all the 1p19q-codeleted gliomas have been shown to be mutated on *IDH1* or *IDH2*; inversely not all *IDH* mutated gliomas present 1p19q chromosomal translocation (Labussiere, 2010).

Combinations of these two molecular alterations in the subgroup of non-GBM (grade 3 and grade) allow definition of three molecular subgroups (*IDH*mutated+1p19q codeleted/*IDH*mutated+non codeleted and *IDH* wild-type gliomas) with marked differences in survival rates (**Figure 5.2**) and differential response to PCV based chemotherapy in addition to radiotherapy, as recently reported (Cairncross, 2014). These observations could explain part of the relevant heterogeneity in clinical course we usually observe in non-glioblastoma patients **(Figure 5.2)** and elige the *IDH* mutation as a major marker for prognostication and for decisions regarding chemo-radiotherapy regimens.

From a metabolic perspective, mutations in *IDH1* and *IDH2* lead not only to the loss of wild-type enzyme activity-interconversion of isocitrate to α-ketoglutarate (α-KG), but also to a gain-of-function that results in the conversion of α-KG to the "oncometabolite" *2-hydroxyglutarate* (2 HG) (Dang, 2009). 2 HG is a competitive inhibitor of multiple α-KG-dependent deoxygenises, such as the prolyl hydroxylases, and histone demethylases, and the TET family of methylcytosine hydroxylases (Xu et al. 2010). As a result, *IDH1*/2 mutant cells undergo extensive epigenetic modifications that ultimately result in tumorigenesis (Lu, 2012; Turcan, 2012; Sasaki, 2012)

According to previous published studies, 2 HG accumulation may be measured on snap frozen tumor samples by liquid chromatography - mass spectrometry (LC/MS) (**Figure 5.3**). *IDH* mutant tumors have been shown to present more 2 HG than *IDH* wild-type (range from 5 and 35 μmol of 2 HG per gram of tumor) by 100 fold, and 0.045 to 0.68 μmol/gr in *IDH* wild-type gliomas. No differences have been observed for α-KG levels and other metabolites (Dang, 2009), **Figure 5.3**.

5.1.2 Noninvasive Detection of 2 HG by 1H-MRS

To date, a total of only 9 studies reported (Pope, 2012; Andronesi, 2012; Choi, 2012; Natsumeda, 2014; de la Fuente, 2016; Lazovic, 2012; Emir, 2016; Heo, 2016) on in-vivo 1H-MRS of 2 HG in gliomas including 2 animal studies (Lazovic, 2012; Heo, 2016). 5 different 1H-MRS methods have already been proposed (**Table 5.2**).

The 2 HG molecule has 5 non-exchangeable protons (5-spin system) with complicated J-coupling interactions (Choi, 2012). These interactions refer to inter-spin interactions through electron bonds in a molecule (de Graaf RA, 2007; Allen, 1997). Such an indirect interaction between spins rather than a direct interaction through space is termed as J-coupling; the spins involved in the interaction are said to be J-coupled (de Graaf RA, 2007; Allen, 1997). J-coupling results in peak splitting (e.g., a singlet into a multiplet) and changes in line shape and signal amplitude as a function of time (typically, echo time [TE]).

The majority of the 1H-MRS-detectable metabolites have coupled spins such as 2 HG, Glu, Gln, gammaaminobutylicacid (GABA), and N-acetylaspartylglutamate (NAAG) (Govind, 2015). On the other hand, water and creatine (Cr) are representative metabolites with uncoupled spins only.

The spectral characteristics of 2 HG are determined by J-coupling in combination with the resonance frequencies of the 5 protons that are determined by chemical

environments of the protons in the molecule (chemical-shift), giving rise to three, non-field-dependent, multiplets centred at ~4.0, ~2.3, and ~1.9 ppm (contributed by 1, 2, and 2 spins, respectively) (**Figure 5.4)** (Choi, 2012). The spins resonating at ~1.9 ppm are J-coupled with the spin resonating at ~4.0 ppm, as well as with those resonating at ~2.3 ppm (Choi, 2012). The multiplet at ~4.0 ppm is relatively small in amplitude as it is contributed by only one proton, it overlaps with signals from lactate (Lac) and myo-inositol (mI), and is close to the strong PCr (~3.9 ppm) and water (~4.7 ppm) signals. The multiplet at ~1.9 ppm also overlaps with signals from other metabolites (**Figure 5.4**), in particular, with N-acetylaspartate (NAA). The multiplet at ~2.3 ppm has the largest signal and is therefore widely used as a target signal for 2 HG quantification (**Figure 5.4**). However, it also overlaps widely with signals from at least 4 other metabolites (**Figure 5.4**) (Andronesi, 2012; Choi, 2012).

Techniques for detection of 2 HG, published so far can vary insofar as:

- pulse sequence (PRESS, LASER, COSY): series of radio frequency pulses applied to the sample, which may vary in number, duration, and shape and are related to the characteristic frequencies of the target signals
- echotime (short TE or long TE): the time between the application of the radiofrequency excitation pulse and the peak of the measured signal (spin-echo).
- different editing method, which allows the signals of specific metabolites in a target spectral region to be cancelled.
- single or multivoxel: single or multiple region(s) of interest for spectral detection.
- size of voxel (ranging from 1.8 and 8 cm^3)
- magnetic field (3 to 7T)

Results from the nine previous studies on 2 HG in-vivo detection by 1H-MRS, including 2 animal studies, are resumed in **Table 5.2**.

Examples of in vivo single-voxel localized PRESS spectra from *IDH* mutated gliomas fro (Choi, 2012) are shown in **Figure 5.5.**

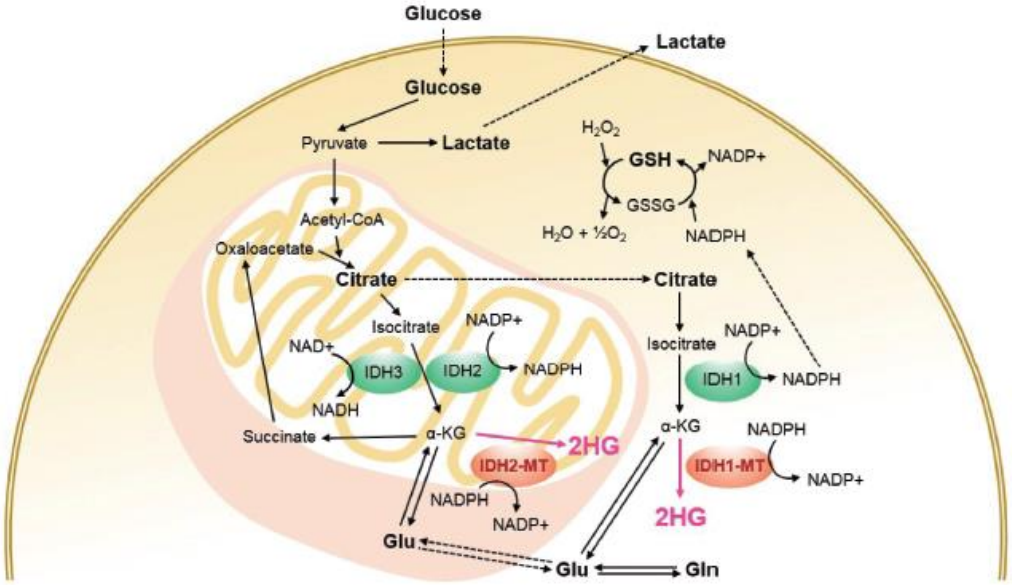

Figure 5.1 Adapted from (Kim, 2016). Simplified metabolic pathways associated with socitrate dehydrogenase (*IDH*) and 2-hydroxyglutarate (2 HG). Mutations of *IDH1* and *IDH2* result in overproduction of 2 HG. 1H-MRS-visible metabolites including 2 HG are marked in bold. Acetyl-CoA = acetyl coenzyme A, Gln = glutamine, Glu = glutamate, GSH = glutathione, GSSG = glutathione disulfide, H2O = water, H2O2 = hydrogen peroxide, *IDH*-MT = mutant isocitrate dehydrogenase, NAD = nicotinamide adenine dinucleotide, NADH = nicotinamide adenine dinucleotide hydrate, NADP = nicotinamide adenine dinucleotide phosphate, NADPH = nicotinamide adenine dinucleotide phosphate hydrate, α-KG = *alpha*-ketoglutarate

Gene	Nucleotide change	Amino acid change	*N* (%)
IDH1	G395A	R132H	664 (92.7%)
	C394T	R132C	29 (4.2%)
	C394A	R132S	11 (1.5%)
	C394G	R132G	10 (1.4%)
	G395T	R132L	2 (0.2%)
IDH2	G515A	R172K	20 (64.5%)
	G515T	R172M	6 (19.3%)
	A514T	R172W	5 (16.2%)

Table 5.1Adapted from (Hartmann, 2009). Type of 716 *IDH1* and 31 *IDH2* mutations and frequency among mutations in 1,010 WHO grades II and III astrocytomas, oligodendrogliomas and oligoastrocytomas. N (%) number of tumors and percentage of mutation among all mutations.

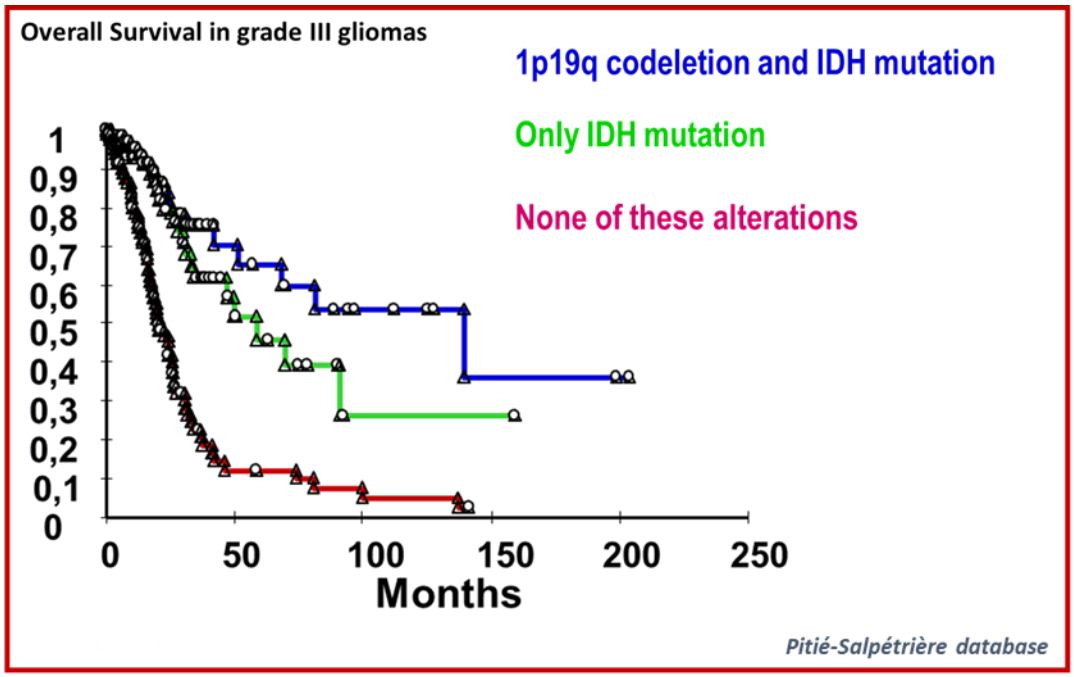

Figure 5.2 Overall survival of 206 grade III gliomas from Pitié Salpétrière database, according *IDH* mutation status and the presence of 1p19q codeletion. Rounds correspond to censored patients.

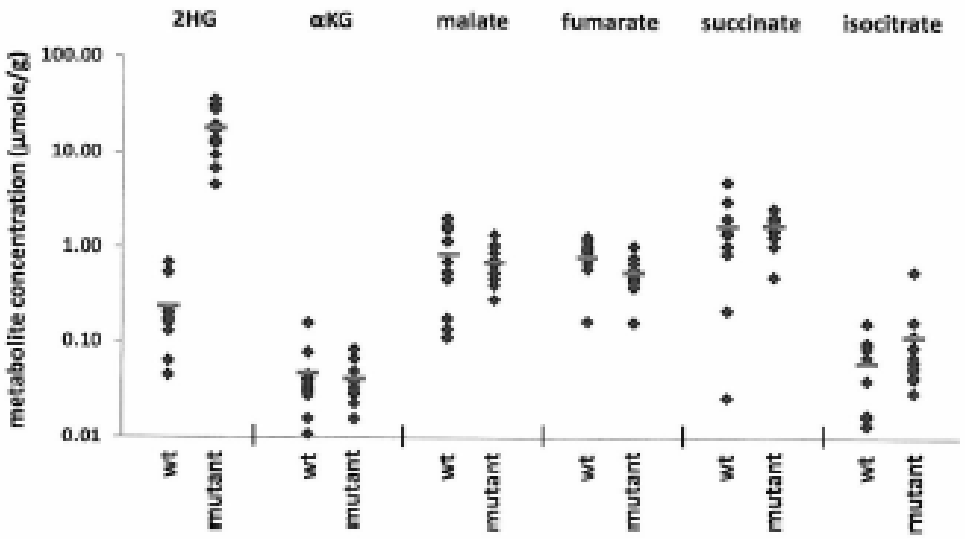

Characterization of human brain tumor samples.

Sample ID	Primary Specimen Diagnosis	WHO Grade	Tumor Cells in Tumor Foci (%)	Genotype	Nucleotide change	Codon	2HG (µmole/g)	αKG (µmole/g)	Malate (µmole/g)	Fumarate (µmole/g)	Succinate (µmole/g)	Isocitrate (µmole/g)
1	Glioblastoma, residual/recurrent	IV	n/a	wild type	wild type	R132	0.18	0.161	1.182	0.923	1.075	0.041
2	Glioblastoma	IV	n/a	wild type	wild type	R132	0.16	0.079	1.708	1.186	3.156	0.100
3	Glioblastoma	IV	n/a	wild type	wild type	R132	0.13	0.028	0.140	0.170	0.891	0.017
4	Oligoastrocytoma	II	n/a	wild type	wild type	R132	0.21	0.016	0.553	1.061	1.731	0.089
5	Glioblastoma	IV	n/a	mutant	G364A	R132H	16.97	0.085	1.091	0.807	1.357	0.058
6	Glioblastoma	IV	n/a	mutant	G364A	R132H	19.42	0.023	0.462	0.590	1.966	0.073
7	Glioblastoma	IV	n/a	mutant	G364A	R132H	31.56	0.068	0.758	0.503	2.019	0.093
8	Oligodendroglioma, anaplastic	III	75	mutant	G364A	R132H	12.49	0.033	0.556	0.439	0.507	0.091
9	Oligodendroglioma, anaplastic	III	90	mutant	G364A	R132H	4.59	0.029	1.377	1.060	1.077	0.574
10	Oligoastrocytoma	II	n/a	mutant	G364A	R132H	6.80	0.038	0.403	0.503	1.561	0.065
11	Glioblastoma	IV	n/a	wild type	wild type	R132	0.686	0.011	0.113	0.990	5.085	0.007
12	Glioblastoma	IV	n/a	mutant	G364A	R132H	18.791	0.016	0.470	0.462	2.673	0.031
13	Glioblastoma	IV	n/a	mutant	G364A	R132H	4.59	0.029	1.377	1.060	1.077	0.043
14	Glioblastoma	IV	n/a	wild type	wild type	R132	0.199	0.046	0.180	0.170	0.221	0.014
15	Glioblastoma	IV	n/a	mutant	C363G	R132G	13.827	0.030	0.905	0.599	1.335	0.046
16	Glioblastoma	IV	n/a	mutant	G364A	R132H	28.364	0.068	0.535	0.488	2.105	0.054
17	Glioblastoma	IV	n/a	mutant	C363A	R132S	9.364	0.029	1.088	0.693	2.151	0.121
18	Glioblastoma	IV	n/a	wild type	wild type	R132	0.540	0.031	0.468	0.608	1.490	0.102
19	Glioma, malignant, astrocytoma	IV	80	mutant	G364A	R132H	19.000	0.050	0.654	0.391	2.197	0.171
20	Oligodendroglioma	III	80	wild type	wild type	R132	0.045	0.027	1.576	0.998	1.420	0.018
21	Glioma, malignant, astrocytoma	IV	95	wild type	wild type	R132	0.064	0.034	0.711	0.710	2.105	0.165
22	Glioblastoma	IV	70	wild type	wild type	R132	0.171	0.041	2.066	1.323	0.027	0.072

Figure 5.3 Adapted from (Dang, 2010). A) Malignant human gliomas containing R132 mutations in *IDH1* contain increased concentrations of 2 HG. Human glioma samples obtained by surgical resection were snap frozen, genotyped to stratify as wild-type (WT) (N=10) or carrying an R132 mutant allele (Mutant) (n=12) and metabolites extracted for LC-MS analysis. Among the 12 mutant tumors, 10 carried a R132H mutation, one an R132S mutation, and one an R132G mutation. Each symbol represents the amount of the listed metabolite found in each tumor sample. Red lines indicate the group sample means. The difference in 2 HG observed between WT and R132 mutant *IDH1* mutant tumors was statistically significant by Student's t-test ($p<0.0001$). There were no statistically significant differences in αKG, malate, fumarate, succinate, or isocitrate levels between the WT and R132 mutant *IDH1* tumors. **B) The clinical characteristics, *IDH1* mutation status, levels of metabolites measurement in the clinical specimens**. **2 HG levels ranged from 5 to 32 µmol/gr** in *IDH* mutated gliomas and from **0.045 to 0.68 µmol/gr in *IDH* wild-type gliomas**.

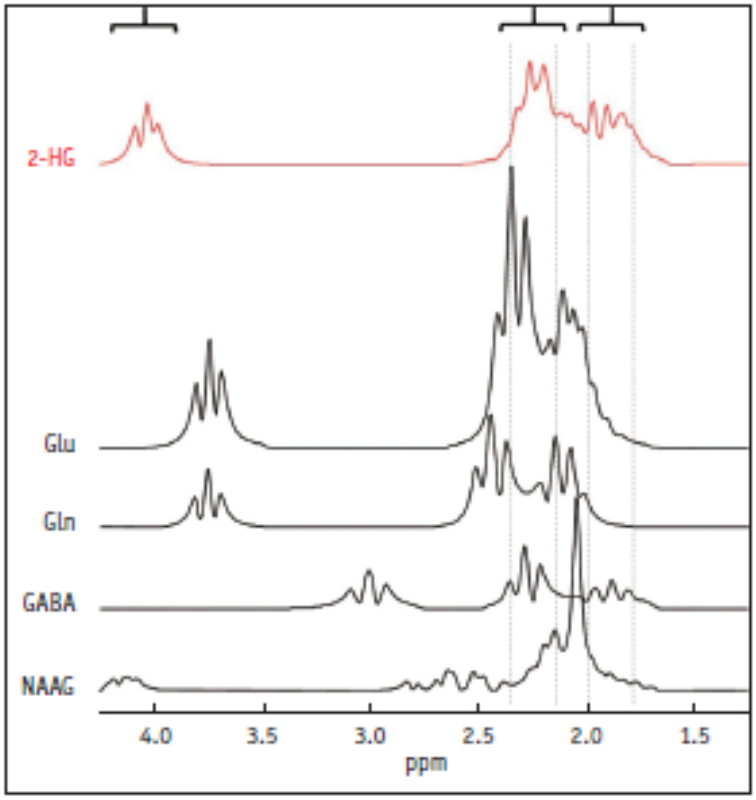

Figure 5.4 Adapted from (Kim, 2016). Simulated spectra of 2 HG and its background metabolites at 3T. Concentration ratio of 5:9.25:4.5:1.5:1.5 (mM) was assumed for *2 HG*:Glu:Gln:GABA:NAAG. Line widths of all spectra were broadened to mimic in-vivo spectra. GABA = gamma-aminobutylic acid, Gln = glutamine, Glu = glutamate, NAAG = N-acetylaspartylglutamate, 2 HG = 2-hydroxyglutarate

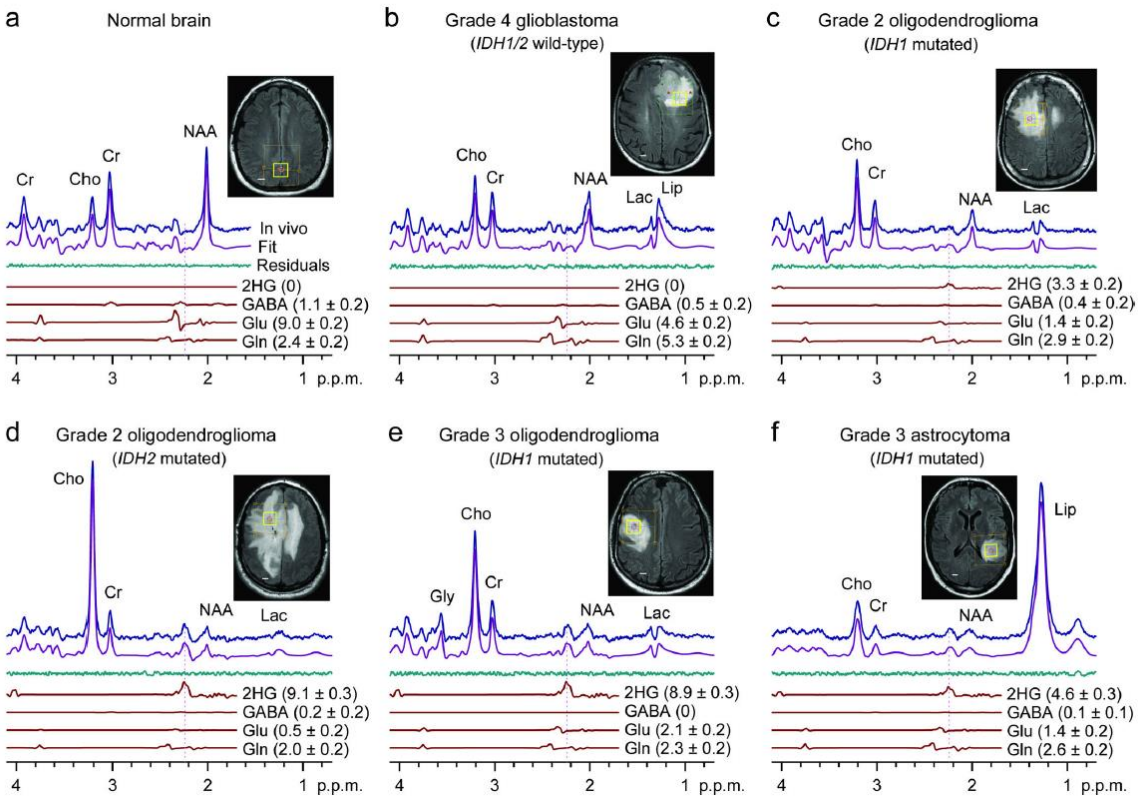

Figure 5.5 Adapted from (Choi, 2012). In vivo single-voxel localized PRESS spectra from normal brain (a) and tumors (b-f), at 3T, are shown together with spectral fits (LCModel) and the components of 2 HG, GABA, glutamate, and glutamine, and voxel positioning (2×2×2 cm3). Spectra are scaled with respect to the water signal from the voxel. Vertical lines are drawn at 2.25 ppm to indicate the *H4* multiplet of 2 HG. Shown in brackets is the estimated metabolite concentration (mM) ± standard deviation. Abbreviations: Cho, choline; Cr, creatine; NAA, N-acetylaspartate; Glu, glutamate; Gln, glutamine; GABA, γ-aminobutyric acid; Gly, glycine; Lac, lactate; Lip, lipids. Scale bars, 1 cm.

Method	Authors (Ref)	Subject	Number of Subjects (Number of Voxels)*			Sensitivity (%)	Specificity (%)†	Cutoff CRLB Peak Y (%)‡	Reference	Scanner	Field Strength (T)	Pulse Sequence	TR/TE (TE1, TE2) (ms)	Scan Time (min)	Voxel Volume (cm^3)
			MT	WT	Healthy										
Short TE	Andronesi et al. (15)	Human	2	4	4	NA	NA	20	Glu + Gln	Siemens	3.0	LASER	1500/45	3.2	27.0, 42.8
	Choi et al. (17)	Human	22	-	7	77	100	19	Water	Philips	3.0	PRESS	2000/35 (21, 14)	4.3	8.0
	Pope et al. (14)	Human	9	15	-	100	73	NA	Water, Cr	Siemens	3.0	PRESS	2000/30	4.3	8.0
	Natsumeda et al. (18)	Human	25 (15)	27 (18)	-	100	72	35§	Water	GE	3.0	PRESS	1500/30	3.2–4.9	(1.2–2.0)§
	Lazovic et al. (20)	Mouse	8	7	-	100	100	20	Cho	Bruker	7.0	PRESS	4000/6.9	34.1	3.0
Short TE with baseline	Hao et al. (22)	Rat	7 (7)	6 (6)	(6)	100	83	20	Water	Agilent	9.4	SPECIAL	4000/2.8	25.6	9.6×10^{-3}
	Choi et al. (16)	Human	15	15	-	100	100	19	Water	Philips	3.0	PRESS	2000/97 (32, 65)	2.1	8.0
	Choi et al. (17)	Human	22	-	7	100	100	19	Water	Philips	3.0	PRESS	2000/97 (32, 65)	4.3	8.0
Long TE	de la Fuente et al. (19)	Human	22	6	-	91	100	30‖	Water	GE	3.0	PRESS	2000/97 (26, 71)	5.5–9.5	8.0
Difference editing	Emir et al. (21)	Human	10 (10)	4 (4)	8 (25)	NA	93	30	Water	Siemens	7.0	Semi-LASER	5000–6000/110	10.7–12.8	8.0
	Andronesi et al. (15)	Human	2	4	4	NA	NA	20	Glu + Gln	Siemens	3.0	MEGA-LASER	1500/75	5.0	27.0, 42.8
	Choi et al. (16)	Human	NA	NA	NA	100	100	NA	Water	Philips	3.0	MEGA-PRESS	2000/106 (26, 80)	13.0	8.0
2D	Andronesi et al. (15)	Human	2	4	4	NA	NA	NA	Glu + Gln	Siemens	3.0	LASER-COSY	1500/45	12.8	27.0, 42.8

Table 5.2 1H-MRS Methods and Their Performance in Identifying *IDH*-mutational Status in Gliomas. †Specificity: estimated from *IDH* wild-type tumor voxels + healthy voxels, ‡Cutoff Cramer-Rao lower bound for successful spectral fitting, §For 2 HG concentrations of > 1 mM, ‖For 2 HG concentrations of ≥ 1 mM. Cho = choline, Cr = creatine, Gln = glutamine, Glu = glutamate, healthy = healthy brain tissue, *IDH* = isocitrate dehydrogenase, MT = tissue from *IDH*mutated tumor, NA = not available, sensitivity = estimated from *IDH*-mutated tumor voxels, TE1 = 1st echo time, TE2 = 2nd echo time, TR = repetition time, WT = tissue from *IDH* wild-type tumor, 1H-MRS = proton magnetic resonance spectroscopy, 2 HG = 2-hydroxyglutarate

5.2 AIMS

The main objective of this study is to setup and optimize non-invasive detection of 2 HG in 1H-MRS by a novel difference spectroscopy sequence (MEGA-PRESS; Mescher-Garwood Point-Resolved Echo Spectroscopy Sequence) in a prospective cohort of patients before surgery for a suspected glioma.

Secondary objectives will be to determine sensitivity and specificity of this technique by comparison with genomic analysis of tumor samples and to correlate with 2 HG tumor levels measured by gas chromatography-tandem mass spectrometry (GC-MS/MS).

Association with grade and genomic background will also be explored.

A supplementary cohort of *IDH* mutant glioma patients will be examined after surgery in order to determine sensitivity of MEGA-PRESS in this setting and to explore 2 HG variations during anti-cancer therapies.

5.3 Diagnostic value of 2-hydroxyglutarate detection by 1H-MR spectroscopy before surgery in patients with glioma: correlations with tumor phenotype and tissue dosage.

5.3.1 INTRODUCTION

The overproduction of the oncometabolite 2-hydroxyglutarate (2 HG) in *IDH* mutated gliomas can be detected non-invasively by magnetic resonance spectroscopy (MRS) (Andronesi, 2012; Choi, 2012).

IDH mutations (involving *IDH1* and *IDH2* isoforms) occur in 70–90% of grade II and grade III gliomas, and depict a molecular background and biological behaviour which differ significantly from *IDH*-wild type gliomas without dependence on the grade (Parsons, 2008; Sanson, 2009).

For these reasons, *IDH* mutational status has been recently integrated in WHO classification of brain tumor (Louis, 2016) as a determinant molecular factor together with 1p19 codeletion for histological diagnosis. Moreover, *IDH* mutant protein may become druggable targets of new therapies that can inhibit the mutant protein.

For these reasons, detection of *IDH* mutations is crucial for diagnosis, prognosis and treatment planification.

Previous studies reported the feasibility of non-invasive detection of 2 HG by MR spectroscopy for concentration >1mM with different spectroscopic methods based on conventional sequences optimized for detection of 2 HG, or spectral editing (Pope, 2012; Andronesi, 2012; Choi, 2012).

Detection of 2 HG by MRS in a preoperative setting proved to be challenging and *IDH* mutant case series reported so far are relatively small. In addition, few data are available on correlations with 2 HG measured in tissue samples, as well as the molecular status and histological phenotype.

In this study, we used a MEGA-PRESS difference spectroscopy sequence (Mescher-Garwood Point-Resolved Echo Spectroscopy Sequence; (Mescher, 1998)), for 2 HG detection in a group of 27 patients before surgery for a suspected grade II and grade III glioma. We assessed specificity and sensitivity and we related the results to 2 HG concentration in tumor as well as tumor molecular status.

5.3.2 METHODS

Patients

We prospectively studied adult patients with intracranial gliomas who went to the *Pitié-Salpétrière* Department of Neurosurgery for surgical resection or brain biopsy of their brain tumors. Collection of patient samples and clinico-pathological information was undertaken with informed consent and ethical board approval in accordance with the tenets of the Declaration of Helsinki. All subjects gave written informed consent. All patients displayed measurable disease on magnetic resonance imaging (MRI) for which surgical resection was warranted. Clinical classification and grading of the tissue was performed by a board-certified neuropathologist (Louis, 2016).

MRI/MRS Protocol

Acquisitions were performed using a 3-T whole-body system (MAGNETOM Verio, Siemens, Erlangen, Germany) equipped with a 32-channel receive-only head coil. The protocol included T2-weighted FLAIR and T1-weighted sequences for voxel placement and tissue segmentation. MRS data were acquired using a single-voxel MEGA-PRESS sequence optimized for 2 HG detection (TR=2s, TE=68ms, 128 averages, scan time = 9 min) with editing pulses applied at 1.9 and 7.5 ppm, for the edited and non-edited condition respectively, which allows for the measure of the 2 HG signal at 4.05 ppm.

Water suppression was performed using VAPOR and outer volume suppression techniques (Tkac, 1999). A non-water suppressed scan was acquired for quantification of absolute metabolite concentrations. Typical VOI size was 2x2x2 cm3 (Fig. 5. 1c, f). VOI size was adapted to tumor size in order to minimize partial volume effects, keeping a minimum size of 6 cm3.

MRS Post-Processing

Frequency and phase corrections were performed on single spectra based on the total choline signal at 3.2 ppm, using in-house written Matlab routines. Spectral quantification was performed using LCModel (Provencher, 2001) based on the water reference scan, assuming a bulk water concentration in tumors of 55.5 mM, and correcting for the water transverse relaxation time T2 (150 ms) (Madan, 2015). The Cramer Rao lower bounds (CRLB) threshold for reliable 2 HG detection was set to 30%.

Tumor analysis and 2 HG tissue dosage

Automated IHC was performed on 4-µm-thick FFPE sections with an avidin–biotin–peroxidase complex on Benchmark XT (Ventana Medical System Inc, Tucson AZ, USA) using the Ventana Kit including DAB reagent to search for the expression of *IDH1* R132H (Dianova, H09), P53 (DAKO, DO.7), and *ATRX* (SIGMA, polyclonal). Labeling was defined as positive (at least one cluster of positive tumor cells) or negative (no positive tumor cells detected) (Tabouret, 2016).

The QIAamp DNA Mini Kit was used to extract tumor DNA from frozen tumors, as described by the manufacturer (Qiagen, Courtaboeuf, France). DNA was extracted from blood samples using a conventional saline method.

Mutational status of *IDH1, IDH2* was determined using the Sanger technique, as previously described (Sanson, 2009). All cases in this series scoring negative for IDH1 R-132H immunostaining were analyzed for *IDH1* and *IDH2*.

The presence of 1p19q codeletion was assessed by CNV analysis by SNP array (9 cases) (Gonzalez-Aguilar, 2012) and a customs next-generation sequencing (NGS) targeted gene capture (11 cases).

Metabolite Extraction and Analysis

2 HG tissue levels were measured by gas chromatography-mass spectrometry (GC-MS/MS) using a Scion TQ instrument (Brüker) in full scan or MRM modes depending on metabolite concentration. Tissue samples were homogenized in bidistilled water and soluble protein concentration was measured by the BCA assay. All samples were treated by organic (ethylacetate) extraction and by a standard silylation protocol (BSTFA + 1% TMCS). Stable isotope internal standards were purchased from Cambridge Isotope Laboratories (2,3,3-D3-*2 HG*). Inter-series coefficients of variation and linearity for 2 HG were <6% and >99% in the ERNDIM external quality control programs (http://www.erndimqa.nl). "D vs. L stereoisomer determination was performed by chiral derivatization and GC-MS/MS in MRM mode as previously reported (Janin, 2014).

5.3.3 RESULTS

Patients

Between October 2014 and July 2016, we prospectively included 27 consecutive patients that were suspected of having a grade II or grade III glioma prior to surgery at *Pitié Salpétriere* Department of Neurosurgery (26 patients) and *Hopital Foch* (1 patient).

Of the 27 patients enrolled in this study, 25 were found to have good quality MRS: one patient was excluded because of a poor compliance during MR and one patient was excluded because of a small residual volume requiring voxel size<6 cm3 established as a minimum size for VOI in this study.

Patient's characteristics and findings are summarized in **Table 5.3.1**. 24 patients underwent MRS before a median interval of 1 day before surgery. Only in one patient (Patient 19) was surgery delayed by 6 months because of the occurrence of pulmonary embolism and the start of anticoagulant therapy. All patients but one were included before their first surgery at initial diagnosis of a suspected glioma. Patient 21 was included before second surgery for a known oligodendroglioma, which was diagnosed and operated on in 2007. Recurring in 2010, he was treated with chemotherapy by temozolomide for 24 months and radiotherapy; after an interval of two years without any treatment he recurred and was then included in this study before undergoing his second surgery.

With the exception of Patient 21, no patients received any cancer therapy before inclusion in this study. Among the 25 patients, all underwent subtotal resection excepted two patients (Patient 23 and Patient 24) who were biopsied. Because of the small size of tumor biopsy, frozen tissue for 2 HG tissue dosage was not available for these two patients.

Median age at diagnosis was 38 years old (range 22-63); sex ratio was 1.2.

Genotyping assay for *IDH* found 21 *IDH*-mutant and 4 *IDH* wild-type. In the *IDH* mutant group integrated diagnosis according to WHO 2016 (Louis, 2016), resulted in diffuse astrocytoma grade II (7 patients), anaplastic astrocytoma (7 patients), oligodendroglioma (2 patients), anaplastic oligodendroglioma (3 patients), and glioblastoma *IDH*-mutant (2 patients) (**Table 5.3.1)**. One patient (Patient 17) showed a particular phenotype *IDH* mutant, ATRX maintained, INA positive, p53 negative, *hTERT* C228T mutated, highly suggestive the presence of 1p19q which was finally not proved by NGS.

In the *IDH* wild-type subgroup, one was a ganglioglioma, two were diffuse astrocytoma grade II and one was a glioblastoma.

Regarding the type of *IDH* mutation, twenty patients harbored *IDH1* mutations (19 patients R132H, 1 patient R132G), one patient (Patient 20) harbored an *IDH2* R172K mutation.

MRI and MRS Studies

Because of the principal inclusion criteria consisting of the suspicion of grade II or grade III glioma, operative structural MRI imaging characteristics were generally indistinguishable between *IDH* mutant and wild-type tumors as shown in **Figure. 5.3.1** in C and D, respectively.

Tumor size, surrounding edema and mass were not associated with *IDH* mutational status.

Localized MR spectroscopy using MEGA-PRESS of the areas of tumor revealed the presence of measurable 2 HG at 4 ppm.

Principal criteria to score patients as 2 HG positives was 2 HG concentration CRLB <30%.

20 patients of this series presented measurable levels of 2 HG and CRLB < 30%: they were then finally scored as 2 HG positives in the pre-operative setting. After surgery, each of these 20 patients were confirmed to harbor an *IDH* mutant glioma.

For these patients, range of 2 HG concentrations by MRS was comprised between 1.42 and 8.56 mM (median 3.34mM) (**Figure 5.3.3** in A**).**

Inversely none of the four *IDH* wild-type glioma patients show any measurable 2 HG with high CRLB (99% in two patients, 65% and 66% in the remaining two).

CRLB value (31%) at limit of sensitivity were found in the remaining *IDH1* R132H mutant patients (Patient 1): in this case, MRS was finally scored negative for 2 HG MRS detection (**Table 5.3.1. and Figure 5.3.4**.).

No false positive for *IDH* mutation were recorded by MRS.

Example of MEGA-PRESS spectra for one *IDH*-mutant and one *IDH* wild-type are shown in **Figure 5.3.1.**

Twenty *IDH* mutant patients had measurable levels of 2 HG by MRS, with low CRLB values, suggesting that the measurement of 2 HG was accurate. They were then scored as "2 HG positive" in MRS according to our quality criteria. Inversely, no false positive was recorded in this series (**Table 5.3.1**).
MEGA-PRESS optimized for 2 HG detection show a sensitivity of 95% and specificity of 100% of prediction of the *IDH* mutation in the tumor. The positive predictive value of the presence of the *IDH* mutation for MEGA-PRESS was 100% (VPN 80%) (**Table 5.3.2**).

Quantitative Measure of 2 HG and Other Metabolites

Quantitative measures of 2 HG were available by MRS for 21 cases. Levels were comprised between a minimum of 1 nmol/mg to a maximum of 613 nmol/mg.
At the tissue level, gas chromatography-tandem mass spectrometry (GC-MS/MS) quantitation of tumor-derived 2 HG shows higher levels of 2 HG in *IDH* mutant compared to *IDH* wild-type samples (**Figure 5.3.3** in B).
Range of tissue 2 HG was comprised between 1.7 nmol/mg and 613 nmol/mg in *IDH* mutant (median 130 nmol/mg).
The two *IDH* wild-type for which a tissue dosage was available show levels at 1.0 and 2.9 nmol/mg.
To note, known ranges from the previous report (Dang, 2009) had 2 HG levels ranging from 5 to 32 µmol/gr in *IDH* mutated gliomas and from 0.045 to 0.68 µmol/gr in *IDH* wild-type gliomas (**Figure 5.3**).
Excepting for Patient 1, (presented in **Figure 5.3.4**), which is the only *IDH1* mutant in this series with 2 HG lower than the range reported by Dang et al., all other *IDH* mutant in this series displayed levels of 2 HG $\geq$ 18 nmol/mg.

2 HG tissue dosages by GC-MS/MS resulted then consistent with 2 HG MRS assessment because Patient 1 is the only *IDH* mutant patient scoring negative by MRS.

Regression analysis showed a significant correlation between 2 HG by MRS and tissue dosage (r^2=0.27; *P*=0.015) **(Figure 5.3.2).**

Next, to determine if histo-molecular background influences 2 HG accumulation we compared 2 HG detectable levels by the *IDH* mutant-1p19 codeleted gliomas (*IDH*+/1p19q+) versus *IDH* mutant-non codeleted gliomas (*IDH*+/1p19q-).

We did not find significant differences in 2 HG levels measured by MRS nor in the tissue between *IDH*+/1p19+ and *IDH*+/1p19-.

MRS 2 HG levels resulted 2.8 mM *IDH*+/1p19+ (range 1.67-8.5 mM; 4 patients) versus 3.8 mM in *IDH*+/1p19- (range 1.76-6.8 mM; 13 patients) (**Figure 5.3.3** in C).

By GC-MS/MS, median tumor 2 HG levels resulted in 79 nmol/mg in *IDH*+/1p19+ (range 45.9-154.0 nmol/mg; 5 patients) versus 135 nmol/mg in *IDH*+/1p19- (range 1.7-613 nmol/mg; 16 patients) (**Figure 5.3.3** in D).

Finally, to determine if glioma grade affected 2 HG levels, we compared detectable levels of 2 HG between glioma grades. We observed a higher median level in grade IV (7.7 mM) than in grade III (3.3 mM) and grade II (3.2 mM). We could not perform the Mann-Whitney test because of the number of grade IV samples <3. A t-test showed a significant difference of means of 2 HG- *P*= 0.0001 (grade IV versus grade II) and *P*=0.003 (grade IV versus grade II)-by MRS (**Figure 5.3.3** in E).

From the tissue dosages analysis, we observed a trend to higher concentration of 2 HG in *IDH* mutant GBM (median 371 nmol/mg; range 130-613 nmol/mg) versus grade III (median 125 nmol/mg; range 23.80-336 nmol/mg) and grade II (median 117 nmol/mg; range 1.7-316 nmol/mg), but these differences did not

raise level of significativity (*P*=0.06 and *P*=0.08 respectively) (**Figure 5.3.3** in F). To note, Patient 25 harboring an *IDH* wild-type glioblastoma showed low levels in the tissue (2.9 nmol/mg) and no measurable 2 HG by MRS.

Impact of Surgery and Anti-Cancer Therapies in a Supplementary Cohort

In order to explore reliability of non-invasive 2 HG measure by MRS in post-operative management of *IDH* mutant glioma patients, we extended our analysis to a supplementary group of 35 patients known to be affected by an *IDH* mutant glioma.

We analyzed these 35 patients by the same MRS protocol, as used in the pre-operative setting and previously describe (15 grade II, 15 grade III and 4 grade IV at the initial tumor).

Sixteen patients were scanned after surgery and before starting an anticancer therapy, 19 patients were scanned post-treatement during or after radiotherapy or chemotherapy.

Interestingly, we observed that sensitivity of non-invasive detection of 2 HG accumulation dramatically decreased to 43%.

Measurable levels of 2 HG, according to good quality criteria (CRLB<30%) were found in 15 patients out of 35.

Among cases scoring positive for 2 HG by MRS, we noticed that a higher fraction of patients 9/15 (60%) were scanned in a pre-treatement phase versus 7/20 (35%) in the group scoring negative of 2 HG at MRS.

Even if insignificant, this trend was consistent with a supplementary finding in the first patient who completed a follow-up period before and during radiotherapy followed by chemotherapy protocol.

This representative case is shown in **Figure 5.3.6**. The patient was affected by an anaplastic oligodendroglioma harboring *IDH* mutation (**Figure 5.3.6**) and 1p19q codeletion and was treated by radiotherapy and adjuvant PCV after surgery. First MRS scan was performed after surgery and before starting radiotherapy, and then

repeated after radiotherapy and during chemotherapy protocol. During the follow-up we observed a striking and progressive reduction of 2 HG levels with regression of detectable levels of 2 HG after radiotherapy (4.1 mM with CRLB 10% at baseline; 2.2 mM with CRLB 24% 1 month after radiotherapy and 1.37 mM CRLB 35%, 5 months after radiotherapy and during PCV chemotherapy) as it showed by subsequent spectra 1 month after radiotherapy and during chemotherapy **Figure 5.3.6**.

Similarly, 9 patients in this series were included in a phase 1 escalating dose trial with specific inhibitors of IDH1 (AG120) and IDH2 (AG221) (Agios). Among them, 6 show measurable levels of 2 HG by MRS at baseline and then continued the follow-up with close MRS scans during the first month after the start of the treatment.

Average levels of 2 HG at different time points are illustrated in plot G in **Figure 5.3.7** and 1 representative for the anti-IDH1 and the anti-IDH2 protocols are illustrated in **Figure 5.3.7**. The follow-up of these representative cases and of mean levels of 2 HG show an important and permanent decrease of 2 HG rapidly after the start of the specific anti- *IDH* target therapy.

Finally, in order to expand our analysis to a putative effect of genomic background of 2 HG levels, we combined 2 HG measurements by MRS in patients harboring glioma with *IDH* mutation from the pre-operative cohort (17 patients) and the post-operative cohort (35 patients).

In this larger series we confirmed the absence of significant differences in 2 HG concentrations by MRS between 1p19 codeleted gliomas (median 2 HG 3.8; range 1.6-9.2mM) versus 1p19 non codeleted gliomas (median 3.9; range 1.76-6.8) but, remarkably, we found that three patients (Patient 20 from the preoperative cohort) and two patients from the post-operative cohort harboring *IDH2* K172 displayed significantly higher levels of 2 HG (median 2 HG 6.8mM, range 4.3-9.2mM) than *IDH1* mutant (3.79mM; range 1.67-8.5mM) (P=0.03). Despite the small sample size (only 3 *IDH2* mutant), differences resulted as being statistically significant and results are shown **Figure 5.3.5.**

Pt	Sex	Age at diagnosis	Histological diagnosis	IDH status	1p19q codeletion	ATRX immunostaining	MRS 2 HG concentration (mM)	CRLB (%)	Tumor 2 HG concentration (nmol/mg)
1	M	31	diffuse astroyctoma grade II	IDH1 R-132H	no	loss	1.2	31	1.7
2	M	32	diffuse astroyctoma grade II	IDH1 R-132H	no	loss	2.26	26	18.0
3	M	33	diffuse astroyctoma grade II	IDH1 R-132H	no	loss	4.48	14	117.0
4	F	32	diffuse astroyctoma grade II	IDH1 R-132H	no	loss	3.79	6	138.0
5	M	33	diffuse astroyctoma grade II	IDH1 R-132G	na	loss	1.76	20	145.0
6	F	27	diffuse astroyctoma grade II	IDH1 R-132H	no	loss	1.47	28	213.0
7	F	49	diffuse astroyctoma grade II	IDH1 R-132H	no	loss	4.33	11	316.0
8	F	39	oligodendroglioma grade II	IDH1 R-132H	yes	maintained	1.42	22	68.0
9	F	51	oligodendroglioma grade II	IDH1 R-132H	yes	maintained	2.47	15	45.9
10	F	48	anaplastic astrocitoma grade III	IDH1 R-132H	no	loss	3.34	14	117.9
11	M	38	anaplastic astrocitoma grade III	IDH1 R-132H	no	loss	2.76	21	68.0
12	F	32	anaplastic astrocitoma grade III	IDH1 R-132H	no	loss	4.06	12	115.0
13	M	40	anaplastic astrocitoma grade III	IDH1 R-132H	no	loss	3.18	15	133.0
14	F	45	anaplastic astrocitoma grade III	IDH1 R-132H	no	loss	2.04	15	209.0
15	F	25	anaplastic astrocitoma grade III	IDH1 R-132H	no	loss	4.11	10	304.0
16	F	30	anaplastic astrocitoma grade III	IDH1 R-132H	no	loss	3.93	9	336.0
17	M	49	anaplastic oligodendroglioma grade III	IDH1 R-132H	no	maintained	1.66	26	23.8
18	M	32	anaplastic oligodendroglioma grade III	IDH1 R-132H	yes	maintained	1.67	18	79.0
19	M	54	anaplastic oligodendroglioma grade III	IDH1 R-132H	yes	maintained	3.3	13	154.0
20	M	56	glioblastoma	IDH2 R-172K	na	loss	6.8	8	613.0
21	M	45	glioblastoma	IDH1 R-132H	yes	maintained	8.56	6	130.0
22	M	22	ganglioglioma grade I	IDH1 and IDH2 wild-type	no	na	0	999	1.0
23	M	48	diffuse astroyctoma grade II	IDH1 and IDH2 wild-type	no	maintained	1.17	69	na
24	F	63	diffuse astroyctoma grade II	IDH1 and IDH2 wild-type	na	maintained	0.07	999	na
25	M	41	glioblastoma	IDH1 and IDH2 wild-type	no	maintained	0.77	65	2.9

Table 5.3.1. Clinical and histo-molecular features of the cohort with corresponding 2 HG by MRS and tissue dosage. CRLB means Cramer Rao lower bounds; na=not available.

	2 HG MRS positive	2 HG MRS negative	Total
IDH mutated glioma	20	1	21
IDH wild-type glioma	0	4	4
Total	20	5	25

Table 5.3.2. Predictive value of 2 HG non-**invasive detection by MRS in a prospective cohort of 25 patients scanned before surgery**. *IDH* mutation status was assessed in *IDH1* and *IDH2*. MRS by MEGA-PRESS proved to be highly specific (100%) and sensitive (95.2%). Positive predictive value was 100% and the negative predictive value 80% (chi2 19.05).

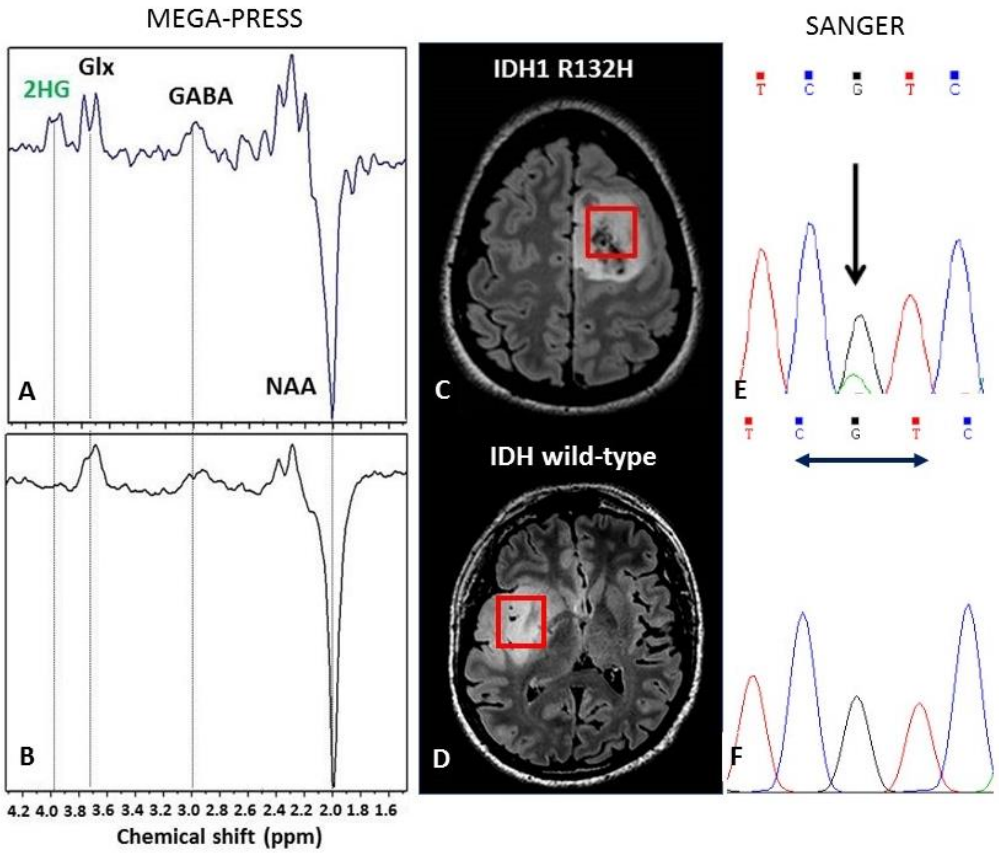

Figure 5.3.1. Examples of MEGA-PRESS Spectra, Voxel positioning and Sanger sequence of *IDH1* codon 132 of the tumor after resection, of one *IDH* mutated glioma patient (in A, C and E) and one *IDH* wild-type glioma patient in (B, D and F). MRS spectrum after differential editing shows a peak of 2 HG at 4ppm (in A) and the absence of the 2 HG peak in B. Sanger sequencing show the presence an hetozygote R-132H mutation of *IDH1* characterized by the appearance of a green peak in chromatogram corresponding to adenine at guanine position (black peak) in F *IDH1* wild-type sequence at codon 132.

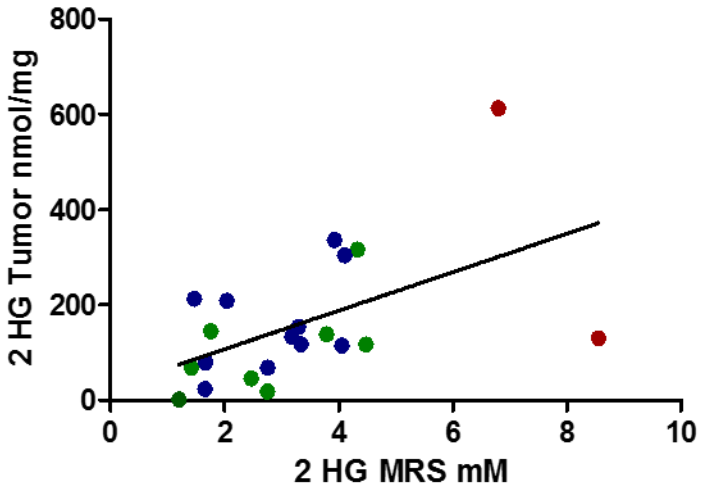

Figure 5.3.2. Regression plot of 2 HG concentrations measured by MRS (X axis) and in the tumor GC-MS/MS (Y axis) in the subgroup of 21 patients with measurable levels of 2 HG **on MRS (and CRLB<30%).** Green Dots correspond to grade II, blue dots to grade III and red dots to grade IV. 2 HG concentrations in MRS display a significant correlation with concentration in the tumor (r2=0.27; *P*=0.015).

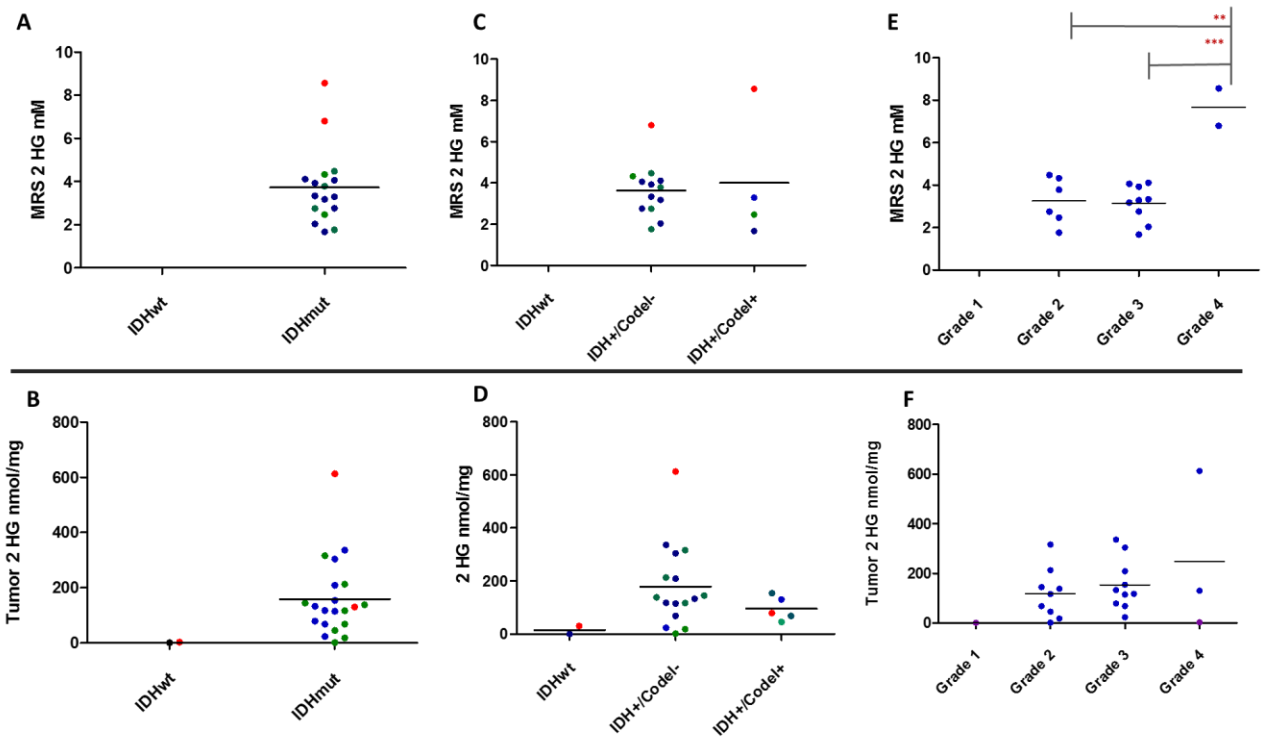

Figure 5.3.3. 2 HG measurable levels in the tissue, and by MRS according to *IDH* status (A and B), molecular subgroup (C and D) and grade (E and F). Each symbol represents the amount of the listed metabolite found in each tumor sample.
Black bars indicate the group sample means.
In plot A, B, C, D green dots correspond to grade II, blue dots correspond to grade III and red dots correspond to grade IV. In plot E and F violets dots correspond to *IDH* wild-type sample.
Plot A, C, D corresponds to dosages by MRS. Only measureable levels of 2 HG with CRLB<30% are reported.
Plots D, E, and F correspond to dosages by GC-MS/MS analysis.
In A and B gliomas are stratified according to the *IDH* status.
IN C and D, gliomas are stratified according to the molecular subgroup (*IDH*wt versus *IDH* mut1p19q codeleted versus *IDH* mutant 1p19q non codeleted).
In E and F, gliomas are stratified according the grade.
In grade IV, by MRS, 2 HG mean level was significantly higher than grade III and grade II by t test (P=0.0001 and 0.003 respectively).
In grade IV, tumor 2 HG shows a trend to higher concentrations (median 371 nmol/mg; range 130-613 nmol/mg) versus grade III (median 125 nmol/mg; range 23.80-336 nmol/mg) and grade II (median 117 nmol/mg; range 1.7-316 nmol/mg) (P=0.06 and P=0.08 respectively).
No differences were observed according to the molecular subgroups *IDH*+/Codel+ versus *IDH*+/Codel- subgroups.

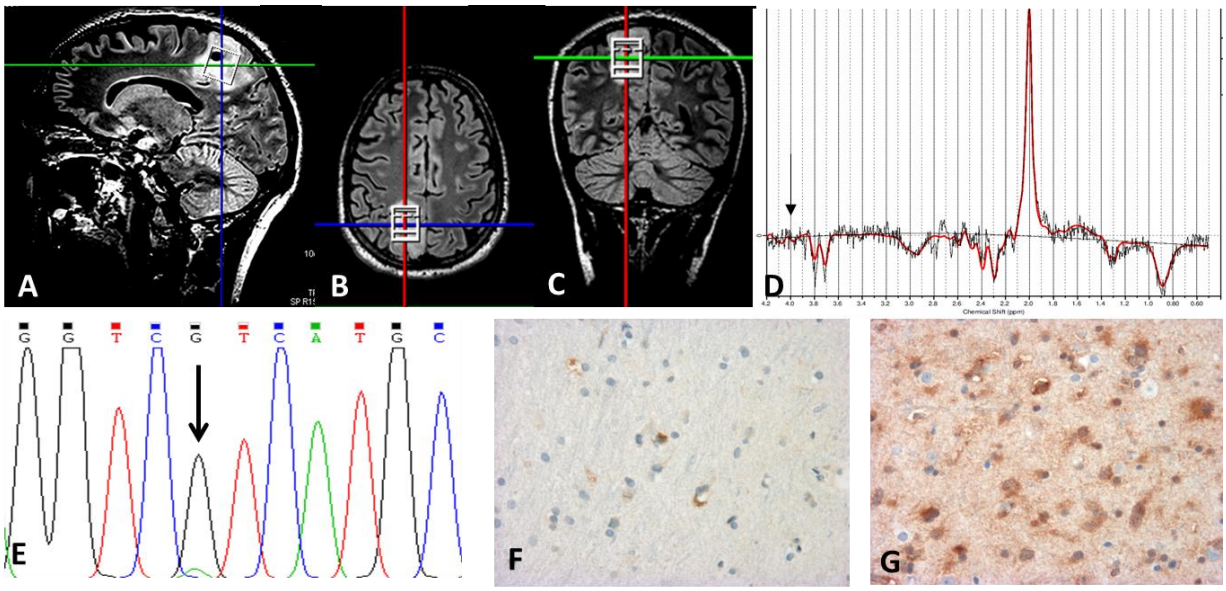

Figure 5.3.4: MRS and Spectra obtained by Mega-Press in Patient 1. Detection of 2 HG peak is at limit of sensitivity (CRBL 31%) and then MRS was scored negative for 2 HG detection. This patient correspond the only false negative case of this series (Tab2). Interestingly, the average percentage of tumor cells expressing the mutant form of *IDH1* R132H was around 10%, with heterogeneous areas scoring from 50% and 1% labeled tumor cells (100% of tumor cells). Contamination by non-tumor cells was present. Molecular analysis showed a small peak in chromatogram corresponding to the mutant allele of *IDH1* in codon 132 and NGS analysis assessed a fraction of 0.048% (37/761) mutant reads. Molecular and histological findings in this patient suggest a sort of dilution with wild-type *IDH1* DNA and protein and could explain in part the negative result of MRS.

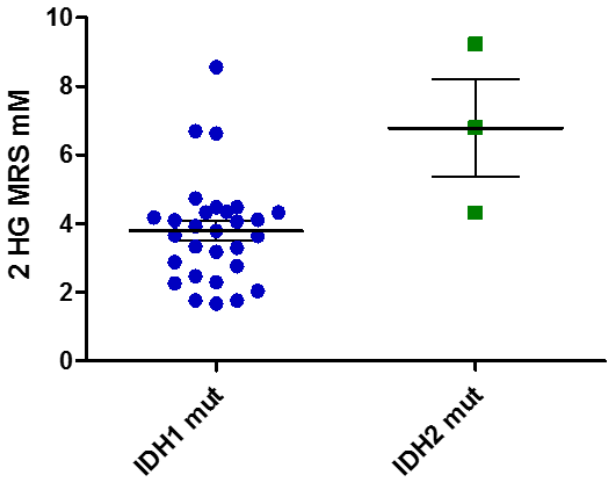

Figure 5.3.5. 2 HG measurable levels by MRS in 32 *IDH* mutant gliomas (17 from the pre-surgery and 15 from the post-surgery subgroups) according to *IDH* mutation. Levels distribution analysis show significant higher levels in the 3 patients harboring *IDH2* K172 mutations (median 2 HG in *IDH1* mutant 3.79mM versus 6.80 mM in *IDH2* mutants; *P*=0.03)

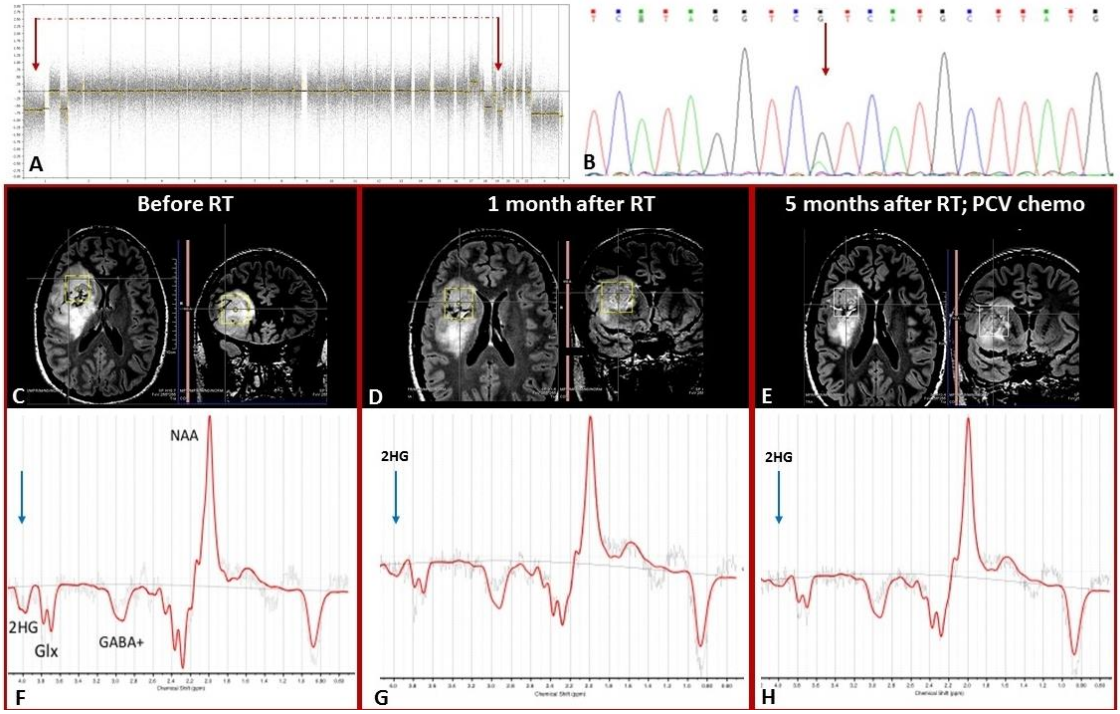

Figure 5.3.6 2 HG permanent decrease during radiothemotherapy. A representative case of a 50-year-old patient affected by an *IDH* mutant 1p19q codeleted anaplastic oligodendroglioma that was scanned by MRS after surgery and then every month during anticancer treatment.
In A) SNV plot of tumor DNA showing a complete loss of small arm of 1p and long arm of 19q (indicated by the arrows), In B) Sanger sequence showing the hetozygous mutation in codon 132 of *IDH1*.
Axial and coronal FLAIR imaging before starting radiotherapy and 1 months later and 5 months later during conomcitant chemotherapy by PCV (are shown in C, D and E respectively).
MRS Spectra obtained by Mega PRESS before RT (in F), 1 month after radiotherapy and 4
5 months after radiotherapy shows a significant decrease of 2 HG from 4.1 mM (CRLB 10%) to undetectable levels.

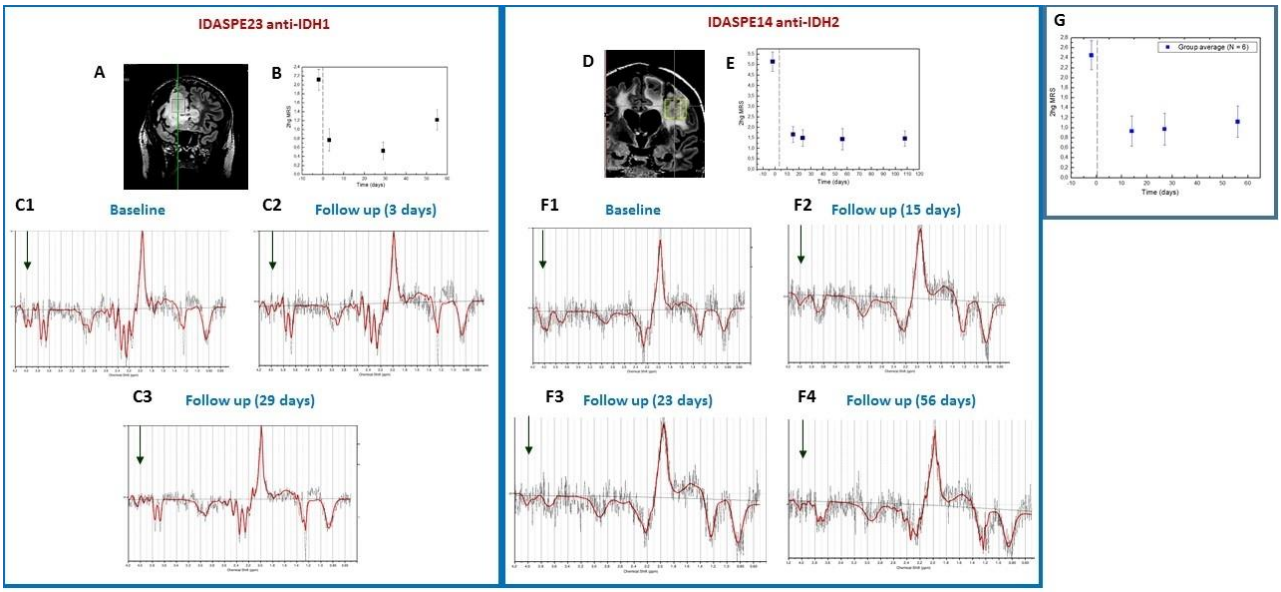

Figure 5.3.7 2 HG decrease specific anti IDH1 and anti IDH2 therapies.
In the left block a representative case of a 36 patient harboring an *IDH* mutant glioma. In A Flair imaging at baseline and in B 2 HG levels measured at different time points are consistent with the reduction of 2 HG peak observed rapidly at 3 days (C2) and 29 days (C3).
A similar results observed in Patient Idaspe 14 (54 years old) harboring an *IDH2* mutation and treated by an anti IDH2. Baseline and subsequent spectra (F1, F2, F3 and F4) showed a prompt and persistent reduction of 2 HG at 4 ppm.
Average levels of the 6 patients included in specific anti-IDH therapies are reported in G, showing the permanent reduction of 2 HG after the start of target therapies.

5.3.4 DISCUSSION

The quantification of the 2 HG metabolite through MRS represents an appealing imaging biomarker in glioma because it directly measures the product of the mutant enzyme, which is highly useful for diagnosis, treatment planification and prognosis. Moreover, the fascinating perspective of realizing the pharmacodynamics measure of activity of anti-IDH therapies at the tumor level in real time makes this technique appealing despite its technical challenges.

A number of approaches and methodologies have been reported (PRESS; LASER, COSY) with high levels of sensitivity (100%) and lower levels of specificity 70-90% (see **Table 5.3.2**).

In this study we report an original technique for 1H-MRS non-invasive detection of 2 HG by MEGA-PRESS as a reliable tool to predict *IDH* mutation. Using stringent criteria as CRLB<30%, MEGA-PRESS proves to be highly precise (100%) and with sensitivity of around 95%.

Consistently, 2 HG levels assessment by MEGA-PRESS resulted in a good correlation with 2 HG tissue dosages.

Based on our data and previous reports (Dang, 2010; Andronesi, 2012) most tumor levels of 2 HG seem to be high enough to grant detection by in vivo MRS, however there may be a number of tumors in which levels could be around or below the 1-mM detection threshold, conclusively affecting sensitivity. Indeed, one *IDH* mutant glioma in our series showed 2 HG levels and CRLB at the lower limit of detectability and was finally judged as negative by MRS. In this patient, we found a very low level of 2 HG in the tissue and an important contamination by non-tumor cells at histological and genomic level. Consistently with our observation, density of tumor cells has been recently suggested as a factor influencing 2 HG measurement by MRS (de la Fuente, 2016).

This point may intuitively explain the dramatic reduction of sensitivity at 43% of MEGA-PRESS in detection of 2 HG after surgery, as we observed in our supplementary series of post-operative patients.

We investigated other potential factors correlating with 2 HG levels and we observed that high-grade *IDH* mutant gliomas show higher levels of 2 HG as well as *IDH2* mutation. The 1p19 codeletion does not seem to influence 2 HG levels. However, the rare *IDH2* mutation, which is associated with 1p19q codeletion, appears associated with higher levels of 2 HG.

Finally, our preliminary result on radiological follow-up of *IDH* mutant patients during radiochemiotherapy suggests that one of the major factors that affect 2 HG level are cancer therapies, as shown in our representative cases and also other reports (Andronesi, 2012). Further studies might elucidate duration of such a decrease, the presence of differential response of 2 HG to specific chemo-radiotherapy regimens and more interestingly if 2 HG decreases may be a predictor of tumor response, clinical benefit and/or tumor progression.

More fascinatingly, we report here our preliminary results on 2 HG as dramatically and rapidly decreasing with anti-IDH therapies. This observation proves that MEGA-PRESS is a reliable and reproducible method for 2 HG assessment and open fascinating field of research on the value of this variation in *IDH* mutant response and resistance to target therapy.

6. CONCLUSIONS AND PERSPECTIVES

To date, driver oncogenes remain the most appealing targets for development of innovating therapies and new diagnostic tools.

In this study, we dichotomized the field of research in the two main nosological entities identified in glioma so far: the *IDH* mutant and *IDH* wild-type, and we developed a novel approach for target therapies and non-invasive molecular diagnosis.

In the first study we proposed a molecular prognostic classification of gliomas basing on *IDH* and *pTERT* mutational status and we also reported a striking parallelism of germ line variants which are differently associated to the risk of developing specific subtypes of glioma mainly according the *IDH* status.

In the second study focused on *IDH* wild-type gliomas, we reported an unbiased screening assay for *FGFR-TACC* fusions that occur in grade II and III glioma harboring wild-type *IDH1*, with frequency similar to glioblastoma (GBM), therefore providing a clue to the aggressive clinical behavior of this glioma subtype in glioma.

Our RT-PCR based assay overcomes the great variability of variants that are generated by *FGFR-TACC* chromosomal translocation in human cancer. Thanks to the largest screening performed so far, we identified the highest number of cases harboring *FGFR-TACC* gene fusions and we were able to show that *FGFR-TACC* fusions display a specific genomic background, which is mutually exclusive with *IDH* and *EGFR* amplification, but co-occurs with *CDK4*, *MDM2* amplification and 10q loss.

We showed that *FGFR-TACC*-positive glioma displays strikingly uniform expression of the fusion protein and, judging from the high specificity of FGFR3 staining, we found that FGFR3 IHC could be considered a reliable method for prescreening. Preclinical experiments with *FGFR3-TACC3*-positive glioma cells treated with an anti-FGFR TK inhibitor (JNJ-42756493) showed strong anti-tumor effects and treatment of two patients with recurrent GBM harboring

FGFR3-TACC3 resulted in clinical improvement and radiological tumor reduction.

We also showed that *FGFR3*-TAC3 fusions are associated with longer survival in GBM and given the promising therapies we are testing in this setting, rechallenge and concomitant administration of target TK inhibitors may be a relevant option to be tested to produce a clinically relevant benefit in this selected subgroup of patient.

In perspective, we will then move to analysis of clinical efficacy of anti-FGFR specific target therapies and of eventual mechanism of resistance.

In the third study, we developed and validated novel methods for 2 HG detection in *IDH* mutant tumors and we showed that this technique is highly specific and sensitive in pre-operative stages and that it could be integrated in diagnostic work-up.
In the post-operative phase 2 HG seems to be, in a number of patients, an interesting new imaging marker to monitor. Further studies will answer the question on the predictor value of this variation of response and survival.

In conclusion, our findings may have contributed to enrich the repertoire of target driver oncogenes of therapeutic relevance in glioma and improve access towards innovating diagnostic tools in the field of neuro-oncology.

7. ANNEXES

In this section, we report twelve articles and studies where we contributed, from November 2013, as authors or co-authors, and that are annexes to the PhD research project on molecular markers of gliomas presented in this thesis.

REVIEW

Predictive biomarkers in adult gliomas: the present and the future

Laure Thomas[a], *Anna L. Di Stefano*[b], *and François Ducray*[a,c]

Purpose of review
This review summarizes recent studies on the predictive value of molecular markers in adult gliomas, including 1p/19q codeletion, *MGMT* methylation, *IDH* mutation and markers identified using omics and next-generation sequencing studies.

Recent findings
The long-term results of the Radiation Therapy Oncology Group and European Organization for Research and Treatment of Cancer trials in anaplastic oligodendroglial glioma have shown that the 1p/19q codeletion predicts an overall survival benefit from early PCV (procarbazine CCNU vincristine) chemotherapy. This benefit can also be predicted using gene expression-based molecular subtypes of gliomas while the predictive value of the *IDH* mutation in this context requires further study. In elderly patients with glioblastoma, the analysis of *MGMT* methylation status in two phase III trials suggests that this alteration may guide treatment decisions; however, this finding still needs confirmation in prospective studies. Omics and next-generation sequencing studies have identified additional potential predictive markers. In particular, *IDH* mutations, *BRAF* V600E mutations and *FGFR* gene fusions might predict efficacy of therapies targeted against these alterations.

Summary
Currently, the 1p/19q codeletion is the only well established predictive marker with clinical utility. However, it is likely that other molecular markers such as *MGMT* methylation, *IDH* mutation and those identified using omics and next-generation sequencing studies will further guide treatment decisions in adult gliomas.

Keywords
1p/19q codeletion, glioma, IDH mutation, MGMT methylation, predictive biomarker

INTRODUCTION

Until recently, treatment decisions in glioma were based on clinical, radiological and histological factors with little use of predictive molecular markers [1]. When treating anaplastic gliomas, many neuro-oncologists used the 1p/19q codeletion status for care decisions but this strategy was not supported by strong evidence [2▪]. In glioblastoma patients less than 70 years, *MGMT* methylation predicts a stronger benefit of temozolomide radiochemotherapy, but is not decisional in this population, as unmethylated patients can benefit from this regimen [3].

Now, the long-term results of the Radiation Therapy Oncology Group (RTOG) and European Organization for Research and Treatment of Cancer (EORTC) trials have clearly established that the 1p/19q codeletion predicts a benefit for early chemotherapy in anaplastic gliomas, and two phase III trials suggest that *MGMT* methylation should guide treatment decisions in elderly patients with glioblastoma [4▪▪–7▪▪]. In addition, omics and next-generation sequencing studies have identified gene expression signatures and molecular markers that could predict treatment efficacy, particularly when using targeted therapies [8▪▪–10▪▪].

[a]Service de Neuro-Oncologie, Hôpital Neurologique, Hospices Civils de Lyon, [b]Université Pierre et Marie Curie-Paris 6, Centre de Recherche de l'Institut du Cerveau et de la Moelle épinière (CRICM), UMR-S975, Paris and [c]INSERM, U1028; CNRS, UMR5292; Lyon Neuroscience Research Center, Neuro-Oncology and Neuro-Inflammation Team, Université Claude Bernard Lyon 1, Lyon, France

Correspondence to François Ducray, Service de Neuro-oncologie, Hôpital Neurologique, 59 boulevard Pinel 69003 Lyon, France. Tel: +33 4 72 68 49 64; fax: +33 4 72 35 73 29; e-mail: francois.ducray@chu-lyon.fr

Curr Opin Oncol 2013, 25:689–694
DOI:10.1097/CCO.0000000000000002

KEY POINTS

- In anaplastic gliomas, 1p/19q codeletion predicts early chemotherapy benefit.
- The predictive value of *MGMT* methylation in elderly glioblastoma patients is promising but needs further confirmation.
- In the near future, predictive biomarkers will likely guide the use of targeted therapies.

CHROMOSOME 1P/19Q CODELETION

In 1998, the 1p/19q codeletion has been associated with response to chemotherapy in anaplastic oligodendrogliomas [11]. However, in contrast to its well established prognostic value, the predictive value of the 1p/19q codeletion had, until recently, remained a topic of debate.

Chromosome 1p/19q codeletion is strongly associated with classical oligodendroglial features. It results from an unbalanced translocation between the entire arm of 19p and 1q [12]. At the genomic level, it corresponds to a complete loss of the 1p and 19q arms, which is important to distinguish from 1p partial distal deletions (typically 1p36) that occur in astrocytic tumors and are associated with a poor prognosis [13–15]. Using fluorescence in-situ hybridization or loss of heterozygosity techniques with probes focusing solely on 1p36 loci (as classically performed) may be insufficient to discriminate between the two types of 1p deletions [13]. 1p/19q codeletion is almost always associated with an *IDH1/IDH2* mutation and is exclusive from *TP53*, *ATRX* mutations and from *EGFR* and other gene amplifications [16,17▪,18▪,19▪▪]. Mutations of *CIC* (located on 19q) and *FUBP1* (located on 1p) occur in approximately 60 and 15% of cases, respectively, and are specific to 1p/19q-codeleted tumors [19▪▪,20▪▪,21]. The recently identified mutations of the *TERT* promoter, which lead to increased telomerase expression, seem to be present in nearly all 1p/19q-codeleted tumors [22▪,23▪,24▪▪]. These mutations are also present in the majority of primary glioblastomas. In contrast, they are rare in *IDH* mutated non1p/19q-codeleted gliomas. These tumors harbor *ATRX* mutations that maintain telomere length independently of telomerase activity (alternative lengthening of telomeres) [24▪▪]. At the gene expression level 1p/19q codeletion is associated with a proneural gene expression profile and the expression of neuronal genes [25]. In particular, internexine alpha expression can be used as a surrogate marker of the 1p/19q codeletion and has a strong prognostic value in anaplastic gliomas [26–28].

In the mid 1990s, two phase III studies – one by the RTOG and the other by the EORTC – were initiated to test if adding PCV (procarbazine CCNU vincristine) chemotherapy to radiotherapy as part of the initial treatment might improve the overall survival (OS) of patients with anaplastic oligodendroglial tumors (AOTs). The first results of these two studies, published in 2006, showed that PCV and radiotherapy increased progression-free survival (PFS) but did not affect OS and that this outcome was true irrespective of 1p/19q status [29,30]. After a median follow-up of 11 years, the long-term results of both studies now clearly demonstrate that 1p/19q codeletion is not only a major prognostic factor but also a major predictive factor of early chemotherapy benefit [4▪▪,5▪▪]. In patients with 1p/19q-codeleted tumors, PCV and radiotherapy resulted in a nearly three-fold increase in median PFS compared with radiotherapy alone (8.4 years versus 2.9 years in the RTOG study; 13 years versus 4.1 years in the EORTC study) and in a two-fold increase of the median OS (14.7 years versus 7.3 years in the RTOG study; median OS not reached versus 9.3 years in the EORTC study). In contrast, early PCV was associated with only a modest increase in PFS with no effect on OS in non1p/19q-codeleted tumors. Therefore, the updated results of the RTOG and EORTC study define radiotherapy and PCV as the new standard of care for newly diagnosed 1p/19q-codeleted AOTs. However, the survival curves of patients with 1p/19q-codeleted AOTs treated with radiotherapy alone or radiotherapy and PCV only began to diverge at 5 years, which suggests that some 1p/19q-codeleted tumors are not sensitive to PCV. As such, additional biomarkers need to be identified within 1p/19q tumors. Although radiotherapy and PCV did not improve median OS in non1p/19q-codeleted tumors, the survival curves indicated a higher rate of long-term survival in this group compared with those in the group that received radiotherapy alone. Because noncodeleted tumors that harbor *IDH* mutations are associated with a far better prognosis than non1p/19q-codeleted tumors that express wild-type IDH, assessing the value of *IDH* status to predict early chemotherapy benefits in non1p/19q-codeleted tumors would be interesting [16]. In the EORTC study, robust conclusions could not be made because of the limited number of patients with AOTs that were both non1p/19q-codeleted and *IDH*-mutated. Further molecular analyses from the RTOG study are expected. Interestingly, a translational study on the EORTC study demonstrated that the benefit of early PCV chemotherapy could be more reliably predicted by tumor gene expression profiles [8▪▪]. One hundred and forty AOTs were assigned to main gliomas subtypes [called intrinsic glioma

subtypes (IGS)] previously identified based on unsupervised gene expression analysis. Tumors assigned to IGS-9 (which was enriched in 1p/19q codeleted tumors) significantly benefited from adjuvant PCV. A similar (although nonsignificant) trend was observed for tumors assigned to IGS-17 (which was enriched in *IDH* mutated but non1p/19q-codeleted tumors).

In low-grade gliomas (LGGs), 1p/19q codeletion also has a strong prognostic value. The median survival duration is 12–15 years in the presence of the 1p/19q codeletion and 5–8 years in the absence of the codeletion [1]. In the largest published series of patients treated with up-front temozolomide, the 1p/19q codeletion was associated with both a higher response rate (72 versus 46%) to chemotherapy and a longer duration of response (>40 versus 20 months) [31]. However, its predictive value needs to be confirmed in prospective clinical trials [32]. Analysis of the outcome according to the 1p/19q codeletion in the RTOG phase III trial (radiotherapy versus radiotherapy and PCV in unfavorable LGGs) and in the EORTC/NCIC phase III trial (up-front radiotherapy versus up-front temozolomide in progressive LGGs) are expected to clarify the predictive and clinical values of 1p/19q in LGGs.

O6-METHYLGUANINE-DNA METHYL TRANSFERASE

MGMT silencing through methylation of its promoter induces low expression of MGMT protein and decreases DNA-repair activity, which increases sensitivity to alkylating agents.

MGMT methylation occurs in approximately 40% of glioblastomas. In 2005, it was identified as both a strong prognostic and predictive marker in glioblastomas treated with temozolomide radiochemotherapy [33]. However, assessment of *MGMT* methylation was not incorporated into treatment decisions because *MGMT* methylation was only demonstrated to be a quantitative predictive marker. Indeed, when the effect of concomitant and adjuvant temozolomide versus radiotherapy alone was evaluated in the EORTC/NCIC 26981/22981 glioblastoma trial, the benefit of radiochemotherapy was higher in *MGMT*-methylated patients (23.4 versus 15.3 months, $P=0.004$) than in *MGMT*-unmethylated patients (12.6 versus 11.8 months, $P=0.035$). However, the latter group still benefited from this treatment, particularly in terms of long-term survival [34].

A retrospective analysis of *MGMT* methylation was recently performed in two phase III trials, the NOA-8 and the Nordic trials, which evaluated the effect of radiotherapy versus temozolomide chemotherapy in elderly glioblastoma patients [6••,7••]. *MGMT* methylation was analyzed in 56 and 69% of patients in the NOA-8 and the Nordic trial, respectively. In the NOA-8 trial (patients >65 years), *MGMT*-methylated patients had a longer PFS when treated with temozolomide as opposed to radiotherapy (8.4 versus 4.6 months, $P=0.01$), whereas *MGMT*-unmethylated patients had a longer PFS when treated with radiotherapy than with temozolomide (4.6 versus 3.3 months, $P=0.01$). A similar yet not significant trend was observed for OS. The Nordic trial (patients >60 years) showed a nonsignificant trend toward longer OS in *MGMT*-methylated patients when treated with temozolomide rather than with radiotherapy (hazard ratio = 0.64, $P=0.07$), but *MGMT*-unmethylated patients did not fare better when treated with radiotherapy than with temozolomide. PFS data were not available for this trial, as these data were deliberately not collected. These results, together with another retrospective study, suggest that *MGMT* methylation could guide treatment decision in elderly patients with glioblastoma [35•]. However, the data are not yet robust enough to be translated into the clinic and need prospective validation. The results of the NCIC/EORTC phase III trial (accelerated radiotherapy versus accelerated radiotherapy and temozolomide) are awaited to clarify the predictive value of this alteration in elderly patients with glioblastomas and the place of combined radiochemotherapy in this population.

Until now, the use of *MGMT* methylation as a predictive factor has also been limited by the fact that the optimal technique to study *MGMT* methylation is still debated. In a recent study, the rate of *MGMT*-methylated patients varied from 33 to 60% depending on the method that was used [36••]. Methylation-specific PCR has been used as a standard to study *MGMT* methylation, but this method is only qualitative and lacks automation. Therefore, alternative semiquantitative and quantitative techniques have been developed. However, these techniques do not study exactly the same regions of the *MGMT* promoter. Therefore, as the methylation pattern of the promoter can be heterogeneous, some patients are classified as methylated or as unmethylated depending on the technique used [36••]. Two recent studies suggested that pyrosequencing was the most reliable technique and had the best predictive value [36••,37•]. Interestingly, both the methylation-specific PCR and the pyrosequencing technique analyze a region of the *MGMT* promoter, wherein methylation was recently shown to display the highest negative correlation with MGMT expression and the highest positive correlation with survival [38••].

In contrast to glioblastomas, *MGMT* methylation in anaplastic gliomas appears until now only as a prognostic factor without predictive value [39,40]. This may be explained by the fact that, in these tumors, *MGMT* methylation is tightly associated with *IDH* mutation and a diffuse hypermethylated phenotype [38••,41].

IDH1/IDH2 MUTATIONS

Isocitrate dehydrogenase mutations have a strong diagnostic and prognostic value in adult diffuse gliomas but no clear predictive value [42]. Whether *IDH* mutated non1p/19q-codeleted anaplastic gliomas benefit from early PCV chemotherapy remains to be determined. The *IDH* mutation has been suggested to predict the response to first-line temozolomide chemotherapy in low-grade gliomas, but this finding requires confirmation [43]. An analysis of the outcome according to the *IDH* mutation in the RTOG phase III trial (radiotherapy versus radiotherapy and PCV in unfavorable LGGs) and the EORTC/NCIC phase III trial (up-front radiotherapy versus up-front temozolomide in progressive LGGs) is expected to clarify the predictive value of *IDH* mutation in LGGs. However, *IDH* mutation might predict the efficacy of mutant *IDH* inhibitors in the future. Important advances have been achieved in the understanding of the pathophysiology of *IDH* mutations. As suggested by the distribution of its mutations, the mutated IDH protein has been shown to be oncogenic [44••]. *IDH* mutations result in the abnormal production of 2-hydroxyglutarate (2-HG) that is structurally similar to α-ketoglutarate. 2-HG competitively inhibits multiple α-ketoglutarate enzymes leading to histone and DNA hypermethylation, altered cell differentiation and activation of enzymes implicated in hypoxia-inducible factor (HIF) degradation [45••–47••]. Most interestingly, a selective R132H-IDH1 inhibitor has recently been shown to specifically impair the growth of *IDH*1-mutant glioma cells and promote their differentiation [48••].

NEW PREDICTIVE BIOMARKERS IDENTIFIED THROUGH OMICS AND NEXT-GENERATION SEQUENCING STUDIES

Omics studies have enabled the classification of gliomas into molecularly homogeneous subgroups that are of prognostic value, independently of histology [49]. These subgroups could also be of predictive value. Erdem-Eraslan *et al.* [8••] demonstrated that the gene expression profiles of anaplastic glioma could be used to predict the benefit of early PCV chemotherapy. In glioblastomas, Verhaak *et al.* [50] suggested that the molecular classification into four subclasses (classical, mesenchymal, proneural and neural) predicts the benefit of a more intensive treatment. Patients with mesenchymal and classical glioblastomas showed increased OS when treated with temozolomide radiochemotherapy and/or more than three cycles of adjuvant temozolomide, which was not the case for patients with proneural glioblastomas. The classical subclass has also been suggested to be associated with a higher response rate to first-line chemotherapy [51]. However, these results require validation in prospective studies. Extensive molecular studies have also identified recurrent alterations that could predict the efficacy of targeted therapies. *BRAF* alterations were first identified in the majority of pilocytic astrocytomas suggesting that these tumors might be candidates for BRAF inhibitors [52,53]. In these tumors, the most frequent alteration is a KIAA1549-BRAF fusion transcript. This alteration is also found in a small subset of diffuse gliomas, in particular 1p/19q-codeleted oligodendrogliomas [54•]. Subsequently, activating *BRAF* V600E mutations were found in two-thirds of pleomorphic xanthoastrocytomas and gangliogliomas as well as in 50% of epithelioid glioblastomas (an uncommon glioblastoma variant not recognized in the WHO 2007 classification) [55,56•,57,58,59•]. However, this mutation is rare (<5%) in other diffuse gliomas, including glioblastomas. Interestingly, this mutation can be easily assessed using a V600E mutation-specific antibody and a small case study suggested that vemurafenib (a potent BRAF inhibitor with clinically meaningful activity against *BRAF*-mutated metastatic melanoma) could be active in adults with recurrent pleomorphic xanthoastrocytomas that showed a *BRAF* mutation [60,61•]. *MET* is amplified in approximately 5% of glioblastomas and could predict the efficacy of crizotinib, an oral small-molecule inhibitor of the MET and anaplastic lymphoma kinase (ALK) tyrosine kinases that is highly effective in lung cancers with ALK translocation [62•]. Oncogenic *EGFR* alterations are much more frequent (40%), but anti-EGFR therapies have failed to demonstrate clinical activity until now. However, new EGFR tyrosine kinase inhibitors could be more effective [63••]. Finally, high-throughput RNA sequencing studies identified recurrent activating FGFR fusion transcripts in a small subset of glioblastomas (3%) that might be good candidates for the use of anti-FGFR-targeted therapies [9••,10••].

CONCLUSION

Major advances have been achieved in the molecular characterization of adult gliomas, which led to

the identification of strong diagnostic and prognostic markers. Predictive biomarkers are more difficult to identify and need to be validated in prospective clinical trials before being translated into the clinic. Currently, the 1p/19q codeletion is the only well established predictive marker with clinical utility. However, it is likely that other molecular markers, such as *MGMT* methylation, *IDH* mutation and those identified using omics and next-generation sequencing studies, will further guide treatment decisions for gliomas in the near future. Because many of these new predictive biomarkers will most likely be present in only small subsets of patients, facilities that can perform prospective high-throughput molecular analyses of gliomas will be necessary [64▪].

Acknowledgements

A.L.D.S. is supported by investigator Fellowship from Collegio Ghislieri, Pavia, Italy.

Conflicts of interest

There are no conflicts of interest.

REFERENCES AND RECOMMENDED READING

Papers of particular interest, published within the annual period of review, have been highlighted as:

- ▪ of special interest
- ▪▪ of outstanding interest

1. Ricard D, Idbaih A, Ducray F, *et al.* Primary brain tumours in adults. Lancet 2012; 379:1984–1996.
2. ▪ Panageas KS, Iwamoto FM, Cloughesy TF, *et al.* Initial treatment patterns over time for anaplastic oligodendroglial tumors. Neuro Oncol 2012; 14:761–767.

This study describes the patterns of treatment over time in a retrospective study of 1013 anaplastic oligodendrogliomas treated between 1987 and 2007.

3. Weller M. Assessing the MGMT status in glioblastoma: one step forward, two steps back? Neuro Oncol 2013; 15:253–254.
4. ▪▪ van den Bent MJ, Brandes AA, Taphoorn MJ, *et al.* Adjuvant procarbazine, lomustine, and vincristine chemotherapy in newly diagnosed anaplastic oligodendroglioma: long-term follow-up of EORTC brain tumor group study 26951. J Clin Oncol 2013; 31:344–350.

The long-term results of the EORTC 26951 trial define radiotherapy and PCV as the new standard of care for newly diagnosed 1p/19q-codeleted anaplastic oligodendroglial gliomas and demonstrate that the 1p/19q codeletion is a strong predictive marker of early PCV chemotherapy benefit in these tumors.

5. ▪▪ Cairncross G, Wang M, Shaw E, *et al.* Phase III trial of chemoradiotherapy for anaplastic oligodendroglioma: long-term results of RTOG 9402. J Clin Oncol 2013; 31:337–343.

The long-term results of the RTOG 9402 trial define radiotherapy and PCV as the new standard of care for newly diagnosed 1p/19q-codeleted anaplastic oligodendroglial gliomas and demonstrate that the 1p/19q codeletion is a strong predictive marker of early PCV chemotherapy benefit in these tumors.

6. ▪▪ Malmstrom A, Gronberg BH, Marosi C, *et al.* Temozolomide versus standard 6-week radiotherapy versus hypofractionated radiotherapy in patients older than 60 years with glioblastoma: the Nordic randomised, phase 3 trial. Lancet Oncol 2012; 13:916–926.

This study demonstrates that temozolomide and hypofractionated radiotherapy are superior to conventional radiotherapy in elderly patients with glioblastoma and suggests that *MGMT* promoter methylation could predict the benefit of temozolomide treatment.

7. ▪▪ Wick W, Platten M, Meisner C, *et al.* Temozolomide chemotherapy alone versus radiotherapy alone for malignant astrocytoma in the elderly: the NOA-08 randomised, phase 3 trial. Lancet Oncol 2012; 13:707–715.

This study demonstrates that temozolomide alone is not inferior to radiotherapy alone in elderly patients with glioblastomas and suggests that *MGMT* promoter methylation could guide decision-making in this population.

8. ▪▪ Erdem-Eraslan L, Gravendeel LA, de Rooi J, *et al.* Intrinsic molecular subtypes of glioma are prognostic and predict benefit from adjuvant procarbazine, lomustine, and vincristine chemotherapy in combination with other prognostic factors in anaplastic oligodendroglial brain tumors: a report from EORTC study 26951. J Clin Oncol 2013; 31:328–336.

This study demonstrates that anaplastic gliomas gene expression profiles can predict the benefit of early PCV chemotherapy.

9. ▪▪ Singh D, Chan JM, Zoppoli P, *et al.* Transforming fusions of FGFR and TACC genes in human glioblastoma. Science 2012; 337:1231–1235.

In this study, the authors show that oncogenic FGFR fusion transcripts occur in a small subset of glioblastoma patients who might be good candidates for anti-FGFR-targeted therapies.

10. ▪▪ Wu YM, Su F, Kalyana-Sundaram S, *et al.* Identification of targetable FGFR gene fusions in diverse cancers. Cancer Discov 2013; 3:636–647.

In this study, the authors identified oncogenic FGFR fusion transcripts in several tumors including a small subset of glioblastomas.

11. Caimcross JG, Ueki K, Zlatescu MC, *et al.* Specific genetic predictors of chemotherapeutic response and survival in patients with anaplastic oligodendrogliomas. J Natl Cancer Inst 1998; 90:1473–1479.
12. Jenkins RB, Blair H, Ballman KV, *et al.* A t(1;19)(q10;p10) mediates the combined deletions of 1p and 19q and predicts a better prognosis of patients with oligodendroglioma. Cancer Res 2006; 66:9852–9861.
13. Idbaih A, Kouwenhoven M, Jeuken J, *et al.* Chromosome 1p loss evaluation in anaplastic oligodendrogliomas. Neuropathology 2008; 28:440–443.
14. Idbaih A, Marie Y, Pierron G, *et al.* Two types of chromosome 1p losses with opposite significance in gliomas. Ann Neurol 2005; 58:483–487.
15. Vogazianou AP, Chan R, Backlund LM, *et al.* Distinct patterns of 1p and 19q alterations identify subtypes of human gliomas that have different prognoses. Neuro Oncol 2010; 12:664–678.
16. Labussiere M, Idbaih A, Wang XW, *et al.* All the 1p19q codeleted gliomas are mutated on IDH1 or IDH2. Neurology 2010; 74:1886–1890.
17. ▪ Kannan K, Inagaki A, Silber J, *et al.* Whole-exome sequencing identifies ATRX mutation as a key molecular determinant in lower-grade glioma. Oncotarget 2012; 3:1194–1203.

This study demonstrates that *ARTX* mutations occur in most *IDH*-mutated non 1p/19q-codeleted gliomas, that these mutations correlate with TP53 expression and that they are associated with the alternative lengthening of telomeres.

18. ▪ Liu XY, Gerges N, Korshunov A, *et al.* Frequent ATRX mutations and loss of expression in adult diffuse astrocytic tumors carrying IDH1/IDH2 and TP53 mutations. Acta Neuropathol 2012; 124:615–625.

The authors demonstrate that *ATRX* mutations are very frequent in grade II/III astrocytomas and mixed gliomas, wherein they are strongly correlated with the presence of *IDH* and *TP53* mutations.

19. ▪▪ Jiao Y, Killela PJ, Reitman ZJ, *et al.* Frequent ATRX, CIC, FUBP1 and IDH1 mutations refine the classification of malignant gliomas. Oncotarget 2012; 3:709–722.

The authors show that three main subgroups of adult gliomas can be distinguished based on their genetic characteristics. Gliomas with *IDH/CIC/FUBP1* mutations have the best prognosis. Gliomas with *IDH/ATRX/TP53* mutation have an intermediary prognosis, whereas gliomas with neither of these two profiles have a poor prognosis.

20. ▪▪ Yip S, Butterfield YS, Morozova O, *et al.* Concurrent CIC mutations, IDH mutations, and 1p/19q loss distinguish oligodendrogliomas from other cancers. J Pathol 2012; 226:7–16.

Using exome sequencing the authors identified *CIC* mutations in 2/3 of 1p/19q-codeleted oligodendrogliomas.

21. Bettegowda C, Agrawal N, Jiao Y, *et al.* Mutations in CIC and FUBP1 contribute to human oligodendroglioma. Science 2011; 333:1453–1455.
22. ▪ Arita H, Narita Y, Fukushima S, *et al.* Upregulating mutations in the TERT promoter commonly occur in adult malignant gliomas and are strongly associated with total 1p19q loss. Acta Neuropathol 2013.

In this study, the authors show that *TERT* promoter mutations are present in almost all 1p/19q-codeleted gliomas and the majority of primary glioblastomas.

23. ▪ Liu X, Wu G, Shan Y, *et al.* Highly prevalent TERT promoter mutations in bladder cancer and glioblastoma. Cell Cycle 2013; 12:1637–1638.

In this study, the authors show that *TERT* promoter mutations are found in the majority of primary glioblastomas.

24. ▪▪ Killela PJ, Reitman ZJ, Jiao Y, *et al.* TERT promoter mutations occur frequently in gliomas and a subset of tumors derived from cells with low rates of self-renewal. Proc Natl Acad Sci U S A 2013; 110:6021–6026.

In addition to showing that *TERT* promoter mutations are present in almost all 1p/19q-codeleted gliomas and the majority of primary glioblastomas, the authors show that *TERT* promoter mutations are associated with increased *TERT* expression and are exclusive of *ATRX* mutations that are associated with an alternative mechanism of telomere maintenance.

25. Ducray F, Idbaih A, de Reynies A, *et al.* Anaplastic oligodendrogliomas with 1p19q codeletion have a proneural gene expression profile. Mol Cancer 2008; 7:41.
26. Buckley PG, Alcock L, Heffernan J, *et al.* Loss of chromosome 1p/19q in oligodendroglial tumors: refinement of chromosomal critical regions and evaluation of internexin immunostaining as a surrogate marker. J Neuropathol Exp Neurol 2011; 70:177–182.

27. Mokhtari K, Ducray F, Kros JM, *et al.* Alpha-internexin expression predicts outcome in anaplastic oligodendroglial tumors and may positively impact the efficacy of chemotherapy: European organization for research and treatment of cancer trial 26951. Cancer 2011; 117:3014–3026.

28. Ducray F, Mokhtari K, Criniere E, *et al.* Diagnostic and prognostic value of alpha internexin expression in a series of 409 gliomas. Eur J Cancer 2011; 47:802–808.

29. Cairncross G, Berkey B, Shaw E, *et al.* Phase III trial of chemotherapy plus radiotherapy compared with radiotherapy alone for pure and mixed anaplastic oligodendroglioma: Intergroup Radiation Therapy Oncology Group Trial 9402. J Clin Oncol 2006; 24:2707–2714.

30. van den Bent MJ, Carpentier AF, Brandes AA, *et al.* Adjuvant procarbazine, lomustine, and vincristine improves progression-free survival but not overall survival in newly diagnosed anaplastic oligodendrogliomas and oligoastrocytomas: a randomized European Organisation for Research and Treatment of Cancer phase III trial. J Clin Oncol 2006; 24:2715–2722.

31. Kaloshi G, Benouaich-Amiel A, Diakite F, *et al.* Temozolomide for low-grade gliomas: predictive impact of 1p/19q loss on response and outcome. Neurology 2007; 68:1831–1836.

32. Viaccoz A, Lekoubou A, Ducray F. Chemotherapy in low-grade gliomas. Curr Opin Oncol 2012; 24:694–701.

33. Hegi ME, Diserens AC, Gorlia T, *et al.* MGMT gene silencing and benefit from temozolomide in glioblastoma. N Engl J Med 2005; 352:997–1003.

34. Stupp R, Hegi ME, Mason WP, *et al.* Effects of radiotherapy with concomitant and adjuvant temozolomide versus radiotherapy alone on survival in glioblastoma in a randomised phase III study: 5-year analysis of the EORTC-NCIC trial. Lancet Oncol 2009; 10:459–466.

35. ▪ Reifenberger G, Hentschel B, Felsberg J, *et al.* Predictive impact of MGMT promoter methylation in glioblastoma of the elderly. Int J Cancer 2012; 131:1342–1350.
A large retrospective study in elderly patients with glioblastomas suggests that *MGMT* promoter methylation could guide decision-making in these patients.

36. ▪▪ Quillien V, Lavenu A, Karayan-Tapon L, *et al.* Comparative assessment of 5 methods (methylation-specific polymerase chain reaction, MethyLight, pyrosequencing, methylation-sensitive high-resolution melting, and immunohistochemistry) to analyze O6-methylguanine-DNA-methyltranferase in a series of 100 glioblastoma patients. Cancer 2012; 118:4201–4211.
A comparative study of five methods for the analysis of MGMT status in glioblastomas demonstrating that pyrosequencing is an interesting alternative technique to methylation-specific PCR.

37. ▪ Christians A, Hartmann C, Benner A, *et al.* Prognostic value of three different methods of MGMT promoter methylation analysis in a prospective trial on newly diagnosed glioblastoma. PLoS ONE 2012; 7:e33449.
A comparative study of three methods for the analysis of MGMT status in glioblastomas demonstrating that pyrosequencing is an interesting alternative technique to methylation-specific PCR.

38. ▪▪ Bady P, Sciuscio D, Diserens AC, *et al.* MGMT methylation analysis of glioblastoma on the Infinium methylation BeadChip identifies two distinct CpG regions associated with gene silencing and outcome, yielding a prediction model for comparisons across datasets, tumor grades, and CIMP-status. Acta Neuropathol 2012; 124:547–560.
In this study, the authors identified two regions of the *MGMT* promoter in which methylation is strongly associated with OS and inversely correlated with MGMT expression.

39. van den Bent MJ, Dubbink HJ, Sanson M, *et al.* MGMT promoter methylation is prognostic but not predictive for outcome to adjuvant PCV chemotherapy in anaplastic oligodendroglial tumors: a report from EORTC Brain Tumor Group Study 26951. J Clin Oncol 2009; 27:5881–5886.

40. Wick W, Hartmann C, Engel C, *et al.* NOA-04 randomized phase III trial of sequential radiochemotherapy of anaplastic glioma with procarbazine, lomustine, and vincristine or temozolomide. J Clin Oncol 2009; 27:5874–5880.

41. van den Bent MJ, Gravendeel LA, Gorlia T, *et al.* A hypermethylated phenotype is a better predictor of survival than MGMT methylation in anaplastic oligodendroglial brain tumors: a report from EORTC study 26951. Clin Cancer Res 2011; 17:7148–7155.

42. Sanson M, Marie Y, Paris S, *et al.* Isocitrate dehydrogenase 1 codon 132 mutation is an important prognostic biomarker in gliomas. J Clin Oncol 2009; 27:4150–4154.

43. Houillier C, Wang X, Kaloshi G, *et al.* IDH1 or IDH2 mutations predict longer survival and response to temozolomide in low-grade gliomas. Neurology 2010; 75:1560–1566.

44. ▪▪ Vogelstein B, Papadopoulos N, Velculescu VE, *et al.* Cancer genome landscapes. Science 2013; 339:1546–1558.
An outstanding review of the advances achieved thanks to comprehensive sequencing efforts in cancer, including brain tumors.

45. ▪▪ Koivunen P, Lee S, Duncan CG, *et al.* Transformation by the (R)-enantiomer of 2-hydroxyglutarate linked to EGLN activation. Nature 2012; 483:484–488.
The authors demonstrate that *IDH* mutation leads to increased degradation of HIF, which would act as a tumor suppressor in this context.

46. ▪▪ Lu C, Ward PS, Kapoor GS, *et al.* IDH mutation impairs histone demethylation and results in a block to cell differentiation. Nature 2012; 483:474–478.
The authors show that 2-HG produced by *IDH* mutant cells can inhibit histone demethylation and that inhibition of histone demethylation can be sufficient to block the differentiation of nontransformed cells.

47. ▪▪ Turcan S, Rohle D, Goenka A, *et al.* IDH1 mutation is sufficient to establish the glioma hypermethylator phenotype. Nature 2012; 483:479–483.
The authors show that IDH mutation is the molecular basis of the CpG island methylator phenotype in gliomas.

48. ▪▪ Rohle D, Popovici-Muller J, Palaskas N, *et al.* An inhibitor of mutant IDH1 delays growth and promotes differentiation of glioma cells. Science 2013; 340:626–630.
In this study, the authors demonstrate that a selective R132H-IDH1 inhibitor could impair the growth of *IDH1*-mutant but not *IDH1*-wild-type glioma cells.

49. Gravendeel LA, Kouwenhoven MC, Gevaert O, *et al.* Intrinsic gene expression profiles of gliomas are a better predictor of survival than histology. Cancer Res 2009; 69:9065–9072.

50. Verhaak RG, Hoadley KA, Purdom E, *et al.* Integrated genomic analysis identifies clinically relevant subtypes of glioblastoma characterized by abnormalities in PDGFRA, IDH1, EGFR, and NF1. Cancer Cell 2010; 17:98–110.

51. Ducray F, de Reynies A, Chinot O, *et al.* An ANOCEF genomic and transcriptomic microarray study of the response to radiotherapy or to alkylating first-line chemotherapy in glioblastoma patients. Mol Cancer 2010; 9:234.

52. Sadighi Z, Slopis J. Pilocytic astrocytoma: a disease with evolving molecular heterogeneity. J Child Neurol 2013; 28:625–632.

53. Horbinski C. To BRAF or not to BRAF: is that even a question anymore? J Neuropathol Exp Neurol 2013; 72:2–7.

54. ▪ Badiali M, Gleize V, Paris S, *et al.* KIAA1549-BRAF fusions and IDH mutations can coexist in diffuse gliomas of adults. Brain Pathol 2012; 22:841–847.
The authors shows that a small subset of oligodendrogliomas harbor KIAA1549-BRAF fusions, which therefore might be candidates for anti-BRAF therapies.

55. Dias-Santagata D, Lam Q, Vernovsky K, *et al.* BRAF V600E mutations are common in pleomorphic xanthoastrocytoma: diagnostic and therapeutic implications. PLoS ONE 2011; 6:e17948.

56. ▪ Kleinschmidt-DeMasters BK, Aisner DL, Birks DK, Foreman NK. Epithelioid GBMs show a high percentage of BRAF V600E mutation. Am J Surg Pathol 2013; 37:685–698.
The authors report *BRAF* V600E mutations in half of epithelioid glioblastomas, an uncommon variant of glioblastomas.

57. Schindler G, Capper D, Meyer J, *et al.* Analysis of BRAF V600E mutation in 1,320 nervous system tumors reveals high mutation frequencies in pleomorphic xanthoastrocytoma, ganglioglioma and extra-cerebellar pilocytic astrocytoma. Acta Neuropathol 2011; 121:397–405.

58. Schmidt Y, Kleinschmidt-DeMasters BK, Aisner DL, *et al.* Anaplastic PXA in adults: case series with clinicopathologic and molecular features. J Neurooncol 2013; 111:59–69.

59. ▪ Koelsche C, Wohrer A, Jeibmann A, *et al.* Mutant BRAF V600E protein in ganglioglioma is predominantly expressed by neuronal tumor cells. Acta Neuropathol 2013; 125:891–900.
The authors report the occurrence of *BRAF* V600E mutations in 70% of gangliogliomas.

60. Capper D, Preusser M, Habel A, *et al.* Assessment of BRAF V600E mutation status by immunohistochemistry with a mutation-specific monoclonal antibody. Acta Neuropathol 2011; 122:11–19.

61. ▪ Chamberlain MC. Salvage therapy with BRAF inhibitors for recurrent pleomorphic xanthoastrocytoma: a retrospective case series. J Neurooncol 2013; 114:237–240.
Among four patients with recurrent pleomorphic xanthoastrocytoma that showed a *BRAF* V600E mutation, one patient achieved a partial response and two patients achieved stable disease.

62. ▪ Chi AS, Batchelor TT, Kwak EL, *et al.* Rapid radiographic and clinical improvement after treatment of a MET-amplified recurrent glioblastoma with a mesenchymal-epithelial transition inhibitor. J Clin Oncol 2012; 30:e30–33.
A case report suggesting crizotinib activity in glioblastomas with *MET* amplification.

63. ▪▪ Vivanco I, Robins HI, Rohle D, *et al.* Differential sensitivity of glioma- versus lung cancer-specific EGFR mutations to EGFR kinase inhibitors. Cancer Discov 2012; 2:458–471.
The present study shows that EGFR-mutated glioblastomas do not respond to EGFR tyrosine kinase inhibitors that are active in EGFR-mutated lung cancer because EGFR mutations occur in the extracellular domain and not in the intracellular kinase domain in glioblastomas. However, these mutations could be effectively targeted using next-generation EGFR tyrosine kinase inhibitors.

64. ▪ Chi AS, Batchelor TT, Dias-Santagata D, *et al.* Prospective, high-throughput molecular profiling of human gliomas. J Neurooncol 2012; 110:89–98.
This study shows that high-throughput molecular profiling incorporated into the routine clinical evaluation of glioma patients may enable the rational selection of patients for targeted therapy clinical trials and thereby improve the likelihood that such trials will succeed.

Neurology®

Acute late-onset encephalopathy after radiotherapy: An unusual life-threatening complication

Paul J. Regal, Anna L. Di Stefano, Giulia Berzero, et al.

Neurology 2014;82;1102
DOI 10.1212/WNL.0000000000000201

Section Editor
Robert C. Griggs, MD

WriteClick: Editor's Choice

Editors' Note: In reference to "White matter hyperintensities on MRI in high-altitude U-2 pilots," Hellmann-Regen et al. identify potentially confounding factors, in addition to hypobaria, that are seen in military pilots, including high Gz stress and radiation exposure, and suggest a "regular pilot" control group. Author McGuire responds by sharing unpublished findings on a group of altitude-chamber technicians.
—Megan Alcauskas, MD, and Robert C. Griggs, MD

ACUTE LATE-ONSET ENCEPHALOPATHY AFTER RADIOTHERAPY: AN UNUSUAL LIFE-THREATENING COMPLICATION

Paul J. Regal, Newcastle, Australia: Di Stefano et al.[1] reported 5 patients who developed steroid-responsive encephalopathy 9 months to 17 years after whole-brain radiotherapy for brain tumors. MRI, CSF, EEG, and other laboratory tests excluded almost all other potential causes for encephalopathy. The favorable response to IV methylprednisolone in 2–6 days further restricted the field of potential causes. The authors decided that brain biopsy, a potential gold standard, was not necessary. Brain autopsy on the 2 patients who died 2–2.5 years after autopsy was not undertaken. I wonder whether the authors estimated the denominator—the number of patients treated with whole-brain radiotherapy—to yield these 5 cases. In addition, it would be interesting to know the incidence of other forms of encephalopathy after radiotherapy. From my research in the Central Coast Australia Delirium Intervention Study—a prospective randomized controlled trial for subjects age 65+—both the informant-rated instrumental activities of daily living and informant-rated apathy evaluation score declined significantly in the days prior to delirium. Perhaps the authors could provide the cognitive scores before encephalopathy, on admission, and after recovery.

Author Response: Anna L. Di Stefano, Giulia Berzero, Enrico Marchioni, Pavia, Italy: We thank Dr. Regal for his comments. Peculiar characteristics of acute late-onset encephalopathy after radiotherapy (ALERT) syndrome are acute onset and rapid response to steroids. We agree with the value of neuropathologic findings in the setting of unusual complications of radiation therapy. These were not available in our retrospective case series. Two patients did not show MRI abnormalities targetable by brain biopsy. In the remaining patients, brain biopsy was not performed because of patients' critical conditions at the time of ALERT syndrome and the subsequent improvement and MRI normalization after high-dose steroids. In this setting, we judged brain biopsy as an invasive procedure exposing patients to a disproportionate risk.

Patients 1 and 3 died at hospitals not within our site of acute respiratory distress due to pulmonary infection. They had no recent neurologic symptoms or MRI alterations. Although autopsy could have been informative, it was not performed. We intend to collect neuropathologic specimens from patients presenting with similar symptoms from all sites wishing to collaborate with us. As a retrospective study, neuropsychological tests were not serially performed.

From 1998 to 2011, patients were admitted into 4 different neurologic sites at the onset of neurologic symptoms. We cannot correctly estimate the number of patients receiving whole-brain radiotherapy in origin departments but we suggest that a more informative denominator would be the number of long-surviving patients after brain irradiation. To answer this, we are conducting a prospective clinical study on long survivors after brain irradiation to explore the underlying mechanisms of acute encephalopathy and its relationship with chronic postradiation complications.

1. Di Stefano AL, Berzero G, Vitali P, et al. Acute late-onset encephalopathy after radiotherapy: an unusual life-threatening complication. Neurology 2013;81:1014–1017.

WHITE MATTER HYPERINTENSITIES ON MRI IN HIGH-ALTITUDE U-2 PILOTS

Julian Hellmann-Regen, Kim Hinkelmann, Francesca Regen, Berlin, Germany: McGuire et al.[1] presented interesting data on the prevalence and location of white matter hyperintensities (WMHs) in MRI scans of high-altitude pilots. The authors demonstrated that WMHs differ between the pilot group and a matched group of healthy controls. They concluded that these differences may be the result of hypobaria in the pilot group. While

Acute late-onset encephalopathy after radiotherapy: An unusual life-threatening complication

Paul J. Regal, Anna L. Di Stefano, Giulia Berzero, et al.

Neurology 2014;82;1102
DOI 10.1212/WNL.0000000000000201

OPEN ACCESS Freely available online

PLOS ONE

Parametric Response Maps of Perfusion MRI May Identify Recurrent Glioblastomas Responsive to Bevacizumab and Irinotecan

Domenico Aquino[1], Anna Luisa Di Stefano[2☯], Alessandro Scotti[1☯], Lucia Cuppini[3], Elena Anghileri[3], Gaetano Finocchiaro[3], Maria Grazia Bruzzone[1], Marica Eoli[3]*

1 Neuro-Radiology Unit, Fondazione IRCCS Istituto Neurologico C. Besta, Milan, Italy, **2** General Neurology Unit, Fondazione IRCCS Istituto Neurologico Nazionale C. Mondino, Pavia, Italy, **3** Molecular Neuro-Oncology Unit, Fondazione IRCCS Istituto Neurologico C. Besta, Milan, Italy

Abstract

Background: Perfusion weighted imaging (PWI) can be used to measure key aspects of tumor vascularity in vivo and recent studies suggest that perfusion imaging may be useful in the early assessment of response to angiogenesis inhibitors. Aim of this work is to compare Parametric Response Maps (PRMs) with the Region Of Interest (ROI) approach in the analysis of tumor changes induced by bevacizumab and irinotecan in recurrent glioblastomas (rGBM), and to evaluate if changes in tumor blood volume measured by perfusion MRI may predict clinical outcome.

Methods: 42 rGBM patients with KPS ≥50 were treated until progression, as defined by MRI with RANO criteria. Relative cerebral blood volume (rCBV) variation after 8 weeks of treatment was calculated through semi-automatic ROI placement in the same anatomic region as in baseline. Alternatively, rCBV variations with respect to baseline were calculated into the evolving tumor region using a voxel-by-voxel difference. PRMs were created showing where rCBV significantly increased, decreased or remained unchanged.

Results: An increased blood volume in PRM (PRM_{CBV+}) higher than 18% (first quartile) after 8 weeks of treatment was associated with increased progression free survival (PFS; 24 versus 13 weeks, $p = 0.045$) and overall survival (OS; 38 versus 25 weeks, $p = 0.016$). After 8 weeks of treatment ROI analysis showed that mean rCBV remained elevated in non responsive patients (4.8 ± 0.9 versus 5.1 ± 1.2, $p = 0.38$), whereas decreased in responsive patients (4.2 ± 1.3 versus 3.8 ± 1.6 $p = 0.04$), and re-increased progressively when patients approached tumor progression.

Conclusions: Our data suggest that PRMs can provide an early marker of response to antiangiogenic treatment and warrant further confirmation in a larger cohort of GBM patients.

Citation: Aquino D, Di Stefano AL, Scotti A, Cuppini L, Anghileri E, et al. (2014) Parametric Response Maps of Perfusion MRI May Identify Recurrent Glioblastomas Responsive to Bevacizumab and Irinotecan. PLoS ONE 9(3): e90535. doi:10.1371/journal.pone.0090535

Editor: Russell O. Pieper, University of California-San Francisco, United States of America

Received September 27, 2013; **Accepted** February 2, 2014; **Published** March 27, 2014

Funding: This work was partially supported by a grant from the Italian Ministry of Health [RF-INN-2008-1142520 to GF]. Drugs were supplied by Roche S.p.A. (Monza, Italy) and Hospira (Napoli, Italy). This work was partially funded by MIUR, FIRB project "Materiali fluorurati nanostrutturati come mezzi di contrasto intelligenti in 19F-RMN (FLUORIMAGING)" project no. RBAP1183B5. The funders had no role in study design, data collection and analysis, decision to publish, or preparation of the manuscript. No additional external funding received for this study.

Competing Interests: The authors have declared that no competing interests exist.

* E-mail: eoli@istituto-besta.it

☯ These authors contributed equally to this work.

Introduction

Glioblastomas (GBM) are highly vascularized tumors, leading to development of therapeutic strategies targeting tumor angiogenesis [1]. Bevacizumab, a monoclonal antibody targeting the vascular endothelial growth factor (VEGF), has recently entered into the clinical arena and represents the front-runner among currently available antiangiogenic drugs [2]. Despite the significant number of studies based on GBM treatment with bevacizumab, alone or in combination with other drugs, in vivo modifications induced by treatment are poorly defined [3]. Moreover, although the highly variable response to bevacizumab, currently there are no prospectively validated predictive or prognostic biomarkers for it [4].

Perfusion weighted imaging (PWI) can be used to measure key aspects of tumor vascularity in vivo and recent studies suggest that perfusion imaging may be useful in the early assessment of response to angiogenesis inhibitors. Sorensen, studying recurrent GBM patients treated with cediranib, an inhibitor of the VEGF receptor tyrosine kinases, calculated a "vascular normalization index" by combining Ktrans (the rate of transfer of the contrast agent (CA)), microvessel volume and circulating collagen IV and found that this index (measured 1 day after treatment initiation) was predictive of overall and progression-free survival (OS and PFS) [5].

Cha et al. studied 18 patients with recurrent malignant gliomas treated with both thalidomide (an antiangiogenic agent) and carboplatin: changes in relative Cerebral Blood Volume (rCBV)

are better correlated with treatment response than enhancing tumor size [6].

In 16 patients with recurrent GBM treated with bevacizumab, Sawlani observed that mean rCBV, mean leakage coefficient and hyperperfusion volume (HPV), defined as the fraction of tumor with an rCBV above a pre-specified threshold, correlate with time to progression [7].

Parametric Response Maps (PRM) are voxel-wise analytic approach to quantify significant regional changes in tumor physiology after therapy [8,9].

Aim of this work is to compare PRMs with the classical Region Of Interest (ROI) approach [10] in the analysis of tumor changes induced by bevacizumab and irinotecan in recurrent GBM, and to evaluate if changes in tumor blood volume measured by perfusion MRI may predict clinical outcome [11].

Methods

Ethics statement

All patients in the current work were part of a study carried out according to the Italian Decree Law of May 8th, 2003 allowing treatment of patients with no other therapeutic option, with drugs not yet approved by the Italian Regulatory Agency, but with evidence of efficacy in phase II clinical trials [11]. The protocol was approved by the Ethics Committee of the Neurological Institute "Carlo Besta" of Milan and registered in the Institute database (#1/08). All patients gave written informed consent. All clinical investigation were conducted according to the principles expressed in the Declaration of Helsinki.

Patients

Forty-two of these patients who underwent the same MRI protocol, were enrolled [11]. All patients underwent prior surgery and radiochemotherapy according to the Stupp's protocol [12], followed by second or third line chemotherapy.

Magnetic Resonance Imaging (MRI) was performed with a 1.5-T MR Unit (Magnetom Avanto; Siemens, Erlangen, Germany) before starting therapy and followed up every 8 weeks until tumor progression or treatment discontinuation.

RANO criteria were used to assess tumor response and tumor progression; however, to assess changes of FLAIR hyperintensity, a threshold of 25% or more of the maximal cross-sectional area was used [13,14]. Baseline tumor volumes were determined on 3D post-gadolinium T1 weighted images by manually outlining the enhancing portion of the lesion using MRIcro (http://www.mccauslandcenter.sc.edu/mricro/). The total enhancing volume was obtained as the product of the number of enhancing voxels and the voxel volume.

We used the following four criteria to assess MR patterns of disease at baseline and at progression [15]. Local disease: unifocal, contiguous with the primary site or resection cavity or within a 3 cm margin. Distant disease: a second non-contiguous lesion in addiction to disease at the primary site. Multifocal disease: three or more non-contiguous lesions including the primary site (cerebro-spinal fluid spread of disease was also defined as multifocal disease). Diffuse disease: extending more than 3 cm beyond the primary site with poor or indistinct contrast enhancement or FLAIR margins.

Acquisition protocol

The radiological MR protocol included: 1) a 3D post-contrast MPRAGE T1-weighted sequence (TR\TE\TI = 1160\4.21\600 ms, matrix = 384×512, voxel size = 0.47×0.47×0.9 mm, 192 slices, AT = 1.42 min); 2) a 3D FLAIR sequence (TR\TE = 5000\477 ms, matrix = 256×256, voxel size = 1×1×1, 160 slices); 3) PWI was performed with a Dynamic Susceptibility Contrast (DSC) GRE echo-planar (EPI) sequence (TR\TE = 2040\53 ms, flip angle = 30°, matrix size = 128×128, voxel size = 2×2×5 mm, 50 dynamic volumes of 17, AT = 1.42 min). Acquisitions were carried out during the injection of the gadolinium-based contrast agent Gadovist (Bayer), 1 mol/L. A bolus injection of 9 cc was administered at 5 mL/s using an automated injector. To minimize T1-shortening effects, a contrast agent predose of 3 cc was used to saturate leaky tissue from the blood–brain barrier breakdown.

Post-processing

Every DSC-MRI volume was spatially co-registered to the first one at baseline by an affine 12 DOF registration. Post-contrast T1-weighted images were co-registered and resampled to match the spatial resolution of the DSC volume of reference.

DSC-MRI data were processed to create rCBV maps. NordicICE (http://www.nordicneurolab.com) was used for perfusion processing, including a CA leakage correction caused by blood-brain barrier disruption, and an automated gamma-variate fitting of first-pass CA concentration curves.

The following two methods were used to evaluate rCBV variation during treatment.

Region Of Interest (ROI). Three separated ROIs were placed in regions of highest perfusion seen on the rCBV color maps at baseline. Size and morphology of ROIs were maintained constant (circular 40 mm^2 area) and the maximum value recorded. Reference ROI was drawn on contralateral normal white matter, with the same size and position [10,16]. rCBV variation after 8 weeks of treatment was calculated through semi-automatic ROI placement in the same anatomic region as baseline.

Parametric Response Maps (PRMs). This technique was previously used to assess DWI variation at two end-points for each patient after radiotherapy in GBM [17] and create rCBV maps of patients with grade III and IV gliomas receiving concurrent radiochemotherapy [8,9].

Two ROIs were drawn by an experienced neuroradiologist on contrast-enhanced T1-weighted images: the first including all tissues into the enhancement area, the second covering the hyperintense area that was judged to be necrotic. This second volume was then subtracted from the first one and the selected region defined as the "tumor region". A control ROI of the same size was drawn contralaterally on frontal, normal white matter.

Perfusion changes over time were quantified by using a voxel-by-voxel analysis in the tumor region, drawn at baseline [17]. In case of progression another ROI was drawn on the new tumor volume and the sum of this ROI and baseline ROI was considered as definitive ROI. The rCBV values of each voxel within the tumor at week 8 and at time of progression were compared with baseline values. To evaluate their difference two thresholds were set: they were determined to be the 95% confidence intervals (C.I.) (1.96xSD) obtained comparing the rCBV values of the two time points in the normal contralateral white matter. The tumor region was then subdivided in three regions represented with different colors: 1) areas with rCBV greater than the upper threshold (increased CBV, iCBV), represented in red; 2) areas with rCBV lower than the lower threshold (decreased CBV, dCBV), represented in blue; 3) areas unchanged (uCBV), represented in black (Figure 1). Colored maps were than overlayed/merged on T2 reference images, allowing a qualitative assessment of perfusion changes in pathological areas. The procedure was repeated at each time point until progression.

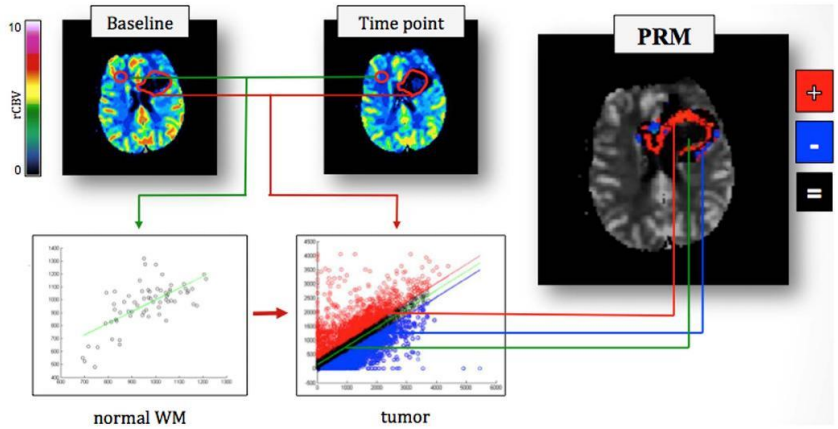

Figure 1. Parametric Response Maps creation process. 1) comparison of the rCBV values of a ROI placed on the normal white matter between the baseline and the time point under examination; 2) Classification of increased, decreased and unchanged differences values in the tumor area on the basis of the previously determined thresholds; 3) Chromatic representation of the difference map obtained by the subtraction of the baseline map from the time point one. Red voxels indicate an increase of rCBV, blue a decrease and black voxels are unchanged.
doi:10.1371/journal.pone.0090535.g001

Statistical analysis

PFS and OS were calculated from treatment onset until disease progression or death/last follow-up, if censored. Kaplan Meier analysis estimated PFS and OS. The log rank test assessed differences in progression or survival in patients with different clinical or radiological parameters. These parameters were set at the 25°, 50°, 75°, 90° percentile and separately evaluated in all patients.

Correlations between radiological and clinical parameters or treatment response were assessed using the Mann-Whitney exact U test. The Wilcoxon rank sum test evaluated differences among radiological parameters at baseline, week 8 or progression. All p-values were two-sided.

A multivariate analysis and a Cox proportional hazard regression model analysis were performed on variables showing statistically significant differences at univariate analysis to investigate their independent prognostic role. In particular, rCBV variation was used as a dichotomic parameter. All statistical analyses were performed using the R software (www.r-project.org).

Results

Clinical results

Patients' clinical and demographical baseline characteristics are reported in Table 1. In particular, MR showed in 31 cases (74%) local disease, in 6 (14%) multifocal and in 5 (12%) distant disease. No patient was previously treated with bevacizumab or other anti-angiogenic drugs.

During treatment three patients discontinued irinotecan before progression due to low tolerance and continued bevacizumab as monotherapy.

Tumor volumes at baseline were significantly lower in patients presenting local disease than in patients presenting distant or multifocal disease (median 17.2 versus 36.7 and 40.8 cm^3, respectively; Mann Whitney $p = 0.01$).

Median follow-up was 33.5 weeks (range 9–111 weeks). At the time of this analysis, four of 42 patients were progression-free, three died before disease progression and four were alive.

Median OS was 35.0 weeks (CI 25.5–44.5); OS at 6 months was 66% (CI 52.0–80.0) and OS at 12 months 22% (CI 9.0–36.0). Median PFS was 20.0 weeks (CI 11.8–28.2), PFS at 6 months was 40%.

Median OS and median PFS were not significantly different when considering: sex, age ≥40 versus <40, age ≥60 versus <60, KPS ≥70 versus <70, and partial response versus stable/progressive disease according to RANO criteria [13].

Patients with local pattern of disease at baseline had longer PFS and OS than patients with distant or multifocal disease at baseline (PFS 28.0 versus 9.0 weeks, $p<0.001$; OS 41.0 versus 18.0 or 19.0 weeks respectively, $p = 0.001$. Figure 2).

All patients underwent MRI at baseline and 8 weeks after treatment onset; 32 patients were also assessed 16 weeks after treatment onset.

Magnetic resonance results

MRI at 8 weeks after treatment onset showed partial responses in 9 cases, stable disease in 23 patients and progressive disease in 10. In this report we define patients showing progression at 8 weeks as *non-responsive*, and patients radiologically improved or with stable disease as *responsive*. No other partial or complete response was observed later.

The analysis of tumor responses to treatment at 8 weeks or later time points was available in 32 patients: other 10 patients died or interrupted treatment before progression or had incomplete neuroimaging.

Table 1. Patients characteristics at baseline.

Characteristic	No. of pts	%
Male	27	64
Female	15	36
Median age [all pts] (range)	53 (15–76)	
<40	9	21
40–60	25	59
>60	8	20
Median [all pts] (range)	70 (50–100)	
<70	5	12
70–80	33	78
90–100	4	10
De novo GBM	36	86
Secondary GBM	6	14
Disease recurrence: $1^{st}/2^{nd}$	27/15	64/36
Radiotherapy	42	100
$1^{st}/2^{nd}$ line chemotherapy	42/15	100/36
Median tumor volume, cm^3 (range)	22.29 (0.97–132.6)	
Local	31	74
Multifocal (Leptomeningeal dissem).	6	14
Distant	5	12
Diffuse	0	0

Abbreviations: cc, cubic centimetres; dissem, dissemination; MR, magnetic resonance; pts, patients.
doi:10.1371/journal.pone.0090535.t001

Twenty patients (16 with local and 4 with multifocal disease) did not show changes when compared to baseline. Seven patients converted to a diffuse pattern of disease (6 patients starting from local and 1 from distant pattern), whereas 5 converted to multifocal disease (2 from local and 3 from distant disease).

Analysis with the ROI method

Results are detailed in Table 2. Mean rCBV of all patients at baseline was 4.4 (±1.2 SD) (Table 2a).

Patients with local disease at baseline showed significantly lower rCBV than patients with distant or multifocal disease at baseline ($p = 0.041$).

In all patients mean rCBV decreased significantly at 8 weeks (4.4±1.2 SD versus 4.1±1.6 SD; $p = 0.040$), but was statistically unchanged at 16 weeks (3.7±1.3 SD; n.s.). The serial measurement of rCBV at all time points until progression, performed in 24 patients, showed that rCBV changes differently within time according to treatment response. After 8 weeks of therapy 32 responsive patients showed a significant decrease of rCBV with respect to the baseline (4.2±1.3 versus 3.8±1.6 $p = 0.04$), whereas 10 non responsive patients, who progressed at 8 weeks maintained elevated rCBV (4.8±0.9 versus 5.1±1.2, $p = 0.38$) (Figure 3a).

Patients who progressed after 8 weeks showed an initial significant decrease of rCBV, followed by a progressive tendency to increased rCBV as long as they approached tumour progression.

In particular, when progression occurred at 16 weeks (8 cases) a new increase in rCBV at 16 weeks occurred after a significant decrease at 8 weeks (Figure 3b); a decrease at 8 weeks in rCBV was also observed in patients who progressed at 24 weeks or later (6 cases), but in the following MR performed before progression a light continuous increase of rCBV was observed (Figure 3c).

The radiological pattern of disease at progression might influence rCBV changes. While patients with local, distant or multifocal disease at progression showed an initial rCBV decrease followed by a new increase, patients with diffuse disease at progression maintained a low rCBV (Table S1 in File S1).

Parametric response maps (PRM)

Increased or decreased blood volume in PRM was defined as PRM_{CBV+} or PRM_{CBV-}, respectively, as in the work of Galbán et al [8]. At 8 weeks we observed a mean PRM_{CBV+} of 30%±16% and a PRM_{CBV-} of 18%±14% in all patients. Similar data were obtained at 16 weeks of treatment: PRM_{CBV+} was 32%±19% and PRM_{CBV-} was 17%±14% (Table 2b).

If we consider PRM results dividing patients into non-responsive and responsive, at 8 weeks we found a lower PRM_{CBV+} value in non-responsive than responsive (23%±19% versus 33%±14%, not significant) (Table 2b). Most of the non-responsive presented PRM_{CBV+} <18% (first quartile, $p = 0.04$).

We also examined perfusion at progression in 24 patients using PRMs: PRM_{CBV+} was 30%±20% and PRM_{CBV-} 20%±18%. No significant difference in PRM at progression was found dividing patients according to treatment response or pattern of disease at progression (see Table S2 in File S1).

Correlation with survival

Median PFS and OS were longer in responsive patients (PFS: 8 versus 17 months, $p<0.0001$; OS:18 versus 39 months, $p<0.0001$).

Tumor volume higher than 75° percentile (44.5 cm^3) was associated with significantly shorted PFS (14 versus 18 weeks, $p = 0.023$) and OS (24 versus 39.00 weeks, $p = 0.049$).

Using the classical ROI method rCBV values (at baseline and 8 weeks) did not correlate with PFS or OS. PRM analysis, on the

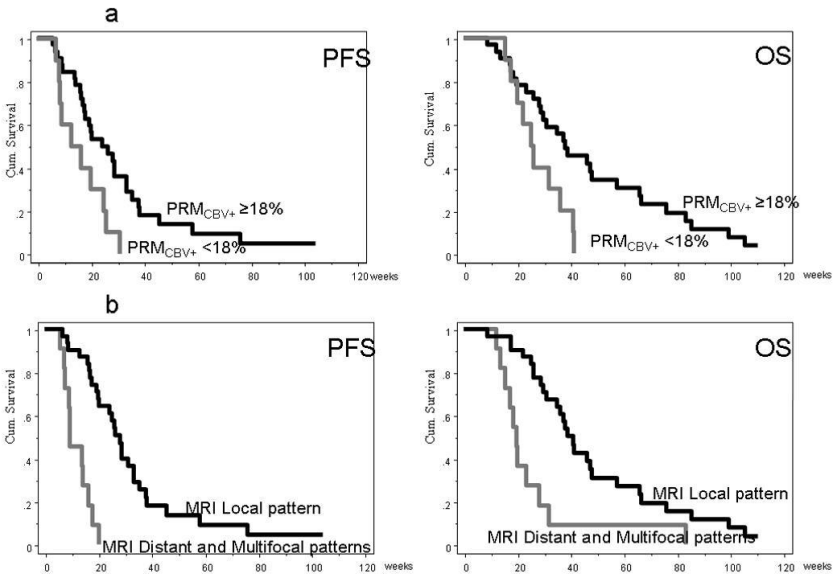

Figure 2. Correlations between PRM$_{CBV+}$ higher than 18% and baseline magnetic resonance disease patterns and PFS/OS. A: Patients with PRM$_{CBV+}$ higher than the first quartile, 18%, had longer survival than the others. B: Patients with local pattern of disease at baseline had longer PFS and OS than those with distant or multifocal disease.
doi:10.1371/journal.pone.0090535.g002

Table 2. a) Mean rCBV max at different timepoints b) mean PRM$_{CBV-}$ and PRM$_{CBV+}$ at different time points.

a.

	No. of pts	Baseline rCBV	8 week-rCBV
All patients	42	4.4±1.2[a]	4.1±1.6 [b]
Non-responsive	10	4.8±0.9	5.1±1.2
Responsive	32	4.2±1.3[c]	3.8±1.6[d]
MR pattern at Baseline			
Local	31	4.2±1.0[e]	4.0±1.5
Multifocal or Distant	11	4.9+1.6[f]	4.5±1.9

a–b $p=0.04$; c–d $p=0.01$; e–f $p=0.04$.

b.

	No. of pts	PRM$_{CBV-}$	PRM$_{CBV+}$
All patients	42	18%±14%	30%±16%
Non-responsive	10	12%±11%	23%±19%
Responsive	32	19%±15%	33%±14%
MR pattern at Baseline			
Local	31	19%±15%	31%±16%
Multifocal or Distant	11	15%±10%	29%±18%

doi:10.1371/journal.pone.0090535.t002

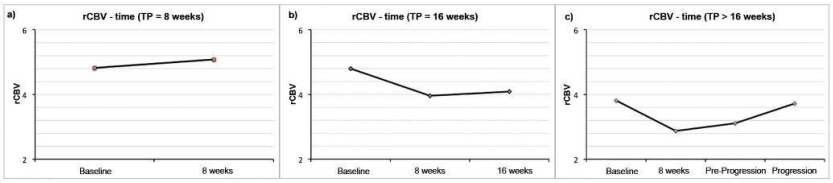

Figure 3. Mean rCBV changes according to treatment response within time. a) Mean rCBV remained elevated in non responsive patients who progressed after 8 weeks of treatment. b) Mean rCBV resulted in a significant decrease at 8 weeks, and in a new increase at 16 weeks, when progression occurred at 16 weeks. c) Mean rCBV showed a decrease at 8 weeks also in patients who progressed at 24 weeks or later but in the following MR performed before progression a light continuous increase of rCBV was observed.
doi:10.1371/journal.pone.0090535.g003

contrary, did show correlations with survival. Patients with PRM_{CBV+} higher than 18% (first quartile) showed a significantly longer survival (Figure 2): median OS was 38.0 weeks in patients with PRM_{CBV+} ≥18% and 25.1 weeks in patients with PRM_{CBV+}<18% ($p=0.016$); median PFS was 24.3 weeks in patients with PRM_{CBV+} ≥18% and 13.1 weeks in patients with PRM_{CBV+} <18% ($p=0.045$).

Multivariate analysis

A multivariate analysis and a Cox proportional hazards regression analysis were performed on variables showing statistically significant differences at univariate analysis to investigate their independent prognostic role. Multifocal or distant pattern of disease at baseline and PRM_{CBV+}<18% were independent predictors of shorter PFS (HR 8.2, $p=$<0.0001 and HR 3.2, $p=0.021$, respectively).

Multifocal and distant pattern at baseline were the only independent predictors of OS (HR 3.1, $p=0.01$), (Table 3).

Discussion

GBM is a tumor characterized by heterogeneous features with different regional expressions of potential therapeutic targets such as EGFR and VEGF [18,19]. The pattern of microvascular proliferation can be various within the tumor with both simple, hyperplastic capillaries with increase endothelial cellularity and lumen patency, and complex, large collections of capillaries with partially thrombosed slit-like lumen, microvascular hyperplasia, resulting in minimal perfusion to the surrounding tumor tissue [20] [17].

MRI and Positron Emission Tomography (PET) can give detailed information about tumor heterogeneity. In particular, advanced MRI techniques could lead to a better microstructural and functional characterization of gliomas. Diffusion MRI giving information about the degree of cellularity in the different portions of tumoral and peritumoral areas could be predictive and prognostic in glioma and seems to correlate with survival in patients treated with bevacizumab [17,21–23]. Spectroscopy MRI (H-MRS) can inform about metabolite concentration in the tumoral portions and could be an early indicator of response to antiangiogenic therapy [24,25].

Dynamic Susceptibility Contrast-MRI (DSC-MRI) gives information about microvascular density and antiangiogenic therapy efficacy and could be helpful in tumor grading. In particular, rCBV may provide a prognostic information complementing histopathology [16,26].

In our work we used DSC-MRI to evaluate the hemodynamic response over time in patients affected by recurrent GBM and treated with bevacizumab and irinotecan. We chose this technique because of its extended use in the clinical practice and due to the characteristics of rCBV. Indeed rCBV is a reliable indicator of microvascularization [27] and can be used to assess glioma grade [16,28] and distinguish progression from pseudo-progression [29]. Moreover, some studies demonstrated that rCBV correlates with overall survival [27,28,30].

The most common methods to evaluate rCBV over time are the ROI-based and the histogram-based. The first one is highly user-dependent but allows a precise identification of the portion of the tumor to be analysed; on the other hand, it cannot accurately characterize the hemodynamic heterogeneity of high grade gliomas. The histogram-based method is less user-dependent and allows a better representation of the tissue heterogeneity, with similar sensitivity but higher specificity than the ROI method [8,16]. Its main limitation is spatial localization: it gives information about glioma heterogeneity and might give indications about glioma grade, but it is not able to spatially localize regions where rCBV changes occur.

In this work the ROI method was used in comparison to PRMs. The PRMs [8,9] is a voxel-wise technique estimating point by point the rCBV differences over time to better inquire the

Table 3. Univariate and multivariate analysis.

	Progression Free Survival		Overall Survival	
Model	**Univariate *p* values**	**Multivariate *p* values**	**Univariate *p* values**	**Multivariate *p* values**
Volume ≥44.47 cm^3	0.02	n.s.	0.04	n.s.
Multifocal and Distant pattern	<0.0001	<0.0001	0.01	0.01
PRM_{CBV+}<18%	0.045	0.02	0.016	n.s.

doi:10.1371/journal.pone.0090535.t003

hemodynamic features of the tumor and to spatially localize the occurrence of hemodynamic changes. We compared PRMs with the classical ROI approach to investigate which one could better characterize the temporal variations of the tumor during therapy and have a better prognostic value.

The main result of the study is the correlation of PRMs with PFS at treatment onset. $PRM_{CBV+} > 18\%$, in particular, proved to be a valid prognostic marker of response whereas rCBV obtained by classical ROI showed no correlation with survival. These results are in accordance with those by Sorensen et al. [5], and Batchelor et al. [31] but different with respect to data published by Galbán et al. [8] where PRM_{CBV-} rather than PRM_{CBV+}, was predictive of OS.

This discrepancy could be mostly due to the different type of therapy used in the two studies: radio-chemotherapy in the study of Galban et al [8], bevacizumab and irinotecan in our population. Ionizing radiation and classical chemotherapy tumor growth through the induction of DNA damnage, while Bevacizumab is a target therapy inducing inhibition of vessel expansion, regression of pre-existing vasculature and inhibition of bone marrow derived cell and/or endothelial progenitor.

Other relevant differences include different kinds of tumors (grade III and IV gliomas versus recurrent high grade gliomas) and time points considered: they studied subjects before therapy and 1–3 weeks after treatment onset, we studied our subjects before therapy and every 8 weeks until progression. More recently Galbán et al. showed the predictive value of the PRMs in association with ADC functional diffusion maps [32]. Using this method, they studied high grade gliomas treated with radio-chemotherapy before the beginning of therapy and three weeks after, finding that the combination of PRM_{ADC+} and PRM_{CBV-} has a predictive value, strongly correlating with OS at 1 year. Moreover, in this study patients received a treatment different from bevacizumab/irinotecan and were observed for a shorter duration.

Using PRMs Batchelor et al. [31] demonstrated that treatment with cediranib, a pan-VEGF receptor tyrosine kinase inhibitor, increases perfusion, in 50% of patients with newly diagnosed GBMs and that these patients survive 9-mo longer than those whose perfusion does not increase.

Differently from the PRMs method, the classical ROI approach did not provide a significant correlation with survival, in accordance with previous results by Galban et al. [8]. In addition, at 8 weeks the classical ROI method showed an initial decrease of the rCBV values, whereas the PRMs method showed greater PRM_{CBV+}. The ROI method registered the mean rCBV variation in three ROIs placed in the points of maximum rCBV in the ehnancement region [16], whereas the PRMs consider a greater volume and analyze differences in a voxel-wise manner. Thus the first method is biased by the user ROI selection as it only takes into consideration the regions of maximum rCBV. Thus, mean rCBV after 8 weeks of treatment remained elevated in non responsive patients, but decreased in responsive patients, followed by a progressive tendency to increase as long as patients approached tumor progression.

On the contrary, the PRM method is less user-dependent as it considers the whole enhancement region, being unaffected by the selection criterias.

As previously reported [30], the PRMs tecnique is preferable because it offers the same sensibility but a higher specificity than the ROI classical approach. Interestingly, in non-responsive patients no major modification of perfusion was observed after treatment, suggesting that in non-responsive patients angiogenesis might be less VEGF dependent [33].

Even if the PRMs approach is affected by intrinsic limitations [8,17], such as the need of a high quality image registration, it provided relevant information. Its potential to predict survival in recurrent GBM treated with bevacizumab and irinotecan, adds to previous results in high grade gliomas treated with radio-chemotherapy [8], making it a promising prognostic biomarker. Moreover, the tecnique (born with the analysis of ADC maps [17]) could be used in combination with other kind of sequences, such as the Dynamic Contrast Enhanced-MRI (DCE-MRI) to obtain more detailed informations about the biology of the disease under treatment.

Supporting Information

File S1 Supplementary tables. Table S1, Mean rCBV changes according to radiological disease pattern at progression. Table S2, Mean PRM_{CBV-} and PRM_{CBV+} changes during treatment.
(DOCX)

Acknowledgments

We thank Dr. Stefania Cuzzubbo (Fondazione IRCCS Istituto Neurologico C. Besta, Milan, Italy) for her support in collecting data; Dr. Serena Pellegatta (Fondazione IRCCS Istituto Neurologico C. Besta, Milan, Italy) for digitizing figures; Roche S.p.A. (Basel, Switzerland) and Hospira Italia Srl (Naples, Italy) for providing the drugs.

Author Contributions

Conceived and designed the experiments: DA ALDS AS ME MGB. Performed the experiments: DA ALDS AS ME. Analyzed the data: DA ALDS AS LC GF MGB ME. Contributed reagents/materials/analysis tools: DA ALDS AS EA. Wrote the paper: DA ALDS LC GF ME. Performed clinical follow up of patients: EA ME.

References

1. McNamara MG, Mason WP (2012) Antiangiogenic therapies in glioblastoma multiforme. Expert Rev Anticancer Ther 12: 643–654.
2. Specenier P (2012) Bevacizumab in glioblastoma multiforme. Expert Rev Anticancer Ther 12: 9–18.
3. Lu KV, Bergers G (2013) Mechanisms of evasive resistance to anti-VEGF therapy in glioblastoma. CNS Oncol 2: 49–65.
4. Maru D, Venook AP, Ellis LM (2013) Predictive biomarkers for bevacizumab: Are we there yet? Clin Cancer Res 19: 2824–2827.
5. Sorensen AG, Emblem KE, Polaskova P, Jennings D, Kim H, et al. (2012) Increased survival of glioblastoma patients who respond to antiangiogenic therapy with elevated blood perfusion. Cancer Res 72: 402–407.
6. Cha S, Knopp EA, Johnson G, Litt A, Glass J, et al. (2000) Dynamic contrast-enhanced T2-weighted MR imaging of recurrent malignant gliomas treated with thalidomide and carboplatin. AJNR Am J Neuroradiol 21: 881–890.
7. Sawlani RN, Raizer J, Horowitz SW, Shin W, Grimm SA, et al. (2010) Glioblastoma: A method for predicting response to antiangiogenic chemotherapy by using MR perfusion imaging—pilot study. Radiology 255: 622–628.
8. Galban CJ, Chenevert TL, Meyer CR, Tsien C, Lawrence TS, et al. (2009) The parametric response map is an imaging biomarker for early cancer treatment outcome. Nat Med 15: 572–576.
9. Tsien C, Galban CJ, Chenevert TL, Johnson TD, Hamstra DA, et al. (2010) Parametric response map as an imaging biomarker to distinguish progression from pseudoprogression in high-grade glioma. J Clin Oncol 28: 2293–2299.
10. Law M, Young R, Babb J, Pollack E, Johnson G (2007) Histogram analysis versus region of interest analysis of dynamic susceptibility contrast perfusion MR imaging data in the grading of cerebral gliomas. AJNR Am J Neuroradiol 28: 761–766.
11. Cuppini L, Calleri A, Bruzzone MG, Prodi E, Anghileri E, et al. (2013) Prognostic value of CD109+ circulating endothelial cells in recurrent glioblastomas treated with bevacizumab and irinotecan. PLoS One In press.

12. Stupp R, Mason WP, van den Bent MJ, Weller M, Fisher B, et al. (2005) Radiotherapy plus concomitant and adjuvant temozolomide for glioblastoma. N Engl J Med 352: 987–996.
13. Wen PY, Macdonald DR, Reardon DA, Cloughesy TF, Sorensen AG, et al. (2010) Updated response assessment criteria for high-grade gliomas: Response assessment in neuro-oncology working group. J Clin Oncol 28: 1963–1972.
14. Pope WB, Lai A, Mehta R, Kim HJ, Qiao J, et al. (2011) Apparent diffusion coefficient histogram analysis stratifies progression-free survival in newly diagnosed bevacizumab-treated glioblastoma. AJNR Am J Neuroradiol 32: 882–889.
15. Chamberlain MC (2011) Radiographic patterns of relapse in glioblastoma. J Neurooncol 101: 319–323.
16. Law M, Young RJ, Babb JS, Peccerelli N, Chheang S, et al. (2008) Gliomas: Predicting time to progression or survival with cerebral blood volume measurements at dynamic susceptibility-weighted contrast-enhanced perfusion MR imaging. Radiology 247: 490–498.
17. Moffat BA, Chenevert TL, Lawrence TS, Meyer CR, Johnson TD, et al. (2005) Functional diffusion map: A noninvasive MRI biomarker for early stratification of clinical brain tumor response. Proc Natl Acad Sci U S A 102: 5524–5529.
18. Van Meter ME, Kim ES (2010) Bevacizumab: Current updates in treatment. Curr Opin Oncol 22: 586–591.
19. Barajas RF,Jr, Cha S (2012) Imaging diagnosis of brain metastasis. Prog Neurol Surg 25: 55–73.
20. Jain RK (2001) Normalizing tumor vasculature with anti-angiogenic therapy: A new paradigm for combination therapy. Nat Med 7: 987–989.
21. Maier SE, Sun Y, Mulkern RV (2010) Diffusion imaging of brain tumors. NMR Biomed 23: 849–864.
22. Pope WB, Qiao XJ, Kim HJ, Lai A, Nghiemphu P, et al. (2012) Apparent diffusion coefficient histogram analysis stratifies progression-free and overall survival in patients with recurrent GBM treated with bevacizumab: A multi-center study. J Neurooncol 108: 491–498.
23. Zulfiqar M, Yousem DM, Lai H (2013) ADC values and prognosis of malignant astrocytomas: Does lower ADC predict a worse prognosis independent of grade of tumor?—a meta-analysis. AJR Am J Roentgenol 200: 624–629.
24. Hashimoto M, Ichihara M, Watanabe T, Kawai K, Koshikawa K, et al. (2004) Expression of CD109 in human cancer. Oncogene 23: 3716–3720.
25. Ratai EM, Zhang Z, Snyder BS, Boxerman JL, Safriel Y, et al. (2013) Magnetic resonance spectroscopy as an early indicator of response to anti-angiogenic therapy in patients with recurrent glioblastoma: RTOG 0625/ACRIN 6677. Neuro Oncol 15: 936–944.
26. Takano S, Kimu H, Tsuda K, Osuka S, Nakai K, et al. (2013) Decrease in the apparent diffusion coefficient in peritumoral edema for the assessment of recurrent glioblastoma treated by bevacizumab. Acta Neurochir Suppl 118: 185–189.
27. Hu LS, Eschbacher JM, Dueck AC, Heiserman JE, Liu S, et al. (2012) Correlations between perfusion MR imaging cerebral blood volume, microvessel quantification, and clinical outcome using stereotactic analysis in recurrent high-grade glioma. AJNR Am J Neuroradiol 33: 69–76.
28. Mills SJ, Soh C, O'Connor JP, Rose CJ, Buonaccorsi G, et al. (2010) Enhancing fraction in glioma and its relationship to the tumoral vascular microenvironment: A dynamic contrast-enhanced MR imaging study. AJNR Am J Neuroradiol 31: 726–731.
29. Sugahara T, Korogi Y, Tomiguchi S, Shigematsu Y, Ikushima I, et al. (2000) Posttherapeutic intraaxial brain tumor: The value of perfusion-sensitive contrast-enhanced MR imaging for differentiating tumor recurrence from nonneoplastic contrast-enhancing tissue. AJNR Am J Neuroradiol 21: 901–909.
30. Young R, Babb J, Law M, Pollack E, Johnson G (2007) Comparison of region-of-interest analysis with three different histogram analysis methods in the determination of perfusion metrics in patients with brain gliomas. J Magn Reson Imaging 26: 1053–1063.
31. Batchelor TT, Gerstner ER, Emblem KE, Duda DG, Kalpathy-Cramer J, et al.(2013) Improved tumor oxygenation and survival in glioblastoma patients who show increased blood perfusion after cediranib and chemoradiation. PNAS,2013 Nov;110(47):19059–64.
32. Galban CJ, Chenevert TL, Meyer CR, Tsien C, Lawrence TS, et al. (2011) Prospective analysis of parametric response map-derived MRI biomarkers: Identification of early and distinct glioma response patterns not predicted by standard radiographic assessment. Clin Cancer Res 17: 4751–4760.
33. Carmeliet P, Jain RK (2011) Molecular mechanisms and clinical applications of angiogenesis. Nature 473: 298–307.

Hindawi Publishing Corporation
BioMed Research International
Volume 2014, Article ID 154350, 5 pages
http://dx.doi.org/10.1155/2014/154350

Clinical Study

Facing Contrast-Enhancing Gliomas: Perfusion MRI in Grade III and Grade IV Gliomas according to Tumor Area

Anna Luisa Di Stefano,[1,2] Niels Bergsland,[3] Giulia Berzero,[1,4] Lisa Farina,[5] Elisa Rognone,[5] Matteo Gastaldi,[6] Domenico Aquino,[7] Alessandro Frati,[8] Francesco Tomasello,[9] Mauro Ceroni,[2,6] Enrico Marchioni,[1] and Stefano Bastianello[2,5]

[1] *Neuro-Oncology Unit, C. Mondino National Neurological Institute, 27100 Pavia, Italy*
[2] *Department of Brain and Behavioral Sciences, University of Pavia, 27100 Pavia, Italy*
[3] *Magnetic Resonance Laboratory, IRCCS Don Gnocchi Foundation, 20148 Milan, Italy*
[4] *Neuroscience Consortium, University of Pavia, Monza Policlinico and Pavia Mondino, 27100 Pavia, Italy*
[5] *Neuroradiological Department, C. Mondino National Neurological Institute, 27100 Pavia, Italy*
[6] *General Neurology Unit, C. Mondino National Neurological Institute, 27100 Pavia, Italy*
[7] *Department of Neuroradiology, IRCCS Foundation Neurological Institute C. Besta, 20133 Milan, Italy*
[8] *Department of Neurosurgery, IRCCS Neuromed, Pozzilli (IS), University of Rome La Sapienza, 00185 Rome, Italy*
[9] *Department of Neurosurgery, University of Messina, 98122 Messina, Italy*

Correspondence should be addressed to Anna Luisa Di Stefano; annaluisadistefano@gmail.com

Received 14 February 2014; Accepted 6 March 2014; Published 3 April 2014

Academic Editor: Lombardi Giuseppe

Tumoral neoangiogenesis characterizes high grade gliomas. Relative Cerebral Blood Volume (rCBV), calculated with Dynamic Susceptibility Contrast (DSC) Perfusion-Weighted Imaging (PWI), allows for the estimation of vascular density over the tumor bed. The aim of the study was to characterize putative tumoral neoangiogenesis via the study of maximal rCBV with a Region of Interest (ROI) approach in three tumor areas—the contrast-enhancing area, the nonenhancing tumor, and the high perfusion area on CBV map—in patients affected by contrast-enhancing glioma (grades III and IV). Twenty-one patients were included: 15 were affected by grade IV and 6 by grade III glioma. Maximal rCBV values for each patient were averaged according to glioma grade. Although rCBV from contrast-enhancement and from nonenhancing tumor areas was higher in grade IV glioma than in grade III (5.58 and 2.68; 3.01 and 2.2, resp.), the differences were not significant. Instead, rCBV recorded in the high perfusion area on CBV map, independently of tumor compartment, was significantly higher in grade IV glioma than in grade III (7.51 versus 3.78, $P = 0.036$). In conclusion, neoangiogenesis encompasses different tumor compartments and CBV maps appear capable of best characterizing the degree of neovascularization. Facing contrast-enhancing brain tumors, areas of high perfusion on CBV maps should be considered as the reference areas to be targeted for glioma grading.

1. Introduction

Gliomas are the most common brain primary neoplasms and are classified based on histologic parameters including atypia, vascular endothelial proliferation, necrosis, and mitosis [1, 2]. A common histopathological characteristic for both grade III and grade IV glioma is vascular endothelial proliferation,which is known to correspond to blood brain barrier disruption and tumoral neoangiogenesis [3, 4] as evidenced by contrast-enhancement observed using conventional Magnetic Resonance Imaging (MRI).Although neuroradiological necrosis is a hallmark of glioblastoma (GBM; grade IV glioma), it is not a constant finding. Therefore it can be difficult to distinguish between grade III and grade IV gliomas using conventional MRI.

Dynamic Susceptibility Contrast (DSC) Perfusion-Weighted Imaging (PWI) measures concentration of a paramagnetic contrast material in the organ, providing reliable information

on blood flow and vascularization. Among other perfusion parameters such as Cerebral Blood Flow (CBF) and Mean Transit Time (MTT), Cerebral Blood Volume (CBV) was shown to best correlate with tumoral neoangiogenesis and subsequently glioma grading. In particular, Relative Cerebral Blood Volume (rCBV), reflecting increased capillary density, was shown to be significantly higher in high grade gliomas (grade III and grade IV gliomas) than low grade gliomas (grade II glioma) and with higher values in grade IV [5].

Although rCBV increase is recognized as a surrogate marker of malignancy [6–8], differentiation between grade III and grade IV glioma is not consistently reproducible [8–11].

Furthermore, rCBV increases in glioblastoma multiforme (GBM) peritumoral area [10] and the peculiar pattern of rCBV increase surrounding glioblastoma contrast-enhancing tumor bed [12, 13] raises the question of where measuring rCBV values may best distinguish between grade III and grade IV gliomas.

In this study we investigated rCBV differences in patients with grade III and grade IV glioma using a Region of Interest- (ROI-) based method in three different tumor areas: the contrast-enhancing area, the nonenhancing tumor, and the high perfusion area on CBV map.

The aim of the study was to determine which tumor compartments showed rCBV differences related to glioma grade.

2. Materials and Methods

We examined perfusion MRI from 21 patients affected by histologically proven high grade gliomas: fifteen patients were affected by grade IV glioma and 6 patients by grade III glioma.

Twelve patients underwent a DSC perfusion examination before surgery and 9 with residual tumor were examined after surgery after a median of 6.8 months. All patients undergoing perfusion after surgery had residual tumor and were not in progression at the time of DSC perfusion examination. All patients in this study were affected by primary disease and in particular grade IV glioma patients were all affected by primary GBM.

Demographical characteristics of patients are detailed in Table 1. Glioma grading was assessed by an experienced neuropathologist according to WHO criteria 2007 [2]. The study was approved by the local Institutional Review Board and all patients provided informed consent.

All participants were scanned using a 1.5T Philips Intera Gyroscan (Philips Medical System, Best, The Netherlands) with a maximum slew rate of 150 Tm^{-1} s^{-1} and a maximum gradient amplitude of 30 mT/m. All scans were performed using an 8-channel SENSE (sensitivity encoding parallel imaging) head coil.

The scanning protocol included the following.

An axial 2D spin-echo (SE) T2-weighted Fluid Attenuated Inversion Recovery (FLAIR) image: echo time (TE)/repetition time (TR)/inversion time (TI) = 140/11000/2800 ms, flip angle (FA) = 90°, echo train length (ETL) = 50, acquisition matrix = 256 × 188, FOV = 250 mm^2 (for an in-plane resolution of 0.9 mm × 1.3 mm), slice thickness = 5 mm, gap = 1 mm, number of excitations (NEX) =2, and number of slices = 24.

Table 1: Patients' clinical data and tumor diagnosis.

WHO glioma grade	Number of patients	Age (years) (median, range)	Sex ratio (male/female)
III	6	49 (24–66)	6.0
IV	15	63 (23–80)	1.5

An axial 2D SE T1-weighted image: TE/TR = 15/649.5 ms, FA = 90°, ETL = 1, acquisition matrix = 260 × 209, FOV = 250 mm^2 (in-plane resolution of 0.9 mm × 1.2 mm), slice thickness = 5 mm, gap = 1 mm, NEX = 2, and number of slices = 24.

An axial 3D perfusion weighted gradient echo (GRE) sequence (Principles of Echo Shifting with a Train of Observations, PRESTO) for Dynamic Susceptibility Contrast MRI: TE/TR = 8/16.72 ms (effective T2 = 23.71 ms), FA = 7°, ETL = 7, acquisition matrix = 64 × 64, FOV = 220 mm^2 (in-plane resolution of 3.44 mm × 3.44 mm), slice thickness = 3 mm, NEX = 1, and number of slices = 30 with 40 temporal localizations. This sequence was acquired with a standard dose of 0.2 mmol/Kg body weight of gadopentetate dimeglumine (Gd-DTPA) contrast agent (Gadovist) which was injected at a rate of 4 mL/s, followed by a 20 mL continuous saline flush. Using a 0.05 mmol/Kg dose, presaturation of the baseline signal prior to the PWI acquisition was done to reduce T1-effects as well as potential contrast leakage effects due to blood brain barrier disruption.

An axial 3D T1-weighted fast field echo (FFE) sequence after the PWI: TE/TR = 4.6/25 ms, FA = 30°, ETL = 1, acquisition matrix = 256 × 256, FOV = 250 mm^2 (in-plane resolution of 0.98 mm × 0.98 mm), slice thickness = 1.6 mm, gap = 0, NEX = 1, and number of slices = 170.

Postprocessing was performed using Olea Medical PerfScape software (version 2.0). The DSC acquisition was corrected for patient motion using the built-in feature of PerfScape. The T1 SE, FLAIR, and T1 3D FFE images were then coregistered and resampled into the space of the DSC MRI. It is well known that disruption of the blood brain barrier, as is common in high grade tumors, can lead to inaccurate measures of CBV [14]. As such, the correction for leakage effects option in PerfScape was employed.

Relative CBV (rCBV) was calculated from three separate ROIs that were placed in three different compartments: the area of contrast-enhancement, the nonenhancing tumor, and high perfusion area seen on the CBV color overlay maps. In the contrast-enhancement area, necrosis was excluded from CBV measure. The nonenhancing surrounding tumor ROIs corresponded to areas of T2/FLAIR hyperintensity outside contrast-enhancement. We ensured that T2/FLAIR ROIs were not placed in areas of contrast-enhancement as all images were coregistered. Placement of ROIs on the CBV map was performed in high perfusion areas independently of the contrast-enhancement and T2/FLAIR ROI locations.

Morphology and size of the ROIs were constant (elliptical-40 mm^2 area) and the maximum value was recorded for each compartment according to Law et al. [15].

Table 2: Mean rCBV values according to histological grading. Relative Cerebral Blood Volume (rCBV) was measured with the ROI-based approach in three distinct areas: the high perfusion area on CBV map ("CBV map" in the table), the contrast-enhanced area ("CE" in the table), and the nonenhancing tumor ("Non-CE" in the table). Only rCBV values measured in the high perfusion area in CBV map showed significant difference between grade III and grade IV gliomas.

WHO glioma grade	rCBV; mean (SD)					
	CBV map	*P*	CE	*P*	Non-CE	*P*
Glioma grade III	3.78 (1.70)	**0.036**	3.01 (1.02)	0.27	2.20 (1.73)	0.71
Glioma grade IV	7.51 (3.84)		5.58 (5.48)		2.68 (2.93)	

All values were normalized to a corresponding ROI placed in contralateral normal brain parenchyma. All ROIs were placed by two operators (A.D, N.B.) via consensus. Maximal rCBV values for each patient were averaged according to glioma grade.

Differences between grades and tumor areas were tested using *t*-test. ANOVA was used in order to compare rCBV values in different subgroups of patients. Contingency analysis was performed by Fisher's exact test. In all analyses we considered a *P* value of 0.05 (two-sided) as being statistically significant.

3. Results

Twelve patients underwent a DSC perfusion examination before surgery (3 patients affected by grade III glioma and 9 patients affected by grade IV glioma) and 9 patients with residual tumor were examined after surgery after a median of 6.8 months (3 patients affected by grade III glioma and 6 by grade IV glioma). Distribution of patients according to the timing of perfusion MRI (presurgery versus postsurgery) was not significantly different between grade III glioma and grade IV ($P = 0.67$).

In the grade III glioma subgroup, 2 patients were affected by anaplastic oligodendroglioma and 4 patients by anaplastic astrocytoma; in the grade IV glioma subgroup all patients were affected by glioblastoma.

Mean rCBV values from patients are detailed in Table 2. In the grade III glioma subgroup, mean rCBV was higher in the contrast-enhanced area than nonenhancing tumor (3.01 and 2.20, resp., $P = 0.11$); rCBV recorded in CBV map, independently of tumor compartment as seen on conventional MRI, was 3.78.

In glioma grade IV, mean rCBV was higher in contrast-enhanced area than nonenhancing tumor (5.58 and 2.68, resp., $P = 0.04$); the mean rCBV recorded in the CBV map was 7.51.

Between glioma grade III and glioma grade IV, no significant differences in rCBV were observed in the contrast-enhancement area and in the nonenhancing tumor ($P = 0.27$ and 0.71, resp.). Inversely, mean rCBV was significantly higher in grade IV gliomas than in grade III ($P = 0.036$) in the high perfusion area of CBV map independently of tumor compartment, as seen on conventional MRI (Figure 1).

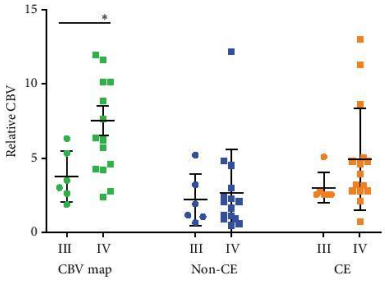

Figure 1: Scatter-plot diagram representing rCBV values according to grade and tumor area. Circles represent grade III, squares grade IV. Green color represents rCBV values measured in CBV map; blue color represents rCBV values measured in the nonenhancing tumor (Non-CE); orange color represents rCBV values measured in enhancing area (CE). Lines correspond to mean value and error bars to standard error of the mean. Only rCBV values measured in the high perfusion area in CBV map showed significant difference between grade III and grade IV gliomas.

4. Discussion

Neovascular proliferation is a hallmark of malignant gliomas and PWI is useful in glioma grading through detection of vascular density and of the grade of tumor-associated neovascularization [7, 16].

The measure of rCBV is commonly used in order to predict glioma grade or to differentiate radionecrosis from tumor recurrence in a diagnostic setting. Several reports on rCBV increases in peritumoral area of glioblastoma [10, 13] have suggested that there is a mismatch between the extension of effective vascular proliferation and area of contrast-enhancement.

In this work we mapped rCBV maximal increase in two different compartments of glioma grade III and glioma grade IV—the contrast-enhancing area and nonenhancing tumor with a ROI-based method. rCBV was also recorded in high perfusion area of CBV map independently of corresponding tumor area on conventional MRI.

Values of rCBV recorded in this work are consistent with the other reports in the literature [6]. As expected we found a significantly higher rCBV in contrast-enhanced area than in nonenhancing tumor in the grade IV glioma subgroup.

Concerning rCBV differences according to the tumor grade, we did not find significant differences of rCBV values recorded in contrast-enhancing area or nonenhancing tumor between grades III and IV.

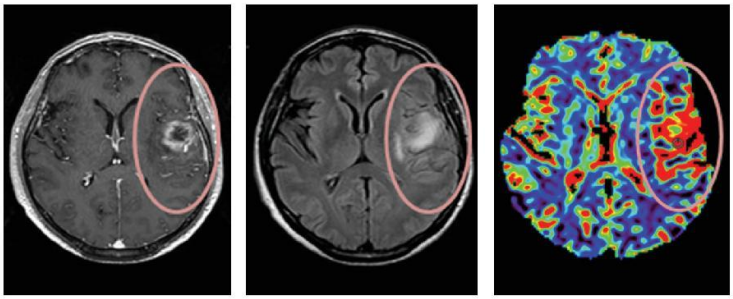

(a) (b) (c)

Figure 2: Axial coregistered contrast-enhanced axial T1-weighted image (a), FLAIR image (b), and CBV map (c) from a patient affected by glioma grade IV. In the CBV map (c) warmer colors indicate higher CBV values suggesting higher perfusion and neovascularization. Comparison of CBV map (c) and contrast-enhanced axial T1-weighted image highlights a mismatch area (surrounded by the circle) corresponding to the extension of the high perfusion area outside the contrast-enhancement: this indicates a more extensive neovascularization than that shown by conventional MRI (a, b).

Only measures of rCBV in the high perfusion area on the CBV map showed a significant difference between grade III glioma and grade IV, with higher values in grade IV.

Taken together, these results support the idea that neoangiogenesis heterogeneously encompasses both contrast-enhancing and nonenhancing tumor areas. The contrast-enhancing areas appear to reflect a higher degree of neoangiogenesis, although the difference with respect to nonenhancing areas was significant only in grade IV glioma subgroup.

Interestingly, we did not find significant differences in maximal rCBV in neither of these two areas when comparing grades III and IV. This suggests that basing rCBV measurements on signal characteristics of conventional MRI may not be sufficient to distinguish between grade III and grade IV gliomas.

Glioblastoma has been shown to present with a more heterogeneous neovascularization than grade III glioma [12]. In particular glioblastoma present, more so than with lower grades, areas with low perfusion due to necrosis, area of focal rCBV increase, and also increased rCBV values in peritumoral normal-appearing parenchyma [14, 17].

In particular, a special pattern of rCBV increase in peritumoral area can occur in a "stripe like" fashion which has been termed a "striate sign." This feature has been described as mostly represented in glioblastoma rather than lower grade gliomas and in particular with respect to grade III glioma [12, 13]. The same authors showed that this specific pattern of rCBV in peritumoral area was significantly associated with normalized choline increase and with the subsequent appearance of contrast-enhancement in the same area [12, 13]. A similar example of mismatch between high perfusion area from CBV map and contrast-enhancement observed in our patients is shown in Figure 2. Histopathologically, these patterns of rCBV may reflect diffuse migration of glioma cells along vascular channels of the white matter tracts spreading beyond the visible tumor border [18].

Taken together, these results support the hypothesis that only the rCBV map represents extensively the neovascular phenomena, its extension into apparently normal surrounding parenchyma, and its quantitative difference among glioma grades.

Limits of the study are the small sample size and potential sampling differences from the ROI-dependent method of measure which may increase interobserver variability. Nevertheless the latter is the most used in clinical routine. Additionally, all ROIs were placed in consensus by two authors. The fact that some patients were scanned before surgery and other patients afterwards presents an additional confound. However, we did not find any significant differences between the pre-/posttreatment groups (results not shown). Nevertheless, we cannot rule out the possibility that surgical intervention in some patients may have influenced the results.

In conclusion, maximal rCBV values measured directly on the CBV map seem to best characterize the extensive neoangiogenesis phenomena of high grade gliomas and quantitative difference of microvascular density between grade III and grade IV glioma. Such measurements should be considered as the reference map for glioma grading and potentially for serial measures of rCBV modification during antiangiogenic treatment.

Conflict of Interests

The authors declare that there is no conflict of interests regarding the publication of this paper.

Acknowledgments

The study was supported by a Grant of the National Ministry of University and Research, PRIN 2008 "2008979 M8 K_003." The authors are grateful to OLEA Medical for providing OLEA PerfScape Software for postprocessing perfusion analysis. Dr. Di Stefano is supported by an investigator Fellowship from Collegio Ghislieri, Pavia, Italy.

References

[1] D. N. Louis, H. Ohgaki, O. D. Wiestler et al., "The 2007 WHO classification of tumours of the central nervous system," *Acta Neuropathologica*, vol. 114, no. 2, pp. 97–109, 2007.

[2] D. N. Louis, H. Ohgaki, O. D. Wiestler, and W. K. Cavenee, *WHO Classification of Tumours of the Central Nervous System*, IARC, Lyon , France, 2007.

[3] R. Felix, W. Schorner, and M. Laniado, "Brain tumors: MR imaging with gadolinium-DTPA," *Radiology*, vol. 156, no. 3, pp. 681–688, 1985.

[4] B. L. Dean, B. P. Drayer, C. R. Bird et al., "Gliomas: classification with MR imaging," *Radiology*, vol. 174, no. 2, pp. 411–415, 1990.

[5] J. R. Petrella and J. M. Provenzale, "MR perfusion imaging of the brain: techniques and applications," *American Journal of Roentgenology*, vol. 175, no. 1, pp. 207–219, 2000.

[6] T. Sugahara, Y. Korogi, M. Kochi et al., "Correlation of MR imaging-determined cerebral blood volume maps with histologic and angiographic determination of vascularity of gliomas," *American Journal of Roentgenology*, vol. 171, no. 6, pp. 1479–1486, 1998.

[7] H. J. Aronen, F. S. Pardo, D. N. Kennedy et al., "High microvascular blood volume is associated with high glucose uptake and tumor angiogenesis in human gliomas," *Clinical Cancer Research*, vol. 6, no. 6, pp. 2189–2200, 2000.

[8] E. A. Knopp, S. Cha, G. Johnson et al., "Glial neoplasms: dynamic contrast-enhanced $T2^*$-weighted MR imaging," *Radiology*, vol. 211, no. 3, pp. 791–798, 1999.

[9] N. Fayed, J. Dávila, J. Medrano, and S. Olmos, "Malignancy assessment of brain tumours with magnetic resonance spectroscopy and dynamic susceptibility contrast MRI," *European Journal of Radiology*, vol. 67, no. 3, pp. 427–433, 2008.

[10] S. Cha, E. A. Knopp, G. Johnson, S. G. Wetzel, A. W. Litt, and D. Zagzag, "Intracranial mass lesions: dynamic contrast-enhanced susceptibility-weighted echo-planar perfusion MR imaging," *Radiology*, vol. 223, no. 1, pp. 11–29, 2002.

[11] R. Sanz-Requena, A. Revert-Ventura, L. Martí-Bonmatí, Á. Alberich-Bayarri, and G. García-Martí, "Quantitative MR perfusion parameters related to survival time in high-grade gliomas," *European Radiology* , vol. 23, no. 12, pp. 3456–3465, 2013.

[12] S. Blasel, K. Franz, M. Mittelbronn et al., "The striate sign: peritumoural perfusion pattern of infiltrative primary and recurrent gliomas," *Neurosurgical Review*, vol. 33, no. 2, pp. 193–203, 2010.

[13] S. Blasel, K. Franz, H. Ackermann, S. Weidauer, F. Zanella, and E. Hattingen, "Stripe-like increase of rCBV beyond the visible border of glioblastomas: site of tumor infiltration growing after neurosurgery," *Journal of Neuro-Oncology*, vol. 103, no. 3, pp. 575–584, 2011.

[14] J. L. Boxerman, K. M. Schmainda, and R. M. Weisskoff, "Relative cerebral blood volume maps corrected for contrast agent extravasation significantly correlate with glioma tumor grade, whereas uncorrected maps do not," *American Journal of Neuroradiology*, vol. 27, no. 4, pp. 859–867, 2006.

[15] M. Law, R. J. Young, J. S. Babb et al., "Gliomas: predicting time to progression or survival with cerebral blood volume measurements at dynamic susceptibility-weighted contrast-enhanced perfusion MR imaging," *Radiology*, vol. 247, no. 2, pp. 490–498, 2008.

[16] B. R. Rosen, J. W. Belliveau, J. M. Vevea, and T. J. Brady, "Perfusion imaging with NMR contrast agents," *Magnetic Resonance in Medicine*, vol. 14, no. 2, pp. 249–265, 1990.

[17] I. C. Chiang, Y. T. Kuo, C. Y. Lu et al., "Distinction betweenhigh-grade gliomas and solitary metastases using peritumoral 3-T magnetic resonance spectroscopy, diffusion, and perfusion imagings," *Neuroradiology*, vol. 46, no. 8, pp. 619–627, 2004.

[18] P. J. Kelly, C. Daumas-Duport, and D. B. Kispert, "Imaging-based stereotaxic serial biopsies in untreated intracranial glial neoplasms," *Journal of Neurosurgery*, vol. 66, no. 6, pp. 865–874, 1987.

Hindawi Publishing Corporation
BioMed Research International
Volume 2014, Article ID 282815, 8 pages
http://dx.doi.org/10.1155/2014/282815

Research Article

An ANOCEF Genomic and Transcriptomic Microarray Study of the Response to Irinotecan and Bevacizumab in Recurrent Glioblastomas

Julien Laffaire,[1] Anna Luisa Di Stefano,[2,3,4,5] Olivier Chinot,[6,7,8] Ahmed Idbaih,[2,3,4,8] Jaime Gallego Perez-Larraya,[2,3,4,8] Yannick Marie,[2,3,4] Nadia Vintonenko,[2,3,4] Blandine Boisselier,[2,3,4] Patrizia Farina,[2,3,4,9] Jean-Yves Delattre,[2,3,4,8] Dominique Figarella-Branger,[7,8,10] Jérôme Honnorat,[8,11,12,13] Marc Sanson,[2,3,4,8] and François Ducray[8,11,12,13]

[1] *Programme Cartes d'Identité des Tumeurs (CIT), Ligue Nationale Contre le Cancer, Paris, France*
[2] *AP-HP, Groupe Hospitalier Pitié-Salpêtrière, Service de Neurologie Mazarin, Paris, France*
[3] *INSERM, U975, Centre de Recherche de l'Institut du Cerveau et de la Moelle, Paris, France*
[4] *Faculté de Médecine Pitié-Salpêtrière, Université Pierre & Marie Curie Paris VI, CNRS UMR 7225 and UMR-S975, Paris, France*
[5] *Neuro-Oncology Unit, C. Mondino National Neurological Institute, Pavia, Italy*
[6] *Assistance Publique-Hôpitaux de Marseille, Service de Neuro-Oncologie, Centre Hospitalier Universitaire Timone, 264 rue Saint Pierre, 13385 Marseille Cedex 05, France*
[7] *Aix-Marseille Université, Inserm, CRO2 UMR_S 911, 13385 Marseille, France*
[8] *ANOCEF (Association des Neuro-Oncologues d'Expression Française (French Speaking NeuroOncologists' Association)), France*
[9] *Medical Oncology 1, Venetian Oncology Institute-IRCCS, Padua, Italy*
[10] *APHM, Hôpital de la Timone, Service d'Anatomie Pathologique et de Neuropathologie, 13385 Marseille, France*
[11] *Service de Neuro-oncologie, Hôpital Neurologique, Hospices Civils de Lyon, 59 Boulevard Pinel, 69394 Lyon Cedex 3, Lyon, France*
[12] *Université de Lyon, Claude Bernard Lyon 1, Lyon, France*
[13] *Lyon Neuroscience Research Center, INSERM U1028/CNRS UMR 5292, Lyon, France*

Correspondence should be addressed to François Ducray; francois.ducray@chu-lyon.fr

Received 11 February 2014; Accepted 25 February 2014; Published 2 April 2014

Academic Editor: Giuseppe Lombardi

Background. We performed a retrospective study to assess whether the initial molecular characteristics of glioblastomas (GBMs) were associated with the response to the bevacizumab/irinotecan chemotherapy regimen given at recurrence. *Results.* Comparison of the genomic and gene expression profiles of the responders ($n = 12$) and nonresponders ($n = 13$) demonstrated only slight differences and could not identify any robust biomarkers associated with the response. In contrast, a significant association was observed between GBMs molecular subtypes and response rates. GBMs assigned to molecular subtype IGS-18 and to classical subtype had a lower response rate than those assigned to other subtypes. In an independent series of 33 patients, neither EGFR amplification nor CDKN2A deletion (which are frequent in IGS-18 and classical GBMs) was significantly associated with the response rate, suggesting that these two alterations are unlikely to explain the lower response rate of these GBMs molecular subtypes. *Conclusion.* Despite its limited sample size, the present study suggests that comparing the initial molecular profiles of responders and nonresponders might not be an effective strategy to identify biomarkers of the response to bevacizumab given at recurrence. Yet it suggests that the response rate might differ among GBMs molecular subtypes.

1. Background

In recurrent glioblastomas (GBMs), studies have shown a high response rate (30–50%) to bevacizumab, a human monoclonal antivascular endothelial growth factor (VEGF) antibody, administered alone or in combination with irinotecan, demonstrating a 35–50% estimated 6-month progression-free survival (PFS) [1–3]. Simple biomarkers that would help in selecting patients most likely to benefit from bevacizumab would be very helpful, but no such markers are available to date. In the present study, we hypothesized that the response to bevacizumab plus irinotecan given at recurrence might be related to the molecular characteristics of the initial tumor. To identify predictive biomarkers, we compared the initial GBM genomic and gene expression profiles of responders and nonresponders to bevacizumab plus irinotecan given at the time of recurrence.

2. Methods

2.1. Patients. We retrospectively identified responders and nonresponders to bevacizumab/irinotecan chemotherapy. This study was approved by the ANOCEF review board. All patients who underwent a genetic analysis of tumor samples collected for this study signed a written informed consent form. The patients' clinical characteristics are summarized in Table 1 and see additional Table 1 in Supplementary Material available online at http://dx.doi.org/10.1155/2014/282815. All of the 25 patients included in this study had *de novo* GBM according to the 2007 World Health Organization Classification [4] and were initially treated according to the Stupp regimen [5]. To exclude patients with possible pseudoprogression, only those patients with a progression occurring more than 3 months after the end of the radiochemotherapy treatment were selected [6]. Patients received bevacizumab (10 mg/kg) plus irinotecan (125 mg/m^2) every two weeks either at the first ($n = 15$), second ($n = 9$), or third ($n = 1$) recurrence (chemotherapy details are available in additional Table 1). To identify clinically meaningful biomarkers of the response, the patients were considered to be responders if they achieved a complete or partial response according to RANO criteria [6] and presented more than 6-month progression-free survival (PFS); the patients were considered to be nonresponders if they progressed within 4 months.

2.2. Samples. The samples were provided as snap-frozen sections of the areas immediately adjacent to the region used for the histopathological diagnosis. Only samples representative of the tumor and from which high-quality DNA and/or RNA could be obtained were selected ($n = 25$). A total of 21 samples were available for the genomic Illumina SNP array study, which included samples from 8 responders and 13 nonresponders. The gene expression array study was performed on 23 samples (including 19 samples common to the SNP array study): 11 responders and 12 nonresponders.

2.3. Genomic and Gene Expression Data

2.3.1. RNA and DNA Extraction. Total RNA was extracted using the RNeasy Lipid Tissue Mini Kit (Qiagen), and DNA was extracted using the QIAamp DNA Mini Kit (Qiagen) following the manufacturer's instructions. Both the RNA and DNA were assessed for integrity and quantity, following stringent quality control criteria (CIT program protocols http://cit.ligue-cancer.net/). The genomic and gene expression analyses were performed using R software (http://www.R-project.org/).

2.3.2. Gene Expression Arrays. The gene expression arrays were performed using the IGBMC microarray platform (Strasbourg, France). Total RNA was amplified, labeled, and hybridized to the Affymetrix Human Genome U133 plus2 GeneChip, following the manufacturer's protocol (Affymetrix, Santa Clara, CA, USA). The microarrays were scanned using an Affymetrix GeneChip Scanner 3000, and the raw intensities were quantified from the subsequent images using GCOS 1.4 software (Affymetrix). The data were normalized using the robust multiarray average method implemented in the R package affinity [9].

Unsupervised hierarchical clustering analysis was performed using the Pearson correlation metric. Only probesets with an Affymetrix annotation class A and located on autosomes were considered. Differences between the sample clusters were tested using the Chi-squared test, and genes differentially expressed between the tumors of responder and nonresponder patients were assessed using the t-test followed by Benjamini and Hochberg correction. The analyses of the gene sets using KEGG and Biocarta pathways and Gene Ontology terms, Molecular Signature Database gene sets, and Stanford Microarray Database gene sets were performed on the 1000 most differentially expressed genes (500 genes upregulated in responders and 500 genes upregulated in nonresponders) using hypergeometric tests [10]. We used the published centroid-based classifier of Verhaak et al. to classify our samples according to their system [7]. Samples were assigned to one of the six molecular subtypes of gliomas (called intrinsic glioma subtypes (IGS)) described by Gravendeel et al. [8] using ClusterRepro (an R package; http://crantastic.org/packages/clusterRepro) [11].

2.3.3. Genomic Arrays. The genomic arrays were performed using the IntegraGen Platform (Evry, France). DNA was hybridized to Illumina SNP Human CNV370 chips according to the instructions provided by the array manufacturer (Illumina, San Diego, CA). The raw fluorescent signals were imported into Illumina BeadStudio software and normalized as previously described [12] to obtain the log R ratio (LRR) and B Allele Frequency (BAF) for each SNP. A supplemental normalization procedure tQN [13] was applied to correct for dye bias. The genomic profiles were then segmented using the circular binary segmentation algorithm (DNAcopy package, Bioconductor) [14] into the LRR and BAF data separately, as previously described [13, 15]. The absolute copy number and genotype status of the segments were then determined using the genome alteration print (GAP) method [15].

Table 1: Patient characteristics.

	Nonresponders	Responders	
Number of patients	13	12	
Median age (years) at diagnosis (range)	56 (37–69)	62 (57–72)	t-test $P = 0.01$
Biopsy/resection (%)	0/100	25/75	
Initial treatment (%)	RTCT (100%)	RTCT (100%)	
Median delay (months) between diagnosis and bev./iri. onset (range)	11 (7–22)	13 (5–27)	Ns
Recurrence number at bev./iri. onset			
First	8	7	
Second	4	5	
Third	1	0	
Median KPS at bev./iri. onset	70	80	Ns
Median PFS after bev./iri. onset (months)	2.4	9.4	$P < 0.0001$
Median OS after bev./iri. onset (months)	6.4	18.9	$P = 0.0001$
Median OS since diagnosis (months)	18.3	36.4	$P = 0.002$

RTCT: temozolomide radiochemotherapy; bev./iri.: bevacizumab/irinotecan chemotherapy; KPS: Karnofsky performance status; PFS: progression-free survival; OS: overall survival; ns: not significant.

The data are available in the ArrayExpress database (http://www.ebi.ac.uk/arrayexpress/), ArrayExpress accession: E-MTAB-951.

2.3.4. RT-PCR. The gene expression of NPTX2, EPHA7, SOCS2, PDGFD, PRKCZ, and ENPP4 in the tumors and nontumor control tissue were analyzed using UPL probe real-time quantitative polymerase chain reaction (QPCR) analysis. The reference gene was PPIA. The sequences of the primers and probes are listed in additional Table 2. The real-time QPCR reactions were performed as follows: 1X LightCycler 480 Probes Master (Roche Applied Science), 4 pmoles each primer, 2 pmoles Universal ProbeLibrary Set, Human, and 8 ng cDNA. The real-time QPCR cycles were as follows: initial denaturation at 95°C for 110 minutes and 45 cycles of 95°C for 10 seconds and annealing at 60°C for 30 minutes. The 2-DeltaDeltaCT method was used to determine the relative expression levels. The calculation of the relative amounts of the studied transcript compared to the reference transcript was performed using the LightCycler 480 Software (Roche applied science). The final results were expressed as a ratio of the expression levels of the studied gene and reference in the sample, normalized to the ratio of the reference gene expression in the calibration RNA.

2.4. Independent Data Set. An independent series of 33 GBMs from the Salpêtrière database treated with the bevacizumab/irinotecan combination at recurrence (31 out of 33 were treated at first recurrence) was used to assess the impact of the *CDKN2A* homozygous deletion and *EGFR* amplification. These alterations were assessed in the initial tumor using CGH arrays as previously described [16]. The response according to RANO criteria was assessable in 29 of the patients. RNA was available for 7 of the responders and 11 nonresponders and was used to study NPTX2, EPHA7, SOCS2, PDGFD, PRKCZ, and ENPP4 gene expression using RT-PCR.

3. Results

3.1. Patients' Characteristics. Twelve responders and thirteen nonresponders were included. All of the MRIs were reviewed. All of the patients exhibited an evaluable disease at the initiation of bevacizumab plus irinotecan treatment. The patients' characteristics are shown in Table 1. After bevacizumab/irinotecan onset, the responders had a longer progression-free survival (PFS) and overall survival (OS) than the nonresponders. The OS since diagnosis was also significantly longer for the responders (Table 1).

3.2. Responders and Nonresponders Have Very Similar Genomic and Gene Expression Profiles. The comparison of the genomic profiles (gains, losses, homozygous deletions, and amplifications) of the responders ($n = 8$) versus nonresponders ($n = 13$) demonstrated only slight genomic differences (Figure 1, additional Tables 3a and 3b), with the most consistent being an entire chromosome 20 gain that was significantly more frequent in the nonresponders (Fisher's exact test $P = 0.04$). *EGFR* amplification (9/13 in nonresponders versus 4/8 in responders) and *CDKN2A* locus homozygous deletion (8/13 in nonresponders versus 4/8 in responders) were also more frequently observed in nonresponders, but the difference was not significant.

Similarly, the comparison of the gene expression profiles of the responders ($n = 11$) and nonresponders ($n = 12$) demonstrated only few differences. Sixty probe sets (fifty-one in responders and nine in nonresponders) were differentially expressed, with a t-test P value < 0.05 and a fold change above 2, though with a very high (95%) false discovery rate (additional Table 4). Neither the expression of VEGF nor its receptors were associated with the response to the treatment. Using RT-PCR we studied the expression of 6 genes implicated in angiogenesis and overexpressed in responders (ENPP4, PRKCZ, and EPHA7) or nonresponders (NPTX2, SOCS2, and PDGFD) in an independent series of 7 responders and 11 nonresponders. EPHA7 [17] is implicated in endothelial

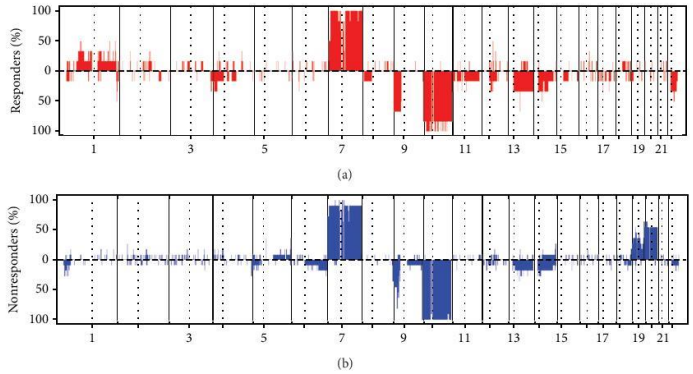

Figure 1: Genomic profiles of responders and nonresponders. Genomic profiles of responders and nonresponders to the bevacizumab/irinotecan regimen. For each chromosome, the telomere of the short arm is on the left and the telomere of the long arm is on the right. The y-axis corresponds to the frequency of gains and losses in each group of patients.

tubulogenesis, and PRKCZ has been implicated in VEGF transcriptional activation [18]. NPTX2 has been shown to be overexpressed in edematous versus nonedematous gliomas in the absence of increased VEGF expression [19]. PDGFD is a proangiogenic factor [20], and SOCS2 is involved in IGF1R signaling and is also a proangiogenic factor [21]. However, with the exception of SOCS2, we failed to confirm similar overexpression in the responders/nonresponders that was significant in this independent series (additional Table 5). Lastly, the pathway analysis performed on the 1000 genes that were most differentially expressed (500 genes upregulated in responders and 500 genes upregulated in nonresponders) demonstrated that these gene lists were significantly enriched in genes with different ontologies (additional Tables 6 and 7). The list of upregulated genes in the responders was significantly enriched in genes upregulated in the normal brain, whereas the list of upregulated genes in the nonresponders was enriched in genes that have been shown to be upregulated during hypoxia [22] and also in genes that might be targets of the transcription factor HIF1.

3.3. GBMs Molecular Subtypes Are Associated with Different Response Rates. As responders and nonresponders had very similar gene expression profiles, we hypothesized that there might be several subgroups of responders and nonresponders. To test this hypothesis, we performed an unsupervised hierarchical clustering analysis of the 23 GBMs included in the gene expression study. As shown in Figure 2, three main subgroups were identified. This clustering was robust and conserved across different gene lists and clustering methods. However, none of the three clusters was enriched in responders or nonresponders, and some responders and nonresponders could have very similar gene expression profiles. Therefore, to assess whether transcriptomic subgroups of GBMs previously identified in larger series of patients were associated with a specific pattern of response to the bevacizumab/irinotecan regimen, we classified our 23 samples according to the transcriptomic classifications of Gravendeel et al. [8] and of Verhaak et al. [7] and estimated the response rate in each subgroup. According to Gravendeel et al. [8], 14 GBMs were assigned to molecular subtype 18 (IGS-18), 3 to molecular subtype 22 (IGS-22), and 6 to molecular subtype 23 (IGS-23). According to Verhaak et al. [7], 9 GBMs were classified as classical, 6 as mesenchymal, 5 as proneural, and 3 as neural. The 9 classical GBMs were also assigned to IGS-18 which in addition consisted of 3 neural and 2 proneural GBMs. Interestingly, the GBMs assigned to IGS-18 were more frequently not responsive than the GBMs assigned to IGS-22 or IGS-23 (10/14 versus 2/9, Fisher's exact test P value = 0.03) and a similar trend was observed for classical versus nonclassical GBMs (7/9 versus 5/14, Fisher's exact test P value = 0.09). Conversely, IGS-18 GBMs had a shorter PFS after bevacizumab/irinotecan than IGS-22/23 GBMs (3.2 months versus 9.4 months, $P = 0.01$) and classical GBMs had a shorter PFS than nonclassical GBMs (2.2 months versus 8.3 months, $P = 0.003$) (Figure 3). Overall survival after bevacizumab/irinotecan also tended to be shorter in IGS-18 than in IGS-22/23 GBMs and in classical than nonclassical GBMs (7 months versus 18.9 months, $P = 0.06$ and 6.6 months versus 14.3 months, $P = 0.06$).

3.4. Neither EGFR Amplification Status Nor CDKN2A Locus Homozygous Deletion Status Is Associated with the Response Rate, the Progression-Free Survival, or the Overall Survival after Bevacizumab/Irinotecan Initiation. Because, in our series, *EGFR* amplification and *CDKN2A* homozygous deletion were more frequent in IGS-18 GBMs than in IGS-22/23 GBMs (11/14 versus 0/5, Fisher's exact test P value <0.01

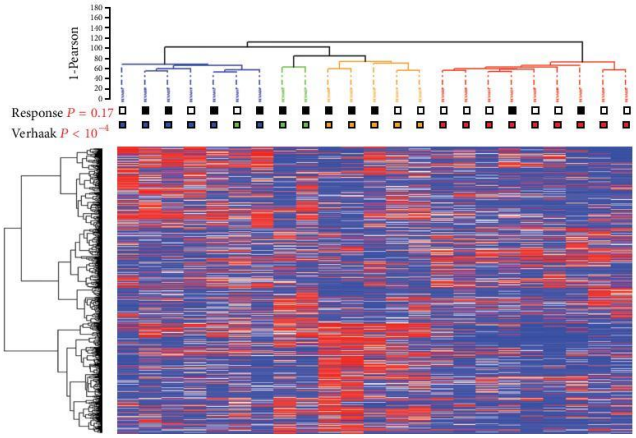

Figure 2: Unsupervised hierarchical clustering of the 23 GBMs. The heatmap was constructed using the 2365 probesets (quantile 0.95), with the greatest robust coefficient of variation between the tumor samples. The samples and genes were clustered using Ward's linkage and Pearson's correlation coefficient. For each probe set, the lowest and highest intensity values are displayed in blue and red, respectively. Response: black = responder, white = nonresponder. Verhaak = class according to Verhaak et al.'s classification [7]: neural = green, classical = red, mesenchymal = blue, and proneural = orange.

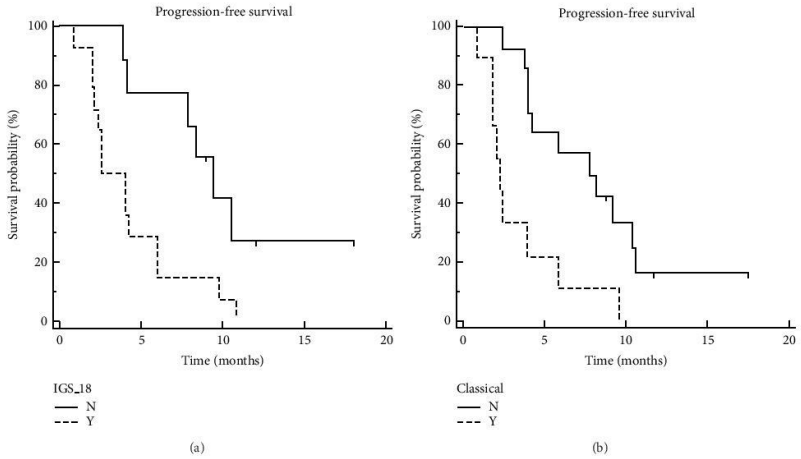

Figure 3: Progression-free survival according to Gravendeel et al. [8] and Verhaak et al. [7] molecular subtypes. GBMs assigned to IGS-18 (dashed line) had a shorter PFS after bevacizumab/irinotecan than those assigned to IGS-22 and IGS-23 (plain line) (3.2 months versus 9.4 months, $P = 0.01$). GBMs classified as classical (dashed line) had a shorter PFS than those classified as nonclassical (2.2 months versus 8.3 months, $P = 0.003$).

Table 2: Characteristics of the 33 patients from the Salpètrière database for whom the impact of EGFR amplification and CDKN2A locus homozygous deletion was assessed.

Characteristics of the 33 patients of the independent dataset	
Number of patients	33
Median age (years) at diagnosis (range)	59 (25–81)
Initial treatment (%)	RTCT (100%)
Median delay (months) between diagnosis and bev./iri. onset (range)	15 (3.5–60)
Recurrence number at bev./iri. onset	
First	31
Second/third	1/1
Response according to RANO	
Complete	4
Partial	11
Stable	7
Progression	7
Not assessable	3
EGFR amplification	13
CDKN2A homozygous deletion	12
Median PFS after bev./iri. onset (months)	5.5
Median OS after bev./iri. onset (months)	9.7
Median OS since diagnosis (months)	29

RTCT: temozolomide radiochemotherapy; bev./iri.: bevacizumab/irinotecan chemotherapy; KPS: Karnofsky performance status; PFS: progression-free survival; OS: overall survival; ns, nonsignificant.

and 10/14 versus 1/5 Fisher's exact test P value = 0.1, resp.) and also more frequent in classical than in nonclassical GBMs (9/9 versus 2/10, Fisher's exact test P value < 0.01 and 10/14 versus 1/5 Fisher's exact test P value = 0.02, resp.), we decided to evaluate the impact of these two genomic abnormalities in an independent series, in order to assess if these genomic abnormalities contribute to the lower response rate of IGS-18 and classical GBMs. This independent series comprised 33 GBMs from the Salpètrière database treated with the combination of bevacizumab/irinotecan at recurrence and for whom the *CDKN2A* locus homozygous deletion and *EGFR* amplification status were available in the initial tumor. The patients' characteristics are shown in Table 2. However, we did not observe any significant association between *EGFR* amplification and/or *CDKN2A* deletion status and the response rate to bevacizumab/irinotecan, the PFS, or the OS after bevacizumab/irinotecan initiation.

4. Discussion

Several studies have identified radiological, plasmatic, or clinical markers of the response to bevacizumab [23–25]. The objective of the present study was to identify biomarkers predictive of the response to bevacizumab/irinotecan given at GBM recurrence based on the transcriptomic and genomic characterization of the initial tumor. Given the dramatically different clinical and radiological response patterns to this treatment, we hypothesized that the comparison of a limited series of well-selected responders and nonresponders would be sufficient to identify robust and clinically useful biomarkers if such markers do exist. However, although the responders and nonresponders had dramatically different response patterns, we found that the two groups of patients had very similar genomic and gene expression profiles and we failed to identify any robust predictive biomarker. There are several possible hypotheses to explain this finding. First, the genomic and transcriptomic characteristics of the initial tumor might not be predictive of the response to bevacizumab/irinotecan given at recurrence because the molecular profile of recurrent GBMs might have significantly changed. However, Sathornsumetee et al. demonstrated that the expression of VEGF and CA9 (a marker of hypoxia) assessed by immunohistochemistry in the initial GBM was associated with the response and survival, respectively, in patients receiving bevacizumab and irinotecan at recurrence [26]. Interestingly, we similarly found that the profile of nonresponders was enriched in genes upregulated during hypoxia, though not influenced by VEGF expression. A second hypothesis to explain the absence of major difference between the profiles of responders and nonresponders is that the criteria used for defining the responders and nonresponders in the present study were not appropriate. These criteria were chosen to discover biomarkers that might be clinically meaningful and that might identify responders that achieve both a radiological response and prolonged PFS (>6 months) and to differentiate these patients from those who progress rapidly, regardless of the radiological response. Another hypothesis (and we suggest the most likely) is that the comparison of responders and nonresponders (regardless of the criteria) might not be the best strategy to identify biomarkers of the response. Indeed, this strategy assumes that all of the responders and nonresponders share common characteristics, which might be inappropriate if there are not one but several subgroups of responders/nonresponders with different mechanisms of response or resistance. In fact, both Verhaak et al. and Gravendeel et al. demonstrated that this is likely to be the case, as they identified transcriptomic subgroups of GBMs that seem to display different patterns of response according to the treatment used [7, 8]. Furthermore, we previously found that mesenchymal GBMs were more likely to respond to radiotherapy, whereas classical GBMs were more likely to respond to first-line alkylating chemotherapy [10]. In our series, though it was not designed to study this association, we observed an interesting association between GBMs molecular classes and the response rates. Using Gravendeel et al. classification, GBMs assigned to IGS-18 had a lower response rate to bevacizumab/irinotecan than the GBMs assigned to IGS-22 and IGS-23 [8]. Using Verhaak et al. classification a similar trend was observed for classical GBMs [7] when compared to nonclassical GBMs. This is in agreement with the fact that IGS-18 GBMs are generally assigned to the classical subtype (9 out of 14 cases in our series) [27]. As *EGFR* amplification and *CDKN2A* deletion status are two genomic hallmarks of IGS-18 and classical GBMs, we next studied the impact of these two genomic abnormalities in an independent series

of 33 patients. However, we did not identify any significant association with the response rate to bevacizumab/irinotecan suggesting that *EGFR* amplification and *CDKN2A* deletion are not responsible for the lower response rate of IGS-18 and classical GBMs to bevacizumab/irinotecan.

Taken together, our findings suggest that comparing the initial genomic and gene expression profiles of responders and nonresponders might not be an effective strategy to identify robust biomarkers of the response to bevacizumab/irinotecan given at recurrence. Yet, they also suggest that GBMs molecular subclasses are associated with the response to this treatment. This result however needs to be validated in a prospective and larger series of patients.

Conflict of Interests

The authors declare that they have no conflict of interests regarding the publication of this paper.

Authors' Contribution

Julien Laffaire and Anna Luisa Di Stefano contributed equally to this work.

Acknowledgments

The authors thank Fabien Petel for his help in managing the microarray database of the CIT3. They thank Pim French for his help in assigning their samples to IGS. This work is part of the Cartes d'Identité des Tumeurs (CIT) national program funded and developed by the Ligue Nationale Contre le Cancer and was also supported in part by the Institut National du Cancer (INCa; ref 2009-126). Di Stefano is supported by an investigator Fellowship from Collegio Ghislieri, Pavia, Italy. Pr Figarella-Branger is supported by a Grant INCa-DGOS-Inserm 6038. Frozen specimens from the AP-HM institution were stored and then provided by the AP-HM tumor bank (authorization no. AC-2013-1786). Frozen specimens from Lyon were stored in NeuroBioTec, Bron, France.

References

[1] H. S. Friedman, M. D. Prados, P. Y. Wen et al., "Bevacizumab alone and in combination with irinotecan in recurrent glioblastoma," *Journal of Clinical Oncology*, vol. 27, no. 28, pp. 4733–4740, 2009.

[2] T. N. Kreisl, L. Kim, K. Moore et al., "Phase II trial of single-agent bevacizumab followed by bevacizumab plus irinotecan at tumor progression in recurrent glioblastoma," *Journal of Clinical Oncology*, vol. 27, no. 5, pp. 740–745, 2009.

[3] J. J. Vredenburgh, A. Desjardins, J. E. Herndon II et al., "Bevacizumab plus irinotecan in recurrent glioblastoma multiforme," *Journal of Clinical Oncology*, vol. 25, no. 30, pp. 4722–4729, 2007.

[4] D. N. Louis, H. Ohgaki, O. D. Wiestler et al., "The 2007 WHO classification of tumours of the central nervous system," *Acta Neuropathologica*, vol. 114, pp. 97–109, 2007.

[5] R. Stupp, W. P. Mason, M. J. van den Bent et al., "Radiotherapy plus concomitant and adjuvant temozolomide for glioblastoma," *The New England Journal of Medicine*, vol. 352, no. 10, pp. 987–996, 2005.

[6] P. Y. Wen, D. R. Macdonald, D. A. Reardon et al., "Updated response assessment criteria for high-grade gliomas: response assessment in neuro-oncology working group," *Journal of Clinical Oncology*, vol. 28, no. 11, pp. 1963–1972, 2010.

[7] R. G. W. Verhaak, K. A. Hoadley, E. Purdom et al., "Integrated genomic analysis identifies clinically relevant subtypes of glioblastoma characterized by abnormalities in PDGFRA, IDH1, EGFR, and NF1," *Cancer Cell*, vol. 17, no. 1, pp. 98–110, 2010.

[8] L. A. M. Gravendeel, M. C. M. Kouwenhoven, O. Gevaert et al., "Intrinsic gene expression profiles of gliomas are a better predictor of survival than histology," *Cancer Research*, vol. 69, no. 23, pp. 9065–9072, 2009.

[9] R. A. Irizarry, B. M. Bolstad, F. Collin, L. M. Cope, B. Hobbs, and T. P. Speed, "Summaries of Affymetrix GeneChip probe level data," *Nucleic Acids Research*, vol. 31, no. 4, article e15, 2003.

[10] F. Ducray, A. de Reyniès, O. Chinot et al., "An ANOCEF genomic and transcriptomic microarray study of the response to radiotherapy or to alkylating first-line chemotherapy in glioblastoma patients," *Molecular Cancer*, vol. 9, article 234, 2010.

[11] A. V. Kapp and R. Tibshirani, "Are clusters found in one dataset present in another dataset?" *Biostatistics*, vol. 8, no. 1, pp. 9–31, 2007.

[12] D. A. Peiffer, J. M. Le, F. J. Steemers et al., "High-resolution genomic profiling of chromosomal aberrations using Infinium whole-genome genotyping," *Genome Research*, vol. 16, no. 9, pp. 1136–1148, 2006.

[13] J. Staaf, J. Vallon-Christersson, D. Lindgren et al., "Normalization of Illumina Infinium whole-genome SNP data improves copy number estimates and allelic intensity ratios," *BMC Bioinformatics*, vol. 9, article 409, 2008.

[14] E. S. Venkatraman and A. B. Olshen, "A faster circular binary segmentation algorithm for the analysis of array CGH data," *Bioinformatics*, vol. 23, no. 6, pp. 657–663, 2007.

[15] T. Popova, E. Manié, D. Stoppa-Lyonnet, G. Rigaill, E. Barillot, and M. H. Stern, "Genome Alteration Print (GAP): a tool to visualize and mine complex cancer genomic profiles obtained by SNP arrays," *Genome Biology*, vol. 10, no. 11, article R128, 2009.

[16] A. Idbaih, Y. Marie, C. Lucchesi et al., "BAC array CGH distinguishes mutually exclusive alterations that define clinicogenetic subtypes of gliomas," *International Journal of Cancer*, vol. 122, no. 8, pp. 1778–1786, 2008.

[17] J. E. Leslie-Barbick, C. Shen, C. Chen, and J. L. West, "Micron-scale spatially patterned, covalently immobilized vascular endothelial growth factor on hydrogels accelerates endothelial tubulogenesis and increases cellular angiogenic responses," *Tissue Engineering A*, vol. 17, no. 1-2, pp. 221–229, 2011.

[18] S. Pal, K. Datta, R. Khosravi-Far, and D. Mukhopadhyay, "Role of protein kinase Czeta in Ras-mediated transcriptional activation of vascular permeability factor/vascular endothelial growth factor expression," *The Journal of Biological Chemistry*, vol. 276, no. 4, pp. 2395–2403, 2001.

[19] M. R. J. Carlson, W. B. Pope, S. Horvath et al., "Relationship between survival and edema in malignant gliomas: role of vascular endothelial growth factor and neuronal pentraxin 2," *Clinical Cancer Research*, vol. 13, no. 9, pp. 2592–2598, 2007.

[20] A. Kumar, X. Hou, C. Lee et al., "Platelet-derived growth factor-DD targeting arrests pathological angiogenesis by modulating glycogen synthase kinase-3β phosphorylation," *The Journal of Biological Chemistry*, vol. 285, no. 20, pp. 15500–15510, 2010.

[21] H. Li, Y. Adachi, H. Yamamoto et al., "Insulin-like growth factor-I receptor blockade reduces tumor angiogenesis and enhances the effects of bevacizumab for a human gastric cancer cell line, MKN45," *Cancer*, vol. 117, no. 14, pp. 3135–3147, 2011.

[22] S. M. Mense, A. Sengupta, M. Zhou et al., "Gene expression profiling reveals the profound upregulation of hypoxia-responsive genes in primary human astrocytes," *Physiological Genomics*, vol. 25, no. 3, pp. 435–449, 2006.

[23] G. Lombardi, F. Zustovich, P. Farina et al., "Hypertension as a biomarker in patients with recurrent glioblastoima treated with antiangiogenic drigs: a single-center experience and a critical review of the literature," *Anticancer Drugs*, vol. 24, pp. 90–97, 2013.

[24] E. Tabouret, F. Boudouresque, M. Barrie et al., "Association of matrix metalloproteinase 2 plasma level with response and survival in patients treated with bevacizumab for recurrent high-grade glioma," *Neuro-Oncology*, vol. 16, pp. 392–399, 2014.

[25] B. M. Ellingson, S. Sahebjam, H. J. Kim et al., "Pretreatment ADChistogram analysis is a predictive biomarker for bevacizumab treatment but not chemotherapy in recurrent glioblastoma," *American Journal of Neuroradiology*, 2013.

[26] S. Sathornsumetee, Y. Cao, J. E. Marcello et al., "Tumor angiogenic and hypoxic profiles predict radiographic response and survival in malignant astrocytoma patients treated with bevacizumab and irinotecan," *Journal of Clinical Oncology*, vol. 26, no. 2, pp. 271–278, 2008.

[27] L. Erdem-Eraslan, L. A. Gravendeel, J. de Rooi et al., "Intrinsic molecular subtypes of glioma are prognostic and predict benefit from adjuvant procarbazine, lomustine, and vincristine chemotherapy in combination with other prognostic factors in anaplastic oligodendroglial brain tumors: a report from EORTC study 26951," *Journal of Clinical Oncology*, vol. 31, pp. 328–336, 2013.

Neuro-oncology

SHORT REPORT

Herpes simplex encephalitis in glioma patients: a challenging diagnosis

Giulia Berzero,[1,2] Anna Luisa Di Stefano,[1,3] Caroline Dehais,[3] Marc Sanson,[3] Paola Gaviani,[4] Antonio Silvani,[4] Andrea Salmaggi,[4,5] Paolo Vitali,[1] Luca Diamanti,[1,2] Fausto Baldanti,[6] Lisa Maria Farina,[1] Mauro Ceroni,[1,7] Enrico Marchioni[1]

► Additional material is published online only. To view please visit the journal online (http://dx.doi.org/10.1136/jnnp-2013-307198).

For numbered affiliations see end of article.

Correspondence to
Dr E Marchioni, C. Mondino Foundation, Via Mondino 2, Pavia 27100, Italy; enrico.marchioni@mondino.it

Received 7 November 2013
Revised 8 April 2014
Accepted 4 May 2014
Published Online First 29 May 2014

ABSTRACT

Objectives In recent years, herpes simplex encephalitis (HSE) has been reported with increasing frequency in settings of immunosuppression, such as acquired immunodeficiency, transplantation and cancer. As observed, in immunocompromised individuals HSE presents peculiar clinical and paraclinical features, and poorer prognosis.

Methods Here we describe a retrospective series of seven cases of HSE in patients with high-grade glioma (HGG), collected among three institutions in a 5-year period (during this time, a total of 1750 patients with HGG were treated).

Results Diagnosis of the condition was particularly challenging due to the confounding clinical presentation and the atypical biological findings. As a result, antiviral treatment was started with a sharp delay compared with immunocompetent hosts. Prognosis was poor, with high short-term mortality and severe residual disability in survivors.

Conclusions The substantial incidence of HSE observed in our centres together with the difficulty in diagnosing the condition suggest that the incidence of this complication may be highly underestimated. The aim of our report is to strengthen the observation of HSE in patients with HGG and outline the key elements that may allow its diagnosis.

INTRODUCTION

Herpes simplex encephalitis (HSE) is the most common form of sporadic encephalitis in the general population, with an incidence of 2–4 cases per million people annually.[1] Although most commonly seen in immunocompetent hosts, in recent years several cases of HSE in settings of immunosuppression—such as acquired immunodeficiency, transplantation and cancer—have now been reported.[2 3] In immunocompromised patients, HSE may present with atypical clinical and biological features,[2 4] making the diagnosis challenging even for expert neurologists. In patients with brain tumours, the diagnosis of HSE is made even more difficult by the presence of neurological signs and symptoms attributable to the tumour itself.

Single cases of HSE in high-grade glioma (HGG) patients are scattered through literature, but the actual incidence of this complication is unknown. Rarity and the difficulty in diagnosing the condition might cause to underestimate the occurrence of HSE in patients with HGG.

We report seven cases of HSE in patients with HGG, collected among three institutions in a 5-year period, and review the existing literature. The aim of our report is to strengthen the observation of HSE in high-grade glioma patients, describe the peculiar clinical and biological profile of HSE in this setting and outline the key elements that may allow its diagnosis.

CASE SERIES

Here we describe a series of seven patients with HGG who developed HSE during cancer treatment, collected among three institutions (C. Mondino National Institute of Neurology Foundation, Pavia, Italy; C. Besta Neurological Institute, Milan, Italy; AP-HP, Groupe Hospitalier Pitié-Salpêtrière, Paris, France). Every centre conducted an Internal Review Board-approved retrospective study using an institutional database of all patients receiving a diagnosis of 'herpes simplex encephalitis' and 'glioma' from the period between 1 January 2008 and 30 September 2013. During this time, a total of 1750 patients with HGG were treated in the three institutions.

Patients developed HSE during different steps of HGG evolution: one patient 2 weeks after surgery (patient 7), four patients during the Stupp protocol (patients 1, 2, 5 and 6) and the remaining two (patients 3 and 4) 4 and 13 months after its conclusion while receiving a first-line or second-line chemotherapy.

Clinical and paraclinical findings in our seven patients are detailed in table 1.

All the patients were receiving daily steroids, and four of the seven patients showed a grade II or III lymphopenia (CTCAE V.3.0). The main clinical features of HSE included fever (7/7), stupor/coma (7/7) and partial seizures (6/7). In two patients (patients 2 and 4), an encephalitis was suspected due to the clinical and electroencephalographic appearance of a new epileptic focus contralateral to the tumour site, and in three others (patients 1, 3 and 7) due to persistent consciousness alteration. In all cases, systemic infections and tumour progression were excluded on the basis of chest X-ray, urine and blood testing, and brain CT scan. Cerebrospinal fluid (CSF) analysis revealed slight blood–brain barrier damage in all seven patients, but lymphomonocytic pleocytosis in only three. The diagnosis of HSE was confirmed by CSF analysis and PCR for herpes simplex virus 1 (HSV-1),

To cite: Berzero G, Di Stefano AL, Dehais C, et al. J Neurol Neurosurg Psychiatry 2015;86:374–377.

Table 1 Clinical and paraclinical findings in our seven patients

		Tumour characteristics											CSF analysis		Delay in antiviral	
Patient	Age/ gender	Type	Location	Side (R/L)	Delay since Stupp	Current CHT	Steroids	Lymphocytes/ mm^3	Clinical features	Seizures	EEG	MRI alterations	WBC/ mm^3	Proteins mg/dL	treatment (days)	Evolution
1	72/F	GBM	P–O	L	Ongoing, 4th week		Dexamethasone 8 mg/day	525	Fever, coma (GCS 6)	Partial	Left subcontinuous slow activity with sharp waves	Left temporomesial and cerebellum	<2	79	7	Death for HSE
2	39/M	Gr. III Astro.	F–T	L	Ongoing, 3rd week		Dexamethasone 8 mg /day	1790	Fever, stupor, aphasia, behavioural alterations	Masticatory seizures, generalised status epilepticus	Right epileptic abnormalities	Bilateral temporomesial	>50	203	8	Survived with residual cognitive impairment and behavioural changes
3	59/F	GBM	Cerebellar vermis		Completed 13 months before	Irinotecan/ bevacizumab (2nd line)	Prednisone 40 mg/day	550	Fever, coma (GCS 5)	No	Bilateral diffuse slow abnormalities with pseudo-periodic pattern	Bilateral frontotemporal	3	141	5	Death for HSE
4	58/F	GBM	T	L	Completed 4 months before	Temozolomide (1st line)	Dosage not available	300	Fever, coma (GCS 8)	Partial	Right epileptic abnormalities	Right temporoinsular	13	109	4	Survived with residual cognitive impairment
5	63/M	GBM	T	R	Ongoing, 4th week		Dosage not available	–	Fever, coma (GCS 6)	Partial status epilepticus, generalised seizures	Left periodic emispheric slowing, right epileptic abnormalities	Bilateral temporoinsular	2	166	3	Death for HSE
6	53/M	Gr. III Astro.	F–I	L	Ongoing, 4th week		Dexamethasone 16 mg/day	500	Fever, stupor	Partial	Bilateral pseudo-periodic frontotemporal slow abnormalities	Right temporomesial and insular	<2	64	3	Survived with residual cognitive impairment
7	63/M	GBM	T	L	Stupp not performed	None	Dexamethasone 4 mg/day	–	Fever, dysphasia, coma (GCS 3)	Partial seizures, generalised status epilepticus	Diffuse epileptic activity	Bilateral frontotemporoinsular	18	153	6	Death for HSE

Astro, astrocytoma; CHT, chemotherapy; CSF, cerebrospinal fluid; F, frontal; GCS, Glasgow Coma Scale; GBM, glioblastoma multiforme; Gr, grade; HSE, herpes simplex encephalitis; I, insular; O, occipital; P, parietal; T, temporal; WBC, white blood cells; –, not available.

positive in all the patients with high CSF/serum replication ratio. MRI showed monolateral or bilateral typical HSE alterations in all cases. Apparent diffusion coefficient (ADC) maps were positive, indicating restricted diffusion in temporomesial/basal areas, in all four patients in whom diffusion weighted imaging (DWI) was acquired (figure 1). Despite treatment (intravenous acyclovir, 10 mg/kg every 8 h/daily), four patients died of the infection, while the three who survived were left with severe residual cognitive impairment and disability.

DISCUSSION

This retrospective study represents the largest series of HSE in high-grade glioma patients and describes the peculiar clinical and paraclinical profile of HSE in this population.

HSE clinical presentation was dominated by the presence of mild to moderate hyperthermia, stupor and recurrent seizures up to status epilepticus. Diffusion-weighted MRI was constantly altered, and resulted in an early and helpful tool to direct the following diagnostic work-up. CSF profile was misleading due to absence or poor evidence of CNS inflammatory markers. This finding may be possibly addressed to an anergic immune compartmental cellular response and has been reported in patients receiving brain irradiation and prolonged steroids.[4] All seven cases were eventually confirmed by PCR testing on CSF, emphasising the importance to perform this test even in the absence of pleocytosis. In addition to the peculiarities attributable to the background of immunosuppression, in patients with HGG the diagnosis of HSE is made even more difficult by the broad spectrum of alternative causes that can produce a similar clinical phenotype: tumour progression, early-onset radiation-induced encephalopathy and systemic infectious or metabolic diseases. Antiviral treatment was started as soon as diagnosis HSE was evoked. Still, the diagnostic delay was remarkable in our series: the median time from admission to starting antiviral treatment was 5 days in our series compared with the average of 7 h reported in immunocompetent hosts.[5] The delay in diagnosis may have possibly contributed to the poor prognosis we observed. On the basis of our experience, we report three key elements that, occurring alone or in combination, should prompt early suspicion of HSE in glioma patients: hyperthermia, acute consciousness alteration rapidly progressing to coma and the appearance of new epileptic foci not corresponding to the site of the primary tumour. In these scenarios, diffusion-weighted MRI and PCR for HSV on CSF, followed by empirical treatment with acyclovir, should be promptly undertaken.

In recent years, the literature is enriching with reports of HSE in immunocompromised patients,[2] including patients with systemic neoplasms[3] and primary CNS tumours.[3 4] We conducted a review of the literature and found 14 previously reported cases of HSE in patients with gliomas,[6–16] with details reported in online supplementary table S2. Consistently with that found in our series, HSE occurred during different steps of cancer history (in five patients perioperatively,[7–9] in six patients during

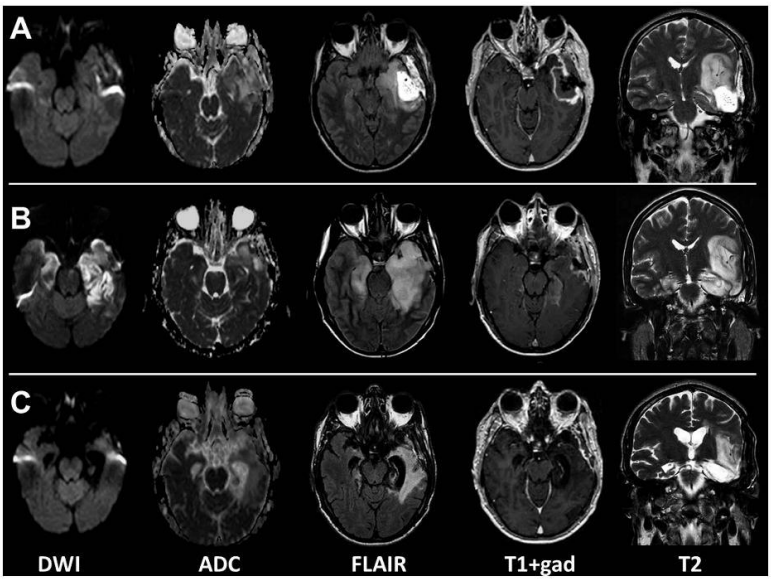

Figure 1 Patient 2 MRI pattern. (A) 22 days after surgical resection in the lateral left temporal lobe, with residual anaplastic astrocytoma in the left insula. (B) During acute herpes simplex encephalitis (HSE), involving bilateral temporomesial structures, more in the left hemisphere, where diffusion restriction and contrast enhancement is also more evident. (C) One year after the acute HSE: significant cerebral atrophy especially in bilateral temporomesial structures, where subtle abnormalities remain but no contrast enhancement. The residual anaplastic astrocytoma is stable.

radiotherapy[10–14] and in the last three patients within 3 months of its completion[6 15 16]), and evolution was characterised by high mortality or severe morbidity despite antiviral treatment.

Regarding aetiology, patients with HGG are surely exposed to a number of conditions predisposing to infections, such as chronic steroid treatment, chemotherapy-induced myelosuppression and the tumour itself. Steroids are known to have profound effects on the distribution and function of lymphocytes. The related risk of infections is proportionate to the dose and duration of steroid administration and patients with HGG usually require steroid treatment for the entire disease duration, and particularly during combined radiochemotherapy. The Stupp protocol[17] is since 2005 the standard of care in patients with HGG. In our experience, temozolomide provokes neutropenia during the concomitant and adjuvant phase, and a peculiar prolonged lymphopenia during the concomitant phase, when associated to chronic steroids. In the case of HSE, lymphopenia is most likely the defect to promote the infection and was observed in four of the seven patients in our series. Additionally, the impairment of cell-mediated immunity induced by steroids and chemotherapy is worsened by the local and systemic immunosuppressive effect of HGG-induced cytokines.[18] Irradiation is known to have a great impact on neurons and immune cells, and all patients with HGG receive radiotherapy as part of the Stupp protocol.[17] Considering HSV elective tropism towards temporomesial structures, it is remarkable that half of the patients reported in literature and in our series suffered from a temporal neoplasm, thus suggesting that direct local irradiation may play a role in promoting viral reactivation. This may also be part of the reason why, of all major viral infections, HSE is the most frequently reported in patients with brain cancer.

On the basis of our observations, we would like to raise the attention of neurologists and oncologists on HSE as an underestimated, rare but non-negligible complication in patients with HGG. Stupp protocol is already recognised to be a time of susceptibility for opportunistic infections, and prophylactic antimicrobial treatment is recommended by a number of oncological guidelines[19] to prevent *Pneumocystis carinii* pneumonia. Conversely, invasive viral infections are considered a rare event in patients with solid tumours, and therefore antiviral prophylaxis is not recommended. Still, compared with other patients with cancer, HGG are contemporary exposed not only to a severe cell-immunity impairment but also to the local insult of radiotherapy. Antiviral prophylaxis with acyclovir has proven effective and is already recommended in a number of haematological malignancies during the period of leucopenia to prevent herpesviruses reactivation.[19] Acyclovir is usually well tolerated, and major side effects are very rare. On these grounds, considering the poor prognosis HSE has shown in patients with HGG, a benefit/risk discussion for the introduction of acyclovir prophylaxis may be pertinent in the neuro-oncology community.

Author affiliations
[1]C. Mondino National Institute of Neurology Foundation, IRCCS, Pavia, Italy
[2]Neuroscience Consortium, University of Pavia, Monza Policlinico and Pavia Mondino, Pavia, Italy
[3]AP-HP, Groupe Hospitalier Pitié-Salpêtrière, Service de Neurologie 2, Paris, France
[4]Neuro-oncology Unit, C. Besta Neurological Institute, Milan, Italy
[5]SC Neurologia, Ospedale A. Manzoni, Lecco, Italy
[6]Molecular Virology Unit, IRCCS Policlinico San Matteo Foundation, Pavia, Italy
[7]Department of Neuroscience, University of Pavia, Pavia, Italy

Acknowledgements The authors would like to thank Georgia Mussati for her able assistance in radiological data collection and commentary.

Contributors All authors made substantial contributions to the conception or design of the work, or the acquisition, analysis or interpretation of data. All authors contributed to drafting the work or revising it critically for important intellectual content. All authors approve the final version published. All authors are accountable for the accuracy and integrity of any part of the work. Specific coauthors responsibilities include the following: patient recruitment: EM, GB, CD, MS, PG, LD, ALDS, MC, AS, AS; neuroradiology: PV, LMF; virology: FB; manuscript drafting: GB, EM; critical revision of the manuscript: MS, ALDS, EM, GB, MC, AS.

Funding This study had no industry funding. This work was supported by Italian Health Ministry grant 'Ricerca Corrente 2012'. ALDS is supported by an investigator fellowship from the Collegio Ghislieri, Pavia, Italy.

Conflict of interest None.

Patient consent Obtained.

Ethics approval Approved by the Institutional Ethics Committee.

Provenance and peer review Not commissioned; externally peer reviewed.

REFERENCES

1 Whitley RJ. Herpes simplex virus. In: Scheld WM, Whitley RJ, Marra CM, eds. *Infections of the central nervous system*. 3rd edn. Philadelphia, PA: Lippincott Williams & Wilkins, 2004:123–44.
2 Tan IL, McArthur JC, Venkatesan A, *et al*. Atypical manifestations and poor outcome of herpes simplex encephalitis in the immunocompromised. *Neurology* 2012;79:2125–32.
3 Graber JJ, Rosenblum MK, DeAngelis LM. Herpes simplex encephalitis in patients with cancer. *J Neurooncol* 2011;105:415–21.
4 Jakob NJ, Lenhard T, Schnitzler P, *et al*. Herpes simplex virus encephalitis despite normal cell count in the cerebrospinal fluid. *Crit Care Med* 2012;40:1304–8.
5 Michael BD, Sidhu M, Stoeter D, *et al*. North West Neurological Infections Network. Acute central nervous system infections in adults—a retrospective cohort study in the NHS North West region. *QJM* 2010;103:749–58.
6 Schiff D, Rosenblum MK. Herpes simplex encephalitis (HSE) and the immunocompromised: a clinical and autopsy study of HSE in the settings of cancer and human immunodeficiency virus-type 1 infection. *Hum Pathol* 1998;29:215–22.
7 Benjamin SP, McCormack LJ, Chatty ME, *et al*. Coexistent herpes simplex encephalitis and malignant astrocytoma. A clinicopathologic study of three cases. *Cleve Clin Q* 1972;39:135–43.
8 Ochsner F. Contamination of a glioma by the herpes virus. *Schweiz Arch Neurol Neurochir Psychiatr* 1981;129:19–30.
9 Sheleg SV, Nedzved MK, Nedzved AM, *et al*. Contamination of glioblastoma multiforme with type 1 herpes simplex virus. Case illustration. *J Neurosurg* 2001;95:721.
10 Riel-Romero RM, Baumann RJ. Herpes simplex encephalitis and radiotherapy. *Pediatr Neurol* 2003;29:69–71.
11 Kocher M, Kunze S, Eich HT, *et al*. Efficacy and toxicity of postoperative temozolomide radiochemotherapy in malignant glioma. *Strahlenther Onkol* 2005;181:157–63.
12 Spacca B, Mallucci C, Riordan A, *et al*. HSV encephalitis in a child with brain stem glioma: a rare complication of therapy. Case report and review of the neurosurgical literature. *Childs Nerv Syst* 2007;23:1347–50.
13 Okada M, Miyake K, Shinomiya A, *et al*. Relapse of herpes encephalitis induced by temozolomide-based chemoradiation in a patient with malignant glioma. *J Neurosurg* 2013;118:258–63.
14 Krieger D, Wendtland B, Brückmann H. Herpes simplex encephalitis following irradiation of a brain stem glioma. *Nervenarzt* 1988;59:50–4.
15 Tohyama Y, Sako K, Daita G, *et al*. Dissociation of 99mTc- ECD and 99mTc-HMPAO distributions in herpes simplex encephalitis. *Childs Nerv Syst* 1997;13:352–5.
16 Lins H, Kanakis D, Heinrichs T, *et al*. Sudden progression of a glioblastoma in partial remission? *Clin Neurol Neurosurg* 2004;106:335–6.
17 Stupp R, Mason WP, van den Bent MJ, *et al*. Radiotherapy plus concomitant and adjuvant temozolomide for glioblastoma. *N Engl J Med* 2005;352:987–96.
18 Dix AR, Brooks WH, Roszman TL, *et al*. Immune defects observed in patients with primary malignant brain tumors. *J Neuroimmunol* 1999;100:216–32.
19 NCCN Clinical Practice Guidelines in Oncology, Prevention and treatment of cancer-related infections, v.2.2011.

JNNP

Herpes simplex encephalitis in glioma patients: a challenging diagnosis

Giulia Berzero, Anna Luisa Di Stefano, Caroline Dehais, Marc Sanson, Paola Gaviani, Antonio Silvani, Andrea Salmaggi, Paolo Vitali, Luca Diamanti, Fausto Baldanti, Lisa Maria Farina, Mauro Ceroni and Enrico Marchioni

J Neurol Neurosurg Psychiatry 2015 86: 374-377 originally published online May 29, 2014
doi: 10.1136/jnnp-2013-307198

Cancer Treatment Reviews 40 (2014) 951–959

Contents lists available at ScienceDirect

Cancer Treatment Reviews

journal homepage: www.elsevierhealth.com/journals/ctrv

Anti-Tumour Treatment

Systemic treatments for brain metastases from breast cancer, non-small cell lung cancer, melanoma and renal cell carcinoma: An overview of the literature

Giuseppe Lombardi [a,1,*], Anna Luisa Di Stefano [b,c,1], Patrizia Farina [a,1], Vittorina Zagonel [a,1], Emeline Tabouret [d,e,1]

[a] Medical Oncology 1 Unit, Veneto Institute of Oncology IOV – IRCCS, Padua, Italy
[b] AP-HP, Groupe Hospitalier Pitié-Salpêtrière, Service de Neurologie 2, Paris 75013, France
[c] National Neurological Institute C. Mondino, University of Pavia, Italy
[d] APHM, Timone Hospital, Neuro-Oncology, Marseille, France
[e] Aix-Marseille University, CRO2, UMR911, Marseille, France

ARTICLE INFO

Article history:
Received 18 April 2014
Received in revised form 16 May 2014
Accepted 19 May 2014

Keywords:
Brain metastases
Melanoma
Lung cancer
Breast cancer
Renal cell carcinoma

ABSTRACT

The frequency of metastatic brain tumors has increased over recent years; the primary tumors most involved are breast cancer, lung cancer, melanoma and renal cell carcinoma. While radiation therapy and surgery remain the mainstay treatment in selected patients, new molecular drugs have been developed for brain metastases. Studies so far report interesting results.

This review focuses on systemic cytotoxic drugs and, in particular, on new targeted therapies and their clinically relevant activities in brain metastases from solid tumors in adults.

Introduction

Metastatic brain tumors are the most common intracranial neoplasms in adults and are a significant cause of deleterious effects on many critical neurological functions. Moreover, morbidity and mortality rates are higher for patients who develop brain metastasis (BM); over the last few years, the frequency of BM has increased due to longer survival of patients through more effective systemic treatment and earlier BM detection by improved neuro-imaging.

Estimates of BM incidence vary from 20% to 50% [1]; analyses of patient data from the Metropolitan Detroit Cancer Surveillance System showed a total incidence proportion of BM of 9.6% [1]; the incidence proportion of BM was highest for lung cancer (19.9%), followed by 6.9% for melanoma, 6.5% for renal cancer, 5.1% for breast cancer. However, as described in various studies, the incidence of BM may be higher than observed, due to asymptomatic BM [2].

Radiation therapy and surgery remain the cornerstone of treatment in selected patients, while cytotoxic drugs have a limited impact. On the other hand, in recent years, advances in the understanding of the biology of BM have led to the development of new targeted therapies and interesting results have been obtained so far.

In this review, we analyzed systemic treatments, both cytotoxic and, in particular, new molecular drugs for BM from solid tumors in adults, such as breast cancer, lung cancer, renal cancer and melanoma.

Breast cancer

Recent improvements in systemic therapy have increased the overall survival of breast cancer (BC) patients, including metastatic patients. In the context of controlled systemic disease, the prevalence of BM from BC is increasing. BC is the second leading cause of BM after lung cancer and accounts for 17–20% of all cases. BM treatment options currently include whole-brain radiotherapy

* Corresponding author. Address: Medical Oncology 1, Veneto Institute of Oncology – IRCSS, via Gattamelata, 64, 35128 Padua, Italy. Tel.: +39 3290048377; fax: +39 0498215904.
E-mail address: giuseppe.lombardi@ioveneto.it (G. Lombardi).
[1] All authors contributed equally to the writing of the paper.

http://dx.doi.org/10.1016/j.ctrv.2014.05.007
0305-7372/

Table 1
Clinical studies of systemic treatments for brain metastases in breast cancer.

Author	PTS	Regimen	RR (%)	PFS (ms)	OS (ms)
Cytotoxic drugs					
Freedman et al. [7]	15	Sagopilone	13.3	1.4	5.3
Siena et al. [5]	51	Temozolomide	4	1.9	NR
Cassier et al. [3]	25	Cisplatin + vinorelbine + RT	76	3.7	6.5
Rivera et al. [6]	24	Capecitabine + temozolomide	18	12 wks	NA
Franciosi et al. [4]	56	Cisplatin + etoposide	38	4	8
Targeted therapies					
Brufsky et al. [8]	258	Trastuzumab vs. no use	NA	NA	17.5 vs. 3.9
Lin et al. [11]	39	Lapatinib	2.6	3	NR
	242	Lapatinib	6	2.4	6.4
Lin et al. [12]	(50)	(Lapatinib + capecitabine)	(20)	(3.6)	
Lin et al. [13]	22	Lapatinib + capecitabine vs. lapatinib + topotecan	38 vs. 0	NA	NA
Bachelot et al. [14]	44	Lapatinib + capecitabine	66	5.5	17
Lin et al. [15]	35	Lapatinib + RT	79	4.8	19

PTS: patients; RR: response rate; PFS: progression free survival; OS: overall survival; RT: radiation therapy; NR: not reached; NA: not available.

(WBRT), surgery, stereotactic radiosurgery (SRS), chemotherapy and a combination of these methods (see Table 1).

Cytotoxic drugs

In the setting of newly or recurrent BM from BC, few prospective trials have evaluated the benefit of cytotoxic agent administration. At the onset of BM, in combination with radiotherapy, the use of cisplatin and vinorelbine was associated with 76% of objective brain response rate (RR) for 25 pts. However, median progression free survival (PFS) remained modest (3.7 months) while median overall survival (OS) was 6.5 months, and half of patients presented with non-hematological grade 3–4 toxicities [3]. In another phase II trial [4], combination of cisplatin and etoposide with radiation therapy (RT) for 56 patients with BM was associated with 13% of complete response and 14 partial responses (25%); however, mPFS and mOS remained modest (4 and 8 months, respectively). In these first-line studies, despite encouraging response rates, effect of combination of RT and cytotoxic agents remained modest.

In another phase II study [5], the authors evaluated temozolomide activity with alternating weekly, dose-dense temozolomide, in pretreated patients with BM, stratified by primary tumor type. In this study, 51 BC patients presented with a mPFS of 1.9 months while mOS was not reached. The disease control rate (responses + stable disease) was 20% while ORR was 4%.

In a phase I trial [6], 24 newly or recurrent patients with BM from BC, were treated with temozolomide plus capecitabine. This regimen was associated with 18% of ORR, an mPFS of 12 weeks and was correlated to improvement or stabilization of neurocognitive function and quality of life.

Sagopilone, an epothilone B analogue that crosses the blood–brain barrier, was evaluated in a phase II trial [7] for 15 patients with recurrent BM from BC. ORR was 13.3%, mPFS and mOS were 1.4 and 5.3 months, respectively; these modest results led to premature stopping of enrollment.

Finally, no prospective trial has evaluated the potential benefit of hormonal therapy for patients with BM from BC.

Human epidermal growth factor receptor (HER) targeted therapies

HER2 is overexpressed in approximately 20% of breast cancer tissue and it represents one of the main molecular targets in the development of new therapies.). Trastuzumab, a monoclonal antibody targeting HER2, was approved for metastatic breast cancer in 1998. Lapatinib is a dual tyrosine kinase inhibitor of both HER1 and HER2, approved by the FDA in 2007. Finally, pertuzumab, a monoclonal antibody that blocks dimerisation of HER2 with HER1, 3 and 4, was approved in 2012.

Overexpression of HER2 is an independent factor for development of BM, which may likely be due to a more aggressive subtype of HER2-positive breast cancer, or to the fact that these patients treated with HER2-targeted therapies live longer. Moreover, these targeted drugs have limited potential to cross the blood–brain-barrier. Hence, in the setting of well-controlled extracranial disease and BM, the best treatment is still unknown and several clinical trials to determine the optimal treatment of BM are ongoing.

In the treatment of BM, several studies have suggested activity of trastuzumab for treatment of BM from BC. However, all studies, except one [8], were retrospective and even in the prospective study, data concerning BM were retrospectively collected. In this study [8], use of trastuzumab was associated with better OS (17.5 vs. 3.8 months). Despite the absence of a prospective and randomized trial, use of trastuzumab at the time of BM could represent an interesting option. Trastuzumab was used in intrathecal treatment in several case reports in association with intrathecal methotrexate or cytarabine. This strategy was associated with stabilization of multiple BM in one case [9,10]. However, the absence of a larger cohort or prospective trial did not allow any conclusion about the potential benefit of the use of intrathecal trastuzumab.

Several studies have evaluated the activity of lapatinib for BM in BC and 5 of these were prospective trials. Lin et al. in 2008 [11] first reported on lapatinib for recurrent BM from BC. In this single-arm phase II study, 39 patients were enrolled. By "*Response Evaluation Criteria In Solid Tumors*" (RECIST) assessment, the ORR was only 2.6%; but by volumetric analysis, 10 pts (26%) achieved at least 10% of volumetric reduction. In this study, mPFS was 3.0 months [11]. In 2009, Lin et al. published a second phase II trial evaluating lapatinib for patients with BC and BM progressing after RT [12]. In this study, lapatinib refractory-patients were treated with lapatinib plus capecitabine. Overall response or volumetric reduction of lesions was observed in 6% and 21% of patients, respectively. In patients with the extension of lapatinib + capecitabine, ORR and volumetric reduction were seen in 20% and 40% of patients, respectively, leading to the preferential use of this association. For patients with lapatinib alone or lapatinib plus capecitabine, mPFS were 2.4 and 3.6 months, respectively, while mOS for the entire cohort was 6.4 months [12].

In a recent randomized phase II trial, the combination of lapatinib and capecitabine versus lapatinib plus topotecan was analyzed [13]. However, this trial was prematurely stopped due to excess toxicity and lack of efficacy in the lapatinib plus topotecan arm (ORR = 0%). In the LANDSCAPE trial [14], the combination of

lapatinib plus capecitabine for the treatment of untreated brain metastases from HER2-positive breast cancer was evaluated. Sixty-six percent of patients had objective brain partial response, delaying the initiation of radiotherapy. In this trial, mPFS was 5.5 months and mOS was 17 months.

At the onset of BM, another phase I trial [15] evaluated the association of lapatinib and RT for newly BM from BC in 35 pts. ORR was 79% by volumetric criteria. In this study, mPFS was 4.8 months and mOS was 19 months. However, this study did not meet the primary objective of feasibility because of toxicity.

Moreover, combination of lapatinib and trastuzumab for BM from BC was only evaluated in retrospective studies. Use of both anti-HER2 agents could be associated to an interesting effect on patient survival [16,17].

Finally, no study is available to date on the evaluation of pertuzumab for BM from BC.

Non-small cell lung cancer

In patients with non-small cell lung cancer (NSCLC), brain metastases develop in approximately 30% of cases [18]. In the literature, BM from NSCLC was treated with various cytotoxic drugs or new molecular drugs with or without RT.

Cytotoxic drugs

Recently, many chemotherapeutic regimens have been tested in phase II or phase III trials for the treatment of brain metastases from NSCLC (see Table 2).

Franciosi et al. [4] analyzed 116 patients receiving cisplatin 100 mg/m^2 on day 1 and Etoposide 100 mg/m^2 on days 1, 3, and 5 or on days 4, 6, and 8 every 3 weeks. The distribution of primary tumor site was breast cancer in 56 patients (52%) and NSCLC in 43 (40%). Among 43 patients with NSCLC, 3 achieved CR (7%), 10 achieved PR, 15 had SD, 7 had PD, and 8 had insufficient treatment or response was not assessed. The median survival was 32 weeks for patients with NSCLC.

Another trial [19] evaluated the efficacy and safety of pemetrexed–cisplatin plus concurrent WBRT in patients with BM from lung adenocarcinoma. Forty-two patients were enrolled in this study. Patients with newly diagnosed NSCLC with BM and Eastern Cooperative Oncology Group (ECOG) performance status (PS) of 0–2 received up to six cycles of cisplatin and pemetrexed (75 and 500 mg/m^2, respectively) every 3 weeks in association with WBRT 30 Gy during the first cycle. Concerning brain lesions, RR was 68.3%, PFS was 10.6 months and OS was 12.6 months. A Spanish study [20] evaluated the activity of paclitaxel–cisplatin with vinorelbine or gemcitabine as front-line therapy in BM from NSCLC. Whole-brain irradiation was offered early in case of progression and later as consolidation treatment. The median OS for all patients was 21.4 weeks and the median PFS was 12.8 weeks. Paclitaxel and cisplatin combined with vinorelbine or gemcitabine as front-line therapy in brain metastases seem to achieve a response similar to that for extracranial disease; intracranial RR was observed in 38% of the patients. Kleisbauer et al. [21] analyzed the response to high dose cisplatin. Twenty-four consecutive patients with BM of lung carcinoma were included in this study. The total dose of cisplatin (200 mg/m^2) was divided into 5 equal daily fractions, infused over 6 h. Failure was observed in 17 cases, ORR in 7 cases (2 cases without injection contrast in the tumor, 3 partial regressions, 2 complete regressions). In conclusion, 30% of patients exhibited an ORR with low toxicity.

In the study by Quantin et al. [22], 23 previously untreated patients suffering from NSCLC BM were prospectively included in this feasibility study. Treatment consisted of three cycles of WBRT (18 Gy in 10 fractions) and vinorelbine, 30 mg/m^2 on days 1 and 8, ifosfamide 1.5 g/m^2 daily from day 1 through day 3, and cisplatin 100 mg/m^2 on day 2. A cycle restarted every 28 days. Specific evaluation of brain response demonstrated complete response for 7 patients, and partial response in 6 (ORR 56%). Median OS from start of protocol was 7.6 months.

In a multicentric phase III trial, Neuhaus et al. [23] analyzed OS, local response and PFS of patients with BM from NSCLC and small cell lung cancer treated with RT alone or RT plus topotecan. The data showed no significant advantage for concurrent radiochemotherapy; however, the recruited number of patients was too low to exhibit advantage of combined treatment.

Temozolomide is an orally administered prodrug that is converted spontaneously to the active alkylating agent. In patients with newly-diagnosed BM or with progression after RT, temozolomide demonstrated an interesting activity.

A phase II study [5], evaluated the efficacy of alternating weekly, dose-dense temozolomide in pretreated patients with BM prospectively stratified by primary tumor type. This study analyzed 53 patients with NSCLC. PFS was 66 days and OS was 172 days. Thrombocytopenia was the most common adverse event causing dose modification or treatment discontinuation.

Giorgio et al. [24] evaluated in a phase II study the efficacy and safety of temozolomide in 30 NSCLC patients pre-treated with WBRT and at least one previous line of chemotherapy for metastatic brain disease. Three patients (10%) achieved an objective response of BM with 2 complete remissions. Stable disease and progressive disease were achieved in 3 (10%) and 24 patients (80%), respectively.

Epidermal growth factor receptor (EGFR) inhibitors

Targeted therapies are undergoing active development as a means to improve treatment efficacy in selected patient populations. Novel agents, such as EGFR tyrosine kinase inhibitors (TKI), have now been included in standard non-small-cell lung cancer

Table 2
Clinical studies of cytotoxic treatments for brain metastases in lung cancer.

Author	PTS	Regimen	RR (%)	mPFS (ms)	OS (ms)
Franciosi et al. [4]	43	Cisplatin–etoposide	30	4	8
Cortes et al. [20]	26	Cisplatin–taxol	38	3.2	5.3
Cotto et al. [77]	31	Cisplatin–fotemustine	23	5	4
Fujita et al. [78]	30	Cisplatine–ifosfamide–CPT11	50	4.6	12
Dinglin et al. [19]	42	Pemetrexed–cisplatin	68	10.6	12.6
Kleisbauer et al. [21]	24	Cisplatin	30	NA	NA
Siena et al. [5]	53	TMZ	NA	66 days	172 days
Giorgio et al. [24]	30	TMZ	10	3.6 ms	6 ms
Quantin et al. [22]	23	RT + vinorelbine–ifosfamide–cisplatin	30	NA	7.6

PTS: patients; RR: response rate; PFS: progression free survival; OS: overall survival; RT: radiation therapy; NR: not reached; NA: not available; TMZ: temozolomide; CPT11: irinotecan.

treatments. In a small subset of patients harboring EGFR-activating mutations, erlotinib and gefitinib administration was followed by RR and a longer PFS and OS than that obtained with standard chemotherapeutic regimens. In recent years however, several authors have reported a growing number of cases of partial and complete response in BM patients treated with EGFR TKIs (see Table 3). Data from retrospective series and phase II studies also suggest that a response can be obtained using EGFR tyrosine kinase inhibitors treatment for patients with BM, especially those harboring EGFR mutations.

Kim et al. [25] analyzed the response of 23 never-smoking Korean patients with adenocarcinoma of the lung with BM treated with EGFR TKI therapy until disease progression. RR was 69.6% and disease control rate 82.6%. Intracranial RR was observed in 17 patients.

Gefinitib is an orally active and reversible inhibitor of EGFR tyrosine kinase. Chiu et al., conducted a prospective study with 76 patients with NSCLC and presence of BM treated with gefitinib showing a RR of 33%. PFS and OS were 5 and 9.9 months, respectively. Severity of skin toxicity was associated with tumor response and patient survival [26].

Moreover, EGFR inhibitors can be safely administered concurrently with WBRT; in fact, a recent phase II randomized study [27] in BM from NSCLC compared WBRT plus gefitinib vs. WBRT plus temozolomide. In this randomised phase II trial, patients with BM from NSCLC were randomly assigned to 30 Gy WBRT with either concomitant gefitinib 250 mg/day continuously or temozolomide 75 mg/m^2 for 21 days every 28 days. The primary end-point was OS but the study failed to show any advantage for gefitinib: 6.3 months in the gefinitib arm and 4.9 months in the temozolomide arm (p not significant).

Ma et al. [28] analyzed the efficacy and toxicity of the treatment with WBRT and gefinitib. In this study, 21 patients were enrolled. Gefitinib was administrated at dosage of 250 mg/day. The primary end points were safety and OS. Concomitant treatment was well tolerated, 4 and 13 patients had a complete and partial response, respectively; 3 patients had stable disease. The concomitant treatment seems to be well tolerated with a significant improvement of quality of life in this Chinese population.

In a recent study, Hsiao et al. [29] analyzed the predictive role of EGFR mutations in BM treatment. In this study, 180 of 505 lung adenocarcinoma patients developed BM during their disease and 139 patients including 89 EGFR-mutant and 50 EGFR wild-type patients were identified for analysis. Among patients eligible for evaluation of treatment response, up to 85% received RT and the remaining took EGFR TKIs. EGFR-mutant patients compared with EGFR wild-type patients had significantly greater intracranial RR of BM and a longer median OS after BM diagnosis.

Erlotinib is a low-molecular weight, orally bio-available drug that selectively and reversibly inhibits the tyrosine kinase activity of EGFR. Welsh et al. [30] analyzed in a phase II trial the median OS of patients with BM from NSCLC treated with erlotinib plus WBRT. Eligible patients had BM from NSCLC, regardless of EGFR status. 40 patients completed erlotinib + WBRT. Median OS of 17 patients with known EGFR status was 9.3 months and 19.1 months for EGFR wild-type and EGFR mutated, respectively.

In another retrospective study [31], 40 NSCLC patients with BM were treated with erlotinib until disease progression, death, or intolerable side effects. For intracranial diseases, partial response was observed in 4 patients (10%), stable disease in 21 (52.5%), and progressive disease in 15 (37.5%), with an RR of 10% and a disease control rate of 62.5%. PFS and OS were 3.0 months and 9.2 months, respectively.

Ceresoli et al. [32] evaluated the activity and safety of gefitinib in 41 NSCLC patients with BM. Thirty-seven patients had received prior chemotherapy and 18 patients had been treated previously with WBRT, completed at least 3 months before entering the trial. Partial response was observed in 4 patients (10%), and stable disease in 7 cases, for a disease control rate of 27%. Median duration of partial response was 13.5 months. PFS was 3 months. Toxicity was mild and consisted of grade 1–2 skin toxicity and diarrhea, occurring in 24% and 10% of patients, respectively.

Wu et al. [33] evaluated the activity of gefitinib in 44 NSCLC patients with BM. Of these patients, 30 were previously treated with WBRT. Partial response was observed in 14 patients (31.8%) and stable disease in 21 (47.7%). PFS and OS were 9 and 13 months, respectively. The difference in disease control rate between the patients who had previous WBRT and those without was not significant (p not significant).

Table 3
Clinical studies of targeted drugs for brain metastases in lung cancer.

Author	PTS	Regimen	RR (%)	mPFS (ms)	OS (ms)
Ceresoli et al. [32]	41	Gefitinib	10	3	5
Chiu et al. [26]	21	Gefitinib	76	5	9.9
Wu et al. [33]	44	Gefitinib	38	9	13
Kim et al [25]	23	Gefitinib/ erlotinib	69	7.1	18.8
Welsh et al. [30]	40	Erlotinib + RT	86	NA	19.1

PTS: patients; RR: response rate; PFS: progression free survival; OS: overall survival; RT: radiation therapy; NA: not available.

Antiangiogenic drug bevacizumab

One of the targeted approaches most widely studied in the treatment of NSCLC is the inhibition of angiogenesis. Angiogenesis is essential for the development and progression of cancer, and vascular endothelial growth factor (VEGF) is a critical mediator of tumor angiogenesis. Bevacizumab, an anti-VEGF recombinant humanized monoclonal antibody, is the first targeted agent which, when combined with chemotherapy, has shown superior efficacy versus chemotherapy alone as first-line treatment of advanced non-squamous NSCLC patients. Patients with BM have initially been excluded from bevacizumab trials for the risk of cerebral hemorrhage as a result of the treatment. Nevertheless, the available data suggest an equal risk of intracranial bleeding in patients with CNS metastases treated with or without bevacizumab therapy [34].

A phase II trial (PASSPORT) [35] specifically addressed bevacizumab safety in patients with NSCLC and previously treated BM. This open-label multicenter trial for first- and second-line treatment of nonsquamous NSCLC enrolled patients with BM. First-line patients received bevacizumab (15 mg/kg) every 3 weeks with platinum-based doublet therapy or erlotinib, and second-line patients received bevacizumab with single-agent chemotherapy or erlotinib, until disease progression or death. The study showed that addition of bevacizumab to various chemotherapy agents or erlotinib in patients with NSCLC and BM is safe and is associated with a low incidence of CNS hemorrhage.

A Japanese study retrospectively identified patients treated with bevacizumab and chemotherapy for BM from NSCLC, including 17 patients with lung adenocarcinoma. In 14 pts with evaluable BM, the response rate for intracranial metastases was 78.6%. In these patients, 2 bleeding events were reported: one was grade 1 intracranial hemorrhage, the other was grade 1 bronchopulmonary hemorrhage. This study showed that chemotherapy and bevacizumab is effective for patients with BM and is a well-tolerated regimen with a favorable toxicity profile [36].

Zustovich et al. [37] analyzed 18 patients with BM mostly from lung and renal adenocarcinoma and the majority of patients had a

treatment-naïve brain disease: 82% of patients had a partial response and 18% had stable disease. PFS was 14 months and OS was 15 months. Toxicity was the same as that in clinical practice and no cerebral hemorrhagic events were reported.

Noroxe et al. [38] analyzed OS, PFS, RR and toxicity in patients who received bevacizumb plus chemotherapy. Median OS and PFS were 8.8 and 4.5 months in patients with ECOG PS of 0–1, while 2.6 and 1.2 months for those with PS 2. Therefore, these data suggest that patients with PS 2 should not receive this treatment.

Melanoma

Melanoma BM are common since at least one patient out of three with advanced melanoma will ultimately develop BM. Survival remains dismal with an expected median OS of 16–22 weeks, probably because of the poor efficacy of conventional treatments due to radioresistency of melanoma cells and the low blood–brain barrier penetrance of systemic cytotoxic agents commonly used in metastatic melanoma. More recently, new therapeutic agents have proven their efficacy in progressing metastatic melanoma and in particular on the basis on molecular status of primary disease (see Table 4).

These recent advantages achieved by small molecules and personalized therapy give rise to the issue of the best sequencing of therapeutical interventions and the need for stratification of patient prognostic factors.

Cytotoxic chemotherapy with nitrosoureas, such as fotemustine and temozolomide, have been tested in melanoma brain metastasis patients because of their ability to penetrate the blood–brain barrier. Response rate of 5.9% was observed for fotemustine and 6% for temozolomide without any added benefit to RT, and with increased toxicity [39–43].

Recently, two systemic agents showed encouraging results in control of melanoma brain metastasis alone or in association with brain irradiation. These preliminary data are very encouraging even if still investigational.

The first is the human CTLA4-antibody, ipilimumab, which inhibits immunologic checkpoints. The mechanism of action involves the blockade of negative signaling in cytotoxic T cells that occurs normally following cytotoxic activation.

Ipilimumab was approved in 2011 for patients with metastatic melanoma based on a survival advantage over a melanoma vaccine, corticosteroid therapy and single agent dacarbazine.

Up to 15% objective response and 25% of stabilization 12 weeks following the initiation of therapy were observed in a phase II open study ipilimumab (10 mg/kg intravenously every 3 weeks for 4 cycles followed by the same dose every 12 weeks) versus corticosteroid therapy. Furthermore, median OS of 1 year was obtained in a phase II trial testing ipilimumab in addition to fotemustine. These results encouraged "proof of principle" that the benefit of CTLA4 blockade extends to central nervous system (CNS) disease with peculiar concordant response in the control of brain and extracranial disease in metastatic melanoma. Ipilimumab is currently undergoing testing as adjuvant therapy after resection of high-risk melanoma, either compared with placebo or compared with interferon. In the short-term, combinations with less toxic agents such as temozolomide as well as other new checkpoint-blocking antibodies and RT need to be explored [44–51].

As other immunostimulatory agents, promising antibodies that block negative signaling through the PD-1/PD-L1 axis continue to be studied and represent a potential tool for the management of CNS disease.

The second systemic agent is BRAF inhibitor. BRAF mutations occur in approximately 50% of melanomas, resulting in constitutive up-regulated signaling through the MAPK pathway, independent of receptor–ligand interactions, that can be targeted by selective small-molecule inhibitors [52,53].

The most common mutation is V600E occurring in 70–90% of BRAF-mutant melanomas; other less frequent mutations include V600K (10–30%), V600R (1–7%), and K601E (1–4%) [52,53].

The first report of activity of BRAF inhibitors for patients with melanoma BM was in 10 patients with V600E (9 patients) and V600K (1 patient) melanoma [54]. Nine patients had a size reduction of BM and four had a complete response.

These results led to the largest trial ever conducted in active melanoma BM: 172 patients with V600E or V600K mutation-positive melanoma were treated with 150 mg twice daily of dabrafenib (BREAK-MB); all patients were divided into two cohorts according to prior local therapy with surgery, WBRT, or stereotactic radiosurgery at progression. Responses were seen in both cohorts, and in both V600E and V600K *BRAF* mutation positive melanoma. Overall intracranial RR were up to 39% with median PFS of 16 weeks and OS of 31 and 33 weeks (according to prior treatment at progression) [55].

Interestingly, the brain is not always the first site of progression: 30% of progression at an extracranial site alone and 40% progression both at intra and extra cranial sites were observed [54].

After the encouraging results of the phase I/II study of dabrafenib, vemurafenib (960 mg twice daily) was studied in 24 patients with V600E BRAF mutation-positive melanoma and symptomatic, progressing and untreated BM. The authors had a median PFS of 4 months and a median OS of 5 months. Only 3 patients (16%) had a confirmed partial response in the brain, whereas 13/21 patients (62%) had extra-cranial responses [56].

Another encouraging observation is the dramatic symptomatic relief of neurological symptoms in patients with active brain metastases treated with dabrafenib [57].

However, it is not clear whether a difference in activity exists between dabrafenib and vemurafenib in BM although, a recent preclinical study suggests that dabrafenib may have a higher concentration and longer acting lipophilic metabolites crossing the BBB in murine model [58]. Regarding safety, liver toxicity, arthralgia, and photosensitivity appear more common with vemurafenib; fever is more frequent with dabrafenib [54].

Table 4
Clinical studies of systemic treatments for brain metastases in melanoma.

Author	PTS	Regimen	RR (%)	mPFS (wks)	mOS (wks)
Jacquillat et al. [39]	36	Fotemustine	25	NA	NA
Avril et al. [40]	22	Fotemustine	5.9	NA	NA
Mornex et al. [41]	37	Fotemustine + RT	10	8	15
Margolin et al. [42]	31	Temozolomide + RT	9	8	24
Atkins et al. [43]	39	Temozolomide + RT + Talidomide	7.6	7	16
Margolin et al. [50]	51	Ipilimumab	16	10.7	28
Queirolo et al. [51]	146	Ipilimumab	11	11.2	17.2
Falchook et al. [54]	10	Dabrafenib	90	16.8	32
Dummer et al. [56]	24	Vemurafenib	52	16	30

PTS: patients; RR: response rate; PFS: progression free survival; OS: overall survival; RT: radiation therapy; NA: not available.

Table 5
Clinical studies of systemic treatments for brain metastases in renal cell carcinoma.

Authors	PTS	Regimen	RR (%)	mPFS (ms)	mOS (ms)
Gore et al. [66]	213	Sunitinib	12	5.6	9.2
Stadler et al. [68]	70	Sorafenib	4	NA	NA
Zustovich et al. [76]	4	Bevacizumab	75	26.3*	33.2*

PTS: patients; RR: response rate; PFS: progression free survival; OS: overall survival; NA: not available.
* The maximum reported value among the four patients.

Development of resistance to treatment occurs in most patients and a new strategy could be the association with other inhibitors of MAPK cascade. In fact, a phase 2 study compared single-agent dabrafenib with the combination of dabrafenib and trametinib showing a superior RR (76% vs. 54%), superior progression-free survival (9.4 vs. 5.8 months), and superior progression free survival at 12 months (41% vs. 9%) for the combination regimen [59].

Interestingly, an "abscopal effect" has been described in a patient receiving RT after discontinuation of vemurafenib because of subsequent progression of metastatic melanoma and appearance of a brain metastasis, which was treated by radiosurgery [60]. After radiosurgery, he showed regression of metastatic disease and also appearance of white hair and vitiligo of the skin suggesting an immune response against normal and neoplastic melanocytes activated after radiosurgery without concomitant vemurafenib, which was stopped before radiosurgery at second melanoma progression. At 18 months after the completion of radiosurgery, the patient showed no evidence of recurrence or regression of other metastasis. The term "abscopal effect" (from the Latin "ab"-position away from- and "scopus"-target- has been used to denote this phenomenon of tumor regression at sites that are remote from an irradiated target). The pathophysiology of the abscopal effect seen in this patient is not completely understood; one hypothesis is that BRAF inhibition could result in increased immunogenicity in melanoma cells with increased expression of melanoma antigens and enhanced reactivity to antigen-specific T lymphocytes which ultimately contribute to the systemic response to stereotactic radiosurgery. The response seen in this patient provides insight into how local ablative strategies can augment a systemic response to targeted therapy [61].

In conclusion, the successful results recently obtained in the treatment of patients with BM from melanoma are an example of the need to redesign the therapeutical attitude and to design new clinical trials in this setting of dismal prognosis. The extended survivals obtained by new therapeutic agents justify consideration of aggressive local therapy for patients with melanoma BM. At the moment, the main remaining issue is to find the optimal sequences and combinations of new molecular drugs and to find other molecular alterations that may candidate patients to personalized target therapy.

Renal cell carcinoma

Brain metastasis from renal cell carcinoma (RCC) occurs in approximately 5–10% of cases; data from Maastricht Cancer Registry showed that the 5-year cumulative incidence of brain metastases from RCC was 9.8% [1,62].

The median survival of patients with untreated RCC BM averages from 3 to 4 months [63]; the outcome for these patients is poor, with median OS of only 4–11 months after diagnosis even after surgical resection, WBRT, or stereotactic radiosurgery [64]. Moreover, metastatic RCC is generally resistant to chemotherapy and thus, immunologic therapy with interferon or interleukin-2 has been the most commonly used treatment, despite low response rates. The advent of TKIs and other targeted therapies has drastically altered the management of metastatic RCC, and some published data suggest that these agents may be effective on BM as well (see Table 5).

Sunitinib is a small, oral, multi-targeted receptor TKI with antitumor and antiangiogenic activity. It has been shown that brain penetration of sunitinib may reach 31%, a higher penetration than other TKIs [65]. Gore et al. [66] reported results from an open-label, expanded access program with sunitinib (50 mg once daily, in repeated 6-week cycles of 4 weeks on treatment, followed by 2 week off) for more than 4500 patients with metastatic RCC. Among these, 213 patients with BM were evaluable for tumor response: 12% had partial response and 1% achieved a complete response, yielding an ORR of 12% compared with an ORR of 17% in the overall population [67]. PFS was 5.6 months (95% CI, 5.2–6.1) and 10.9 months (95% CI. 10.3–11.2) in patients with and without BM, respectively. Similarly, median OS was 9.2 months (95% CI, 7.8–10.9) in patients with BM, compared with 18.4 months (95% CI, 17.4–19.2) in the overall population. However, the median OS observed in patients with BM compares favorably with historical survival data for untreated patients with BM [64]. Regarding toxicity, the incidence of severe adverse events and treatment-related adverse events was not different between the two groups of patients. The most common adverse events were diarrhea and fatigue. Cerebral hemorrhage was reported in only one patient. Moreover, the tolerability of sunitinib in patients with BM was similar to that reported in the prior phase II/III trials.

Sorafenib is a multikinase inhibitor of receptor tyrosine kinases VEGF receptors 1, 2, and 3 and platelet-derived growth factor receptors α and β as well as the Raf/MEK/ERK pathway at the level of Raf kinase. In the sorafenib expanded access program [68], of the 1891 evaluable patients with metastatic RCC, 70 had BM. Among these, 4% out of patients obtained a partial response; no patient achieved a complete response, yielding an ORR of 4%. No data on PFS and OS was reported for patients with BM. Toxicity was comparable to that observed with sunitinib.

Massard et al. [69] retrospectively analyzed the incidence of BM in 139 patients treated with sorafenib compared with that in the placebo group in a subgroup of patients from TARGET trial (Treatment Approaches in Renal Cancer Global Evaluation Trial); this study was a randomized phase III trial, involving 903 patients with metastatic RCC, 451 treated with sorafenib and 452 received placebo. The overall incidence of BM was 3% and 12% in patients treated with sorafenib and placebo, respectively ($p = 0.04$). The incidence of BM was also significantly lower in the sorafenib group after one and two years of treatment compared with placebo group ($p = 0.045$). On univariate analyses, the administration of sorafenib therapy was the only predictive factor to affect the occurrence of BM in patients with metastatic RCC. However, some patients in the TKI group were also treated with other targeted agents: erlotinib, temsirolimus and bevacizumab; these agents likely had a protective role with regard to BM as well.

Another retrospective study [70], evaluated the impact of sunitinib and sorafenib on incidence of BM and OS in patients with metastatic RCC. Among 338 patients who were identified (patients were included in the TKI group only if they had received the agent before BM was diagnosed), 154 (46%) were treated with a TKI before brain metastases and 184 (54%) were not. No significant differences in prognostic factors between the two groups were observed. Median OS was longer in the TKI-treated group (25 vs. 12.1 months, $p < 0.0001$). In multivariate analysis, TKI therapy was associated with improved OS (HR 0.53; 95% CI, 0.38–0.74; $p < 0.001$). The 5-year actuarial rate of BM was 40% vs. 17% ($p < 0.001$); on multivariate analysis, TKI treatment was associated with lower incidence of BM (HR, 0.39; 95% CI, 0.21–0.73; $p = 0.003$). This retrospective study found sunitinib and sorafenib to be protective with regard to BM development.

Bastos et al. [71] analyzed 65 patients treated with targeted therapy after BM diagnosis; 52 patients (80) were treated with anti-angiogenic agents and 13 (20%) with mTOR inhibitors. Median OS from start of TKI was 12.2 months (95% CI 8–15.5); median PFS was 3.4 months for first line TKI therapy and 1.9 months for second line TKI.

Larkin et al. [72] retrospectively identified 21 patients (7%) out of 294 patients with RCC developing symptomatic BM while on treatment with sorafenib or sunitinib; the median time from starting TKI to BM was 4 months (range 1–44); the median OS from starting TKI was 11 months (95% CI, 5–17 months). Verma et al. [73], in another retrospective study, confirmed that the development of symptomatic BM is rare but a significant problem in advanced RCC during therapy with sorafenib or sunitinib; in fact, they analyzed 81 patients with BM: 41 patients never received TKI and the remaining 40 received TKI therapy; the median OS from BM diagnosis was 5.4 months for the whole group: 4.4 vs. 6.7 months ($p = 0.07$) in the never-TKI versus TKI groups, respectively. However, patients who received TKI therapy post BM development had a median OS of 23.6 months vs. 2.08 and 4.41 months for the patients who received TKIs pre-BM or never-TKI, respectively ($p = 0.0001$).

A few case reports described the efficacy of other targeted agents on BM from RCC; pazopanib, a potent and selective multi-targeted receptor tyrosine kinase inhibitor of VEGFR-1, VEGFR-2, VEGFR-3, PDGFR-a/β, and c-kit, demonstrated efficacy in a patient who developed more than 20 brain metastases plus multiple bone, lymph node, and soft tissue metastases, and who survived 23 months [74].

Vickers et al. [75], in a retrospective study, analyzed prognostic factors of survival for patients with BM from RCC treated with targeted therapy; they studied 106 patients: 77 treated with sunitinib, 23 with sorafenib, 5 with bevacizumab and 1 patient with temsirolimus. On multivariate analysis, Karnofsky performance status <80% (HR 2.07; 95% CI, 1.2–3.6), RCC diagnosis to treatment with targeted therapy <1 year (HR 2.6; 95% CI, 1.5–4.5) and higher number (>4) of BM (HR 3.1; 95% CI, 1.3–7.5) were associated with worse survival from the time of BM diagnosis. Moreover, patients treated with targeted therapy after BM diagnosis had survived longer than patients who developed BM while receiving targeted therapy, 19.1 vs. 6.3 months, respectively.

Finally, Zustovich et al. [76] described 4 cases of RCC patients with BM treated with bevacizumab with or without α-interferon. They reported a maximum PFS of 26.3 months and a maximum OS of 33.2 months from start of bevacizumab treatment.

Conclusions

In recent years, the frequency of metastatic brain tumors has been increasing and primitive lung cancer is the most common cause. Radiation therapy and surgery can be used in selected patients but can be responsible for acute or delayed neurological deficits. Recently, new targeted drugs have been developed and employed either on established brain metastases or in a preventive setting. Interestingly, these new molecular drugs reported interesting activity and safety in selected cases and in retrospective or prospective studies, with or without radiation therapy in BM from common solid tumors in adults. However, a multidisciplinary collaboration is always required to obtain the appropriate treatment that balances a good quality of life with the prolongation of survival in these patients.

Conflict of interest

None.

Acknowledgment

We thank Ms. Christina Drace for English support.

References

[1] Barnholtz-Sloan JS, Sloan AE, Davis FG, Vigneau FD, Lai P, Sawaya RE. Incidence proportions of brain metastases in patients diagnosed (1973–2001) in the Metropolitan Detroit Cancer Surveillance System. J Clin Oncol 2004;22:2865–72.
[2] Tabouret E, Chinot O, Metellus P, Tallet A, Viens P, Goncalves A. Recent trends in epidemiology of brain metastases: an overview. Anticancer Res 2012;32:4655–62.
[3] Cassier PA, Ray-Coquard I, Sunyach MP, Lancry L, Guastalla JP, Ferlay C, et al. A phase 2 trial of whole-brain radiotherapy combined with intravenous chemotherapy in patients with brain metastases from breast cancer. Cancer 2008;113:2532–8.
[4] Franciosi V, Cocconi G, Michiara M, Di Costanzo F, Fosser V, Tonato M, et al. Front-line chemotherapy with cisplatin and etoposide for patients with brain metastases from breast carcinoma, nonsmall cell lung carcinoma, or malignant melanoma: a prospective study. Cancer 1999;85:1599–605.
[5] Siena S, Crino L, Danova M, Del Prete S, Cascinu S, Salvagni S, et al. Dose-dense temozolomide regimen for the treatment of brain metastases from melanoma, breast cancer, or lung cancer not amenable to surgery or radiosurgery: a multicenter phase II study. Ann Oncol 2010;21:655–61.
[6] Rivera E, Meyers C, Groves M, Valero V, Francis D, Arun B, et al. Phase I study of capecitabine in combination with temozolomide in the treatment of patients with brain metastases from breast carcinoma. Cancer 2006;107:1348–54.
[7] Freedman RA, Bullitt E, Sun L, Gelman R, Harris G, Ligibel JA, et al. A phase II study of sagopilone (ZK 219477; ZK-EPO) in patients with breast cancer and brain metastases. Clin Breast Cancer 2011;11:376–83.
[8] Brufsky AM, Mayer M, Rugo HS, Kaufman PA, Tan-Chiu E, Tripathy D, et al. Central nervous system metastases in patients with HER2-positive metastatic breast cancer: incidence, treatment, and survival in patients from registHER. Clin Cancer Res 2011;17:4834–43.
[9] Lombardi G, Zustovich F, Farina P, Della Puppa A, Manara R, Cecchin D, et al. Neoplastic meningitis from solid tumors: new diagnostic and therapeutic approaches. Oncologist 2011;16:1175–88.
[10] Colozza M, Minenza E, Gori S, Fenocchio D, Paolucci C, Aristei C, et al. Extended survival of a HER-2-positive metastatic breast cancer patient with brain metastases also treated with intrathecal trastuzumab. Cancer Chemother Pharmacol 2009;63:1157–9.
[11] Lin NU, Carey LA, Liu MC, Younger J, Come SE, Ewend M, et al. Phase II trial of lapatinib for brain metastases in patients with human epidermal growth factor receptor 2-positive breast cancer. J Clin Oncol 2008;26:1993–9.
[12] Lin NU, Dieras V, Paul D, Lossignol D, Christodoulou C, Stemmler HJ, et al. Multicenter phase II study of lapatinib in patients with brain metastases from HER2-positive breast cancer. Clin Cancer Res 2009;15:1452–9.
[13] Lin NU, Eierman W, Greil R, Campone M, Kaufman B, Steplewski K, et al. Randomized phase II study of lapatinib plus capecitabine or lapatinib plus topotecan for patients with HER2-positive breast cancer brain metastases. J Neurooncol 2011;105:613–20.
[14] Bachelot T, Romieu G, Campone M, Dieras V, Cropet C, Dalenc F, et al. Lapatinib plus capecitabine in patients with previously untreated brain metastases from HER2-positive metastatic breast cancer (LANDSCAPE): a single-group phase 2 study. Lancet Oncol 2013;14:64–71.
[15] Lin NU, Freedman RA, Ramakrishna N, Younger J, Storniolo AM, Bellon JR, et al. A phase I study of lapatinib with whole brain radiotherapy in patients with human epidermal growth factor receptor 2 (HER2)-positive breast cancer brain metastases. Breast Cancer Res Treat 2013;142:405–14.
[16] Yap YS, Cornelio GH, Devi BC, Khorprasert C, Kim SB, Kim TY, et al. Brain metastases in Asian HER2-positive breast cancer patients: anti-HER2 treatments and their impact on survival. Br J Cancer 2012;107:1075–82.
[17] Gori S, Montemurro F, Spazzapan S, Metro G, Foglietta J, Bisagni G, et al. Retreatment with trastuzumab-based therapy after disease progression following lapatinib in HER2-positive metastatic breast cancer. Ann Oncol 2012;23:1436–41.
[18] Kelly K, Bunn Jr PA. Is it time to reevaluate our approach to the treatment of brain metastases in patients with non-small cell lung cancer? Lung Cancer 1998;20:85–91.
[19] Dinglin XX, Huang Y, Liu H, Zeng YD, Hou X, Chen LK. Pemetrexed and cisplatin combination with concurrent whole brain radiotherapy in patients with brain metastases of lung adenocarcinoma: a single-arm phase II clinical trial. J Neurooncol 2013;112:461–6.
[20] Cortes J, Rodriguez J, Aramendia JM, Salgado E, Gurpide A, Garcia-Foncillas J, et al. Front-line paclitaxel/cisplatin-based chemotherapy in brain metastases from non-small-cell lung cancer. Oncology 2003;64:28–35.
[21] Kleisbauer JP, Guerin JC, Arnaud A, Poirier R, Vesco D. Chemotherapy with high-dose cisplatin in brain metastasis of lung cancers. Bull Cancer 1990;77:661–5.
[22] Quantin X, Khial F, Reme-Saumon M, Michel FB, Pujol JL. Concomitant brain radiotherapy and vinorelbine–ifosfamide–cisplatin chemotherapy in brain metastases of non-small cell lung cancer. Lung Cancer 1999;26:35–9.

[23] Neuhaus T, Ko Y, Muller RP, Grabenbauer GG, Hedde JP, Schueller H, et al. A phase III trial of topotecan and whole brain radiation therapy for patients with CNS-metastases due to lung cancer. Br J Cancer 2009;100:291–7.

[24] Giorgio CG, Giuffrida D, Pappalardo A, Russo A, Santini D, Salice P, et al. Oral temozolomide in heavily pre-treated brain metastases from non-small cell lung cancer: phase II study. Lung Cancer 2005;50:247–54.

[25] Kim JE, Lee DH, Choi Y, Yoon DH, Kim SW, Suh C, et al. Epidermal growth factor receptor tyrosine kinase inhibitors as a first-line therapy for never-smokers with adenocarcinoma of the lung having asymptomatic synchronous brain metastasis. Lung Cancer 2009;65:351–4.

[26] Chiu CH, Tsai CM, Chen YM, Chiang SC, Liou JL, Perng RP. Gefitinib is active in patients with brain metastases from non-small cell lung cancer and response is related to skin toxicity. Lung Cancer 2005;47:129–38.

[27] Pesce GA, Klingbiel D, Ribi K, Zouhair A, von Moos R, Schlaeppi M, et al. Outcome, quality of life and cognitive function of patients with brain metastases from non-small cell lung cancer treated with whole brain radiotherapy combined with gefitinib or temozolomide. A randomised phase II trial of the Swiss Group for Clinical Cancer Research (SAKK 70/03). Eur J Cancer 2012;48:377–84.

[28] Ma S, Xu Y, Deng Q, Yu X. Treatment of brain metastasis from non-small cell lung cancer with whole brain radiotherapy and gefitinib in a Chinese population. Lung Cancer 2009;65:198–203.

[29] Hsiao SH, Lin HC, Chou YT, Lin SE, Kuo CC, Yu MC, et al. Impact of epidermal growth factor receptor mutations on intracranial treatment response and survival after brain metastases in lung adenocarcinoma patients. Lung Cancer 2013;81:455–61.

[30] Welsh JW, Komaki R, Amini A, Munsell MF, Unger W, Allen PK, et al. Phase II trial of erlotinib plus concurrent whole-brain radiation therapy for patients with brain metastases from non-small-cell lung cancer. J Clin Oncol 2013;31:895–902.

[31] Bai H, Han B. The effectiveness of erlotinib against brain metastases in non-small cell lung cancer patients. Am J Clin Oncol 2013;36:110–5.

[32] Ceresoli GL, Cappuzzo F, Gregorc V, Bartolini S, Crino L, Villa E. Gefitinib in patients with brain metastases from non-small-cell lung cancer: a prospective trial. Ann Oncol 2004;15:1042–7.

[33] Wu C, Li LY, Wang MZ, Zhang L, Zhang XT, Zhong W, et al. Gefitinib in the treatment of advanced non-small cell lung cancer with brain metastasis. Zhonghua Zhong Liu Za Zhi 2007;29:943–5.

[34] Soffietti R, Trevisan E, Ruda R. Targeted therapy in brain metastasis. Curr Opin Oncol 2012;24:679–86.

[35] Socinski MA, Langer CJ, Huang JE, Kolb MM, Compton P, Wang L, et al. Safety of bevacizumab in patients with non-small-cell lung cancer and brain metastases. J Clin Oncol 2009;27:5255–61.

[36] Ichiki M, Yoshida T, Nakamura M, Kumano T, Hoshino T. Efficacy and safety of bevacizumab in nonsquamous non-small cell lung cancer with brain metastases. J Clin Oncol 2013;31. suppl; abstr e19134.

[37] Zustovich F, Ferro A, Lombardi G, Zagonel V, Fiduccia P, Farina P. Bevacizumab as front-line treatment of brain metastases from solid tumors: a case series. Anticancer Res 2013;33:4061–5.

[38] Noroxe DS, Wallerek S, Sorensen JB. Platinum-based doublet chemotherapy plus bevacizumab without bevacizumab maintenance in advanced non-small cell lung cancer (NSCLC). Anticancer Res 2013;33:3275–8.

[39] Jacquillat C, Khayat D, Banzet P, Weil M, Fumoleau P, Avril MF, et al. Final report of the French multicenter phase II study of the nitrosourea fotemustine in 153 evaluable patients with disseminated malignant melanoma including patients with cerebral metastases. Cancer 1990;66:1873–8.

[40] Avril MF, Aamdal S, Grob JJ, Hauschild A, Mohr P, Bonerandi JJ, et al. Fotemustine compared with dacarbazine in patients with disseminated malignant melanoma: a phase III study. J Clin Oncol 2004;22:1118–25.

[41] Mornex F, Thomas L, Mohr P, Hauschild A, Delaunay MM, Lesimple T, et al. A prospective randomized multicentre phase III trial of fotemustine plus whole brain irradiation versus fotemustine alone in cerebral metastases of malignant melanoma. Melanoma Res 2003;13:97–103.

[42] Margolin K, Atkins B, Thompson A, Ernstoff S, Weber J, Flaherty L, et al. Temozolomide and whole brain irradiation in melanoma metastatic to the brain: a phase II trial of the Cytokine Working Group. J Cancer Res Clin Oncol 2002;128:214–8.

[43] Atkins MB, Sosman JA, Agarwala S, Logan T, Clark JI, Ernstoff MS, et al. Temozolomide, thalidomide, and whole brain radiation therapy for patients with brain metastasis from metastatic melanoma: a phase II Cytokine Working Group study. Cancer 2008;113:2139–45.

[44] Hodi FS, O'Day SJ, McDermott DF, Weber RW, Sosman JA, Haanen JB, et al. Improved survival with ipilimumab in patients with metastatic melanoma. N Engl J Med 2010;363:711–23.

[45] Robert C, Thomas L, Bondarenko I, O'Day S, Weber J, Garbe C, et al. Ipilimumab plus dacarbazine for previously untreated metastatic melanoma. N Engl J Med 2011;364:2517–26.

[46] Hodi FS, Oble DA, Drappatz J, Velazquez EF, Ramaiya N, Ramakrishna N, et al. CTLA-4 blockade with ipilimumab induces significant clinical benefit in a female with melanoma metastases to the CNS. Nat Clin Pract Oncol 2008;5:557–61.

[47] Bot I, Blank CU, Brandsma D. Clinical and radiological response of leptomeningeal melanoma after whole brain radiotherapy and ipilimumab. J Neurol 2012;259:1976–8.

[48] Schartz NE, Farges C, Madelaine I, Bruzzoni H, Calvo F, Hoos A, et al. Complete regression of a previously untreated melanoma brain metastasis with ipilimumab. Melanoma Res 2010;20:247–50.

[49] Di Giacomo AM, Ascierto PA, Pilla L, Santinami M, Ferrucci PF, Giannarelli D, et al. Ipilimumab and fotemustine in patients with advanced melanoma (NIBIT-M1): an open-label, single-arm phase 2 trial. Lancet Oncol 2012;13:879–86.

[50] Margolin K, Ernstoff MS, Hamid O, Lawrence D, McDermott D, Puzanov I, et al. Ipilimumab in patients with melanoma and brain metastases: an open-label, phase 2 trial. Lancet Oncol 2012;13:459–65.

[51] Queirolo P, Spagnolo F, Ascierto PA, Simeone E, Marchetti P, Scoppola A, et al. Efficacy and safety of ipilimumab in patients with advanced melanoma and brain metastases. J Neurooncol 2014;118:109–16.

[52] Long GV, Menzies AM, Nagrial AM, Haydu LE, Hamilton AL, Mann GJ, et al. Prognostic and clinicopathologic associations of oncogenic BRAF in metastatic melanoma. J Clin Oncol 2011;29:1239–46.

[53] Thomas NE, Edmiston SN, Alexander A, Millikan RC, Groben PA, Hao H, et al. Number of nevi and early-life ambient UV exposure are associated with BRAF-mutant melanoma. Cancer Epidemiol Biomarkers Prev 2007;16:991–7.

[54] Falchook GS, Long GV, Kurzrock R, Kim KB, Arkenau TH, Brown MP, et al. Dabrafenib in patients with melanoma, untreated brain metastases, and other solid tumours: a phase 1 dose-escalation trial. Lancet 2012;379:1893–901.

[55] Long GV, Trefzer U, Davies MA, Kefford RF, Ascierto PA, Chapman PB, et al. Dabrafenib in patients with Val600Glu or Val600Lys BRAF-mutant melanoma metastatic to the brain (BREAK-MB): a multicentre, open-label, phase 2 trial. Lancet Oncol 2012;13:1087–95.

[56] Dummer R, Goldinger SM, Turtschi CP, Eggmann NB, Michielin O, Mitchell L, et al. Vemurafenib in patients with BRAF(V600) mutation-positive melanoma with symptomatic brain metastases: final results of an open-label pilot study. Eur J Cancer 2014;50:611–21.

[57] Klein O, Clements A, Menzies AM, O'Toole S, Kefford RF, Long GV. BRAF inhibitor activity in V600R metastatic melanoma. Eur J Cancer 2013;49:1073–9.

[58] Mittapalli RK, Vaidhyanathan S, Dudek AZ, Elmquist WF. Mechanisms limiting distribution of the threonine-protein kinase B-RaF(V600E) inhibitor dabrafenib to the brain: implications for the treatment of melanoma brain metastases. J Pharmacol Exp Ther 2013;344:655–64.

[59] Flaherty KT, Infante JR, Daud A, Gonzalez R, Kefford RF, Sosman J, et al. Combined BRAF and MEK inhibition in melanoma with BRAF V600 mutations. N Engl J Med 2012;367:1694–703.

[60] Sullivan RJ, Lawrence DP, Wargo JA, Oh KS, Gonzalez RG, Piris A. Case records of the Massachusetts General Hospital. Case 21-2013. A 68-year-old man with metastatic melanoma. N Engl J Med 2013;369:173–83.

[61] Mole RH. Whole body irradiation; radiobiology or medicine? Br J Radiol 1953;26:234–41.

[62] Schouten LJ, Rutten J, Huveneers HA, Twijnstra A. Incidence of brain metastases in a cohort of patients with carcinoma of the breast, colon, kidney, and lung and melanoma. Cancer 2002;94:2698–705.

[63] Decker DA, Decker VL, Herskovic A, Cummings GD. Brain metastases in patients with renal cell carcinoma: prognosis and treatment. J Clin Oncol 1984;2:169–73.

[64] Shuch B, La Rochelle JC, Klatte T, Riggs SB, Liu W, Kabbinavar FF, et al. Brain metastasis from renal cell carcinoma: presentation, recurrence, and survival. Cancer 2008;113:1641–8.

[65] Hu S, Chen Z, Franke R, Orwick S, Zhao M, Rudek MA, et al. Interaction of the multikinase inhibitors sorafenib and sunitinib with solute carriers and ATP-binding cassette transporters. Clin Cancer Res 2009;15:6062–9.

[66] Gore ME, Szczylik C, Porta C, Bracarda S, Bjarnason GA, Oudard S, et al. Safety and efficacy of sunitinib for metastatic renal-cell carcinoma: an expanded-access trial. Lancet Oncol 2009;10:757–63.

[67] Gore ME, Hariharan S, Porta C, Bracarda S, Hawkins R, Bjarnason GA, et al. Sunitinib in metastatic renal cell carcinoma patients with brain metastases. Cancer 2011;117:501–9.

[68] Stadler WM, Figlin RA, McDermott DF, Dutcher JP, Knox JJ, Miller Jr WH, et al. Safety and efficacy results of the advanced renal cell carcinoma sorafenib expanded access program in North America. Cancer 2010;116:1272–80.

[69] Massard C, Zonierek J, Gross-Goupil M, Fizazi K, Szczylik C, Escudier B. Incidence of brain metastases in renal cell carcinoma treated with sorafenib. Ann Oncol 2010;21:1027–31.

[70] Verma J, Jonasch E, Allen P, Tannir N, Mahajan A. Impact of tyrosine kinase inhibitors on the incidence of brain metastasis in metastatic renal cell carcinoma. Cancer 2011;117:4958–65.

[71] Bastos D, Molina AM, Jia X, Velasco S, Patil S, Voss MH, et al. Targeted therapy for renal cell carcinoma with brain metastasis: overall survival and safety. J Clin Oncol 2013;31. suppl; abstr e15517.

[72] Larkin JM, Hess V, Pickering LM, Ferguson T, Forrest R, Gore ME. Symptomatic brain metastases from renal cell carcinoma during treatment with sunitinib or sorafenib. J Clin Oncol 2010;28. suppl; abstr e15023.

[73] Verma J, Jonasch E, Allen PK, Weinberg JS, Tannir N, Chang EL, et al. The impact of tyrosine kinase inhibitors on the multimodality treatment of brain metastases from renal cell carcinoma. Am J Clin Oncol 2013;36:620–4.

[74] Jacobs C, Kim DW, Straka C, Timmerman RD, Brugarolas J. Prolonged survival of a patient with papillary renal cell carcinoma and brain metastases using pazopanib. J Clin Oncol 2013;31:e114–7.

[75] Vickers MM, Al-Harbi H, Choueiri TK, Kollmannsberger C, North S, Mackenzie M, et al. Prognostic factors of survival for patients with metastatic renal cell carcinoma with brain metastases treated with targeted therapy: results from the international metastatic renal cell carcinoma database consortium. Clin Genitourin Cancer 2013;11:311–5.
[76] Zustovich F, Ferro A, Farina P. Bevacizumab as first-line therapy for patients with brain metastases from renal carcinoma: a case series. Clin Genitourin Cancer 2014;12:e107–10.
[77] Cotto C, Berille J, Souquet PJ, Riou R, Croisile B, Turjman F, et al. A phase II trial of fotemustine and cisplatin in central nervous system metastases from non-small cell lung cancer. Eur J Cancer 1996;32A:69–71.
[78] Fujita A, Fukuoka S, Takabatake H, Tagaki S, Sekine K. Combination chemotherapy of cisplatin, ifosfamide, and irinotecan with rhG-CSF support in patients with brain metastases from non-small cell lung cancer. Oncology 2000;59:291–5.

HMG Advance Access published August 11, 2014

Human Molecular Genetics, 2014 ***1–18***
doi:10.1093/hmg/ddu363

Imputation and subset-based association analysis across different cancer types identifies multiple independent risk loci in the *TERT-CLPTM1L* region on chromosome 5p15.33

Zhaoming Wang[1,5], Bin Zhu[1], Mingfeng Zhang[1], Hemang Parikh[1], Jinping Jia[1], Charles C. Chung[1,5], Joshua N. Sampson[1], Jason W. Hoskins[1], Amy Hutchinson[1,5], Laurie Burdette[1,5], Abdisamad Ibrahim[1], Christopher Hautman[1,5], Preethi S. Raj[1], Christian C. Abnet[1], Andrew A. Adjei[6,7], Anders Ahlbom[8], Demetrius Albanes[1], Naomi E. Allen[11], Christine B. Ambrosone[12], Melinda Aldrich[13,14], Pilar Amiano[15,16], Christopher Amos[17], Ulrika Andersson[18], Gerald Andriole Jr[23], Irene L. Andrulis[24], Cecilia Arici[25], Alan A. Arslan[26,27,28], Melissa A. Austin[29], Dalsu Baris[1], Donald A. Barkauskas[30], Bryan A. Bassig[1,32], Laura E. Beane Freeman[1], Christine D. Berg[2], Sonja I. Berndt[1], Pier Alberto Bertazzi[33,34], Richard B. Biritwum[6,7], Amanda Black[1], William Blot[13,14,35], Heiner Boeing[36], Paolo Boffetta[37], Kelly Bolton[1,38], Marie-Christine Boutron-Ruault[39], Paige M. Bracci[40], Paul Brennan[41], Louise A. Brinton[1], Michelle Brotzman[42], H. Bas Bueno-de-Mesquita[43,44], Julie E. Buring[45], Mary Ann Butler[46], Qiuyin Cai[13,14], Geraldine Cancel-Tassin[47,49], Federico Canzian[50], Guangwen Cao[51], Neil E. Caporaso[1], Alfredo Carrato[52], Tania Carreon[46], Angela Carta[24], Gee-Chen Chang[53,54], I-Shou Chang[55], Jenny Chang-Claude[50], Xu Che[58], Chien-Jen Chen[60,61], Chih-Yi Chen[62], Chung-Hsing Chen[55], Constance Chen[63], Kuan-Yu Chen[66], Yuh-Min Chen[67,69,70], Anand P. Chokkalingam[71], Lisa W. Chu[72], Francoise Clavel-Chapelon[73], Graham A. Colditz[74], Joanne S. Colt[1], David Conti[30], Michael B. Cook[1], Victoria K. Cortessis[30], E. David Crawford[75], Olivier Cussenot[47,48,49], Faith G. Davis[76], Immaculata De Vivo[63,77,78], Xiang Deng[1,5], Ti Ding[79], Colin P. Dinney[80], Anna Luisa Di Stefano[85], W. Ryan Diver[86], Eric J. Duell[87], Joanne W. Elena[88], Jin-Hu Fan[89], Heather Spencer Feigelson[90], Maria Feychting[8], Jonine D. Figueroa[1], Adrienne M. Flanagan[91,92], Joseph F. Fraumeni Jr[1], Neal D. Freedman[1], Brooke L. Fridley[93], Charles S. Fuchs[94,95], Manuela Gago-Dominguez[98], Steven Gallinger[99], Yu-Tang Gao[101], Susan M. Gapstur[86], Montserrat Garcia-Closas[1,102], Reina Garcia-Closas[103], Julie M. Gastier-Foster[104], J. Michael Gaziano[96,97,105], Daniela S. Gerhard[4], Carol A. Giffen[106], Graham G. Giles[107], Elizabeth M. Gillanders[108], Edward L. Giovannucci[63,64], Michael Goggins[110,111,112], Nalan Gokgoz[100], Alisa M. Goldstein[1], Carlos Gonzalez[113], Richard Gorlick[114], Mark H. Greene[1], Myron Gross[115], H. Barton Grossman[80], Robert Grubb III[116], Jian Gu[81], Peng Guan[117], Christopher A. Haiman[31], Goran Hallmans[19], Susan E. Hankinson[95], Curtis C. Harris[109], Patricia Hartge[1], Claudia Hattinger[118], Richard B. Hayes[1,119,120], Qincheng He[117], Lee Helman[3], Brian E. Henderson[31],

*To whom correspondence should be addressed at: Laboratory of Translational Genomics, Division of Cancer Epidemiology and Genetics, National Cancer Institute, Advanced Technology Center, 8717 Grovemont Circle, Bethesda, MD 20892-4605, USA. Email: amundadottirl@mail.nih.gov
†Present address: Center for Pediatrics and Adolescent Medicine, Department of Pediatric Hematology and Oncology, Hannover Medical School, Hannover, Germany

Roger Henriksson[18], Judith Hoffman-Bolton[121], Chancellor Hohensee[122], Elizabeth A. Holly[40], Yun-Chul Hong[123,124], Robert N. Hoover[1], H. Dean Hosgood III[126], Chin-Fu Hsiao[56,57], Ann W. Hsing[72,127], Chao Agnes Hsiung[56], Nan Hu[1], Wei Hu[1], Zhibin Hu[128], Ming-Shyan Huang[66], David J. Hunter[63,77,78,129], Peter D. Inskip[1], Hidemi Ito[130], Eric J. Jacobs[86], Kevin B. Jacobs[4,5,131], Mazda Jenab[41], Bu-Tian Ji[1], Christoffer Johansen[132,133], Mattias Johansson[41,20], Alison Johnson[134], Rudolf Kaaks[50], Ashish M. Kamat[80], Aruna Kamineni[135], Margaret Karagas[17], Chand Khanna[3], Kay-Tee Khaw[137], Christopher Kim[1], In-Sam Kim[138,139], Yeul Hong Kim[140,141,142], Young-Chul Kim[143], Young Tae Kim[125], Chang Hyun Kang[125], Yoo Jin Jung[125], Cari M. Kitahara[1], Alison P. Klein[110,111,112,144], Robert Klein[145], Manolis Kogevinas[147,148,149,150], Woon-Puay Koh[151,68], Takashi Kohno[152], Laurence N. Kolonel[153], Charles Kooperberg[122], Christian P. Kratz[1,†], Vittorio Krogh[154], Hideo Kunitoh[152,155], Robert C. Kurtz[145], Nilgun Kurucu[156], Qing Lan[1], Mark Lathrop[157,158], Ching C. Lau[159], Fernando Lecanda[162], Kyoung-Mu Lee[124,222], Maxwell P. Lee[3], Loic Le Marchand[153], Seth P. Lerner[160], Donghui Li[82], Linda M. Liao[1], Wei-Yen Lim[68], Dongxin Lin[59], Jie Lin[81], Sara Lindstrom[63], Martha S. Linet[1], Jolanta Lissowska[163], Jianjun Liu[164,165], Börje Ljungberg[21], Josep Lloreta[149], Daru Lu[166,167], Jing Ma[77,78], Nuria Malats[168], Satu Mannisto[169], Neyssa Marina[170], Giuseppe Mastrangelo[171], Keitaro Matsuo[130,172], Katherine A. McGlynn[1], Roberta McKean-Cowdin[81], Lorna H. McNeill[83], Robert R. McWilliams[173], Beatrice S. Melin[18], Paul S. Meltzer[3], James E. Mensah[6,7], Xiaoping Miao[174], Dominique S. Michaud[175], Alison M. Mondul[1], Lee E. Moore[1], Kenneth Muir[176], Shelley Niwa[42], Sara H. Olson[146], Nick Orr[177], Salvatore Panico[179], Jae Yong Park[138,139,180], Alpa V. Patel[86], Ana Patino-Garcia[162], Sofia Pavanello[171], Petra H. M. Peeters[181,182], Beata Peplonska[184], Ulrike Peters[122], Gloria M. Petersen[173], Piero Picci[118], Malcolm C. Pike[31,146], Stefano Porru[25], Jennifer Prescott[63,77,78], Xia Pu[81], Mark P. Purdue[1], You-Lin Qiao[185], Preetha Rajaraman[1], Elio Riboli[182], Harvey A. Risch[186], Rebecca J. Rodabough[122], Nathaniel Rothman[1], Avima M. Ruder[46], Jeong-Seon Ryu[187], Marc Sanson[85], Alan Schned[17], Fredrick R. Schumacher[31], Ann G. Schwartz[188], Kendra L. Schwartz[189], Molly Schwenn[190], Katia Scotlandi[118], Adeline Seow[68], Consol Serra[191,192], Massimo Serra[118], Howard D. Sesso[45], Gianluca Severi[107], Hongbing Shen[128], Min Shen[1], Sanjay Shete[193], Kouya Shiraishi[152], Xiao-Ou Shu[13,14], Afshan Siddiq[183], Luis Sierrasesumaga[162], Sabina Sierri[194], Alan Dart Loon Sihoe[195], Debra T. Silverman[1], Matthias Simon[196], Melissa C. Southey[197], Logan Spector[198], Margaret Spitz[161], Meir Stampfer[77,78], Par Stattin[21], Mariana C. Stern[31], Victoria L. Stevens[86], Rachael Z. Stolzenberg-Solomon[1], Daniel O. Stram[31], Sara S. Strom[84], Wu-Chou Su[199], Malin Sund[22], Sook Whan Sung[136], Anthony Swerdlow[102,178], Wen Tan[59], Hideo Tanaka[130], Wei Tang[1], Ze-Zhang Tang[79], Adonina Tardon[200], Evelyn Tay[6,7], Philip R. Taylor[1], Yao Tettey[6,7], David M. Thomas[201], Roberto Tirabosco[92], Anne Tjonneland[202], Geoffrey S. Tobias[1], Jorge R. Toro[1], Ruth C. Travis[11], Dimitrios Trichopoulos[65], Rebecca Troisi[1], Ann Truelove[42], Ying-Huang Tsai[203], Margaret A. Tucker[1], Rosario Tumino[204], David Van Den Berg[31], Stephen K. Van Den Eeden[205], Roel Vermeulen[206], Paolo Vineis[207,208], Kala Visvanathan[121], Ulla Vogel[209,210], Chaoyu Wang[1], Chengfeng Wang[58], Junwen Wang[1,5,211], Sophia S. Wang[214], Elisabete Weiderpass[215,216,9,217], Stephanie J. Weinstein[1], Nicolas Wentzensen[1], William Wheeler[106], Emily White[122], John K. Wiencke[218], Alicja Wolk[10], Brian M. Wolpin[94,95], Maria Pik Wong[212], Margaret Wrensch[218], Chen Wu[59], Tangchun Wu[171], Xifeng Wu[81], Yi-Long Wu[219], Jay S. Wunder[23], Yong-Bing Xiang[101], Jun Xu[213], Hannah P. Yang[1], Pan-Chyr Yang[66], Yasushi Yatabe[220],

Yuanqing Ye[81], Edward D. Yeboah[6,7], Zhihua Yin[117], Chen Ying[68], Chong-Jen Yu[199], Kai Yu[1], Jian-Min Yuan[221], Krista A. Zanetti[88], Anne Zeleniuch-Jacquotte[27,28], Wei Zheng[13,14], Baosen Zhou[117], Lisa Mirabello[1], Sharon A. Savage[1], Peter Kraft[63,65], Stephen J. Chanock[1,5], Meredith Yeager[1,5], Maria Terese Landi[1], Jianxin Shi[1], Nilanjan Chatterjee[1] and Laufey T. Amundadottir[1,*]

[1]Division of Cancer Epidemiology and Genetics, [2]Division of Cancer Prevention, [3]Center for Cancer Research and [4]Office of Cancer Genomics, Department of Health and Human Services, National Cancer Institute, National Institutes of Health, Bethesda, MD, USA, [5]Cancer Genomics Research Laboratory, National Cancer Institute, Division of Cancer Epidemiology and Genetics, SAIC-Frederick, Inc., Frederick National Laboratory for Cancer Research, Frederick, MD, USA, [6]Korle Bu Teaching Hospital, PO BOX 77, Accra, Ghana, [7]University of Ghana Medical School, PO Box 4236, Accra, Ghana, [8]Unit of Epidemiology, Institute of Environmental Medicine, [9]Department of Medical Epidemiology and Biostatistics and [10]Unit of Nutritional Epidemiology, Institute of Environmental Medicine, Karolinska Institutet, Stockholm, Sweden, [11]Clinical Trial Service Unit and Epidemiological Studies Unit, University of Oxford, Oxford, UK, [12]Department of Cancer Prevention and Control, Roswell Park Cancer Institute, Buffalo, NY, USA, [13]Division of Epidemiology, Department of Medicine, Vanderbilt Epidemiology Center, [14]Vanderbilt-Ingram Cancer Center, Vanderbilt University School of Medicine, Nashville, TN, USA, [15]Public Health Division of Gipuzkoa, Basque Regional Health Department, San Sebastian, Spain, [16]CIBERESP, CIBER Epidemiologia y Salud Publica, Madrid, Spain, [17]Geisel School of Medicine at Dartmouth, Hanover, NH, USA, [18]Department of Radiation Sciences, Oncology, [19]Department of Public Health and Clinical Medicine/Nutritional Research, [20]Department of Public Health and Clinical Medicine, [21]Department of Surgical and Perioperative Sciences, Urology and Andrology and [22]Department of Surgical and Perioperative Sciences/Surgery, Umeå University, Umeå, Sweden, [23]Division of Urologic Surgery, Washington University School of Medicine, St Louis, MO, USA, [24]Litwin Centre for Cancer Genetics, Samuel Lunenfeld Research Institute, Mt Sinai Hospital, University of Toronto, Toronto, ON, Canada, [25]Department of Medical and Surgical Specialties, Radiological Sciences and Public Health, University of Brescia, Italy, [26]Department of Obstetrics and Gynecology and [27]Department of Population Health, New York University School of Medicine, New York, NY, USA, [28]New York University Cancer Institute, New York, NY, USA, [29]Department of Epidemiology, University of Washington, Seattle, WA, USA, [30]Department of Preventive Medicine, Biostatistics Division, Keck School of Medicine and [31]Department of Preventive Medicine, Keck School of Medicine, University of Southern California, Los Angeles, CA, USA, [32]Division of Environmental Health Sciences, Yale School of Public Health, New Haven, Connecticut, USA, [33]Department of Clinical Sciences and Community Health, University of Milan, [34]Department of Preventive Medicine, Fondazione IRCCS Ca' Granda Policlinico Hospital, Milan, Italy, [35]International Epidemiology Institute, Rockville, MD, USA, [36]Department of Epidemiology, German Institute of Human Nutrition, Potsdam-Rehbruecke, Germany, [37]Institute for Translational Epidemiology, Hematology and Medical Oncology, Mount Sinai Hospital School of Medicine, New York, NY, USA, [38]Department of Oncology, University of Cambridge, Cambridge CB2 2RE, UK, [39]Institut National de la Sante et de la Recherche Medicale (INSERM) and Institut Gustave Roussy, Villejuif, France, [40]Department of Epidemiology and Biostatistics, University of California San Francisco, San Francisco, CA, USA, [41]International Agency for Research on Cancer (IARC-WHO), Lyon, France, [42]Westat, Rockville, MD, USA, [43]National Institute for Public Health and the Environment (RIVM), Bilthoven, The Netherlands, [44]Department of Gastroenterology and Hepatology, University Medical Centre Utrecht, Utrecht, The Netherlands, [45]Division of Preventive Medicine, Brigham and Women's Hospital, Boston, MA, USA, [46]Centers for Disease Control and Prevention, National Institute for Occupational Safety and Health, Cincinnati, OH, USA, [47]CeRePP, Paris, France, [48]AP-HP, Department of Urology, Tenon Hospital, GHU-Est, Paris, France, [49]UPMC Univ Paris 06, GRC n°5, ONCOTYPE-URO, Paris, France, [50]Genomic Epidemiology Group, German Cancer Research Center (DKFZ), Heidelberg, Germany, [51]Department of Epidemiology, Second Military Medical University, Shanghai, China, [52]Medical Oncology Department, Hospital Ramón y Cajal, Madrid, Spain, [53]Faculty of Medicine, School of Medicine, National Yang-Ming University, Taipei, Taiwan, [54]Division of Chest Medicine, Department of Internal Medicine, Taichung Veterans General Hospital, Taichung, Taiwan, [55]National Institute of Cancer Research, [56]Division of Biostatistics and Bioinformatics, Institute of Population Health Sciences and [57]Taiwan Lung Cancer Tissue/Specimen Information Resource Center, National Health Research Institutes, Zhunan, Taiwan, [58]Department of Abdominal Surgery and [59]State Key Laboratory of Molecular Oncology, Cancer Institute and Hospital, Chinese Academy of Medical Sciences and Peking Union Medical College, Beijing, China, [60]Genomics Research Center, Academia Sinica, Taipei, Taiwan, [61]Graduate

Institute of Epidemiology, College of Public Health, National Taiwan University, Taipei, Taiwan, [62]Cancer Center, China Medical University Hospital, Taipei, Taiwan, [63]Program in Molecular and Genetic Epidemiology, [64]Department of Nutrition and [65]Department of Epidemiology, Harvard School of Public Health, Boston, MA, USA, [66]Department of Internal Medicine, National Taiwan University Hospital and National Taiwan University College of Medicine, Taipei, Taiwan, [67]Department of Epidemiology and Public Health, Yong Loo Lin School of Medicine and [68]Saw Swee Hock School of Public Health, National University of Singapore, Singapore, [69]Chest Department, Taipei Veterans General Hospital, Taipei, Taiwan, [70]College of Medical Science and Technology, Taipei Medical University, Taiwan, [71]School of Public Health, University of California, Berkeley, CA, USA, [72]Cancer Prevention Institute of California, Fremont, CA, USA, [73]Inserm, Centre for Research in Epidemiology and Population Health (CESP), Villejuif, France, [74]Washington University School of Medicine, St. Louis, MO, USA, [75]Urologic Oncology, University of Colorado, Aurora, CO, USA, [76]Department of Public Health Sciences, School of Public Health, University of Alberta, Edmonton, AB, Canada T6G 2R3, [77]Department of Medicine, Channing Division of Network Medicine and [78]Brigham and Women's Hospital and Harvard Medical School, Boston, MA, USA, [79]Shanxi Cancer Hospital, Taiyuan, Shanxi, People's Republic of China, [80]Department of Urology, [81]Department of Epidemiology, [82]Department of Gastrointestinal Medical Oncology, [83]Department of Health Disparities Research, Division of OVP, Cancer Prevention and Population Sciences, and Center for Community-Engaged Translational Research, Duncan Family Institute and [84]Department of Epidemiology, Division of Cancer Prevention and Population Sciences, The University of Texas MD Anderson Cancer Center, Houston, TX, USA, [85]Service de Neurologie Mazarin, GH Pitie-Salpetriere, APHP, and UMR 975 INSERM-UPMC, CRICM, Paris, France, [86]Epidemiology Research Program, American Cancer Society, Atlanta, GA, USA, [87]Unit of Nutrition, Environment and Cancer, Cancer Epidemiology Research Program, Bellvitge Biomedical Research Institute, Catalan Institute of Oncology (ICO-IDIBELL), Barcelona, Spain, [88]Epidemiology and Genomics Research Program, Division of Cancer Control and Population Sciences, Bethesda, MD, USA, [89]Shanghai Cancer Institute, Shanghai, People's Republic of China, [90]Institute for Health Research, Kaiser Permanente, Denver, CO, USA, [91]UCL Cancer Institute, Huntley Street, London WC1E 6BT, UK, [92]Royal National Orthopaedic Hospital NHS Trust, Stanmore, Middlesex HA7 4LP, UK, [93]Department of Biostatistics, University of Kansas Medical Center, Kansas City, KS, USA, [94]Department of Medical Oncology, Dana-Farber Cancer Institute, Boston, MA, USA, [95]Channing Laboratory, Department of Medicine, [96]Division of Preventive Medicine, Department of Medicine and [97]Division of Aging, Department of Medicine, Brigham and Women's Hospital and Harvard Medical School, Boston, MA, USA, [98]Genomic Medicine Group, Galician Foundation of Genomic Medicine, Complejo Hospitalario Universitario de Santiago, Servicio Galego de Saude (SERGAS), Instituto de Investigación Sanitaria de Santiago (IDIS), Santiago de Compostela, Spain, [99]Samuel Lunenfeld Research Institute and [100]Lunenfeld-Tanenbaum Research Institute, Mount Sinai Hospital, Toronto, ON, Canada, [101]Department of Epidemiology, Shanghai Cancer Institute, Renji Hospital, Shanghai Jiaotaong University School of Medicine, Shanghai, China, [102]Division of Genetics and Epidemiology, Institute of Cancer Research, Sutton, UK, [103]Unidad de Investigación, Hospital Universitario de Canarias, La Laguna, Spain, [104]Nationwide Children's Hospital, and The Ohio State University Department of Pathology and Pediatrics, Columbus, OH, USA, [105]Massachusetts Veteran's Epidemiology, Research and Information Center, Geriatric Research Education and Clinical Center, Veterans Affairs Boston Healthcare System, Boston, MA, USA, [106]Information Management Services Inc., Calverton, MD, USA, [107]Cancer Epidemiology Centre, The Cancer Council Victoria & Centre for Molecular, Environmental, Genetic, and Analytic Epidemiology, The University of Melbourne, Victoria, Australia, [108]Division of Cancer Control and Population Sciences and [109]Laboratory of Human Carcinogenesis, Center for Cancer Research, National Cancer Institute, Bethesda, MD, USA, [110]Department of Oncology, [111]Department of Pathology and [112]Department of Medicine, The Sol Goldman Pancreatic Research Center, The Johns Hopkins University School of Medicine, Baltimore, MD, USA, [113]Unit of Nutrition, Environment and Cancer, Cancer Epidemiology Research Programme, Catalan Institute of Oncology (ICO), Barcelona, Spain, [114]Albert Einstein College of Medicine, The Children's Hospital at Montefiore, Bronx, NY, USA, [115]Department of Laboratory Medicine and Pathology, School of Medicine, University of Minnesota, Minneapolis, MN, USA, [116]Department of Urology, Washington University School of Medicine, St. Louis, MO, USA, [117]Department of Epidemiology, School of Public Health, China Medical University, Shenyang, China, [118]Laboratory of Experimental Oncology, Orthopaedic Rizzoli Institute, Bologna, Italy, [119]Department of Population Health, New York University Langone Medical Center and [120]Department of Environmental Medicine, New York University Langone Medical Center, New York University Cancer Institute, New York, NY, USA, [121]Johns Hopkins Bloomberg School of Public Health, Baltimore, MD, USA, [122]Division of Public Health Sciences, Fred Hutchinson Cancer Research Center, Seattle, WA, USA, [123]Institute of Environmental Medicine, Seoul National University Medical

Research Center, Seoul, Republic of Korea, [124]Department of Preventive Medicine and [125]Cancer Research Institute, Seoul National University College of Medicine, Seoul, Republic of Korea, [126]Department of Epidemiology and Population Health, Albert Einstein College of Medicine, Bronx, NY, USA, [127]Stanford Cancer Institute, Stanford University, Stanford, CA, USA, [128]Department of Epidemiology and Biostatistics, Cancer Center, Nanjing Medical University, Nanjing, China, [129]Broad Institute of Harvard and MIT, Cambridge, MA, USA, [130]Division of Epidemiology and Prevention, Aichi Cancer Center Research Institute, Nagoya, Japan, [131]Bioinformed, LLC, Gaithersburg, MD, USA, [132]Department of Oncology, Finsen Center, Rigshospitalet, Copenhagen, Denmark, [133]Unit of Survivorship, Danish Cancer Society Research Center, Copenhagen, Denmark, [134]Vermont Cancer Registry, Burlington, VT, USA, [135]Group Health Research Institute, Seattle, WA, USA, [136]Department of Thoracic and Cardiovascular Surgery, Seoul St Mary's Hospital, Seoul, South Korea, [137]School of Clinical Medicine, University of Cambridge, UK, [138]Department of Biochemistry and [139]Department of Cell Biology, School of Medicine, Kyungpook National University, Daegu, Republic of Korea, [140]Genomic Research Center for Lung and Breast/Ovarian Cancers, Korea University Anam Hospital, Seoul, Republic of Korea, [141]Department of Internal Medicine and Division of Brain and [142]Division of Oncology/Hematology, Department of Internal Medicine, Korea University College of Medicine, Seoul, Republic of Korea, [143]Lung and Esophageal Cancer Clinic, Chonnam National University Hwasun Hospital, Hwasun-eup, Republic of Korea, [144]Department of Epidemiology, Johns Hopkins Bloomberg School of Public Health, Baltimore, MD, USA, [145]Department of Medicine and [146]Department of Epidemiology and Biostatistics, Memorial Sloan-Kettering Cancer Center, New York, NY, USA, [147]Centre for Research in Environmental Epidemiology (CREAL), Barcelona, Spain, [148]IMIM (Hospital del Mar Medical Research Institute), Barcelona, Spain, [149]CIBER Epidemiología y Salud Pública (CIBERESP), Barcelona, Spain, [150]National School of Public Health, Athens, Greece, [151]Duke-NUS Graduate Medical School, Singapore, Singapore, [152]Division of Genome Biology, National Cancer Center Research Institute, Tokyo, Japan, [153]Epidemiology Program, University of Hawaii Cancer Center, Honolulu, HI, USA, [154]Fondazione IRCCS Istituto Nazionale dei Tumori, Milano, Italy, [155]Department of Respiratory Medicine, Mitsui Memorial Hospital, Tokyo, Japan, [156]Department of Pediatric Oncology, A.Y. Ankara Oncology Training and Research Hospital, Yenimahalle- Ankara, Turkey, [157]Centre National de Genotypage, IG/CEA, Evry Cedex, France, [158]Centre d'Étude du Polymorphism Humain (CEPH), Paris, France, [159]Texas Children's Cancer and Hematology Centers, [160]Scott Department of Urology and [161]Dan L. Duncan Center, Baylor College of Medicine, Houston, TX, USA, [162]Department of Pediatrics, University Clinic of Navarra, Universidad de Navarra, Pamplona, Spain, [163]Department of Cancer Epidemiology and Prevention, Maria Sklodowska-Curie Cancer Center and Institute of Oncology, Warsaw, Poland, [164]Human Genetics Division, Genome Institute of Singapore, Singapore, [165]School of Life Sciences, Anhui Medical University, Hefei, China, [166]Ministry of Education Key Laboratory of Contemporary Anthropology, School of Life Sciences, Fudan University, Shanghai, China, [167]State Key Laboratory of Genetic Engineering, School of Life Sciences, Fudan University, Shanghai, China, [168]Centro Nacional de Investigaciones Oncologicas, Melchor Fernández Almagro, 3, Madrid E-28029, Spain, [169]National Institute for Health and Welfare, Helsinki, Finland, [170]Lucile Packard Children's Hospital, Stanford University, Palo Alto, CA, USA, [171]Department of Cardiac, Thoracic and Vascular Sciences, University of Padova, Padua, Italy, [172]Department of Preventive Medicine, Kyushu University Faculty of Medical Scicence, Fukuoka, Japan, [173]Department of Health Sciences Research, Mayo Clinic, Rochester, MN, USA, [174]Key Laboratory for Environment and Health, School of Public Health, Tongji Medical College, Huazhong University of Sciences and Technology, Wuhan, China, [175]Department of Epidemiology, Division of Biology and Medicine, Brown University, Providence, RI, USA, [176]Health Sciences Research Institute, University of Warwick, Coventry, UK, [177]Complex Traits Genetics Team and [178]Division of Breast Cancer Research, Institute of Cancer Research, London, UK, [179]Dipartimento di Medicina Clinica e Chirurgia, Federico II University, Naples, Italy, [180]Lung Cancer Center, Kyungpook National University Medical Center, Daegu, Republic of Korea, [181]Julius Center for Health Sciences and Primary Care, University Medical Center, Utrecht, Utrecht, The Netherlands, [182]Department of Epidemiology and Biostatistics, School of Public Health, Imperial College London, London, UK, [183]Department of Genomics of Common Disease, School of Public Health, Imperial College London, London, UK, [184]Nofer Institute of Occupational Medicine, Lodz, Poland, [185]Department of Epidemiology, Cancer Institute (Hospital), Chinese Academy of Medical Sciences, Beijing, People's Republic of China, [186]Yale School of Public Health, New Haven, CT, USA, [187]Department of Internal Medicine, Inha University College of Medicine, Incheon, Korea, [188]Karmanos Cancer Institute and Department of Oncology and [189]Karmanos Cancer Institute and Department of Family Medicine and Public Health Sciences, Wayne State University School of Medicine, Detroit, MI, USA, [190]Maine Cancer Registry, Augusta, ME, USA, [191]Centre for Research in Occupational Health, Universitat Pompeu Fabra, Barcelona, Spain, [192]CIBER of Epidemiology and Public Health (CIBERESP), [193]Department of Biostatistics, MD

Anderson Cancer Center, Houston, TX, USA, [194]Nutritional Epidemiology Unit, Fondazione IRCCS Istituto Nazionale dei Tumori, Milan, Italy, [195]Department of Surgery, Division of Cardiothoracic Surgery, Queen Mary Hospital, Hong Kong, China, [196]Department of Neurosurgery, University of Bonn Medical Center, Bonn, Germany, [197]Department of Pathology, The University of Melbourne, Melbourne, VIC, Australia, [198]University of Minnesota, Minneapolis, MN, USA, [199]Department of Internal Medicine, National Cheng Kung University Hospital and College of Medicine, Tainan, Taiwan, [200]Instituto Universitario de Oncología, Universidad de Oviedo, Oviedo, Spain, [201]Sir Peter MacCallum Department of Oncology, University of Melbourne, St Andrew's Place, East Melbourne, VIC, Australia, [202]Danish Cancer Society Research Center, Copenhagen, Denmark, [203]Department of Pulmonary Medicine, Chang Gung Memorial Hospital, Chiayi, Taiwan, [204]Cancer Registry Associazione Iblea Ricerca Epidemiologica, Onlus and Asp Ragusa, Ragusa Italy, [205]Kaiser Permanente Northern California, Oakland, CA, USA, [206]Division of Environmental Epidemiology, Institute for Risk Assessment Sciences (IRAS), Utrecht University, Utrecht, The Netherlands, [207]Imperial College, London, UK, [208]Human Genetics Foundation (HuGeF), Torino Italy, [209]National Research Centre for the Working Environment, Copenhagen, Denmark, [210]National Food Institute, Technical University of Denmark, Soborg, Denmark, [211]Department of Biochemistry and Centre for Genomic Sciences, LKS Faculty of Medicine, The University of Hong Kong, Hong Kong SAR, China, [212]Department of Pathology and [213]School of Public Health, Li Ka Shing (LKS) Faculty of Medicine, The University of Hong Kong, Hong Kong, China, [214]Division of Cancer Etiology, Department of Population Sciences, City of Hope and the Beckman Research Institute, Duarte, CA, USA, [215]Department of Community Medicine, Faculty of Health Sciences, University of Tromsø, The Arctic University of Norway, Tromsø, Norway, [216]Department of Research, Cancer Registry of Norway, Oslo, Norway, [217]Samfundet Folkhälsan, Helsinki, Finland, [218]University of California San Francisco, San Francisco, CA, USA, [219]Guangdong Lung Cancer Institute, Medical Research Center and Cancer Center of Guangdong General Hospital, Guangdong Academy of Medical Sciences, Guangzhou, China, [220]Department of Pathology and Molecular Diagnostics, Aichi Cancer Center Hospital and [221]University of Pittsburgh Cancer Institute, Pittsburgh, PA, USA and [222]Department of Environmental Health, Korea National Open University, Seoul, Republic of Korea

Received April 22, 2014; Revised June 30, 2014; Accepted July 8, 2014

Genome-wide association studies (GWAS) have mapped risk alleles for at least 10 distinct cancers to a small region of 63 000 bp on chromosome 5p15.33. This region harbors the *TERT* and *CLPTM1L* genes; the former encodes the catalytic subunit of telomerase reverse transcriptase and the latter may play a role in apoptosis. To investigate further the genetic architecture of common susceptibility alleles in this region, we conducted an agnostic subset-based meta-analysis (association analysis based on subsets) across six distinct cancers in 34 248 cases and 45 036 controls. Based on sequential conditional analysis, we identified as many as six independent risk loci marked by common single-nucleotide polymorphisms: five in the *TERT* gene (Region 1: rs7726159, $P = 2.10 \times 10^{-39}$; Region 3: rs2853677, $P = 3.30 \times 10^{-36}$ and $P_{Conditional} = 2.36 \times 10^{-8}$; Region 4: rs2736098, $P = 3.87 \times 10^{-12}$ and $P_{Conditional} = 5.19 \times 10^{-6}$, Region 5: rs13172201, $P = 0.041$ and $P_{Conditional} = 2.04 \times 10^{-6}$; and Region 6: rs10069690, $P = 7.49 \times 10^{-15}$ and $P_{Conditional} = 5.35 \times 10^{-7}$) and one in the neighboring *CLPTM1L* gene (Region 2: rs451360; $P = 1.90 \times 10^{-18}$ and $P_{Conditional} = 7.06 \times 10^{-16}$). Between three and five cancers mapped to each independent locus with both risk-enhancing and protective effects. Allele-specific effects on DNA methylation were seen for a subset of risk loci, indicating that methylation and subsequent effects on gene expression may contribute to the biology of risk variants on 5p15.33. Our results provide strong support for extensive pleiotropy across this region of 5p15.33, to an extent not previously observed in other cancer susceptibility loci.

INTRODUCTION

Genome-wide association studies (GWAS) have identified independent susceptibility loci in a region on chromosome 5p15.33 that are associated with at least 10 distinct cancers. The published findings include bladder (1), estrogen-negative breast (2), glioma (3), lung (4–7), ovary (8), melanoma (9), non-melanoma skin (10,11), pancreas (12), prostate (13) and testicular germ cell cancer (14). This degree of pleiotropy for common susceptibility alleles suggests that the region harbors an important set of elements that could influence multiple cancers. It has been observed previously that one allele may be protective for one cancer while conferring susceptibility to another (15). These independent loci map to ~63,000 bp of 5p15.33 that harbors two plausible candidate genes: *TERT*, which encodes the catalytic subunit of telomerase reverse transcriptase (16) and *CLPTM1L*, which encodes the cleft lip and palate-associated transmembrane 1 like protein (also called cisplatin resistance

related protein, CRR9). *CLPTM1L* appears to play a role in apoptosis and cytokinesis, is overexpressed in both lung and pancreatic cancer and is required for KRAS driven lung cancer (17–21). Germline mutations in *TERT* can cause dyskeratosis congenita (DC), a cancer-prone inherited bone marrow failure syndrome caused by aberrant telomere biology (22). Clinically related telomere biology disorders, including idiopathic pulmonary fibrosis and acquired aplastic anemia, can also be caused by germline *TERT* mutations (reviewed in 23).

To investigate the genetic architecture of common susceptibility alleles across this region of 5p15.33 in multiple cancer sites, we utilized a recently developed method called association analysis based on subsets (ASSET) that combines association signals for an SNP across multiple traits by exploring subsets of studies for true association signals in the same, or the opposite direction, while accounting for the multiple testing required (24). The method has been shown to be more powerful than the standard meta-analysis in the presence of heterogeneity, where the effect of a specific SNP might be restricted to only a subset of traits or/and may have different directions of associations for different traits (24).

RESULTS

In this study, we conducted a cross-cancer fine-mapping analysis of a region on chromosome 5p15.33 known to be associated with multiple cancer sites. We imputed each dataset across a 2 Mb window (chr5: 250 000–2 250 000; hg19) using the 1000 Genomes (1000G) and DCEG reference datasets (25,26) and applied a subset-based meta-analysis method (ASSET) (24) to combine results across six cancers (11 studies) (see Materials and Methods for details). This method has been shown to improve power and interpretation when compared with other traditional methods for the analysis of heterogeneous traits (24).

In the first analysis, we focused on six distinct cancer sites in which 5p15.33 had previously been reported and had a nominal *P*-value in our dataset ('Tier-I studies' scans, see Materials and Methods). We performed the analysis across all studies (77% European, 7% African American and 16% Asian ancestry, ALL scans), and, because the majority of studies and subjects were of European ancestry, we conducted parallel analyses in this group only (EUR scans). Bonferroni correction was used to assess significance, using the threshold at 1.3×10^{-5}, based on the number of single-nucleotide polymorphisms (SNPs) analyzed across the region ($n = 1924$) and the two analyses performed (ALL or EUR scans) (see Materials and Methods). In the second analysis, we examined the regions identified above in eight cancers in which 5p15.33 had not been reported in the literature (NHGRI Catalog of Published GWAS studies: http://www.genome.gov/gwastudies/), or did not show a nominal *P*-value in our dataset ('Tier-II studies').

Application of ASSET by sequential conditioning of associated SNPs revealed up to six independent loci on 5p15.33, each influencing risk of multiple cancers (Fig. 1, Table 1; Supplementary Material, Table S1). In the primary analysis of all subjects, we performed the ASSET meta-analysis based on unconditional association results from each of the six cancer scans (11 studies). This identified rs7726159 with the lowest *P*-value ($P = 2.10 \times 10^{-39}$), thus marking Region 1. The next four SNPs, ranked by *P*-values, were highly correlated with the index SNP based on 1000G CEU data: rs7725218 ($P = 2.98 \times 10^{-39}$, pair-wise $r^2 = 0.90$), rs4449583 ($P = 3.37 \times 10^{-39}$, pair-wise $r^2 = 1.0$), rs7705526 ($P = 1.00 \times 10^{-36}$, pair-wise $r^2 = 0.74$) and rs4975538 ($P = 4.11 \times 10^{-32}$, pair-wise $r^2 = 0.76$). These five SNPs reside in the second and third intron of the *TERT* gene and are common, with effect allele frequencies ranging between 0.18 and 0.43 in African (AFR), 0.35–0.37 in Asian (ASN) and 0.32–0.38 in European (EUR) populations, each estimated in the 1000G project (Supplementary Material, Table S2). A search for surrogates using an r^2 threshold of 0.7 across a 1 Mb window centered on the index SNP did not identify additional highly correlated SNPs. The effect allele (A) of rs7726159 was positively associated with glioma (Glioma Scan) and lung cancer (Asian Lung) ($P = 4.38 \times 10^{-36}$, $OR_{Combined} = 1.47$; 95% CI = 1.38–1.56), but negatively associated with testicular cancer (TGCT NCI), prostate cancer (Pegasus and AdvPrCa) and pancreatic cancer (ChinaPC) ($P = 5.07 \times 10^{-6}$, $OR_{Combined} = 0.85$; 95% CI = 0.80–0.91) (Fig. 2A).

The most significant SNP after conditioning on rs7726159 was rs451360 ($P = 1.90 \times 10^{-18}$; $P_{Conditional} = 7.06 \times 10^{-16}$), residing in intron 13 of *CLPTM1L* and marking Region 2 (Fig. 1, Table 1). Six SNPs were correlated with rs451360 with an $r^2 > 0.7$, all located within 500 kb of this SNP and spanning the entire length of *CLPTM1L*: rs380145, rs13170453, rs37004, rs36115365, rs35953391 and rs7446461. This effect allele (rs451360-A) was positively associated with pancreatic cancer (PanScan) and testicular cancer (TGCT NCI) ($P = 4.38 \times 10^{-13}$, $OR_{Combined} = 1.34$; 95% CI = 1.24–1.45), but negatively associated with lung cancer (AA Lung, Asian Lung and Eur Lung) ($P = 9.50 \times 10^{-8}$, $OR_{Combined} = 0.85$; 95% CI = 0.80–0.90) (Fig. 2B). Although large differences were seen in the effect allele frequencies across the 1000G continental populations, 0.02–0.03 in AFR, 0.12 in ASN and 0.17–0.24 in EUR (Supplementary Material, Table S2), the signal was still sufficiently strong to be detected, particularly in African and Asian lung studies, suggesting its importance in lung cancer etiology.

In our sequential conditional analysis, rs2853677 (located in the first intron of *TERT*) was the most significant SNP after conditioning on both rs7726159 and rs451360, thus marking Region 3 ($P = 3.30 \times 10^{-36}$; $P_{Conditional} = 2.36 \times 10^{-8}$) (Fig. 1, Table 1). No additional SNPs with an $r^2 > 0.7$ were located within 500 kb of this SNP, which has relatively low LD with both rs7726159 ($r^2 = 0.13$) and rs451360 ($r^2 = 0.12$) in 1000G CEU data. Region 3 (rs2853677-A) was positively associated with testicular cancer (TGCT NCI) and pancreatic cancer (PanScan and ChinaPC) ($P = 1.36 \times 10^{-7}$, $OR_{Combined} = 1.22$; 95% CI = 1.13–1.31), but negatively associated with lung cancer (Asian Lung and AA Lung) and glioma (Glioma scan) ($P = 2.79 \times 10^{-31}$, $OR_{Combined} = 0.73$; 95% CI = 0.70–0.77) (Fig. 2C). The effect allele frequency for rs2853677 was consistent across the three continental 1000G populations corresponding to the studies included in this analysis: 0.60 in EUR, 0.67 in ASN and 0.71 in AFR (Supplementary Material, Table S2).

A conditional analysis based on the three SNPs above (rs7726159, rs451360 and rs2853677) yielded Region 4, marked by rs2736098 ($P = 3.87 \times 10^{-12}$; $P_{Conditional} = 5.19 \times 10^{-6}$), a synonymous variant (A305A) in the second exon of *TERT* (Fig. 1, Table 1). Three additional SNPs with an

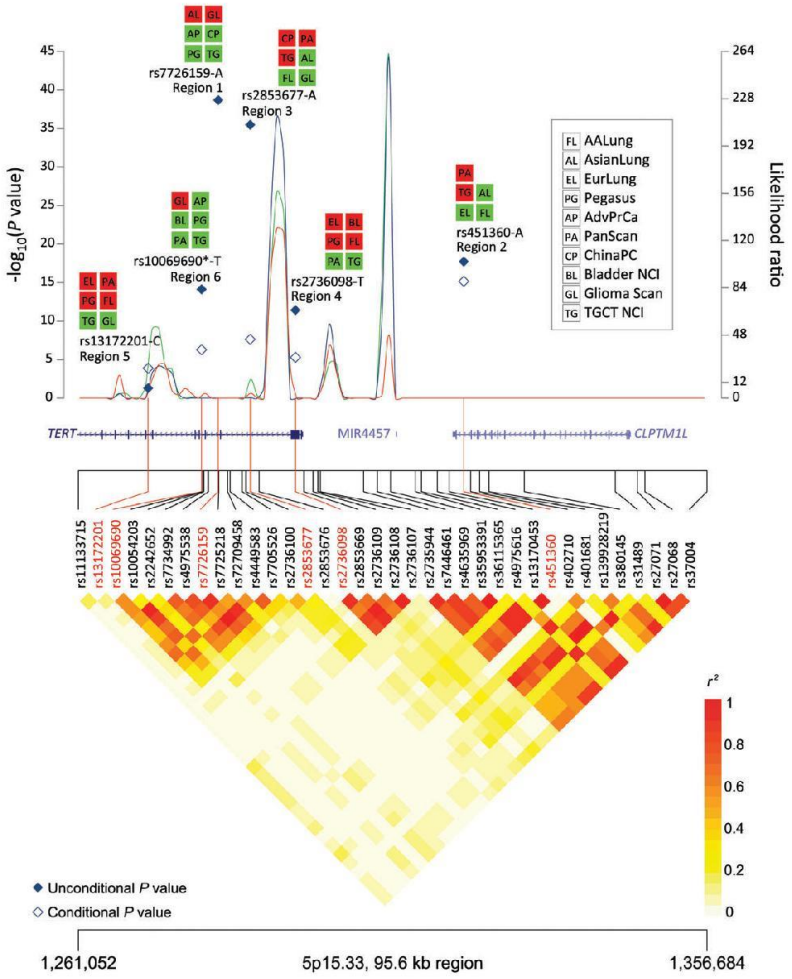

Figure 1. Sequential conditional analyses and ASSET meta-analyses identified up to six independent signals for the *TERT-CLPTM1L* region on chromosome 5p15.33. SNPs marking each region are plotted in the upper panel with two *P*-values (solid diamonds correspond to an unconditional test and open diamonds correspond to a conditional test) on a negative log scale (left *y*-axis) against genomic coordinates (*x*-axis, hg19). Cancers from different GWAS scans (acronyms detailed in box in top panel) that are associated within each region in the subset meta-analysis are listed (red, positively associated; green, negatively associated) from the unconditional ASSET meta-analysis. Effect alleles are shown next to SNP identifiers. Recombination hotspots (curved lines, top panel) were inferred from three populations from the DCEG Imputation Reference Set version 1 (red, CEU; green, ASN; blue, YRI) as the likelihood ratio statistics (right *y*-axis). Also shown are the gene structures for *TERT*, *MIR4457* and *CLPTM1L* (middle panel), and LD heat map based on r^2 using the 1000 Genomes CEU population (lower panel). Results are shown for the ALL analysis except the region marked by rs10069690 (top panel) and labeled with a '*' that was identified in the European ancestry-only analysis (EUR).

Table 1. Association results for SNPs on chromosome 5p15.33 with the risk of cancer

SNP	Gene	Region	Position	Unconditional OR (95% CI) Positively associated	Negatively associated	Unconditional *P*-value	Significant phenotype clusters Positively associated	Negatively associated	Conditional OR (95% CI) Positively associated	Negatively associated	Conditional *P*-value
ALL											
rs7726159	*TERT*	1	1282319	1.47 (1.38–1.56)	0.85 (0.80–0.91)	2.10×10^{-39}	AsianLung, Glioma Scan	TGCT NCI, Pegasus, AdvPrCa, ChinaPC			
rs451360	*CLPTM1L*	2	1319680	1.34 (1.24–1.45)	0.85 (0.80–0.90)	1.90×10^{-18}	PanScan, TGCT NCI	EurLung, AfrAmLung, AsianLung	1.33 (1.23–1.44)	0.86 (0.81–0.92)	7.06×10^{-16}
rs2853677	*TERT*	3	1287194	1.22 (1.13–1.31)	0.73 (0.70–0.77)	3.30×10^{-36}	TGCT NCI, PanScan, ChinaPC	AsianLung[a], Glioma Scan, AfrAmLung	1.11 (0.94–1.30)	0.80 (0.74–0.86)	2.36×10^{-8}
rs2736098	*TERT*	4	1294086	1.15 (1.10–1.21)	0.81 (0.74–0.89)	3.87×10^{-12}	AfrAmLung, Pegasus, EurLung[a], Bladder NCI	PanScan, TGCT NCI[a]	1.18 (1.10–1.25)	0.94 (0.67–1.31)	5.19×10^{-6}
rs13172201	*TERT*	5	1271661	1.06 (0.80–1.41)	0.84 (0.73–0.96)	5.00×10^{-2}	EurLung, Pegasus[a], PanScan, AfrAmLung[a]	TGCT NCI, Glioma Scan	1.13 (1.03–1.23)	0.81 (0.70–0.92)	1.31×10^{-4}
EUR											
rs4449583	*TERT*	1	1284135	1.50 (1.35–1.68)	0.89 (0.83–0.94)	1.02×10^{-15}	Glioma Scan	TGCT NCI, Pegasus, AdvPrCa, PanScan			
rs13170453	*CLPTM1L*	2	1317481	1.34 (1.24–1.45)	0.87 (0.80–0.95)	6.69×10^{-15}	PanScan, TGCT NCI	EurLung	1.33 (1.22–1.44)	0.86 (0.80–0.93)	6.67×10^{-14}
rs10069690	*TERT*	6	1279790	1.48 (1.31–1.67)	0.87 (0.83–0.92)	7.49×10^{-15}	Glioma Scan[a]	AdvPrCa, TGCT NCI[a], PanScan[a], Bladder NCI, Pegasus[a]	NA	0.77 (0.69–0.85)	5.35×10^{-7}
rs13172201	*TERT*	5	1271661	1.07 (0.88–1.29)	0.84 (0.73–0.96)	4.08×10^{-2}	EurLung, Pegasus[a], PanScan	TGCT NCI, Glioma Scan	1.13 (1.04–1.22)	0.82 (0.75–0.90)	2.04×10^{-6}
rs2736098	*TERT*	4	1294086	1.14 (1.08–1.20)	0.81 (0.74–0.89)	5.73×10^{-10}	Pegasus, EurLung[a], Bladder NCI[a]	PanScan, TGCT NCI	1.23 (1.11–1.35)	0.88 (0.75–1.02)	6.31×10^{-5}

The results from the imputation and subset-based ASSET meta-analysis is shown for the 'ALL' scans that include 11 GWAS scans performed in subjects of European, Asian and African American ancestry; and for the 'EUR' scans that include eight scans performed in subjects of European ancestry. Scan acronyms are detailed in Materials and Methods. Listed are SNPs that mark each of the regions identified, gene, genomic location, unconditional and conditional *P*-values and GWAS scans that were positively or negatively associated with the minor allele for each SNP/region. Note that different highly correlated SNPs may mark the same region in the 'ALL' vs. the 'EUR' analysis (Regions 1 and 2). NA indicates that no scan was associated with a particular region.
[a]Cancer sites that were no longer significant in the conditional analysis.

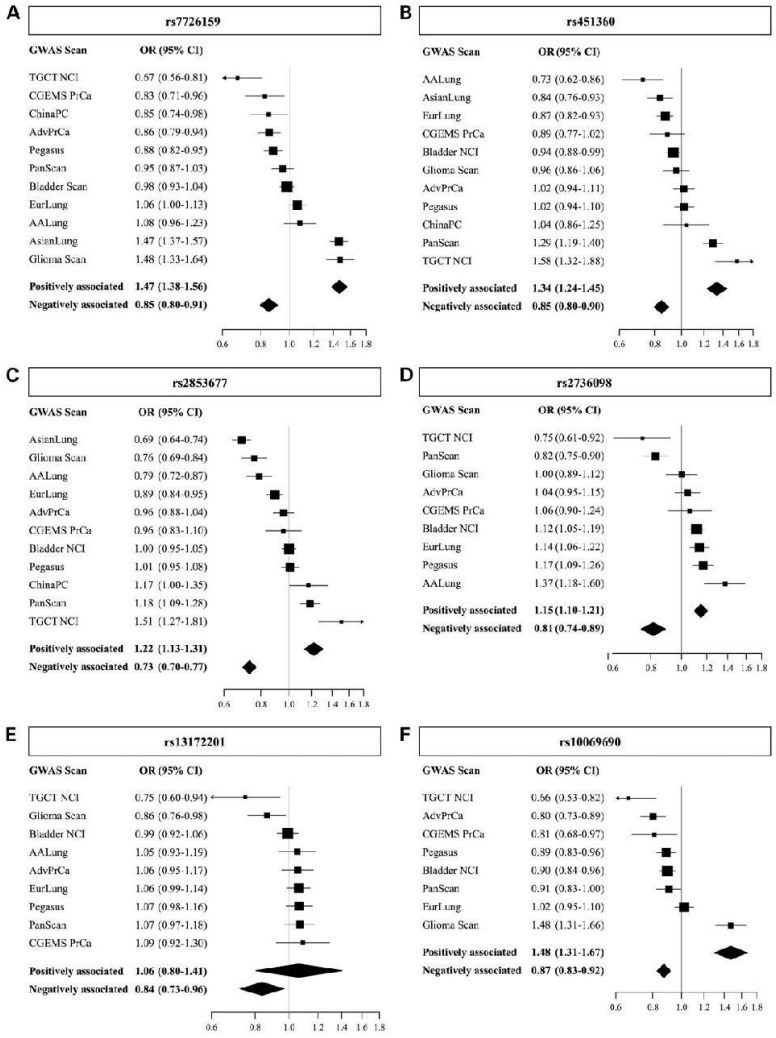

Figure 2. (**A**–**F**) Forest plots for individual risk loci on chr5p15.33 for the unconditional ASSET meta-analysis. For each cancer/GWAS scan, OR and 95% CI were listed and plotted along each line as per the unconditional association analysis. A vertical line of OR = 1 indicates the null. Two summary lines list ORs for the positively or negatively associated subsets as estimated by the ASSET program. (A) rs7726159, (B) rs451360, (C) rs2853677, (D) rs2736098, (E) rs13172201 and (F) rs10069690 in the analysis of European-ancestry studies only. Forest plots for the conditional analyses are shown in Supplementary Material, Figure S1A–E.

$r^2 > 0.7$ were located within 500 kb of this SNP: rs2853669, rs2736108 and rs2736107, all in the promoter of *TERT*, from ~200 to 2700 bp upstream of the transcriptional start site. This region (rs2736098-T) was positively associated with lung cancer (Eur Lung and AA Lung), prostate cancer (Pegasus) and bladder cancer (Bladder NCI) ($P = 2.58 \times 10^{-8}$, $OR_{Combined} = 1.15$; 95% CI = 1.10–1.21), and negatively associated with testicular cancer (TGCT NCI) and pancreatic cancer (PanScan) ($P = 4.89 \times 10^{-6}$, $OR_{Combined} = 0.81$; 95% CI = 0.74–0.89) (Fig. 2D). The effect allele frequencies displayed a wide range across the three continental populations in 1000G, interestingly with the lowest frequency in the most ancient population, 0.06–0.08 (AFR), whereas the other two populations were comparably high: 0.23–0.29 (EUR) and 0.22–0.33 (ASN) (Supplementary Material, Table S2).

An additional suggestive region (Region 5) marked by rs13172201 ($P = 0.05$; $P_{Conditional} = 1.31 \times 10^{-4}$) was determined by our sequential conditional analyses (Fig. 1, Table 1), unmasked mainly due to conditioning on rs7726159 (Region 1). The risk alleles for rs13172201 and rs7726159 were negatively correlated ($r = -0.27$, based on 1000G CEU data) and, in an exploratory analysis of rs13172201 in the Eur Lung scan, this SNP appeared to have a stronger association in rs7726159 CC carriers ($P = 7.0 \times 10^{-4}$, OR = 1.21 95% CI = 1.08–1.35) when compared with rs7726159 AC/AA carriers ($P = 0.10$, OR = 1.12 95% CI = 0.98–1.27).

Region 5 (rs13172201-C) was positively associated with lung cancer (Eur Lung and AA Lung), prostate cancer (Pegasus) and pancreatic cancer (PanScan) and negatively associated with testicular cancer (TGCT NCI) and glioma (Glioma scan) (Fig. 2E). The effect allele for rs13172201, the sentinel SNP in Region 5, was the minor allele in European (0.26 in EUR) and African (0.39 in AFR) populations, while it has become the major allele in Asians (0.85 in ASN).

In an analysis restricted to studies of European ancestry (EUR scans), we noted strong associations for Regions 1, 2, 4 and 5 (Table 1) but not Region 3 (marked by rs2853677). The conditional *P*-value for Region 5, suggestive in the analysis based on all ethnic groups, improved in this subset and surpassed the threshold of 1.3×10^{-5} (rs13172201: $P = 0.041$; $P_{Conditional} = 2.04 \times 10^{-6}$). An additional region, Region 6, marked by rs10069690 ($P = 7.49 \times 10^{-15}$; $P_{Conditional} = 5.35 \times 10^{-7}$) in intron 4 of *TERT* was identified in the European ancestry-only analysis (Fig. 1, Table 1). The significance for this region did not reach our Bonferroni-corrected *P*-value threshold in the analysis of all studies ($P = 5.4 \times 10^{-4}$ after conditioning on rs7726159, rs451360, rs2853677 and rs2736098). As Regions 3 and 6 were located between the same two recombination hotspots (Fig. 1), we assessed correlation in 1000G CEU subjects and noted virtually no LD (rs10069690, rs2853677, $r^2 = 0.0052$), thus supporting the notion that they are independent signals. Low LD existed for these two SNPs in the 1000G YRI ($r^2 = 0.098$) and CHB/JPT ($r^2 = 0.048$) populations (Supplementary Material, Table S3). Region 6 (rs10069690-T) was positively associated with glioma (Glioma scan) ($P = 4.07 \times 10^{-10}$, $OR_{Combined} = 1.48$; 95% CI = 1.31–1.67) and negatively associated with testicular (TGCT NCI), prostate (Pegasus and AdvPrCa), bladder (Bladder NCI) and pancreatic cancer (PanScan) ($P = 4.95 \times 10^{-7}$, $OR_{Combined} = 0.87$; 95% CI = 0.83–0.92) (Fig. 2F). Highly correlated SNPs ($r^2 > 0.7$) were not observed within 500 kb of rs10069690. Notably, the *P*-value for rs10069690 in the Advanced Prostate cancer scan improved from 1.64×10^{-5} to 2.03×10^{-10} after conditioning on Region 1. The correlation between rs10069690 and rs7726159 (Region 1) is $r^2 = 0.13$ in the 1000G CEU, $r^2 = 0.30$ in YRI and $r^2 = 0.42$ in CHB/JPT populations (Supplementary Material, Table S3). SNP rs10069690 was nominally significant in the other two prostate cancer scans with unconditional *P*-values of 0.003 (Pegasus) and 0.02 (CGEMS PrCa) but was not significant after conditioning on the first region in these scans ($P = 0.36$ in Pegasus, $P = 0.078$ in CGEMS PrCa).

For the six signals noted, Regions 1, 3 and 6 are flanked by two recombination hotspots that separate them from Region 5 on the telomeric side and from Region 4 on the centromeric side. Recombination hotspots also separate Regions 2 and 4 (Fig. 1). The LD between SNPs in loci 1, 3 and 6 was low to moderate ($r^2 = 0.0052$, 0.131 and 0.449 in 1000G CEU, $r^2 = 0.0981$, 0.298 and 0.0765 in YRI and $r^2 = 0.0484$, 0.415 and 0.341 in CHB/JPT); however, the conditional analyses supported the presence of three signals bounded by strong recombination hotspots on either side. Region 5 is the most telomeric one and separated from the rest by a strong recombination hotspot. Supplementary Material, Table S1 shows *P*-values for the six regions along each step of the sequential conditional analysis to reflect the change in significance in the analysis.

We also assessed the associations for each of the regions in the 'Tier-II studies' comprising nine GWAS datasets across eight cancers, including 11 385 cases and 18 322 controls. None of the regions showed significant association (data not shown).

In addition to characterizing independent signals in the *TERT-CLPTM1L* region, we have fine-mapped previously reported signals. For pancreatic cancer, the reported GWAS SNP rs401681 had a *P*-value of 3.7×10^{-7} and an OR of 1.19 (12). After imputation, an improved *P*-value was seen for rs451360 (marking Region 2) ($P = 2.0 \times 10^{-10}$; OR = 1.29). After conditioning on rs451360, the *P*-value for rs401681 was no longer significant ($P = 0.1$). The LD between these two SNPs is moderate ($r^2 = 0.35$). For glioma, the GWAS SNP rs2736100 had a *P*-value of 8.49×10^{-9} and OR of 1.08 in the Glioma scan (27). The best imputed SNP rs449583 ($r^2 = 1$ with rs7726159, marking Region 1) showed a much improved *P*-value of 4.1×10^{-14} with an OR of 1.50, and the *P*-value of rs2736100 was no longer significant after conditioning on rs449583 ($P = 0.64$). The LD between these two SNPs was moderate ($r^2 = 0.39$).

Bioinformatic analyses using public data bases (ENCODE and TCGA) were performed to investigate the possible function of SNPs that mark each of the six regions as regulators of expression of *TERT*, or *CLPTM1L*, as well as other genes. Based on ENCODE data, the strongest evidence for putative regulatory functions was seen for SNPs in Regions 1 (rs7725218 and rs4975538), 2 (rs36115365 and rs380145), 4 (rs2736108 and rs2853669) and 5 (rs13172201) with evidence of an open chromatin conformation, regulatory histone modification marks and transcription factor binding in multiple cell types such as prostate, pancreas, breast, lung and brain (Supplementary Material, Table S2).

We next examined the TCGA datasets for expression (eQTL) and methylation (meQTL) quantitative trait loci for lung adenocarcinoma (LUAD), prostate adenocarcinoma (PRAD) and

glioblastoma multiforme (GBM). We did not observe significant eQTLs ($P > 0.41$, data not shown) but noted multiple meQTLs in LUAD and PRAD tumor samples (Supplementary Material, Tables S5 and S6). Methylation at a subset of CpG probes with meQTLs correlated with expression of *TERT* and/or *CLPTM1L*, including two for Region 4 in TCGA LUAD samples (cg26209169: $\beta = -0.47$, $P = 1.18 \times 10^{-5}$; cg11624060: $\beta = -0.36$, $P = 0.001$). These CpGs are located ~1800 bp downstream of *CLPTM1L* (227 bp apart), overlap with key transcription factor binding sites (e.g. TCF3, TCF4, HNF3A, MAX, RUNX3/AML2, ATF-2 and USF1/USF2) and active histone modification marks from ENCODE, and are negatively correlated with expression of *TERT* and *CLPTM1L* (Supplementary Material, Table S5 and Fig. S2). Replication was seen in normal lung samples (cg26209169 and Region 4, $\beta = -0.650$, $P = 5.17 \times 10^{-5}$; cg11624060 and Region 4, $\beta = -0.493$, $P = 0.0027$) from EAGLE (28). The most significant meQTLs in TCGA PRAD samples were seen for Region 1 (cg03935379: $\beta = -1.06$, $P = 8.47 \times 10^{-15}$; cg06531176: $\beta = -1.18$, $P = 2.61 \times 10^{-15}$). These replicated in EAGLE ($P = 5.93 \times 10^{-8}$ and $P = 0.002$, respectively), did not correlate with expression of *TERT* or *CLPTM1L*, and were both located within exon 3 of *TERT* (Supplementary Material, Table S6).

Analysis of TCGA data also revealed increased expression of *TERT* and *CLPTM1L* in tumors compared with normal tissues for lung and prostate cancer (on average 1.29- to 2.02-fold change for paired samples). Copy number differences were more evident in lung tumors (average number of copies was 2.02 in normal and 2.54 in tumors for 51 paired samples, $P = 1.10 \times 10^{-7}$) (Supplementary Material, Fig. S3).

DISCUSSION

Chr5p15.33 harbors a unique cancer susceptibility region that contains at least two plausible candidate genes: *TERT* and *CLTPM1L*. Through a subset-based meta-analysis of GWAS data drawn from six different cancers from three continental populations, we have characterized up to six independent, common, susceptibility alleles, all with evidence of both risk-enhancing and protective effects, differing by cancer type.

TERT encodes the catalytic subunit of the telomerase reverse transcriptase, which, in combination with an RNA template (*TERC*), adds nucleotide repeats to chromosome ends (29). Although telomerase is active in germ cells and in early development, it remains repressed in most adult tissues. Telomeres shorten with each cell division and when they reach a critically short length, cellular senescence or apoptosis is triggered. Cancer cells can continue to divide despite critically short telomeres, by upregulating telomerase or by alternative lengthening of telomeres (16,30,31). While studies investigating the relationship between surrogate tissue (i.e. buccal or blood cell DNA) telomere length and cancer risk have been contradictory, larger prospective studies have not reported an association for risk but only survivorship (32–35). Heritability estimates of telomere length in twin studies suggest a significant genetic contribution, between 36 and 78% (36,37). GWAS SNPs on 5p15.33 have been associated with telomere length implying that *TERT* may indeed be the gene targeted by at least some risk variants in this region (38–40). In addition, germline *TERT* promoter mutations have been identified in familial melanoma as well as somatic mutations in multiple cancers (41,42).

The most commonly reported SNP in the *TERT* gene, rs2736100, was first reported in several GWAS: glioma (3,43), lung cancer in European and Asians (7,44–46) and testicular cancer (14). We have fine-mapped this locus (Region 1) to a set of five correlated SNPs in the second and third intron of *TERT* (marked by rs7726159). In addition to the cancers listed above, we noted novel contributions to this locus by prostate and pancreatic cancer. Fine-mapping efforts in lung (47) and ovarian cancer (48) have reported the same SNP. Region 3 (rs2853677), located in the first intron of *TERT*, has been associated with glioma in Chinese subjects (49) and lung cancer in Japanese subjects (50), in agreement with the strong contribution to this region seen in our analysis by scans performed in individuals of Asian ancestry. In addition to lung cancer and glioma, we noted novel associations for Region 3 with pancreatic and testicular cancer. Region 4 was marked by a synonymous SNP (rs2736098) located in the second exon of *TERT*, with three additional highly correlated SNPs in the promoter region. This region has been reported via fine-mapping in lung, bladder, prostate, ovarian and breast cancer, and shown to influence *TERT* promoter activity (8). Novel contributions to Region 4 were noted for pancreatic and testicular cancer.

In our analysis, we uncovered a new susceptibility locus, Region 5 (marked by rs13172201, Fig. 1), which surpassed the Bonferroni threshold in European studies. We found evidence for a negative correlation between this SNP and rs7726159 (Region 1), indicating a possible interaction. This locus is not significant at a GWAS threshold and requires confirmation in independent samples. Region 6 (marked by rs10069690) has previously been associated with estrogen- and progesterone receptor-negative breast cancer in populations of European and African ancestry (2,51); our analysis adds five cancers to this list: glioma, prostate, testicular germ cell, pancreas and urinary bladder.

The gene adjacent to *TERT*, namely *CLPTM1L*, encodes a protein that is overexpressed in lung and pancreatic cancer, promotes growth and survival, and is required for KRAS driven lung cancer, indicating that it is a plausible candidate gene in this region (17–21). The locus in *CLPTM1L* (Region 2) has previously been associated with risk of cancer in multiple GWAS, marked by rs401681 or rs402710 in pancreatic, lung and bladder cancer as well as in melanoma (1,4,5,12,52). Our subset-based approach has fine-mapped this signal to a set of seven correlated SNPs that span the entire length of *CLPTM1L*.

Two recent papers from the Collaborative Oncology Gene-Environment Study (COGs) fine-mapped 5p15.33 in prostate, breast and ovarian cancer and identified four of the six loci noted in the current study (53,54). In prostate cancer, COGs identified three regions that corresponded to our Region 1 (COGs Region 1, rs7725218), Region 3 (COGs Region 2, rs2853676, $r^2 = 0.32$ with rs2853677) and Region 4 (COGs Region 3, rs2853669) (54). Interestingly, COGs reported protective alleles in Region 1 associated with increased *TERT* expression in benign prostate tissue samples. The fourth COGs prostate cancer locus, marked by rs13190087, was not significant in our study ($P = 0.089$), possibly due to a more specific effect for prostate cancer for this locus where our study had less power.

In breast and ovarian cancer, COGs identified three regions corresponding to our Region 1 (COGs Region 2, rs7705526, associated with risk of ovarian cancer with low malignant potential, telomere length and promoter activity), Region 4 (COGs Region 1, rs2736108, associated with risk of ER-negative and *BRCA1* mutation carrier breast cancer, telomere length and altered promoter activity) and Region 6 (COGs Region 3, rs10069690, associated with risk of ER-negative breast cancer, breast cancer in *BRCA1* carriers and invasive ovarian cancer) (53). Regions 2 (in *CLPTM1L*) and 5 (in *TERT*) were not observed in the COGs reports, perhaps due to the choice of SNPs by COGs for fine-mapping as well as the more comprehensive reference set for 1000 Genomes used to conduct our imputation, or because of cancer-specific effects for these loci.

It is becoming increasingly clear that DNA methylation is under genetic control. Regions of variable methylation exist across tissues and individuals, tend to be located in intergenic regions, overlapping known regulatory elements. Notably, these are enriched for disease-associated SNPs (28,55,56). Analysis of TCGA data, while not uncovering significant eQTLs, indicated that DNA methylation could play a role in the underlying biology at 5p15.33. Methylation in a small region downstream of *CLPTM1L*, with features supporting an active regulatory function, was consistent with lower methylation levels in carriers of risk alleles for lung cancer (Region 4) and higher expression of *TERT* and *CLPTM1L*. Increased expression of both genes is consistent with a pro-tumorigenic role in lung cancer (19,21,31). For prostate cancer, the most notable meQTLs were located within exon 3 of *TERT* with increased rates of methylation for carriers of risk alleles in Regions 1 and 6. Although gene-body methylation has been observed to positively correlate with gene expression (57), we did not see evidence to support this for this particular set of CpGs. As a large fraction of meQTLs does not overlap with eQTLs (55), they may influence molecular phenotypes other than gene expression such as alternative promoter usage, splicing and even mutations (58–60). It is intriguing that methylation QTLs observed in TCGA data differ to some degree between lung and prostate cancer, and that none were observed in glioblastoma. This indicates that the *TERT-CLPTM1L* region may harbor multiple elements that have the capacity to influence molecular phenotypes that in turn impact cancer development. However, only a subset of these elements may be active in each organ, thus leading to different mechanistic avenues for risk modulation in different tissues. It is possible that the interplay between risk variants, multiple biological mechanisms and attributed genes, in addition to environmental and lifestyle factors that differentially influence various cancers may eventually come to explain how the same alleles at this complex locus can mediate opposing cancer risk in different organs.

In summary, we report up to six independent loci on chr5p15.33, each influencing the risk of multiple cancers. We observed pleiotropy for common susceptibility alleles in this region, defined as the phenomenon wherein a single genetic locus affects multiple phenotypes (61). These alleles could influence multiple cancers distinctly, perhaps in response to environmental factors or in interactions with other genes. Our cardinal observations underscore the complexity of the alleles and suggest the importance of tissue-specific factors that contribute to cancer susceptibility. Further laboratory analysis is needed to validate our findings using TCGA data, and investigate the optimal functional variants in each of the six independent loci in order to provide a clearer understanding of each of the loci in this multi-cancer susceptibility region.

MATERIALS AND METHODS

Study participants

Participants were drawn from a total of 20 previous GWAS scans of 13 distinct cancer types: bladder, breast, endometrial, esophageal squamous, gastric, glioma, lung, osteosarcoma, ovarian, pancreatic, prostate, renal cancer and testicular germ cell tumors. We first assessed a set of 11 GWAS representing six distinct cancers ('Tier-I studies') in which 5p15.33 had previously been implicated (NHGRI Catalog of Published GWAS studies: http://www.genome.gov/gwastudies/). The GWAS scans and their acronyms were: Asian lung cancer scan (AsianLung), European lung cancer scan (EurLung), African American lung (AA Lung), PanScan, China pancreatic cancer scan (ChinaPC), Testicular germ cell tumor (TGCT NCI) scan, glioma scan, Bladder NCI scan, Pegasus prostate cancer scan (Pegasus), CGEMS prostate cancer scan (CGEMS PrCa) and Advanced prostate cancer scan (Adv PrCa) (see case and control counts in Supplementary Material, Tables S4A–D). In a second analysis, we separately assessed a set of nine GWAS scans representing eight cancers ('Tier-II studies') in which 5p15.33 had not been previously reported in the literature (NHGRI Catalog of Published GWAS studies: http://www.genome.gov/gwastudies/). These studies were: Asian esophageal scan (Asian EsoCa), Asian gastric cancer scan (Asian GastCa), CGEMS Breast cancer scan (CGEMS Breast), Endometrial cancer scan (EndomCa), ER negative breast cancer scan (ERneg BPC3 BrCa), Ghana prostate cancer scan (Ghana PrCa), Osteosarcoma scan (OS), Ovarian cancer scan (OvCa) and Renal cancer scan (Renal US) (see case and control counts in Supplementary Material, Tables S4E–H). Studies were conducted in individuals of European background (EUR scans) but we did include studies in populations of Asian ancestry (i.e., esophageal squamous, gastric, non-smoking lung and pancreatic cancers) and African ancestry (i.e. lung and prostate cancer) (ALL scans). Study characteristics, genotyping and quality control have been previously published for all studies listed by cancer type and GWAS scan acronym: bladder cancer/Bladder NCI (1,62), breast cancer/CGEMS BrCa (63), breast cancer/ERneg BPC3 BrCa (64), endometrial cancer/EnCa (65), gastric cancer and esophageal squamous cell carcinoma/Asian UpperGI (66), glioma/Glioma scan (27), lung cancer in Europeans/EurLung (7), lung cancer in African Americans/AALung (67), lung cancer in non-smoking women from Asia/AsianLung (68,69), osteosarcoma/OS (70), ovarian cancer/OvCa (71), pancreatic cancer/PanScan (12,72), pancreatic cancer in Asians/ChinaPC (73), prostate cancer/Pegasus (unpublished data), prostate cancer/CGEMS PrCa (74), advanced prostate cancer/AdvPrCa (75), prostate cancer in Africans/GhanaPrCa (unpublished data), renal cancer/Renal US (76) and testicular germ cell tumors/TGCT NCI (77).

Each participating study obtained informed consent from study participants and approval from its Institutional Review Board (IRB) including IRB certification permitting data

sharing in accordance with the National Institutes of Health (NIH) Policy for Sharing of Data Obtained in NIH Supported or Conducted GWAS.

Genotyping

Arrays used for scanning included the Illumina HumanHap series (317 + 240S, 550, 610 K, 660 W and 1 M), as well as the Illumina Omni series (OmniExpress, Omni1M, Omni2.5 and Omni5M). The majority of the studies were genotyped at the Cancer Genomics Research Laboratory (formerly Core Genotyping Facility) of the National Cancer Institute (NCI) of the NIH. The ChinaPC GWAS (Affymetrix 6.0) was genotyped at CapitalBio in Beijing, China. This necessitated imputation before the cross-cancer subset-based meta-analysis. We used a combination of public resources, 1000 Genomes (1000G) (25) and DCEG (26) reference datasets, to impute existing GWAS datasets (78) using IMPUTE2 (79).

In addition to the standard QC procedures previously applied in the primary GWAS publications, we further filtered SNPs as follows: (i) completion rate per locus < 90%, (ii) MAF < 0.01, (iii) Hardy–Weinberg proportion P-value $< 1 \times 10^{-6}$, (iv) exclusion of A/T or G/C SNPs.

Lift over the genomic coordinates to NCBI genome build 37 or hg19

Because the March 2012 release of the 1000 Genomes Project data is based on NCBI genome build 37 (hg19), we utilized the LiftOver tool (http://hgdownload.cse.ucsc.edu/) to convert genomic coordinates for scan data from build 36 to build 37. The tool re-maps only coordinates, but not SNP identifiers. We prepared the inference.bed file and then performed the lift over as follows:

~/tools/liftover/liftOver inference.bed ~/tools/liftover/hg18ToHg19.over.chain.gz output.bed unlifted.bed

A small number of SNPs that failed LiftOver, mostly because they could not be unambiguously mapped to the genome by NCBI, were dropped from each imputation inference set.

Strand alignment with 1000 Genomes reference data set

Since A/T or G/C SNPs were excluded, strand alignment for the scan data required checking allele matches between the inference set and reference set locus by locus. If they did not match, alleles were complemented and checked again for matching. SNPs that failed both approaches were excluded from the inference data. Locus identifiers were normalized to those used in the 1000 Genomes data based on genomic coordinates, although the IMPUTE2 program uses only the chromosome/location to align each locus overlapping between the imputation inference and reference set.

Conversion of genotype files into WTCCC format

After LiftOver to genome build 37 and ensuring that alleles were reported on the forward strand, we converted the genotype data into IMPUTE2 format using GLU. We split the genotype file into one per chromosome and sorted SNPs in order of genomic location using the GLU *transform* module.

Imputation of a 2Mb window on chr5p15.33

We used both the 1000G data (March 2012 release) (25) and the DCEG imputation reference set (26) as reference datasets to improve overall imputation accuracy. The IMPUTE2 program (79) was used to impute a 2 Mb window on chr5p15.33 from 250 000 to 2 250 000 (hg19) with a 250 kb buffer on either side as well as other recommended default settings. For the association analysis, we focused on a smaller region from chr5: 1 250 000–1 450 000 delineated by recombination hotspots (discussed below).

Post-imputation filtering and association analysis

We excluded imputed loci with INFO < 0.5 from subsequent analyses. SNPTEST (79) was used for the association analysis with covariate adjustment and score test of the log additive genetic effect. The same adjustments as used originally in each individual scan were used. Note that the per SNP imputation accuracy score (IMPUTE's INFO field) is calculated by both IMPUTE2 and SNPTEST. The two INFO metrics calculated during imputation by IMPUTE2 and during association testing by SNPTEST are strongly correlated, especially when the additive model is fitted (78). We chose the INFO metric calculated by SNPTEST for post-imputation SNP filtering.

Subset and conditional analyses

Association outputs from SNPTEST were reformatted and subsequently analyzed using the ASSET program, an R package (http://www.bioconductor.org/packages/devel/bioc/html/ASSET.html; https://r-forge.r-project.org/scm/viewvc.php/*checkout*/pkg/inst/doc/vignette.Rnw?root=asset) for subset-based meta-analyses (24). ASSET is a suite of statistical tools specifically designed to be powerful for pooling association signals across multiple studies when true effects may exist only in a subset of the studies and could be in opposite directions across studies. The method explores all possible subset (or a restricted set if user specifies so) of studies and evaluates fixed-effect meta-analysis-type test-statistics for each subset. The final test-statistics is obtained by maximizing the subset-specific test-statistics over all possible subsets and then evaluating its significant after efficient adjustment for multiple testing, taking into account the correlation between test-statistics across different subsets due to overlapping subjects. The method not only returns a P-value for significance for the overall evidence of association of an SNP across studies, but also outputs the 'best subset' containing the studies that contributed to the overall association signal. For detection of SNP association signals with effects in opposite directions, ASSET allows subset search separately for positively and negatively associated studies and then combines association signals from two directions using a chi-square test-statistics. The method can take into account correlation due to overlapping subject across studies (e.g. share controls). More details about these and other features of the method can be found elsewhere [22].

For our current study, the matrices of the overlapping counts for cases–controls across datasets, which are utilized by ASSET to adjust for possible correlation across studies, were constructed and passed into the ASSET program (Supplementary Tables S4A–H). We used a two-sided test P-value, which

can combine association signals in opposite directions, to assess the overall significance of whether an SNP was associated with the cancers under study. For detection of independent susceptibility SNPs, we performed sequential conditional analysis in which in each step the ASSET analysis is repeated by conditioning on SNPs that have been detected to be most significant in previous steps. The process was repeated until the *P*-value for the most significant SNP for a step remained $< 1.3 \times 10^{-5}$, a conservative threshold that corresponds to Bonferroni adjustment for the 1924 SNPs used in the analysis for an alpha level of 0.05 and the two analyses performed (for the ALL vs. the EUR scans).

In the primary analysis, we included all GWAS scans in which one or more susceptibility alleles on 5p15.33 had been previously noted at genome-wide significant threshold ('Tier-I studies'). We further required a nominal signal in our data ($P < 0.05$). This yielded 11 GWAS across six distinct cancer sites and includes 34 248 cases and 45 036 cancer-free controls (Supplementary Material, Tables S4A–D). In a secondary analysis, we assessed the associations for each of the six regions in scans in which 5p15.33 had not been previously reported in the literature (http://www.genome.gov/gwastudies/), or did not show a nominal *P*-value in the GWAS datasets used in the current study ('Tier-II studies'). This yielded nine GWAS datasets across eight cancers, including a total of 11 385 cases and 18 322 controls (Supplementary Material, Tables S4E–H).

Recombination hotspot estimation

Recombination hotspots were identified in the region of 5p15.33 harboring *TERT* and *CLPTM1L* (1 264 068–1 360 487) using SequenceLDhot (80), a program that uses the approximate marginal likelihood method (81) and calculates likelihood ratio statistics at a set of possible hotspots. We tested three sample sets from East Asians ($n = 88$), CEU ($n = 116$) and YRI ($n = 59$) from the DCEG Imputation Reference Set. The PHASE v2.1 program was used to calculate background recombination rates (82,83).

Validation of imputation accuracy

Imputation accuracy was assessed by direct TaqMan genotyping. TaqMan genotyping assays (ABI, Foster City, CA, USA) were optimized for six SNPs (rs7726159, rs451360, rs2853677, rs2736098, rs10069690 and rs13172201) in the independent regions. In an analysis of 2327 samples from the Glioma brain tumor study (Glioma BTS, 330 samples) (27), testicular germ cell tumor (TGCT STEED study, 865 samples) (77) and Pegasus (PLCO, 1132 samples) (unpublished data), the allelic R^2 (84) measured between imputed and assayed genotypes were 0.88, 0.98, 0.86, 0.85, 0.81 and 0.61 for the six SNPs listed in the same order as above.

Bioinformatic analysis of functional potential

HaploReg v2 (http://www.broadinstitute.org/mammals/haploreg/haploreg.php) was used to annotate functional and regulatory potential of highly significant and highly correlated SNPs that mark each of the regions identified (using ENCODE data) (85). RegulomeDB (http://regulome.stanford.edu/) was used to assess and score regulatory potential of SNPs in each locus (86). eQTL effects were assessed using the Multiple Tissue Human Expression Resource database (http://www.sanger.ac.uk/resources/software/genevar/) but significant findings at a $P < 1 \times 10^{-3}$ threshold were not noted (data not shown) (87). Predicted effects of SNPs on splicing were assessed using NetGene2 (http://www.cbs.dtu.dk/services/NetGene2/) (88) but no effect were seen for any of the SNPs in the six regions (data not shown).

We carried out eQTL and methylation quantitative trait locus (meQTL) analyses to assess potential functional consequences of SNPs in the six regions identified in normal and tumor derived tissue samples from TCGA: LUAD (52/403 normal/tumor samples for eQTL analysis: 26/354 normal/tumor samples for meQTL analysis), PRAD (31/133 normal/tumor for eQTL; 39/158 normal/tumor for meQTL) and GBM (109 tumor for eQTL; 83 tumor for meQTL; normal GBM samples were not available). Transcriptome (Illumina HiSeq 2000, level 3), methylation (Illumina Infinium Human DNA Methylation 450 platform, level 3), genotype data (Affymetrix Genome-Wide Human SNP Array 6.0 platform, level 2) and phenotypes were downloaded from the TCGA data portal (https://tcga-data.nci.nih.gov/tcga/). Methylation probes located on X/Y chromosomes, annotated in repetitive genomic regions (GEO GPL16304), with SNPs (Illumina dbSNP137.snpupdate.table.v2) with MAF > 1% in the respective TCGA samples, with missing rate >5%, as well as 65 quality control probes on the 450 K array. We excluded transcripts on X/Y chromosomes and those with missing rate >5%. A principle component analysis was conducted on a genome-wide level in R using gene expression and methylation data (separately in normal and tumor tissues, and after excluding transcripts with variance $< 10^{-8}$ and methylation probes with variance <0.001). Genotype imputation was performed as described above for the 2 Mb window centered on *TERT* and *CLPTM1L*. For eQTL analysis, normalized transcript counts for *CLPTM1L* and *TERT* were normal quantile transformed and regressed against the imputed dosage of minor allele for each risk locus (six loci, 19 SNPs). The regression model included age, gender (not for PRAD), stage (only for tumor samples), copy number, top five principle components (PCs) of imputed genotype dosage and top five PCs of transcript counts to account for possible measured or unmeasured confounders and to increase detection power. The meQTL analysis was conducted in a similar manner in TCGA LUAD, PRAD GBM samples; beta-values of methylation at 169 CpG probes in the region encompassing *TERT* and *CLPTM1L* were normal quantile transformed and regressed as described above with the exception of inclusion of the top five PCs of methylation instead of expression values. We report the estimate of regression coefficient of imputed dosage, its standard error and *P*-values, adjusted by the Benjamini–Hochberg procedure for controlling false discovery rate (89). Spearman's rank-order correlation was calculated to assess the relationship between the methylation and gene expression for TCGA LUAD ($n = 486$), PRAD ($n = 186$) and GBM ($n = 126$) tumor samples. *P*-values were adjusted by the Benjamini–Hochberg procedure as described above. For the purpose of visualizing meQTLs, the most likely genotype was selected from the imputed genotype dosages.

Methylation QTLs were assessed in EAGLE normal lung tissue samples ($n = 215$) as previously described with the

addition of imputation of the 19 SNPs in the 6 regions under study here (28).

AUTHORS' CONTRIBUTIONS

Conceived and designed the experiments: Z.W., N.C., L.T.A. Performed the experiments: Z.W., B.Z., M.Z., H.P., J.J., C.C.C., J.N.S., J.W.H., A.H., L.B., A.I., C.H., L.T.A. Analyzed the data: Z.W., B.Z., M.Z., H.P., J.J., C.C.C., J.N.S., J.W.H., M.Y., N.C., L.T.A. Contributed reagents/materials/analysis tools: all authors. Wrote the paper: ZW and LTA. Contributed to the writing of the paper: all authors.

SUPPLEMENTARY MATERIAL

Supplementary Material is available at *HMG* online.

ACKNOWLEDGEMENTS

The authors acknowledge the contribution of the staff of the Cancer Genomics Research Laboratory for their invaluable help throughout the project.

Conflict of Interest statement: None declared.

FUNDING

This work was supported by the Intramural Research Program and by contract number HHSN261200800001E of the US National Institutes of Health (NIH), National Cancer Institute. The content of this publication does not necessarily reflect the views or policies of the Department of Health and Human Services nor does mention of trade names, commercial products or organizations imply endorsement by the U.S. Government. Additional funding acknowledgements are listed in Supplementary Material. The funders had no role in study design, data collection and analysis, decision to publish or preparation of the manuscript.

REFERENCES

1. Rothman, N., Garcia-Closas, M., Chatterjee, N., Malats, N., Wu, X., Figueroa, J.D., Real, F.X., Van Den Berg, D., Matullo, G., Baris, D. *et al.* (2010) A multi-stage genome-wide association study of bladder cancer identifies multiple susceptibility loci. *Nat. Genet.*, **42**, 978–984.
2. Haiman, C.A., Chen, G.K., Vachon, C.M., Canzian, F., Dunning, A., Millikan, R.C., Wang, X., Ademuyiwa, F., Ahmed, S., Ambrosone, C.B. *et al.* (2011) A common variant at the TERT-CLPTM1L locus is associated with estrogen receptor-negative breast cancer. *Nat. Genet.*, **43**, 1210–1214.
3. Shete, S., Hosking, F.J., Robertson, L.B., Dobbins, S.E., Sanson, M., Malmer, B., Simon, M., Marie, Y., Boisselier, B., Delattre, J.Y. *et al.* (2009) Genome-wide association study identifies five susceptibility loci for glioma. *Nat. Genet.*, **41**, 899–904.
4. Wang, Y., Broderick, P., Webb, E., Wu, X., Vijayakrishnan, J., Matakidou, A., Qureshi, M., Dong, Q., Gu, X., Chen, W.V. *et al.* (2008) Common 5p15.33 and 6p21.33 variants influence lung cancer risk. *Nat. Genet.*, **40**, 1407–1409.
5. McKay, J.D., Hung, R.J., Gaborieau, V., Boffetta, P., Chabrier, A., Byrnes, G., Zaridze, D., Mukeria, A., Szeszenia-Dabrowska, N., Lissowska, J. *et al.* (2008) Lung cancer susceptibility locus at 5p15.33. *Nat. Genet.*, **40**, 1404–1406.
6. Broderick, P., Wang, Y., Vijayakrishnan, J., Matakidou, A., Spitz, M.R., Eisen, T., Amos, C.I. and Houlston, R.S. (2009) Deciphering the impact of common genetic variation on lung cancer risk: a genome-wide association study. *Cancer Res.*, **69**, 6633–6641.
7. Landi, M.T., Chatterjee, N., Yu, K., Goldin, L.R., Goldstein, A.M., Rotunno, M., Mirabello, L., Jacobs, K., Wheeler, W., Yeager, M. *et al.* (2009) A genome-wide association study of lung cancer identifies a region of chromosome 5p15 associated with risk for adenocarcinoma. *Am. J. Hum. Genet.*, **85**, 679–691.
8. Beesley, J., Pickett, H.A., Johnatty, S.E., Dunning, A.M., Chen, X., Li, J., Michailidou, K., Lu, Y., Rider, D.N., Palmieri, R.T. *et al.* (2011) Functional polymorphisms in the TERT promoter are associated with risk of serous epithelial ovarian and breast cancers. *PLoS ONE*, **6**, e24987.
9. Rafnar, T., Sulem, P., Stacey, S.N., Geller, F., Gudmundsson, J., Sigurdsson, A., Jakobsdottir, M., Helgadottir, H., Thorlacius, S., Aben, K.K. *et al.* (2009) Sequence variants at the TERT-CLPTM1L locus associate with many cancer types. *Nat. Genet.*, **41**, 221–227.
10. Stacey, S.N., Sulem, P., Masson, G., Gudjonsson, S.A., Thorleifsson, G., Jakobsdottir, M., Sigurdsson, A., Gudbjartsson, D.F., Sigurgeirsson, B., Benediktsdottir, K.R. *et al.* (2009) New common variants affecting susceptibility to basal cell carcinoma. *Nat. Genet.*, **41**, 909–914.
11. Yang, X., Yang, B., Li, B. and Liu, Y. (2013) Association between TERT-CLPTM1L rs401681[C] allele and NMSC cancer risk: a meta-analysis including 45,184 subjects. *Arch. Dermatol. Res.*, **1**, 49–52.
12. Petersen, G.M., Amundadottir, L., Fuchs, C.S., Kraft, P., Stolzenberg-Solomon, R.Z., Jacobs, K.B., Arslan, A.A., Bueno-de-Mesquita, H.B., Gallinger, S., Gross, M. *et al.* (2010) A genome-wide association study identifies pancreatic cancer susceptibility loci on chromosomes 13q22.1, 1q32.1 and 5p15.33. *Nat. Genet.*, **42**, 224–228.
13. Kote-Jarai, Z., Olama, A.A., Giles, G.G., Severi, G., Schleutker, J., Weischer, M., Campa, D., Riboli, E., Key, T., Gronberg, H. *et al.* (2011) Seven prostate cancer susceptibility loci identified by a multi-stage genome-wide association study. *Nat. Genet.*, **43**, 785–791.
14. Turnbull, C., Rapley, E.A., Seal, S., Pernet, D., Renwick, A., Hughes, D., Ricketts, M., Linger, R., Nsengimana, J., Deloukas, P. *et al.* (2010) Variants near DMRT1, TERT and ATF7IP are associated with testicular germ cell cancer. *Nat. Genet.*, **42**, 604–607.
15. Mocellin, S., Verdi, D., Pooley, K.A., Landi, M.T., Egan, K.M., Baird, D.M., Prescott, J., De Vivo, I. and Nitti, D. (2012) Telomerase reverse transcriptase locus polymorphisms and cancer risk: a field synopsis and meta-analysis. *J. Natl. Cancer Inst.*, **104**, 840–854.
16. Kim, N.W., Piatyszek, M.A., Prowse, K.R., Harley, C.B., West, M.D., Ho, P.L., Coviello, G.M., Wright, W.E., Weinrich, S.L. and Shay, J.W. (1994) Specific association of human telomerase activity with immortal cells and cancer. *Science*, **266**, 2011–2015.
17. Yamamoto, K., Okamoto, A., Isonishi, S., Ochiai, K. and Ohtake, Y. (2001) A novel gene, CRR9, which was up-regulated in CDDP-resistant ovarian tumor cell line, was associated with apoptosis. *Biochem. Biophys. Res. Commun.*, **280**, 1148–1154.
18. James, M.A., Wen, W., Wang, Y., Byers, L.A., Heymach, J.V., Coombes, K.R., Girard, L., Minna, J. and You, M. (2012) Functional characterization of CLPTM1L as a lung cancer risk candidate gene in the 5p15.33 locus. *PLoS ONE*, **7**, e36116.
19. Ni, Z., Tao, K., Chen, G., Chen, Q., Tang, J., Luo, X., Yin, P. and Wang, X. (2012) CLPTM1L is overexpressed in lung cancer and associated with apoptosis. *PLoS ONE*, **7**, e52598.
20. Jia, J., Bosley, A.D., Thompson, A., Hoskins, J.W., Cheuk, A., Collins, I., Parikh, H., Xiao, Z., Ylaya, K., Dzyadyk, M. *et al.* (2014) CLPTM1L promotes growth and enhances aneuploidy in pancreatic cancer cells. *Cancer Res.*, **74**, 2785–2795.
21. James, M.A., Vikis, H.G., Tate, E., Rymaszewski, A.L. and You, M. (2014) CRR9/CLPTM1L Regulates Cell Survival Signaling and Is Required for Ras Transformation and Lung Tumorigenesis. *Cancer Res.*, **74**, 1116–1127.
22. Ballew, B.J. and Savage, S.A. (2013) Updates on the biology and management of dyskeratosis congenita and related telomere biology disorders. *Expert Rev. Hematol.*, **6**, 327–337.
23. Armanios, M. and Blackburn, E.H. (2012) The telomere syndromes. *Nat. Rev. Genet.*, **13**, 693–704.
24. Bhattacharjee, S., Rajaraman, P., Jacobs, K.B., Wheeler, W.A., Melin, B.S., Hartge, P., Yeager, M., Chung, C.C., Chanock, S.J. and Chatterjee, N. (2012) A subset-based approach improves power and interpretation for the combined analysis of genetic association studies of heterogeneous traits. *Am. J. Hum. Genet.*, **90**, 821–835.

25. Genomes. (2010) A map of human genome variation from population-scale sequencing. *Nature*, **467**, 1061–1073.
26. Wang, Z., Jacobs, K.B., Yeager, M., Hutchinson, A., Sampson, J., Chatterjee, N., Albanes, D., Berndt, S.I., Chung, C.C., Diver, W.R. *et al.* (2012) Improved imputation of common and uncommon SNPs with a new reference set. *Nat. Genet.*, **44**, 6–7.
27. Rajaraman, P., Melin, B.S., Wang, Z., McKean-Cowdin, R., Michaud, D.S., Wang, S.S., Bondy, M., Houlston, R., Jenkins, R.B., Wrensch, M. *et al.* (2012) Genome-wide association study of glioma and meta-analysis. *Hum. Genet.*, **131**, 1877–1888.
28. Shi, J., Marconett, C.N., Duan, J., Hyland, P.L., Li, P., Wang, Z., Wheeler, W., Zhou, B., Campan, M., Lee, D.S. *et al.* (2014) Characterizing the genetic basis of methylome diversity in histologically normal human lung tissue. *Nat. Commun.*, **5**, 3365.
29. Cheung, A.L. and Deng, W. (2008) Telomere dysfunction, genome instability and cancer. *Front. Biosci.*, **13**, 2075–2090.
30. Cesare, A.J. and Reddel, R.R. (2010) Alternative lengthening of telomeres: models, mechanisms and implications. *Nat. Rev. Genet.*, **11**, 319–330.
31. Shay, J.W. and Bacchetti, S. (1997) A survey of telomerase activity in human cancer. *Eur. J. Cancer*, **33**, 787–791.
32. Hou, L., Zhang, X., Gawron, A.J. and Liu, J. (2012) Surrogate tissue telomere length and cancer risk: shorter or longer? *Cancer Lett.*, **319**, 130–135.
33. Pooley, K.A., Sandhu, M.S., Tyrer, J., Shah, M., Driver, K.E., Luben, R.N., Bingham, S.A., Ponder, B.A., Pharoah, P.D., Khaw, K.T. *et al.* (2010) Telomere length in prospective and retrospective cancer case-control studies. *Cancer Res.*, **70**, 3170–3176.
34. De Vivo, I., Prescott, J., Wong, J.Y., Kraft, P., Hankinson, S.E. and Hunter, D.J. (2009) A prospective study of relative telomere length and postmenopausal breast cancer risk. *Cancer Epidemiol. Biomarkers Prev.*, **18**, 1152–1156.
35. Weischer, M., Nordestgaard, B.G., Cawthon, R.M., Freiberg, J.J., Tybjaerg-Hansen, A. and Bojesen, S.E. (2013) Short telomere length, cancer survival, and cancer risk in 47102 individuals. *J. Natl. Cancer Inst.*, **105**, 459–468.
36. Slagboom, P.E., Droog, S. and Boomsma, D.I. (1994) Genetic determination of telomere size in humans: a twin study of three age groups. *Am. J. Hum. Genet.*, **55**, 876–882.
37. Andrew, T., Aviv, A., Falchi, M., Surdulescu, G.L., Gardner, J.P., Lu, X., Kimura, M., Kato, B.S., Valdes, A.M. and Spector, T.D. (2006) Mapping genetic loci that determine leukocyte telomere length in a large sample of unselected female sibling pairs. *Am. J. Hum. Genet.*, **78**, 480–486.
38. Nan, H., Qureshi, A.A., Prescott, J., De Vivo, I. and Han, J. (2011) Genetic variants in telomere-maintaining genes and skin cancer risk. *Hum. Genet.*, **129**, 247–253.
39. Melin, B.S., Nordfjall, K., Andersson, U. and Roos, G. (2012) hTERT cancer risk genotypes are associated with telomere length. *Genet. Epidemiol.*, **36**, 368–372.
40. Hsu, C.P., Hsu, N.Y., Lee, L.W. and Ko, J.L. (2006) Ets2 binding site single nucleotide polymorphism at the hTERT gene promoter – effect on telomerase expression and telomere length maintenance in non-small cell lung cancer. *Eur. J. Cancer*, **42**, 1466–1474.
41. Horn, S., Figl, A., Rachakonda, P.S., Fischer, C., Sucker, A., Gast, A., Kadel, S., Moll, I., Nagore, E., Hemminki, K. *et al.* (2013) TERT promoter mutations in familial and sporadic melanoma. *Science*, **339**, 959–961.
42. Killela, P.J., Reitman, Z.J., Jiao, Y., Bettegowda, C., Agrawal, N., Diaz, L.A. Jr, Friedman, A.H., Friedman, H., Gallia, G.L., Giovanella, B.C. *et al.* (2013) TERT promoter mutations occur frequently in gliomas and a subset of tumors derived from cells with low rates of self-renewal. *Proc. Natl. Acad. Sci. USA*, **110**, 6021–6026.
43. Simon, M., Hosking, F.J., Marie, Y., Gousias, K., Boisselier, B., Carpentier, C., Schramm, J., Mokhtari, K., Hoang-Xuan, K., Idbaih, A. *et al.* (2010) Genetic risk profiles identify different molecular etiologies for glioma. *Clin. Cancer Res.*, **16**, 5252–5259.
44. Yang, P., Li, Y., Jiang, R., Cunningham, J.M., Zhang, F. and de Andrade, M. (2010) A rigorous and comprehensive validation: common genetic variations and lung cancer. *Cancer Epidemiol. Biomarkers Prev.*, **19**, 240–244.
45. Hu, Z., Wu, C., Shi, Y., Guo, H., Zhao, X., Yin, Z., Yang, L., Dai, J., Hu, L., Tan, W. *et al.* (2011) A genome-wide association study identifies two new lung cancer susceptibility loci at 13q12.12 and 22q12.2 in Han Chinese. *Nat. Genet.*, **43**, 792–796.
46. Miki, D., Kubo, M., Takahashi, A., Yoon, K.A., Kim, J., Lee, G.K., Zo, J.I., Lee, J.S., Hosono, N., Morizono, T. *et al.* (2010) Variation in TP63 is associated with lung adenocarcinoma susceptibility in Japanese and Korean populations. *Nat. Genet.*, **42**, 893–896.
47. Pande, M., Spitz, M.R., Wu, X., Gorlov, I.P., Chen, W.V. and Amos, C.I. (2011) Novel genetic variants in the chromosome 5p15.33 region associate with lung cancer risk. *Carcinogenesis*, **32**, 1493–1499.
48. Johnatty, S.E., Beesley, J., Chen, X., Macgregor, S., Duffy, D.L., Spurdle, A.B., deFazio, A., Gava, N., Webb, P.M., Rossing, M.A. *et al.* (2010) Evaluation of candidate stromal epithelial cross-talk genes identifies association between risk of serous ovarian cancer and TERT, a cancer susceptibility 'hot-spot'. *PLoS Genet.*, **6**, e1001016.
49. Zhao, Y., Chen, G., Song, X., Chen, H., Mao, Y. and Lu, D. (2012) Fine-mapping of a region of chromosome 5p15.33 (TERT-CLPTM1L) suggests a novel locus in TERT and a CLPTM1L haplotype are associated with glioma susceptibility in a Chinese population. *Int. J. Cancer*, **131**, 1569–1576.
50. Shiraishi, K., Kunitoh, H., Daigo, Y., Takahashi, A., Goto, K., Sakamoto, H., Ohnami, S., Shimada, Y., Ashikawa, K., Saito, A. *et al.* (2012) A genome-wide association study identifies two new susceptibility loci for lung adenocarcinoma in the Japanese population. *Nat. Genet.*, **44**, 900–903.
51. Palmer, J.R., Ruiz-Narvaez, E.A., Rotimi, C.N., Cupples, L.A., Cozier, Y.C., Adams-Campbell, L.L. and Rosenberg, L. (2012) Genetic susceptibility loci for subtypes of breast cancer in an African American population. *Cancer Epidemiol. Biomarkers Prev.*, **22**, 127–34.
52. Barrett, J.H., Iles, M.M., Harland, M., Taylor, J.C., Aitken, J.F., Andresen, P.A., Akslen, L.A., Armstrong, B.K., Avril, M.F., Azizi, E. *et al.* (2011) Genome-wide association study identifies three new melanoma susceptibility loci. *Nat. Genet.*, **43**, 1108–1113.
53. Bojesen, S.E., Pooley, K.A., Johnatty, S.E., Beesley, J., Michailidou, K., Tyrer, J.P., Edwards, S.L., Pickett, H.A., Shen, H.C., Smart, C.E. *et al.* (2013) Multiple independent variants at the TERT locus are associated with telomere length and risks of breast and ovarian cancer. *Nat. Genet.*, **45**, 371–384.
54. Kote-Jarai, Z., Saunders, E.J., Leongamornlert, D.A., Tymrakiewicz, M., Dadaev, T., Jugurnauth-Little, S., Ross-Adams, H., Al Olama, A.A., Benlloch, S., Halim, S. *et al.* (2013) Fine-mapping identifies multiple prostate cancer risk loci at 5p15, one of which associates with TERT expression. *Hum. Mol. Genet.*, **22**, 2520–2528.
55. Grundberg, E., Meduri, E., Sandling, J.K., Hedman, A.K., Keildson, S., Buil, A., Busche, S., Yuan, W., Nisbet, J., Sekowska, M. *et al.* (2013) Global analysis of DNA methylation variation in adipose tissue from twins reveals links to disease-associated variants in distal regulatory elements. *Am. J. Hum. Genet.*, **93**, 876–890.
56. Irizarry, R.A., Ladd-Acosta, C., Wen, B., Wu, Z., Montano, C., Onyango, P., Cui, H., Gabo, K., Rongione, M., Webster, M. *et al.* (2009) The human colon cancer methylome shows similar hypo- and hypermethylation at conserved tissue-specific CpG island shores. *Nat. Genet.*, **41**, 178–186.
57. Jjingo, D., Conley, A.B., Yi, S.V., Lunyak, V.V. and Jordan, I.K. (2012) On the presence and role of human gene-body DNA methylation. *Oncotarget*, **3**, 462–474.
58. Rideout, W.M. III, Coetzee, G.A., Olumi, A.F. and Jones, P.A. (1990) 5-Methylcytosine as an endogenous mutagen in the human LDL receptor and p53 genes. *Science*, **249**, 1288–1290.
59. Maunakea, A.K., Nagarajan, R.P., Bilenky, M., Ballinger, T.J., D'Souza, C., Fouse, S.D., Johnson, B.E., Hong, C., Nielsen, C., Zhao, Y. *et al.* (2010) Conserved role of intragenic DNA methylation in regulating alternative promoters. *Nature*, **466**, 253–257.
60. Shen, H. and Laird, P.W. (2013) Interplay between the cancer genome and epigenome. *Cell*, **153**, 38–55.
61. Solovieff, N., Cotsapas, C., Lee, P.H., Purcell, S.M. and Smoller, J.W. (2013) Pleiotropy in complex traits: challenges and strategies. *Nat. Rev. Genet.*, **14**, 483–495.
62. Figueroa JD, Y.Y., Siddiq, A., Garcia-Closas, M., Chatterjee, N. *et al.* (2014) Genome-wide association study identifies multiple loci associated with bladder cancer risk. *Hum. Mol. Genet.*, **23**, 1387–1398.
63. Hunter, D.J., Kraft, P., Jacobs, K.B., Cox, D.G., Yeager, M., Hankinson, S.E., Wacholder, S., Wang, Z., Welch, R., Hutchinson, A. *et al.* (2007) A genome-wide association study identifies alleles in FGFR2 associated with risk of sporadic postmenopausal breast cancer. *Nat. Genet.*, **39**, 870–874.
64. Siddiq, A., Couch, F.J., Chen, G.K., Lindstrom, S., Eccles, D., Millikan, R.C., Michailidou, K., Stram, D.O., Beckmann, L., Rhie, S.K. *et al.* (2012) A meta-analysis of genome-wide association studies of breast cancer identifies two novel susceptibility loci at 6q14 and 20q11. *Hum. Mol. Genet.*, **21**, 5373–5384.

65. De Vivo, I., Prescott, J., Setiawan, V.W., Olson, S.H. and Wentzensen, N., Australian National Endometrial Cancer Study Group, Attia, J., Black, A., Brinton, L., Chen, C. *et al.* (2014) Genome-wide association study of endometrial cancer in E2C2. *Hum. Genet. 133*, 211–24.
66. Abnet, C.C., Freedman, N.D., Hu, N., Wang, Z., Yu, K., Shu, X.O., Yuan, J.M., Zheng, W., Dawsey, S.M., Dong, L.M. *et al.* (2010) A shared susceptibility locus in PLCE1 at 10q23 for gastric adenocarcinoma and esophageal squamous cell carcinoma. *Nat. Genet.*, **42**, 764–767.
67. Hinch, A.G., Tandon, A., Patterson, N., Song, Y., Rohland, N., Palmer, C.D., Chen, G.K., Wang, K., Buxbaum, S.G., Akylbekova, E.L. *et al.* (2011) The landscape of recombination in African Americans. *Nature*, **476**, 170–175.
68. Hsiung, C.A., Lan, Q., Hong, Y.C., Chen, C.J., Hosgood, H.D., Chang, I.S., Chatterjee, N., Brennan, P., Wu, C., Zheng, W. *et al.* (2010) The 5p15.33 locus is associated with risk of lung adenocarcinoma in never-smoking females in Asia. *PLoS Genet.*, **6**.
69. Lan, Q., Hsiung, C.A., Matsuo, K., Hong, Y.C., Seow, A., Wang, Z., Hosgood, H.D. 3rd, Chen, K., Wang, J.C., Chatterjee, N. *et al.* (2012) Genome-wide association analysis identifies new lung cancer susceptibility loci in never-smoking women in Asia. *Nat. Genet.*, **44**, 1330–1335.
70. Savage, S.A., Mirabello, L., Wang, Z., Gastier-Foster, J.M., Gorlick, R., Khanna, C., Flanagan, A.M., Tirabosco, R., Andrulis, I.L., Wunder, J.S. *et al.* (2013) Genome-wide association study identifies two susceptibility loci for osteosarcoma. *Nat. Genet.*, **45**, 799–803.
71. Bolton, K.L., Tyrer, J., Song, H., Ramus, S.J., Notaridou, M., Jones, C., Sher, T., Gentry-Maharaj, A., Wozniak, E., Tsai, Y.Y. *et al.* (2010) Common variants at 19p13 are associated with susceptibility to ovarian cancer. *Nat. Genet.*, **42**, 880–884.
72. Amundadottir, L., Kraft, P., Stolzenberg-Solomon, R.Z., Fuchs, C.S., Petersen, G.M., Arslan, A.A., Bueno-de-Mesquita, H.B., Gross, M., Helzlsouer, K., Jacobs, E.J. *et al.* (2009) Genome-wide association study identifies variants in the ABO locus associated with susceptibility to pancreatic cancer. *Nat. Genet.*, **41**, 986–990.
73. Wu, C., Miao, X., Huang, L., Che, X., Jiang, G., Yu, D., Yang, X., Cao, G., Hu, Z., Zhou, Y. *et al.* (2012) Genome-wide association study identifies five loci associated with susceptibility to pancreatic cancer in Chinese populations. *Nat. Genet.*, **44**, 62–66.
74. Thomas, G., Jacobs, K.B., Yeager, M., Kraft, P., Wacholder, S., Orr, N., Yu, K., Chatterjee, N., Welch, R., Hutchinson, A. *et al.* (2008) Multiple loci identified in a genome-wide association study of prostate cancer. *Nat. Genet.*, **40**, 310–315.
75. Schumacher, F.R., Berndt, S.I., Siddiq, A., Jacobs, K.B., Wang, Z., Lindstrom, S., Stevens, V.L., Chen, C., Mondul, A.M., Travis, R.C. *et al.* (2011) Genome-wide association study identifies new prostate cancer susceptibility loci. *Hum. Mol. Genet.*, **20**, 3867–3875.
76. Purdue, M.P., Johansson, M., Zelenika, D., Toro, J.R., Scelo, G., Moore, L.E., Prokhortchouk, E., Wu, X., Kiemeney, L.A., Gaborieau, V. *et al.* (2011) Genome-wide association study of renal cell carcinoma identifies two susceptibility loci on 2p21 and 11q13.3. *Nat. Genet.*, **43**, 60–65.
77. Schumacher, F.R., Wang, Z., Skotheim, R.I., Koster, R., Chung, C.C., Hildebrandt, M.A., Kratz, C.P., Bakken, A.C., Timothy Bishop, D., Cook, M.B. *et al.* (2013) Testicular germ cell tumor susceptibility associated with the UCK2 locus on chromosome 1q23. *Hum. Mol. Genet.*, **22**, 48–53.
78. Marchini, J. and Howie, B. (2010) Genotype imputation for genome-wide association studies. *Nat. Rev. Genet.*, **11**, 499–511.
79. Marchini, J., Howie, B., Myers, S., McVean, G. and Donnelly, P. (2007) A new multipoint method for genome-wide association studies by imputation of genotypes. *Nat. Genet.*, **39**, 906–913.
80. Fearnhead, P. (2006) SequenceLDhot: detecting recombination hotspots. *Bioinformatics*, **22**, 3061–3066.
81. Fearnhead, P. and Donnelly, P. (2002) Approximate likelihood methods for estimating local recombination rates. *J. R. Stat. Soc.*, **64**, 657–680.
82. Li, N. and Stephens, M. (2003) Modeling linkage disequilibrium and identifying recombination hotspots using single-nucleotide polymorphism data. *Genetics*, **165**, 2213–2233.
83. Crawford, D.C., Bhangale, T., Li, N., Hellenthal, G., Rieder, M.J., Nickerson, D.A. and Stephens, M. (2004) Evidence for substantial fine-scale variation in recombination rates across the human genome. *Nat. Genet.*, **36**, 700–706.
84. Browning, B.L. and Browning, S.R. (2009) A unified approach to genotype imputation and haplotype-phase inference for large data sets of trios and unrelated individuals. *Am. J. Hum. Genet.*, **84**, 210–223.
85. Ward, L.D. and Kellis, M. (2012) HaploReg: a resource for exploring chromatin states, conservation, and regulatory motif alterations within sets of genetically linked variants. *Nucleic Acids Res.*, **40**, D930–934.
86. Boyle, A.P., Hong, E.L., Hariharan, M., Cheng, Y., Schaub, M.A., Kasowski, M., Karczewski, K.J., Park, J., Hitz, B.C., Weng, S. *et al.* (2012) Annotation of functional variation in personal genomes using RegulomeDB. *Genome Res.*, **22**, 1790–1797.
87. Grundberg, E., Small, K.S., Hedman, A.K., Nica, A.C., Buil, A., Keildson, S., Bell, J.T., Yang, T.P., Meduri, E., Barrett, A. *et al.* (2012) Mapping cis- and trans-regulatory effects across multiple tissues in twins. *Nat. Genet.*, **44**, 1084–1089.
88. Hebsgaard, S.M., Korning, P.G., Tolstrup, N., Engelbrecht, J., Rouze, P. and Brunak, S. (1996) Splice site prediction in Arabidopsis thaliana pre-mRNA by combining local and global sequence information. *Nucleic Acids Res.*, **24**, 3439–3452.
89. Benjamini, Y. and Hochberg, Y. (1995) Controlling the false discovery rate – a practical and powerful approach to multiple testing. *J. R. Stat. Soc. B*, **57**, 289–300.

Hindawi Publishing Corporation
BioMed Research International
Volume 2014, Article ID 470523, 2 pages
http://dx.doi.org/10.1155/2014/470523

Editorial

Gliomas

Giuseppe Lombardi,[1] Alessandro Della Puppa,[2] Anna Luisa Di Stefano,[3,4] Andrea Pace,[5] Roberta Rudà,[6] Emeline Tabouret,[7] and Vittorina Zagonel[1]

[1] *Medical Oncology 1, Veneto Institute of Oncology-IRCCS, Via Gattamelata 64, 35128 Padua, Italy*
[2] *Neurosurgery Department, Padua Hospital, 35128 Padua, Italy*
[3] *Department of Neuro-Oncology, UPMC, GH Pitié-Salpétrière, 75005 Paris, France*
[4] *DBBS, National Neurological Institute C. Mondino, University of Pavia, 27100 Pavia, Italy*
[5] *Neurology Unit, National Cancer Unit, Regina Elena, 00144 Rome, Italy*
[6] *Department of Neuro-Oncology, Città della Salute e della Scienza, University of Turin, 10126 Turin, Italy*
[7] *Department of Neuro-Oncology, Hopitaux de Marseille, Marseille, France*

Correspondence should be addressed to Giuseppe Lombardi; giuseppe.lombardi@ioveneto.it

Received 25 June 2014; Accepted 25 June 2014; Published 26 August 2014

Gliomas are a heterogeneous group of tumors developing from glial cells in the central nervous system. Gliomas are divided into two histopathological subgroups: low and high grade gliomas. High-grade gliomas, such as glioblastoma and anaplastic astrocytoma, are extremely aggressive lesions and represent the most common primary malignant brain tumors.

In the last years, there have been important developments about their biologic mechanism, their surgical and drug treatment, and their diagnosis and genetic mutations; indeed, the recent IDH gene mutation identification in gliomas has been an important contribution to the knowledge improvement of biological mechanism and prognosis of these tumors. Through the analysis of IDH gene mutation it is possible to add molecular characteristics to refine the WHO classification in order to define more homogeneous gliomas subgroups. X.-W. Wang et al. showed that IDH mutation is almost constant in 1p19q codeleted tumors and they stratified low- and high-grade gliomas according to the codeletion of 1p19q and IDH mutation to define three prognostic subgroups: 1p19q and IDH mutated, IDH mutated alone, and none of these alterations; they demonstrated that the presence of IDH mutation combined with other genomic markers can be used to refine the prognostic classification of gliomas, independently of tumor grade. Noteworthy, X.-W. Wang et al., in another work, showed that IDH1-R132H mutation could be predictive of response to radiation therapy; indeed, they suggested that IDH mutation could increase radiosensitivity in hypoxic conditions, underlining the primordial IDH mutation determination whatever the diagnostic approach. Indeed, in a recent work, G. Lombardi et al. [1] reported the possibility to discriminate IDH mutation analyzing the concentration of 2-hydroxyglutarate in urinary and plasma samples.

As described by P. Gonzalez-Gomez et al., another signaling pathway such as bone morphogenetic proteins (BMPs) could present with both prognostic value and promising therapeutic tools for gliomas.

A very interesting study about the use of 5-aminolevulinic acid (5-ALA) fluorescence in high-grade gliomas surgery was reported by A. Della Puppa et al.; they analyzed 94 patients who underwent surgery guided by 5-ALA fluorescence and stratified data for recurrent surgery, tumor location, tumor size, and tumor grade; they concluded that this surgical approach enables a gross total resection in 100% of cases and recurrent surgery, location, size, and tumor grade can be predictor of surgical outcome. The role of salvage radiosurgery in patients with recurrent malignant gliomas was studied by M. Martínez-Carrillo et al.; retrospectively, they analyzed 87 patients with recurrent anaplastic astrocytoma

and glioblastoma who underwent stereotactic radiosurgery; although the population was very heterogeneous and various prior studies showed conflicting results about the efficacy of reirradiation, they concluded that this treatment was safe and may be a potential treatment option in selected patients.

New technological instruments such as brain magnetic resonance imaging (MRI) with spectroscopy and perfusion can help in the right diagnosis for these tumors; in fact, A. L. Di Stefano et al., evaluating perfusion MRI in grades III and IV gliomas, showed that any significant difference in rCBV between grade III and grade IV is detectable in the contrast-enhancement area while areas of high perfusion on CBV map appear capable of best characterizing the degree of neovascularization and should be considered as the reference areas to be targeted for gliomas grading. The role of diffusion tensor histogram analysis was studied in pediatric diffuse intrinsic pontine gliomas by E. A. Steffen-Smith et al. from National Institutes of Health in Bethesda; they evaluated tumor structure in children using histogram analyses of mean diffusivity, concluding that this method can show significant interpatient and intratumoral differences and quantifiable changes in tumor structure.

Finally, an Italian study by V. Vaccaro et al. analyzed the efficacy of bevacizumab in association with fotemustine in patients with recurrent malignant gliomas. Antiangiogenic treatments for glioma patients have been tested in numerous clinical trials, both retrospective and prospective studies, with conflicting results; indeed, recently, two randomized prospective phase III studies failed to demonstrate the bevacizumab efficacy when added to temozolomide and radiation therapy for new glioblastoma patients [2, 3]. The combination treatment with bevacizumab and fotemustine was previously studied by R. Soffietti et al. [4] in recurrent glioblastoma patients, although with a different dosage and schedule. In both studies, this regimen showed interesting results with good safety in these patients.

In conclusion, gliomas represent an important subject of study and in this special issue very interesting works on recent developments about diagnosis, molecular biology, surgical treatment, and new targeted therapies for gliomas were selected.

Giuseppe Lombardi
Alessandro Della Puppa
Anna Luisa Di Stefano
Andrea Pace
Roberta Rudà
Emeline Tabouret
Vittorina Zagonel

References

[1] G. Lombardi, G. Corona, P. Farina et al., "Diagnostic value of plasma and urinary 2-hydroxyglutarate to identify patients with IDH-mutated glioma," *Journal of Clinical Oncology*, vol. 32, article 5s, 2014.

[2] O. L. Chinot, W. Wick, and T. Cloughesy, "Bevacizumab for newly diagnosed glioblastoma," *The New England Journal of Medicine*, vol. 370, article 2049, 2014.

[3] M. R. Gilbert, E. P. Sulman, and M. P. Mehta, "Bevacizumab for newly diagnosed glioblastoma," *The New England Journal of Medicine*, vol. 370, pp. 2048–2049, 2014.

[4] R. Soffietti, E. Trevisan, L. Bertero et al., "Bevacizumab and fotemustine for recurrent glioblastoma: a phase II study of AINO (Italian Association of Neuro-Oncology)," *Journal of Neuro-Oncology*, vol. 116, pp. 533–541, 2014.

J Neurooncol
DOI 10.1007/s11060-014-1677-x

LABORATORY INVESTIGATION

VEGFA SNP rs2010963 is associated with vascular toxicity in recurrent glioblastomas and longer response to bevacizumab

Anna Luisa Di Stefano · Marianne Labussiere · Giuseppe Lombardi · Marica Eoli · Donata Bianchessi · Francesco Pasqualetti · Patrizia Farina · Stefania Cuzzubbo · Jaime Gallego-Perez-Larraya · Blandine Boisselier · Francois Ducray · Caroline Cheneau · Arrigo Moglia · Gaetano Finocchiaro · Yannick Marie · Amithys Rahimian · Khe Hoang-Xuan · Jean Yves Delattre · Karima Mokhtari · Marc Sanson

Received: 15 May 2014 / Accepted: 30 November 2014

Abstract Although anti-VEGF therapy is widely used in high-grade gliomas, no predictor of response or toxicity has been reported yet. We investigated here the association of the functional single nucleotide polymorphism (SNP) rs2010963, located in the 5′ untranslated terminal region of the *VEGFA* gene, with survival, response to bevacizumab (BVZ) and vascular toxicity. The rs2010963 was genotyped by Taqman assay in blood DNA from 954 glioma patients with available survival data, including 225 glioblastoma (GBM) patients treated with BVZ. VEGFA plasma levels were assessed by ELISA in 87 patients before treatment. Thrombo-hemorragic adverse events were recorded during BVZ treatment or not, and in an independent population of 92 GBM patients treated with temozolomide. The CC genotype was associated with the occurrence of thrombo-hemorragic events (CC 25 versus CG 13.5 and GG 5.2 %; $P = 0.0044$) during BVZ. A similar but weaker and non significant trend was observed in patients not receiving BVZ. A CC genotype was associated with higher levels of plasma VEGFA at baseline (107.6 versus 57.50 pg/mL in heterozygotes (CG) and 52.75 pg/mL in GG patients, $P = 0.035$ and $P = 0.028$ respectively). The CC genotype tended to be associated to longer PFS when treated with BVZ ($P = 0.05$), but not

Electronic supplementary material The online version of this article (doi:10.1007/s11060-014-1677-x) contains supplementary material, which is available to authorized users.

A. L. Di Stefano · M. Labussiere · J. Gallego-Perez-Larraya · B. Boisselier · F. Ducray · C. Cheneau · A. Rahimian · K. Hoang-Xuan · J. Y. Delattre · K. Mokhtari · M. Sanson
UMPC Univ Paris VI, Centre de Recherche de l'Institut du Cerveau et de la Moelle épinière, INSERM U 1127, CNRS, UMR 7225; GH Pitié-Salpêtrièr, Sorbonne Universités, 75013 Paris, France

A. L. Di Stefano · P. Farina · S. Cuzzubbo · J. Gallego-Perez-Larraya · K. Hoang-Xuan · J. Y. Delattre · M. Sanson
Service de Neurologie 2, AP-HP, Groupe Hospitalier Pitié-Salpêtrière, 75013, Paris, France

A. L. Di Stefano · A. Moglia
National Neurological Institute C. Mondino, DBBS, University of Pavia, Pavia 27100, Italy

G. Lombardi · P. Farina
Department of Experimental Oncology, Medical Oncology 1, Veneto Institute of Oncology - IRCCS, Padua, Italy

M. Eoli · D. Bianchessi · S. Cuzzubbo · G. Finocchiaro
Neuro-oncology Unit, National Neurological Institute C. Besta, Milan, Italy

F. Pasqualetti
Deptartment Radiotherapy, University Hospital of Pisa, Pisa, Italy

J. Gallego-Perez-Larraya
Department of Neurology, Clinic of the University of Navarra, University of Navarra School of Medicine, Pamplona, Spain

Y. Marie
Institut du Cerveau et de la Moelle épinière (ICM), Plateforme de Génotypage Séquençage, 75013 Paris, France

A. Rahimian · J. Y. Delattre · K. Mokhtari · M. Sanson
Onconeurothèque, 75013 Paris, France

K. Mokhtari
Laboratoire de Neuropathologie R. Escourolle, AP-HP, Groupe Hospitalier Pitié-Salpêtrière, 75013 Paris, France

M. Sanson (✉)
Service de Neurologie 2, Groupe Hospitalier Pitié-Salpêtrière, 75651 Paris Cedex 13, France
e-mail: marc.sanson@psl.aphp.fr

Published online: 07 December 2014

when treated with the temozolomide treatment. Our data suggest that the rs2010963 genotype is associated with longer PFS, higher risk of vascular events in recurrent GBM especially treated with BVZ, and higher plasma VEGFA concentration. It may help to identify patients at risk of vascular adverse events during BVZ treatment.

Keywords Glioblastoma · VEGF · Bevacizumab · SNP · rs2010963

Abbreviations

VEGFA	(Vascular endothelial factor A)
OS	(Overall survival)
PFS	(Progression free survival)
W.H.O.	(World Health Organization)
KPS	(Karnofsky performance status)
SNP	(Single nucleotide polymorphism)

Introduction

Glioblastoma (GBM), the most frequent and malignant glioma subtype, is characterized by both hyper vascularisation and endothelial proliferation [1]. VEGFA is the most important pro-angiogenic factor in GBM and VEGFA concentrations in gliomas correlate with vascularity [2]. A high response rate (30–50 %) has been observed in recurrent GBMs treated with bevacizumab (BVZ), a human monoclonal anti-vascular endothelial growth factor-A (VEGFA) antibody, administered alone or in combination with irinotecan, with a 35–50 % estimated 6-month progression-free survival (PFS) [3–5]. Unpredictably, some patients experience drug resistance, limited antitumor activity, or toxicity. The most frequent grades 3–4 adverse events include hypertension, asthenia, diarrhea and severe thrombo-hemorragic events in about 5 % of patients [3, 6]. Therefore there is a need for markers predictive of response and toxicity.

The *VEGFA* gene, located at 6p21.1 [7], spans approximately 14 kilobases and encodes 8 exons [8, 9]. The 5′ and 3′ untranslated regions (UTR) contain key regulatory elements responsive to hypoxia [10], and contribute to a high variability in VEGF production among tissues [11]. SNP rs2010963 (G+405C, G-634C) in the 5′-UTR enhances *VEGFA* expression at both transcriptional and translational levels and may hypothetically influence tumor aggressiveness or the response to anti-angiogenic therapies [12, 13]. Moreover, the G+405C allele was found to be correlated with a higher risk of developing different solid cancers, such as non-small cell lung cancer (NSCLC) [14], prostate cancer [15] and glioma [16]. The rs2010963 SNP has also been associated to vascular disorders (Ref 20–24) and higher VEGF plasma levels (Ref 20). However, the prognostic value of SNP rs2010963 in glioma patients is not known, neither an eventual predictive value of response and tolerance to therapies that specifically target VEGF.

We explored the association of *VEGFA* SNP rs2010963 with vascular events and response to BVZ in glioblastoma patients. We also explored the correlation with plasma levels of VEGF and outcome in a large population of glioma patients.

Patients and methods

Populations

Bevacizumab treated glioblastoma population

We retrospectively investigated response and tolerance to a BVZ-based regimen in patients with recurrent glioblastoma (GBM), according to the following criteria: histological diagnosis of primary GBM, initially treated with the Stupp regimen [17], Karnofsky Performance Status Score (KPS) > 40, receiving BVZ (10 mg/kg every 14 days) at recurrence in monotherapy or in association with chemotherapy for at least two administrations.

Clinical and radiological responses were assessed according to the RANO criteria [18].

Patients that discontinued BVZ before tumor progression because of toxicity were censored for survival analyses. Adverse events were graded according to CTCAE v 4.0 (Common Terminology Criteria for Adverse Events: http://ctep.cancer.gov/protocolDevelopment/electronic_applications/ctc.htm).

Whole glioma population and independent data set

Patients were selected according to the following criteria: histological diagnosis of grade II to grade IV glioma, clinical data and follow-up available and written informed consent. Clinical data were retrieved from a prospectively maintained database; clinical data used included: age at surgery, sex, histology according to the 2007 World Health Organization Classification (WHO) [19].

Collection of blood samples and clinico-pathological information was undertaken with informed consent and relevant ethical board approval in accordance with the tenets of the Declaration of Helsinki.

Methods

The *VEGF* SNP rs2010963 genotype was assessed from blood DNA using a Taqman SNP Genotyping Assay (assay ID: C_8311614_10, Applied Biosystems). Plasma VEGFA

concentrations were assessed using Quantikine® Sandwich ELISA kits (R&D Systems) following manufacturer instructions at baseline before initiation of bevacizumab.

Statistical analysis

Statistical analyses were undertaken using the R software (www.r-project.org). The independence of alleles (Hardy–Weinberg equilibrium) was confirmed using the Chi squared test at one degree of freedom for each polymorphism (chi-2 < 3.84; p value > 0.05). Progression-free survival (PFS) was defined as the time between the diagnosis and recurrence or last follow-up. Patients who were recurrence-free at the last follow-up were considered as a censored event in the analysis. Overall survival (OS) was defined as the time between the diagnosis and death or last follow-up. Patients who were still alive at the last follow-up were considered as a censored event in the analysis. Survival curves were calculated according to the Kaplan–Meier method and differences between curves were assessed using the log-rank test. The difference in distribution of categorical variables was analyzed using Fisher exact and the Chi square test for trend and logistic regression. The Mann–Whitney method was employed to test the distribution of the VEGFA plasma level and the Spearman test was used to assess any correlation with age and body mass index (BMI). We considered a P value ≤ 0.05 (two-sided) to be statistically significant.

Results

Vascular events in GBM patients treated with bevacizumab at recurrence

A population of 225 glioblastoma patients treated with BVZ at recurrence was analyzed; characteristics are listed in Supplementary Table 1. Median PFS was 19.42 weeks. Median OS was 37.86 weeks. No significant difference in PFS and OS was observed between patients receiving BVZ in monotherapy, or in association with fotemustine and irinotecan.

Thirty-four patients out of 225 (15.1 %) presented adverse events during BVZ treatment. Twenty-five patients (11.1 %) had thrombo-hemorragic (TH) complications and 9 patients (4 %) had other complications. Among them, two patients presented a sudden death. Characteristics, frequency and grading of adverse events is reported in Supplementary Table 4. Eleven out of the 25 patients with TH complications and 4 out of the 9 patients with other complications discontinued BVZ and shifted towards other chemotherapies.

Impact of rs2010963 on outcome and vascular events in GBM patients during bevacizumab treatment

VEGFA rs2010963 genotypes are shown in Table 1. Minor allele frequency was 0.34. The distribution of allele frequencies in our population met the H–W equilibrium ($\chi^2 = 0.16$; $P = 0.68$). PFS was better in CC (median = 28.3 weeks) than CG (18.1 weeks) and GG patients (19.0 weeks; log-rank $P = 0.05$) (Fig. 1a, Table 1, Supplementary Fig. 1a), but not overall survival (CC patients 40.6 weeks, CG 41.7 weeks, GG patients 36.28 weeks) (Fig. 1b, Table 1, Supplementary Fig. 1b). rs2010963 genotypes did not show significantly different response rates according to the RANO criteria.

Twenty-five patients experienced TH events during BVZ, 6 of 25 CC (24.0 %), 14 of 104 CG (13.5 %) and 5 of 96 GG (5.2 %) (Fig. 2) ($P = 0.0044$; Hazard *Ratio* 2.44, $P = 0.006$).

rs2010963 status and thrombo-hemorragic events in patients not receiving BVZ

To determine if vascular events were dependent on BVZ-based therapy, we analyzed available clinical files from our cohort of 141 genotyped GBM patients not receiving BVZ: thrombo-hemorragic events were reported in 2/14 CC patients (14 %: one pulmonary embolism, one phlebitis), 5/66 CG (8 %: two pulmonary embolism, three intratumoral hematomas) and 7/61 GG (11 %: two pulmonary embolism, three phlebitis, two intratumoral hematomas), during the whole course of the disease ($p = 0.3$). We then

Table 1 Median progression free survival (PFS) and overall survival (OS) according to rs2010963 genotype

	All	*VEGFA* rs2010963 genotype				*VEGFA* rs2010963 allele		
		CC	CG	GG	*P*	C(CC)	G (CG + GG)	*P*
N	225	25	104	96		25	200	–
Median PFS (weeks)	19.42	26.82	18.00	19.00	*0.15*	26.82	18.00	0.06
Median OS (weeks)	37.86	41.71	40.57	36.28	*0.32*	41.71	37.71	0.60

CG means heterozygotes. In the right part, the C subgroup corresponds to CC genotype carriers and the G subgroup corresponds to heterozygotes (CG) and GG genotype carriers

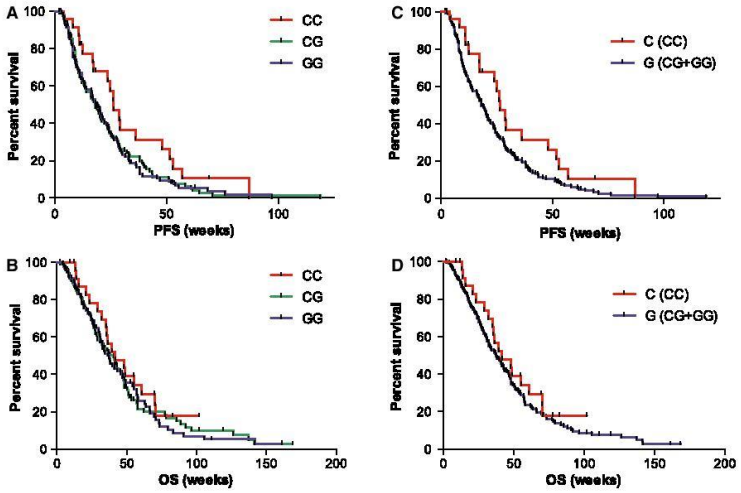

Fig. 1 Progression-free survival (PFS; *upper panels*) and overall survival (OS; *lower panels*) in GBM patients treated with BVZ at recurrence according to rs2010963 genotype (C = CC; G = Het + GG patients)

tested the impact of rs2010963 genotypes in an additional independent population of 92 GBM patients during their first-line chemotherapy with temozolomide. The clinical and demographic characteristics of this population are reported in Supplementary Table 2. Eleven thrombo-hemorragic events were observed: five deep venous thrombosis and six pulmonary embolisms. One patient with a pulmonary embolism also presented a concomitant intratumoral bleeding. Again we observed an over-representation of CC (3/10 = 30 %), compared to CG (3/42 = 7 %) and GG (5/40 = 12 %) ($p = 0.1$). Even pooling the two populations, the over-representation of CC (5/24) compared to CG + GG (20/209) remains non significant ($p = 0.15$).

rs2010963 is not prognostic per se in glioma

We then evaluated the prognostic value of rs2010963 in a large independent population of glioma patients. Blood DNA samples from 954 adult glioma patients (323 WHO grade IV, 269 WHO grade III and 362 WHO grade II) were analyzed for *VEGFA* SNP 2010963. Clinical and demographic characteristics are reported in Supplementary Table 3. The distribution of allele frequencies in our population met the Hardy–Weinberg equilibrium ($P = 0.33$). Minor allele frequency was 33.2 %. Allelic frequencies were independent of sex, age at diagnosis, grade and histology. No difference was observed for PFS and OS between the three genotypes for the whole population, and after stratification for grade (Table 2 and Supplementary Figs 1, 2).

rs2010963 genotype affects VEGFA plasma levels

Since rs2010963 is located in a regulatory region *VEGFA* gene, it may affect VEGFA expression. We looked therefore for differences in baseline VEGF plasma levels before the onset of BVZ between the three genotypes. 87 plasma samples were available (12 CC, 35 CG and 40 GG). Baseline VEGF plasma level was significantly higher in CC patients (median = 107.6 pg/mL), as compared to CG (57.50 pg/mL) ($P = 0.035$) and GG (52.75 pg/mL) ($P = 0.028$) (Fig. 3). The VEGF plasma level was not correlated with age, body mass index (BMI), sex or hypertension. The baseline VEGF plasma level did not differ significantly in patients who developed TH adverse events during BVZ and did not affect PFS and OS during BVZ.

Discussion

We found that the *VEGFA* rs2010963 CC genotype was associated with thrombo-hemorragic events in patients

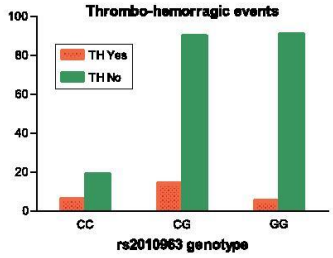

Fig. 2 Distribution of thrombo-hemorragic (TH) events during BVZ among rs2010963 genotypes

treated with BVZ at recurrence. There are several limitations due to the retrospective analysis of the data, the missing data in the whole GBM cohort, and also the limited cohort of GBM patients treated with temozolomide alone. In these populations not receiving BVZ, we could not demonstrate an impact of genotype on thrombo-hemorragic events. Although the two populations presented similar clinical characteristics such as age, KPS and BMI, they cannot be compared because of the different stages of the disease: the impact of the rs2010963 CC genotype was then analyzed separately in the two populations.

The *VEGFA* rs2010963 polymorphism has been associated with susceptibility to vascular disorders, such as diabetic retinopathy, myocardial infarction and impaired prognosis in patients with chronic heart failure [20–24], and may therefore play a role in thrombo-hemorragic events occurring in patients receiving anti-VEGF therapies.

The functional consequences of the rs2010963 variant are still a matter of debate. Located in the regulatory region of the gene, the rs2010963 polymorphism is believed to alter VEGFA expression. Indeed, we found a higher plasma level of VEGFA in CC patients. In line with our own findings, higher *VEGFA* expression has been reported in post-mortem retina from individuals with the rs2010963 C allele [25], and a CC genotype has been associated with higher serum VEGF levels [2, 20].

In a cohort of 954 gliomas, both PFS and OS for grade II to IV gliomas were independent of the rs2010963 status, suggesting that the rs2010963 SNP is not per se a prognostic marker. In contrast, patients with the rs2010963 CC genotype had a longer PFS after BVZ treatment (median PFS 28.3 weeks), as compared to CG and GG patients (18.1 and

Table 2 Median progression free survival (PFS) and overall survival (OS) according to rs2010963 genotype and glioma grade

VEGFA rs2010963 genotype	CC	CG	GG	*P*
All gliomas	99	437	418	
N				
Median PFS, months	19.81	19.86	18.01	0.43
Median OS, months	63.86	70.51	46.26	0.18
Grade II	42	165	155	
N				
Median PFS, months	37.16	37.46	39.53	0.78
Median OS, months	153.43	161.73	150.06	0.81
Grade III	25	112	132	
N				
Median PFS, months	22.86	20.46	16.56	0.61
Median OS, months	46.56	55.21	37.91	0.34
Grade IV	32	140	151	
N				
Median PFS, months	8.36	9.73	8.56	0.43
Median OS, months	17.03	19.86	16.96	0.51

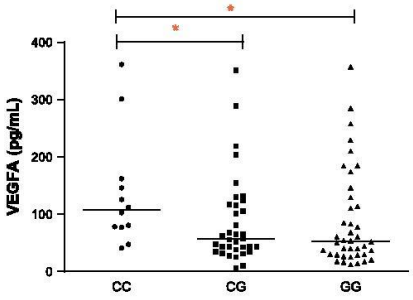

Fig. 3 Baseline VEGFA plasma levels according to rs2010963 genotypes

19.0 weeks, respectively). Our results suggest that patients with the rs2010963 CC genotype may have an improved response to BVZ, but are also more prone to develop thrombo-hemorragic events. One may speculate that the rs2010963 CC genotype, resulting in higher VEGFA production, promotes the development of a VEGFA-dependent angiogenesis, and explains, at least in part, the improved responsiveness to BVZ. On the other hand, BVZ is associated with an increased risk of developing venous thrombo-embolisms [26] and hemorrhage in cancer patients [27], but the specific link between rs2010963 status and the vascular toxicities remains unexplained.

From a practical point of view, if these data are confirmed by an independent study, a more systematic thrombo-

embolic prevention may be warranted in rs2010963 CC patients with gliomas, especially when treated with BVZ.

Acknowledgments Work supported by a Grant from the Institut National du Cancer (INCa; Angiogli- RAFc0209). A.L. Di Stefano received an investigator fellowship from PRIN 2010ZESJWN_008. The research leading to these results has received funding from the program "investissements d'avenir" ANR-10-IAIHU-06. The authors are indebted to Alexandru Agachi for English Editing.

Conflict of interest None.

References

1. Kunnakkat S, Narayana A (2011) Bevacizumab in the treatment of high-grade gliomas: an overview. Angiogenesis 14:423–430
2. Jensen RL (1998) Growth factor-mediated angiogenesis in the malignant progression of glial tumors: a review. Surg Neurol 49:189–195; discussion 196
3. Friedman HS, Prados MD, Wen PY et al (2009) Bevacizumab alone and in combination with irinotecan in recurrent glioblastoma. J Clin Oncol 27:4733–4740
4. Kreisl TN, Kim L, Moore K et al (2009) Phase II trial of single-agent bevacizumab followed by bevacizumab plus irinotecan at tumor progression in recurrent glioblastoma. J Clin Oncol 27:740–745
5. Vredenburgh JJ, Desjardins A, Herndon JE 2nd et al (2007) Bevacizumab plus irinotecan in recurrent glioblastoma multiforme. J Clin Oncol 25:4722–4729
6. Gil MJ, de Penas Las R, Reynes G et al (2012) Bevacizumab plus irinotecan in recurrent malignant glioma shows high overall survival in a multicenter retrospective pooled series of the Spanish neuro-oncology research group (GEINO). Anticancer Drugs 23:659–665
7. GKB P. http://www.pharmgkb.org/ [online]. Available at: http://www.pharmgkb.org/
8. Brogan IJ, Khan N, Isaac K, Hutchinson JA, Pravica V, Hutchinson IV (1999) Novel polymorphisms in the promoter and 5′ UTR regions of the human vascular endothelial growth factor gene. Hum Immunol 60:1245–1249
9. Tischer E, Mitchell R, Hartman T et al (1991) The human gene for vascular endothelial growth factor. Multiple protein forms are encoded through alternative exon splicing. J Biol Chem 266:11947–11954
10. Minchenko A, Salceda S, Bauer T, Caro J (1994) Hypoxia regulatory elements of the human vascular endothelial growth factor gene. Cell Mol Biol Res 40:35–39
11. Schultz A, Lavie L, Hochberg I et al (1999) Interindividual heterogeneity in the hypoxic regulation of VEGF: significance for the development of the coronary artery collateral circulation. Circulation 100:547–552
12. Jain L, Vargo CA, Danesi R et al (2009) The role of vascular endothelial growth factor SNPs as predictive and prognostic markers for major solid tumors. Mol Cancer Ther 8:2496–2508
13. Watson CJ, Webb NJ, Bottomley MJ, Brenchley PE (2000) Identification of polymorphisms within the vascular endothelial growth factor (VEGF) gene: correlation with variation in VEGF protein production. Cytokine 12:1232–1235
14. Zhai R, Liu G, Zhou W et al (2008) Vascular endothelial growth factor genotypes, haplotypes, gender, and the risk of non-small cell lung cancer. Clin Cancer Res 14:612–617
15. Sfar S, Hassen E, Saad H, Mosbah F, Chouchane L (2006) Association of VEGF genetic polymorphisms with prostate carcinoma risk and clinical outcome. Cytokine 35:21–28
16. Li R, Zhao Y, Fan W et al (2011) Possible association between polymorphisms of human vascular endothelial growth factor a gene and susceptibility to glioma in a Chinese population. Int J Cancer 128:166–175
17. Stupp R, Mason WP, van den Bent MJ et al (2005) Radiotherapy plus concomitant and adjuvant temozolomide for glioblastoma. N Engl J Med 352:987–996
18. Wen PY, Macdonald DR, Reardon DA et al (2010) Updated response assessment criteria for high-grade gliomas: response assessment in neuro-oncology working group. J Clin Oncol 28:1963–1972
19. Louis DN, Ohgaki H, Wiestler OD, Cavenee WK (2007) WHO Classification of tumours of the central nervous system. Acta Neuropathol 114:97–109
20. Petrovic D, Verhovec R, Globocnik Petrovic M, Osredkar J, Peterlin B (2007) Association of vascular endothelial growth factor gene polymorphism with myocardial infarction in patients with type 2 diabetes. Cardiology 107:291–295
21. Awata T, Inoue K, Kurihara S et al (2002) A common polymorphism in the 5′-untranslated region of the VEGF gene is associated with diabetic retinopathy in type 2 diabetes. Diabetes 51:1635–1639
22. Inoue M, Itoh H, Ueda M et al (1998) Vascular endothelial growth factor (VEGF) expression in human coronary atherosclerotic lesions: possible pathophysiological significance of VEGF in progression of atherosclerosis. Circulation 98:2108–2116
23. Petrovic MG, Korosec P, Kosnik M et al (2008) Local and genetic determinants of vascular endothelial growth factor expression in advanced proliferative diabetic retinopathy. Mol Vis 14:1382–1387
24. van der Meer P, De Boer RA, White HL et al (2005) The VEGF +405 CC promoter polymorphism is associated with an impaired prognosis in patients with chronic heart failure: a MERIT-HF substudy. J Card Fail 11:279–284
25. Vailati FB, Crispim D, Sortica DA, Souza BM, Brondani LA, Canani LH (2012) The C allele of -634G/C polymorphism in the VEGFA gene is associated with increased VEGFA gene expression in human retinal tissue. Invest Ophthalmol Vis Sci 53:6411–6415
26. Nalluri SR, Chu D, Keresztes R, Zhu X, Wu S (2008) Risk of venous thromboembolism with the angiogenesis inhibitor bevacizumab in cancer patients: a meta-analysis. JAMA 300:2277–2285
27. Hapani S, Sher A, Chu D, Wu S (2010) Increased risk of serious hemorrhage with bevacizumab in cancer patients: a meta-analysis. Oncology 79:27–38

Hindawi Publishing Corporation
BioMed Research International
Volume 2015, Article ID 948497, 6 pages
http://dx.doi.org/10.1155/2015/948497

Research Article

Meningeal Melanomatosis: A Challenge for Timely Diagnosis

Giulia Berzero,[1,2] Luca Diamanti,[1,2] Anna Luisa Di Stefano,[1,3] Paola Bini,[1] Diego Franciotta,[1] Ilaria Imarisio,[4] Paolo Pedrazzoli,[4] Lorenzo Magrassi,[5] Patrizia Morbini,[6] Lisa Maria Farina,[1] Stefano Bastianello,[1,7] Mauro Ceroni,[1,7] and Enrico Marchioni[1]

[1] *C. Mondino National Neurological Institute, Via Mondino 2, 27100 Pavia, Italy*
[2] *Neuroscience Consortium, University of Pavia, Monza Policlinico and Pavia Mondino, 27100 Pavia, Italy*
[3] *AP-HP, Groupe Hospitalier Pitié-Salpêtrière, Service de Neurologie Mazarin, 75013 Paris, France*
[4] *Oncology Unit, Policlinico San Matteo Foundation IRCCS, 27100 Pavia, Italy*
[5] *Neurosurgery Unit, Policlinico San Matteo Foundation IRCCS, 27100 Pavia, Italy*
[6] *Department of Molecular Medicine, Unit of Pathology, University of Pavia and Policlinico San Matteo Foundation IRCCS, 27100 Pavia, Italy*
[7] *Department of Brain and Behavioral Sciences, University of Pavia, 27100 Pavia, Italy*

Correspondence should be addressed to Enrico Marchioni; enrico.marchioni@mondino.it

Received 27 June 2014; Accepted 5 October 2014

Academic Editor: Athanasios G. Pallis

Neoplastic meningitis is a central nervous system complication that occurs in 3–5% of patients with cancer. Although most commonly seen in patients with disseminated disease, in a small percentage of patients, it may be the initial manifestation of cancer or even primitive in origin. In the absence of cancer history, the diagnosis of neoplastic meningitis may be challenging even for expert neurologists. Prognosis is poor, with a median overall survival of weeks from diagnosis. In the retrospective study herein, we described three cases of meningeal melanomatosis in patients without previous cancer history. The patients were diagnosed with significant delay (17 to 47 weeks from symptom onset) mainly due to the deferral in performing the appropriate testing. Even when the diagnosis was suspected, investigations by MRI, cerebrospinal fluid, or both proved at times unhelpful for confirmation. Prognosis was dismal, with a median survival of 4 weeks after diagnosis. Our observations are a cue to analyze the main pitfalls in the diagnosis of neoplastic meningitis in patients without cancer history and emphasize key elements that may facilitate early diagnosis.

1. Introduction

Neoplastic meningitis is a central nervous system complication that occurs in 3–5% of patients with cancer [1], and it is most commonly seen in patients with disseminated progressive systemic disease due to spread of malignant cells to the leptomeninges. The most common primary tumors to metastasize to the meninges are lung cancer (9–25% of patients) [2] and melanoma (23%) [3], due to a distinctive neurotropism. More rarely neoplastic meningitis is the initial manifestation of systemic cancer (5–10%) [1] or it is primitive in origin, as it occurs in primary leptomeningeal melanomatosis [4]. In patients without cancer history, diagnosis may be challenging even for expert neurologists due to the lack of specific signs and symptoms. Prognosis of neoplastic meningitis is poor, as most untreated patients die within 1–9 weeks from diagnosis (median 3 weeks) [1, 5], as a result of neurological disease or tumor progression. The timeliness of diagnosis is crucial to start the appropriate treatment before sudden neurological deterioration.

Here, we present a retrospective series of three patients with meningeal melanomatosis without history of cancer,

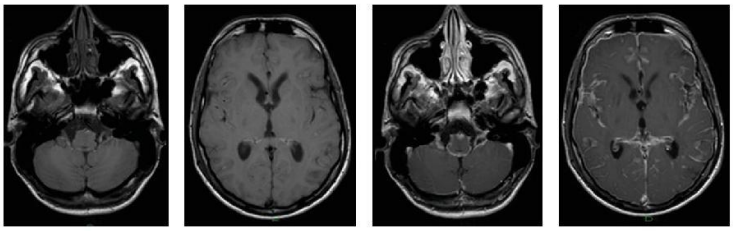

(a) (b) (c) (d)

Figure 1: Brain diffuse leptomeningeal melanomatosis in patient 1. (a), (b): T1 weighted axial image (TR/TE 1157 ms/45 ms) shows diffuse sulcal signal hyperintensity due to melanin products which cause T1 shortening signal. (c), (d): contrast-enhanced T1-weighted volume image (TR/TE 25 ms/4,6 ms) shows prominent and extensive leptomeningeal enhancement.

characterized by a dramatic diagnostic delay. We also propose an algorithm focused on the diagnosis of neoplastic meningitis in naïve patients.

2. Materials and Methods

We describe a retrospective series of three patients with meningeal melanomatosis recruited from our two institutions (C. Mondino National Neurological Institute and Policlinico San Matteo Foundation IRCCS, Pavia, Italy) in four years. We conducted an Internal Review Board approved study using an institutional oncological database of all patients receiving a diagnosis of meningeal melanomatosis from January 2010 to January 2014. The medical records were reviewed and clinical, biological, and radiological data collected for details.

3. Results

The clinical and paraclinical characteristics of our three patients are summarized in Table 1. Patients were aged between 17 and 65. All patients had no previous cancer history and arrived to our centers after several neurologic evaluations. Clinical presentation included diffuse and/or multifocal neurological signs and symptoms: headache, nausea and/or vomiting, monoparesis, and cranial nerve palsies. One patient (patient 3) presented recurrent isolated confusional episodes but was completely asymptomatic in between. Electroencephalogram showed bilateral/diffuse slow abnormalities without epileptic activity in all cases. Brain MRI performed within the first 4 weeks from symptom onset was normal in both patients in whom it was acquired (pt 1 and 3). Alternatively, focal or diffuse nodular enhancement of leptomeninges and cranial nerves was documented (Figure 1). Spine MRI revealed nodular contrast enhancement of meninges, conus, and cauda, suggesting neoplastic infiltration (Figure 2). Cerebrospinal fluid (CSF) analysis showed severe blood-CSF barrier (B-CSF B) damage in all patients but inconstant pleocytosis. In patient 2, despite repeated lumbar punctures, CSF cytology remained negative and diagnosis was confirmed on leptomeningeal tissue obtained from biopsy. In all other patients, the presence of melanoma cells in the CSF (Figures 3 and 4) was eventually documented by means of repeated lumbar punctures. After the diagnosis of meningeal melanomatosis was confirmed, all patients underwent a chest-abdomen CT scan and a dermatological and an ophthalmological assessment. In two patients, the final diagnosis was of probable primary leptomeningeal melanomatosis (pt 1 and 2), while in patient 3 a cutaneous melanoma of right eyelid was documented. The diagnostic delay was remarkable in our series, with a median delay of 32 weeks from symptom onset (range: 17–47 weeks). Prognosis was dismal, with a median survival of 4.14 weeks from diagnosis (range: 2–6.29 weeks).

4. Discussion

Although restricted, our series offers several insights into the diagnosis of neoplastic meningitis in naïve patients. These patients, without a previous cancer history, can present with diffuse/multifocal clinical signs and symptoms and represent a real diagnostic challenge. On these grounds, we propose an algorithm (Figure 5) to guide the clinician in the complex process of differential diagnosis, regarding as opening scenario a naïf patient presenting with subacute headache and/or encephalopathy plus one or more focal signs, and negative or inconclusive MRI, as we have observed in our series. In this setting, CSF analysis should be promptly performed to exclude other dysimmune/infectious disorders such as autoimmune and paraneoplastic encephalitides, primary CNS vasculitis, and chronic infectious meningitis, which can course without MRI alterations. Besides, it is important to consider that a delay in the diagnosis of the above-mentioned conditions may strongly affect final outcome and long-term sequelae.

Furthermore, even when the diagnosis of neoplastic meningitis has been suspected, paraclinical findings could be inconclusive. According to the literature, brain MRI has an estimated sensitivity of 40–60% in demonstrating

Table 1: Clinical and paraclinical findings in our three patients.

Pt	1				2				3			
Age/gender	17/M				55/M				65/M			
Clinical presentation at onset	Headache, nausea and vomiting, diplopia, and weight loss				Left leg monoparesis, headache, nausea and vomiting				Recurrent confusional episodes			
MRI												
Time from symptom onset (weeks)	4	30	47		8.2		12.9		1	21.4		
Hydrocephalus	No	Modest dilation of ventricular system	*Tetra*-ventricular		Triventricular		Triventricular		No	Triventricular		
Leptomeningeal contrast enhancement	No	Contrast not administered	Supra- and infratentorial, cranial nerves, spinal cord, conus, and cauda equina		Supratentorial, conus, and cauda equina		Supratentorial, spinal cord, conus, and cauda equina		No	Supra- and infratentorial, cranial nerves, conus, and cauda equina		
Dural melanin deposits	No	No	Yes		No		No		No	Yes		
CSF												
Time from symptom onset (weeks)	40.6	42.9	44.9	8.1	10.6	14.9			21.4			
Glucose (mg/dL)	—	92	83	—	—	29			8			
Proteins (mg/dL)	—	2366	2773	370	—	431			535			
Cell count (cells/uL)	4	110	174	2	<2	10			36			
Cytology	n.p.	Nonspecific	Melanoma cells	n.p.	No identifiable cells	Nonspecific			Melanoma cells			
EEG	Poorly organized background activity with bilateral slow abnormalities				Diffuse bilateral slowing				Bilateral fronto-centrotemporal slow abnormalities with left prevalence			
Extra CNS visceral met	No				No				No			
Final diagnosis	**Primary leptomeningeal melanomatosis**				**Primary leptomeningeal melanomatosis**				**Leptomeningeal carcinomatosis and cutaneous melanoma**			
Time to diagnosis (weeks)	47				17				23.4			
Clinical evolution	Confusion, visual hallucinations, partial seizures, and behavioral alterations				Urinary retention, progressive paraparesis, and visual hallucinations				Vigilance impairment, generalized seizures, headache, and backache			
Treatment	Temozolomide (1 cycle)				Dacarbazine (1 cycle)				None			
Overall survival (weeks)	49.1				23.4				30			

Legend to Table 1: CNS = central nervous system, CSF = cerebrospinal fluid, EEG = electroencephalogram, met = metastases, MRI = magnetic resonance imaging, n.p. = not performed, and — = not available.

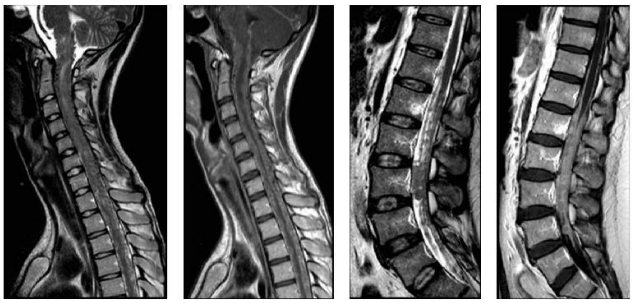

(a) (b) (c) (d)

Figure 2: Primary leptomeningeal melanomatosis in patients 1 ((a), (b)) and 2 ((c), (d)). (a), (c): Sagittal T2-weighted images (TR/TE 3500 ms/120 ms) of cervical-dorsal spine and cauda equina show hypertrophic leptomeninges with crowded subarachnoid space and multinodular appearance of the cauda equina. (b), (d): Sagittal T1-weighted images (TR/TE 65 ms/9 ms) of cervical-dorsal spine and cauda equina show diffuse leptomeningeal enhancement and thickening.

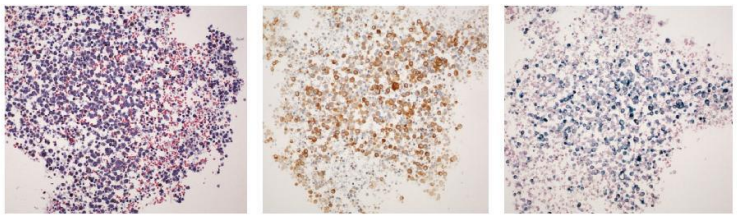

(a) (b) (c)

Figure 3: Light microscopy pictures of the cytological specimen of cerebrospinal fluid obtained from patient 1: (a) hematoxylin and eosin staining of the hypercellular sample, with large, hyperchromatic cells associated with erythrocytes; (b) atypical cells stained with Melan-A, a melanoma-specific marker; (c) Schmorl staining confirmed the presence of melanin (blue granular stain) in the cytoplasm; magnification, 20x.

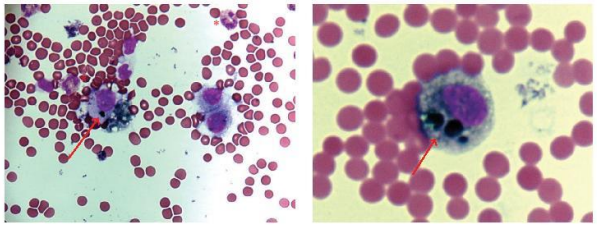

(a) (b)

Figure 4: Light microscopy pictures of the cytospin of the cerebrospinal fluid cells from patient 1: (a) hematoxylin and eosin staining of large, hyperchromatic cells, along with erythrocytes, lymphoma monocytoid cells, and eosinophils (asterisks); (b) an atypical cell at larger magnification; arrows indicate granules of melanin.

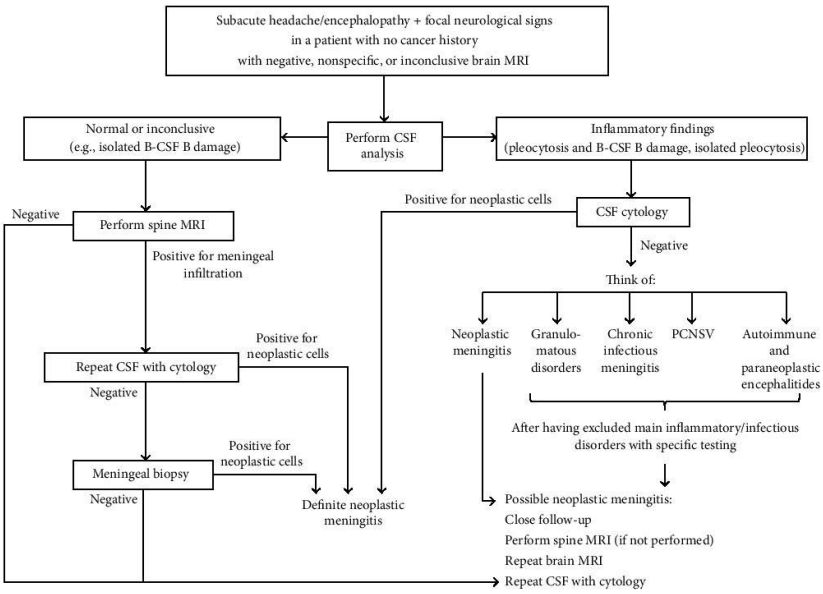

Figure 5: The proposed algorithm for the diagnosis of neoplastic meningitis in naïve patients. B-CSF B = blood-cerebrospinal fluid barrier, CSF = cerebrospinal fluid, and PCNSV = primary CNS vasculitis.

meningeal neoplastic infiltration [1, 6, 7], but data correlating sensitivity of MRI to the timing of its execution are currently unavailable. In our series, brain MRI performed within the first month from onset was normal despite the clinical pattern was dominated by cerebral involvement. In the absence of meningeal contrast enhancement, dilation of the ventricular system or reduction of subarachnoid sulci may be indirect signs of neoplastic meningitis and should be valued in all cases.

CSF analysis, which was performed with remarkable delay in our series, showed a significant protein increase due to severe B-CSF B damage in all patients. Noteworthy, despite the delay and repeated sampling, in patient 2 CSF results were inconclusive for the detection of neoplastic cells, leading to performing a meningeal biopsy. Interestingly, CSF cytology can be persistently negative even in the presence of disseminated cranial and spinal disease on MRI. These data are consistent with current evidence that malignant cells are detected in the CSF in 50–70% of patients with neoplastic meningitis by initial lumbar puncture [1, 8, 9], a rate that increases with repeated sampling. In the case of normal or inconclusive CSF findings, a spine MRI may be helpful to demonstrate meningeal infiltration of cauda roots, even in the absence of spinal symptoms.

Overall, diagnostic difficulties resulted in a dramatic diagnostic delay, ranging from 17 to 47 weeks after clinical onset. These data are remarkable considering the poor short-term prognosis of these patients [10], who could access only palliative or even no treatment.

In conclusion, the difficulty in both posing the clinical suspicion and confirming the diagnosis of neoplastic meningitis contributed to the sharp diagnostic delay observed in our series. Early recognition is fundamental to make differential diagnosis and start appropriate therapies. Thus, improving the handle of these patients and the current diagnostic algorithms for neoplastic meningitis is of capital importance to offer them appropriate treatments.

Conflict of Interests

The authors declare that there is no conflict of interests regarding the publication of this paper.

Acknowledgments

Anna Luisa Di Stefano was supported by PRIN 2010-2011, 2010ZESJWN_008.

References

[1] B. Gleissner and M. C. Chamberlain, "Neoplastic meningitis," *The Lancet Neurology*, vol. 5, no. 5, pp. 443–452, 2006.

[2] S. T. Rosen, J. Aisner, R. W. Makuch et al., "Carcinomatous leptomeningitis in small cell lung cancer: a clinicopathologic review of the National Cancer Institute experience," *Medicine*, vol. 61, no. 1, pp. 45–53, 1982.

[3] M. H. Amer, M. Al-Sarraf, L. H. Baker, and V. K. Vaitkevicius, "Malignant melanoma and central nervous system metastases. Incidence, diagnosis, treatment and survival," *Cancer*, vol. 42, no. 2, pp. 660–668, 1978.

[4] S. V. Liubinas, N. Maartens, and K. J. Drummond, "Primary melanocytic neoplasms of the central nervous system," *Journal of Clinical Neuroscience*, vol. 17, no. 10, pp. 1227–1232, 2010.

[5] M. Balm and J. Hammack, "Leptomeningeal carcinomatosis: presenting features and prognostic factors," *Archives of Neurology*, vol. 53, no. 7, pp. 626–632, 1996.

[6] R. J. Freilich, G. Krol, and L. M. DeAngelis, "Neuroimaging and cerebrospinal fluid cytology in the diagnosis of leptomeningeal metastasis," *Annals of Neurology*, vol. 38, no. 1, pp. 51–57, 1995.

[7] L. M. DeAngelis, "Current diagnosis and treatment of leptomeningeal metastasis," *Journal of Neuro-Oncology*, vol. 38, no. 2-3, pp. 245–252, 1998.

[8] R. J. Van Oostenbrugge and A. Twijnstra, "Presenting features and value of diagnostic procedures in leptomeningeal metastases," *Neurology*, vol. 53, no. 2, pp. 382–385, 1999.

[9] M. E. Olson, N. L. Chernik, and J. B. Posner, "Infiltration of the leptomeninges by systemic cancer: a clinical and pathologic study," *Archives of Neurology*, vol. 30, no. 2, pp. 122–137, 1974.

[10] L. Harstad, K. R. Hess, and M. D. Groves, "Prognostic factors and outcomes in patients with leptomeningeal melanomatosis," *Neuro-Oncology*, vol. 10, no. 6, pp. 1010–1018, 2008.

J Neurooncol
DOI 10.1007/s11060-015-1999-3

LABORATORY INVESTIGATION

TERT promoter mutations and rs2853669 polymorphism: prognostic impact and interactions with common alterations in glioblastomas

Umberto Nencha[1] · Amithys Rahimian[1,2] · Marine Giry[1] · Andrea Sechi[1] · Karima Mokhtari[3] · Marc Polivka[4] · Yohann Schmitt[1] · Anna-Luisa Di Stefano[1,5] · Agusti Alentorn[1,5] · Marianne Labussière[1] · Marc Sanson[1,5,6]

Received: 6 June 2015 / Accepted: 19 November 2015

Abstract *TERT* promoter (*TERT*p) mutation is the most common mutation in glioblastomas. It creates a putative binding site for Ets/TCF transcription factors, enhancing telomerase expression and activity, whereas the rs2853669 variant disrupts another Ets/TCF binding. We explore here the interaction between these two alterations, tumor genomic profile and the impact on prognosis. The *TERT*p and rs2853669 statuses were determined and confronted with the outcome and molecular profile, i.e., loss of chromosome 10q, *CDKN2A* deletion, *IDH* mutation, *EGFR* amplification, *MGMT* promoter methylation. 651 glioblastomas were selected (sex ratio = 1.35, median age 60.4 years, median survival 13.5 months). The *TERT*p mutation found in 481 patients (74 %) was independent from rs2853669 genotypes. *TERT*p mutation, but not rs2853669 status, was associated with older age (61.4 vs. 52.8 years). rs2853669 status had no impact on overall survival (OS) either in mutated *TERT*p or wild-type *TERT*p. Neither rs2736100 (*TERT*, 5q15.33) nor rs192011116 (*TERC*, 3q26.2) status had any impact on survival or showed any association with a *TERT*p mutation. The *TERT*p mutation was associated with *EGFR* amplification chromosome 10q loss, *CDKN2A* deletion and *IDH* wt. *EGFR* amplification was associated with a better outcome in TERTp mutated GBM, and a worse outcome in TERTp WT. This study—the largest analyzing the *TERT*p mutation and the rs2853669 polymorphism—fails to find any prognostic impact of rs2853669. It confirms the dual prognostic impact of *EGFR* amplification depending on *TERT*p status.

Keywords Glioblastoma · TERT · Polymorphism · EGFR · rs2853669

Umberto Nencha, Amithys Rahimian and Marine Giry have contributed equally to the data presented in this paper.

Electronic supplementary material The online version of this article (doi:10.1007/s11060-015-1999-3) contains supplementary material, which is available to authorized users.

✉ Marc Sanson
marc.sanson@psl.aphp.fr

[1] Sorbonne Universités UPMC Univ Paris 06, INSERM CNRS, U1127, UMR 7225, ICM, 75013 Paris, France

[2] OncoNeuroTek, 75013 Paris, France

[3] Laboratoire de neuropathologie R Escourolle, GH Pitié-Salpêtrière, 75013 Paris, France

[4] Laboratoire d'anatomie pathologique, Hôpital Lariboisière, 75010 Paris, France

[5] AP-HP, GH Pitié-Salpêtrière, Service de Neurologie 2, 75013 Paris, France

[6] Service de Neurologie 2, Groupe Hospitalier Pitié-Salpêtrière, 75651 Paris cedex 13, France

Introduction

Increasing telomerase activity promotes immortalization through telomere lengthening. Telomerase consists of a reverse transcriptase, encoded by *TERT*, and an RNA component, encoded by *TERC*, which serves as a template for the telomere repeat. Interestingly, the Single Nucleotide Polymorphisms (SNPs) rs2736100, which maps to the *TERT* region (5q15.33), and the rs192011116, which maps near *TERC* (3q26.2), have both been associated with a glioblastoma risk and with longer mean leukocyte telomere length [1–3]. In addition, somatic mutations of the *TERT* promoter gene have been reported in numerous cancers and particularly in gliomas. They are present in 80 % of

Published online: 25 November 2015

oligodendrogliomas and 75 % of glioblastomas (GBM) [4]. The two most common mutations (*TERTp* C250T and C228T) create a putative binding site for the Ets/TCF transcription factors, which results in a two to fourfold increase in telomerase expression [5]. These mutations are an independent negative prognostic factor in glioblastomas [6–10]. On the other hand, the SNP rs2853669 at −245 bp from the *TERT* gene ATG, disrupts another binding site for Ets/TCF, through a C/T substitution, and it has been associated with lower *TERT* expression and decreased telomerase activity [11–14]. Whereas a former study found the poor predictive impact of a *TERTp* mutation confined to the patients who did not carry the variant C-allele of rs2853669 polymorphism [8], another paper reached the opposite conclusions and showed that the prognostic impact of a *TERTp* mutation was much stronger in carriers compared to non carriers of the C-allele [15].

Here we determined the distribution of the different rs2853669 variants in 651 patients affected by primary GBMs. We analyzed the interaction between *TERTp* mutational status and the rs2853669, rs2736100 (5q15.33) and rs192011116 (3q26.2) status in terms of overall survival. We also explored the interaction with other common molecular markers of GBMs: *EGFR* amplification, chromosome 10q loss, *CDKN2A* loss, *IDH1* or *IDH2 (IDH)* mutation and *MGMT* promoter (*MGMT*p) methylation.

Patients and methods

Patients selection

Patients' informed consent and ethical board approval were required for collection of tumor samples and clinical-pathological information, as stated by the Declaration of Helsinki. Patient inclusion criteria were: histologic diagnosis of primary glioblastoma; availability of tumor DNA; and complete clinical data from the neuro-oncology database (OncoNeuroTek, Paris).

DNA extraction, amplification, purification and Sanger sequencing

DNA from cryopreserved or formalin-fixed paraffin embedded (FFPE) tumor samples was extracted using the QIAmp Midi Kit (Qiagen) or iPrep ChargeSwitch Forensic kit (Life Technologies) respectively, as previously described [13].

DNA amplification was performed using the mix FastStart™ PCR Master (Roche®) as follows: 3 min at 94 °C; 35 cycles at 94 °C-15 s, 60 °C-45 s, 72 °C-1 min, with a final step at 72 °C for 8 min. Primer sequences were as follows: SNP_TERT_F: ATTCGACCTCTCTCCGCTGG; SNP_TERT_R: CTGGAAGGTGAAGGGGCAG; TERTp_F: GGATTCGCGGGCACAGAC; C228_250T_R: CAGCGCTGCCTGAAACTC.

DNA sequencing was performed by the Sanger technique.

The rs2736100 (5q15.33) and rs192011116 (3q26.2) SNP statuses were available from a previous study for a subset of patients [1]. *IDH* status, *EGFR* amplification, 10q loss, *CDKN2A* deletion and *MGMT*p methylation were available in the OncoNeuroTek database or were determined as previously described [6, 16].

Statistical analysis

The χ^2 test or Fisher exact test were used to compare the genotype distribution. The Man-Whitney-Wilcoxon test was used to compare continuous variables (i.e., age) between distinct categories.

Overall survival (OS) was defined as the time between diagnosis and death or last follow up. Living patients at the time of the last follow up were considered as censored events in the analysis. Progression free survival (PFS) was defined as the time between the diagnosis and recurrence or last follow-up. Patients who were recurrence-free at the last follow-up were considered as a censored event in the analysis. Survival curves were calculated according to the Kaplan–Meier method and differences between curves were assessed using the log-rank test. Variables with a significant p-value were used to build a multivariate Cox model. p-values <0.05 were considered significant.

Results

Patients characteristics and outcomes

651 glioblastomas were selected (sex ratio = 1.35, median age at diagnosis 60.4 years). Median survival was 13.5 months. The patients' characteristics are reported in Table 1. As expected, age ($p < 10^{-12}$) and Karnofsky performance status (KPS) ($p < 10^{-5}$) were strong predictors of outcome. Upfront treatment modalities were also associated with outcome, i.e., surgery (biopsy vs. partial or gross total removal, $p < 10^{-7}$) (supplementary Fig. 1) and radiotherapy-temozolomide versus radiotherapy versus chemotherapy alone ($p < 10^{-12}$).

These parameters were entered into a Cox model (supplementary Table 1 a, b). This multivariate analysis suggests that treatment modalities are related to KPS while age remains the strongest independent prognostic factor.

Table 1 Clinical and molecular characteristics of the patients

Age at diagnosis	60.4 (15–90)
Gender	375 M, 276 F. Sex ratio = 1.35
KPS	Median 80 (20–100)
	<70: 56
	≥70: 451
	ND: 144
Surgery	Biopsy: 173
	Partial removal: 209
	Total removal: 269
Upfront treatment	Radiotherapy-TMZ: 239
	Radiotherapy: 238
	Chemotherapy: 56
	ND: 118
PFS	5.5 months
OS	13.5 months
TERTp mutational status	492 mut/159 wt
	C228T: 360
	C132T: 127
	C228T and C250T: 5
rs2853669 status	CC: 65
	CT: 270
	TT: 316
rs192011116 status	AA: 13
	GA: 85
	GG: 117
	ND: 436
rs2736100 status	A A: 29
	C A: 136
	C C: 91
	ND: 393
IDH1/2	Mutated: 50
	Wt: 600
	ND:1
Chromosome 10q status	Loss: 453
	No loss: 103
	ND: 96
EGFR status	Amplification: 221
	Normal: 375
	ND: 55
p16/CDKN2A status	Deletion: 248
	No deletion: 343
	ND: 60
MGMTp status	Methylated: 212
	Unmethylated: 239
	ND: 200

*TERT*p mutation status is independent from rs2853669 genotypes

We found 492 (76 %) patients with *TERT*p mutation, 365 (56.0 %) had the C228T substitution, and 132 (20 %) the C250T, five cases harboring both mutations. rs2853669 status was TT in 316 (48.5 %) patients, CT in 270 (41.5 %) and CC in 65 (10 %). *TERTp* mutation was associated with a poorer outcome both in carriers (allele C: OR = 1.41; $p = 0.027$) and non-carriers of the rs2853669 variant (allele T: OR = 1.7; $p = 0.00085$). There was no difference in the relative distribution of the rs2853669 genotypes between different *TERTp* mutated GBM and *TERTp* wild type GBM ($\chi^2 = 0.92$; $p = 0.63$). Relative genotype frequencies were CC 47/492 (9.6 %) CT 209/492 (42.5 %) TT 236/492 (47.9 %) for *TERTp* mutated patients and CC 18/159 (11.3 %) CT 61/159 (38.4 %) TT 80/159 (50.3 %) for *TERTp* wild type (wt), fulfilling the Hardy–Weinberg equilibrium ($p = 0.9$; $p = 0.2$).

TERTp mutation but not rs2853669 status is associated with older age

We looked for an association between age at diagnosis and rs2853669 status in both *TERTp* mutated and wild type patients. Whereas *TERTp* mutation was correlated with older age (mean age 61.4, vs. 52.8 years, $p < 0.0001$), age distribution did not differ between rs2853669 CC, CT or TT genotypes ($p = 0.13$) (Fig. 1).

rs2853669 Status has no impact on overall survival (OS)

We first compared the CC and CT carriers versus the TT carriers groups and found no difference in OS ($p = 0.3$, Fig. 2).

We then analyzed separately the impact of rs2853669 status on OS in *TERTp* mutated patients and in *TERTp* wt patients. While a *TERT*p mutation is clearly associated with a poorer survival ($p < 0.0001$), we found no prognostic impact of rs2853669 status in both *TERTp* mutated and *TERTp* wt populations (Fig. 3). However, C carriers (i.e., CC+CT patients) tended to have a better outcome in the *TERT*p mutated group ($p = 0.18$), but not in the *TERT*p wt group. rs2736100 (5q15.33) and rs192011116 (3q26.2) statuses were available for 215 GBM patients. None of them had an impact on survival ($p = 0.6$) and we found no association with the *TERTp* mutation ($p = 0.55$ and 0.7 respectively).

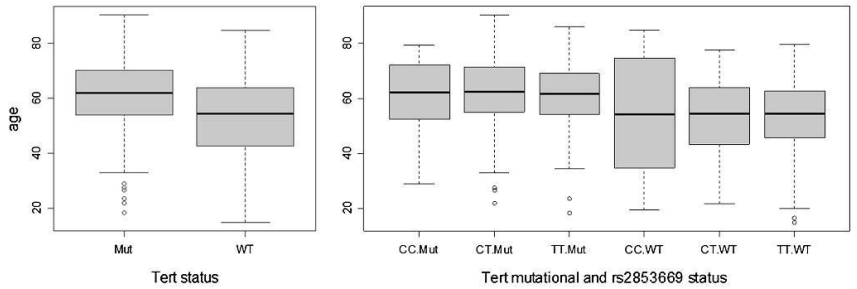

Fig. 1 Age distribution according to *TERT*p mutational status ($p < 10^{-9}$) and rs2853669 (p = NS)

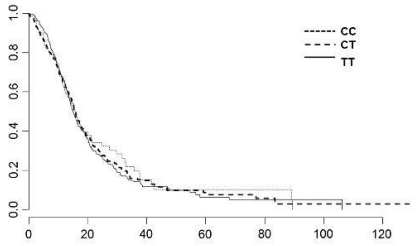

Fig. 2 Survival curves according to the rs2853669 status CC, CT and CT

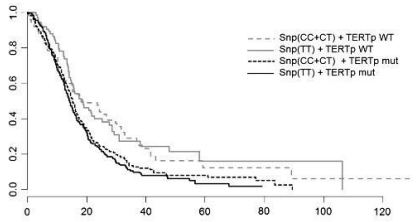

Fig. 3 Survival curves according to the rs2853669 status (CC+CT vs. TT) and *TERT*p mutational status

Association with the main molecular alterations and prognostic impact

We first looked for associations between *TERTp* status and the following molecular alterations: chromosome 10q loss, found in 385/429 of *TERTp* mutated versus 67/126 in *TERTp* wt ($p < 10^{-15}$), *EGFR* amplification, found in 197/454 versus 24/142 ($p < 10^{-8}$), *CDKN2A/P16* deletion, found in 203/450 versus 45/139 (p = 0.02), *IDH* mutation, found in 11/491 versus 39/159 ($p < 10^{-15}$), and MGMT promoter status, found methylated in 156/347 versus 56/104 (p = 0.13).

We then analyzed the prognostic impact of each of these alterations (suppl. Figs. 2a–f). As expected, only *TERTp* mutation, *IDH* mutation and *MGMTp* methylation status had a prognostic impact. The prognostic impact was independent of treatment modalities, except for the *MGMTp* methylation status, which showed a clear benefit of RT-TMZ versus RT alone in *MGMTp* methylated ($p < 10^{-4}$), but not *MGMTp* unmethylated patients (p = 0.2) (suppl Fig. 3). This confirms previous data [17].

We then investigated the prognostic impact of these combined alterations. While *EGFR* amplification has no prognostic impact per se, we consolidated here our previous data [6], showing that *EGFR* amplification is associated with a better outcome in *TERTp* mutated GBM (median survival = 16.1 months vs. 13 months; p = 0.001), and a poorer outcome in *TERTp* wt GBM (median survival = 13.3 months vs. 26.5 months; p < 0.01) (Fig. 4a). Whereas IDH mutation is probably associated with better outcome in the context of *TERTp*wt (median survival 29 months vs. 17.3 months p = 0.09) this may be not the case for the *IDH*wt-*TERTp*mut (median survival 20 months vs. 14.1 months p = 0.3) (Fig. 4b).

rs2853669 status was not associated with *IDH* status, Chromosome 10q loss (p = 0.13), *CDKN2A* deletion (p = 0.5), or *MGMTp* status (p = 0.99). *EGFR* amplification tended to be more frequent in GBM patients bearing the variant allele C (123/305 vs. 98/291, p = 0.08).

Multivariate analysis

We first entered all the significant prognostic markers in a Cox model (suppl. Table 2 a, b). We found that only *MGMTp* was an independent factor, while *TERTp* status,

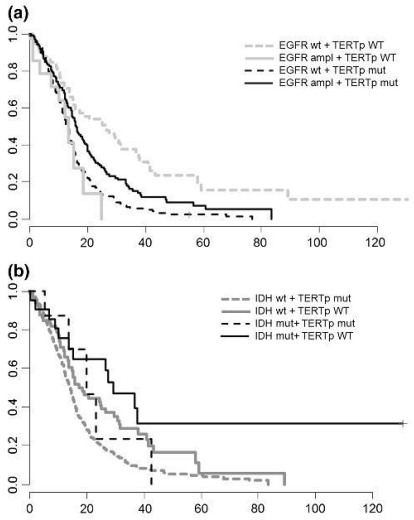

Fig. 4 Survival curves according to *TERT*p and *EGFR* status (**a**). Survival curves according to *TERT*p and *IDH* status (**b**)

and to a lesser extend IDH status, were dependent on age.

Because we found *EGFR* associated with *TERTp* mutation, and *EGFR* prognostic impact dependent on *TERTp* status (Fig. 4a), we investigated the relation between *EGFR* status and *TERTp* using multivariate analysis (suppl. Table 3). We found indeed that *EGFR* amplification is related to better outcome in GBM patients (OR = 0.756, p = 0.02 when entering *TERTp* vs. OR = 0.983 for *EGFR* alone).

Discussion

Because previous works have generated conflicting data, we first investigated here, on a larger series of primary glioblastomas, the interaction between *TERTp* status and rs2853669. The rs2853669 minor allele disrupts a site for the ETS transcription factor family, whereas the *TERTp* mutation creates a new site. While mutation results in an increase of TERT activity, the variant rs2853669 allele is associated with lower TERT expression and activity [13, 14]. We may therefore suspect that the two variants – constitutional and somatic-, having opposite biological effects, will also have an opposite prognostic impact. And indeed in bladder cancer, the variant G has been associated with better outcome in *TERT*p mutated bladder cancers and with poorer outcome in non-mutated cancers [12]. In glioblastomas, data are more conflicting. Based on 178 glioblastomas, Simon et al. found that the poor prognostic effect of *TERTp* mutation was confined to the 84 non-carriers of the C-allele for the rs2853669 polymorphism [8]. In contrast, Spiegl et al. found an opposite result in a series of 126 glioblastoma patients, with a poor prognostic effect of *TERTp* mutation only in the 67 carriers of the C-allele polymorphism rs2853669 [15]. Here we showed that the presence of a *TERTp* mutation is associated with a poor prognosis both in carriers and non-carriers of the rs2853669 variant. In addition this study, based on the largest series of glioblastomas of any such studies, does not show any significant prognostic impact of rs2853669 independently of age, or to the presence of a *TERT*p mutation (although the C variant tended to be associated with better outcome in *TERTp* mut GBMs, the trend was clearly not significant).

Since telomere lengthening is critical to tumor survival, and telomere lengthening has been associated with higher glioma risk, we also investigated the potential relation between the *TERTp* mutation and two variants rs2736100 on 5q15.33 (TERT region) and rs192011116 on 3q26.2(TERC region), associated with higher glioblastoma risk and telomere lengthening. Although this analysis was conducted on a smaller number of samples, once more we found no association.

We extended here our previous analysis showing that *TERT*p mutation is associated with a poor outcome, loss of chromosome 10q, *CDKN2A* deletion and *EGFR* amplification [6]. We confirmed here, in contrast to earlier studies [7], that the *TERTp* mutation's poor prognosis impact is not related to the lack of *IDH* mutation: we rather suggest that *IDH* mutation is associated with poor prognosis in the presence of a *TERTp* mutation [6] (Fig. 4b): supporting our data. A similar result (although not mentioned by the authors) can be extracted from the data presented in a recent, independent publication from Eckel-Passow et al. (cf their Fig. 3b) [18]. Finally we show that *EGFR* amplification has an opposite prognostic impact according to *TERTp* status: positive in *TERTp* mutated GBM, and negative in *TERTp* GBM (Fig. 4a).

Acknowledgments Work supported by the Fondation ARC. UN was supported by a grant from the University of Pavia and the Association pour la Recherche sur les Tumeurs Cérébrales. The research leading to these results has received funding from the program "investissements d'avenir" ANR-10-IAIHU-06. The authors are indebted to Alexandru Agachi for English Editing.

Compliance with ethical standards

Conflict of interest None.

References

1. Shete S, Hosking FJ, Robertson LB et al (2009) Genome-wide association study identifies five susceptibility loci for glioma. Nat Genet 41:899–904
2. Walsh KM, Codd V, Smirnov IV et al (2014) Variants near TERT and TERC influencing telomere length are associated with high-grade glioma risk. Nat Genet 46:731–735
3. Jones AM, Beggs AD, Carvajal-Carmona L et al (2012) TERC polymorphisms are associated both with susceptibility to colorectal cancer and with longer telomeres. Gut 61:248–254
4. Killela PJ, Reitman ZJ, Jiao Y et al (2013) TERT promoter mutations occur frequently in gliomas and a subset of tumors derived from cells with low rates of self-renewal. Proc Natl Acad Sci U S A 110:6021
5. Huang FW, Hodis E, Xu MJ, Kryukov GV, Chin L, Garraway LA (2013) Highly recurrent TERT promoter mutations in human melanoma. Science 339:957–959
6. Labussière M, Boisselier B, Mokhtari K et al (2014) Combined analysis of TERT, EGFR, and IDH status defines distinct prognostic glioblastoma classes. Neurology 83:1200–1206
7. Nonoguchi N, Ohta T, Oh JE, Kim YH, Kleihues P, Ohgaki H (2013) TERT promoter mutations in primary and secondary glioblastomas. Acta Neuropathol 126:931–937
8. Simon M, Hosen I, Gousias K et al (2015) TERT promoter mutations: a novel independent prognostic factor in primary glioblastomas. Neuro Oncol 17:45–52
9. Arita H, Narita Y, Fukushima S et al (2013) Upregulating mutations in the TERT promoter commonly occur in adult malignant gliomas and are strongly associated with total 1p19q loss. Acta Neuropathol 126:267–276
10. Killela PJ, Pirozzi CJ, Healy P et al (2014) Mutations in IDH1, IDH2, and in the TERT promoter define clinically distinct subgroups of adult malignant gliomas. Oncotarget 5:1515–1525
11. Hsu CP, Hsu NY, Lee LW, Ko JL (2006) Ets2 binding site single nucleotide polymorphism at the hTERT gene promoter–effect on telomerase expression and telomere length maintenance in non-small cell lung cancer. Eur J Cancer 42:1466–1474
12. Rachakonda PS, Hosen I, de Verdier PJ et al (2013) TERT promoter mutations in bladder cancer affect patient survival and disease recurrence through modification by a common polymorphism. Proc Natl Acad Sci U S A 110:17426–17431
13. Labussière M, Di Stefano AL, Gleize V et al (2014) TERT promoter mutations in gliomas, genetic associations and clinicopathological correlations. Br J Cancer 111:2024–2032
14. Park CK, Lee SH, Kim JY et al (2014) Expression level of hTERT is regulated by somatic mutation and common single nucleotide polymorphism at promoter region in glioblastoma. Oncotarget 5:3399–3407
15. Spiegl-Kreinecker S, Lotsch D, Ghanim B et al (2015) Prognostic quality of activating TERT promoter mutations in glioblastoma: interaction with the rs2853669 polymorphism and patient age at diagnosis. Neuro Oncol 17:1231
16. Sanson M, Marie Y, Paris S et al (2009) Isocitrate dehydrogenase 1 codon 132 mutation is an important prognostic biomarker in gliomas. J Clin Oncol 27:4150–4154
17. Hegi ME, Diserens AC, Gorlia T et al (2005) MGMT gene silencing and benefit from temozolomide in glioblastoma. N Engl J Med 352:997–1003
18. Eckel-Passow JE, Lachance DH, Molinaro AM et al (2015) Glioma Groups Based on 1p/19q, IDH, and TERT Promoter Mutations in Tumors. N Engl J Med 372:2499–2508

8. REFERENCES

Allen, P. S., Thompson, R. B., & Wilman, A. H. (1997). Metabolite-specific NMR spectroscopy in vivo. *NMR Biomed, 10*(8), 435-444.

Andronesi, O. C., Kim, G. S., Gerstner, E., Batchelor, T., Tzika, A. A., Fantin, V. R., Sorensen, A. G. (2012). Detection of 2-hydroxyglutarate in IDH-mutated glioma patients by in vivo spectral-editing and 2D correlation magnetic resonance spectroscopy. *Sci Transl Med, 4*(116), 116ra114. doi:10.1126/scitranslmed.3002693

Andronesi, O. C., Loebel, F., Bogner, W., Marjanska, M., Vander Heiden, M. G., Iafrate, A. J., Cahill, D. P. (2016). Treatment Response Assessment in IDH-Mutant Glioma Patients by Noninvasive 3D Functional Spectroscopic Mapping of 2-Hydroxyglutarate. *Clin Cancer Res, 22*(7), 1632-1641. doi:10.1158/1078-0432.CCR-15-0656

Arcaro, A., & Guerreiro, A. S. (2007). The phosphoinositide 3-kinase pathway in human cancer: genetic alterations and therapeutic implications. *Curr Genomics, 8*(5), 271-306. doi:10.2174/138920207782446160

Brennan, C. W., Verhaak, R. G., McKenna, A., Campos, B., Noushmehr, H., Salama, S. R., Network, T. R. (2013). The somatic genomic landscape of glioblastoma. *Cell, 155*(2), 462-477. doi:10.1016/j.cell.2013.09.034

Cairncross, J. G., Ueki, K., Zlatescu, M. C., Lisle, D. K., Finkelstein, D. M., Hammond, R. R., Louis, D. N. (1998). Specific genetic predictors of chemotherapeutic response and survival in patients with anaplastic oligodendrogliomas. *J Natl Cancer Inst, 90*(19), 1473-1479.

Cairncross, J. G., Wang, M., Jenkins, R. B., Shaw, E. G., Giannini, C., Brachman, D. G., Curran, W. J., Jr. (2014). Benefit from procarbazine, lomustine, and vincristine in oligodendroglial tumors is associated with mutation of IDH. *J Clin Oncol, 32*(8), 783-790. doi:10.1200/JCO.2013.49.3726

Capper, D., Zentgraf, H., Balss, J., Hartmann, C., & von Deimling, A. (2009). Monoclonal antibody specific for IDH1 R132H mutation. *Acta Neuropathol, 118*(5), 599-601. doi:10.1007/s00401-009-0595-z

Chell, V., Balmanno, K., Little, A. S., Wilson, M., Andrews, S., Blockley, L., Cook, S. J. (2013). Tumour

cell responses to new fibroblast growth factor receptor tyrosine kinase inhibitors and identification of a gatekeeper mutation in FGFR3 as a mechanism of acquired resistance. *Oncogene, 32*(25), 3059-3070. doi:10.1038/onc.2012.319

Chesi, M., Nardini, E., Brents, L. A., Schrock, E., Ried, T., Kuehl, W. M., & Bergsagel, P. L. (1997). Frequent translocation t(4;14)(p16.3;q32.3) in multiple myeloma is associated with increased expression and activating mutations of fibroblast growth factor receptor 3. *Nat Genet, 16*(3), 260-264. doi:10.1038/ng0797-260

Choi, C., Ganji, S. K., DeBerardinis, R. J., Hatanpaa, K. J., Rakheja, D., Kovacs, Z., Maher, E. A. (2012). 2-hydroxyglutarate detection by magnetic

resonance spectroscopy in IDH-mutated patients with gliomas. *Nat Med, 18*(4), 624-629. doi:10.1038/nm.2682

Dang, C. V. (2010). Glutaminolysis: supplying carbon or nitrogen or both for cancer cells? *Cell Cycle, 9*(19), 3884-3886. doi:10.4161/cc.9.19.13302

Dang, L., White, D. W., Gross, S., Bennett, B. D., Bittinger, M. A., Driggers, E. M., Su, S. M. (2009). Cancer-associated IDH1 mutations produce 2-hydroxyglutarate. *Nature, 462*(7274), 739-744. doi:10.1038/nature08617

de la Fuente, M. I., Young, R. J., Rubel, J., Rosenblum, M., Tisnado, J., Briggs, S., Thakur, S. B. (2016). Integration of 2-hydroxyglutarate-proton magnetic resonance spectroscopy into clinical practice for disease monitoring in isocitrate dehydrogenase-mutant glioma. *Neuro Oncol, 18*(2), 283-290. doi:10.1093/neuonc/nov307

Di Stefano, A. L., Enciso-Mora, V., Marie, Y., Desestret, V., Labussiere, M., Boisselier, B., Sanson, M. (2013). Association between glioma susceptibility loci and tumour pathology defines specific molecular etiologies. *Neuro Oncol, 15*(5), 542-547. doi:10.1093/neuonc/nos284

Di Stefano, A. L., Fucci, A., Frattini, V., Labussiere, M., Mokhtari, K., Zoppoli, P., Iavarone, A. (2015). Detection, Characterization, and Inhibition of FGFR-TACC Fusions in IDH Wild-type Glioma. *Clin Cancer Res, 21*(14), 3307-3317. doi:10.1158/1078-0432.CCR-14-2199

Eckel-Passow, J. E., Lachance, D. H., Molinaro, A. M., Walsh, K. M., Decker, P. A., Sicotte, H., Jenkins, R. B. (2015). Glioma Groups Based on 1p/19q, IDH, and TERT Promoter Mutations in Tumors. *N Engl J Med, 372*(26), 2499-2508. doi:10.1056/NEJMoa1407279

Emir, U. E., Larkin, S. J., de Pennington, N., Voets, N., Plaha, P., Stacey, R., Ansorge, O. (2016). Noninvasive Quantification of 2-Hydroxyglutarate in Human Gliomas with IDH1 and IDH2 Mutations. *Cancer Res, 76*(1), 43-49. doi:10.1158/0008-5472.CAN-15-0934

Enciso-Mora, V., Hosking, F. J., Di Stefano, A. L., Zelenika, D., Shete, S., Broderick, P., Houlston, R. S. (2013). Low penetrance susceptibility to glioma is caused by the TP53 variant rs78378222. *Br J Cancer, 108*(10), 2178-2185. doi:10.1038/bjc.2013.155

Gonzalez-Aguilar, A., Idbaih, A., Boisselier, B., Habbita, N., Rossetto, M., Laurenge, A., Hoang-Xuan, K. (2012). Recurrent mutations of MYD88 and TBL1XR1 in primary central nervous system lymphomas. *Clin Cancer Res, 18*(19), 5203-5211. doi:10.1158/1078-0432.CCR-12-0845

Govind, V., Young, K., & Maudsley, A. A. (2015). Corrigendum: proton NMR chemical shifts and coupling constants for brain metabolites. Govindaraju V, Young K, Maudsley AA, NMR Biomed. 2000; 13: 129-153. *NMR Biomed, 28*(7), 923-924. doi:10.1002/nbm.3336

Graaf, R. d. (2007). *In vivo NMR spectroscopy: principles and techniques,* (2nd ed. ed.). Chichester: John Wiley & Sons,.

Gross, S., Cairns, R. A., Minden, M. D., Driggers, E. M., Bittinger, M. A., Jang, H. G., Mak, T. W. (2010). Cancer-associated metabolite 2-hydroxyglutarate accumulates in acute myelogenous leukemia with

isocitrate dehydrogenase 1 and 2 mutations. *J Exp Med, 207*(2), 339-344. doi:10.1084/jem.20092506

Hartmann, C., Meyer, J., Balss, J., Capper, D., Mueller, W., Christians, A., von Deimling, A. (2009). Type and frequency of IDH1 and IDH2 mutations are related to astrocytic and oligodendroglial differentiation and age: a study of 1,010 diffuse gliomas. *Acta Neuropathol, 118*(4), 469-474. doi:10.1007/s00401-009-0561-9

Hemminki, K., Tretli, S., Sundquist, J., Johannesen, T. B., & Granstrom, C. (2009). Familial risks in nervous-system tumours: a histology-specific analysis from Sweden and Norway. *Lancet Oncol, 10*(5), 481-488. doi:10.1016/S1470-2045(09)70076-2

Heo, H., Kim, S., Lee, H. H., Cho, H. R., Xu, W. J., Lee, S. H., Kim, H. (2016). On the Utility of Short Echo Time (TE) Single Voxel 1H-MRS in Non-Invasive Detection of 2-Hydroxyglutarate (2 HG); Challenges and Potential Improvement Illustrated with Animal Models Using MRUI and LCModel. *PLoS One, 11*(1), e0147794. doi:10.1371/journal.pone.0147794

Houillier, C., Wang, X., Kaloshi, G., Mokhtari, K., Guillevin, R., Laffaire, J., Delattre, J. Y. (2010). IDH1 or IDH2 mutations predict longer survival and response to temozolomide in low-grade gliomas. *Neurology, 75*(17), 1560-1566. doi:10.1212/WNL.0b013e3181f96282

Idbaih, A., Aimard, J., Boisselier, B., Marie, Y., Paris, S., Criniere, E., Delattre, J. Y. (2009). Epidermal growth factor receptor extracellular domain mutations in primary glioblastoma. *Neuropathol Appl Neurobiol, 35*(2), 208-213. doi:10.1111/j.1365-2990.2008.00977.x

Idbaih, A., Kouwenhoven, M., Jeuken, J., Carpentier, C., Gorlia, T., Kros, J. M., Hoang-Xuan, K. (2008). Chromosome 1p loss evaluation in anaplastic oligodendrogliomas. *Neuropathology, 28*(4), 440-443. doi:10.1111/j.1440-1789.2008.00863.x

Idbaih, A., Marie, Y., Lucchesi, C., Pierron, G., Manie, E., Raynal, V., Delattre, O. (2008). BAC array CGH distinguishes mutually exclusive alterations that define clinicogenetic subtypes of gliomas. *Int J Cancer, 122*(8), 1778-1786. doi:10.1002/ijc.23270

Idbaih, A., Marie, Y., Pierron, G., Brennetot, C., Hoang-Xuan, K., Kujas, M., Delattre, J. Y. (2005). Two types of chromosome 1p losses with opposite significance in gliomas. *Ann Neurol, 58*(3), 483-487. doi:10.1002/ana.20607

Janin, M., Mylonas, E., Saada, V., Micol, J. B., Renneville, A., Quivoron, C., de Botton, S. (2014). Serum 2-hydroxyglutarate production in IDH1- and IDH2-mutated de novo acute myeloid leukemia: a study by the Acute Leukemia French Association group. *J Clin Oncol, 32*(4), 297-305. doi:10.1200/JCO.2013.50.2047

Jenkins, R. B., Blair, H., Ballman, K. V., Giannini, C., Arusell, R. M., Law, M., Buckner, J. C. (2006). A t(1;19)(q10;p10) mediates the combined deletions of 1p and 19q and predicts a better prognosis of patients with

oligodendroglioma. *Cancer Res, 66*(20), 9852-9861. doi:10.1158/0008-5472.CAN-06-1796

Jenkins, R. B., Xiao, Y., Sicotte, H., Decker, P. A., Kollmeyer, T. M., Hansen, H. M., Wrensch, M. R. (2012). A low-frequency variant at 8q24.21 is strongly associated with risk of oligodendroglial tumors and astrocytomas with IDH1 or IDH2 mutation. *Nat Genet, 44*(10), 1122-1125. doi:10.1038/ng.2388

Killela, P. J., Pirozzi, C. J., Healy, P., Reitman, Z. J., Lipp, E., Rasheed, B. A., Bigner, D. D. (2014). Mutations in IDH1, IDH2, and in the TERT promoter define clinically distinct subgroups of adult malignant gliomas. *Oncotarget, 5*(6), 1515-1525. doi:10.18632/oncotarget.1765

Killela, P. J., Reitman, Z. J., Jiao, Y., Bettegowda, C., Agrawal, N., Diaz, L. A., Jr., Yan, H. (2013). TERT promoter mutations occur frequently in gliomas and a subset of tumors derived from cells with low rates of self-renewal. *Proc Natl Acad Sci U S A, 110*(15), 6021-6026. doi:10.1073/pnas.1303607110

Kim, H., Kim, S., Lee, H. H., & Heo, H. (2016). In-Vivo Proton Magnetic Resonance Spectroscopy of 2-Hydroxyglutarate in Isocitrate Dehydrogenase-Mutated Gliomas: A Technical Review for Neuroradiologists. *Korean J Radiol, 17*(5), 620-632. doi:10.3348/kjr.2016.17.5.620

Kinnersley, B., Labussiere, M., Holroyd, A., Di Stefano, A. L., Broderick, P., Vijayakrishnan, J., Houlston, R. S. (2015). Genome-wide association study identifies multiple susceptibility loci for glioma. *Nat Commun, 6*, 8559. doi:10.1038/ncomms9559

Labussiere, M., Boisselier, B., Mokhtari, K., Di Stefano, A. L., Rahimian, A., Rossetto, M., Sanson, M. (2014). Combined analysis of TERT, EGFR, and IDH status defines distinct prognostic glioblastoma classes. *Neurology, 83*(13), 1200-1206. doi:10.1212/WNL.0000000000000814

Labussiere, M., Di Stefano, A. L., Gleize, V., Boisselier, B., Giry, M., Mangesius, S., Sanson, M. (2014). TERT promoter mutations in gliomas, genetic associations and clinico-pathological correlations. *Br J Cancer, 111*(10), 2024-2032. doi:10.1038/bjc.2014.538

Labussiere, M., Idbaih, A., Wang, X. W., Marie, Y., Boisselier, B., Falet, C., Sanson, M. (2010). All the 1p19q codeleted gliomas are mutated on IDH1 or IDH2. *Neurology, 74*(23), 1886-1890. doi:10.1212/WNL.0b013e3181e1cf3a

Larjavaara, S., Mantyla, R., Salminen, T., Haapasalo, H., Raitanen, J., Jaaskelainen, J., & Auvinen, A. (2007). Incidence of gliomas by anatomic location. *Neuro Oncol, 9*(3), 319-325. doi:10.1215/15228517-2007-016

Law, M., Yang, S., Wang, H., Babb, J. S., Johnson, G., Cha, S., Zagzag, D. (2003). Glioma grading: sensitivity, specificity, and predictive values of perfusion MR imaging and proton MR spectroscopic imaging compared with conventional MR imaging. *AJNR Am J Neuroradiol, 24*(10), 1989-1998.

Lazovic, J., Soto, H., Piccioni, D., Lou, J. R., Li, S., Mirsadraei, L., Pope, W. B. (2012). Detection of 2-hydroxyglutaric acid in vivo by proton magnetic resonance spectroscopy in U87 glioma cells overexpressing isocitrate dehydrogenase-1 mutation. *Neuro Oncol, 14*(12), 1465-1472. doi:10.1093/neuonc/nos258

Louis, D. N., Ohgaki, H., Wiestler, O. D., Cavenee, W. K., Burger, P. C., Jouvet, A., Kleihues, P. (2007). The 2007 WHO classification of tumours of the central nervous system. *Acta Neuropathol, 114*(2), 97-109. doi:10.1007/s00401-007-0243-4

Louis, D. N., Perry, A., Reifenberger, G., von Deimling, A., Figarella-Branger, D., Cavenee, W. K., Ellison, D. W. (2016). The 2016 World Health Organization Classification of Tumors of the Central Nervous System: a summary. *Acta Neuropathol, 131*(6), 803-820. doi:10.1007/s00401-016-1545-1

Lu, C., Ward, P. S., Kapoor, G. S., Rohle, D., Turcan, S., Abdel-Wahab, O., Thompson, C. B. (2012). IDH mutation impairs histone demethylation and results in a block to cell differentiation. *Nature, 483*(7390), 474-478. doi:10.1038/nature10860

Madan, A., Ganji, S. K., An, Z., Choe, K. S., Pinho, M. C., Bachoo, R. M., Choi, C. (2015). Proton T2 measurement and quantification of lactate in brain tumors by MRS at 3 Tesla in vivo. *Magn Reson Med, 73*(6), 2094-2099. doi:10.1002/mrm.25352

Natsumeda, M., Igarashi, H., Nomura, T., Ogura, R., Tsukamoto, Y., Kobayashi, T., Fujii, Y. (2014). Accumulation of 2-hydroxyglutarate in gliomas correlates with survival: a study by 3.0-tesla magnetic resonance spectroscopy. *Acta Neuropathol Commun, 2*, 158. doi:10.1186/s40478-014-0158-y

Olshen, A. B., Venkatraman, E. S., Lucito, R., & Wigler, M. (2004). Circular binary segmentation for the analysis of array-based DNA copy number data. *Biostatistics, 5*(4), 557-572. doi:10.1093/biostatistics/kxh008

Omuro, A., & DeAngelis, L. M. (2013). Glioblastoma and other malignant gliomas: a clinical review. *JAMA, 310*(17), 1842-1850. doi:10.1001/jama.2013.280319

Ostrom, Q. T., Gittleman, H., Fulop, J., Liu, M., Blanda, R., Kromer, C., Barnholtz-Sloan, J. S. (2015). CBTRUS Statistical Report: Primary Brain and Central Nervous System Tumors Diagnosed in the United States in 2008-2012. *Neuro Oncol, 17 Suppl 4*, iv1-iv62. doi:10.1093/neuonc/nov189

Parsons, D. W., Jones, S., Zhang, X., Lin, J. C., Leary, R. J., Angenendt, P., Kinzler, K. W. (2008). An integrated genomic analysis of human glioblastoma multiforme. *Science, 321*(5897), 1807-1812. doi:10.1126/science.1164382

Pope, W. B., Prins, R. M., Albert Thomas, M., Nagarajan, R., Yen, K. E., Bittinger, M. A., Liau, L. M. (2012). Non-invasive detection of 2-hydroxyglutarate and other metabolites in IDH1 mutant glioma patients

using magnetic resonance spectroscopy. *J Neurooncol, 107*(1), 197-205. doi:10.1007/s11060-011-0737-8

Powers, C. J., McLeskey, S. W., & Wellstein, A. (2000). Fibroblast growth factors, their receptors and signaling. *Endocr Relat Cancer, 7*(3), 165-197.

Provencher, S. W. (2001). Automatic quantitation of localized in vivo 1H spectra with LCModel. *NMR Biomed, 14*(4), 260-264.

Quillien, V., Lavenu, A., Karayan-Tapon, L., Carpentier, C., Labussiere, M., Lesimple, T., Figarella-Branger, D. (2012). Comparative assessment of 5 methods (methylation-specific polymerase chain reaction, MethyLight, pyrosequencing, methylation-sensitive high-resolution melting, and immunohistochemistry) to analyze O6-methylguanine-DNA-methyltranferase in a series of 100 glioblastoma patients. *Cancer, 118*(17), 4201-4211. doi:10.1002/cncr.27392

Reyes-Botero, G., Giry, M., Mokhtari, K., Labussiere, M., Idbaih, A., Delattre, J. Y., Sanson, M. (2014). Molecular analysis of diffuse intrinsic brainstem gliomas in adults. *J Neurooncol, 116*(2), 405-411. doi:10.1007/s11060-013-1312-2

Rigau, V., Zouaoui, S., Mathieu-Daude, H., Darlix, A., Maran, A., Tretarre, B., Association des Neuro-Oncologues d'Expression, F. (2011). French brain tumor database: 5-year histological results on 25 756 cases. *Brain Pathol, 21*(6), 633-644. doi:10.1111/j.1750-3639.2011.00491.x

Sanson, M., Hosking, F. J., Shete, S., Zelenika, D., Dobbins, S. E., Ma, Y., Simon, M. (2011). Chromosome 7p11.2 (EGFR) variation influences glioma risk. *Hum Mol Genet, 20*(14), 2897-2904. doi:10.1093/hmg/ddr192

Sanson, M., Marie, Y., Paris, S., Idbaih, A., Laffaire, J., Ducray, F., Delattre, J. Y. (2009). Isocitrate dehydrogenase 1 codon 132 mutation is an important prognostic biomarker in gliomas. *J Clin Oncol, 27*(25), 4150-4154. doi:10.1200/JCO.2009.21.9832

Sasaki, M., Knobbe, C. B., Munger, J. C., Lind, E. F., Brenner, D., Brustle, A., Mak, T. W. (2012). IDH1(R132H) mutation increases murine haematopoietic progenitors and alters epigenetics. *Nature, 488*(7413), 656-659. doi:10.1038/nature11323

Shete, S., Hosking, F. J., Robertson, L. B., Dobbins, S. E., Sanson, M., Malmer, B., Houlston, R. S. (2009). Genome-wide association study identifies five susceptibility loci for glioma. *Nat Genet, 41*(8), 899-904. doi:10.1038/ng.407

Siegel, R., Ward, E., Brawley, O., & Jemal, A. (2011). Cancer statistics, 2011: the impact of eliminating socioeconomic and racial disparities on premature cancer deaths. *CA Cancer J Clin, 61*(4), 212-236. doi:10.3322/caac.20121

Singh, D., Chan, J. M., Zoppoli, P., Niola, F., Sullivan, R., Castano, A., Iavarone, A. (2012). Transforming fusions of FGFR and TACC genes in human

glioblastoma. *Science, 337*(6099), 1231-1235. doi:10.1126/science.1220834

Stupp, R., Mason, W. P., van den Bent, M. J., Weller, M., Fisher, B., Taphoorn, M. J., National Cancer Institute of Canada Clinical Trials, G. (2005). Radiotherapy plus concomitant and adjuvant temozolomide for glioblastoma. *N Engl J Med, 352*(10), 987-996. doi:10.1056/NEJMoa043330

Suzuki, H., Aoki, K., Chiba, K., Sato, Y., Shiozawa, Y., Shiraishi, Y., Ogawa, S. (2015). Mutational landscape and clonal architecture in grade II and III gliomas. *Nat Genet, 47*(5), 458-468. doi:10.1038/ng.3273

Tabernero, J., Bahleda, R., Dienstmann, R., Infante, J. R., Mita, A., Italiano, A., Soria, J. C. (2015). Phase I Dose-Escalation Study of JNJ-42756493, an Oral Pan-Fibroblast Growth Factor Receptor Inhibitor, in Patients With Advanced Solid Tumors. *J Clin Oncol, 33*(30), 3401-3408. doi:10.1200/JCO.2014.60.7341

Tabouret, E., Nguyen, A. T., Dehais, C., Carpentier, C., Ducray, F., Idbaih, A., For, P. N. (2016). Prognostic impact of the 2016 WHO classification of diffuse gliomas in the French POLA cohort. *Acta Neuropathol, 132*(4), 625-634. doi:10.1007/s00401-016-1611-8

Thomson, R. E., Kind, P. C., Graham, N. A., Etherson, M. L., Kennedy, J., Fernandes, A. C., Iwata, T. (2009). Fgf receptor 3 activation promotes selective growth and expansion of occipitotemporal cortex. *Neural Dev, 4*, 4. doi:10.1186/1749-8104-4-4

Tkac, I., Starcuk, Z., Choi, I. Y., & Gruetter, R. (1999). In vivo 1H NMR spectroscopy of rat brain at 1 ms echo time. *Magn Reson Med, 41*(4), 649-656.

Turcan, S., Rohle, D., Goenka, A., Walsh, L. A., Fang, F., Yilmaz, E., Chan, T. A. (2012). IDH1 mutation is sufficient to establish the glioma hypermethylator phenotype. *Nature, 483*(7390), 479-483. doi:10.1038/nature10866

Turner, N., & Grose, R. (2010). Fibroblast growth factor signalling: from development to cancer. *Nat Rev Cancer, 10*(2), 116-129. doi:10.1038/nrc2780

van Rhijn, B. W., van Tilborg, A. A., Lurkin, I., Bonaventure, J., de Vries, A., Thiery, J. P., Radvanyi, F. (2002). Novel fibroblast growth factor receptor 3 (FGFR3) mutations in bladder cancer previously identified in non-lethal skeletal disorders. *Eur J Hum Genet, 10*(12), 819-824. doi:10.1038/sj.ejhg.5200883

Vogazianou, A. P., Chan, R., Backlund, L. M., Pearson, D. M., Liu, L., Langford, C. F., Ichimura, K. (2010). Distinct patterns of 1p and 19q alterations identify subtypes of human gliomas that have different prognoses. *Neuro Oncol, 12*(7), 664-678. doi:10.1093/neuonc/nop075

Waitkus, M. S., Diplas, B. H., & Yan, H. (2016). Isocitrate dehydrogenase mutations in gliomas. *Neuro Oncol, 18*(1), 16-26. doi:10.1093/neuonc/nov136

Walsh, K. M., Codd, V., Smirnov, I. V., Rice, T., Decker, P. A., Hansen, H. M., Wrensch, M. R. (2014). Variants near TERT and TERC influencing telomere length are associated with high-grade glioma risk. *Nat Genet, 46*(7), 731-735. doi:10.1038/ng.3004

Weathers, S. P., & Gilbert, M. R. (2014). Advances in treating glioblastoma. *F1000Prime Rep, 6*, 46. doi:10.12703/P6-46

Wrensch, M., Jenkins, R. B., Chang, J. S., Yeh, R. F., Xiao, Y., Decker, P. A., Wiencke, J. K. (2009). Variants in the CDKN2B and RTEL1 regions are associated with high-grade glioma susceptibility. *Nat Genet, 41*(8), 905-908. doi:10.1038/ng.408

Xu, W., Yang, H., Liu, Y., Yang, Y., Wang, P., Kim, S. H., Xiong, Y. (2011). Oncometabolite 2-hydroxyglutarate is a competitive inhibitor of alpha-ketoglutarate-dependent dioxygenases. *Cancer Cell, 19*(1), 17-30. doi:10.1016/j.ccr.2010.12.014

Yan, H., Parsons, D. W., Jin, G., McLendon, R., Rasheed, B. A., Yuan, W., Bigner, D. D. (2009). IDH1 and IDH2 mutations in gliomas. *N Engl J Med, 360*(8), 765-773. doi:10.1056/NEJMoa0808710

Yang, H., Ye, D., Guan, K. L., & Xiong, Y. (2012). IDH1 and IDH2 mutations in tumorigenesis: mechanistic insights and clinical perspectives. *Clin Cancer Res, 18*(20), 5562-5571. doi:10.1158/1078-0432.CCR-12-1773

Zonari, P., Baraldi, P., & Crisi, G. (2007). Multimodal MRI in the characterization of glial neoplasms: the combined role of single-voxel MR spectroscopy, diffusion imaging and echo-planar perfusion imaging. *Neuroradiology, 49*(10), 795-803. doi:10.1007/s00234-007-0253-x